Dipartimento di / Department of

Scienza dei Materiali

Dottorato di Ricerca in / PhD program Scienza e Nanotecnologia dei Materiali Ciclo / Cycle XXXIII

SUSTAINABLE SYNTHETIC METHODOLOGIES FOR THE PREPARATION OF ORGANIC SEMICONDUCTING MATERIALS: ORGANIC (OPTO)ELECTRONICS GROWING "GREEN"

Cognome / Surname: Calascibetta Nome / Name: Adiel Mauro

Matricola / Registration number: 769698

Tutore / Tutor: Prof. Luca Beverina

Coordinatore / Coordinator: Prof. Marco Bernasconi

ANNO ACCADEMICO / ACADEMIC YEAR 2019/2020

Table of Contents

Introduction

Organic Electronics en Route Toward a Sustainable Future

We live immersed in an electronic world where it becomes increasingly difficult to imagine a single day without the assistance of modern technology. Whether we talk about electronic circuits, processors, sensors, lasers, memory elements, displays, photodiodes, solar cells and so forth, those devices are indispensable tools of our daily routine. Electronics, and more specifically integrated circuits (IC), have dramatically changed our lives and the way we interact with the world. Economic, health, and national security rely on and are positively impacted by electronic technology. The commercial success of integrated electronics is based on a mutual development of technology and applications, where technical progress and economic growth support each other. The impressive technological achievements of our time are the result of more than fifty years of ongoing electronics revolution, where inorganic semiconductors with their archetypical examples silicon and gallium arsenide remain fundamental. Nevertheless, modern silicon microelectronics and its manufacturing technology are characterized by extremely expensive and complicated processes; they generally require high-temperature and vacuum-based manufactures limiting the technology throughput. Even if novel electronic products become more and more energy efficient in application, it is not their power consumption that creates an energy imbalance, but actually the energy expended in their production phase and stored (embodied) in their inner constituents, i.e. microchips, processors, displays, etc.[1,2] The higher the demand of the market, the more versatile the offer, and the higher the energy consumption expended in the manufacturing processes. Modern electronic technology has turned the relationship energy consumed during fabrication vs. energy consumed during exploitation of the product to a complete imbalance: just think that a simple laptop or a smart phone contains more embodied energy than a 1980s or 1990s edition automobile.[3] The manufacturing process of a significant amount of a high-quality inorganic semiconductor or other nanomaterial of any modern electronic gadget requires up to six orders of magnitude or more energy than the energy required for processing a plastic or a metal component.[1] The colossal demand of electronics is leading not only to an energy imbalance, but also to a series of unfortunate and undesirable consequences: (i) a massive amount of wastes, including both electrical and electronic equipment (WEEE) and manufacturing refuses, besides (ii) a rapid exhaustion of already scarce natural elements, such as gallium (annual production of ~215 tons) and indium (annual production of ~1100 tons including recycling) both of which have an estimated availability of about 20 years until they will run out completely.[4] The resources and methodologies used to manufacture electronic devices raise urgent questions about the negative environmental impacts of the production, use, and disposal of electronic devices. A paradigm shift of the way we control both the resource exploitation, and the electronics manufacturing/disposal is required in order to minimize the negative impact of our present and future generations on the environment and to create a sustainable future. As defined by the *United Nations World Commission on Environment and Development*, a sustainable development is established when humanity ensures its present needs without compromising the ability of future generations to meet their own needs.[5]

For most people, the expression "sustainable electronics" concerns about energy efficiency, resource use, and waste disposal or recycling, that is building an electronic world which enables sustainable management of natural resources. Creating more sustainable electronic products is not just about

introducing "eco-friendly" device platforms, but also using more "eco-friendly" manufacturing methods to do so. In fact, sustainability cuts across the entire life cycle of an electronic product, from raw resources to disposal. In this regard, the use of organic materials to construct electronic devices offers a more eco-friendly and cost-affordable approach to grow our electronic world.[6] Organic-based technologies consisting of "soft" conjugated small molecules and polymers as the core semiconductor element are meant to address the energy, cost-inefficiency and sustainability issues posed by their inorganic counterparts. Organic electronics (OE) entered the research field in 1977 with the discovery of highly conducting polyacetylene by Shirakawa, MacDiarmid, and Heeger,[7] opening up new fields of science and research of huge interest. The progress in those fields has grown exponentially and nowadays π-conjugated organic structures, called organic semiconductors (OSCs), can be successfully implemented in several electronic devices, including organic light-emitting diodes (OLEDs), organic field-effect transistors (OFETs), sensors, integrated circuits, solar energy storage, memories, organic photovoltaic cells (OPVs), RF-ID tags etc.[8–12] The growing list of applications reflects the complexity of the topic and the wide possible uses for organic electronics, and it is likely that the list will even grow in the future. The first examples, such as displays in mobile appliances, have already found their way to market as replacements for traditional components in existing products. Today, OLEDs are widely used in mobile phones and it is possible to buy printed organic photovoltaic modules and simple printed memories. In particular, OE distinguishes itself from traditional electronics because it is possible to explore a limitless library of materials through structural design and functionalization at molecular level, as well as process active materials from solution and form functional films to realize light displays and circuits that are completely flexible. Furthermore, owing to the key features of low-cost, low-temperature and processability from solution over arbitrary substrates, OSCs are amenable to inexpensive, fast, and high-throughput manufacturing processes; for example, they are compatible with all-in-line roll-to-roll printing techniques to fulfil the constantly increasing demand for large-area electronics.[13] Finally, biocompatible and biodegradable electronic devices may be realized only with organic materials, which have the potential to interface with biological systems in a way not possible with today's silicon-based electronics. This opens a vast world of possibility with respect to medical, sensing, and other human interface applications.

Despite intense efforts of the scientific community during the past 30 years, the performance[14–16] and stability[17] of organic semiconductors remain at current times major hurdles in their development as solid competitors of the inorganic counterparts. As a consequence, the large-scale immediate replacement of hard core inorganic components with organic counterparts is not immediately foreseen.[14–18] Nevertheless, the versatile nature of OE combined with the promise the field holds forth for environmental and social sustainability point the way to a very long-lived set of technologies. It is not just the devices themselves that promise to be more eco-friendly (ending with potentially biodegradable or recyclable devices) than silicon-based electronics, but also their manufacture processes. With OLEDs already making a large footprint in the market of flat panel displays and with OFETs and OPVs entering small scale commercial production in e-books and roll-to-roll fabricated photovoltaics, the research field of OE is mature enough to focus on achieving ambitious goals of generating "green" avenues for a sustainable electronic future.

As already discussed, OE is a platform technology that enables multiple applications, which vary widely in their specifications. Since the technology is still in its early stage but aiming to a transition from lab-to-fab scale of production, it is important to develop a common opinion about what kind of products, processes and materials will be available and when. "Green" chemistry and technologies are carving avenues towards achieving the ambitious goal of sustainability in the field of electronics,[19] by identifying (i) highly abundant, low cost and natural organic precursors, with (ii) economically feasible and high throughput synthetic routes that avoid (or at least that remarkably reduce) the usage of toxic solvents for the production of performing materials and do not generate toxic waste requiring expensive handling and disposal. In addition, active materials should ensure (iii) low-cost processes for practical devices fabrication (ideally either at room temperature from benign solvents or at low sublimation temperatures), and (iv) ideally render electronics that feature biodegradability in mild degradation conditions at the end of their life cycle and/or electronics that are suitable for performing

complex biological functions (e.g. transduction, sensing, recognition, event triggering, etc.) as a tool for interfacing electronics with various forms of life. Since green materials and technologies are now in the stage of emerging concepts, offering at this time a clear definition of "greenness" is not unequivocal; that is because achieving industrial green synthesis of green organic materials by means of green technologies remains truly challenging at this time. For example, many benign dyes and pigments commonly employed in textile, cosmetic, and food coloring industries are produced through industrially attractive, low-cost and high throughput synthesis;[20] nevertheless, in many cases their manufacture involves and generates environmentally unfriendly by-products and waste. However, the field of OE is in its infancy with respect to class of devices on the market. Realizing the vision of OE as a more innovative, accessible, and sustainable approach to grow our electronic world will require overcoming key research challenges for advancing the field in a way that will maximize its potential positive impact on society.

In their quest to achieve electronics sustainability by solving the above-mentioned energy deficiency puzzle and redressing the unfolding environmental disaster, scientists are often inspired both by the apparent simplicity and by the true complexity of nature. Nature is an extremely efficient energy consumption engine that we could use for infinite inspirations.

Image with Copyright © of The Royal Society of Chemistry 2014. [6]

Bibliography

1. Gutowski, T. G. *et al.* Thermodynamic analysis of resources used in manufacturing processes. *Environ. Sci. Technol.* **43**, 1584–1590 (2009).
2. Allwood, J. M., Ashby, M. F., Gutowski, T. G. & Worrell, E. Material efficiency: A white paper. *Resour. Conserv. Recycl.* **55**, 362–381 (2011).
3. Williams, E. D. Revisiting energy used to manufacture a desktop computer: Hybrid analysis combining process and economic input-output methods. *IEEE Int. Symp. Electron. Environ.* 80–85 (2004) doi:10.1109/isee.2004.1299692.
4. Zoeteman, B. C. J., Krikke, H. R. & Venselaar, J. Handling WEEE waste Hows: On the effectiveness of producer responsibility in a globalizing world. *Int. J. Adv. Manuf. Technol.* **47**, 415–436 (2010).
5. Chatterjee, D. K. World Commission on Environment and Development. *Encycl. Glob. Justice* 1163–1163 (2011) doi:10.1007/978-1-4020-9160-5_1126.
6. Irimia-Vladu, M. 'Green' electronics: Biodegradable and biocompatible materials and devices for sustainable future. *Chem. Soc. Rev.* **43**, 588–610 (2014).
7. Chiang, C. K. *et al.* Electrical conductivity in doped polyacetylene. *Phys. Rev. Lett.* **39**, 1098–1101 (1977).
8. Guo, X., Baumgarten, M. & Müllen, K. Designing π-conjugated polymers for organic electronics. *Prog. Polym. Sci.* **38**, 1832–1908 (2013).
9. Dou, L., Liu, Y., Hong, Z., Li, G. & Yang, Y. Low-Bandgap Near-IR Conjugated Polymers/Molecules for Organic Electronics. *Chem. Rev.* **115**, 12633–12665 (2015).
10. Groves, C. Organic light-emitting diodes: Bright design. *Nat. Mater.* **12**, 597–598 (2013).
11. Wang, C., Dong, H., Hu, W., Liu, Y. & Zhu, D. Semiconducting π-conjugated systems in field-effect transistors: A material odyssey of organic electronics. *Chem. Rev.* **112**, 2208–2267 (2012).
12. Facchetti, A. π-Conjugated polymers for organic electronics and photovoltaic cell applications. *Chem. Mater.* **23**, 733–758 (2011).
13. Zvezdin, A., Di Mauro, E., Rho, D., Santato, C. & Khalil, M. En route toward sustainable organic electronics. *MRS Energy Sustain.* **7**, 3–10 (2020).
14. Ma, H., Acton, O., Hutchins, D. O., Cernetic, N. & Jen, A. K. Y. Multifunctional phosphonic acid self-assembled monolayers on metal oxides as dielectrics, interface modification layers and semiconductors for low-voltage high-performance organic field-effect transistors. *Phys. Chem. Chem. Phys.* **14**, 14110–14126 (2012).
15. Mei, J., Diao, Y., Appleton, A. L., Fang, L. & Bao, Z. Integrated materials design of organic semiconductors for field-effect transistors. *J. Am. Chem. Soc.* **135**, 6724–6746 (2013).
16. Janssen, R. A. J. & Nelson, J. Factors limiting device efficiency in organic photovoltaics. *Adv. Mater.* **25**, 1847–1858 (2013).
17. Jørgensen, M. *et al.* Stability of polymer solar cells. *Adv. Mater.* **24**, 580–612 (2012).
18. Ante, F. *et al.* Contact resistance and megahertz operation of aggressively scaled organic transistors. *Small* **8**, 73–79 (2012).
19. Lee, E. K., Lee, M. Y., Park, C. H., Lee, H. R. & Oh, J. H. Toward Environmentally Robust Organic Electronics: Approaches and Applications. *Adv. Mater.* **29**, 1–29 (2017).
20. Irimia-Vladu, M., Głowacki, E. D., Voss, G., Bauer, S. & Sariciftci, N. S. Green and biodegradable electronics. *Mater. Today* **15**, 340–346 (2012).

Chapter 1

Organic Semiconducting Materials for (Opto)Electronic Applications

Photoactive and electroactive organic systems, known as organic semiconductors (OSCs), have been playing a crucial role as functional materials in the development of organic electronic, photonic and optoelectronic devices mainly concerned with thin-films and flexible architectures.[1,2] Among these technologies organic photovoltaic devices (OPVs), organic light-emitting diodes (OLEDs) and organic thin-film transistors (OTFTs) have been the central topics of current research and development.[3–5] OPVs have been receiving a great deal of interest as promising candidates for next-generation solar cells helping facing current global issues of non-abundant materials, environment and energy. OLEDs have already found their way to market with the successful practical application as portable flat-panel displays in smartphones and televisions and are expected to accomplish next-generation solid-state lighting. OTFTs are key components for driving various devices to a cheap and practical fabrication of thin-film, light-weight and flexible architectures by use of printing techniques.

OSCs consist of both small-molecular and polymeric materials and they are generally characterized by low-cost, lightweight, wide availability of raw materials, synthetic flexibility, low production and energy costs, easy processibility, and infinite possibilities of chemical engineering and functionalization for tailoring physical properties to achieve specific functions.[6] Actually, OSCs are expected to be key materials for 21st-century industries: they can be solution processed, low-temperature evaporated or sublimed (at relatively low vacuum levels), self-assembled and formulated in functional inks which are compatible with flexible plastic substrates. These advantages allow to deploy organic-based devices in large-area through low cost roll-to-roll printing or coating processes, profiting from well-established know-how about printing processes, papers, and photographic films production for example.[7] Digital printing (such as inkjet) makes it even possible to produce custom-designed plastic electronics on a massive scale by remarkably cost-effective continuous reel-to reel processes.

The science of organic and printed (opto)electronics include wide areas, from the structural design and synthesis of photoactive and electroactive materials, to the elucidation of their physical and chemical properties as well as the structures, fabrication, and performance evaluation of the devices, and the creation of new knowledge derived from the operation of such devices. Overall, the technology has already entered in a small market reality with first relatively simple products,[10] however further growth could be reached in the near future depending on progress in materials, processes, devices, circuit designs and environmental impact.

This chapter gives an overview of organic semiconducting materials, including both molecular materials and polymers, with applications in electronic and optoelectronic devices such as OTFTs, OLEDs and OPVs, focusing on the recent progress in these fields. The characteristic features and molecular design concepts for molecular and polymeric materials, with examples of various kinds of OSCs for use in such devices, fabrication and performance are also discussed.

1.1. Organic π-Conjugated Systems: Structures and Properties

Organic semiconductors are π-electron systems with the capability to absorb and emit light in the wavelength region from ultraviolet to near infrared, generate and transport charge carriers and often exhibit excellent nonlinear optical properties. These materials possess a π-conjugated backbone (generally represented by the alternation of single and double bonds) which can be simplified to a system of linked diene units leading to extended p-orbitals that, by resonance effect, confer electron delocalization and the ability to transport charge. The conjugation extension and functionalization of this backbone have a dramatic impact on optical and electrical properties of the material. Conversely, non-conjugated structures such as polyethylene or teflon are excellent insulators. The solid-state structure of conjugated systems is dominated by individual molecular units bound together by weak interactions, principally Van der Waals forces such as dipole-dipole and π-π stacking, which impart unique electronic properties depending on the packing structure.[8] These should be contrasted with the far stronger intramolecular covalent interactions, which nevertheless allow for soft bonded degrees of freedom, notably torsional motion along the backbone and side chains.[9] As a result, structure packing is governed by both energy and entropy, giving rise to complex morphologies that incorporate amorphous, liquid-crystalline, and crystalline ordering.

The description of optical and electrical properties of organic semiconductors is generally performed by considering the energy and electronic distribution of the corresponding frontier molecular orbitals (FMOs): the highest occupied molecular orbital (HOMO) and the lowest unoccupied molecular orbital (LUMO). Considering a given structure, as its conjugation length increases the HOMO-LUMO energy gap decreases, complemented by the reduction in distance between bond and anti-bond molecular orbitals until they are so close to become indiscernible from each other (**Figure 1**). This leads to the formation of two bands: the valence band where the electrons are located, and the conduction band, where the electrons can jump as soon as they receive enough energy to overcome the energy gap. The limit of this representation is reached when the gap between HOMO and LUMO is so small that the two orbitals basically overlap, as in the case of a metal. Organic materials are identified as semiconductors an energy gap (E_G) is always present, even in the case of Polyacetylene the simplest example of conjugated polymer. Indeed, even if in principle the linear combination of an infinite number of conjugated double bonds would lead to a completely delocalized structure where all carbon atoms are equivalents, a fundamental result of solid-state physics (the Peierls theorem) forbids the existence of a monodimensional metal. As such, a finite bond length alternation between adjacent double and single bonds is formed with the consequent opening of a small band gap.

Carful control over HOMO-LUMO energy levels, energy gap and solid-state packing, by means of structural design engineering, enable defining specific optical, electrical, and optoelectronic properties of organic materials, such as absorption/emission characteristics and charge carrier mobility, leading to define an active material as most suitable for a specific (opto)electronic application.[10]

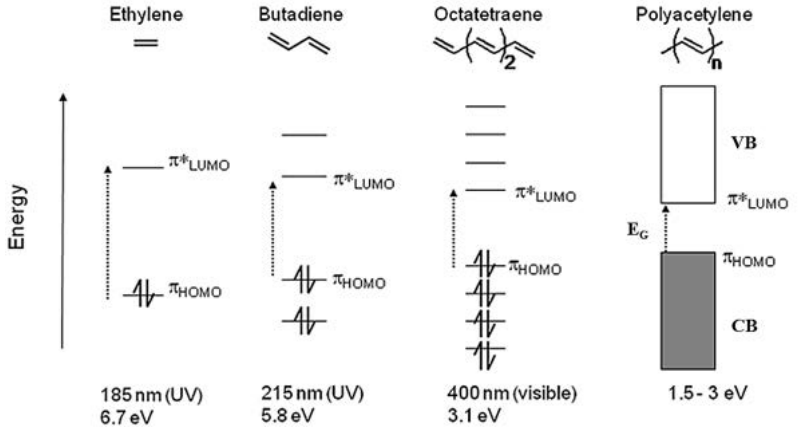

***Figure 1**. Diagram of electronic levels distribution as function of the number of conjugated double bonds.*

1.1.1. Structural Engineering of the Energy Gap in π-Conjugated Systems

As previously discussed, the energy gap $\mathbf{E_G}$ between the HOMO-LUMO levels of a specific material decreases as a negative function of the extent of conjugation of the structure. However, this trend is not linear, but it tends asymptotically to a set value given by several energy contributions. This concept was formalized by Roncali[11] in the following equation:

$$\mathbf{E_G} = E_{bla} + E_{Res} + E_{sub} + E_{\theta} + E_{Int}$$

These contributions can be represented by five parameters:

- The bond-length alternation energy (E_{bla}), which usually represent the major contribution and depends on the difference between single and double bond lengths of the π-conjugated core. This parameter is particularly pronounced in aromatic systems, where the two limiting mesomeric forms aromatic and quinoid (**Figure 2)** obtained by the flip of the double bonds are not energetically equivalent.
- The aromatic stabilisation resonance energy (E_{Res}) of cyclic π-systems. There is a competition between π-electron confinement within the aromatic rings and delocalization along the whole conjugated chain. The energy needed to switch from the aromatic to the quinoid form directly depends on E_{Res} of a given aromatic unit. Typically, highly delocalized π-electrons are essential to achieve optimal electronic properties.
- The electronic effect of substituents (E_{sub}). The introduction of electron-withdrawing or electron-releasing substituents strongly affect the HOMO-LUMO levels.
- The planarity of the molecule (E_{θ}). The degree of interannular rotations relates to different conformations of the conjugated core. Any distortion from backbone planarity due to interannular rotations about single bonds will increase E_G because the orbital overlap varies with the cosine of the torsional angle θ.
- The solid-state interactions between individual molecules (E_{Int}). Intermolecular interactions can influence the properties of a single conjugated molecule by tuning E_G when assembling.

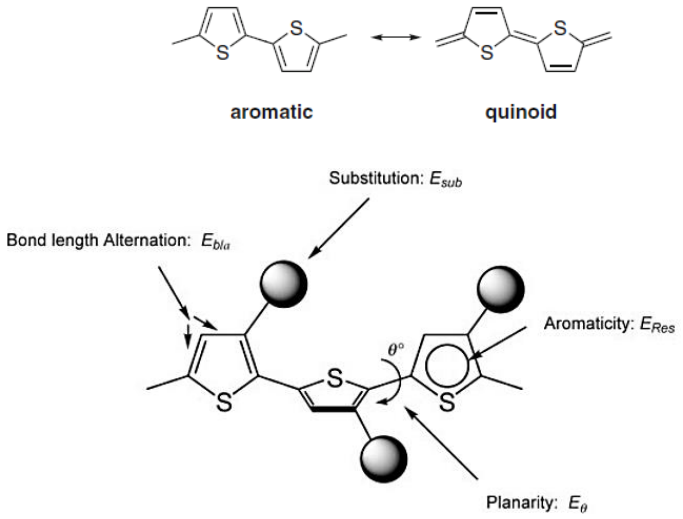

***Figure 2**. Top: schematic representation of aromatic and quinoidal structures of bithiophene. Bottom: structural factors determining the HOMO-LUMO energy gap of linear π-conjugated systems. Reported with permission from ref. [11]; © 2007 WILEY-VCH Verlag GmbH & Co. KGaA, Weinheim.*

Since (opto)electronic devices require active materials with a specific combination of properties (for instance specific visible light interactions and efficient charge transport) the engineering of the energy gap of π-conjugated structures is the obvious solution to obtain materials with tailored physical properties. The molecular architecture useful to construct functional materials is related to one or several of these contributions. First, energy gap restriction only through conjugation length extension is a restricted strategy since at some point the effective conjugation length becomes saturated and the energy gap begins to level off.[12,13] The following are synthetic principles useful to module and in particular to narrow the energy gap of semiconducting materials in order to control (opto)electronic properties.

Resonance energy reduction

The contribution given by E_{bla} explains why conjugated aromatic rings are highly employed to achieve suitable (opto)electronic properties. Thiophenes are one of the most essential classes of aromatic heterocyclic compounds in the field of materials chemistry. Thiophene-based materials are beneficial due to their semiconducting nature, nonlinear optical responses and effective electron transport properties.[14] Considering the contribution of E_{Res} in the E_G tuning, the choice of less aromatic thiophene rings over benzene rings and the insertion of double bonds between the conjugated aromatic rings represents a simple and straightforward way to reduce E_G and improve charge delocalization. This structural design include two well-studied families of organic semiconductors: poly(p-phenylenevinylenes) (PPVs)[15] and poly(thienylenevinylenes) (PTVs)[16]. In particular, the insertion of double bonds leads to a decrease of the overall aromaticity of the system and thus to a reduction of the gap. Moreover, in both cases the ethylenic linkages eliminate the rotational freedom around the ring-ring single bonds and lead to a more planar geometry (favouring also E_θ) and thus further helps in reducing E_G. These effects can be evidenced by comparing the λ_{max} of absorbance of conjugated oligomers reported in **Figure 3** containing a constant number of π-electrons in different combinations of thiophene and ethylene units.[17]

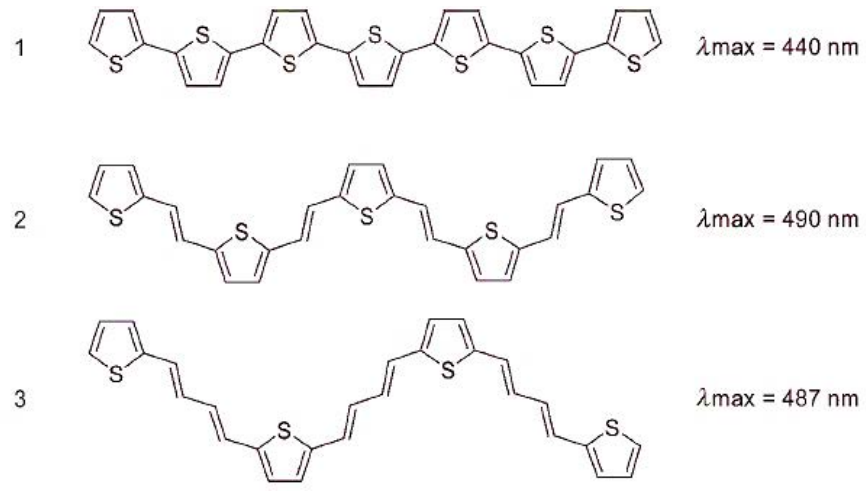

***Figure 3**. Chemical structures of oligomers 1–3 showing the effect on E_G (λmax of absorbance) by adding double bonds between the thiophene units in the molecule. Reported with permission from ref .[11]; © 2007 WILEY-VCH Verlag GmbH & Co. KGaA, Weinheim.*

While the insertion of ethylenic linkages between the thiophene rings generates the expected decrease of E_G, as shown by a 50 nm red shift of λ_{max} between 1 and 2, insertion of two adjacent double bonds (3) does not produce the expected further narrowing of the gap but contrary a slightly blue shift of λ_{max} from 490 to 487 nm between 2 and 3. This result shows that the decrease of aromaticity is in fact

counterbalanced by an increase of the vibrational freedom of the system, in which small changes in bond length alternation become possible.

Furthermore, the use of conjugated systems with an enhanced quinoid character is another popular approach for energy-gap restriction. Considering a conjugated polythiophene structure, the most immediate way to increase the quinoid character of the neutral state includes the fusion of the thiophene ring with an aromatic system with a higher resonance energy (E_{Res}). Since the aromatic character tends to localize in the system of highest $E_{Res,}$ it follows that the thiophene ring tends to dearomatize to adopt a quinoid structure. Therefore, comparison of the E_{Res} values for thiophene and benzene shows that the [c]fusion of the two rings should contribute to confer a quinoid character on the thiophene system (**Figure 4**).[18]

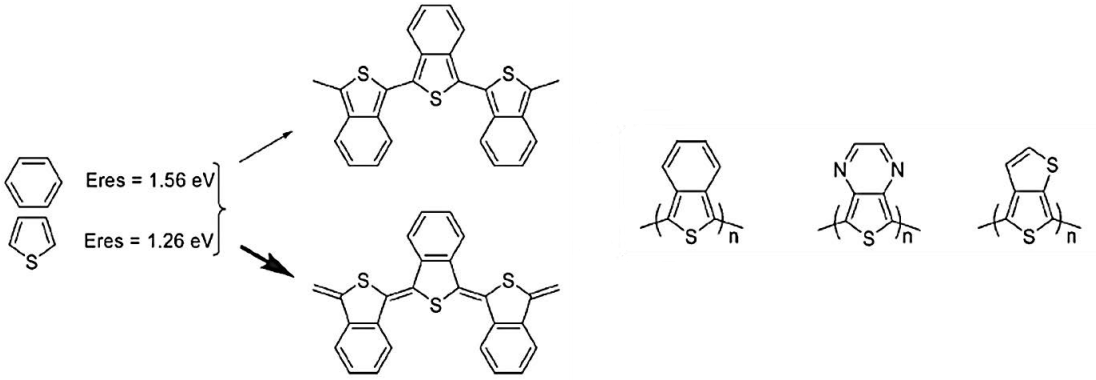

***Figure 4**. Left: comparison of the E_{Res} values for thiophene and benzene. The [c]fusion of the two rings contribute to confer quinoid character on the thiophene system, that in this case correspond to poly(benzo[c]thiophene). Right: examples of chemical structures of other typical low-band-gap polymers based on fused ring systems. Reported with permission from ref [11]; © 2007 WILEY-VCH Verlag GmbH & Co. KGaA, Weinheim.*

The electronic effect of substituents

Modulation of FMO levels and E_G can be done by introducing electron-releasing (ERG) or electron-withdrawing (EWG) groups as described for $E_{sub.}$ The introduction of ERGs to a conjugated structure decreases the oxidation potential of the system raising the HOMO level and reducing the E_G, while introducing EWGs increase the electron affinity of the system reducing both HOMO and LUMO levels as well as reducing the E_G.[11] The impact of the substituent on FMO levels depends on its electron-releasing/withdrawing strength. Alkoxy, alkylsulfanyl or amino groups are very popular electron-releasing substituents, while nitro, carboxy or cyano groups are very common electron-withdrawing substituents (**Figure 5**). The introduction of alkyl chains of sufficient length (typically 6–9 carbons) is crucial to confer solubility to highly conjugated materials in common organic solvents. Moreover, alkyl chains have a slightly inductive effect in raising its HOMO level and indirectly contribute to reduce the E_G by enhancing the long-range order in the structure, through lipophilic interactions between the alkyl chains (E_{Int});[19] this effect is remarkably important in regioregular polymers.[20,21]

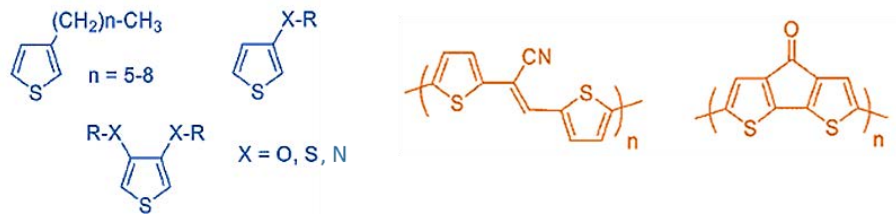

***Figure 5**. The introduction of ERGs such as e alkyl, alkoxy, alkylsulfanyl and amino groups (blue) or EWGs such as cyano or keto groups (orange) can module the energy gap. Adapted with permission from ref .[11].*

Alternation of Donor-Acceptor units

Further energy gap engineering can be performed though the "Donor-Acceptor" (D-A) approach. The alternation of electron rich (donor D) and electron poor (acceptor A) units along the π-conjugated structure leads to a molecular orbital hybridization broadening the HOMO-LUMO levels and thus reducing the E_G (**Figure 6**). This strategy introduces push-pull driving forces to facilitate electron delocalization within the conjugated structure and leads to materials with tailored FMO levels and E_G suitable for various optoelectronic applications depending on the donor and acceptor relative strength of the corresponding building blocks.[22]

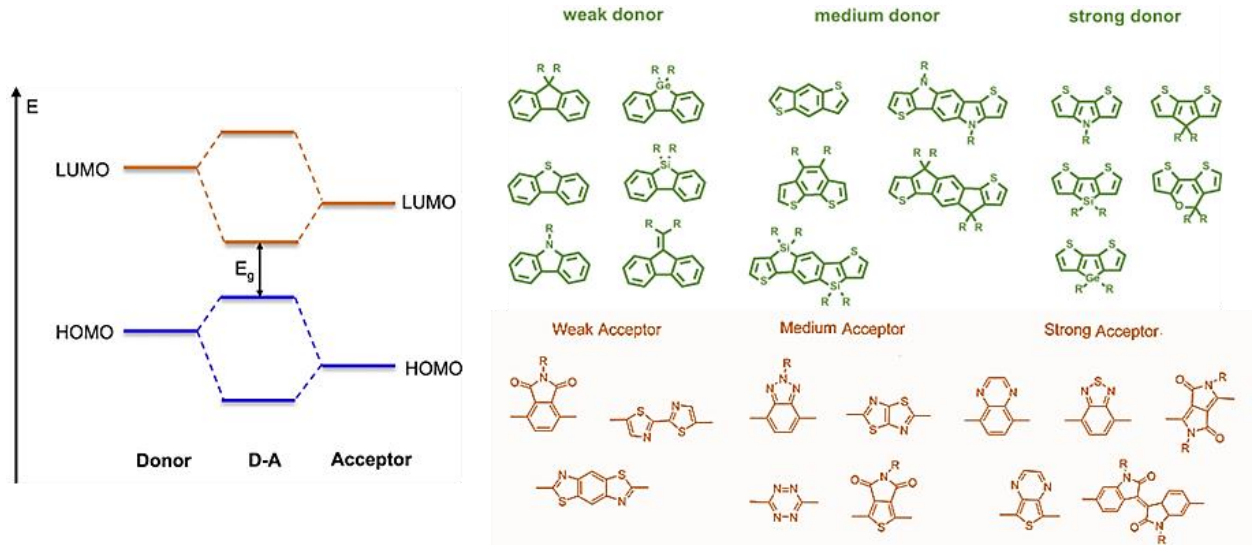

***Figure 6**. Left: diagram showing reduced E_G in donor-acceptor (D-A) structures via molecular orbital hybridization. Right: representative D and A π-electronic units.*

Rigidification of the Conjugated System

Controlling the structural conformation of conjugated materials in order to achieve high planarity is another strategy useful to finetune FMOs and reduce E_G as described for E_θ. An increase in the planarization of the π-conjugated framework allows a more efficient intermolecular π-π orbital overlap (rising the contribution of E_{Int}), π-electrons delocalization and charge transport.[23] Three general methods can be employed to achieve highly planar conjugated conformations (**Figure 7**). The first involves the increase of the number of fused aromatic rings in the structure, e.g. acenes (**A**); the second consist of connect the neighboring aromatic rings via covalent bonds to restrict the rotation about single bonds (**B**); and the third requires noncovalent through-space intramolecular interactions to enhance the planarity and rigidity of conjugated backbones, implementing O···S, N···S, X···S (where X = halide), and hydrogen-bonding interactions (**C**).[24]

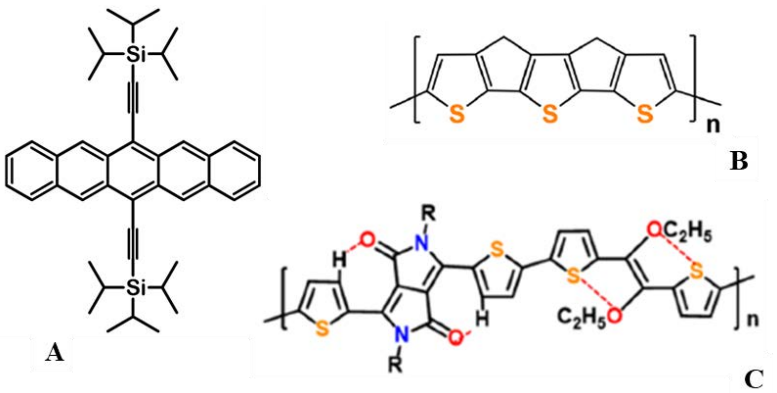

***Figure 7.** Examples of structural strategies to achieve planar conformations.*

Structural analysis of the systems with the smallest band gaps reported so far shows that their design implicitly or explicitly leads to various combinations of some of the just discussed synthetic tools. Yamashita[25] and co-workers synthesized a series of tricyclic systems involving a median proquinoid acceptor groups such as dithienylthienopyrazine (i), dithienylthienothiadiazole (ii), and dithienylthiadiazolothienopyrazine (iii) (**Figure 8**) and showed that the corresponding polymers obtained exhibit E_G values as low as 0.50 eV for iii for example.

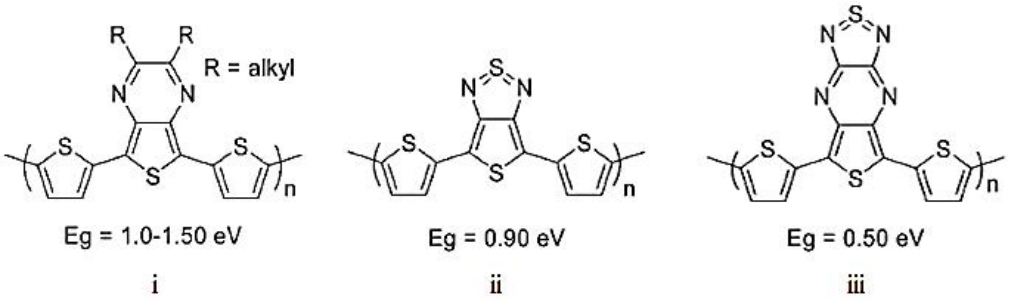

Figure 8. *Chemical structures of example tricylcic repeat units with a median proquinod acceptor group. Reported with permission from ref .[11]; © 2007 WILEY-VCH Verlag GmbH & Co. KGaA, Weinheim.*

These tricyclic systems represent a synergistic combination of alternant D-A groups, quinoidization of the polythiophene backbone by the proquinoid median groups and rigidification by intramolecular sulfur-nitrogen interactions. Even lower E_G values can be obtained replacing the thiophene unit with EDOT.[26] The results can be attributed to the stronger donor strength of EDOT, the additive sulfur-nitrogen and sulfur-oxygen noncovalent interactions and to the regular 1:1 alternation of the D-A groups.

To date, numerous small-molecule and polymeric π-conjugated organic semiconductors having diverse electronic and conformational structures have been realized, with the goals of manipulating device-specific optoelectronic properties by tuning E_G, controlling the solid-state packing, solution processability, and the resulting thin-film morphology and microstructure. The choice between molecular or polymeric semiconductors generally depends on the device to be realized, the performance required and the type of process that it is meant to be employed for its manufacture.

1.1.2. Control of Structures and Morphologies: Small-Molecules VS Polymers

Careful control over the structures and morphologies of materials is of vital importance to ensure high performance in device operation.[27] In this context, it is important to consider that processing, properties and functions of π-conjugated polymers are quite different from the corresponding small molecular units. Conjugated materials exist as either crystals, amorphous glasses, or mesophase structures such as liquid crystals and plastic crystals. Small-molecular semiconductors usually exist as crystals and generally they are not able to form smooth films. On the other hand, conjugated polymers usually contain both crystalline and amorphous phases, ranging from highly crystalline polymers to fully amorphous polymers, and usually they can form uniform films. Examples of the representative classes of crystalline molecular materials are given by polycondensed aromatic hydrocarbons, such as anthracene and pentacene (1); metal and metal-free phthalocyanines (2,3); porphyrines (3); fullerenes and their derivatives (4); perylenebisdiimides, such as PTCBI (5); and oligothiophenes with well-defined structures (6), among other substances (**Figure 9,** on the left in the blue square).[28] Furthermore, it is noteworthy that certain kinds of small molecules exhibit polymorphism (e.g., CuPc (2), TiOPc (3), and perylene pigments (5)) thus packing into crystal structures with different properties.[29] In the late 1980s, research in small organic conjugated molecules that readily form stable, amorphous glasses above room temperature became very popular for OLEDs applications.[30] Like polymers, amorphous conjugated molecular materials form stable, amorphous glasses with definite glass-transition temperatures (Tg) above room temperature, and they

does form smooth, uniform, amorphous films. Amorphous molecular materials have nonplanar molecular structures and take different conformers. The incorporation of bulky and heavy substituents and the enlargement of molecular size make glass formation easier and enhance the stability of the glassy state. The introduction of structurally rigid moieties such as biphenyl, terphenyl, carbazole, and truxene increases the Tg.[31] Representative classes of amorphous molecular materials include π-electron starburst molecules, such as the TDATA family (7), end-capped systems with the dimesitylboryl group such as TMB-TB (8), tetraphenylmethane derivatives (9), the family of spiro-linked molecules (10) and systems containing phosphorus atoms such as POAPF (11) (**Figure 9,** on the right in the orange square).[28]

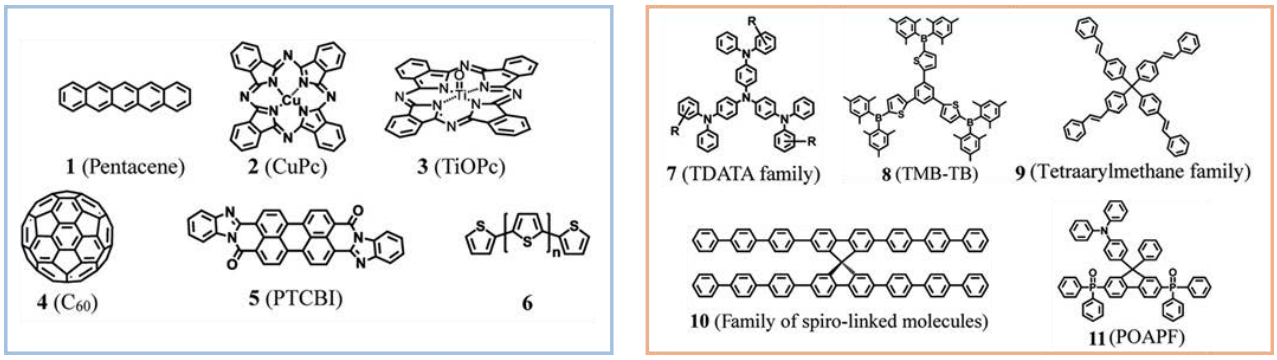

Figure 9. *Chemical structures of representative classes of crystalline molecular materials (in blue, left) and amorphous molecular materials (in red, right). Adapted with permission from ref.* [28].

On the other hand, linear π-conjugated polymers mostly consist of a crystalline phase and generally they are hard to solubilize. The representative classes of linear π-conjugated polymers are given by polyacetyrene (12), poly(p-phenylene)s (13), poly(p-phenylene vinylene)s (14, PPV), poly(9,9-dialkylfluorene)s (15), polythiophenes (16), polypyrroles (17), polyanilines (18), among other substances (**Figure 10**).

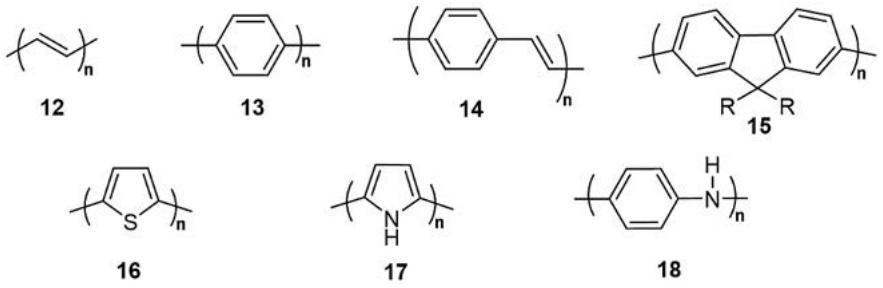

Figure 10. *Chemical structures of representative classes of linear π-conjugated polymers. Reported with permission from ref.* [28].

As already discussed, to make π-conjugated polymers soluble in organic solvents, alkyl groups are often introduced as substituents. The improved synthetic methods have enabled the synthesis of highly regioregular poly(3-alkylthiophene)s with high degrees of the head-to-tail (HT) structure.[32] They exhibited superior charge-carrier mobility and electric conductivity after doping relative to those of corresponding regiorandom polymers.

Generally, polymers readily form large-area, uniform films with mechanical strength and low surface roughness by solution processing. This film-forming ability of polymers makes them well suited to a number of practical applications. In order to increase morphological control and reduce batch-to-batch variability, various processing techniques have been developed. Solution-based approaches[33] (exactly suited for conjugated small-molecules and polymers bearing solubilizing alkyl chains) include spin and spray coating, solution-coating with fluid control, epitaxy, solvent-annealing, and nucleation techniques, to just name a few. Vacuum processing[34], by contrast, is only applicable to

small-molecular semiconductors, where vapour-phase deposition enables the fabrication of high-purity thin films with good control over thickness and chemical composition.

Summarizing, considering both conjugated small molecules and polymers, each possesses their own advantages and disadvantages, also depending on the application to be accomplished. For example, small molecules are generally easier to purify and allow high-vacuum based processing, enabling the fabrication of defined multilayer devices of high performance. High-vacuum fabrication of electronic devices on the other hand is slow and costly and offers limited scalability towards bigger substrates. Moreover, small-molecular crystalline materials might prevent smooth, uniform thin-film formation, which can cause damage to devices. On the other hand, grain boundary-free amorphous materials, including both molecular materials and polymers, allow smooth, uniform amorphous thin-film formation. In addition, solution-processable semiconducting polymers are of good flexibility and consistent with numerous printing techniques for fast, cost-effective, low-temperature and large-area fabrication such as plastic circuits and electronic papers. However, a major problem that restrains the development of polymer-based devices (in addition to the limited purification techniques that can be employed for polymers syntheses) concerns the low mobilities generally observed for polymeric materials, which are several orders of magnitude lower than that of organic small molecules. In general, either crystalline or amorphous materials are used, and the choice of which one depends on the kind of device to be realized. While polycrystalline materials have been widely used in OPVs and OFETs because of their higher charge carrier mobilities than those of amorphous materials, amorphous molecular materials have been applied successfully in OLEDs and solution-processed bulk-heterojunction OPVs.

1.1.3. Charge Transport in OSCs

The basic principle underlying charge transport in organic semiconductors is strictly related to both charge delocalization and solid-state packing. As already discussed, the solid-state structure of OSCs is built from individual molecular or polymeric units assembled by weak interactions, principally van der Waals forces (aromatic π-π stacking, dipole-dipole interactions, hydrogen bonds etc.). Thus, the electronic interaction between its individual units is generally low and the electronic structure of the individual constituents dictates the solid-state architecture. While charge carriers in inorganic semiconductors are generally delocalized, on the other hand charge carriers in organic semiconductors are generally rather localized on distinct sites (e.g. single molecules portions or small coherent chain segments for polymers).[35] As such, the HOMO and LUMO levels of the conjugated material are often used to discuss the behaviour of the solid itself. Charge carriers can be injected electrically or generated photonically (forming excitons) and they can diffuse through the system via hopping charge transport mechanism.[36] . The hopping mechanism involves the transport of the charge through a "jumping" process of charge carriers between localized states (HOMO or LUMO) of adjacent molecules/polymeric chains within the lattice. Hopping can happen due to the electronic coupling driven by weak intermolecular interactions which mediate the transfer above FMOs overlap of neighbours in π-conjugated systems. During the process, the single localized charge moves accompanied by the polarization created from the distortion of the electron density, the reorientation of the dipoles of the adjacent molecules and lattice and molecular vibrations (phonons). The effect of localization is that the mean free path of charges is typically of the order of the spacing between adjacent molecular sites, and charges moving through the disordered lattice are scattered at each molecular site.[37] If localization is dominated by molecular conformational changes, then charge transfer is thermally activated with an activation energy that is dependent on the active molecular deformations. These models are known as polaron models.

Organic semiconductors can be divided in two categories according to their redox properties and the nature of charge carriers they can transport: p-type materials and n-type materials. The former consists of electron-rich molecules or polymers having low ionization potential (IP) and with high propensity upon oxidation as their HOMO is remarkably high in energy. In these materials it is possible to inject holes (h^+) that are the species responsible of the transport of charge. Vice-versa, n-type materials are

generally electron-poor molecules or polymers having high electron affinity (EA) and with high tendency upon reduction as their LUMO is quite low in energy. In these materials it is possible to inject electrons (e^-) which are the species responsible of the transport of charge. Other type of OSCs are called "ambipolar" since these materials are both p- and n- type and they can generate both charge carriers h^+ and e^-.[37] Considering the hopping mechanism, once a p-type material oxidizes it loses an electron from the HOMO and a radical cation specie is formed. This specie can receive an electron from an adjacent neutral molecule, which in turn becomes a radical cation. More specifically, the electron is transferred from the HOMO of the closed neutral molecule to the HOMO of the radical cation specie, causing the movement of a hole charge-carrier associated with the radical cation. On the other way around, upon reduction of an n-type material a radical anion is formed, and an electron can be transferred from the LUMO of the radical anion specie to the LUMO of an adjacent neutral molecule favouring the transport of charge (**Figure 11**) along the material.[38]

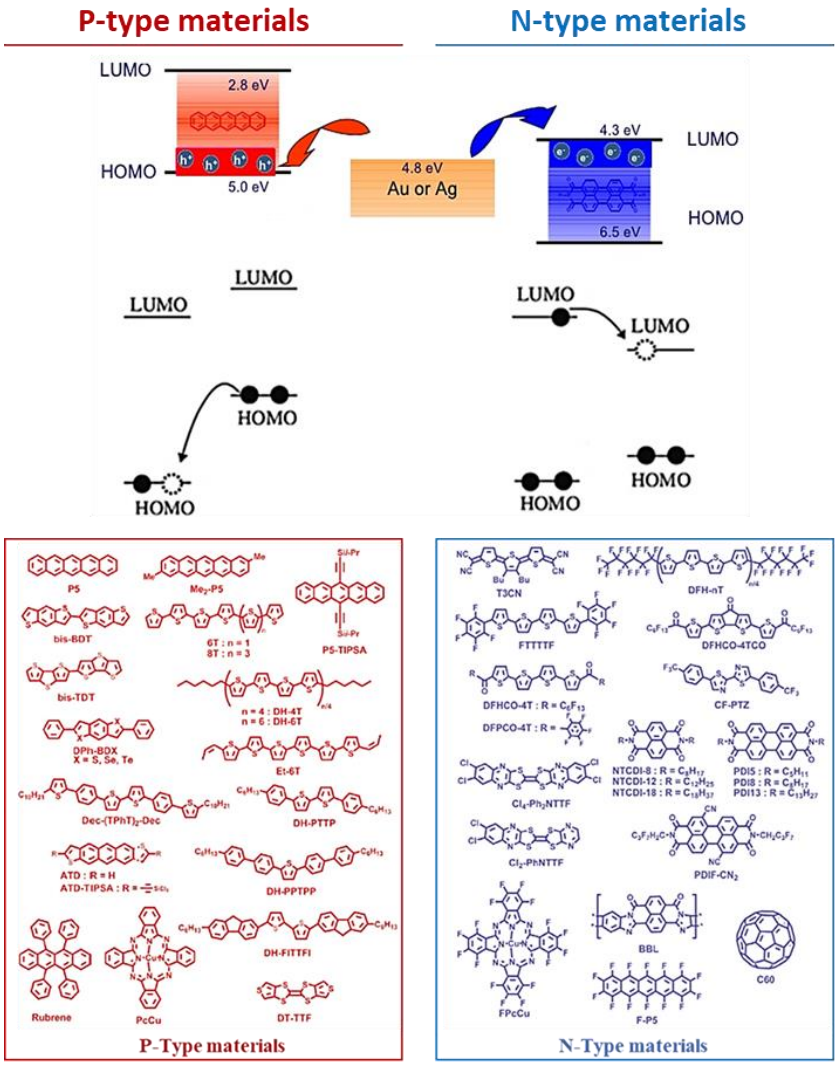

Figure 11. *Top: hopping charge transport through the material's FMO energy levels. Bottom: illustration of P-type and N-type materials structures. Reported with permission from ref.* [38]*; © Elsevier Ltd 2007.*

The charge carrier mobility is an important electronic feature of semiconductors and metals as it defines the quality of charge carrier transport of a given material. The mobility (μ) relates the drift velocity of free carriers, h^+ or e^-, to the driving force of an applied electric field. The charge carrier mobility is often measured as a figure of merit describing the semiconductors ability to conduct charges which is of vital importance for efficient device operation. In both OLEDs and OPVs for example, device efficiency can be hindered by imbalanced mobilities of electrons and holes in their respective n-type and p-type layers.[39] In transistors the mobility determines parameters such as the

maximum current through the device (at a given voltage) and the maximum achievable switching speed.[38] There are in principle two methods to determine this crucial parameter. Either the charge carrier mobility can be measured for a known at a given applied field (e.g. in a transit time experiment) or the current at known field and charge carrier density is recorded (e.g. in a transistor).[36] OSCs are often highly disordered (both spatially and energetically) especially in the amorphous state, and hence, their charge-carrier mobility is smaller than their covalently-bonded, highly-ordered crystalline inorganic counterparts such as C-Si. The main factors influencing the performance of devices can be divided into two categories: factors related to device physics and factors related to the semiconducting materials. The factors related to device physics involve the device configuration, the quality of the semiconductor/dielectric or semiconductor/electrode interfaces, film morphology and deposition conditions. On the other hand, factors associated to the semiconductor material relate to: (i) the band structure and FMOs' energies, which should have enough molecular orbital overlap to ensure that the charge transferring between adjacent molecules does not have to overcome a high energy barrier; (ii) the match between the energy levels of the material and the electrodes to facilitate charge injection; (iii) the solid-state packing structures should form compact, orderly stacking, which facilitates the charge transport between molecules; (iv) the electrical, optical and chemical stability (v) the molecular weights and defects for polymeric materials and (vi) the degree of purity. Generally, OSCs exhibit poor mobility and stability and therefore for now they can only find use in niche applications where high performances are not required. However, doping techniques have been highly exploited in order to improve OSCs conductivity and anyway, OSCs are remarkably interesting also for their excellent optical properties.

1.1.4. Doping in OSCs

Doping is a popular technique widely used to enhance conductivity of both organic and inorganic semiconductors. The introduction of defects by doping in organic semiconductors leads to the insertion of additional energy levels between the HOMO and LUMO of the material and thus reduces its energy gap. Careful control on dopant concentration allows to finetune the conductivity of the material. Doping in organic semiconductors consist in the addition of specific molecular species able to induce the formation of mobile charge carriers along the conjugated structure. In a nutshell, the doping process is a redox reaction. Depending on the conducting channel of the material (p-type or n-type) the dopant corresponds to a highly electron donating or accepting specie able to promote charge transfer in a more efficient way thanks to the right match of frontier energy levels.[40] A p-type dopant can be figured as a strong electron accepting agent which oxidizes the p-semiconducting material by removing an electron from its HOMO and so introducing a positive hole in the structure. On the other hand, a n-type dopant is a strongly electron donating agent which reduces the n-semiconducting material by adding an electron to its LUMO and so introducing a negative charge in the structure.[41] The integer charge transfer model and the molecular orbital levels involved in the doping processes (p-type and n-type) are schematically represented in **Figure 12**.

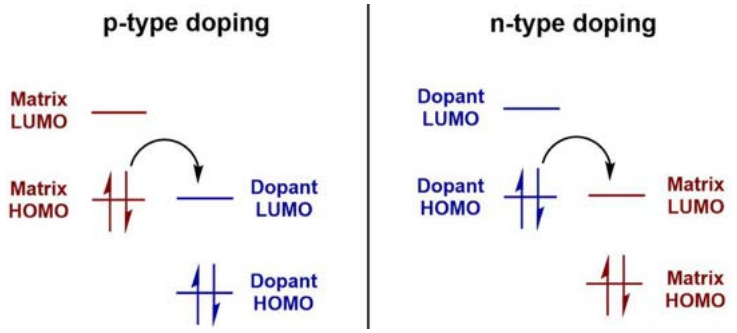

***Figure 12**. Organic semiconductor doping via integer charge transfer model. Efficient electron transfer requires suitable energy level alignment of p- and n-type dopants. Reported with permission from ref.*[41]*. © The Author(s) 2017.*

Some of the earliest examples of conducting organic materials come from the p-type doping of polyacetylene with halogens.[42] In these early conducting polymers, dopants were introduced via exposure to halogen vapours leading to diffusion problems during processing. A more popular and practical approach is the use of small molecules as dopants. P-type doping has been widely investigated with strong Lewis acids being employed.[43] N-doping of materials is much more difficult to achieve since the HOMO of the dopant must be high enough to allow it to donate electrons to the LUMO of various materials. N-doping has previously been achieved using alkali metals, mostly lithium,[44] and molecules with extremely high HOMO levels such as tetrathianaphthacene (TTN, E_{HOMO}=−4.7 eV). Anyway, similar energies in the HOMO of the dopant and LUMO of the accepting material are essential to achieve efficient results.[45]

Considering the p-type doping in in *trans*-polyacetylene for example, the oxidation of the system by the dopant produces a cation and a free radical electron on the material, and the charge neutrality is maintained by the formation of an anion on the reduced dopant. If this process occurs twice the two radical anions can recombine to form what is known as a spinless soliton, a positive or negative charge carrier free to independently move around the polymer chain. The process of forming solitons is unique to *trans*-polyacetylene due to it containing a doubly degenerate ground state which allows the soliton charges to move independently of each other (**Figure 13**).

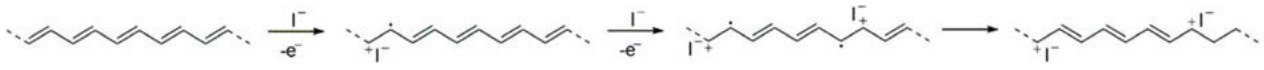

Figure 13*. Soliton formation using iodine as the dopant trans-polyacetylene. Reported with permission from ref.*[41].

However, most of the conjugated structures with applications in modern optoelectronic devices do not exhibit the same symmetry as *trans*-polyacetylene and therefore do not contain the degenerate ground state necessary for independent solitons to act as charge carriers. In this case, during the p-doping an electron is removed from the material and the cation and radical are again formed; the resulting cation and radical electron are partially delocalized over the π-conjugated system and is termed a polaron. An illustrative example of p-doping in polythiophene with BF_4^- as dopant is reported in **Figure 14.** The polaron induces the formation of the quinoidal structure leading to a distortion in bond lengths over the section of the material linking the radical and cation. This distortion is not energetically favoured and is therefore usually stabilized over more than one repeating unit. Upon further oxidation, which can be induced by increasing dopant concentration, the unpaired radical electron of the polaron can be removed which leads to a sequence of quinoid type monomer units along the polymer which are separated from the normal aromatic monomer units by the two cationic charges. These sections of the material are known as bipolarons and at high dopant levels are responsible for charge transport across the structure.[46]

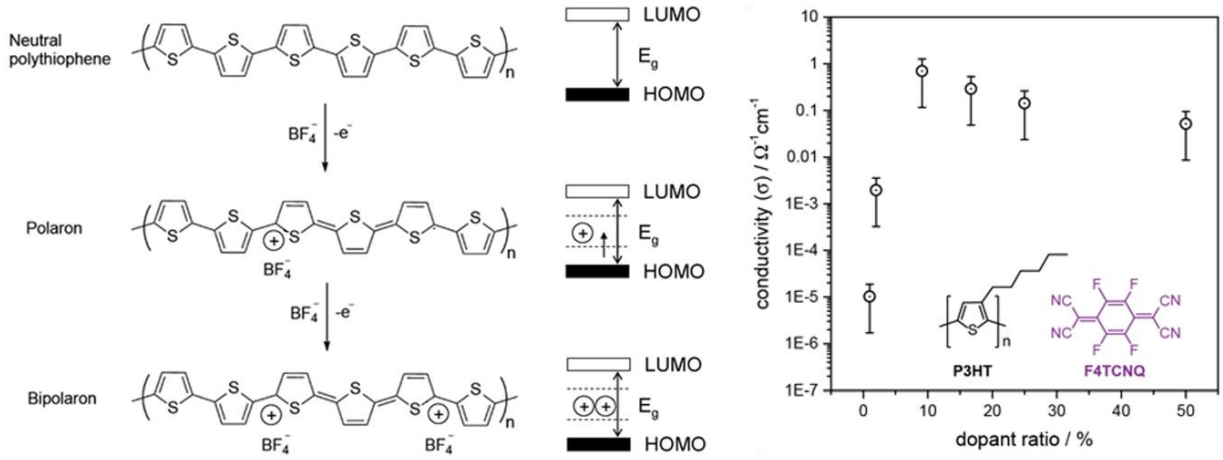

Figure 14*. On the left: example of polaron and bipolaron formation in polythiophene upon doping with BF_4^- and the consequent effect of inserting additional energy levels between the HOMO and LUMO of the material. On the right: sheet conductivities (σ) of poly(3-hexylthiophene) (P3HT) thin films upon p-doping*

concentrations of the strong electron acceptor F4TCNQ. Adapted with permission from ref.[40] *and ref.*[41]*; © The Author(s) 2017.*

With this approach the conductivity of conjugated materials can be tuned over several orders of magnitude as shown in **Figure 14** for the p-doping of P3HT. Today, molecular doping enables the high performance of modern benchmark organic devices by concurrently reducing ohmic losses in charge transport layers and injection barriers at interfaces to electrodes.[47]

1.1.5. Optical Properties of OSCs

Organic semiconducting materials possess fascinating optical properties and they have been extensively investigated and exploited for many applications associated with light interactions. Conjugated structures are able to absorb photons and may have many vibronic possibilities depending on the structural dipoles, which can give rise to anisotropy and several distinct absorption bands.[48] Interacting with light, highly ordered materials generally exhibit sharp absorption bands associated with different vibronic features. On the other hand, amorphous materials generally display broad and smoothed Gaussian absorption distribution due to the disorder in the film or in solution (**Figure 15**).

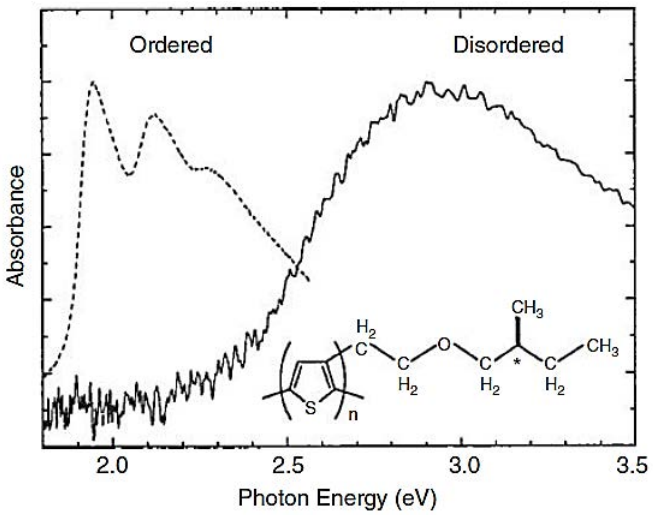

Figure 15*. Absorption spectra of ordered and disordered films of a polythiophene derivative. The inset is the chemical structure of the derivative. Source: Reprinted Figure 1 with permission from T. Kobayashi et al., Phys. Rev. B 62, 8580. Copyright (2000) The American Physical*

Specifically, the absorption of a photon of appropriate energy promotes the excitation of an electron from the HOMO to the LUMO in the absorbing molecule leading to the formation of an electron-hole pair system, also known as exciton. As previously discussed, excitons can be formed photonically or electrically and they can diffuse through the system via hopping charge transport mechanism.[36] In the first case, the exciton population is directly related to the number of absorbed photons. The exciton can be described as a molecular excited state, represented by an electron-hole system connected together by a Coulombic electrostatic interaction. In order to have current flowing along the material after light exposure, the excitons must dissociate before they could recombine (possibly with the emission of a photon), and to do that it is necessary to provide them with enough energy to break their electrostatic bonds. For an organic photodiode, for instance, the photo-generated excitons are broken by the internal electric field due to the difference of the working functions of the two electrodes.

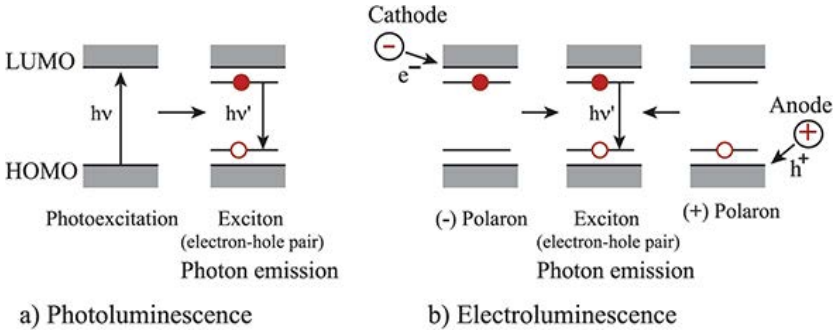

Figure 16. *a) Exciton formation upon photoexcitation and (b) exciton formation upon electroexcitation. Copyright © 2018 Morgan & Claypool Publishers*

Organic semiconductors generally have high absorption coefficients at the peak of their absorption spectrum and, as such, the exciton generation rate can be maximised by increasing the overlap between the absorption profile and the source spectrum. According to their spatial extent and binding energy, excitons can be divided in (a) small, tightly bound excitons referred to as Frenkel excitons, and (b) large and loosely bound excitons referred to as Wannier–Mott excitons.[49] Large or small, in this context it is related to the lattice constant. Exciton transport is governed by diffusion processes, with transport directed away from regions of high exciton concentration. The lack of molecular interaction in organic semiconductors influences exciton transport, which occurs through a hopping mechanism as already discussed. Excitons can move across the lattice through either dipole–dipole interactions (Förster resonance energy transfer) or wave function overlap (Dexter energy transfer); recombine radiatively (emitting a photon) or nonradiatively; or separate into free carriers.[50,51] Almost all organic materials have relatively high (higher than the thermal energy) exciton-binding energies, and this is of fundamental importance for, for example, OPV applications where optical excitations need to be separated into free carriers.

Atomic movement influences the relative positions of the atoms in a molecule and this affects the electronic states that absorb and emit light. In disordered materials, there are usually too many small variations to be identified, but in ordered systems there are particular vibrational modes that can even dominate the optical properties.[48] Since both absorption and emission favourably occurs from the vibronic state with the lowest energy, the absorption and photoluminescence spectra should be, in the ideal case, mirrored. Actually, since several defects are typically present in the solid-state and some of the vibronic transitions may be forbidden for, for example, symmetry reasons, the absorption and emission spectra are in reality rather dissimilar. The exciton migration toward a lower energy level also means that ordered domains will have a bigger impact on emission than absorption. Absorption and emission from the lowest vibronic level do usually not take place at the same energy despite the same states being involved. The reason for this is the reorganization energy. Both the energy of the excited electron and that of the resulting hole are shifted into the energy gap by one reorganization energy (**Figure 17**).[48]

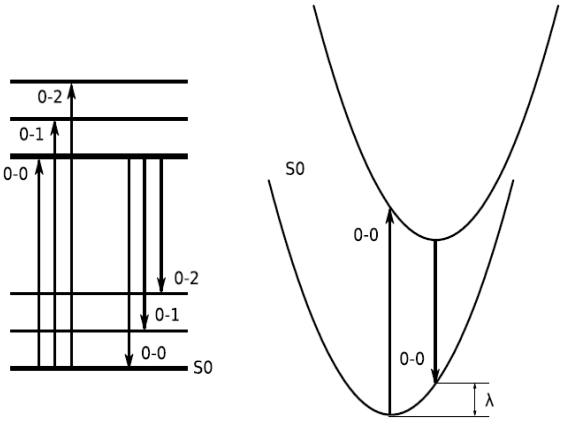

Figure 17. *Left: excitation (light absorption) from the ground state (S0) to a vibronically splitted excited state (arrows pointing up) and relaxation (light emission) from the excited state's energy minimum to the vibronically splitted ground state (arrows pointing down). Right: energy parabolas of the ground state and the excited state involved, where λ is the reorganization energy. The total shift in energy between absorption and emission is 2λ. Copyright (2016) by Taylor & Francis Group, LLC.*[48]

In short, this means that the emission is shifted by two reorganization energies associated to the absorption. The disorder in the structure, and the fact that there are many distinct electronic states that can absorb light in a solid, usually make it difficult or impossible to identify the appropriate transitions, and thus the reorganization energy, at room temperature. The qualitative correlation remains, however, and materials with a large so-called Stokes shift (i.e., a large red shift of the emission spectrum compared to the absorption spectrum) tend to have large reorganization energies.

As already mentioned, excitons can recombine radiatively or non-radiatively. The rate of exciton recombination depends, among other things, on the spatial overlap of the electronic wavefunctions of the constituent hole and electron. Variations in electronegativity along the structure due to molecular asymmetry can cause alterations in the electron and hole charge densities and thus increase the exciton lifetime. Excitons can also be an intermediate in recombination processes. Electrons are spin -1/2 particles, that is, fermions, and the total spin of the exciton can therefore be either 1 or 0. No two fermions can occupy the same quantum state. Excitons with a total spin of 0 are called singlet excitons and excitons with a total spin of 1 triplet excitons. Photoexcitation typically generates singlets, which can recombine quickly and radiatively (fluorescence). In a random population, such as in an electroluminescent device, however, there will also be triplets. Mathematically, the ratio between singlets and triplets is 1:3. Triplets are more long lived and do not recombine radiatively in organic semiconductors. Without intersystem crossing, for example, electroluminescent devices are thus limited to a quantum efficiency of at most 25%.[52] Hence, metal–organic molecules capable of emitting light from triplet decay (phosphorescence) are typically used together with fluorescent organic semiconductors in OLEDs.[53] However, room-temperature phosphorescence emission is observed not only for transition metal complexes, but also for some metal-free molecular crystals, where intramolecular motions are suppressed by several intermolecular interactions in the crystal lattice, thereby minimizing nonradiative decay from the electronically excited triplet state. The search for room-temperature phosphorescent organic compounds in the crystalline state and the establishment of guidelines for designing room-temperature phosphorescent organic molecules, along with crystal engineering, have been of crucial research for efficient electroluminescent devices.

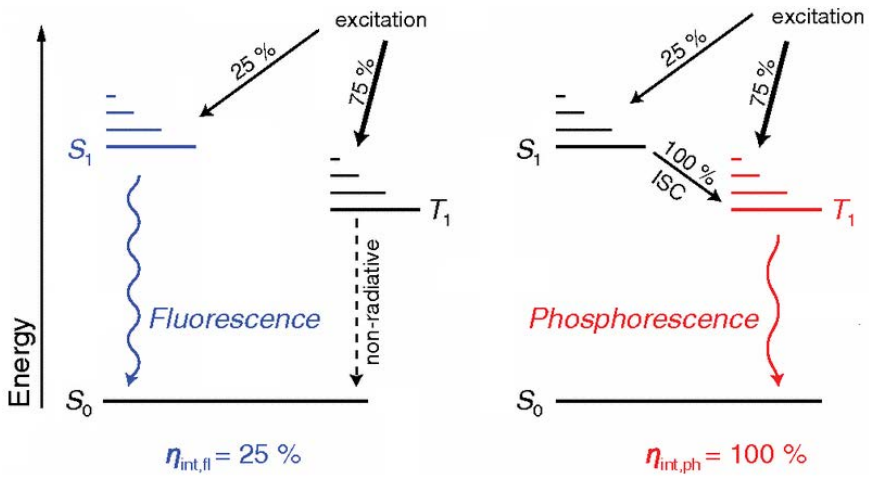

Figure 18. *Population scheme of singlet and triplet levels of organic materials after electro- or photo-excitation. For fluorescent emitter materials, the internal quantum efficiency (η_{int}) can be maximum 25%. For phosphorescent emitter materials, the singlet excitons created are efficiently transferred to the triplet state via intersystem crossing (ISC) and the internal quantum efficiency can ideally reach 100%.*

Since the exciton-binding energy typically exceeds the thermal energy in organic semiconductors, separation of optical excitons into free charges is relatively inefficient. The charge separation is expected to be proportional to the relative recombination and dissociation rates. Both of these rates are strongly dependent on the nature of the material and the external electric field applied. Just as excitons can dissociate into free carriers, on the other way around free carriers can be reformed into excitons. The rate with which free carriers recombine is proportional to the sum of the electron and hole charge carrier mobilities and the permittivity of the material. Although relatively slow, the

recombination rate is still generally much faster than the dissociation rate at reasonable electric fields. To solve this, it is possible to use two-phase systems, where there is a suitable energetic offset between the respective FMOs of the two materials (**Figure 19**). When one of the materials is excited, either the hole or the electron will transfer to the other phase while still being electrostatically tightly bound. Such a state is called a charge transfer state and the corresponding exciton a charge transfer exciton. The electron and hole of a charge transfer exciton becomes (even more) spatially separated and the wave function overlap reduced, which results in an increased lifetime that is proportional to the frontier orbital offset. Many material combinations can reach close to 100% charge separation efficiency in this way.[54]

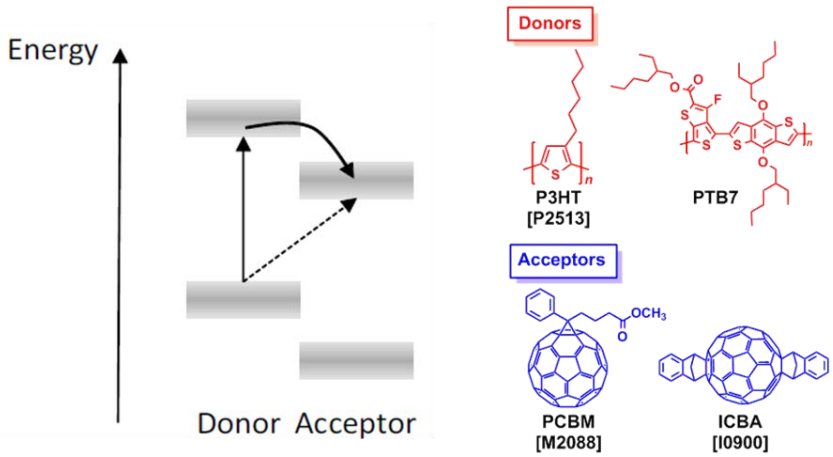

***Figure 19**. Sketch of light absorption–induced charge transfer exciton formation either by formation of an exciton on the donor molecule followed by transfer of the excited electron into the acceptor molecule LUMO (solid arrows) or direct formation where an electron from the donor HOMO is excited into the acceptor LUMO.*

1.2. Devices: "The Big Three"

Among the different organic (opto)electronic devices, this section deals with "The Big Three", i.e. OFETs, OLEDs and OPVs, and mainly focuses on their working principles and the corresponding functional materials typically used. As discussed so far, the electronic and optical properties of a given material are affected by film order, and film order is to a large extent controlled by the chemical structure of the molecule or polymer as well as the film-forming process conditions. In general, the choice of which material is most suitable for a chosen application depends on many aspects, which makes design and screening of materials for a chosen application a remarkably complex and multivariate task. It is hard to predict the functionality of a material in a device solely on the basis of the properties of the isolated system, thus the "perfect" material for a given application is an ambitious target that requires significant trial-and-error work.[48]

1.2.1. Large Area Electronics with Organic Field-Effect Transistors

The transistors that make up the integrated circuits of the electronic devices we use daily are mainly made from inorganic semiconducting materials and among them, silicon is the most popular. In fact, the well-known silicon MOSFET (metal-oxide-semiconductor field-effect transistor) is the basic building block of modern integrated circuits. However, since silicon requires expensive manufacturing processes, such as thin film deposition and patterning, the cost of the current silicon transistor technology is relatively high.[55] The need for large area, flexible and low-cost electronics has stimulated the development of a new category of transistors, which are made from solution-based

conductor, semiconductor, and dielectric materials. Organic materials are attracting attention for cost-effective and large-area pervasive electronics applications. Organic thin-film transistors (OTFTs) can be fabricated with printing technologies on arbitrary substrates, enabling both high-throughput and low-cost production (**Figure 20**). In particular, the most widely used are the organic "field-effect" transistors (OFETs) which exploit an electric field to modulate the conduction of a channel located at the interface between a dielectric and a semiconductor. The first OFETs based solely on organic materials had field-effect charge-carrier mobilities (μ_{FET}) of less than 10^{-2} $cm^2V^{-1}s^{-1}$ and were still vastly inferior compared to amorphous silicon (a-Si) MOSFET ($\mu_{FET} = 10^{-1}$ $cm^2V^{-1}s^{-1}$). Nevertheless, after 10 years of intensive research solution-processed OFET components are now approaching the field mobilities of amorphous silicon (maximum mobilities μ_{FET} of 0.6 $cm^2V^{-1}s^{-1}$).[56] In OFETs, solution-processable active materials allow cost-effective and large-area processing in roll-to-roll methods, for example, for the electronic control of large active-matrix displays or in electronic labels. Moreover, the avoidance of slow and cost-intensive vapor deposition methods in high vacuum brings cost advantages. For instance, the use of OFET in electronic labels, so-called RFID tags (radio frequency identification tags), requires a production cost of less than one cent per label.[57]

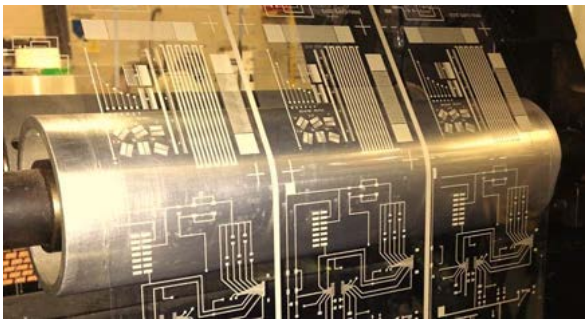

Figure 20. Roll-to-roll production of flexible integrated circuits.

The structure of an OTFT generally consists of five parts: a source (S) electrode, a drain (D) electrode, a gate (G) electrode, an organic semiconductor (OS) layer, and a dielectric layer, deposited on a substrate (that could be a flexible plastic or paper). The most common OFET device configuration contains a thin film of the organic semiconductor deposited on top of a dielectric with an underlying gate electrode (**Figure 21**). Charge-injecting source-drain (S-D) electrodes providing the contacts are defined either on top of the organic film (top-contact configuration) or on the surface of the FET substrate prior to deposition of the semiconductor film (bottom-contact configuration). Other device structures are shown in **Figure 21**.[38]

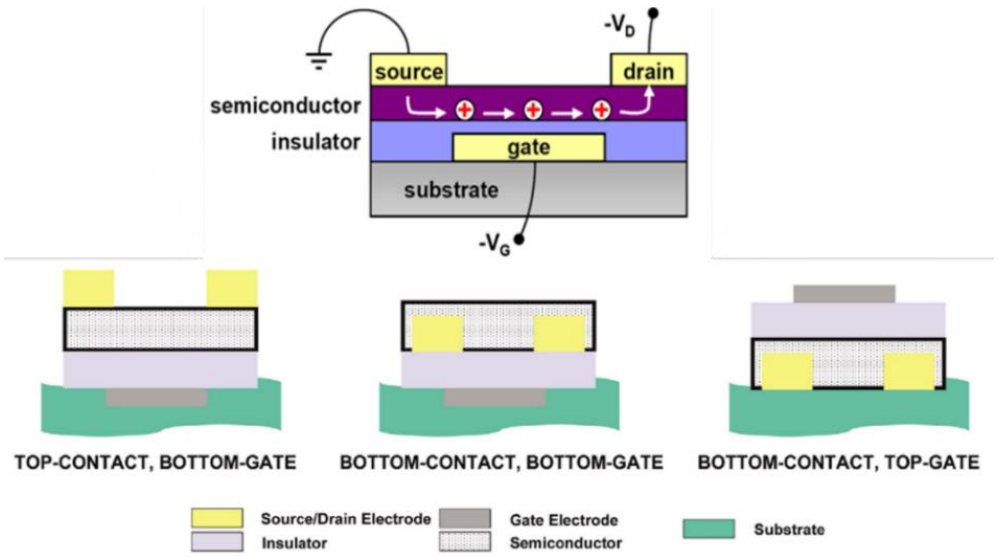

Figure 21. *Top: schematic cross-section of a typical OFET structure. Bottom: schematic representation of three different thin-film transistor structures.*

The three terminals (S, D and G electrodes) are connected to an external circuit and the device can act as an amplifier, switch, oscillator, or frequency converter. The conductive channel length is determined by the distance between the S-D electrodes. OFETs uses the gate-source voltage (V_{GS}) to control the drain current (I_D), resulting in the output current being proportional to the input voltage (in the linear region). This operation is controlled by an electric field generated by the input gate voltage, called the "field effect". OFETs can be divided into unipolar and bipolar (or ambipolar) according to the type of charge transport carrier they use. A unipolar transistor, that is an n-type or p-type, is a transistor in which electrons (in an n-channel transistor) or holes (in a p-channel transistor) are mobile inside the conducting channel. Bipolar transistors use both holes and electrons for conduction.

Minimal current between S and D electrodes is measured when no voltage is applied between the G and S electrodes (device 'off' state). When a voltage is applied to the G, electrons or holes can be induced at the semiconducor-dielectic interface and the S-D current increases (device 'on' state). When an OFET is active, upon the application of negative V_{GS} and V_{DS}, the organic material is *p*-channel since holes are the majority charge carriers (**Figure 22**). On the other hand, when a (positive) D-S current is observed upon the application of positive V_{GS} and V_{DS}, the semiconductor is n-channel since the electrons are mobile (**Figure 22**). In the case that the device operates for both V_{GS} and V_{DS} polarities the semiconductor is ambipolar. Note the fundamental difference between n-/p-organic and n-/p-inorganic semiconductors is that the former is based on the gate voltage sign at which they are active whereas the latter is based on the majority carrier type because of the (chemical) doping process. Therefore it is important to take into a count that the categorization of an organic semiconductor as 'p-' or 'n-' channel has no absolute meaning but is strongly related to the FET device structure/material combination on which the transport characteristics are measured.[38]

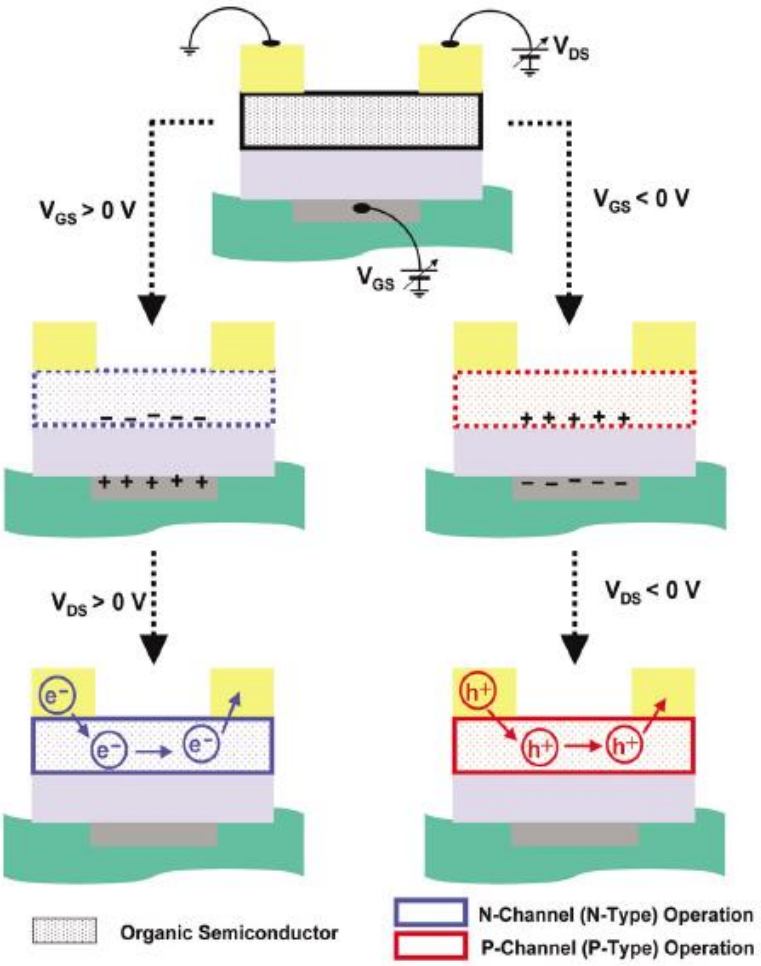

***Figure 22**. Schematic of p- and n-channel thin-film transistor operation. © Elsevier Ltd 2007.*

Generally, to evaluate the performance of an OFET device it is necessary to take into account the following parameters[58]:

- The charge-carrier mobility (μ), which describes how fast the charge carriers can move along the semiconductor layer in relation to the electric field applied by the gate. Thus, it characterizes the critical voltage at which the field effect is operative. This parameter is strictly related to the impurity concentrations, defect concentration, temperature, and charge carriers' concentrations (conductivity is proportional to the product of mobility and carrier concentration).

- The threshold voltage (V_T), which is the minimum value of V_G required to induce a barely effective field effect and observe current flow between the S-D terminals. The V_T in an ideal accumulation-type OFET is zero because ideally all induced charge is necessarily mobile. However, real OTFTs are usually nonideal and they have a threshold voltage.

- The current modulation ratio (I_{on}/I_{off}), defined as the ratio between the I_{DS} output when the transistor is in the "on" state at $V_G \neq 0$ (I_{on}) and the I_{DS} output when it is in the "off" state at $V_{GS} = 0$ (I_{off}). For an optimal functioning of the OFET the transport of the charges should be much fast as possible through the conduction channel and at the semiconductor/dielectric interface when the transistor is in the "on" state (high I_{on} is necessary). Conversely, when the electric field is switched off, it is proper that the semiconductor is no longer polarized and therefore no current flow is observed when the transistor is in the "off" state (the I_{off} observed should be as low as possible).

While the latter parameter can be obtained from the measurement of two currents, the first two must be extrapolated from the classic model of the MOSFET, which is described by two limit formulas:

$$(I_D)_{lin} = \frac{W}{L}\mu_{lin}C_i\left(\frac{V_G - V_T - V_D}{2}\right)V_D \quad \cap \quad |V_D| < |V_G - V_T|$$

$$(I_D)_{sat} = \frac{W}{2L}\mu_{sat}C_i(V_G - V_T)^2 \quad \cap \quad |V_D| > |V_G - V_T|$$

Where: μ_{lin} and μ_{sat} are the mobilities of the charge carriers (which flow in the semiconductor because of the electric field generated by the V_G applied) in the linear and saturation regime respectively, W is the channel width, L is the channel length, Ci is the capacitance of the dielectric per unit area , V_T is the threshold voltage, V_{DS} is the voltage between the source and drain electrodes and V_G is the voltage applied at the gate. In the output characteristics, two operation regions can be differentiated: a linear region at low drain voltage and a saturation region at high drain voltage. For both of the linear and saturation operating regimes of the OFET, by setting the geometries of the device, the type of dielectric and the V_G applied, it is possible to construct the transfer characteristics curves from which μ_{lin}, μ_{sat} and V_T can be obtained.[59]

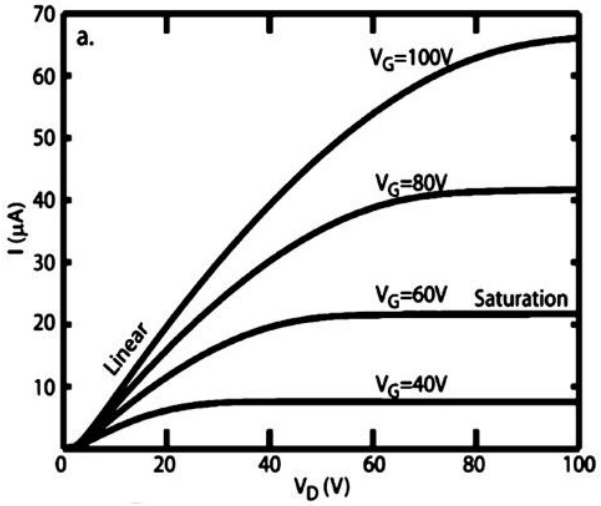

***Figure 23**. Example of a transfer characteristic I–V curve (I_D vs V_D) for various values of V_G. Thick lines indicate the saturation regime.*

OFETs' performances are related to both devices physics (device configuration, contact resistance, interfaces, deposition, channel length and width modulation) and semiconductor material employed (charge carrier mobility, morphological order, purity, stability). They deviate from the traditional Si-based MOSFETs mainly for the low carrier mobilities and inferior stability. However, research in these field is working hard to bridge the gap with the traditional cost-inefficient inorganic technology and today we can see how far organic materials have gone.[60]

Considering the enormous impact that the nature of semiconducting layer has on device performances and lifetime, it is important to understand which organic structures of choice are best suited for OFETs applications and why. Following are reported the most important features that OSCs must fulfil to ensure high performance in OFETs devices, as well as the organic semiconducting structures that can be commonly found in OFETs.

1.2.1.1. Organic Materials for OFETs

Both conjugated low molecular weight compounds (small molecules and oligomers with well-defined structures) and polymeric semiconductors are suitable organic semiconductors for OFET applications. Owing to their crystallinity, small molecules often have the advantage that they pack themselves in a very orderly manner in the solid state. This generally leads to a higher charge-carrier mobility, as the mobility depends primarily on the intermolecular interactions; however, high order also leads to a limited solubility. When making transistors by printing techniques, the OSC must be processed from solution and should be able to form high quality film as well as be environmentally stable. Polymers are of good flexibility, which renders them the most promising materials for flexible devices (such as plastic circuits and electronic papers). The low charge carrier mobilities of OSCs compared to traditional silicon represent an important challenge the scientific community in this field want to overcome. Current research in the field of materials for OFETs focus on improving charge carriers mobility, and thus OFET's performance, by structural engineering upon the semiconductor material structure in order to finetune some key parameters:[58]

- The HOMO and LUMO energy levels. These values have a significant influence on both the injection and current-carrying characteristics: they must match with the work functions electrodes source and drain, be at levels where holes/electrons can be induced at accessible applied electric fields and be able to efficient overlap between neighbours. Moreover, HOMO and LUMO energy levels also have an important influence on the device stability. Nowadays,

there are fewer accounts of n-type than p-type organic semiconductors, primarily because of the inherent instability of organic anions in the presence of air and water and problems with oxygen trapping within these materials.[61–63] For this reason, in some cases, the mobilities of the n-type OFETs can be one or even several orders of magnitude higher when taking precautionary measures to exclude atmospheric oxygen and water in vacuum or inert atmosphere.

- The solid-state packing structures. This parameter strongly affects charge mobility since it defines the degree of molecular orbital overlap between adjacent molecules, and better the overlap, more efficient is the charge transfer. The solid-state packing of small-molecular OSCs can be divided into four types[64] as shown in **Figure 24**: (**A**) herringbone (face-to-edge) packing without π–π overlap between adjacent molecules (for example in pentacene); (**B**) herringbone (face-to-edge) packing with slipped π-π stacking between adjacent molecules (for example in rubrene); (**C**) one-dimensional (face-to-face) lamellar packing (for example in N,N'-dihexyl-naphthalenediimide) and (**D**) two-dimensional (face-to-face) lamellar packing (for example in TIPS-pentacene). The latter two types of packings, because of the high overlap between MOs of neighbour molecules, represent the more promising solid-state structures to favour efficient charge carrier hopping pathways a with enhanced mobilities. In the case of conjugated polymers, the solid-state packing includes both face-on and edge-on orientation of the polymer chain with respect to the substrates (**Figure 25**). The possible charge transport pathways in polymeric films can be divided into: intrachain transport along the π-conjugation direction, interchain transport along the π-stacking direction, and alkyl stacking direction. In particular, best performances are reached when the structure is preferentially oriented with the conjugation direction approximately parallel to the FET substrate (edge-on), since the most efficient charge transport occurs along the direction of intermolecular π-π stacking. Finally, the crystalline domains of the conjugated polymer must cover the area between the S and D contacts uniformly, hence the film should possess a single-crystal-like morphology. [65]

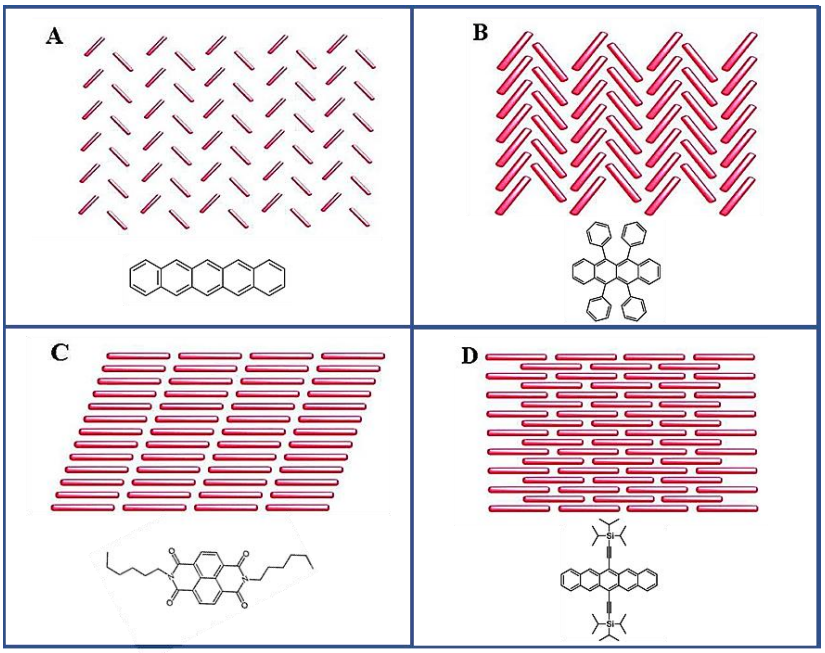

***Figure 24**. Solid-state packing possibilities of small-molecular OSCs. (**A**) herringbone (face-to-edge) packing without π–π overlap between adjacent molecules (example: pentacene); (**B**) herringbone (face-to-edge) packing with slipped π-π stacking between adjacent molecules (example: rubrene); (**C**) one-dimensional (face-to-face) lamellar packing (example: N,N'-dihexyl-naphthalenediimide) and (**D**) two-dimensional (face-to-face) lamellar packing (example: TIPS-pentacene). Copyright 2008 b Wiley-VCH Verlag GmbH & Co. K Ga A and Copyright 2010 Royal Society Chemistry.*[64]

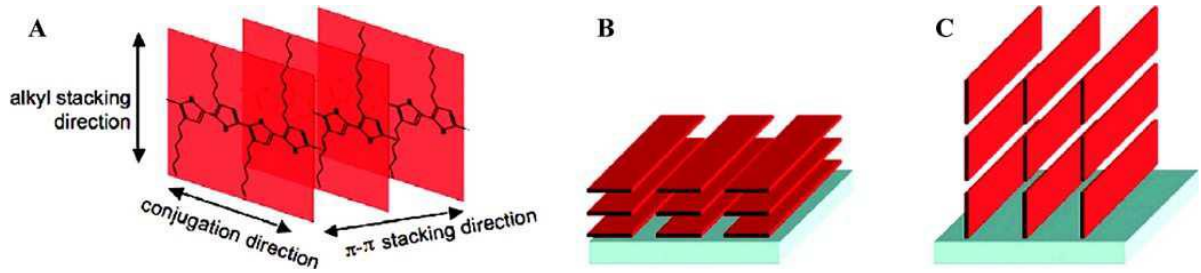

***Figure 25**. (**A**)Possible charge transport mechanisms of conjugated polymer films. (**B**)Face-on and (**C**) edge-on orientation of the polymer chains with respect to the substrate. Reprinted with permission of ref. 64 Copyright 2007 Elsevier B. V.*

- The conjugation extension of polymeric materials. The increased molecular weights of conjugated polymers (or alternated co-polymers) generally leads to superior field-effect mobilities.[66] The increased performances are accompanied by important changes in the thin film morphology: polymeric structures with high molecular weights often exhibit reduced crystallinity and lead to more homogeneous films, favouring the charge transport in the device.

- The purity of the OSC material, which should be extremely pure since impurities act as charge carrier traps and this has a negative impact on the function of the device. Thus, novel synthetic routes that facilitate the purification process to access extremely pure materials are growing importance.[67]

- The doping technique employed. OSC doping can be used for a variety of purposes, including mobility enhancement, charge transport polarity modulation, trap passivation, threshold voltage adjustment, ohmic contacts enhancement, ambipolar charge injection suppression, short channel effect suppression, and stability improvement.[68]

A wide variety of organic semiconductors classes have proved suitable for finding application in the field of OFETs.[38,69–71] At present, the mobilities and I_{on}/I_{off} ratio of OSC materials have exceed 1 $cm^2 V^{-1} s^{-1}$ and 10^6–10^8, respectively.[56,71] However, several conjugated materials show poor solubility in common organic solvents because of their strong π–π interactions. For this reason, as already discussed, the introduction of solubilizing alkyl chains is essential to ensure processability from solution. Relevant p-type structures of application include polycyclic aromatic hydrocarbons and derivatives (acenes, pyrenes, perylenes), heterocyclic and chalcogen aromatic hydrocarbons and derivatives (thienoacenes, selenoacenes), oligothiophenes, thienoacene-based oligomers, polythiophenes, alternated co-polymers. Relevant n-type structures of application include fullerenes, diimides molecules (naphthalene diimide and derivatives, perylene diimide and derivatives) and polymers or alternated co-polymers.

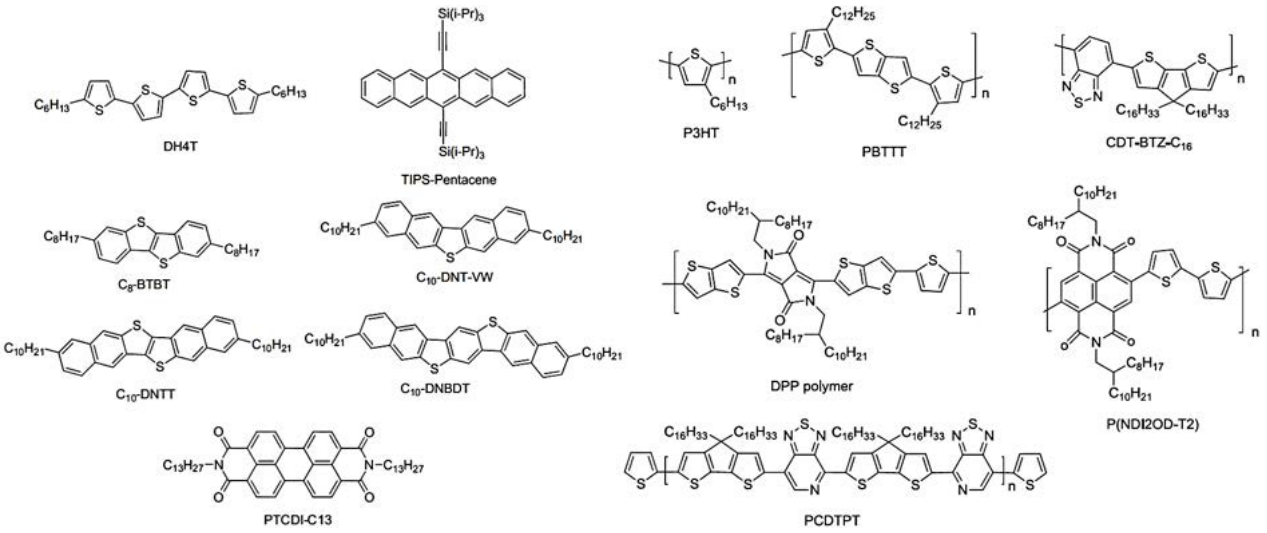

***Figure 26**. Chemical structures of typical soluble crystalline small-molecule and polymeric materials (both p- and n- type) with good charge carries mobilities for organic transistors.*

Still remain many fundamental research challenges that need to be addressed but it appears likely that OTFTs efficient can still grow.

1.2.2. High-Performance Organic Light-Emitting Displays

Organic Light-Emitting Diode (OLED) technology is developing as a promising choice for large area lighting applications, with basic properties such as efficiency, colour stability and lifetime approaching and, in some cases, even exceeding those of conventional inorganic LED technology and with various relevant additional complementing features. Unlike classic light emitting diodes (LEDs), OLEDs consist of several thin stacked layers and do not rely on small, point-shaped single crystals. OLEDs have the notable potential for devices performing as a flexible display by asset of their attractive features such as organic constituents, ultrathin and planar device structure self-emission, and low-temperature fabrication procedure that is compatible with plastic substrates, triggering tremendous studies of OLEDs in flexible configurations.[72,73] Flexible OLEDs have been truly driven close to the level of commercialization, yet technical issues hindering their reliability and durability still remain. OLEDs are now used for various flat-panel displays such as smartphones and televisions owing to their characteristic features: (i) planar emission; (ii) excellent quality image due to high brightness, wide view angle, and good contrast resulting from selfemission; (iii) portability; (iv) suitability for moving-image display owing to fast response; and (v) capability of full-color emission.

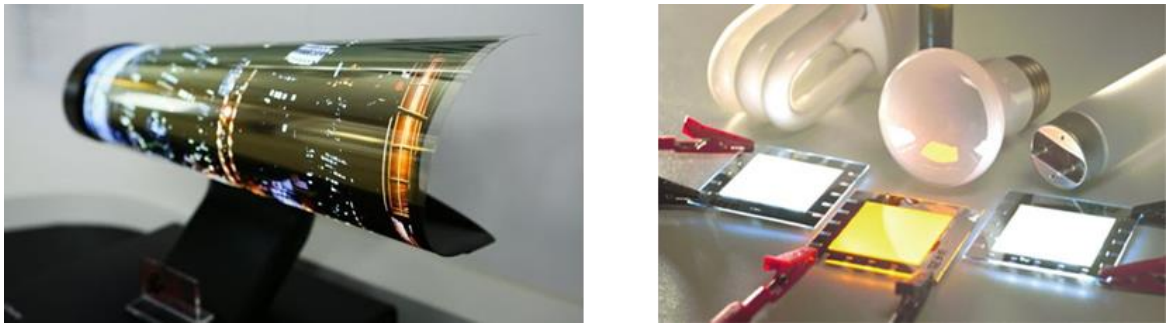

***Figure 28**. Left: Flexible OLED display. Right: OLEDs (warm and cold white) as compared to conventional light sources (compact fluorescent (CFL), incandescent and fluorescent (TL) lamps).*

The basic OLED structure consists of one, two or more organic layers sandwiched between a transparent anode (ITO: indium tin oxide) and a metal cathode, all deposited on a substrate. It can be designed to emit a single color of light, white light, or even tunable colors.[74] OLED utilizes the principle of electroluminescence, where a visible light is emitted by a specific material in response to an electric current or voltage applied. During operation, a bias is applied at electrodes and the anode is positive charged with respect to the cathode. A current of electrons flows through the device from the cathode to the anode: electrons are injected into the LUMO of the organic layer at the cathode and withdrawn from the HOMO at the anode. This latter process may also be described as the injection of holes into the HOMO of the molecule. The device can have specific layers for the injection process between the electrode and the corresponding organic transport layer to improve the process: the hole injection layer (HIL) and electron injection layer (EIL). Electrostatic forces bring the electrons and the holes towards each other (the charges can move by hopping mechanism between neighbours molecules through the corresponding transport layer) and they recombine forming an exciton. This happens closer to the emissive layer, because in organic semiconductors holes are generally more mobile than electrons. The decay of this excited state results in a relaxation of the energy levels of the electron, accompanied by emission of radiation whose frequency is in the visible region (**figure 29**).[74] The frequency of this radiation depends on the energy gap of the material. As electrons and holes are fermions with half integer spin, an exciton may either be in a singlet state or a triplet state depending on how the spins of the electron and hole have been combined. Statistically three triplet excitations will be formed for each singlet exciton. Decay from triplet states (phosphorescence) is spin forbidden, increasing the time scale of the transition and limiting the internal efficiency of fluorescent devices. Phosphorescent organic light-emitting diodes make use of spin-orbit coupling (by using heavy metal atoms such as platinum and iridium) to mix the singlet and triplet states and facilitate intersystem crossing (ISC), thus obtaining emission from both singlet and triplet states and improving the performance of the device allowing theoretically quantum efficiencies up to 100%

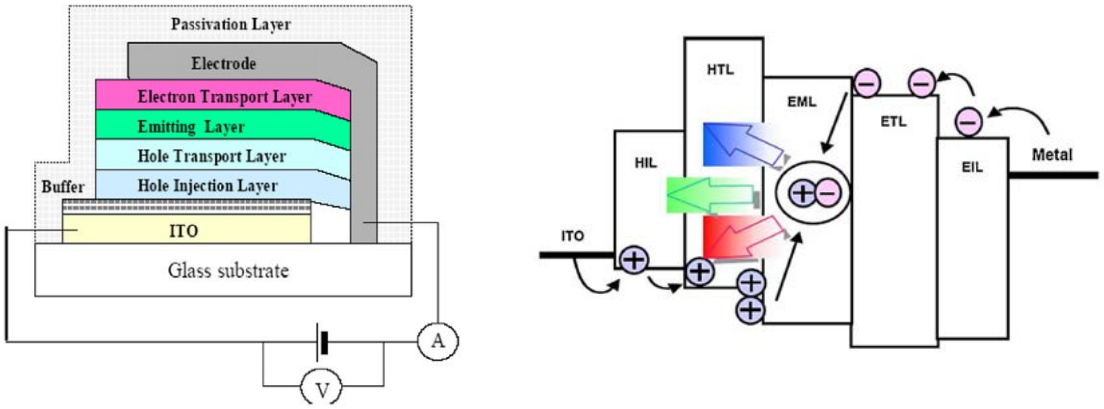

Figure 29. *<u>Left</u>: Structure of a multilayer OLED. It consists of a transparent carrier substrate, a transparent anode, followed by a hole injection layer (HIL), which supports efficient charge injection into the organic material. The HIL is followed by a hole transport layer (HTL), which acts as a mediator between the injection layer and the emissive layer (EML), in the center of the device. The EML converts the incoming charges, holes and electrons, into so-called excitons, charge pairs that can be then converted into photons by the emitter molecules. The electrons are transported into the EML by the electron transport layer (ETL). The ETL is then followed by an electron injection layer (EIL), with the function of enhancing electron injection from the metallic cathode. <u>Right</u>: light emitting mechanism from an OLED device. Light emitting from the OLEDs involves six processes:(i) an external direct current (DC) bias is applied (ii) Injection of holes and electrons. (iii) Transport of holes and electrons into the emitting layer. (iv) Combination of the holes and electrons into excitons. (v) Migration of the excitons under the external electric field and transfer of their energy to emissive molecules to make them excited. (vi) The excited molecules return to their ground states and release energy as electroluminescence. The colour of the light depends on the energy difference between the excited state and ground state of excitons.*

The performance of OLED is characterized by luminous efficacy, quantum efficiency, colour, and lifetime.[74,75] For display and lighting, the luminous efficacy is normally defined by the current efficiency (cd A^{-1}) and luminous power efficiency (lm W^{-1}), respectively. The current efficiency indicates the light-emitting ability of a material, while the power efficiency defines the energy consumption of device. Quantum efficiency is the ratio of emitted photons to injected charges. Quantum efficiency is usually expressed separately as internal quantum efficiency (IQE) and external quantum efficiency (EQE). IQE is the ratio of emitted photons to injected electrons in the emitting layer, which indicates the luminance and charge transport properties of material itself. EQE is the ratio of emitted photons from the direction of observation to injected electrons, which is the summary of IQE and many factors influencing the efficiency, such as output coupling of light. It reflects more accurately the overall performance of OLED. For high purity single colour OLEDs, several requirements should be considered. (i) A narrower emission spectrum is beneficial for colour purity. (ii) Confinement of excitons within the emitting layer is important. If the excitons migrate to the neighbouring layers, it will cause strayed emission, leading to bad colour purity. (iii) A good match of energy levels between layers is needed.[75]

To generate white light from OLEDs with different colours, different strategies can be applied. Since white light is composed of several individual colours, once can either use two or three colours to create white light. The quality of the light can be described by the colour CIE coordinates (x and y) and the color-rendering index (CRI) (**Figure 30**).[76] In particular, these parameters are mainly affected by the shape of the emission spectrum of the emitting compound. The CIE coordinates describe the color composition, that is, the relative intensities of the included colours, while the CRI describes the impression of colours when illuminated by the given light source. The lower the CRI, the worse is the color impression. Instead of using the CIE coordinates, it is common in the lighting industry to use the color temperature. It is represented by the black-body curve and has higher values towards the blue side of the CIE diagram. While 2000 K represents a warm light impression, 6000 K is a value for cold blueish light, like known from fluorescent tubes. The modification of the CRI is also crucial for a nice color perception. It is desirable to have an overly broad emission spectrum to have a high CRI. The stack design of WOLEDs is a very important topic because it has to take into account the aforementioned points, while maximizing the device efficiency to reduce the cost per light output. Consequently, WOLEDs mostly consist of so-called tandem devices, where two or three OLEDs are directly stacked on top of each other and then connected to an external circuit. This maximizes the device efficiency but makes the production more complex because tens of layers have to be deposited on top of each other with perfect alignment and no defects. In between such stacked OLEDs charge generation layers (CGLs) are used to generate holes for one diode and electrons for the other one.[76]

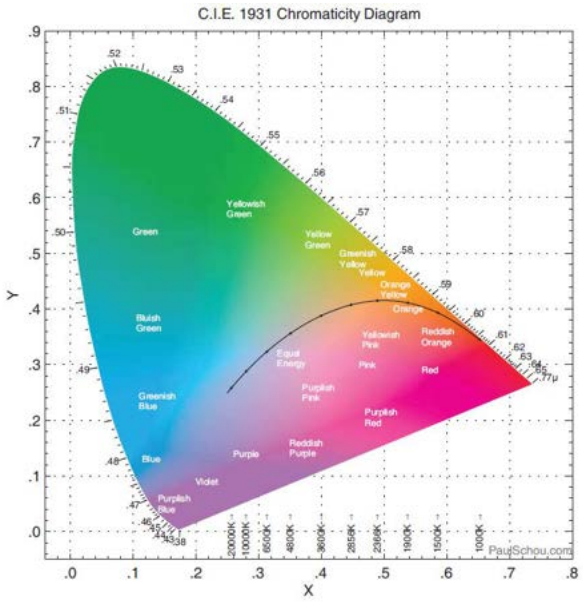

***Figure 30**. Chromaticity coordinates of CIE 1931. Reprinted from ref. 74 with permission from Nature Publishing Group*

More recently, thermally activated delayed fluorescence (TADF) materials have attracted great attention as the new generation of OLED devices. This technology can achieve 100% IQE by harvesting both singlet and triplet excitons using pure organic materials without requiring the use of expensive and scarce metals such as iridium or platinum.[77] Efficient TADF systems requires the "dark" triplet excited states to be easily harvested back to the emissive singlet manifold, using the thermal energy to assist reverse intersystem crossing (RISC) and promote the up-conversion of lower-energy triplet states into the emissive singlet manifold (**Figure 31**). The efficiency of this mechanism is controlled by two main parameters: (i) the energy splitting between the singlet and triplet states (ΔE_{ST}), which needs to be minimized, and (ii) the suppression of non-radiative pathways available for the excited singlet and triplet states to decay, in order to obtain high fluorescence quantum yields and long triplet excited state lifetimes. To achieve a small energy splitting between the singlet and triplet excited states, as it is required to maximize triplet har-vesting by reverse intersystem crossing, molecules should possess excited states of strong charge transfer character, so a small overlap can be obtained between HOMO and LUMO energy levels. However, increasing the charge transfer character of the excited state leads in general to lower fluorescence yields which impact on device efficiencies. One way to solve this dilemma is to use electron-donor (D) and electron-acceptor (A) units linked in nearly perpendicular relative orientation in the TADF emitter, and forming "rigid" molecular structures, which suppresses the non-radiative decay due to the internal conversion channels. This arrangement is able to give fluorescence with high efficiency, while retaining negligible ΔE_{ST}, and thus achieve efficient triplet harvesting.[77]

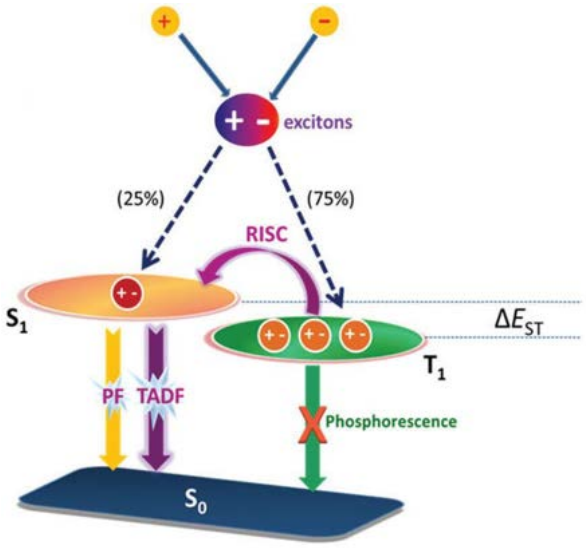

***Figure 31**. TADF mechanism through reverse intersystem crossing (RISC)*

1.2.2.1 Organic Materials for OLEDs

Generally, materials for use in OLEDs should meet the following requirements:[28,78]

1. They should form uniform, homogeneous, pinhole-free thin films by either thermal deposition in vacuum or by solution processing.
2. They should have thermal stability with high Tgs.
3. They should be morphologically stable.
4. The choice of HTL and ETL materials should take into a count similar charge carrier mobilities for efficient exciton forming process in the emitting layer and increase the EQE.

Amorphous molecular materials that form smooth, uniform, amorphous films have proved to be well suited for use in OLEDs. A variety of hole- and electron- transporting, hole- and electron-blocking, and emitting amorphous molecular materials have been designed and synthesized.

Hole-transporting materials should have proper HOMO energy levels so they may accept hole carriers from the anode through the hole-injection layer. The injected hole carriers (i.e., the cation-radical species of hole-transporting molecules) should be stable. In other words, the anodic oxidation

processes of hole-transporting molecules should be reversible. They should have hole-transporting ability, along with electron-blocking. Hole carriers injected from the anode are then injected into the emitting layer in a stepwise process via the hole-transport layer. Between the hole-transporting materials, those with low ionization potential can be used for the hole-injection layer in contact with the anode.

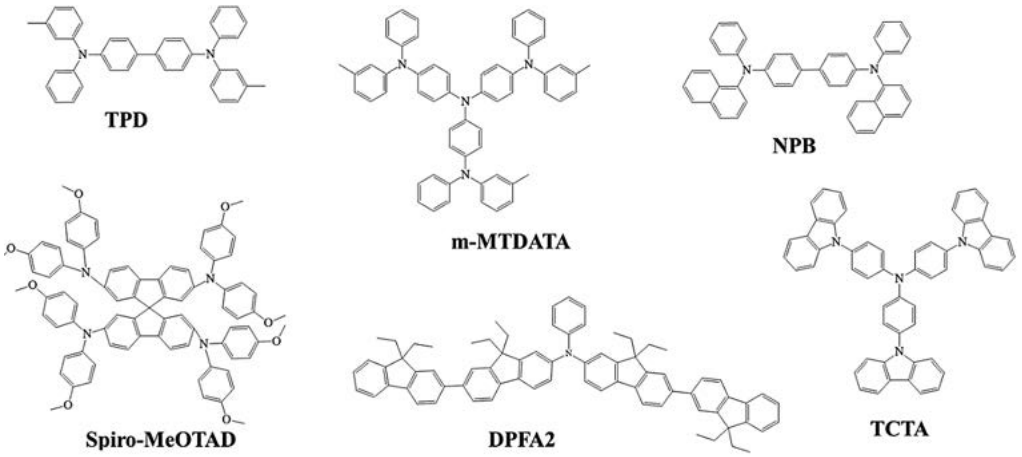

***Figure 32**. Representative chemical structures of hole-transporting materials.*

Electron-transporting materials should have proper LUMO energy levels to accept electron carriers injected from the cathode through the electron-injection layer. Injected electron carriers (i.e., the anion radical species of electron-transporting molecules) should be stable. In other words, the cathodic reduction processes of electron-transporting molecules should be reversible. They should have electron-transporting ability along with hole-blocking. Electron carriers injected from the cathode are then injected into the emitting layer in a stepwise process via the electron-transport layer.

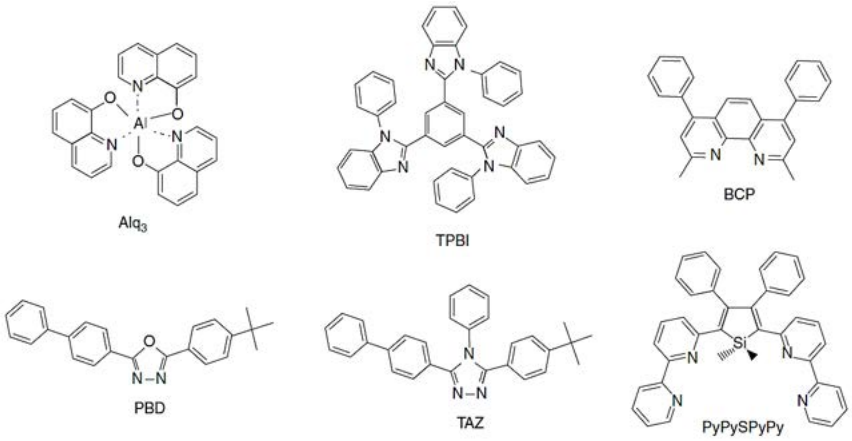

***Figure 33**. Representative chemical structures of electron-transporting materials.*

The emitting layer functions as the recombination centre for holes and electrons injected from the anode and cathode, respectively. Therefore, emitting materials should possess a bipolar character, with proper HOMO and LUMO energy levels so as to accept both holes and electrons injected through the hole- and electron-transport layers, respectively. In addition, injected charge carriers (namely, the cation- and anion-radical species of emitting molecules) should be stable; in other words, the anodic oxidation and cathodic reduction processes of emitting molecules should be reversible. Furthermore, emitting materials should have high-luminescence quantum efficiencies. When emitting materials with high quantum efficiencies for either fluorescence or phosphorescence lack good film-forming ability, they can be used as emitting dopants by being dispersed in the host amorphous molecular materials.

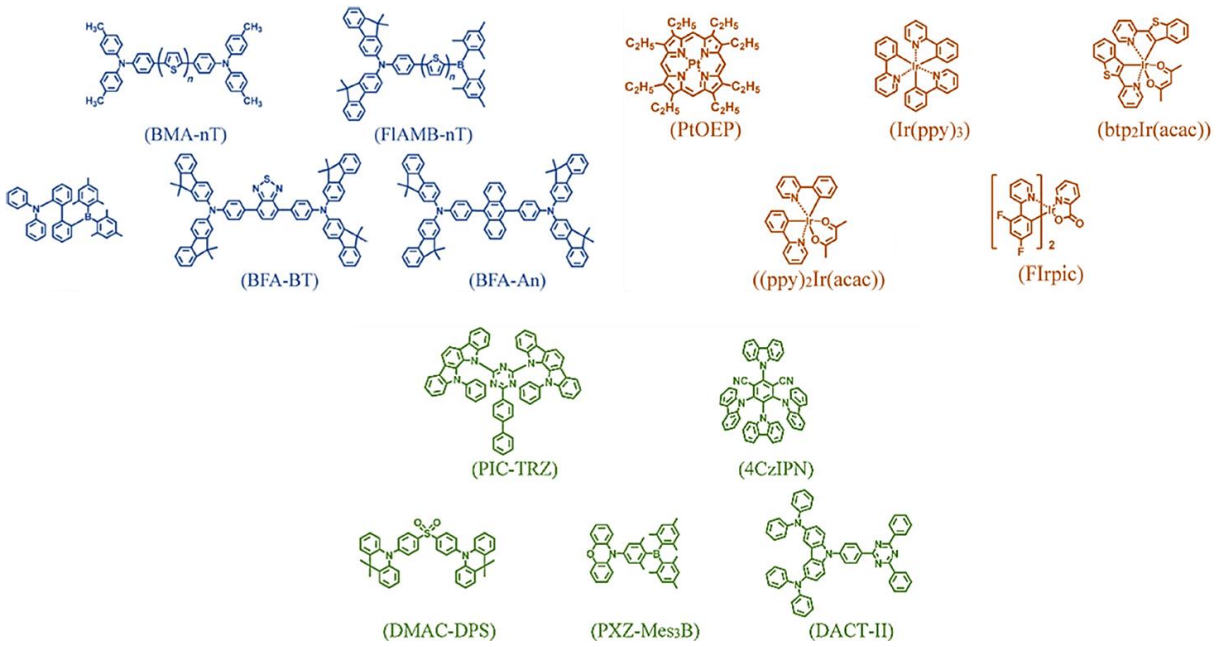

***Figure 34**. Representative chemical structures of emitting materials. In blue: fluorescence-emitting materials; in orange: phosphorescence-emitting materials; in green: TADF-emitting materials.*

1.2.3. Solution-Processed Organic Photovoltaics

Photovoltaics are devices focused on transforming light energy into electrical energy. In recent years, the growing requirement for clean energy resources has led to a remarkable growth in the research, development, and manufacturing of solar cells. Silicon-based devices have been the front competitors in bringing solar cell technology to the consumer market. However, fabrication processes are complex and involve a number of steps that make solar panels expensive and the energy they produce uncompetitive compared to traditional energy sources (e.g., coal, natural gas, hydropower, etc.). Moreover, silicon solar cells are rigid and feature a distinctive reflective look, which limits integration for example in buildings, fabric and other everyday objects. During the past few years solution-processed organic photovoltaics (OPVs) have gained big attention and now they are expected to be one of the future photovoltaic technologies for the low-cost, ease-manufactured, large-scale production of flexible and light-weight devices.[79] The significant progress reached in OPV performance and stability shows the potential of this technology to be one of the crucial technologies for future power generation. OPVs are usually classified into small-molecule solar cells and polymer solar cells. Currently, polymer-based OPVs have been shown to achieve higher power conversion efficiencies than small molecule-based OPVs. However, small molecule-based OPVs have several advantages, such as simple synthesis and purification methods, uniform and defined molecular structures, higher open circuit voltages (Voc), and better batch-to-batch reproducibility.[80]

***Figure 35**. Flexible and light-weight OPV technology for large area applications.*

The photovoltaic process is made up of five steps[81]:

1. Photon absorption and exciton generation. Photons with energy above the optical gap are absorbed by the photoactive organic semiconductor (generally the donor layer). Electrons move from the HOMO energy level to the LUMO energy level, and consequently generate high energy electron-hole pairs bonded by Coulomb attraction, known as excitons.

2. Diffusion of excitons. The excitons can diffuse freely within their lifetime to the donor-acceptor interface. One of the major problems that influences device performance is the annihilation of excitons during the diffusion process.

3. Exciton dissociation and charge carrier generation. When the exciton diffuses to the D-A interface, intermolecular electron transfer between donor and acceptor occurs if the LUMO energy level of the donor is higher than the LUMO of the acceptor. The energetic offset between the HOMO–HOMO and LUMO–LUMO between D and A, generated by stacking the materials between two electrodes, drives exciton dissociation into free charge carriers, where electrons live in the acceptor layer while holes in the donor layer.

4. Charge transport. After dissociation, the free electrons and holes move via the acceptor and donor pathways towards the cathode and anode, respectively. During the movement, the free electrons and holes can potentially be quenched or recombined, which is another key factor causing poor device performance.

5. Charge carriers collection and current formation. The electrons and holes are finally collected by their corresponding electrodes and consequently an electrical current flow is generated.

The earliest version of OPV devices was just a single-layer device structure with an organic photosensitive semiconductor sandwiched between two electrodes. Then, in order to efficiently dissociate the excitons into free charge carriers upon light absorption, bilayer p-/n- heterojunctions are introduced by using electron donor (p-type semiconductor) and electron acceptor (n-type semiconductor) in organic solar cells. Most often, the donor is a conjugated polymer, and the acceptor is a fullerene derivative, both soluble in common organic solvents. Depending on the layer structure between the donor and acceptor, organic solar cells can be divided into two types: planar heterojunction solar cell (PHJ), and bulk heterojunction solar cell (BHJ) as shown in **Figure 36**. In a PHJ cell, the donor and acceptor layers are sequentially stacked layer by layer, whereas in a BHJ cell, the electron donor and acceptor materials form interpenetrating network morphology with a phase separation at nanoscale. As the diffusion length of excitons for most organic semiconductors is only about 4~20 nm, the donor or acceptor layers cannot be too thick, which negatively reduces the photon absorption length and thus leads to low quantum efficiency.[82] The relatively small D/A interface area is also a limiting factor of charge dissociation efficiency in planar heterojunction. In contrast to a PHJ cell, the nanoscale interlacing network of donor and acceptor in a BHJ cell decreases the distance between donor and acceptor, and consequently reduces the necessary diffusion length for the excitons as well as increases the effective D/A interfacial area. Both factors would be beneficial to the device performance. It has been proved that charge dissociation efficiency in a BHJ solar cell can reach to 100%.[83] Nevertheless, recombination of free electrons and holes cannot be suppressed during the charge transport process, which could affect the device performance as well. In general, BHJ photoactive layers can be deposited in solution process with a mixed solution of donor and acceptor and the nanoscale phase separation occurs spontaneously during the thin-film deposition. However, it is more difficult to deposit organic layers by solution process in a layer-by-layer manner since the solvent of each newly deposited layer might destroy the pre-deposited organic layer. Nevertheless, with careful selection of solvents, planar heterojunction solar cells can be fabricated.

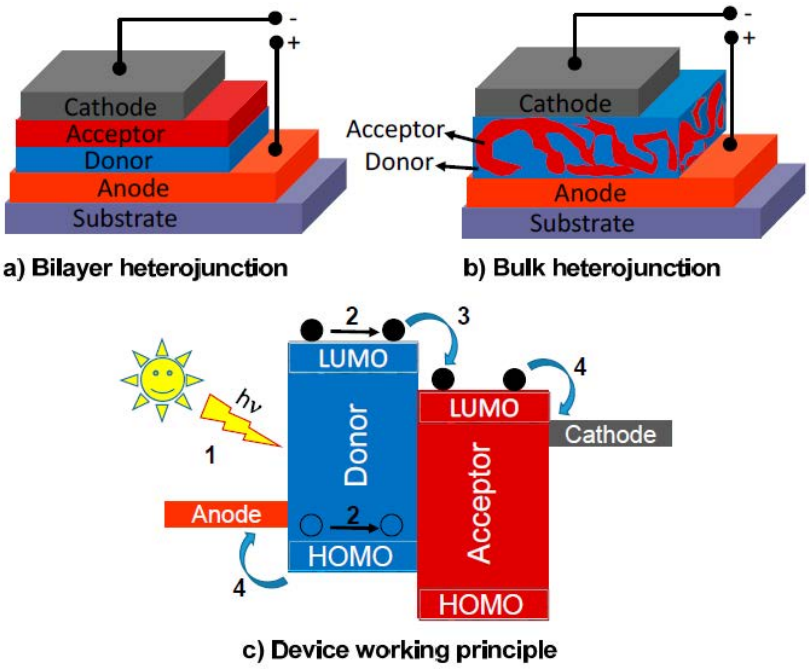

***Figure 36**. Device structures of (**a**) bilayer heterojunction, (**b**) bulk heterojunction, (**c**) device working principle. Copyright of Polymers 2014.*

In summary, PHJ photovoltaic cells collect very small amounts of excitons created near the D-A interface, while BHJ OPV cells, which have an intermixed composite of donor and acceptor, have an advantage in terms of their having a much larger interface area between donor and acceptor. Efficient charge separation results from photo-induced electron transfer from the donor to the acceptor at the large interface, and the high collection efficiency results from a bicontinuous network of internal donor–acceptor heterojunctions.

According to the working principle of organic solar cells, the loss of efficiency in an organic solar cell is caused by optical losses, exciton losses due to insufficient transport of exciton, non-radiative recombination losses, and charge carrier collection losses due to insufficient motilities. The current-voltage curve (I-V) is generally used to characterize an organic solar cell. In the dark, the solar cell should act as a simple diode, and the ideal factor of this cell can be evaluated (**Figure 37**).[84] Under illumination, the whole I-V characteristics curve moves to the 3rd and 4th quadrants. Several important parameters, including open circuit voltage (V_{OC}), short circuit current (I_{SC}), fill factor (FF), maximum power point (P_{max}), and power conversion efficiency (η) can be derived from the I-V characteristics.

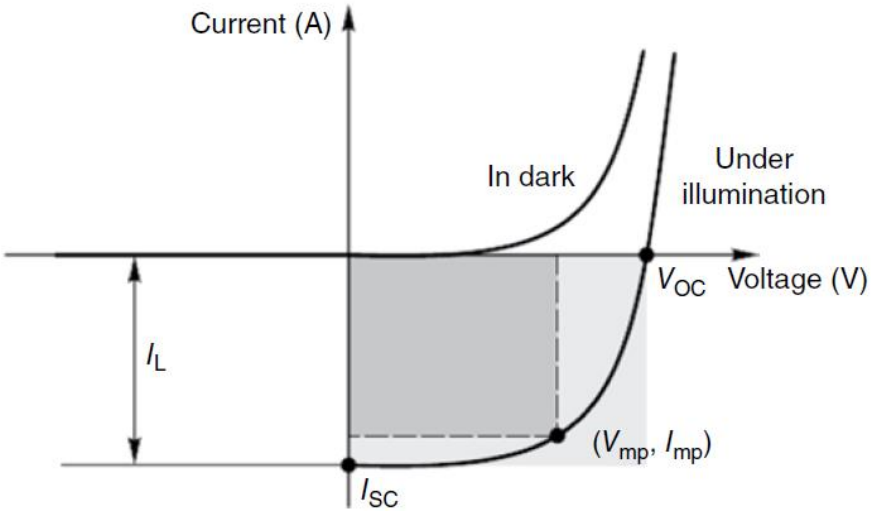

***Figure 37**. Typical I-V characteristics of organic solar cells.*

The open-circuit voltage (V_{OC}) is the maximum voltage at zero current. The V_{OC} is the voltage difference between heterojunction interfaces on the open circuit condition under light illumination. In an organic solar cell, the V_{OC} is linearly dependent on the HOMO level of the donor and the LUMO level of the acceptor. The short-circuit current (I_{SC}) is the maximum current through the solar cell under light illumination when the bias voltage across the cell is zero. I_{SC} is directly related to the number of charge carriers generated within the photoactive layer. Therefore, I_{SC} depends on the efficiencies of three steps: photon absorption, exciton dissociation and charge transport. Fill factor (FF) is defined as the ratio of maximum power (P_{max}) and the product of V_{OC} and I_{SC}. In **Figure 37**, the FF is the area ratio of the rectangle with a length of *V*max and a width of *I*max to the large rectangle with a length and width of V_{OC} and I_{SC}, respectively. A good solar cell usually has an FF of 60–65%. Power conversion efficiency (η) is defined as the ratio of P_{max} to the input solar power P_{in}. It is worth mentioning that the above parameters are usually measured at 25° C under the illumination of AM1.5G solar spectrum, which has a standard light intensity of 100 mW/cm^2.[84]

1.2.3.1. Organic Materials for OPVs

OPVs are based on the idea of the dissociation of electron-hole pairs generated from excitons to yield charge carriers. One photon absorbed by an organic molecule produces at most one pair consisting of a free hole and an electron, which is transported in the donor and acceptor layers, respectively, and collected at each electrode. To observe a good working efficiency in the device, both D and A materials should meet the following requirements:[28,85]

1. Large molar extinction coefficient. Materials should absorb as much of the sunlight as possible, and hence should have broad spectral sensitivity from the visible to near-infrared wavelength region. In an organic solar cell, the thickness of photoactive layer is usually limited due to the low charge carrier mobility of organic semiconductors. Thus, the molar extinction coefficient can provide important information about the light absorption ability of organic semiconductors.

2. Mismatch between the absorption spectrum of an organic semiconductor and the solar radiation spectrum. Most organic semiconductors have a large band-gap (~2 eV) and narrow absorption width. For example, the absorption spectrum of P3HT covers from 400 to 700 nm, which is not matched with the condensed energy range of the solar spectrum (500~900 nm). This means that better light harvesting organic semiconductors via lowering the optical band-gap.

3. Materials with suitable HOMO and LUMO energy levels should be chosen as D and A, respectively, so as to reduce as much as possible the excitation energy loss in the electron-transfer process from the exciton and to give high V_{OC}. A driving force of more than 0.30 eV (energy difference between the LUMO of donor and the HOMO of acceptor) is required to achieve efficient electron transfer. An increase in the HOMO level of the donor will lead to a lower V_{OC}, whereas a decrease in the LUMO level of the donor will lead to insufficient electron transfer between donor and acceptor. So, besides the reduction of the band-gap, the donor and acceptor materials for high efficiency organic solar cells must be designed to optimize the D/A combination with matched HOMO and LUMO levels.

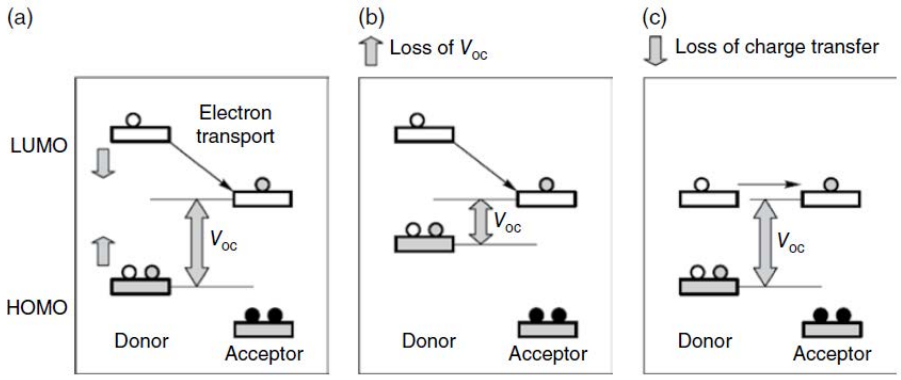

***Figure 38**. The dependence of device performance on the energy level arrangement of donor and acceptor.*

4. Materials should have high charge carrier mobilities for efficient charge separation and transport and reducing series resistance.

5. Thin-film morphology control. The energy conversion efficiency of solar cells is significantly dependent on the nanoscale morphology of the photoactive layer. An ideal nanophase separation structure of the photoactive layer in a BHJ solar cell, where the donor and acceptor form an interpenetrating network morphology to minimize the charge recombination losses, and the interface distance is less than the exciton diffusion length. This is beneficial for efficient charge separation. Additionally, such a nanoscale interlacing network increases the D/A interfacial area enormously, resulting in improved device performance. However, due to the fact that the nanostructure forms spontaneously during the deposition of the photoactive layer, it is quite a challenge to design or to have exact control of the nanoscale morphology.

The main task in developing organic semiconductors is to find the appropriate donor and acceptor combination to reduce the energy losses for each process, therefore, to improve the power conversion efficiency. In order to gain higher power conversion efficiency, semiconductors with reduced optical band-gap. With this aim, several novel low band-gap polymers have been developed. **Figure 39** shows the chemical structure of some low band-gap p-type polymers to use as the donor layer.

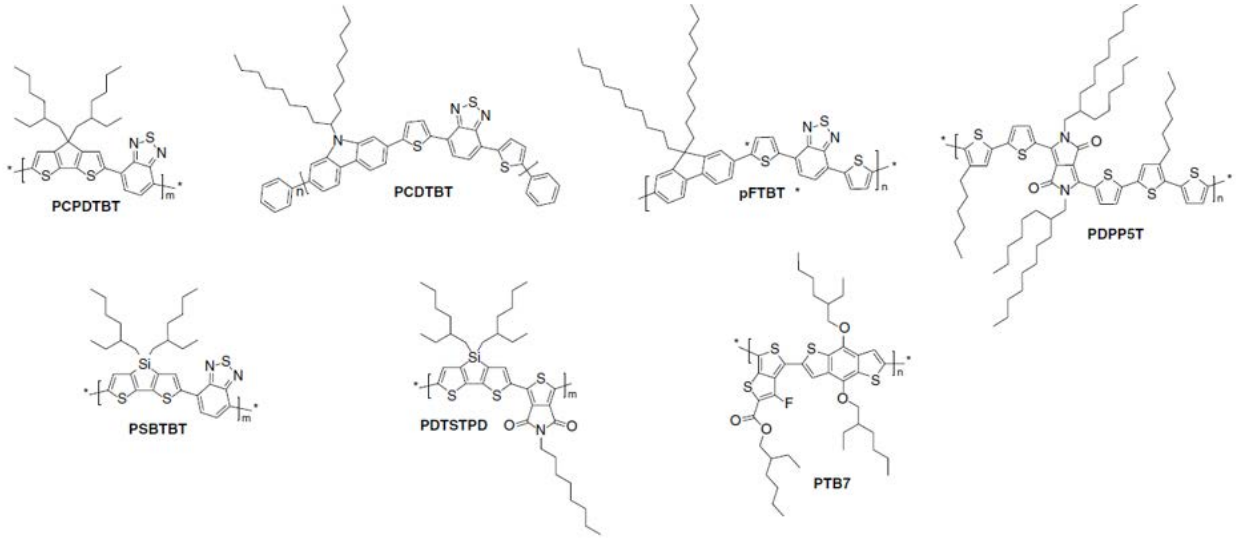

***Figure 39**. Representative chemical structures of low band-gap donor-acceptor alternated conjugated co-polymers as donor layer for flexible OPVs applications.*

Following are reported a series of examples of semiconducting materials as acceptor layer for OPV devices.

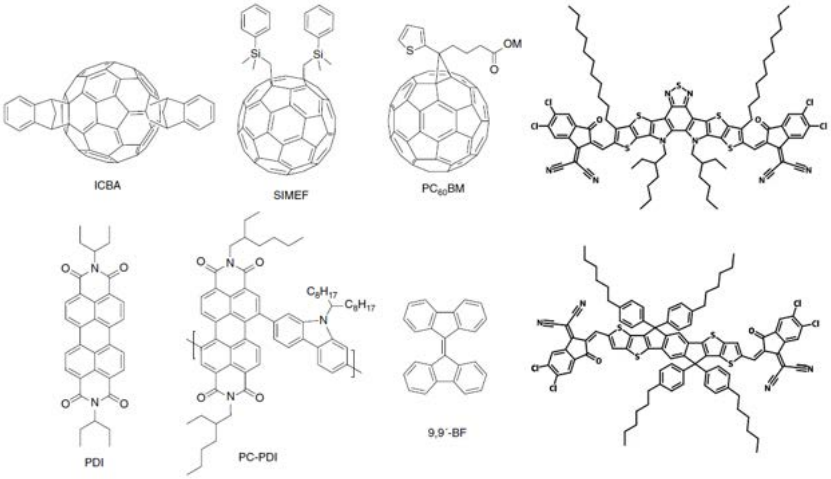

Figure 40. *Representative chemical structures of semiconducting materials as acceptor layer for OPVs applications.*

Bibliography

1. Logothetidis, S. Flexible organic electronic devices: Materials, process and applications. *Mater. Sci. Eng. B Solid-State Mater. Adv. Technol.* **152**, 96–104 (2008).
2. Root, S. E., Savagatrup, S., Printz, A. D., Rodriquez, D. & Lipomi, D. J. Mechanical Properties of Organic Semiconductors for Stretchable, Highly Flexible, and Mechanically Robust Electronics. *Chem. Rev.* **117**, 6467–6499 (2017).
3. Sekitani, T., Zschieschang, U., Klauk, H. & Someya, T. Flexible organic transistors and circuits with extreme bending stability. *Nat. Mater.* **9**, 1015–1022 (2010).
4. Han, T. H. *et al.* Extremely efficient flexible organic light-emitting diodes with modified graphene anode. *Nat. Photonics* **6**, 105–110 (2012).
5. Sun, Y. *et al.* Flexible organic photovoltaics based on water-processed silver nanowire electrodes. *Nat. Electron.* **2**, 513–520 (2019).
6. Torres Sevilla, G. A. & Hussain, M. M. Printed organic and inorganic electronics: Devices to systems. *IEEE J. Emerg. Sel. Top. Circuits Syst.* **7**, 147–160 (2017).
7. Wu, Y., Liu, P., Li, Y. & Ong, B. S. Enabling materials for printed electronics. *Conf. Proc. - Lasers Electro-Optics Soc. Annu. Meet.* **6**, 434–435 (2006).
8. Bromley, S. T., Mas-Torrent, M., Hadley, P. & Rovira, C. Importance of intermolecular interactions in assessing hopping mobilities in organic field effect transistors: Pentacene versus dithiophene-tetrathiafulvalene. *J. Am. Chem. Soc.* **126**, 6544–6545 (2004).
9. Sutton, C., Risko, C. & Brédas, J. L. Noncovalent Intermolecular Interactions in Organic Electronic Materials: Implications for the Molecular Packing vs Electronic Properties of Acenes. *Chem. Mater.* **28**, 3–16 (2016).
10. Facchetti, A. π-Conjugated polymers for organic electronics and photovoltaic cell applications. *Chem. Mater.* **23**, 733–758 (2011).
11. Roncali, J. Molecular engineering of the band gap of π-conjugated systems: Facing technological applications. *Macromol. Rapid Commun.* **28**, 1761–1775 (2007).
12. Brisset, H., Thobie-Gautier, C., Gorgues, A., Jubault, M. & Roncali, J. Novel narrow bandgap polymers from sp3 carbon-bridged bithienyls: Poly(4,4-ethylenedioxy-4H-cyclopenta[2,1-b;3,4-b′]dithiophene). *J. Chem. Soc. Chem. Commun.* 1305–1306 (1994) doi:10.1039/C39940001305.
13. Hamlen, S. Advanced materials. *Offshore Eng.* **42**, 38–39 (2017).
14. Torruellas, W. E. *et al.* Dispersion measurements of the third-order nonlinear susceptibility of polythiophene thin films. *Chem. Phys. Lett.* **175**, 11–16 (1990).
15. Tanase, C., Blom, P. W. M. & De Leeuw, D. M. Origin of the enhanced space-charge-limited current in poly(p-phenylene vinylene). *Phys. Rev. B - Condens. Matter Mater. Phys.* **70**, 1–4 (2004).
16. Hou, J., Tan, Z., He, Y., Yang, C. & Li, Y. Branched poly(thienylene vinylene)s with absorption spectra covering the whole visible region. *Macromolecules* **39**, 4657–4662 (2006).
17. Frère, P. *et al.* Effect of local molecular structure on the chain-length dependence of the electronic properties of thiophene-based π-conjugated systems. *J. Org. Chem.* **68**, 7254–7265 (2003).
18. Wudl, F., Kobayashi, M. & Heeger, A. J. Poly(isothianaphthene). *J. Org. Chem.* **49**, 3382–3384 (1984).
19. Roncali, J. *et al.* Effects of steric factors on the electrosynthesis and properties of conducting poly(3-alkylthiophenes). *J. Phys. Chem.* **91**, 6706–6714 (1987).
20. McCullough, R. D. The chemistry of conducting polythiophenes. *Adv. Mater.* **10**, 93–116 (1998).
21. Bechgaard, K. & Spiering, A. J. H. Two-dimensional charge transport in conjugated polymers. *October* 685–688 (1999).

22. Zhang, Z. G. & Wang, J. Structures and properties of conjugated Donor-Acceptor copolymers for solar cell applications. *J. Mater. Chem.* **22**, 4178–4187 (2012).
23. Blanchard, P., Brisset, H., Riou, A., Hierle, R. & Roncali, J. Bridged 1,6-dithienylhexa-1,3,5-trienes as highly photoluminescent and stable thiophene-based π-conjugated systems. *J. Org. Chem.* **63**, 8310–8319 (1998).
24. Guo, X. *et al.* Materials Design via Optimized Intramolecular Noncovalent Interactions for High-Performance Organic Semiconductors. *Chem. Mater.* **28**, 2449–2460 (2016).
25. Karikomi, M., Kitamura, C., Tanaka, S. & Yamashita, Y. New Narrow-Bandgap Polymer Composed of Benzobis(1,2,5-thiadiazole) and Thiophenes. *J. Am. Chem. Soc.* **117**, 6791–6792 (1995).
26. Akoudad, S. & Roncali, J. Electrogenerated poly(thiophenes) with extremely narrow bandgap and high stability under n-doping cycling. *Chem. Commun.* 2081–2082 (1998) doi:10.1039/a804992k.
27. Virkar, A. A., Mannsfeld, S., Bao, Z. & Stingelin, N. Organic semiconductor growth and morphology considerations for organic thin-film transistors. *Adv. Mater.* **22**, 3857–3875 (2010).
28. Shirota, Y. & Kageyama, H. *Organic materials for optoelectronic applications: Overview*. *Handbook of Organic Materials for Electronic and Photonic Devices* (Elsevier Ltd., 2019). doi:10.1016/b978-0-08-102284-9.00001-2.
29. Jurchescu, O. D. *et al.* Effects of polymorphism on charge transport in organic semiconductors. *Phys. Rev. B - Condens. Matter Mater. Phys.* **80**, 21–23 (2009).
30. Yasuhiko Shirota, Tomakazu Kobata, N. N. Starburst Molecules for Amorphous Molecular Materials. 1145–1148 (1989).
31. Shirota, Y. Photo- and electroactive amorphous molecular materials - Molecular design, syntheses, reactions, properties, and applications. *J. Mater. Chem.* **15**, 75–93 (2005).
32. Bao, Z., Dodabalapur, A. & Lovinger, A. J. Soluble and processable regioregular poly(3-hexylthiophene) for thin film field-effect transistor applications with high mobility. *Appl. Phys. Lett.* **69**, 4108–4110 (1996).
33. Shank, M. H. Made to order. *Isis* **105**, 167–176 (2014).
34. Locklin, J., Roberts, M. E., Mannsfeld, S. C. B. & Bao, Z. Optimizing the thin film morphology of organic fieldeffect transistors: The influence of molecular structure and vacuum deposition parameters on device performance. *Polym. Rev.* **46**, 79–101 (2006).
35. Guo, X., Facchetti, A. & Marks, T. J. Imide- and amide-functionalized polymer semiconductors. *Chem. Rev.* **114**, 8943–9012 (2014).
36. Coropceanu, V. *et al.* Charge transport in organic semiconductors. *Chem. Rev.* **107**, 926–952 (2007).
37. Zaumseil, J. & Sirringhaus, H. Electron and ambipolar transport in organic field-effect transistors. *Chem. Rev.* **107**, 1296–1323 (2007).
38. Facchetti, A. Semiconductors for organic transistors. *Mater. Today* **10**, 28–37 (2007).
39. Jørgensen, M. *et al.* Stability of polymer solar cells. *Adv. Mater.* **24**, 580–612 (2012).
40. Salzmann, I., Heimel, G., Oehzelt, M., Winkler, S. & Koch, N. Molecular Electrical Doping of Organic Semiconductors: Fundamental Mechanisms and Emerging Dopant Design Rules. *Acc. Chem. Res.* **49**, 370–378 (2016).
41. Cowen, L. M., Atoyo, J., Carnie, M. J., Baran, D. & Schroeder, B. C. Review—Organic Materials for Thermoelectric Energy Generation. *ECS J. Solid State Sci. Technol.* **6**, N3080–N3088 (2017).
42. Shirakawa, H., Louis, E. J., MacDiarmid, A. G., Chiang, C. K. & Heeger, A. J. Synthesis of electrically conducting organic polymers: Halogen derivatives of polyacetylene, (CH)x. *J. Chem. Soc. Chem. Commun.* 578–580 (1977) doi:10.1039/C39770000578.
43. Pingel, P. *et al.* P-Type Doping of Poly(3-hexylthiophene) with the Strong Lewis Acid Tris(pentafluorophenyl)borane. *Adv. Electron. Mater.* **2**, 1–7 (2016).
44. Parthasarathy, G., Shen, C., Kahn, A. & Forrest, S. R. Lithium doping of semiconducting organic charge transport materials. *J. Appl. Phys.* **89**, 4986–4992 (2001).

45. Tanaka, S. *et al.* Doping effect of tetrathianaphthacene molecule in organic semiconductors on their interfacial electronic structures studied by UV photoemission spectroscopy. *Japanese J. Appl. Physics, Part 1 Regul. Pap. Short Notes Rev. Pap.* **44**, 3760–3763 (2005).
46. Bredas, J. L. & Street, G. B. Polarons, Bipolarons, and Solitons in Conducting Polymers. *Acc. Chem. Res.* **18**, 309–315 (1985).
47. Salzmann, I. & Heimel, G. Toward a comprehensive understanding of molecular doping organic semiconductors (review). *J. Electron Spectros. Relat. Phenomena* **204**, 208–222 (2015).
48. Nisato, G., Lupo, D. & Ganz, S. *Organic and Printed Electronics*. *Organic and Printed Electronics* (2016). doi:10.1201/b20043.
49. Blumstengel, S., Sadofev, S., Xu, C., Puls, J. & Henneberger, F. Converting Wannier into Frenkel excitons in an inorganic/organic hybrid semiconductor nanostructure. *Phys. Rev. Lett.* **97**, 8–11 (2006).
50. Feron, K., Belcher, W. J., Fell, C. J. & Dastoor, P. C. Organic solar cells: Understanding the role of förster resonance energy transfer. *Int. J. Mol. Sci.* **13**, 17019–17047 (2012).
51. Mikhnenko, O. V., Blom, P. W. M. & Nguyen, T. Q. Exciton diffusion in organic semiconductors. *Energy Environ. Sci.* **8**, 1867–1888 (2015).
52. Segal, M., Baldo, A., Holmes, J., Forrest, R. & Soos, G. Excitonic singlet-triplet ratios in molecular and polymeric organic materials. *Phys. Rev. B - Condens. Matter Mater. Phys.* **68**, 1–14 (2003).
53. Reineke, S., Thomschke, M., Lüssem, B. & Leo, K. White organic light-emitting diodes: Status and perspective. *Rev. Mod. Phys.* **85**, 1245–1293 (2013).
54. Deibe, C., Strobe, T. & Dyakonov, V. Role of the charge transfer state in organic donor-acceptor solar cells. *Adv. Mater.* **22**, 4097–4111 (2010).
55. Tinivella, R., Shen, S., Pirola, M., Ghione, G. & Camarchia, V. A device-level analog and digital subsystem SPICE library for the design of low-cost pentacene OFET RFIDs. *IEEE MTT-S Int. Microw. Symp. Dig.* 848–851 (2010) doi:10.1109/MWSYM.2010.5517804.
56. Allard, S., Forster, M., Souharce, B., Thiem, H. & Scherf, U. Organic semiconductors for solution-processable field-effect transistors (OFETs). *Angew. Chemie - Int. Ed.* **47**, 4070–4098 (2008).
57. Shen, S., Tinivella, R., Pirola, M., Ghione, G. & Camarchia, V. SPICE library for low-cost RFID applications based on pentacene organic FET. *2010 6th Int. Conf. Wirel. Commun. Netw. Mob. Comput. WiCOM 2010* 23–26 (2010) doi:10.1109/WICOM.2010.5601134.
58. Torsi, L., Magliulo, M., Manoli, K. & Palazzo, G. Organic field-effect transistor sensors: A tutorial review. *Chem. Soc. Rev.* **42**, 8612–8628 (2013).
59. Deen, M. J., Kazemeini, M. H. & Holdcroft, S. Contact effects and extraction of intrinsic parameters in poly(3-alkylthiophene) thin film field-effect transistors. *J. Appl. Phys.* **103**, (2008).
60. Tang, W. *et al.* Recent progress in printable organic field effect transistors. *J. Mater. Chem. C* **7**, 790–808 (2019).
61. Dimitrakopoulos, C. D. & Malenfant, P. R. L. Organic thin film transistors for large area electronics. *Adv. Mater.* **14**, 99–117 (2002).
62. De Leeuw, D. M., Simenon, M. M. J., Brown, A. R. & Einerhand, R. E. F. Stability of n-type doped conducting polymers and consequences for polymeric microelectronic devices. *Synth. Met.* **87**, 53–59 (1997).
63. Brown, A. R., Leeuw, D. M. De, Lous, E. J. & Havinga, E. E. Organic n-type field-effect transistor. **66**, 257–261 (1994).
64. Wang, C., Dong, H., Hu, W., Liu, Y. & Zhu, D. Semiconducting π-conjugated systems in field-effect transistors: A material odyssey of organic electronics. *Chem. Rev.* **112**, 2208–2267 (2012).
65. Salleo, A. Charge transport in polymeric transistors. *Mater. Today* **10**, 38–45 (2007).
66. Henson, Z. B., Müllen, K. & Bazan, G. C. Design strategies for organic semiconductors beyond the molecular formula. *Nat. Chem.* **4**, 699–704 (2012).

67. Berrouard, P. *et al.* Synthesis of 5-alkyl[3,4-c]thienopyrrole-4,6-dione-based polymers by direct heteroarylation. *Angew. Chemie - Int. Ed.* **51**, 2068–2071 (2012).
68. Xu, Y. *et al.* Doping: A Key Enabler for Organic Transistors. *Adv. Mater.* **30**, 13–19 (2018).
69. Arias, A. C., MacKenzie, J. D., McCulloch, I., Rivnay, J. & Salleo, A. Materials and applications for large area electronics: Solution-based approaches. *Chem. Rev.* **110**, 3–24 (2010).
70. Paterson, A. F. *et al.* Recent Progress in High-Mobility Organic Transistors: A Reality Check. *Adv. Mater.* **30**, 1–33 (2018).
71. Takimiya, K., Osaka, I., Mori, T. & Nakano, M. Organic semiconductors based on [1]benzothieno[3,2- B][1]benzothiophene substructure. *Acc. Chem. Res.* **47**, 1493–1502 (2014).
72. Lee, S. M., Cho, Y., Kim, D. Y., Chae, J. S. & Choi, K. C. Enhanced Light Extraction from Mechanically Flexible, Nanostructured Organic Light-Emitting Diodes with Plasmonic Nanomesh Electrodes. *Adv. Opt. Mater.* **3**, 1240–1247 (2015).
73. Leo, K. Organic light-emitting diodes: Efficient and flexible solution. *Nat. Photonics* **5**, 716–718 (2011).
74. Thejo Kalyani, N. & Dhoble, S. J. Organic light emitting diodes: Energy saving lighting technology - A review. *Renew. Sustain. Energy Rev.* **16**, 2696–2723 (2012).
75. Thejokalyani, N. & Dhoble, S. J. Novel approaches for energy efficient solid state lighting by RGB organic light emitting diodes - A review. *Renew. Sustain. Energy Rev.* **32**, 448–467 (2014).
76. Kamtekar, K. T., Monkman, A. P. & Bryce, M. R. Recent advances in white organic light-emitting materials and devices (WOLEDS). *Adv. Mater.* **22**, 572–582 (2010).
77. Chen, X. K., Kim, D. & Brédas, J. L. Thermally Activated Delayed Fluorescence (TADF) Path toward Efficient Electroluminescence in Purely Organic Materials: Molecular Level Insight. *Acc. Chem. Res.* **51**, 2215–2224 (2018).
78. Jhulki, S. & Moorthy, J. N. Small molecular hole-transporting materials (HTMs) in organic light-emitting diodes (OLEDs): structural diversity and classification. *J. Mater. Chem. C* **6**, 8280–8325 (2018).
79. Lipomi, D. J., Tee, B. C. K., Vosgueritchian, M. & Bao, Z. Stretchable organic solar cells. *Adv. Mater.* **23**, 1771–1775 (2011).
80. Yan, F., Noble, J., Peltola, J., Wicks, S. & Balasubramanian, S. Semitransparent OPV Modules Pass Environmental Chamber Test Requirements. *Sol. Energy Mater. Sol. Cells* **114**, 214–218 (2013).
81. Yang, X. & Loos, J. Toward high-performance polymer solar cells: The importance of morphology control. *Macromolecules* **40**, 1353–1362 (2007).
82. You, A., Be, M. A. Y. & In, I. Modeling photocurrent action spectra of photovoltaic devices based on organic thin films. **487**, (2005).
83. Brabec, C. J. *et al.* Tracing photoinduced electron transfer process in conjugated polymer / fullerene bulk heterojunctions in real time. **340**, 232–236 (2001).
84. Brabec, B. C. J. *et al.* Origin of the Open Circuit Voltage of Plastic Solar Cells.
85. Li, G., Chang, W. & Yang, Y. Low-bandgap conjugated polymers enabling solution-processable tandem solar cells. *Nat. Publ. Gr.* **2**, 1–13 (2017).

Chapter 2

Modern Sustainable Synthetic Strategies to the Green Access of Semiconducting π-Conjugated Molecular Structures

The worldwide demand for energy-efficient and high-performing (opto)electronics, along with the increasing need for economically feasible and environmentally friendly chemistry, both require semiconducting materials that are both scalable and sustainable. The concern with waste generation and toxic/hazardous chemicals usage has already moulded many operations in chemical and manufacturing industries. To date, common syntheses to access organic semiconductors require the use of large quantities of toxic and/or flammable organic solvents, often involving reagents and by-products that are harmful to health and environment. Research in the field of organic electronics is now increasingly focusing on the development of new sustainable methodologies that allow to prepare active materials in a more efficiently way, caring further on safety and sustainability associated with production processes.[1,2] The immediate approach applicable consist on the removal, or at least on the minimization, of harmful and toxic substances commonly employed within standard processes. The big elephant in the room in the synthesis of active materials is the amount of organic solvent employed, which could ideally be reduced by using aqueous solution of surfactants: in these nano/micro heterogeneous environments organic transformations can happen and often with unprecedent efficiency. Clearly, the process occur not through the dissolution of the reagents (starting materials and catalyst) but from their dispersion in water. Kwon as "micellar catalysis", this strategy has proven to be highly effective on improving sustainability becoming a prominent topic in modern organic synthesis.[3] In particular, the micellar catalysis strategy is compatible with the most common modern strategies employed for C-C and C-heteroatom bonds forming reactions and allow to perform reactions with high yields, in water and under very mild conditions.[4] Nonetheless, the use of such method in the field of organic semiconductors is still limited, with only few relevant examples reported in literature concerning the preparation of π-conjugated molecular and polymeric materials.

This chapter will first give readers an overview of the importance of introducing sustainability in the synthesis of organic semiconductors, satisfying several principles of the green chemistry guidance. Our research purpose is not to provide an exhaustive list of examples of such chemistry, but rather to identify a few key developments in the field that seem especially suited to large-scale synthesis. Then, the discussion will consider the synthetic approaches typically employed to access semiconducting materials with extended π-conjugated structures. In particular, the discussion will involve the well-known Pd-catalysed cross-coupling techniques. Finally, the topic of the work will focus on micro-heterogeneous environments as a new tool for introducing sustainability in the preparation of active materials in water, satisfying several criteria relevant to green chemistry. On my opinion, the micellar catalysis approach constitute today the more promising method to lower the overall cost and environmental impact in the production of organic semiconductors without affecting yields, purity, and device performance.

2.1. Organic Materials: The Lab to Fab Transition

Improvements in organic optoelectronic devices performances and stabilities over the past few years have demonstrated that such technologies are getting closer to a large-scale market production reality. OLEDs have already reached this goal while OFETs and OPVs are expected to reach commercial applications in the near future.[5] However, in the pursuit of high-performance devices, the concept of sustainable optoelectronics has often been neglected. It is essential that continual improvements in device performance and stability are complemented by sustainable and cost-effective processes to ensure a successful and full-potential industrial future.[6] To date, most of the research efforts in the field have been focused at maximizing the field-effect mobility for TFTs, the light emission/vertical conductivity in OLED/diodes, and the light absorption/transport of charge in OPVs, with limited care on the environmental impact and costs associated with the synthetic methodology employed for preparing active materials. Beyond performances, most of the synthetic methodologies currently used to access functional π-conjugated structures are demanding from raw materials/chemical costs, synthetic complexity (number of synthetic steps and purification required), environmental impact, and their large-scale production may present serious limitations.[7] One of the main concerns when moving from the Lab to the Fab environment regards the overall sustainability and environmental impact of the synthetic methodologies employed to access functional materials. Another main subject for Fab developments involves the cost per gram of the active material, which increases linearly with the number of synthetic steps and the purification required for the preparation.[8] The materials, energy, and time put into workup and purification for any multistep chemical synthesis are considerable. Workup and purification includes quenching (i.e., neutralization of reactive species), extraction, chromatography, recrystallization, and distillation or sublimation. To produce active materials efficiently the minimization of workup procedures in the scaled production, as well as solvent and reagent consumption, is essential, ruling out the recourse to column chromatographic purifications. The high purity of active materials is still a characteristic that must be guaranteed. It is possible that a reaction that is in many ways "green" may lead to a product which cannot be isolated in a sequence that is environmentally benign. For instance, besides column chromatography requires the use of high quantities of organic solvent, which is expensive, not safe, and impossible at the industrial scale. The same troubles are found with halogenated solvents which do not respect the environmentally and safety requirements for large scale applications.[9] However, failure in purifying completely active materials can have deleterious effects on the electronic properties. In particular, particles from residual palladium catalysts have negative effects on electrical performance.[10] The analysis by Osedach et al.[11] suggests that workup and purification contributes ~50% of the cost for the laboratory-scale synthesis of P3HT and a considerably greater fraction of the cost (≤90%) for conjugated polymers with greater structural complexity. An acceptable cost, which leads to commercially viable modules, is around 10 €/g.[12] Thus, challenges in this matter mostly consider the elimination (or at least the remarkable reduction) of the use of toxic reagents and solvents, the limitation of undesired side reactions that may include the formation of potentially toxic by-products, the reduction of waste and costs by reducing the number of synthetic steps, the use of abundant or renewable resources and energies, recycling. Research working in the field of organic and printed optoelectronics is now becoming increasingly aware of the need for materials combining reasonable performances with low synthetic complexity and sustainable synthetic approaches.[1,2,13]

In the interest of a robust organic electronic industry, the development of environmentally and economically benign approaches to prepare active semiconducting materials including the principles of green chemistry is essential. The term green chemistry was coined by Paul Anastas[14] of the Environmental Protection Agency (EPA) as "innovative chemical technologies that reduce or eliminate the use or generation of hazardous substances in the design, manufacture and use of chemical products". Using the so-called 12 principles of green chemistry as guidelines, chemists can evaluate and improve current procedures and develop new ones that will have a limited impact on the environment and therefore be more sustainable and economical in the long run.

The 12 principles can be summarized as follows:[14]

1. Prevent waste.
2. Design synthetic methods to maximize the incorporation of all materials used in the process into the final product (i.e., atom economy).
3. Design less hazardous chemical synthesis.
4. Design safer chemicals and other products.
5. Use safer solvents/auxiliaries.
6. Increase energy efficiency.
7. Use renewable raw materials/feedstock.
8. Avoid derivatization (e.g., protecting groups, temporary modification of physical/chemical processes) because it requires additional reagents and can generate waste.
9. Use selective catalysts, not stoichiometric reagents.
10. Design chemical products considering their degradation after use.
11. Analyse in real time to prevent pollution.
12. Minimize the potential for accidents, including releases, explosions, and fires

A green process is tantamount to an efficient one. Green chemistry is a strategy that cut off hazards to prevent waste with a shift in risk management from limiting exposure to toxic substances eliminating them to the extent possible. There are several approaches to evaluating the greenness of a synthetic process. To cite some, first the atom economy (introduced by Trost in 1991)[15] which is the ratio of the molecular weight of the isolated product over the total reactant molecular weight. The higher the atom economy, the greener the reaction is considered. Though, this approach is theoretical in that it assumes exactly stoichiometric quantities of all materials and 100% yield. Another important metric, which considers the actual yield, solvents, and catalysts is the environmental factor (E-factor). This concept was developed by Sheldon[16] after noting that the cost of disposing of waste in the fine chemical industry was comprising an increasing fraction of the revenue generated by the product. The E-factor is defined as the ratio of the mass of waste over the mass of the desired product. Thus, the lower the E Factor, the more environmentally acceptable the process. However, some wastes are more harmful to the environment than others, but currently there are few assessments of the level of greenness of different wastes. In the drug industry, where commercial products often require a number of synthetic steps comparable with those of printable semiconductors, acceptable processes feature E-factors in the 10^2-10^3 range.[17] The corresponding value for organic semiconductors (without even considering processing) is in the excess of 10^4. A dumping of at least one order of magnitude is crucial for successful industrialization of the technology. Given that in our opinion the E-factor represents a good estimate of the synthetic efficiency in terms of sustainability it will always be evaluated within this thesis work.

Industry sector	Annual production (t)	E-factor	Waste produced (t)
Oil refining	10^6-10^8	<0.1	10^5-10^7
Bulk chemicals	10^4-10^6	<1–5	10^4 - 5×10^6
Fine chemicals	10^2–10^4	5–50	5×10^2 – 5×10^5
Pharmaceuticals	10–10^3	25–100	2.5×10^2–10^5

Figure 41. *E-factor values across the chemical industries.*

Unfortunately, at the moment the most successful synthetic methodologies generally used for preparing functional organic semiconductors are affected by cost, safety, and environmental issues which may seriously prevent the large-scale development. In this regard, the application of principles of green chemistry is essential for boost the field of organic optoelectronics. Particular attention should be directed toward organic solvents, which are commonly the major input in industrial and lab-based procedures as reaction medium, in addition to their use for purification. In this context, waste production should be reduced using minimal amounts of toxic solvents which represent the so-called "big elephant in the room". Moreover, traditional solvents commonly used in the production of organic semiconductors (such as 1-methylpyrrolidone (NMP), dimethylformamide (DMF), dimethylacetamide (DMA), pyridine, chlorinated solvents such as dichloromethane (CH_2Cl_2) or chlorobenzene) increase air pollution; most of them are toxic, flammable, or both. Indeed, these solvents are not compliant with relevant legislation, ranking high on the list of harmful chemicals.[18]Therefore their substitution with more environmentally friendly ones can directly have a positive effect on both emissions and safety issues. Synthetic processes should include the use of sustainable mediums which can be easily recovered/reused by exploitation of heterogeneous catalytic systems to simplify workup procedures and reduce energy, waste, and production time.

2.2. Palladium-Catalysed Cross-Coupling Reactions

Transition-metal-catalysed cross-coupling reactions, mainly concerning palladium catalyst, are the cornerstone of the $C(sp^2)$-$C(sp^2)$ and $C(sp^2)$-heteroatom(sp^2) bond forming reactions for the construction of relevant π-conjugated structures with applications in pharmaceuticals, agrochemicals and materials sciences.[19–21] The impact of this powerful technology on organic synthesis and its significant growth over the past two decades was recognized in 2010 with the awarding of the Nobel Prize in Chemistry to Professors Heck, Negishi, and Suzuki.[21] Amongst them, the Migita-Kosugi-Stille and Suzuki-Miyaura cross-couplings, together with the Buchwald-Hartwig amination and direct arylation via C-H bond activation, have achieved great success and popularity in recent literature for the preparation of functional small-molecular and polymeric semiconductors with extended π-conjugated backbones.[1,22] This class of reactions have the merits of producing C–C bonds in high yields under relative mild conditions, good reproducibility and reliability, and high stereo- and regioselectivity, as well as using readily available starting materials. Cross-coupling reactions generally involve the Pd-catalysed cross-coupling of aryl halides (Ar-X) with stoichiometric amounts of aromatic organometallic derivatives (Ar'-M) for the formation of new C-C bonds. The generally accepted mechanism of the reaction with its catalytic cycle is reported in **Figure 42**.

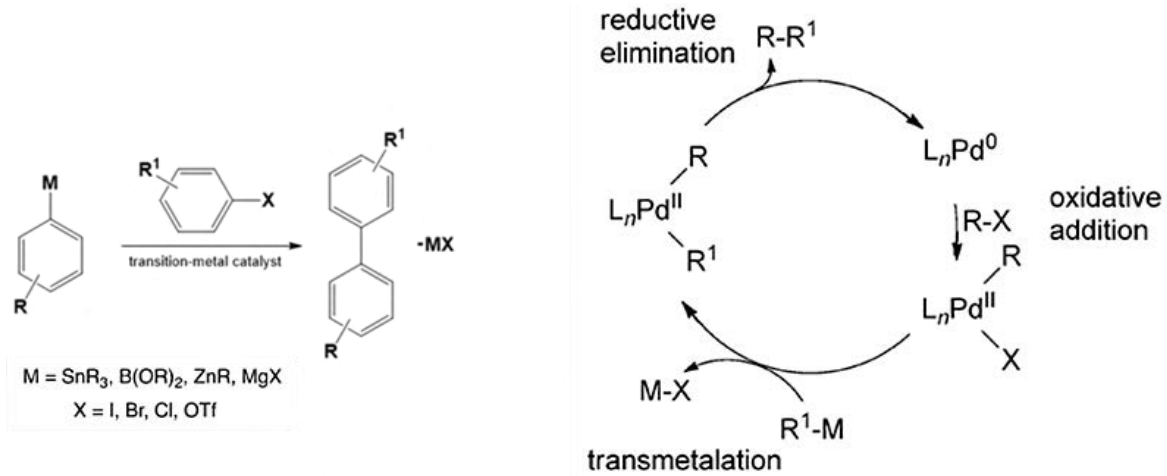

Figure 42. *Pd-catalyzed cross-coupling process (left) and its simplified catalytic cycle (right).*

The catalytic cycle can be described for all the processes by three key steps:[20] the organic halide reacts with the palladium(0) centre through an (i) oxidative addition, giving a palladium(II) complex; subsequently, the (ii) transmetallation takes place, yielding a different Pd(II) complex that contains the two moieties to be coupled; finally, a (iii) reductive elimination occurs, leading to the coupling product with the associated regeneration of the active Pd(0) catalyst. In this mechanistic approach the transmetallation represents the rate determining step, which is strongly affected by the nature of the organometallic partner, making a generalization for the whole process almost impossible.[20] The palladium catalysts that carry out these transformations are typically stabilized by phosphine ligands; however, they are often sensitive to oxygen, moisture, and elevated temperatures. The instability of such catalysts when dissolved restricts their utility to inert atmosphere conditions with rigorously deoxygenated solvents, and renders them to single use. In addition, separation of these homogeneous metal catalysts from the organic product is often challenging but is of utmost importance to prevent trace metal contamination in organic materials that are utilized in electronic devices.

The various type of possible cross-couplings (Suzuki-Miyaura, Stille, Negishi, Kumada-Tamao-Corriu) differ from each other from the organometallic specie involved and so the transmetallation step. Among the cross-coupling reactions there are also the Buchwald-Hartwig reactions (for the formation of C-N bonds), Heck (for double bonds couplings) and Sonogashira (for triple bonds couplings) but unlike the previous ones, one of the two coupling partners is not an organometallic derivative. Considering the formation C-C bond between aromatics, for instance, the Suzuki-Miyaura coupling requires the use of Csp^2-substituted organoborane derivatives (-BOR_2), while the Stille coupling involves Csp^2-substituted organostannyl derivatives (-SnR_3). From the standpoint of environmental concerns, the Stille coupling is particularly problematic due to the use and formation of stoichiometric amounts of highly toxic tin compounds. The Suzuki coupling poses no intrinsic toxicity concern with the boron compounds, which anyway offers high tolerance to functional groups, are relatively inert toward moisture and oxygen, besides they can generally be prepared efficiently from readily available halide precursors under mild Miyaura conditions avoiding lithiation.[23] These features combined with high efficiency of Suzuki cross-coupling reaction in terms of C–C bond formation between aryl moieties has turned Suzuki coupling into one of the most powerful tools for conjugated materials synthesis. However, the Suzuki coupling shares with the Stille coupling the need for the activation of one of the two counterparts by the introduction of an organometallic functionality. The organometallic functionalization requires extra synthetic steps which are time-consuming, cost-ineffective, environmentally harmful, and may be challenging depending on the substrate. Moreover, for the Stille coupling, the compounds involved have safety issues related to (i) lithiation reaction needed to introduce the functionality and (ii) the intrinsic toxicity of the tin compounds involved (think about the contamination of industrial metal reactor walls by tin). This safety, environmentally and economic drawbacks represent an obstacle that may prevent its industrial application.[24]

More recently, palladium-catalysed direct (hetero)arylation (DHA) reactions through C-H bond activation have been extensively explored as a valuable, economical, and environmentally friendly alternative to conventional cross-coupling methods for the atom-economical construction of new C-C bonds.[25] Indeed, the DHA protocol enables the direct coupling between C-H activated (hetero)aryls and (hetero)aryl-halides (commonly -I and -Br) without the need of further functionalization. The advantage in terms of atom economy, number of synthetic steps required, and amount of toxic waste is obvious (**Figure 43)**. These advantges call comparison to the typical Stille coupling, which typically requires bromination, followed by lithiation and then stannylation. At minimum, assuming 100 percent yield at each step, DHAP saves two steps, equivalents of trimethyltinchloride, and either equivalents of n-BuLi or t-BuLi.[26] The determination of the mechanisms involved in DHA reactions is still a subject of investigation, however it is believed to follow a base-assisted, concerted metalation-deprotonation (CMD) pathway.[25,27–30] During this process, carboxylate or carbonate anions coordinate to the metal centre in situ and assist in the C-H bond cleavage which is the rate determining step of the process (transition states 2-TS and 4 in **Figure 44**). Research has proven the

C–H bond activation to be extremely versatile for numerous arenes and heteroarenes, including substituted benzenes, perfluorinated benzenes, and thiophenes.[25]

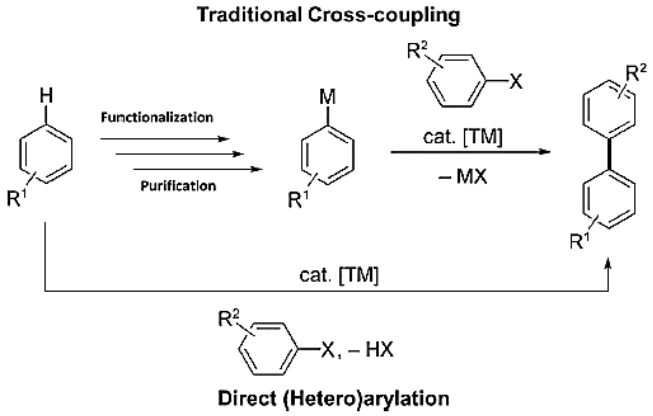

Figure 43. *Comparison between classical cross-coupling and direct arylation. With permission of ref* [25].

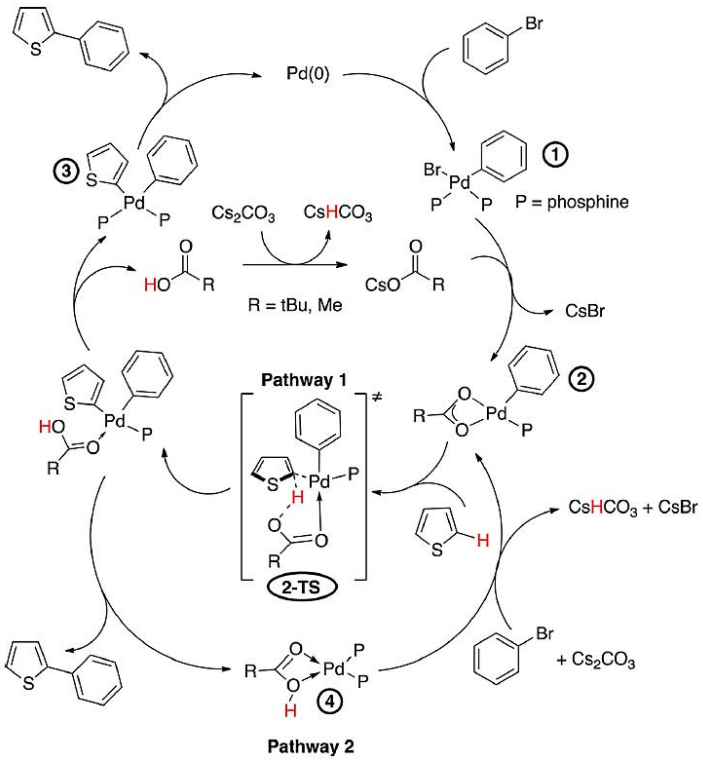

Figure 44. *Catalytic cycles for direct (hetero)arylation concerning the CMD pathway assisted by sterically hindered carboxylic acids as proton shuttles. Reprinted with permission of ref* [30].

On the other hand, the major issues related to the direct arylation protocol is the lack of high C–H bond selectivity and generality. Selectivity is of crucial importance feature, especially in the case of popular conjugated copolymers synthesis (direct (hetero)arylation polymerization, DHAP) since structural defects, branching and/or homocouplings (**Figure 45**), cannot be removed by further purification processes; they are chemically fixed within the polymer chains. It is worth noting that among the many factors that affect the overall performance of a polymer, the structural regularity and the molecular weight are most decisive. This is particularly true for heterocycles such as thiophene derivatives where the aromatic C–H bonds are more reactive than those present in aryl (benzenes, fluorenes, carbazoles, etc.) groups.[31] Additionally, each monomers couple requires reaction-condition optimization (e.g., additives, ligands, catalysts, reaction time and temperature). To date, there is no general DHAP condition that is applicable to all monomer types; the quest to find robust DHAP conditions is of the utmost interest to many research groups.

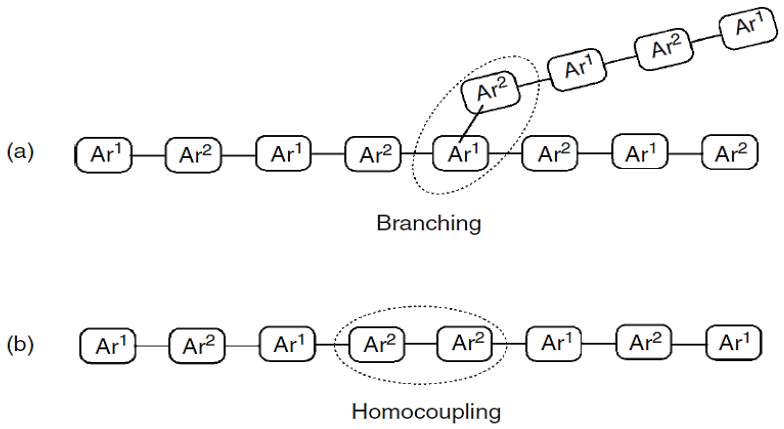

Figure 45. *Structural defects in conjugated alternating copolymers: (a) branching and (b) homocoupling.*

However, continuous improvements in the field have driven the finetuned method to seriously compete with the Stille and Suzuki couplings, in particular for the manufacturing of thiophene containing molecules and polymers.[28,32–36] Careful tuning of reaction conditions enables selective arylation at the α-positions of the thiophene ring with good tolerance over a wide range of electronic structures and electron-donating and electron-withdrawing groups.[37] Because of the pervasive use of thiophene derivatives in materials for organic optoelectronics, DHA is becoming a prominent tool in the field.[26,32,38,39] As a matter of fact, providing that the reaction conditions can be optimized and with general efficiency for a large variety of materials, direct arylation promises to become a powerful methodology for the preparation of conjugated polymers with different electronic structures having high molecular weights, low defects concentration and good regioregularity on the industrial plant scale.[40–42]

2.3. Introducing Sustainability with Aqueous Solutions of Surfactants

Achieving a greener chemical synthesis using less hazardous solvents is imperative. Cross-coupling reactions are often conducted in aprotic solvents (e.g., DMF, DMA, THF, toluene, including halogenated solvents such as chloroform, chlorobenzene and o-dichlorobenzene) because they readily solubilize many reagents involved, facilitating a wide range of reactions.[43] These solvents pose the greatest risk towards human health and environmental sustainability because of their volatility and high-toxicity. Chemical purification is usually the major source of solvent waste and column chromatography is often unavoidable in organic synthesis. Many efforts are required to bypass excess of waste by requiring minimal purification steps; the need of alternative strategies for a robust industrial future is of crucial importance. In recent years, the use of alternative, greener solvents has been applied.[2,44] However, a major challenge in solvent selection lies precisely with solubility. The current strategy to enhance solubility in a given solvent is to attach side chains or other solubilizing groups suitable with the polarity of the solvent employed. Although there has been progress in using greener solvents for processing organic electronics (e.g., organic photovoltaics),[45,46] there are fewer studies exploring semiconductors synthesis in greener-solvent reaction mediums. This is due to the low solubility of extended π-conjugated structures, or degradation of active species and catalysts in alternative solvents.

Replacement of the use of organic solvents in the synthesis of organic semiconductors with water would provide more economically and environmentally sustainable process.[47] The emerging field of micellar catalysis and surfactant enhanced chemistry is playing noticeably in improving the sustainability of organic synthesis.[48] The possibility of use water as reaction medium would have undoubted crucial advantages; water is cheap, widely available, inert, clean, non-flammable, non-toxic, non-polluting, of safe-handling and can be stored indefinitely without any hazard occurring. The use of water as reaction medium opens the way to biphasic extraction of products and recycle of the catalysts, which may remain confined in the micellar aggregates during product removal: the product is insoluble and can be filtered off from the reaction mixture or extracted with the aid of a very little amount of organic water immiscible solvent. Although the hydrophobicity of the organic compounds is not consistent with the polarity of water (particularly for polyconjugated derivatives whose solubility in water is extremely poor), the cornerstones of formulation chemistry allow to adapt organic species in water avoiding segregation through micro/nano lipophilic compartments. The job can be done by peculiar molecules known as surfactants. Surfactants (surface active agents) are amphiphilic molecules generally composed by a polar head and an apolar tail covalently bonded. When dissolved in water, above a certain concentration threshold (called critical micellar concentration CMC), surfactants spontaneously self-assemble in supramolecular aggregates, among which the most popular micelles. The established micelles are core-shells systems with dimensions in the range of nano/micro in which the apolar tails aggregate and interact through non-covalent interactions, while the polar heads form a "protective layer" which preserves the tails from seeing water (**Figure 46**). Surfactants and micelles are in thermodynamic equilibrium and they exchange from each other with lifetimes in the order of 10^{-3}-10^{-2} s.[48]

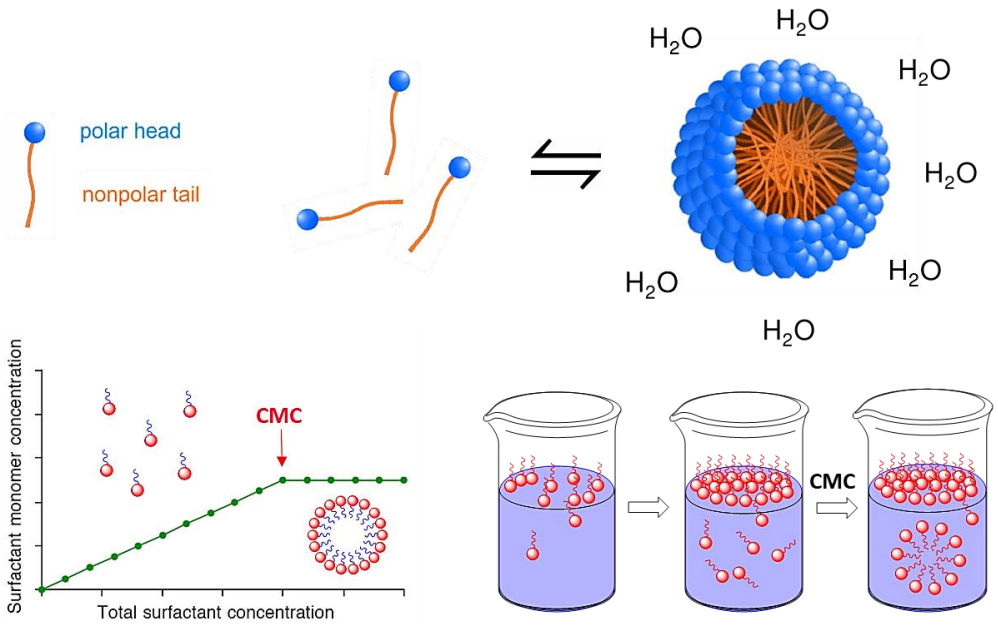

Figure 46. *Representative scheme of the surfactants assembling into micelles in aqueous environment.*

Organic species added to a micellar aqueous solution are distributed between bulk water and micelles depending on their polarity, charge, and dimensions. Lipophilic substrates are almost exclusively hosted within micelles with a local concentration in the supramolecular aggregates that correspond to some orders of magnitudes higher with respect to that considering the entire volume of the solution. Similar to enzymes micelles are characterized by a hydrophobic core, shielded from the contact with water, and a hydrophilic surface where the hydrophilic groups remain exposed to water ensuring organics solubility and/or dispersion within the pockets. Surfactants play the role in reducing the interfacial tension between the two phases stabilizing the micro/nano heterogeneous "oil-in-water" environment. Still, in oil-in-water environments the available space of the lipophilic cores is generally

limited with respect to the amount of the organic phase; thus, the water phase acts as a real reservoir of substrates which continuously get in/get out of the micellar core because of the equilibrium of interconversion between single amphiphiles and aggregates.

Currently, the use of surfactants under micellar conditions represents one of the simplest methods to achieve water compatibility since surfactants are in most cases very economical and safe thanks to their extensive everyday use in detergency. Most of the commercially available surfactants are derived from petroleum feedstock. They can be ionic (cationic, anionic, zwitterionic) or non-ionic structures; the difference lies in the polar head which may or may not have a localized charge. Following **Figure 47** shows the chemical structures of a selection of popular industrial surfactants generally employed to create such micro/nano heterogeneous environments.

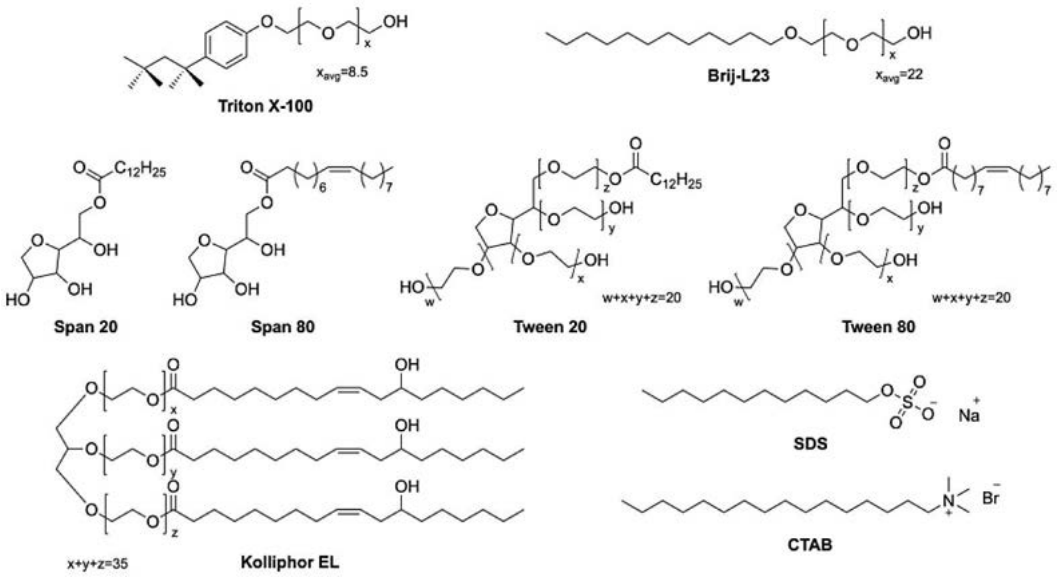

Figure 47. *Chemical structures of popular commercially available surfactants.*

At increased surfactant concentrations much above the CMC other possible types of aggregates are formed, including spherical or ellipsoidal micelles, rods, microemulsions, lamellar or hexagonal liquid crystal phases, vesicles and tubules, and eventually, reverse phases "water in oil" are possible. The kind of aggregate formed is related to several variables: the nature of the amphiphile including the ration between the hydrophilic/hydrophobic portions, the nature of the substrate (liquid or solid), the geometry of the molecule, and the experimental conditions such as temperature, pH and ionic strength.[49] However, literature generally reports the term micellar catalysis not caring which kind of specific aggregation state the surfactant is assuming. The common characteristic of all such associated stable colloids is the formation of lipophilic pockets within the water's polar environment where lipophilic organic species can be accommodated.

2.3.1. Organic Transformations in Water Through the Micellar Catalysis Approach

The dispersion/emulsification of organic molecules in water with surfactants doing the job, does not imply an obstacle on their reactivity. On the contrary, it is possible to exploit the lipophilic cores of micelles as real nano/micro reactors, where chemical transformations can happen regardless the hydrophobicity of the organic species involved, setting aside the use of organic solvents.[47] Micellar reactions are well-known methods of increasing popularity, and to date, the number of reactions reported in literature compatible with these conditions is quite impressive.[50] Representative examples include oxidations, reductions, dehydratations, condensations.[3] In particular, micellar aqueous

solutions have proved to be efficient also in promoting transition-metal-catalysed cross-coupling reactions in water, including Suzuki-Miyaura, Stille, Buchwald-Hartwig, Heck, and Sonogashira couplings, and moreover, often with unprecedent efficiency.[4,51,52] Micellar Stille couplings are as well documented, yet there is little room in the context of green chemistry for a reaction involving highly toxic organo-tin compounds. The enhanced reactivity often observed in micellar catalysis can be explained by the hydrophobic effect generated by the accumulation/segregation of the reagents within the limited volume of the lipophilic micellar cores. Since slight solubilization of substrates occurs predominantly within the apolar core of micelles and not in the entire volume of the liquid phase, the local concentration is higher even if the overall concentration of substrates in the micellar solution is smaller than general concentrations in traditional organic solvents which usually concern in the range of 10^{-1}-10^{-3} M.[48] Specifically, association colloids can be described as a simplified analogous of enzymes: reagents can be hosted and selectively localized in an environment with specific polarity, where the details of the chemical nature of both the hydrophilic and hydrophobic domains of a surfactant can lead to precise noncovalent interactions. Recent literature in the field is increasing becoming aware that water molecules surround the polar external surface of the aggregate have behaviours and properties rather different from water molecules in the bulk. Their peculiar assistance through specific interactions may play a major role.[53]

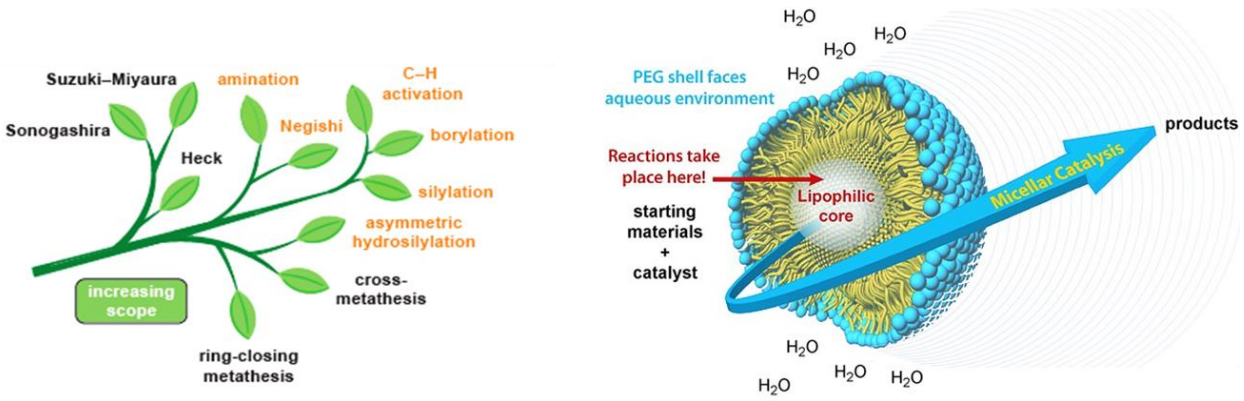

Figure 48. *Left: increasing field of research of micellar catalysis in transition-metal-catalysed reactions; right: schematic representation of a micellar nano/micro reactor.*

All early work in the field of micellar catalysis mostly employed existing industrial surfactants as they are readily available, cheap, and efficient in providing stable formulations. One of the challenges of using commercial surfactants is the need for guidelines to select the most appropriate depending on purpose. Commercial surfactants are complex molecules with a wide structural variety concerning functional groups of different polarities. In order to qualitatively describe the affinity of a given surfactant with respect to the phase to be dispersed/emulsified, some formulation chemistry principles have to be taken into a count. In particular, the Hydrophilic Lipophilic Balance (HLB), which is a completely empirical number not necessarily linearly correlated with the dielectric constant of the medium, gives a qualitative idea of the affinity of a surfactant for water (HLB > 10) or for oil (HLB < 10). Indeed, the HLB is defined as the ratio between the hydrophilic portion and the lipophilic portion of the surfactant structure, determined by calculating values for the different regions of the molecule. For example, the HLB of Triton-X-100 is 13.4, which classifies it as water soluble specie and suitable for the preparation of oil-in-water environments. In contrast, the HLB of Span 80 is 4.3, which identifies it as water insoluble specie and appropriate for the preparation of water-in-oil environments. According to the affinity principle, a correct surfactant should have an HLB similar to that of substrates rather than products to promote complete conversion of chemical transformations.[54]

Later, Prof. Lipshutz and co-workers started to investigate in depth the effective impact of the surfactant's structure and nature on promoting organic reactions, in particular cross-couplings. They demonstrated that careful control on the surfactant's structure, specifically designed and synthetized to have specific non-covalent interactions with the substrates, can play a major role in enhance the reaction course (**Figure 49**).[55] Prof. Lipshutz's work proved that surfactants should be exclusively

selected and designed in order to boost micellar reactions, and not used only as simply hosts like in standard formulation chemistry.

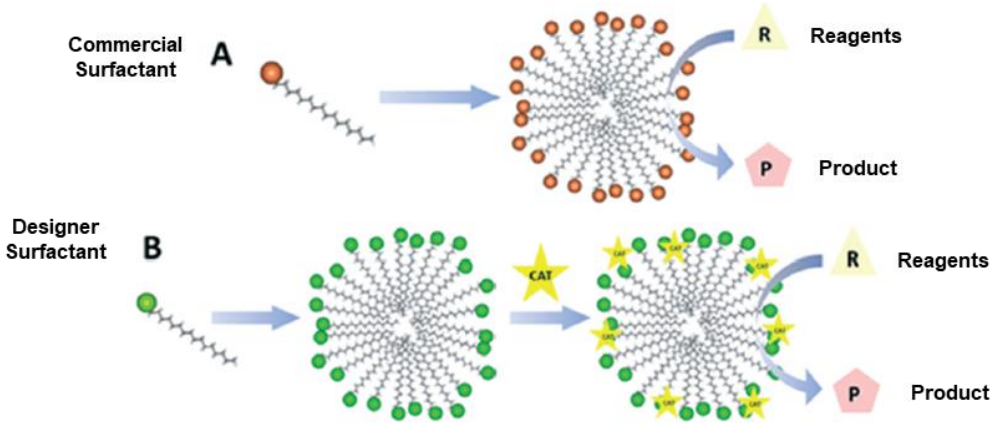

Figure 49. *Different examples of catalysis by micelles of designer surfactants: A) the micellar aggregate directly promotes a chemical transformation; B) the micellar aggregate hosts the real catalysts and imparts specific properties and selectivities. Reported with permission of ref* [55].

The first so called "designer" surfactant reported was DL-α-tocopherol alkoxy-polyethylene glycol sebacate (PTS), obtained through a slightly straightforward synthesis from mostly renewable resources like racemic vitamin E, sebacic acid and a polyethylene glycol derivative with a terminal hydroxyl unit as a hydrophilic moiety. PTS dissolved in water forms both spherical aggregates of 8–10 nm and larger worm- or rod-like aggregates with an overall average size of 25 nm by the DLS analisys.[56] This surfactant supported exceptional catalytic performances in reactions like metathesis, Sonogashira, Suzuki–Miyaura, Heck, amination, silylation reactions and many other Pd-catalyzed transformations at room temperature. Further developments in this context were based on the employment of a shorter linker between the hydrophobic and hydrophilic portions, leading to the introduction of DL-α-tocopherol methoxypolyethylene glycol succinate (TPGS-750-M) as a second generation amphiphile. This surfactant is characterized by the presence of succinic acid as a shorter spacer between the hydrophobic and the hydrophilic portions, and with the PEG unit capped as a methyl ether terminal group. TPGS-750-M dissolved in water provides very sharp spherical aggregates of 12–13 nm by DLS analisys.[57] The success of the latter designer surfactant led its application to a wide range of chemical transformations, in particular for organo metallic catalysis in water at room temperature, with metal nanoparticles, or with ppm amounts of metal catalysts, and also in combination with bio-catalysis.[55] Recently, again the group of Lipshutz developed a much more economical alternative designer surfactant, replacing the hydrophobic unit with the cheap β-sitosterol. The third generation designer surfactant β-sitosterol methoxypolyethylene glycol succinate (SPGS-550-M, also called Nok) enabled comparable catalytic properties to TPGS-750-M for several Ru and Pd catalyzed reactions at room temperature, thus representing a more economically viable alternative.[55] Nok dissolved in water provides very sharp spherical aggregates of 45 nm by DLS analisys.[58] Summarizing, Prof. Lipshutz and co-workers with their designer surfactants observed enhanced reactivity in Pd-catalysed cross-couplings in terms of higher reaction conversion/yield, less catalyst loading need, room temperature working and few hours required compared with several commercially available surfactants or parallel reactions carried out in organic solvent, demonstrating the importance of substrate-surfactant interactions.[55] Such impressive work inspired the community of the field to develop additional designer surfactants for other specific purposes.[55,59,60]

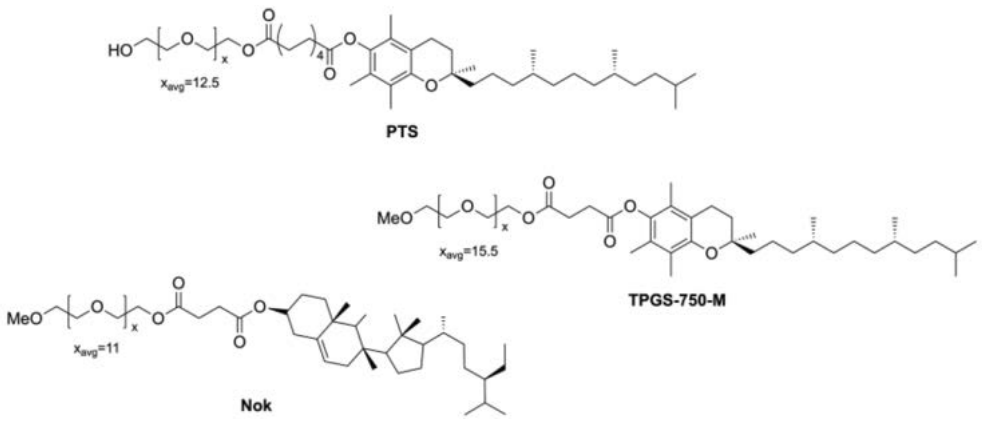

Figure 50. *Chemical structures of Lipshutz's designer surfactants for enhanced reactivity in water.*

2.3.2. Micellar Enhanced Suzuki-Miyaura Couplings

Literature reporting the use of micellar cross-couplings as sustainable alternative solution for the construction of new C-C bonds mostly concerns with the Suzuki-Miyaura (S-M) protocol. Among the many, the S-M reaction remains the favourite for its economic and sustainable advantages in both the pharmaceuticals, agrochemicals, and electronics. The first examples of S-M reaction carried out in micellar environment were reported by Prof. Oehme[61] and co-worker, who employed commercially available ionic surfactants CTAB (hexadecyltrimethylammonium bromide) and SDS (sodium lauryl sulfate) with specifically synthetized water-soluble Pd–phosphine complexes. Later, Arcadi and Cerichelli[62] improved the method employing common palladium sources such as Pd-Tetrakis [$Pd(PPh_3)_4$]and Pd/C (palladium supported on carbon) with several readly available commercial surfactants. The micellar S-M coupling was also one of the first reactions studied by Prof. Lipshutz, and on which he tested the efficacy of designers. He demonstrated that micellar S-M coupling carried out in 1–2wt% PTS water solutions with bis(di-tertbutylphosphino)ferrocene]dichloro palladium (II) [$Pd(dtbpf)Cl_2$] as the catalyst can be efficiently carried out also on thiophene derivatives, well-known systems to be very tedious in this kind of reactions.[63] Prof. Lipshutz research group further improved efficiency of micellar S-M reactions with second (TPGS-750-M) and third (Nok) generations of designer surfactants, proving high reactions efficiency at room temperature and with low catalyst loading.[57,58]

On this point, considering traditional S-M reactions, as well the other kind of couplings, when carried out in solution using organic solvents, they usually require high temperatures, which are often the source of by-products formation and raise the overall cost of the synthesis. Scalability is a major issue when reactions require massive energy inputs for synthesis and fabrication. Although more difficult to achieve, mild synthesis at room temperature is ideal to preserve energy efficiency. Additionally, anaerobic conditions are mandatory and of crucial importance to avoid catalysts poisoning (Pd^0 can be oxidized by the oxygen present in air), so that long degas/purges of inert gases to achieve air-free environments are always required. Running reactions under nitrogen or argon atmosphere is very usual in fine chemical laboratories, however removal of oxygen from water remains a particularly tedious operation everyone would be glad to avoid, particularly when scaling up. In the past few years, my research group reported the use of a commercially available, FDA approved Kolliphor EL (K-EL) to provide a nano heterogeneous environment with oxygen-free micellar cores.[64] In particular, the 2%wt K-EL solution has proven to be an excellent medium to provide efficient S-M couplings in water, at room temperature and under air, so in an oxygenated environment.[64] K-EL is a non-ionic surfactant derived from castor-oil with a main structure of the mixture sold composed of glycerol polyethylene glycol ricinoleate with fatty acid esters (structure reported in **Figure 51**) . It is very popular in medicinal chemistry as excellent emulsifier for poorly soluble drugs, most notably Taxol. The peculiar property of K-EL micelles in keeping out the oxygen from the core, was confirmed by the platinum porphyrin luminescence method;[65] also the fact that the commercially-available K-EL

contains fair quantities of free PEG (polyetheleneglicol), which can act as oxygen-barrier at the two phases interface, should be considered. In details, the work reported the comparison of the micellar S-M coupling on a model reaction (**Figure 51**) between the commercials K-EL and Triton X-100 with Lipshutz's designer surfactants TPGS-750-M. The reactions were performed under identical experimental conditions, apart from the reaction atmosphere. Reactions carried out in K-EL solutions were performed under standard laboratory environment under air, while the reactions in Triton X-100 and TPGS-750-M were performed under a nitrogen saturated environment. The results displayed similar reaction yields, however the reaction carried out using K-EL allows to obtain excellent yields without requiring a deoxygenated environment unlike the other two. Entry 2 in **Figure 51** represents the successful result for the reaction carried out with K-EL in a second consecutive test with the recycled aqueous phase recovered by filtration without adding further fresh catalyst. This actually represents another relevant advantage of the method.[64] Moreover, the convenience of using a commercial surfactant compared to a synthetic one is indisputable. K-EL cost is around 0.23 €/g against TPGS-750-M price of 17.23 €/g from the same supplier (Merck).

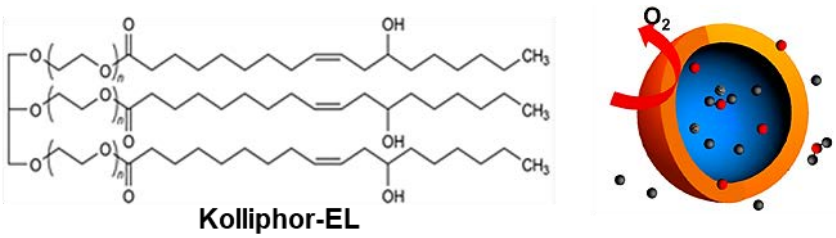

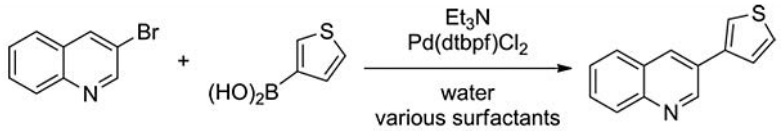

11

Entry	Medium	Run	Atmosphere	Time [h]	Yield [%]
1	Kolliphor EL	I	air	1	90
2	Kolliphor EL	II	air	2	70
3	Triton X-100	I	air	2	68
4	Triton X-100	I	N_2	2	80
5	TPGS-750-M	I	air	2	69
6	TPGS-750-M	I	N_2	2	95

Figure 51. *Test reaction between 3-bromoisoquinoline and 3-thienylboronic acid using different surfactants.*

In details, the reactions were performed under the general conditions reported in familiar literature: works: a 2 wt % solution of the surfactant in distilled water, 0.5 M concentration of the limiting reagent, Pd(dtbpf)Cl_2 2 mol % with respect to the bromide as the catalyst, triethylamine as the base, at room temperature. The conditions including the K-EL were reproduced for other derivatives, again without removing oxygen from the environment, proving a general efficiency for all the reactions as shown in **Figure 52**.

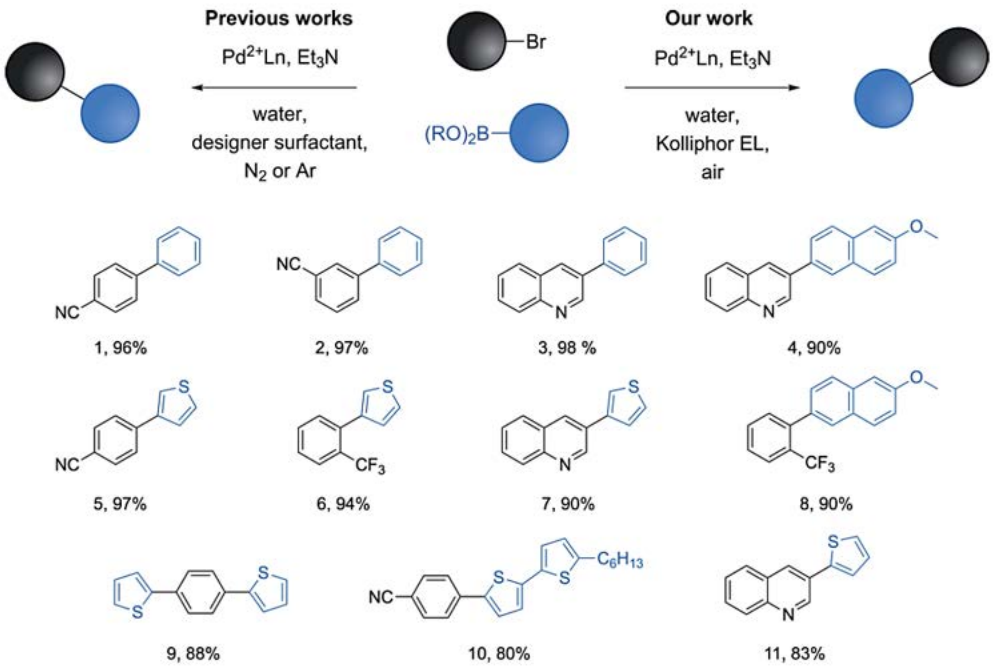

Figure 52. *Set of micellar S-M couplings carried out in a 2 wt% K-EL aqueous solution at room temperature and under air. Reported with permission of ref* [64].

2.3.3. Organic Semiconductors Access in Water and Under Air

My boss Prof. Beverina and his group were the first to attempt to increase the scope of the micellar catalysis approach to the synthesis of organic semiconductors with extended π-conjugated structures. The synthesis of highly conjugated, rigid and poorly soluble organic semiconductors is particularly challenging in the above-mentioned respects. Starting from the impressive results described in the previous paragraph, the group decided to challenge the K-EL dispersion ability with a set of micellar S-M cross-coupling reactions involving organic semiconductors relating to the classes of 9,10-diarylanthracenes, diketopyrrolopyrroles, diarylbenzothiadiazoles, perylenediimides, and isoindigos.[64] One relevant and general characteristic observed in structures with increased conjugation lengths is the poor solubility. To overcome this problem functionalization of functional materials with long or branched alkyl chains to gain reasonable solubility is necessary. From the perspective of micellar catalysis, the use of such highly crystalline, strongly aggregated and poorly soluble precursors represents a challenge. Micellar reactions are commonly performed at a formal 0.5–1.0 M concentration of the reacting substrates in the presence of 1-5 wt% of surfactant in water. Thus, micellar reaction vessels contain much more water insoluble material than the maximum amount that can be incorporated within the micelles at a given time. Actually, micellar synthesis is not a completely appropriate term as the reaction mixture is a suspension. The capability to successfully carry out a micellar coupling is connected with the colocalization of reactive species within the lipophilic compartment of micelles where the Pd^0 catalyst is believed to be localized. Only a minor fraction of reagents at any given time is accessing the lipophilic pockets to chemically evolve. Rigidly packed crystalline materials make the mass exchange from substate suspended microparticles to the catalytic site within the aggregates particularly laborious and slow, thus limiting conversion and yield.[66] These problems are commonly encountered in the semiconductor classes considered by Prof. Beverina. Impressively, his work reported a wide number of complex π-conjugated semiconducting structures reachable with the micellar catalysis method with yields ranging from good to optimal.[64] As expected, the more complex the target, the lower the yield and longer the

reaction time required (**Figure 53**). This study represents the first approach ever reported in the literature for the synthesis of molecular organic semiconductors using only water as reaction medium and under oxygenated environment. These remarkable results opened a new and very promising research field, of which the real heart of this thesis work.

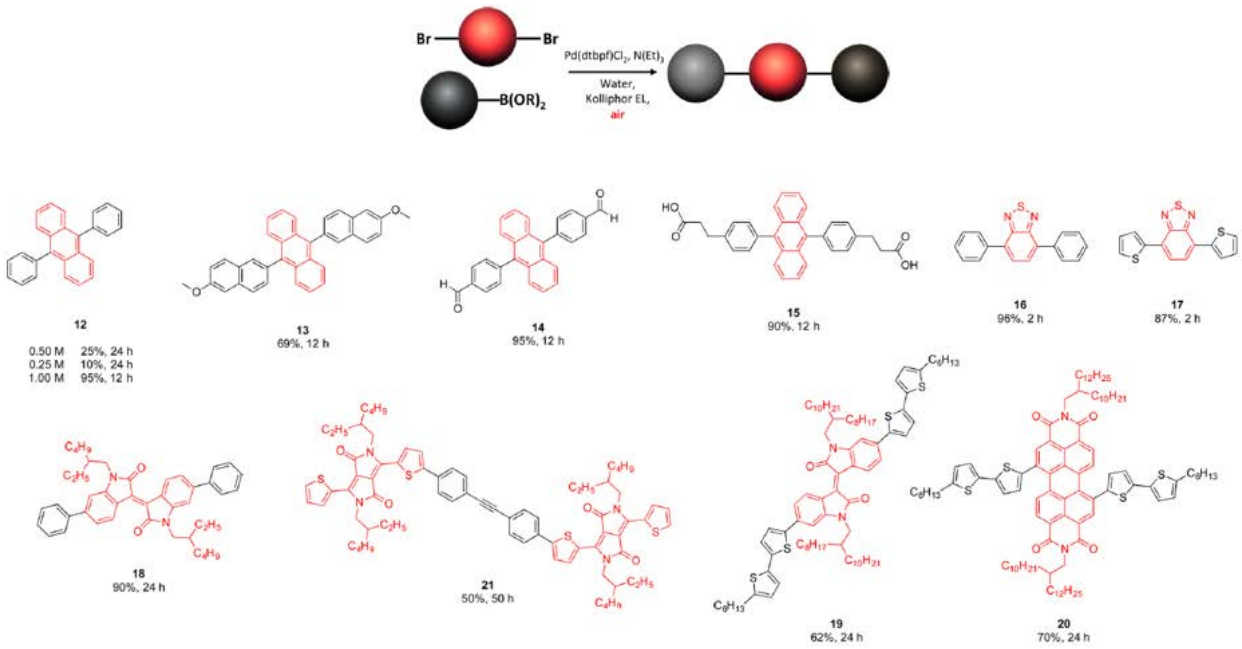

Figure 53. *First examples of organic semiconductors prepared in water and under air. Reported with permission of ref.* [64].

Another relevant literature report describing the preparation of highly conjugated molecular semiconductors in water environment is a Sonogashira coupling performed in TPGS-750-M with $Pd(OAc)_2$ and HandaPhos, a phosphine specifically designed for micellar catalysis.[67,68]

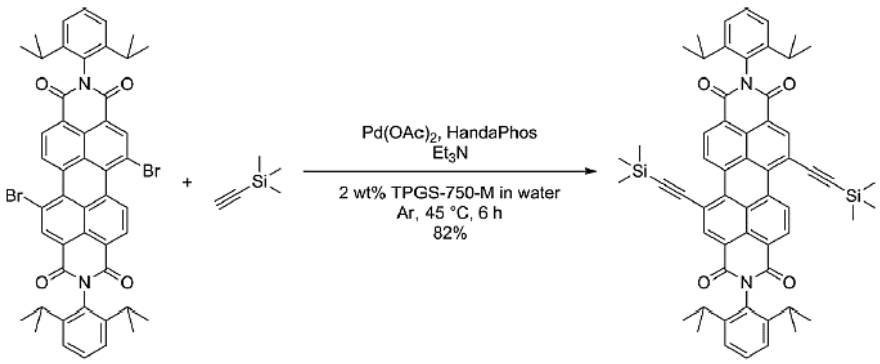

Figure 54. *Sonogashira coupling between a perylenediimide derivative and trimethylsilylacetylene carried out with HandaPhos ligand in 2 wt% TPGS-750-M designer surfactant.*[68]

2.3.4. Effect of Co-Solvents on Micellar Catalysis

Not always the micellar S-M conditions described so far have exhibited high efficiencies. Specifically, more complex the reacting substrates terms of conjugation extension, bulkiness, and functionalization, more difficult the promotion of the reaction in terms of conversion and time. This trouble was particularly observed by my research group in the synthesis of a series of isoindigo based latent pigments of interest for printed electronics applications.[69] Latent pigments are thermosensitive soluble dyes that can be thermally transformed though deprotection (with or without acid catalyst)

into insoluble pigments of application in high performance, ink-based OLEDs and OPVs. The latent pigments method is a practical method of interest as it is a more convenient alternative to vacuum deposition.[70,71]

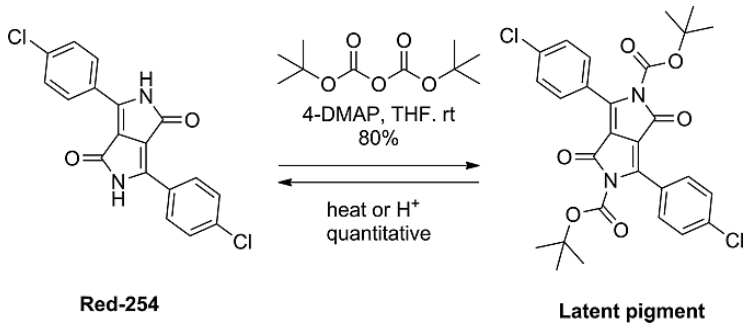

Figure 55. *Representative example of the latent pigment approach.*

Aiming at sustainably extend the conjugation of a serie of isoindigo-based latent pigments, my group explored the S-M micellar approach on a model reaction (**Figure 56**):

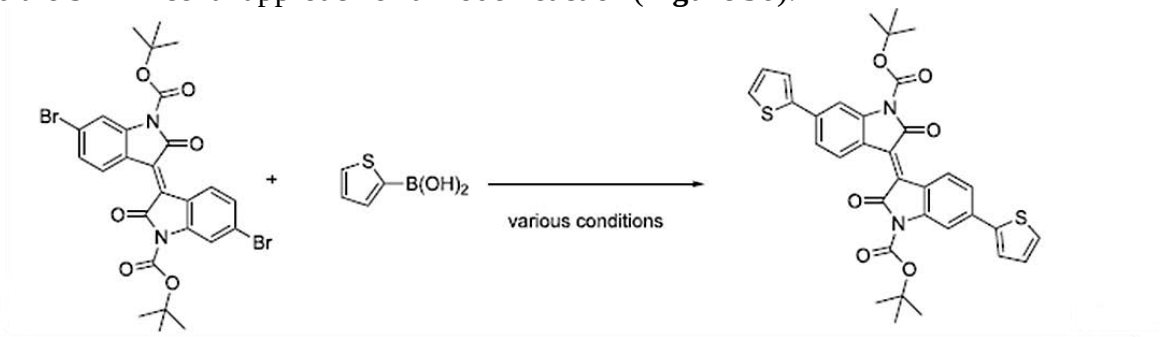

n°	medium	catalyst	atm.	time, h/temperature, °C	Outcome
1	Kolliphor EL	$Pd(dppf)Cl_2$	Air	24/rt	Partial deprotection
2	Kolliphor EL	$Pd(dtpbf)Cl_2$	Air	12/rt	No reaction
3	Kolliphor EL	$Pd(dtpbf)Cl_2$	N_2	12/rt	No reaction
4	TPGS-750-M	$Pd(dtpbf)Cl_2$	Air	12/rt	No reaction
5	TPGS-750-M	$Pd(dtpbf)Cl_2$	N_2	12/rt	No reaction
6	Kolliphor EL	$Pd(AcO)_2$/CyJohnphos	Air	24/rt	Partial deprotection
7	Kolliphor EL	$Pd_2(dba)_3$/Tri(o-tolyl)phosphone	N_2	24/rt	Partial deprotection
8	Kolliphor EL	$Pd_2(dba)_3$/dppf	Air	24/rt	Partial deprotection
9	Kolliphor EL	$Pd_2(dba)_3$/Tris(2-methoxyphenyl)phosphine	N_2	24/rt	Partial deprotection
10	Kolliphor EL	$Pd_2(dba)_3$/XPhos	N_2	24/rt	Partial deprotection
11	Kolliphor EL	$Pd_2(dba)_3$/CyJohnphos	N_2	24/rt.	Partial deprotection
12	Kolliphor EL	$Pd(dtpbf)Cl_2$	Air	12/60	Deprotection

Figure 56. *Model reaction between boc-protected 6,6-dibromoisoindigo and thiophene-2-boronic acid carried out in several micellar S-M conditions.*

As shown in the table of results in **Figure 56**, none of the attempts led to conversion to product, neither with K-EL, nor with the designer TPGS-750-M. Actually, it should be considered that this is a complicated reaction also concerning the use of an organic solvent (refluxing THF reported in literature for this reaction) since the product can be isolated with a yield of nearly 30%.[72] In the case of my group, reaction conditions were varied in the nature and stoichiometry of the catalyst, the concentration of the reaction medium, the temperature, the reaction time and the reaction atmosphere (air vs N_2), however no satisfactory results were observed at all. Nevertheless, the reaction course was dramatically improved by approaching the formulation state of the system.[69] In particular, the main problem related to this particular reaction was the failure in providing a suitable formulative environment where reagents and catalyst could colocalize and react, probably due to the BOC protecting group which altered the correct partitioning of the reagent in the micellar compartments. Thus, the introduction of a small amount of organic co-solvent (only a 10 vol% with respect to water) to the micellar environment allowed to benefit the reaction. The use of organic co-solvents in micellar catalysis is a documented strategy to sizably improve the efficiency and kinetics of surfactant enhanced cross-coupling reactions.[73] The advantages and sizably improvements derived from the co-

solvent approach on micellar couplings were already reported by Prof. Lipshutz.[73] In particular, the organic co-solvents studied by the group were both water miscible (THF and acetone) and immiscible (toluene) introduced in 2%wt K-EL solutions. The test reaction was repeated for all the three co-solvents considered. The reaction temperature was raised from room temperature to 60 °C, a temperature still well below of both the thermal cleavage temperature of latent pigments and the cloud point of the system. The Cloud Point represents the temperature threshold value above which the micellar stability collapse; the equilibrium is totally shifted to free amphiphiles that are not able to aggregate anymore. The results of this approach are following reported in **Figure 57**:

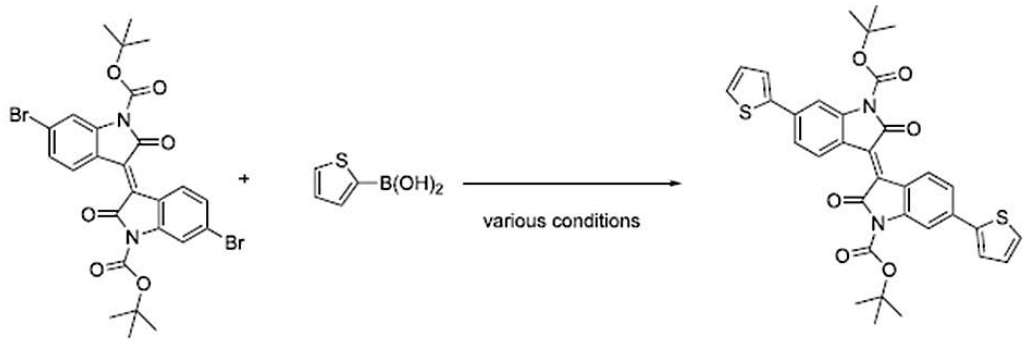

n°	medium	catalyst	atm.	time, h/ temperature, °C	Yield (%)
1	Kolliphor EL/ acetone 9:1	$Pd(dtbpf)Cl_2$	Air	2/60	42
2	Kolliphor EL/ acetone 9:1	$Pd(dtbpf)Cl_2$	N_2	2/60	40
3	Kolliphor EL/THF 9:1	$Pd(dtbpf)Cl_2$	Air	2/60	38
4	Kolliphor EL/THF 9:1	$Pd(dtbpf)Cl_2$	N_2	2/60	39
5	Kolliphor EL/ toluene 9:1	$Pd(dtbpf)Cl_2$	Air	1/60	80
6	Kolliphor EL/ toluene 9:1	$Pd(dtbpf)Cl_2$	N_2	1/60	79
7	Water/toluene 9:1	$Pd(dtbpf)Cl_2$	N_2	1/60	traces

Figure 57. *Model reaction between boc-protected 6,6-dibromoisoindigo and thiophene-2-boronic acid carried out in the presence of organic co-solvents.*

Impressively, the co-solvent strategy led to a remarkable improvement on both reaction yield and time. The use of THF and acetone moderately improved the reaction, leading to 42 and 39% yields respectively. Toluene was the real revolutionary, leading to a satisfactory 80% yield of isolated product. Surprisingly, even in the presence of toluene, reactions did not require a nitrogen atmosphere.

For each K-EL 2 %wt cosolvent solution it was collected the DLS analysis in order to determine the size distribution of the aggregates within the mixtures. As shown in **Figure 58**, the add of water-miscible solvents THF and Acetone led to microemulsions/swollen micelles of increased sizes. On the other hand, the use of a water-immiscible solvent such as toluene led to a sizably increased aggregates shifting the formulation state of the system from a micellar environment to an emulsion environment (**Figure 58**).

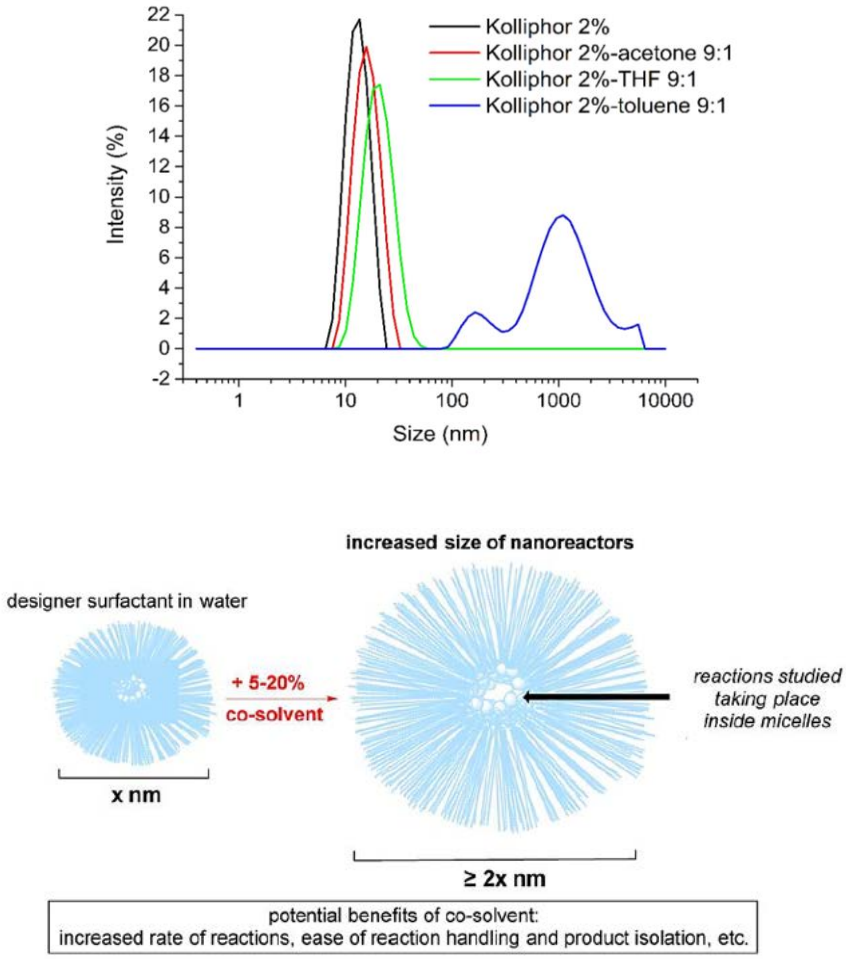

Figure 58. *On top: DLS spectra of K-EL 2 %wt in water (black) and of the corresponding 10 % by volume mixtures with acetone (red), THF (green) and toluene (blue). On bottom: micellar swelling effect by the addition of an amount of an organic co-solvent. Reported with permission of ref* [73].

Oil-in-water emulsions are biphasic mixtures, more or less stable over time, where the oil phase is dispersed in water as tiny droplets. The presence of a surfactant improves their stability: thanks to its amphiphilic properties it surrounds the oil droplets, decreasing the surface tension between the two phases and reducing the coalescence rate. Emulsion reactions may take place within these droplets, where the organic substrates can be partially dissolved and favour of the increased contact surface between each other and the water acts a reservoir of reactants.

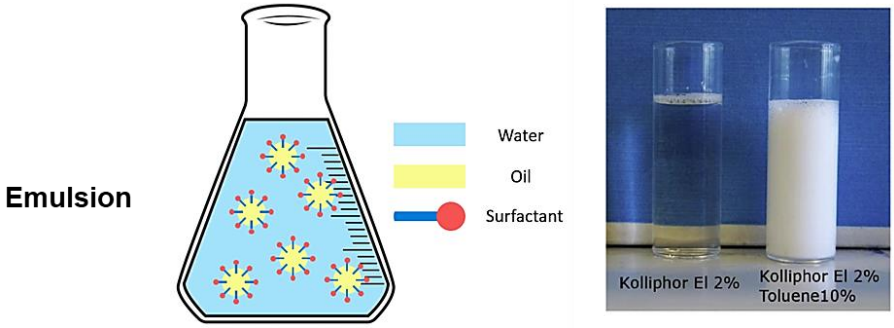

Figure 59. *Schematic representation of emulsions. The picture show how the K-EL 2%wt in H_2O looks like.*

Among the main advantage of adding organic co-solvents to micellar solution, that is the increased solubilization of the substrates, especially helpful for highly crystalline and poorly soluble species as organic semiconductors, the enhanced reactivity of the model reaction can be rationalized by the

changes in the chemical-physical properties of the formulation. The difference between the two formulation states is notable: while micellar solutions and microemulsions are single-phase systems thermodynamically stable below the corresponding Cloud Point, emulsions require both exhaustive and energetic mixing and heat to be kept stable and avoid flocculation and coalescence. Precisely for this reason, the possibility of heating kinetically slow organic reactions to favour their outcome is only that beneficial for emulsions stability while a disadvantage for that of micellar solutions. Still, in the synthesis of organic semiconductors where very complex structures of tedious reactivity are often involved, the practical need to heat the reaction environment to make the reaction work may not be negligible. Under the very same emulsion conditions best suited for the model reaction, a series of isoindigo and diketopirrolepirrole derivatives were prepared with satisfactory yields to prove the generality of the method (**Figure 59**).[69]

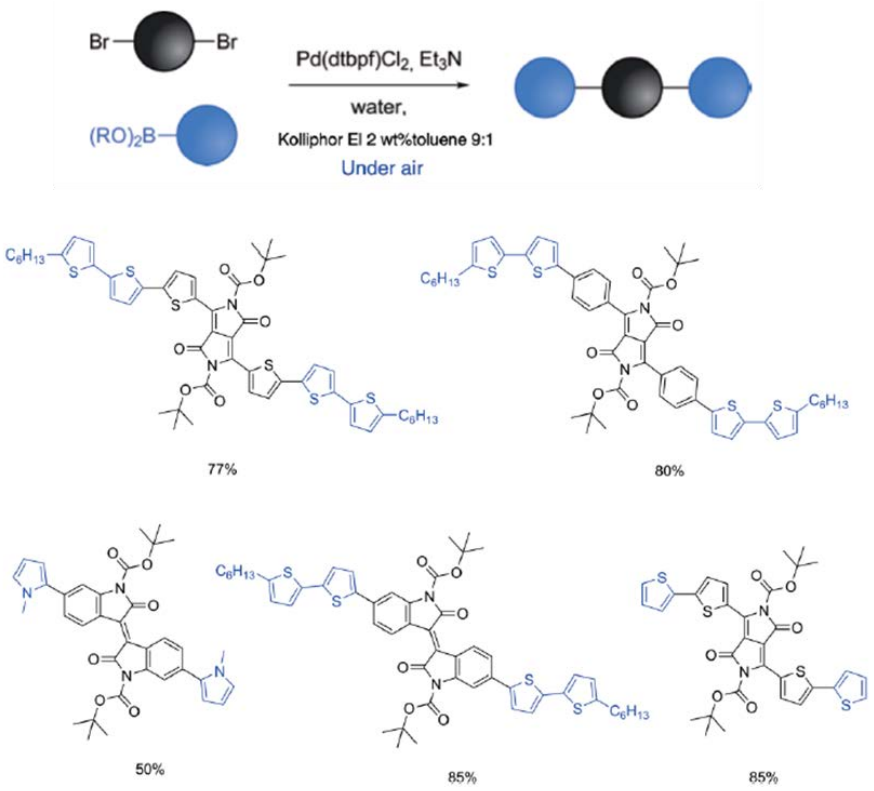

Figure 60. *Examples of latent pigments prepared via emulsion S–M coupling in a Kolliphor EL 2 wt%:toluene, 9:1 vol/vol mixture. Reported with permission of ref.* [69].

Moreover, my group showed the co-solvent approach was efficient in the preparation of other relevant conjugated structures, in particular showing compatibility also with other kind of cross-couplings like Buchwald-Hartwig (B-H) amination.[74] The Pd-catalysed Buchwald-Hartwig amination involves the coupling between an aryl halide and a primary or secondary amine, thus leading to the formation of a new C-N bond. The reaction mechanism is analogous to that of S-M protocol but instead of the trasmetallation process (there is no organometallic precursor but an amine), after the oxidative addition it follows the coordination of the amine to the Pd^{2+} catalytic centre, which is subsequently deprotonated from the base and final elimination of HX lead to the catalytic intermediate previous of the reductive elimination. In particular, the molecular rotor reported in ***Figure 61*** was successfully prepared with the emulsion obtained by mixing the micellar K-EL 2 %wt solution with toluene 10 %vol like in the case previously reported. As for the previous example no reaction or very low conversion was observed under any attempt run under micellar conditions (neither with K-EL, nor with the designer TPGS-750-M.);[74] the only way to satisfyingly obtain the product (with an optimal yield of 89% of isolated product) was to employ emulsion approach heating up the reaction at 60°C.[74]

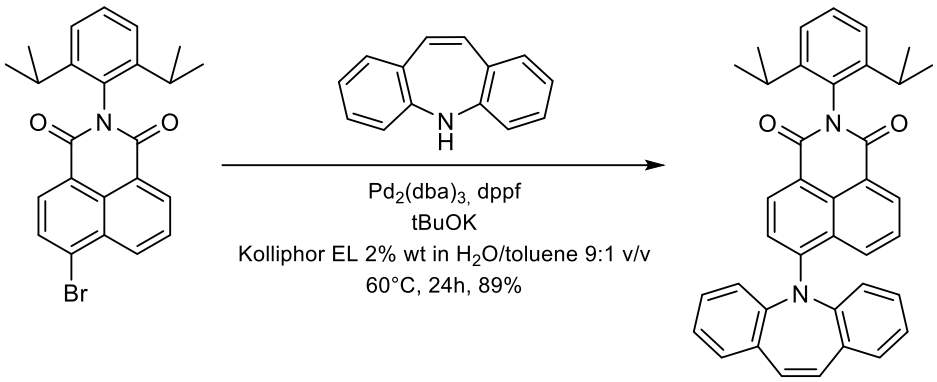

Figure 61. *B-H amination reaction of a naphthalenemonoimide derivative with dibenzoazepine in a K-EL 2 wt%/toluene 9:1 vol/vol mixture. Reported with permission of ref.*[74].

The traditional synthesis of this target compound consisted in a B-H amination in refluxing in toluene under microwave irradiation and nitrogen atmosphere.[75] My group successfully prepared the same compound in 89% yield using a milder and sustainable alternative solution under air.
Although the addition of an organic co-solvent to micellar solutions may seem contradictory to the principles of Green Chemistry, its use is limited to small quantities; its impact is only minimally on the gain in terms of the overall sustainability.

2.4. Aim of the Work

The work concerning this PhD thesis relates to the extension of the impressive and inspiring preliminary results reported by my research group about the possibility to synthetize active and functional optoelectronic materials in water through surfactant enhanced sustainable syntheses. In particular, the aim of the work focus on developing new reaction and formulation conditions that allow to prepare well-established and innovative organic semiconductors through environmentally friendly and industrially feasible methods. The use of micellar or emulsion Pd-catalysed cross-couplings in the field of organic semiconductors is still limited with only very few examples reported in the literature. Each topic of research will show that careful tuning over both reaction conditions and formulation state allows to efficiently perform organic transformations in water with high yields, high purities, minimal and simple purification steps, and with significantly decreased E-factor values compared with standard procedures requiring the use of organic solvents. The methods are Green Chemistry compliant and represent good synthetic and practical alternatives for a large-scale industrial production breakthrough. The full work can be divided in 6 macro topics:

The first part of this thesis work highlights the first study of efficient surfactant enhanced direct (hetero)arylation reactions in water and under air for the synthesis of relevant examples of π-conjugated molecular materials. Careful control over the repartition of substrates in the micro-heterogeneous reactive environment plays a key role on the progress of the reaction. The developed method enables the preparation of a large variety of thiophene-flanked conjugated building blocks with high efficiency along with E-factors in the 10^2-order including purification.

The second part of the work involves the micellar enhanced Suzuki–Miyaura one-pot synthesis of symmetrical and unsymmetrical 4,7-diaryl-5,6-difluoro-2,1,3-benzothiadiazole luminescent derivatives in water and under air. Careful control of the chemical nature of the surfactant-system used, thus tuning the polarity of the micellar compartments plays a key role in determining the

reactivity of the involved species. The syntheses developed for these luminescent building blocks displayed E-factors values in the 10^1-10^2 order including purification.

The third part of the work relates to the sustainable synthesis of conjugated, highly crystalline, poorly soluble planar [1]benzothieno[3,2-b][1]benzothiophene (BTBT) derivatives in water and under mild conditions by micellar and emulsion Suzuki-Miyaura couplings. In particular, the study considers the use of semiconducting designer surfactants to efficiently extend the conjugation of the BTBT core in only water as reaction medium. The work highlights enhanced reactivity in terms of yield and reaction time considering in detail the effects of specific π-π stacking interactions. Several extended π-conjugated BTBT derivatives can be obtained through sustainable methods displaying E-factors in the 10^2-order.

The fourth part of the work consist of developing a sustainable and cost-effective alternative pathway for the multi-step synthesis of Spiro-OMeTAD, a popular and highly efficient hole transporting molecular material (HTM) used in perovskites organic solar cells (PSCs). The whole Spiro-OMeTAD synthesis from commercially available and cheap substrates involves three steps, concerning E-factors values around 10^3-10^4. The sustainable alternative synthetic pathway developed in this work allow to obtain the same quality performer material reducing the E-factor by 1 order of magnitude, making the compound more available to industry.

The fifth section of the thesis concerns with the extension of the previous developed sustainable methods to the preparation of semiconducting conjugated polymers. Exemplified by the two well-known and commercially available luminescent polymers poly(9,9-dioctylfluorene-alt-bithiophene) (PF8T2) and poly(9,9-dioctylfluorene-alt-benzothiadiazole) (PF8BT), this section describes the first examples of efficient Suzuki-Miyaura polycondensations in water, under air, with minimal amount of organic solvent and with moderate heating. The synthetic approach enables a reduction of the E-factor by 1 order of magnitude, without negatively affecting molecular weight, dispersity, chemical structure, or photochemical stability of PF8T2 or PF8BT.

Finally, the last part of the work entails the extension of the sustainable approaches developed to the synthesis of 3D conjugated porous polymers. This class of materials can combine microporosity and high surface areas with extended conjugation, suggesting a range of potential applications in energy related areas such as light-harvesting, fluorescence enhancement, batteries, supercapacitors, photocatalysts or molecular sensing. CPPs can find a broad range of applications including gas adsorption, storage, separation, heterogeneous catalysis, biological functions and so forth.[76] The CPPs prepared exhibit different electronic structures, including fully donor, donor-acceptor, and borderline systems. Likewise, the approach allow to obtain same quality materials as those prepared in solution using organic solvents, however with E-factor values reduced by 1 order of magnitude. The gas adsorbing capacities of such systems are still under investigation.

2.5. Direct (Hetero)Arylation Reactions in Water and under Air

This work has already been published and it is entitled *"Sustainable Access to π-Conjugated Molecular Materials via Direct (Hetero)Arylation Reactions in Water and under Air"*, Molecules **2020**, 25, 3717; doi:10.3390/molecules25163717.[77]

2.5.1. Introduction

Palladium-catalysed direct (hetero)arylation (DHA) reaction is nowadays playing a key role in improving the efficiency and atom economy of C-C cross couplings with a considerable impact in pharmaceuticals, agrochemicals, materials chemistry and so forth. As previously discussed, this protocol represents a more eco-friendly alternative respect to conventional coupling reactions since it does not require tedious pre-functionalization of C–H bonds with extra reagents such as organoboranes and organotins that are needed in Suzuki and Stille couplings. Current research aims at further improving the DHA protocol in terms of efficiency, generality, and selectivity by careful tuning of the reaction conditions and catalytic system, thus at making it competitive or even better with respect to the traditional coupling strategies both in scope of accessible structures and synthetic efficiency. Comparatively, very fewer studies are dedicated to the improvement of such protocol in terms of overall sustainability, mostly concerning with the replacement of high-boiling-point organic solvents normally employed. Among the increasing influence of micellar catalysis over Pd-catalysed cross-coupling reactions, very few examples are currently reported about direct arylation couplings in water. The methods are applied to a truly short class of molecules concerning substituted biaryls and through directing group assistance.[78–80] Even more, no reports on the extension of surfactant enhanced DHA couplings for the synthesis of organic semiconductors are documented in the literature. Additionally, all known palladium catalyzed DHA reactions require the use of inert atmosphere. Recently, Professor M. Leclerc and co-workers[81] have reported the first example of a DHAP protocol using water/toluene 1:1 vol/vol biphasic conditions to generate high-molecular-weight and almost defect-free polymers, even in the presence of oxygen. However, the water is not the reaction medium but only the reservoir of some reactants; the process requires the use of enough organic solvent to completely dissolve the reagents and this is not really beneficial for the reduction of the E-factor of the reaction with respect to homogeneous phase processes. In order to boost the sustainability of direct (hetero)arylation protocol, me and my research group developed a new methodology which avoids the use of large quantities of toxic organic solvent and employs mostly water as reaction medium. As the C-H bond activation is a thermally promoted process, oil-in-water emulsion was employed as reaction medium. In particular, the emulsion obtained by mixing the surfactant Kolliphor 2%wt in H_2O with toluene 9:1 v/v allows to perform the coupling in air by the dispersion of the starting materials at high nominal concentration in the water/toluene mixture. The work herein highlights the first study of efficient surfactant enhanced DHA reactions in water and under air to prepare a variety of thiophene-flanked π-conjugated building blocks in high yield and purity through an industrially feasible, environmentally friendly and synthetically powerful coupling technique. The use of only stoichiometric amounts of organic solvents leads to a significant decrease, by 1 order of magnitude, of the E-factor of the synthetic process compared with standard protocols in organic solvents.

2.5.2. Results and Discussion

2.5.2.1. Optimization of Surfactant Enhanced DHA Coupling on a Model Reaction

In this work we mainly focused on boosting the sustainability of the DHA trough the surfactant enhanced micellar catalysis approach. Actually, the term "micellar" is not the most appropriate in this case as micelles are not really employed. Since high temperatures are normally required to activate (hetero)aromatic C-H bonds (T ≥ 100 °C), an oil-in-water emulsion was employed as reaction medium. Unlike aqueous micellar solutions, where the associated colloids are stable below the corresponding cloud point, emulsions can be heated up generally at much higher temperatures preserving, indeed improving, the stability of the formulation; moreover, the possibility to heat the micro heterogeneous environment favours the kinetics of slow chemical reactions. The cloud point is pH dependent and under the basic conditions required by DHA generally does not exceed 40–50 °C, .[82] Previous experience of my group with emulsion S-M couplings revealed that the use of 2 wt% K-EL micellar solution/emulsion is an ideal reaction medium to drive reactions to completion in a short time, at a low temperature and with a high yield, even working under an oxygenated environment.[54,64,69,74,83] Analogously, we selected the mixture of K-EL 2 wt% in water with toluene 9:1 v/v as the preferred reaction medium. The amount of organic solvent involved in such reactions is really minimal. Indeed, the molarity of toluene is 0.13, to be compared with the 0.5 formal molarity of the halide to be arylated. Toluene helps with making the reaction possible but does not act as a solvent-rather, as a stabilizer for the emulsion. As model reaction we chose the arylation of 2-hexylthiophene with 4-bromoanisole (**Figure 62**) in standard formulative conditions using a 2 wt % solution of surfactant in the presence of 0.5 M solutions of the reagents. The choice was motivated by the vast amount of DHA literature on both thiophene derivatives as reactants and 4-bromoanisole as the arylating species.

Surfactant enhanced Pd-catalyzed cross-coupling reactions are very practical and profitable but qualitatively different from corresponding transformations carried out in homogeneous phase. As the reaction requires colocalization of counterparts and catalysts within the same pocket of a micro heterogeneous mixture, the hydrophilic/lipophilic balance (HLB) and diffusion coefficients of all species are at least as important as the intrinsic reactivity. Here we show that careful tuning of the reactions conditions and formulation control leads to find out a good degree of conversion to the heteroarylated product **1** for the model reaction.

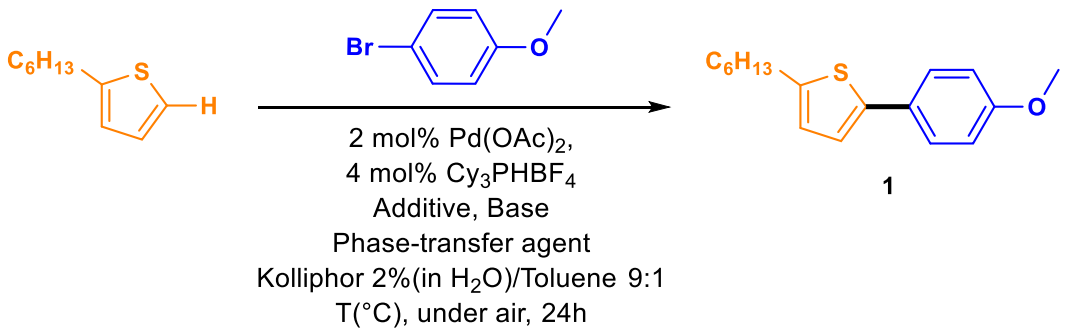

Figure 62. *DHA model coupling between 2-hexylthiophene and 4-bromoanisole in emulsion medium*

Entry	Additive (30 mol%)	Base 1.5 eq	Phase-transfer agent (30 mol%)	T(°C)	Conversion to product (%)
1	PivOH	Na_2CO_3	_	80	trace
2	PivOK	_	_	80	trace
3[a]	$PivONBu_4$	_	_	80	trace
4[a]	$PivONBu_4$	_	_	130	10
5	PivOH	Na_2CO_3	_	130	30
6	PivOH	Cs_2CO_3	_	130	27
7	PivOH	Na_2CO_3	Aliquat 336	130	53 (44 is.)
8	PivOH	Ag_2CO_3	Aliquat 336	130	35
9	PivOH	Et_3N	_	130	32
10	PivOH	TMP	_	130	35
11	PivOH	TMEDA	_	130	7
12	PivOH	Na_2CO_3	Aliquat HTA-1	130	55
13	PivOH	K_3PO_4	Aliquat HTA-1	130	13
14	PivOH	NaOH	Aliquat HTA-1	130	48
15	PivOH	tBuONa	Aliquat HTA-1	130	59
16	NDA	tBuONa	Aliquat HTA-1	130	80 (72 is.)
17	NDA	Na_2CO_3	Aliquat HTA-1	130	68
18[b]	**NDA**	**tBuONa**	**Aliquat HTA-1**	**130**	**88 (86 is.)**
19[b]	NDA	tBuONa	-	130	59

[a]: 1 eq. amount of $PivONBu_4$ was employed; [b] 3 eq. of tBuONa employed.

Table 1. *Screening of suitable reaction conditions and formulation of the DHA model coupling between 2-hexylthiophene and 4-bromoanisole in emulsion medium. All reactions were carried out in a pressure-tight 10 mL screw-cap glass tube under magnetic stirring at 1000 rpm for 24 h and at a nominal concentration for the reagents of 0.5 mol/L.*

The reaction was initially screened to investigate the effects of different proton shuttles, bases, phase-transfer agents, and temperatures in the emulsion medium studied. The catalytic system chosen to generate Pd^0 in situ correspond to the combination of $Pd(OAc)_2$ (2 mol%) and bulky PCy_3, present in the form of the air stable salt Cy_3PHBF_4 (4 mol%), as it is a well-known efficient couple for C-H bond activation of a large variety of thiophene derivatives in apolar solvents like toluene and xylenes.[84–86] Since the catalytic cycle is supposed to take place within the dispersed droplets of toluene in the micro heterogeneous mixture, we referred at toluene system conditions. Entry 1 shows the most general conditions used to perform Pd-catalysed direct arylations of thiophenes: pivalic acid (PivOH, 30 mol%) as proton shuttle assistant between the base and the catalytic specie, and Na_2CO_3 (1.5 eq) as the base. On the first try, the reaction was performed at 80°C but the product was detected only in traces by GC-MS analysis. The lack of efficiency of the reaction could be associated to the difficulty of the inorganic base to colocalize with respect counterparts within the same pocket of the micro-heterogeneous mixture. In entries 2 and 3 we studied the effect of potassium pivalate (PivOK) and tetrabutylammonium pivalate ($PivONBu_4$) as an alternative of $PivOH/Na_2CO_3$ among localization. The use of PivOK as direct source of carboxylate instead of $PivOH/K_2CO_3$ in the presence of PCy_3 as ligand was studied by Professor M. Sommer in DHAP.[87] However, even in these conditions the signal of the product was detected only in traces.

The C-H bond activation of the thiophene ring started to be effective when the temperature was raised significantly from 80 °C to 130 °C as shown in entries 4 and 5. In entry 4 we used $PivONBu_4$ as direct

carboxylate source but the conversion to product turned out to be lower with respect to PivOH/Na_2CO_3. Probably, charged pivalate anions prefer to remain in the aqueous phase without diffuse into toluene droplets, where the catalytic cycle is supposed to take place. We chose tetrabutylammonium specie as pivalate counter ion properly because we thought it could effectively act as phase transfer agent for the pivalate anions. In these conditions the pivalate anions are not catalytically regenerated because of the absence of a base, and so a stoichiometric amount of $PivONBu_4$ is required. The use of the couple PivOH/Na_2CO_3 turned out to be more efficient with respect to conversion to product as shown in entry 5. The couple probably can majorly diffuse in toluene droplets before proton dissociation and at same stay after regeneration. In entry 6, we studied the counterion effect by employing cesium carbonate as the base. Cs_2CO_3 has a lower partition coefficient water/toluene with respect to Na_2CO_3 and this should increase the presence of CO_3^{2-} anions in the toluene droplets phase for catalytic cycle to have place. However, no significant deviation was detected by the GC-MS analysis with respect to entry 5. This could be explained by colocalization of counterparts, and that probably the catalytic cycle takes place at the interface of the two phases and not really inside the toluene droplets. For a better understanding of reaction localization and behavior, it is necessary to have a general formulation screening.

In entry 7 we repeated the conditions of entry 5, employing the more cost-effective base Na_2CO_3, but introducing Aliquat 336 as phase-transfer agent. Aliquat 336 (trioctylmethylammonium chloride) is a quaternary ammonium salt and it is amphiphilic, due the long alkyl chains and the positive charge of the nitrogen atom, so it can act as a surfactant, helping the system to avoid coalescence or flocculation. Compared to entry 4, where $PivONBu_4$ was employed in order to exploit the tetrabutylammonium counter ion effect of phase transfer agent, Aliquat 336 has a lower hydrophilic/lipophilic balance (HLB), due the longer alkyl chains, and so the distribution and location of CO_3^{2-} anions and reactive counterparts may vary. Under these conditions, a moderate yield of 44% (53% conversion by GC-MS analysis) of model product was obtained. In entry 8, we repeated the conditions of entry 7 but in the presence of silver salts, in the form of Ag_2CO_3, since is known in literature that silver salts often enhance DHA reactions rate and selectivity as mild oxidant species and halide scavenger in the palladium catalytic cycle.[35-88] However, the reaction showed less efficient in the presence of Ag_2CO_3 instead of Na_2CO_3 with a marked presence of homocoupling by-products because of the oxidant power of the Ag^+ cations.

In entry 9 we studied the formulative effect by replacing the inorganic base Na_2CO_3, with organic base such as Et_3N. The main impact of NEt_3 is in the nature of the formulation achieved: being liquid, the amine can act as an organic co-solvent, thus helping in partially dissolving the lipophilic reagents. Moreover, the K-EL surfactant is a good emulsifier but not a good dispersant agent, thus in these conditions, liquid organic bases can be more efficiently emulsified with respect to the dispersion of solid inorganic bases such as Na_2CO_3, achieving a better formulation state. The use of organic bases does not need the use of phase-transfer agents, so Aliquat 336 was not employed. Anyhow, the GC-MS analysis of the reaction carried out with NEt_3 showed a markable lower product conversion (32%) with respect to the Na_2CO_3/Aliquat 336 system.[35-89] When Aliquat 336 was employed as phase-transfer agent in previous entries, the GC-MS revealed the presence of large quantities of side insaturated alkyl species derived from the Hoffmann elimination decomposition of Aliquat 336. For this reason, we investigated the effect of another organic base, in order to prevent the possible degradation of triethylamine (ethylene is not revealed by GC-MS analysis). In entry 10 we employed 2,2,6,6-tetramethylpiperidine (TMP), which pKb is comparable with that of triethylamine (pKa TMP = 11.1 vs pKa Et_3N = 10.8). Since the saturated substitution of methyl group in alpha positions respect to the nitrogen atom, TMP cannot undergo Hoffmann elimination. However, even in this case the efficiency was lower respect to entry 7 (35% vs 53% of conversion). In entry 11 we studied the effect of tetramethylethylenediamine (TMEDA) as base in DHA protocol. Recent literature reported that the introduction of TMEDA enhance DHA reactions in terms of selectivity.[90] The role of TMEDA is

rationalized by the authors concerning the intramolecular deprotonation process competition between the diamine and the carboxylate ligands of Pd^0 center. However, the reaction showed very bad result with a conversion to product of only 7%. In entry 12 we employed the more stable to high temperatures phase-transfer agent, Aliquat HTA-1. No significant deviation in terms of reaction conversion was detected replacing Aliquat 336 with Aliquat HTA-1 (55% vs 53% product conversion) and effectively no decomposition byproducts of Aliquat HTA-1 were observed.

In entries 13-15 we investigated the effect of different bases, replacing Na_2CO_3 with K_3PO_4, NaOH and tBuONa respectively. The use of K_3PO_4 as base led to markedly worse result (13% of conversion), NaOH showed slightly lower conversion (48%), while sodium tert-butoxide tBuONa led to a slightly higher conversion (59%). It is noticeable that tBuONa exhibited a 10% more efficient result in terms of reaction conversion since tBuONa in water rapidly reacts to give NaOH + tBuOH. The result could be explained by the benign formulative effect of the non-ionic hydrotrope tert-butanol, which can act as an organic cosolvent, thus helping in partially dissolving the lipophilic reagents. In formulation chemistry hydrotropes are effectively used as cosurfactants for stabilization of microemulsions by reducing the interfacial tension between water and oil.[91] Unlike surfactants, hydrotropes do not form stable micelles in aqueous solutions because the hydrophobic parts of their molecules are too small but they form dynamic noncovalent molecular clusters in aqueous solutions. Those clusters are stabilized by hydrogen bonds between hydrophilic parts of hydrotrope molecules and water. Moreover, the possibility of heteroaryl C-H bond activation/cleavage transition state assistance from tert-butanol in CMD mechanism, by means of supramolecular H-bonds interactions, should not be excluded (Scheme 2). The energy necessary to attain the transition state involved in the rate determining step of DHA can be decomposed into two categories.[27,28] The first corresponds to the energy necessary to distort the C–H bond (E_{dist}) and the second to the energy necessary to counter the electronic interaction between the distorted substrate and the metal center (E_{int}) (**Figure 64**). The transition state proposed (***Figure 63, B***) may involve a supramolecular distorted 8 membered ring via hydrogen bonds, in which the tert-butanol inserts between the activated C-H bond and the carboxylate ligand. From an energetic point of view this should lead to a raised E_{dist} for the increased tension derived by tBuOH insertion. By such interactions, the tert-butanol can transfer faster its acid proton to the carboxylate ligand. Concerted, the tert-butoxide transient specie formed, which is a stronger Lewis base compared to the carboxylate with delocalized electrons, can cleavage the activated heteroaromatic C-H bond with a faster proton transfer, reducing the transition energy cost E_{int} in the CMD process.

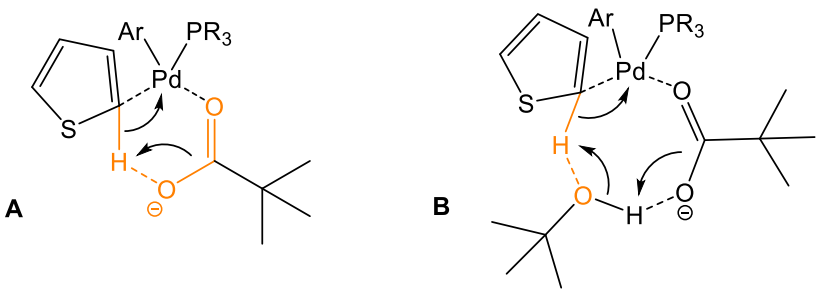

Figure 63. ***A)*** *Carboxylate assistance C-H bond activation/cleavage in CMD transition state.* ***B)*** *Proposed C-H bond activation/cleavage transition state tert-butanol assisted in CMD mechanism.*

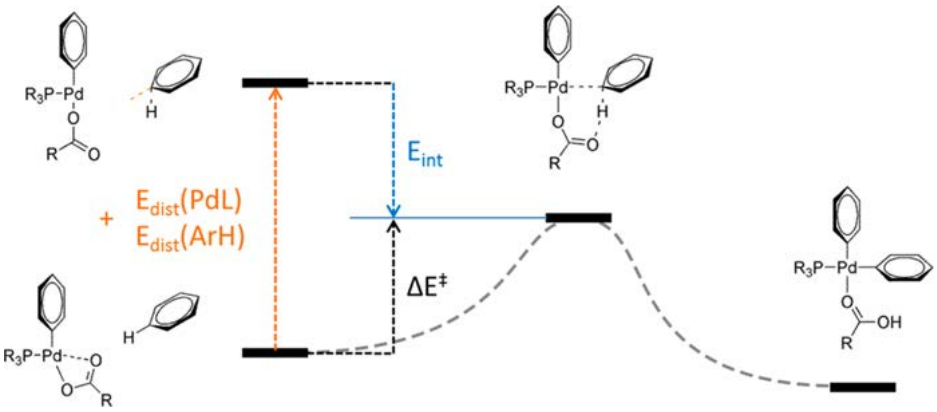

Figure 64. *Diagram illustrating the two principal factors (E_{dist} and E_{int}) that contribute to the energy level of* the transition state (ΔE). Reprinted with permission from ref [29]. Copyright © 2016 American Chemical Society.

The real breakthrough in the optimization of the method came with the introduction of neodecanoic acid (NDA, a mixture of carboxylic acids with the common structural formula $C_{10}H_{20}O_2$, a molecular weight of 172.26 g/mol, and the CAS number 26896-20-8. Components of the mixture are acids with the common property of a "trialkyl acetic acid" having three alkyl groups at carbon two) in the place of pivalic acid in entry 16. NDA possesses a lipophilic character (logP = 3.6) much more pronounced than that of pivalic acid (logP = 1.5). Besides, the use of bulkier NDA instead of PivOH in DHA reactions is reported to improve efficiency and selectivity for a variety of thiophene substrates.[41,92] In these conditions, the couple tBuONa/NDA displayed a good conversion to arylated model product of 80% by GC-MS analysis (72% yield of isolated product). From the formulation point of view, the good result could be explained by the fact that NDA, unlike pivalic acid, is characterized by long alkyl chains turning the carboxylate derived specie amphiphilic and with a markedly reduced HLB value. In this way the neodecanocate specie can act as co-surfactant helping avoiding coalescence or flocculation. Moreover, the associated specie neodecanoate-Aliquat HTA-1 can diffuse more easily within the toluene phase being more lipophilic than pivalate-Aliquat HTA-1. Besides, the use of bulkier NDA instead of PivOH in DHA reactions is reported to improve efficiency and selectivity for a variety of thiophene subtrates.[93,94] In entry 17 we studied the couple NDA/Na_2CO_3 and the product conversion resulted 68%. The result proves that for emulsion conditions tBuONa is the best choice as the base compared with entry 16 (tBuONa/NDA), while NDA the base choice of proton shuttle if compared with entry 12 (PivOH/Na_2CO_3). According to recent reports, the use of a large excess of base is beneficial; we thus doubled the amount of tBuONa (entry 18[b]).[95] Indeed, the yield was further improved to 88%. Having assessed the relevant role of the partition of the carboxylic additive, we wondered whether the presence of the phase transfer agent was still necessary. Its complete removal (Entry 19[b]) proved to be unfavourable, as the yield dropped to 59%, mostly due to limited conversion. Having identified satisficing conditions to carry out the reaction, we then turned to the identification of the by-products and to a further fine tuning of conditions aimed at suppressing the most unfavourable processes in view of a possible extension of the method to polymerizations: dehalogentation (formation of anisole **3**), homocoupling of the bromide (4,40-dimethoxybiphenyl **4**), oxidative homocoupling of the aryl (5,50-dihexyl-2,20-bithiophene **5**), double arylation of thiophene (derivatives **6**, mixture of regioisomers) and oxidative coupling of product **4** and 2-hexylthiophene (derivatives **7**, mixture of regioisomers). The following **Figure 65** shows the results.

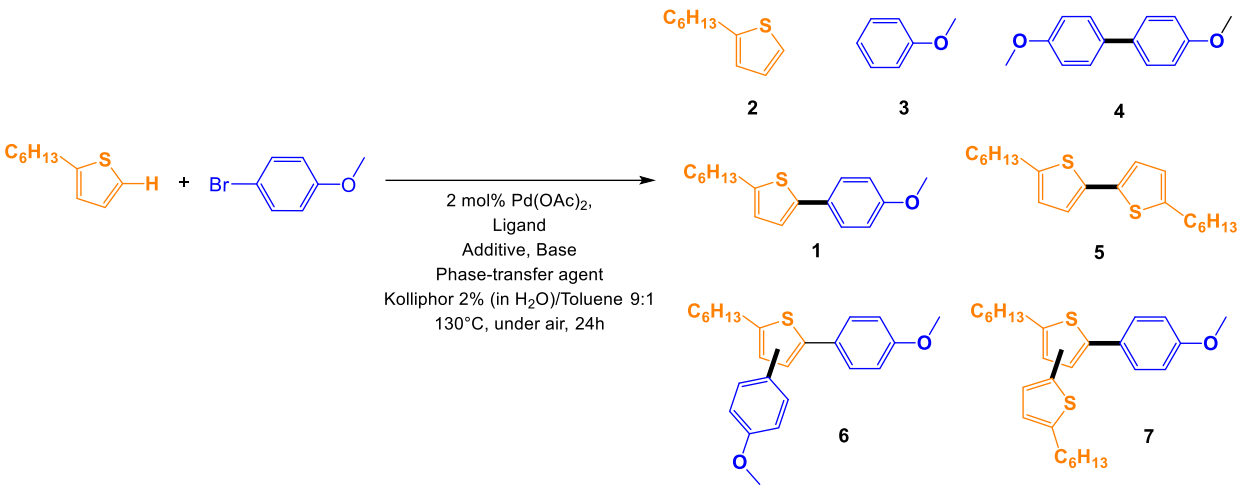

Entry	Ligand (4 mol%)	RCOOH (eq)	Base (eq)	Phase-transfer agent (eq)	1	2	3	4	5	6	7
1	Cy_3PHBF_4	NDA 0.3	tBuONa 3	Aliquat HTA-1 0.3	88%	3%	2%	1%	2%	4%	0%
2	Cy_3PHBF_4	NDA 1	tBuONa 3	Aliquat HTA-1 1	87%	3%	1%	2%	2%	3%	1%
3	tBu_3PHBF_4	NDA 0.3	tBuONa 3	Aliquat HTA-1 0.3	83%	9%	3%	1%	2%	2%	0%
4[a]	Cy_3PHBF_4	NDA 0.3	tBuONa 3	Aliquat HTA-1 0.3	85%	3%	1%	1%	4%	4%	3%
5[b]	Cy_3PHBF_4	NDA 0.3	tBuONa 3	Aliquat HTA-1 0.3	86%	4%	2%	1%	2%	4%	1%

[a] Reaction performed without K-EL; [b] reaction performed under nitrogen atmosphere

Figure 65, Table 2. *Optimization of reaction conditions for the DHA coupling between 2-hexylthiophene and 4-bromoanisole in the emulsion medium. All reactions were carried out in a pressure-tight 10 mL screw-cap glass tube under magnetic stirring at 1000 rpm for 24 h and at a nominal concentration for the reagents of 0.5 mol/L. RCOOH stands for the carboxylic additive.*

Entry 1 shows that under the best experimental conditions identified, the most sizable impurities are the unreacted 2-hexylthiophene (3%) and the double arylation derivative (4%). The increase in the amounts of carboxylic additive and phase transfer agent did not affect the product distribution in a significant way as shown in entry 2; as such we continued using the usual 0.3 eq stoichiometry of both for the remaining attempts. The exchange of Cy_3PHBF_4 with tri-tert-butylphosphine tetrafluoroborate salt (tBu_3PHBF_4), another popular sterically-hindered phosphine employed in DHA, led to a vaguely lower conversion without affecting the product distribution (entry 3). Considering that NDA potassium salt is also a surfactant, in entry 4 we decided to remove the K-EL. The reaction worked very similarly to entry 1, with a noticeable increase in the formation of the bithiophenes **5** and **7**. Both derivatives are formed according to an oxidative coupling of thiophene derivatives, requiring the presence of a Pd^{2+} species. According to our previous experience with K-EL in S-M and B-H couplings, the major benefit of using such a surfactant is exactly the suppression of oxidative side reactions even under an oxygenated environment.[64] In order to verify this, we repeated the reaction in absence of K-EL under nitrogen atmosphere and with nitrogen saturated solvents (entry 5), precisely observing basically the same product distributions of entry 1 reaction. Even if in absolute terms, the impact of all by-products is minimal, thus the influence of their formation in a

polymerization reaction would be sizeable, as the pathway leading to derivative **3** is a termination reaction. those leading to **4** and **5** would introduce defects and those leading to **6** and **7**, crosslinking.

2.5.2.2. Scope and Generality of the Method in the Preparation of Conjugated Building Blocks

After having optimized the method on the model reaction we turned to prove the scope and generality of the method synthetizing a set of representative molecular derivatives with different electronic features. The semiconducting molecular materials selected possess general structures featuring the alternation of aromatic and heteroaromatic rings having electron accepting, donating and borderline characteristics due to the presence of substituents or to the intrinsic characteristics of the various heteroaromatics. Such attributes impact on the efficiency and selectivity of the DHA reaction. We thus studied the synthesis of eight chosen compounds considering the most representative electronic patterns generally found in biaryls for organic semiconductors (**Figure 66**). Following are reported the chemical structures of the semiconductors synthetize under the optimized conditions with their optical and electrochemical characteristics (LUMO levels are not reported as no reversible reduction peak was observed for any compound except derivative **13**).
Derivatives **8** and **9** are p-type organic semiconductors with a low oxidation potential having the HOMO levels of -5.18 and -5.49 eV respectively. They were synthetized by coupling 3,4-ethylenedioxythiophene (EDOT) with electron rich bromides: 4-bromoanisole and 1-bromo-4-methylnaphthalene leading to derivatives **8** and **9** in 82% and 85% yields, respectively. Derivatives **8** and **9** can be synthetized by classical DHA protocol in organic solvent employing refluxed toluene obtaining comparable yields but with an E-factor of the synthesis of nearly 1200.[96] Our method lead to the comparable yields and purity but with an E-factor of the synthesis of only 200. Derivative **10** is also a p-type semiconductor having a high planar core [1]benzothieno[3,2-b][1]benzothiophene (BTBT) very efficient in performing π-π stacking thus increasing the charge carrier mobility. BTBT derivatives are remarkably interesting and fully studied systems for OFET devices. Literature synthesis of derivative **10** require a Stille coupling in organic solvent leading to 77% yield and an E-factor of nearly 1200.[97] Under DHA emulsion conditions, we isolated **10** in 54% yield by the reaction of 2-bromo-BTBT with 2-hexylthiophene. The comparison seems to be unfavorable for emulsion DHA, however, the same purity derivative can be obtained in only a slight lower yield (consider the further steps and related yields and waste to functionalize the thiophene ring with stannyl derivatives) but with an E-factor of only 475 after unavoidable chromatographic purification, thus enabling a direct evaluation of the advantages of the emulsion DHA protocol. Derivatives **11**–**13** also have a potential p-type character, with corresponding HOMO levels of -5.44, -5.54 and -5.59. Derivatives **11** and **12**, concerning a bithiophene and a thienothiophene bridge, support the robustness of the method with more extended conjugated bridges. They were synthetized reacting bithiophene and thienothiophene with 3-bromohexylbenzene to obtain **11** in 71% yield and **12** in 73% yield and with E-factors of 185 and 232 respectively, maintaining the order of magnitude of the E-factor impact compared with the other derivatives. Derivative **13** is a well-known fluorescent probe with a p-type character obtained by reacting 2-hexylthiophene with 9,10-dibromoanthracene in 62% yield and with an E-factor of 256; again comparable yield and purity but with the standard protocol but with a far reduced E-factor.[98] Finally, derivatives **14** and **15** are examples of donor–acceptor building blocks with moieties very popular in low-band gap conjugated alternated copolymers. Derivative **14** was prepared in emulsion DHA conditions by coupling 2-hexylthiophene with 2,1,3-benzothiadiazole in 54% yield with an E-factor of only 556 after an unavoidable chromatographic purification. Again, respect to the literature report, our method has undisputable advantages in terms of sustainability and efficiency.[99] Finally, derivative **15** was obtained by the reaction of 3-bromohexylbenzene with 2,20,3,30,5,50,6,60-octafluorobiphenyl in 82% and with an E-factor of the synthesis of only 174, proving again the efficiency and benefits of the emulsion method.

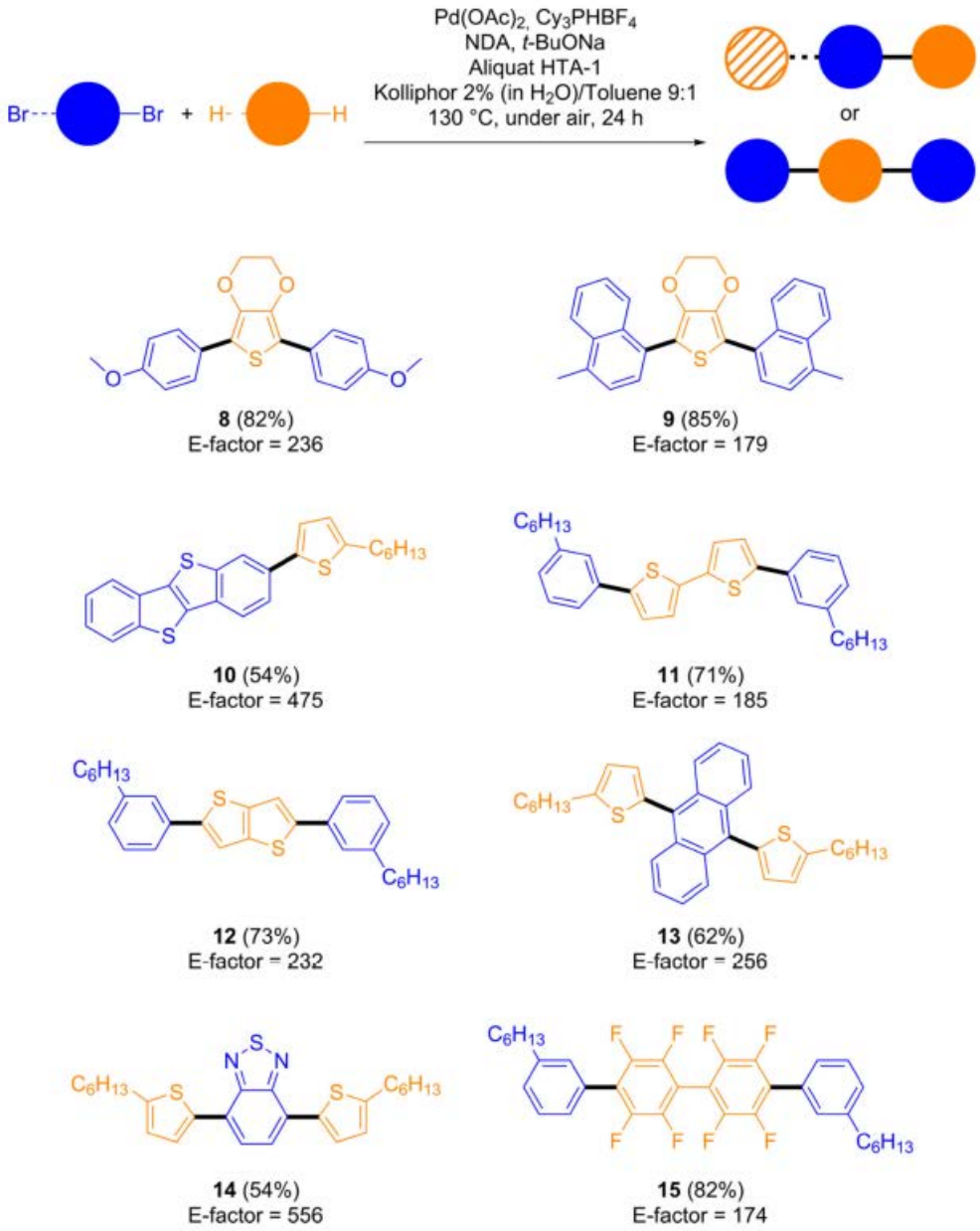

Derivative	λ_{max} (abs) [nm]	λ_{max} (em) [nm]	Stokes Shift [eV]	$E_{1/2}$ (V)	HOMO (eV)
8	351	392	0.37	0.38	−5.18
9	334	430	0.83	0.69	−5.49
10	364	379	0.14	0.78	−5.58
11	375	430	0.43	0.64	−5.44
12	351	391	0.36	0.74	−5.54
13	401	461	0.40	0.78	−5.59
14	469	603	0.58	−1.78	−3.00
15 [a]	267	341	1.00	-	-

[a] The compound has no redox processes within the stability window of the electrolyte.

Figure 66. *Chemical structures of π-conjugated building blocks synthetized by DHA with the emulsion optimized conditions. Optical and electrochemical properties of compounds* ***1***, ***8–15*** *in CH_2Cl_2: linear absorption maxima (λmax(abs)), steady state emission maxima(λmax(em), half-wave potentials ($E_{1/2}$ vs. Fc/Fc+, supporting electrolyte tetrabutylammonium perchlorate 0.1 M) and electrochemical HOMO levels (eV).*

2.5.3. Conclusion

This works highlights the first study of efficient surfactant enhanced DHA reactions in water and under air useful to easily and efficiently prepare a variety of thiophene-flanked π-conjugated building blocks with good yields and purities. In particular, the emulsion obtained by mixing the surfactant K-EL 2%wt in H_2O with toluene 9:1 v/v has demonstrated to be efficient in carrying out DHA reactions on thiophene derivatives. The work demonstrated that micro heterogeneous environments require an accurate finetuning of the colocalization of reagents, catalyst and additives becomes the key factor in achieving high conversions clearly differing from the common homogeneous phase reactions in high-boiling-point organic solvents. The use of NDA instead of pivalic acid was the real breakthrough, leading to a better repartition of reactive species between the water and toluene under emulsion conditions. Once optimized for the model reaction, the method was successfully extended to the preparation of representative molecular semiconductors possessing structural characteristics commonly found in organic semiconductors with application in plastic (opto)electronics, thus proving scope and generality. All the synthetized compounds were characterized in terms of optical and electrochemical properties. Efficiency in terms of yield, purity and E-factor value has been evaluated by the comparison with standard methods using organic solvents, if reported, to prepare same derivatives of interest. The use of only stoichiometric amounts of toluene, required to obtain the emulsion environment, has a significant impact in decrease the E-factor of the synthetic process, leading to reduce the E-factors by 1 order of magnitude respect to the counterpart in homogeneous phase. The method led to values in the 10^2 order, which is a compatible range with the requirements for scaling up.

2.5.4. Experimental Section

2.5.4.1. Materials and Instruments

All reagents, chemical compounds and solvents were purchased from TCI Europe (Haven, Belgium), Fluorochem Europe (Hadfield, Derbyshire, United Kingdom), Alfa Aesar Europe (Kandel, Germany) and Merck Life Science S.r.l. (Milano, Italy) and used as received without any further purification. In particular, for the catalysts, $Pd(OAc)_2$ was purchased from Fluorochem, Cy_3PHBF_4 was purchased from Alfa Aesar Europe (Kandel, Germany) and tBu_3PHBF_4 was purchased from Fluorochem Europe (Hadfield, Derbyshire, United Kingdom). Chromatographic purifications were performed using Davisil LC 60A silica gel (pore size 60 Å, 70-200 μm). Compositions of solvent mixtures used as eluents are indicated as volume/volume ratios. Melting points were determined using a Buchi M-560 (BUCHI Italia s.r.l, Cornaredo, Italy) apparatus and are uncorrected. GC–MS spectra were collected on a Clarus 560 S PerkinElmer (Perkin Elmer Italia, Milano, Italy) having an Elite-5MS 30.0 m x 250 μm column. Helium was used as carrier gas. ^{1}H-NMR and ^{13}C-NMR spectra were collected on a Bruker NMR Avance 400 NEO spectrometer; coupling constants are reported in Hz. Absorption spectra of derivatives **1** and **8**–**15** were collected on a Cary 60 UV□Vis Agilent spectrophotometer in a 10 mm path length quartz cuvette. Photoluminescence (PL) spectra of derivatives **1**, **8**–**15** were collected on a Cary Eclipse Fluorescence
Agilent spectrophotometer (Santa Clara, Califoria, United States) in a 10 mm path length quartz cuvette. Differential pulsed voltammetry (DPV) characterizations were performed in glove box in a three-electrode glass cell using a glassy carbon pin as the working electrode (WE, diameter of 2 mm), a platinum mesh as the counter electrode (CE) and Ag/AgCl wire as the quasi-reference electrode (QRE), using an EG&G Princeton Applied 2273 potentiostat/galvanostat. The electrolyte solution ($(Bu_4N)ClO_4$ 0.1 M in CH_2Cl_2, referred to as TCDCM01), sample solutions (0.005 M in TCDCM01) and the calibration solution (Ferrocene 0.001 M in TCDCM01), were prepared and stored in the glove box. HOMO values were calculated from the half-wave maximum of the DPV plot. The potential

values of -4.6 eV for NHE vs. vacuum and of 0.2 V for Fc/Fc+ vs. NHE were used in potential/energy conversions.[77]

2.5.4.2. General Procedure for Emulsion Couplings and E-factor Calculations

1 L of K-EL 2 wt%:toluene (9:1 v/v) emulsion is prepared homogenizing a 2 wt% aqueous dispersion of K-EL (18 g of Kolliphor EL in 882 mL of deionized water) with 100 mL of toluene using a T 25 digital ULTRA-TURRAX® until a stable, milky dispersion is obtained. All reactions were carried out in a pressure-tight 10 mL screw-cap glass tube equipped with a cylindrical stirring bar in vertical position, under magnetic stirring at 1000 rpm for 24 h and at a nominal concentration for the reagents of 0.5 mol/L. Reactions were extracted with CH_2Cl_2, filtered on a pad of silica gel and submitted to GC–MS characterization. Yields of product and by-products were assessed by GC–MS using a simple semiquantitative area normalization method. As the reported reactions are palladium mediated C-C couplings, water has always been taken into account for the calculation of the E-factor. In fact, it can be contaminated with palladium, and it therefore must be considered an hazardous waste. For this reason, inorganic bases used in the reactions are included as well in the waste calculation, as they remain dissolved in the aqueous phase. For waste calculations, standard conditions for flash chromatography were applied (column dimensions: d=2 cm, h=15 cm, SiO_2 50 g and 200 mL of eluent mixture for around 1 g of reagents mixture).

2.5.4.2.1. Synthesis of 2-(4-methoxyphenyl)-5-hexylthiophene (model compound, 1)

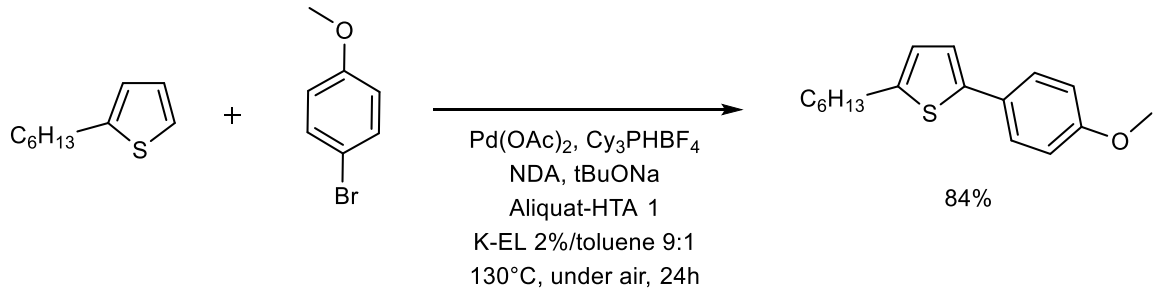

2-hexylthiophene (0.168 g, 1.0 mmol), 4-bromoanisole (0.187 g, 1.0 mmol), $Pd(OAc)_2$ (0.005 g, 0.02 mmol), Cy_3PHBF_4 (0.015 g, 0.04 mmol), *t*BuONa (0.288 g, 3.0 mmol), neodecanoic acid (0.052 g, 0.3 mmol), Aliquat HTA-1 35%wt in H_2O (0.226 g, 0.3 mmol) are weighted in the pressure-tight 10 mL screw-cap glass tube, then 2 mL of K-EL 2 wt%-toluene (9:1 v/v, 2 mL) oil-in-water emulsion are added. The reaction mixture is stirred and allowed to homogenize for 5 min at RT, subsequently it is heated under stirring at 130°C through oil bath for 24 h. The mixture is cooled, then diluted with 8 mL of water and filtered. The crude was purified by column chromatography (17.75 g of silica) using a mixture of petroleum ether/ dichloromethane 7:3 (71 mL) as eluent. The pure product was isolated as a brownish solid in 84% yield (231 mg, 0.84 mmol). Mp: 58-59 °C.

^{1}H-NMR (400 MHz, CDCl3): δ 7.52 (d, J=8.4 Hz, 2H), 7.03 (d, J=3.6 Hz, 1H), 6.92 (d, J=8.4 Hz, 2H), 6.74 (d, J=3.6 Hz, 1H), 3.84 (s, 3H), 2.84 (t, J=7.5 Hz, 2H), 1.77–1.70 (m, 2H), 1.45–1.32 (m, 6H), 0.95 (t, J=7.5 Hz, 3H).

^{13}C-NMR (100 MHz, CDCl3): δ 158.8, 144.7, 141.5, 127.7, 127.5, 127.3, 126.9, 126.7, 124.8, 121.6, 114.5, 114.2, 113.8, 55.3, 31.63, 31.59, 30.2, 28.8, 22.6, 14.1.

E-factor calculation

$$E_{factor} = \frac{mass\ of\ reagents + mass\ of\ auxiliaries - mass\ of\ product}{mass\ of\ product} = \\ = \frac{2.9144 + 86.881 - 0.231}{0.231} = 388$$

UV-Vis absorption and PL spectra for derivative 1

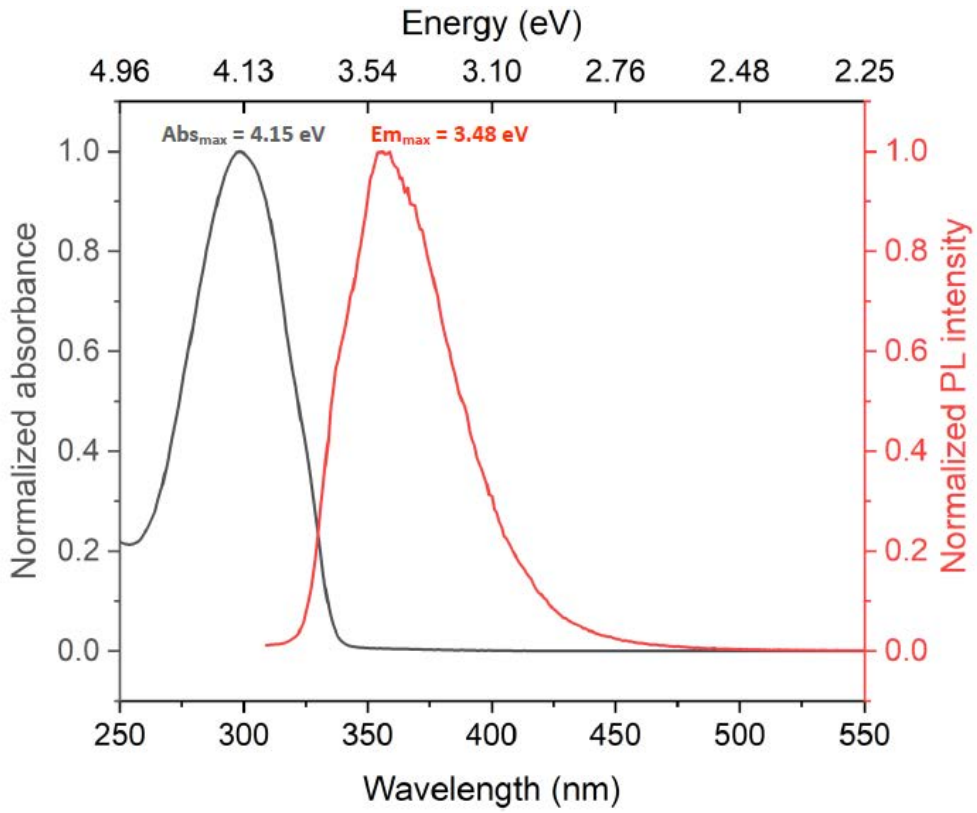

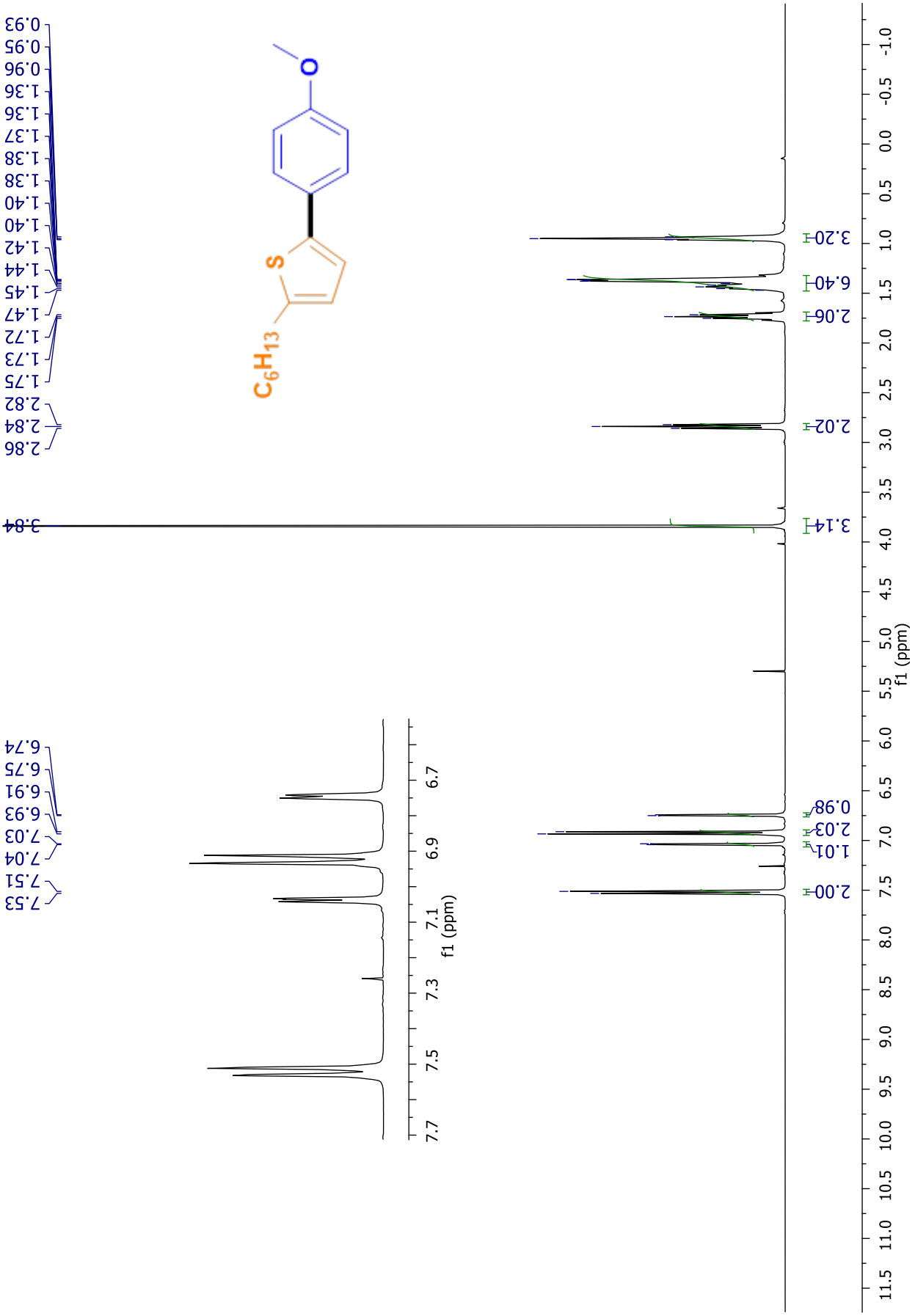

^{1}H-NMR spectrum of derivative 1.

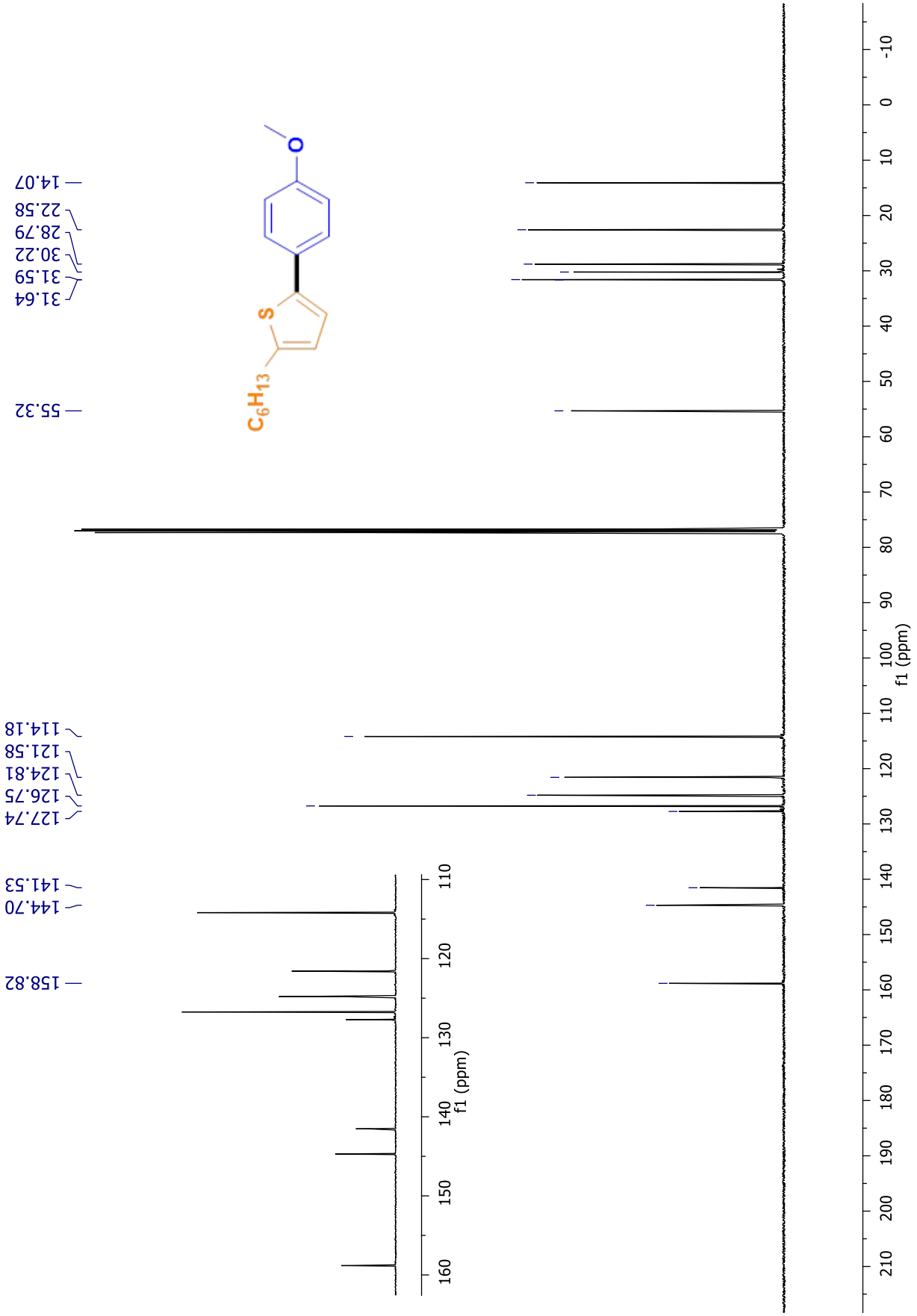

^{13}C-NMR spectrum of derivative 1.

2.5.4.2.2. Synthesis of 2,3-dihydro-5,7-bis(4-methoxyphenyl)thieno[3,4 b][1,4] dioxine (8)

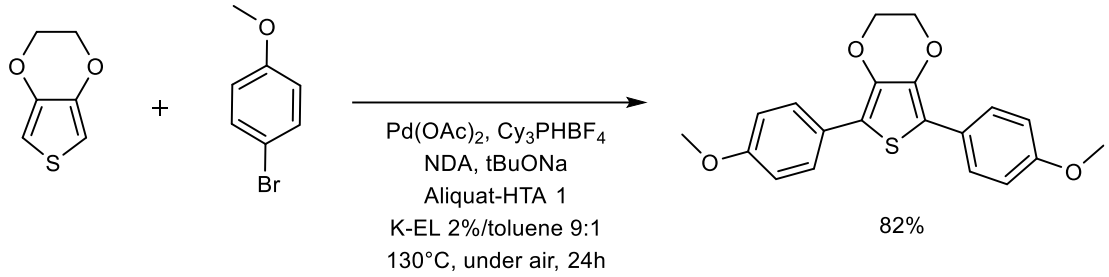

3,4-ethylenedioxythiophene (0.142 g, 1.0 mmol), 4-bromoanisole (0.374 g, 2.0 mmol), Pd(OAc)2 (0.009 g, 0.04 mmol), Cy3PHBF4 (0.030 g, 0.08 mmol), *t*BuONa (0.288 g, 3.0 mmol), neodecanoic acid (0.104 g, 0.6 mmol), Aliquat HTA-1 35%wt in H2O (0.452 g, 0.6 mmol) are weighted in the pressure-tight 10 mL screw-cap glass tube, then 2 mL of K-EL 2 wt%-toluene (9:1 v/v, 2 mL) oil-in-water emulsion are added. The reaction mixture is stirred and allowed to homogenize for 5 min at RT, subsequently it is heated under stirring at 130°C through oil bath for 24 h. The mixture is cooled, then diluted with 8 mL of methanol and filtered. The crude was purified by filtration on a pad of silica gel (15 g) with CH2Cl2 (30 mL). The pure product was obtained by recrystallization from toluene (5 mL) and isolated as a yellowish solid in 82% yield (291 mg, 0.82 mmol). Mp: 178-179 °C.

^{1}H-NMR (400 MHz, CD2Cl2): δ 7.70 (d, J = 8.82 Hz, 4H), 6.95 (d, J = 8.82 Hz, 4H), 4.37 (s, 4H), 3.86 (s, 6H).

^{13}C-NMR (100 MHz, CD2Cl2): δ 158.4, 137.8, 127.2, 125.8, 114.0, 113.8, 64.6, 55.3.

E-factor calculation for derivative 8

$$E_{factor} = \frac{mass\ of\ reagents + mass\ of\ auxiliaries - mass\ of\ product}{mass\ of\ product} = \\ = \frac{3.3724 + 65.571 - 0.291}{0.291} = 236$$

UV-Vis absorption, PL spectra and DPV plot for derivative 8

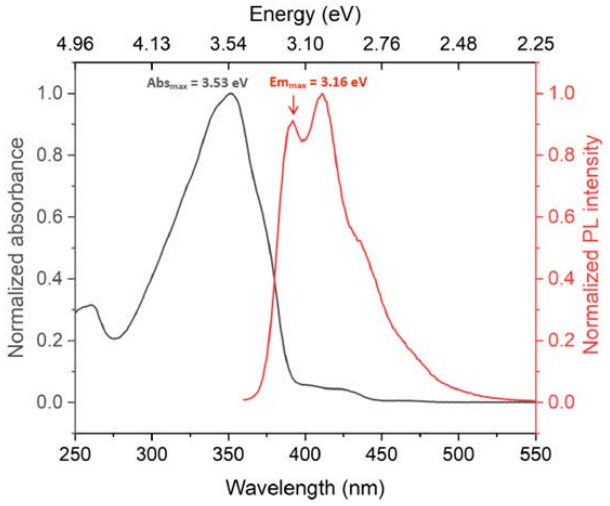

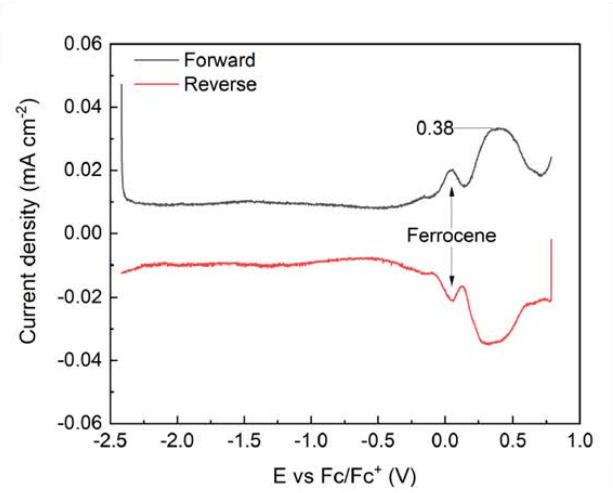

Stokes shift = 0.37 eV.

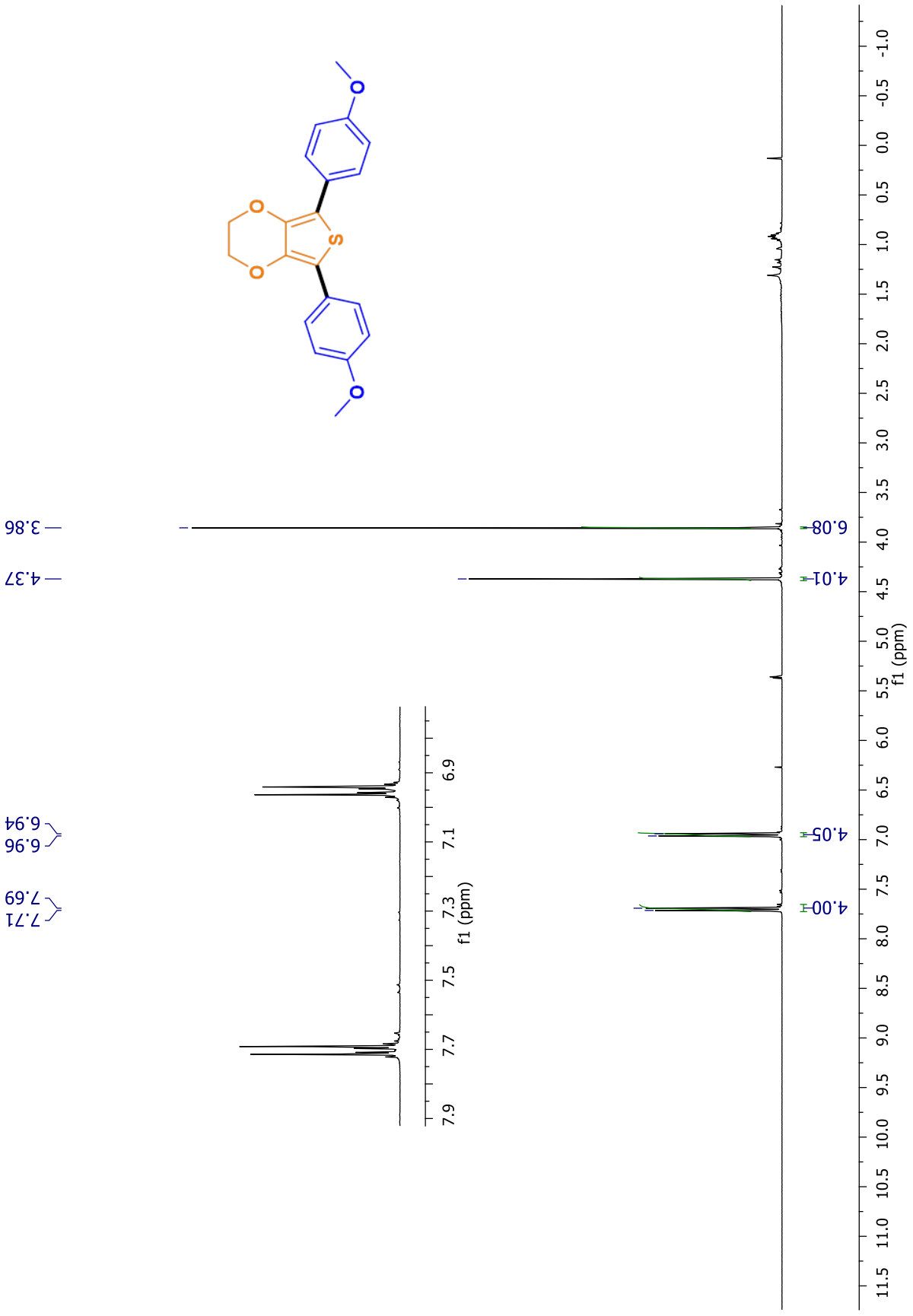

[1]H-NMR spectrum of derivative 8.

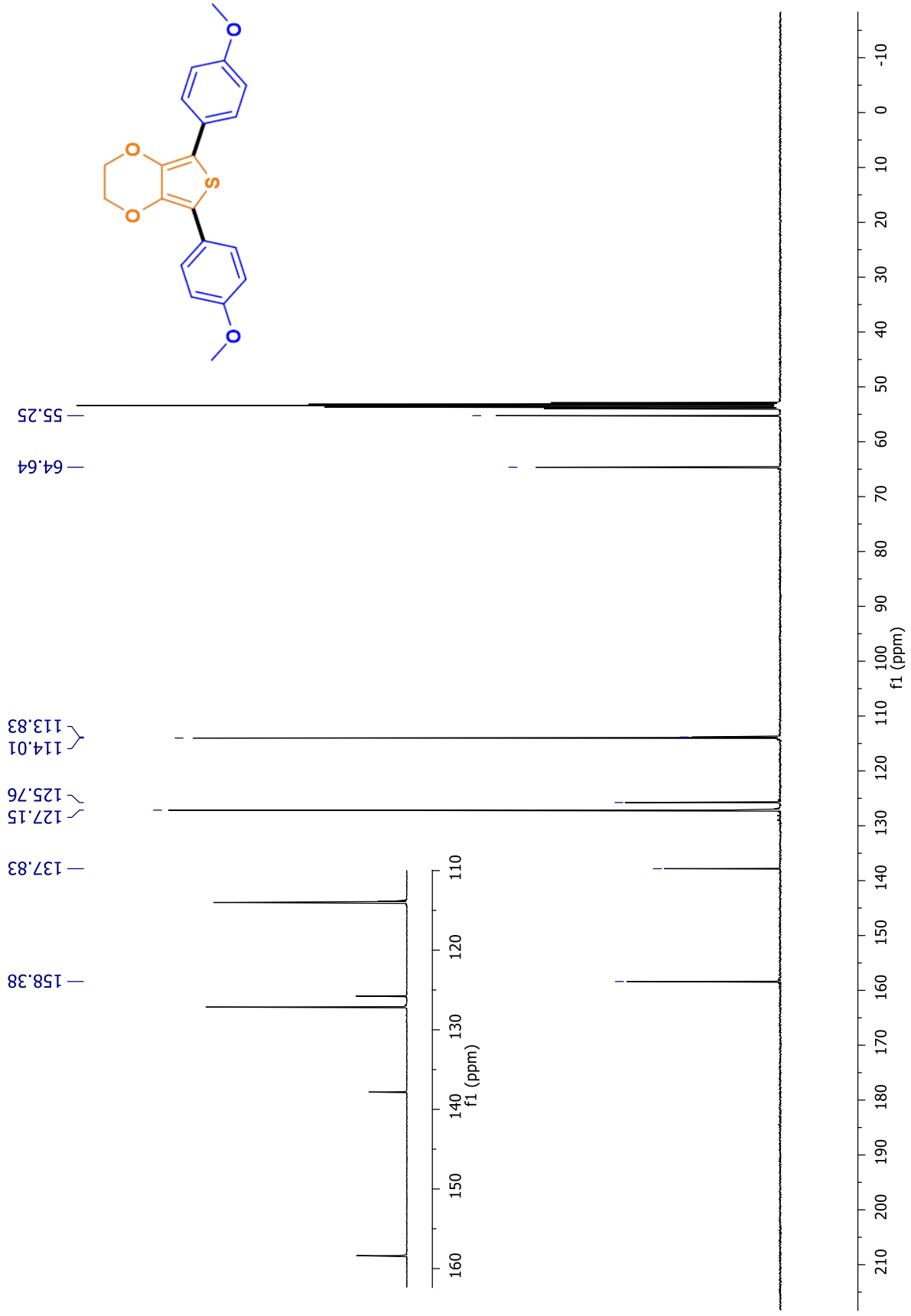

^{13}C-NMR spectrum of derivative 8.

2.5.4.2.3. Synthesis of 2,3-dihydro-5,7-bis(4-methylnaphthyl)thieno[3,4-b][1,4]dioxine (9)

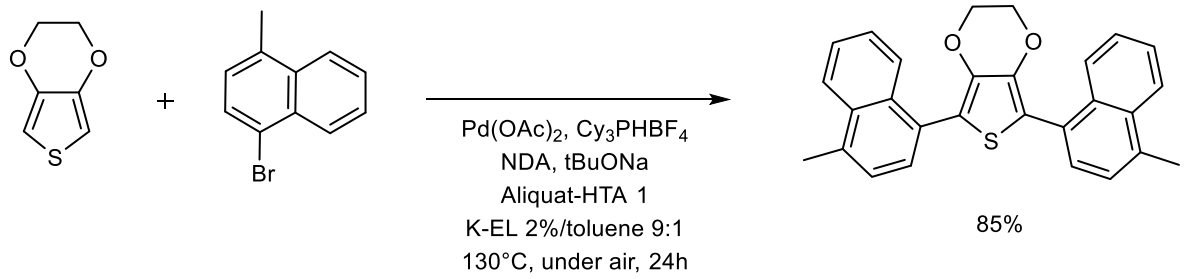

3,4-ethylenedioxythiophene (0.142 g, 1.0 mmol), 1-bromo-4-methylnaphtalene (0.442 g, 2.0 mmol), Pd(OAc)2 (0.009 g, 0.04 mmol), Cy3PHBF4 (0.030 g, 0.08 mmol), *t*BuONa (0.288 g, 3.0 mmol), neodecanoic acid (0.104 g, 0.6 mmol), Aliquat HTA-1 35%wt in H2O (0.452 g, 0.6 mmol) are weighted in the pressure-tight 10 mL screw-cap glass tube, then 2 mL of K-EL 2 wt%-toluene (9:1 v/v, 2 mL) oil-in-water emulsion are added. The reaction mixture is stirred and allowed to homogenize for 5 min at RT, subsequently it is heated under stirring at 130°C through oil bath for 24 h. The mixture is cooled, then diluted with 8 mL of methanol and filtered. The crude was purified by filtration on a pad of silica gel (15 g) with CH2Cl2 (30 mL). The pure product was isolated as a pale-yellow solid in 85% yield (360 mg, 0.85 mmol). Mp: 240-241 °C. Anal. Calcd for $C_{28}H_{22}O_2S$: C, 79.59; H, 5.25; O, 7.57. Found: C, 79.73; H, 5.43; O, 7.28.

^{1}H-NMR (400 MHz, CDCl3) δ 8.26 – 8.24 (m, 2H), 8.10 – 8.07 (m, 2H), 7.61 – 7.58 (m, 6 H), 7.41 (d, *J* = 7.2 Hz, 2H), 4.27 (s, 4H), 2.76 (s, 6H).

^{13}C-NMR (100 MHz, CDCl3) δ 137.72, 135.05, 132.95, 131.90, 128.80, 128.09, 127.13, 126.28, 125.88, 125.87, 124.47, 114.79, 64.71, 19.65.

E-factor calculation for derivative 9

$$E_{factor} = \frac{mass\ of\ reagents + mass\ of\ auxiliaries - mass\ of\ product}{mass\ of\ product} = \\ = \frac{3.4404 + 61.236 - 0.360}{0.360} = 179$$

UV-Vis absorption, PL spectra and DPV plot for derivative 9

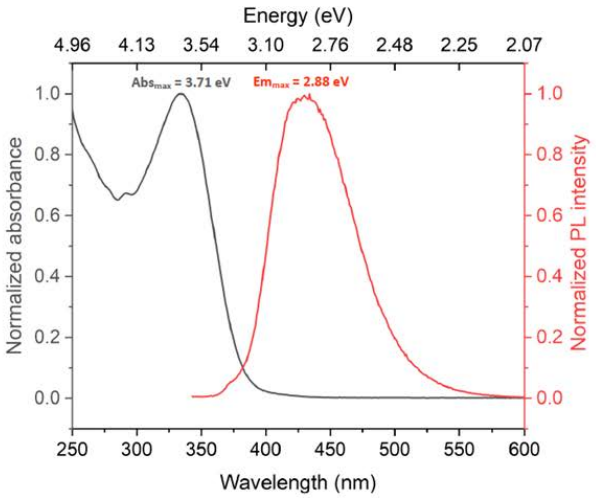

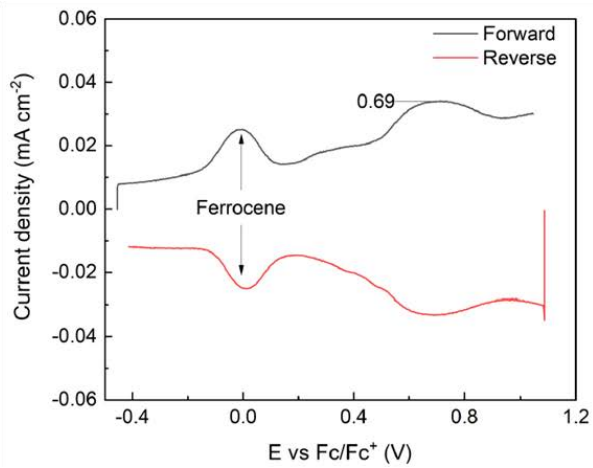

Stokes shift = 0.83 eV.

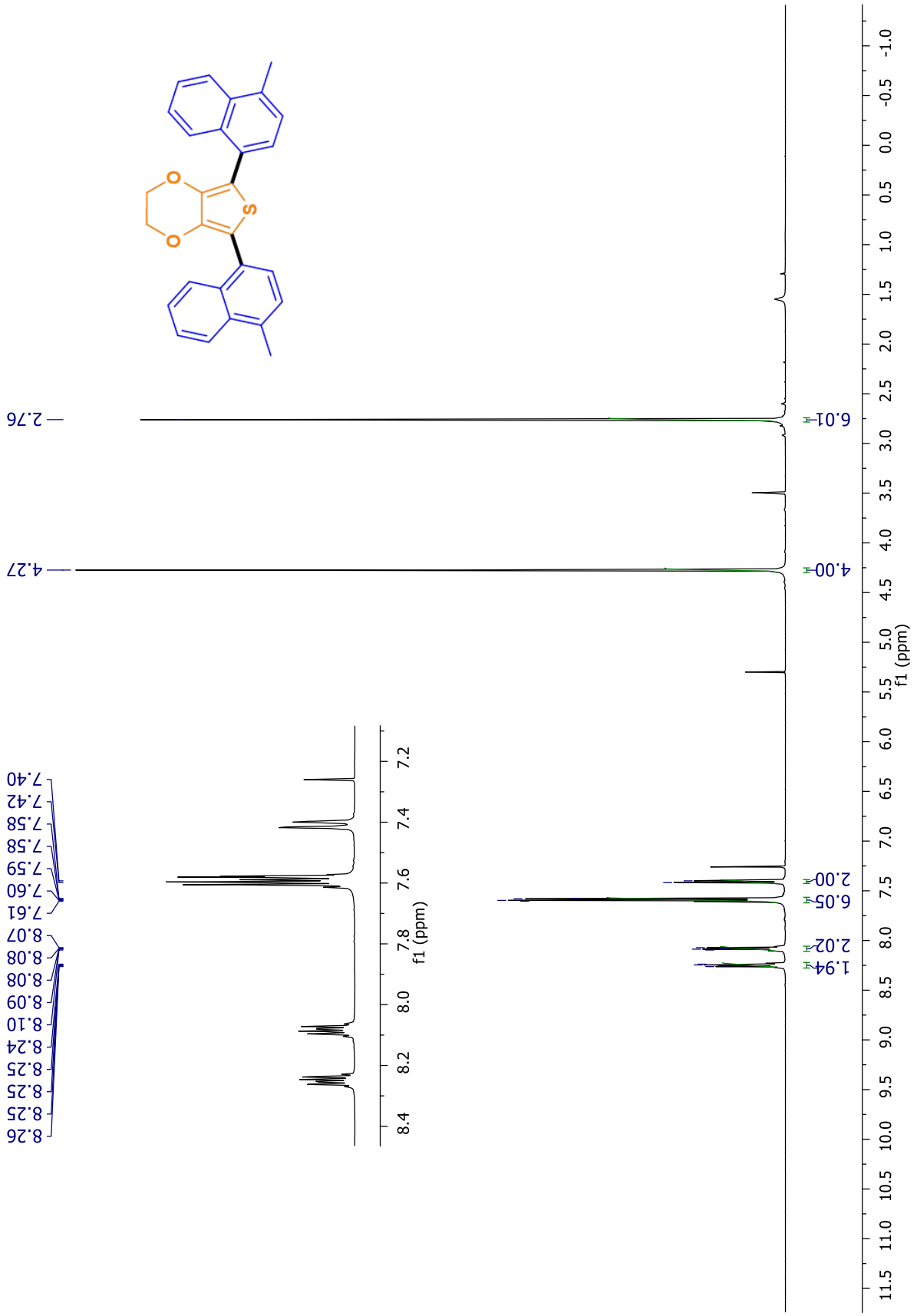

^{1}H-NMR spectrum of derivative 9.

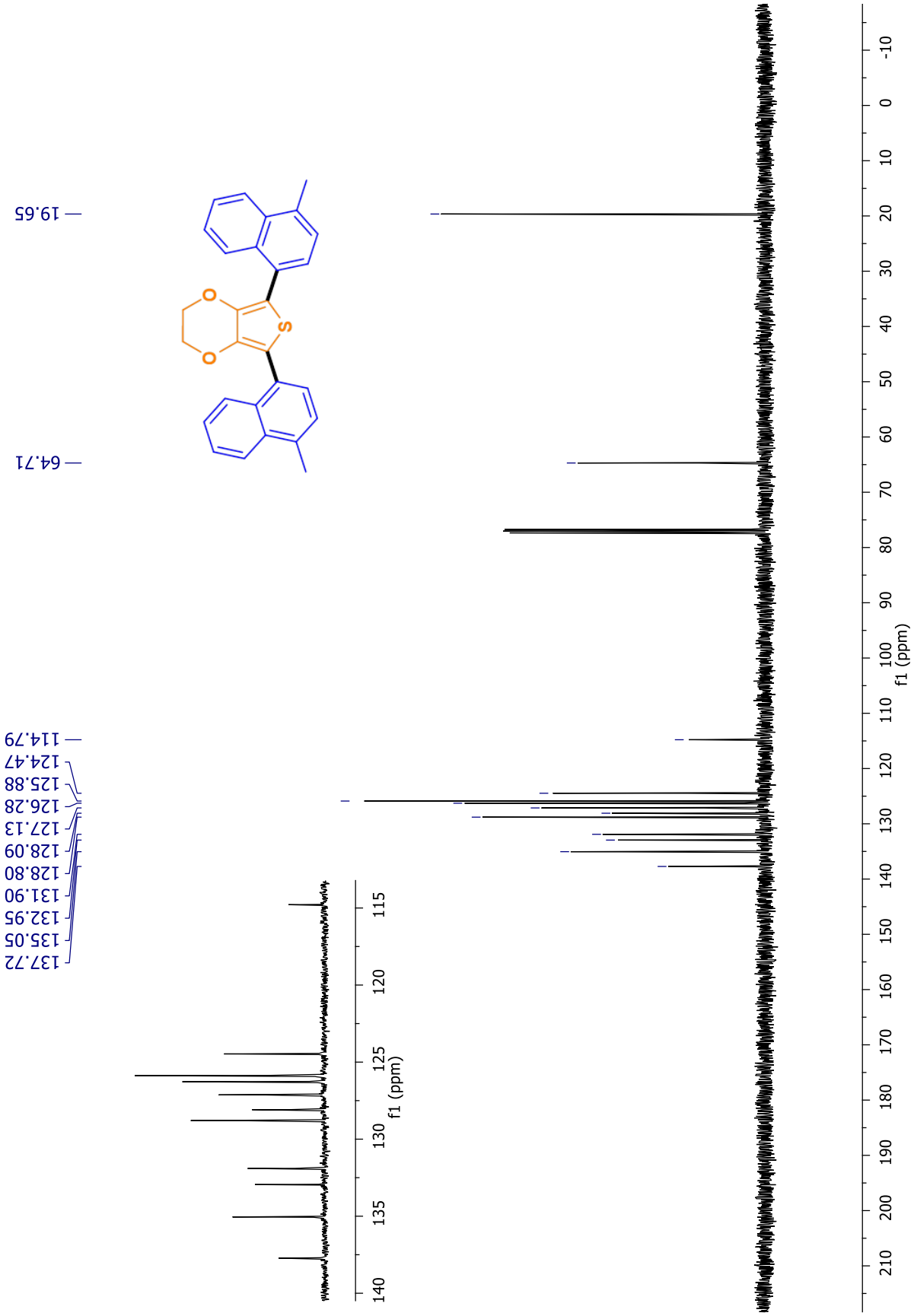

^{13}C-NMR spectrum of derivative 9.

2.5.4.2.4. Synthesis of 2-(5-hexyl)-2-thienyl-[1]benzothieno[3,2-b][1]benzothiophene (10)

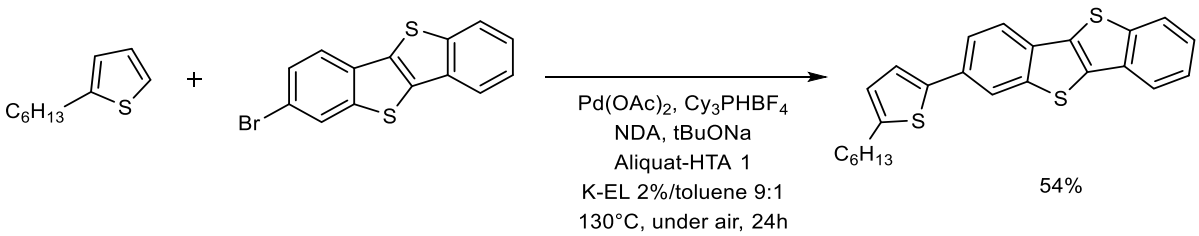

2-bromo-[1]benzothieno[3,2-b][1]benzothiophene (0.320 g, 1.0 mmol), 2-hexylthiophene (0.168 g, 1.0 mmol), Pd(OAc)2 (0.005 g, 0.02 mmol), Cy3PHBF4 (0.015 g, 0.04 mmol), *t*BuONa (0.288 g, 3.0 mmol), neodecanoic acid (0.052 g, 0.3 mmol), Aliquat HTA-1 35%wt in H2O (0.226 g, 0.3 mmol) are weighted in the pressure-tight 10 mL screw-cap glass tube, then 2 mL of K-EL 2 wt%-toluene (9:1 v/v, 2 mL) oil-in-water emulsion are added. The reaction mixture is stirred and allowed to homogenize for 5 min at RT, subsequently it is heated under stirring at 130°C through oil bath for 24 h. The mixture is cooled, then diluted with 8 mL of methanol and filtered. The crude was purified by column chromatography (24.4 g of silica) using a mixture of petroleum ether/dichloromethane 9:1 (97.5 mL) as eluent. The pure product was isolated as a pale-yellow solid in 54% yield (0.220 g, 0.54 mmol). Mp: 184-185 °C.

^{1}H-NMR (400 MHz, CDCl3) δ 8.08 (d, *J* = 1.3 Hz, 1H), 7.92 (d, *J* = 8.0 Hz, 1H), 7.88 (d, *J* = 7.7 Hz, 1H), 7.84 (d, *J* = 8.3 Hz, 1H), 7.66 (dd, *J* = 8.3, 1.6 Hz, 1H), 7.48 – 7.44 (m, 1H), 7.43 – 7.38 (m, 1H), 7.22 (d, *J* = 3.5 Hz, 1H), 6.79 (d, *J* = 3.6 Hz, 1H), 2.85 (t, *J* = 7.6 Hz, 2H), 1.73 (dt, *J* = 15.3, 7.6 Hz, 2H), 1.46 – 1.29 (m, 6H), 0.91 (t, *J* = 7.1 Hz, 3H).

^{13}C-NMR (126 MHz, CDCl3) δ 147.10, 143.97, 143.13, 142.04, 134.37, 134.20, 133.99, 132.89, 132.72, 126.11, 125.85, 125.80, 124.90, 123.98, 123.82, 122.61, 122.41, 121.26, 32.50, 32.47, 31.19, 29.67, 23.47, 14.97.

E-factor calculation for derivative 10

$$E_{factor} = \frac{mass\ of\ reagents + mass\ of\ auxiliaries - mass\ of\ product}{mass\ of\ product} = \\ = \frac{3.0474 + 101.691 - 0.220}{0.220} = 475$$

UV-Vis absorption, PL spectra and DPV plot for derivative 10

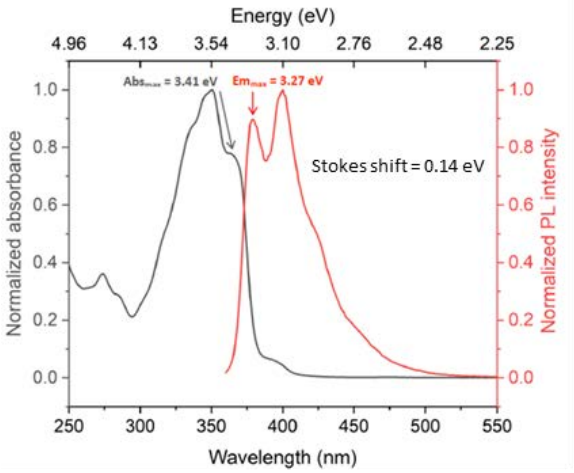

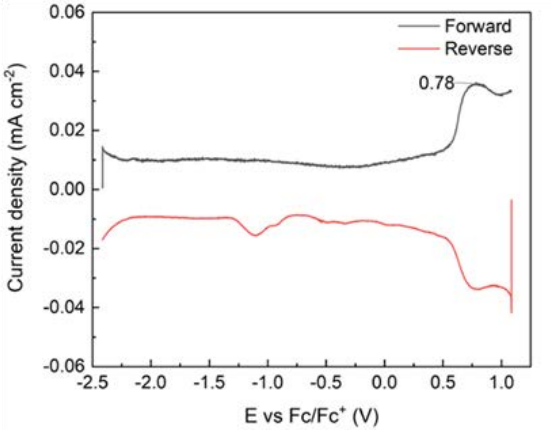

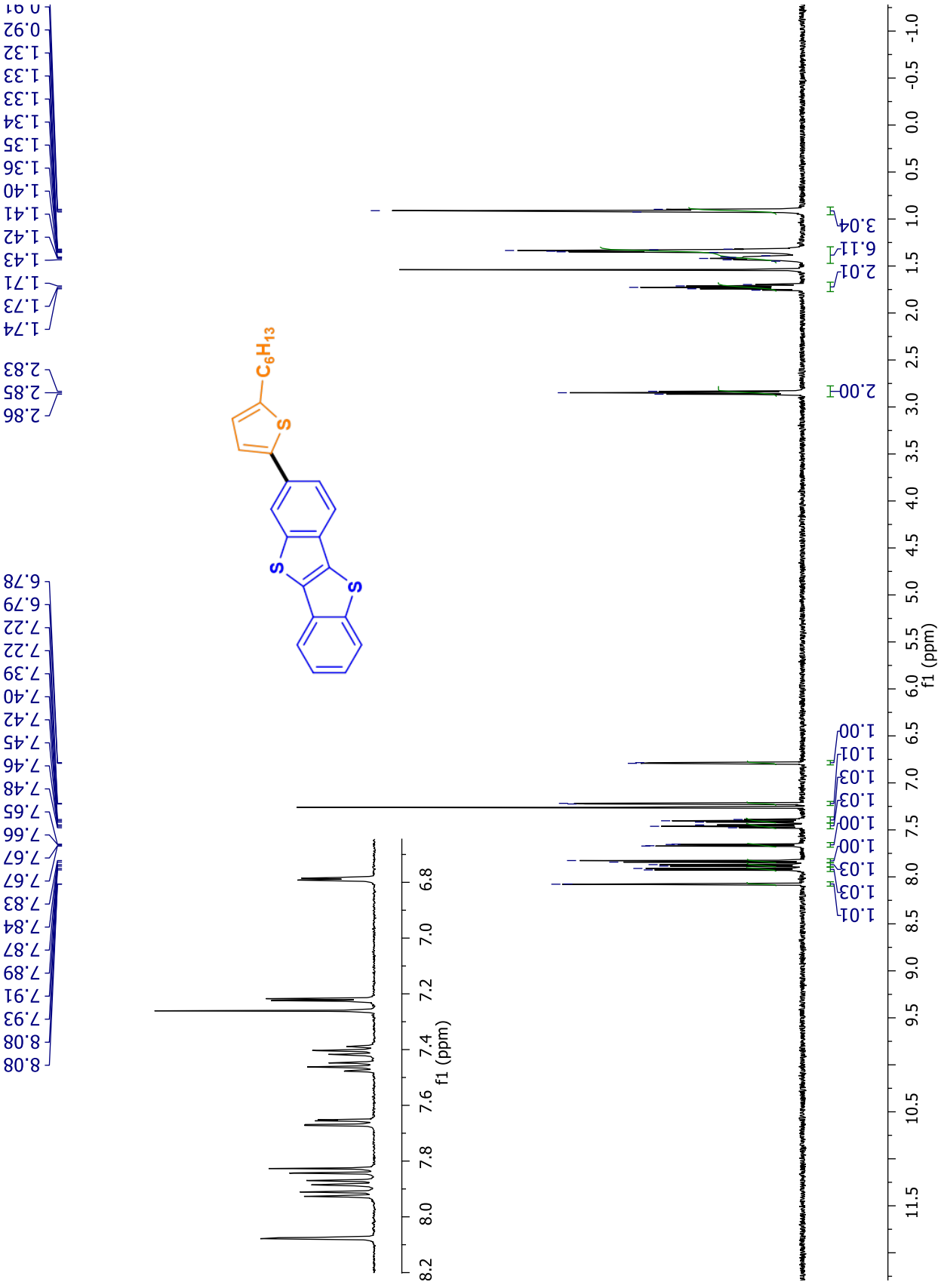

^{1}H-NMR spectrum of derivative 10.

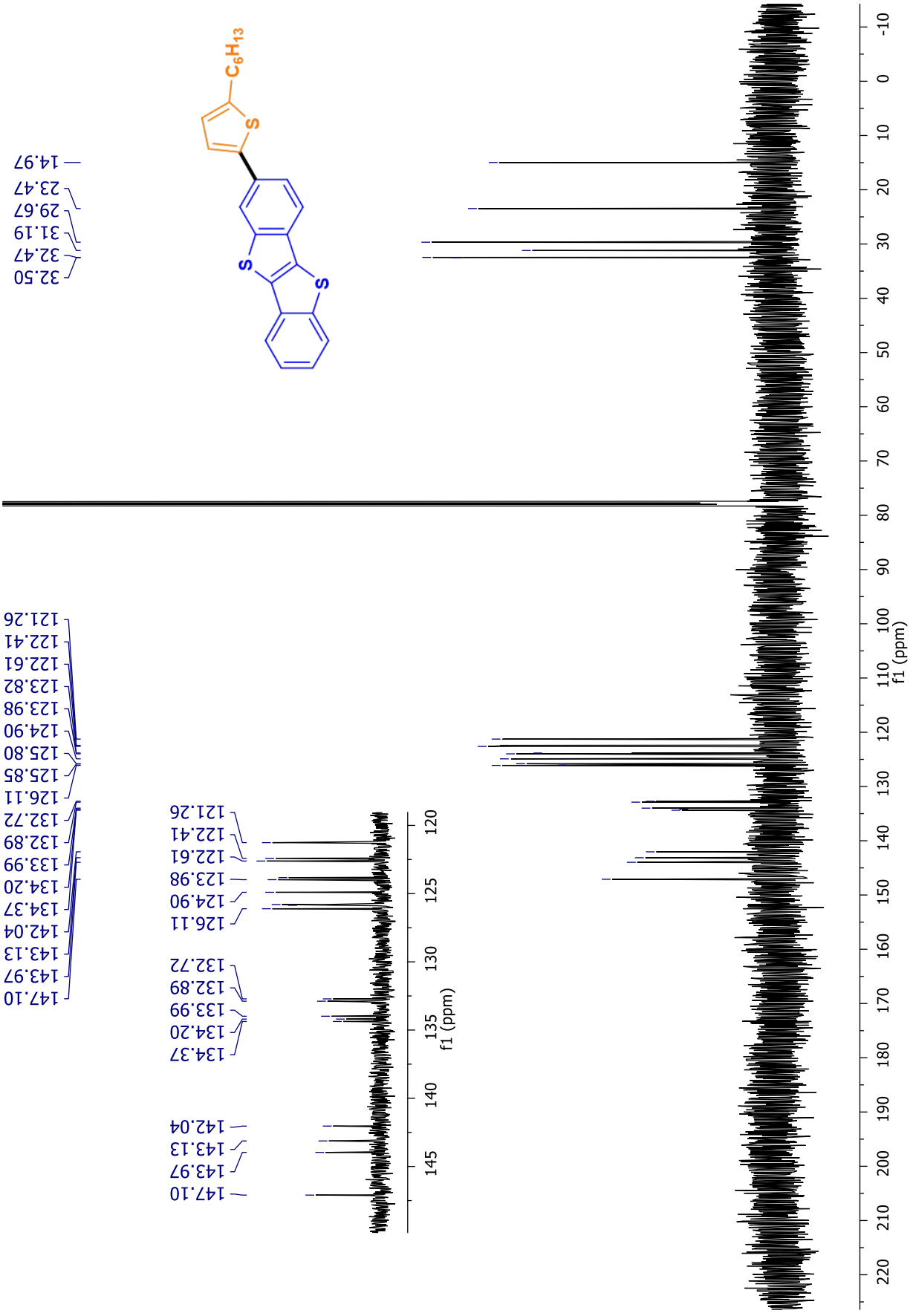

^{13}C-NMR spectrum of derivative 10.

2.5.4.2.5. Synthesis of 5,5'-bis(3-hexylphenyl)-2,2'-bithiophene (11)

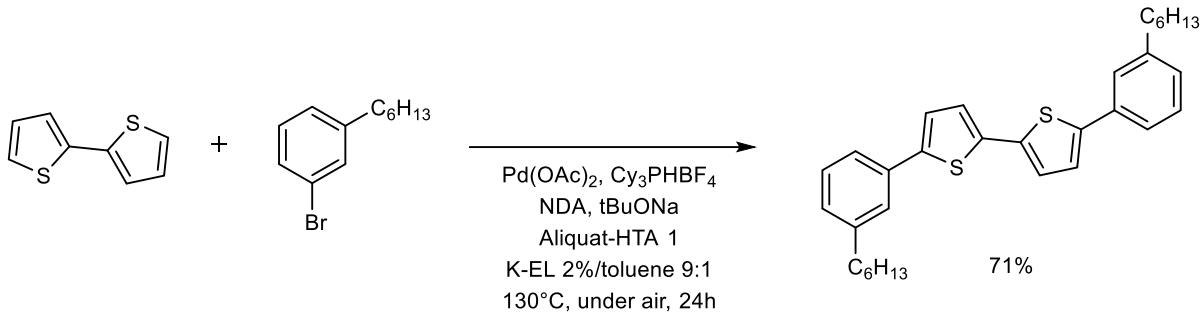

2,2'-bithiophene (0.166 g, 1.0 mmol), 1-bromo-3-hexylbenzene (0.482 g, 2.0 mmol), Pd(OAc)2 (0.009 g, 0.04 mmol), Cy3PHBF4 (0.030 g, 0.08 mmol), *t*BuONa (0.288 g, 3.0 mmol), neodecanoic acid (0.104 g, 0.6 mmol), Aliquat HTA-1 35%wt in H2O (0.452 g, 0.6 mmol) are weighted in the pressure-tight 10 mL screw-cap glass tube, then 2 mL of K-EL 2 wt%-toluene (9:1 v/v, 2 mL) oil-in-water emulsion are added. The reaction mixture is stirred and allowed to homogenize for 5 min at RT, subsequently it is heated under stirring at 130 °C through oil bath for 24 h. The mixture is cooled, then diluted with 8 mL of methanol and filtered. The crude was purified by filtration on a pad of silica gel (15 g) with CH2Cl2 (30 mL). The pure product was isolated as a yellowish solid in 71% yield (348 mg, 0.71 mmol). Mp: 111-112 °C. Anal. Calcd for $C_{32}H_{38}S_2$: C,78.96; H, 7.87. Found: C, 78.60; H, 7.91.

^{1}H-NMR (400 MHz, CDCl3) δ 7.45 – 7.41 (m, 4H), 7.32 – 7.27 (m, 2H), 7.24 (d, *J* = 3.8 Hz, 2H), 7.17 (d, *J* = 3.8 Hz, 2H), 7.12 (dt, *J* = 7.6, 1.2 Hz, 2H), 2.65 (t, *J* = 7.6 Hz, 4H), 1.66 (m, 4H), 1.44 – 1.27 (m, 12H), 0.90 (t, *J* = 7.1 Hz, 6H).

^{13}C-NMR (100 MHz, CDCl3) δ 143.72, 143.37, 136.58, 133.93, 128.82, 127.80, 125.71, 124.32, 123.65, 122.98, 35.97, 31.73, 31.44, 29.02, 22.61, 14.10.

E-factor calculation for derivative 11

$$E_{factor} = \frac{mass\ of\ reagents + mass\ of\ auxiliaries - mass\ of\ product}{mass\ of\ product} = \\ = \frac{3.5044 + 61.236 - 0.348}{0.348} = 475$$

UV-Vis absorption, PL spectra and DPV plot for derivative 11

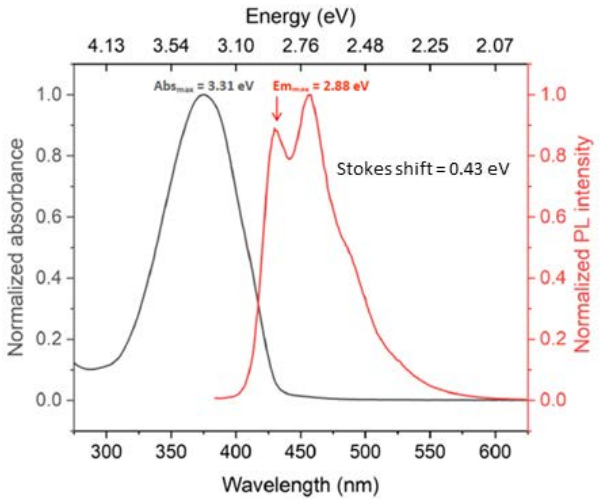

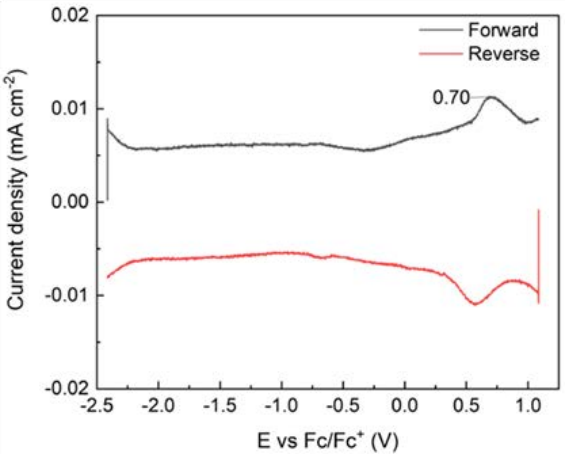

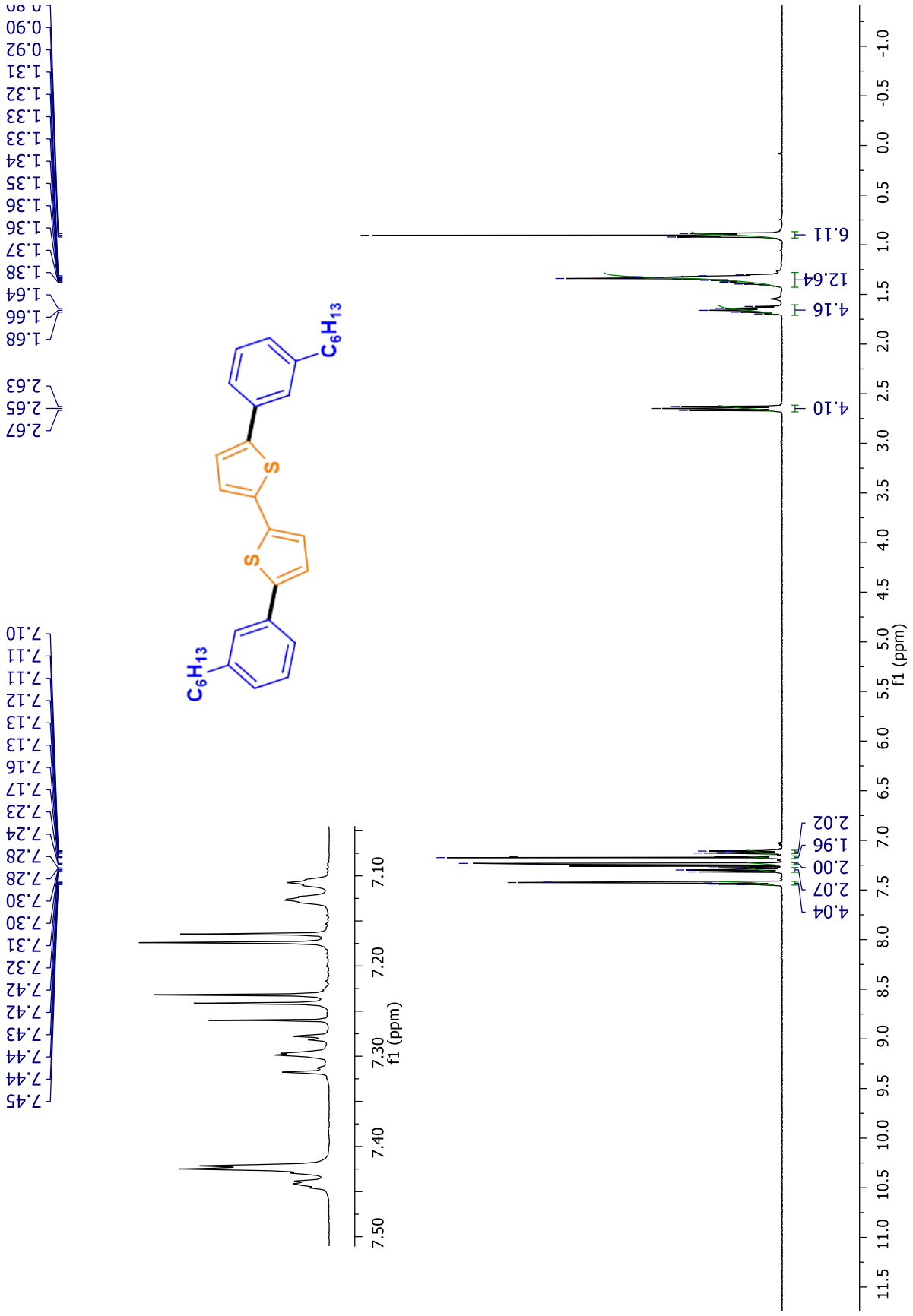

^{1}H-NMR spectrum of derivative 11.

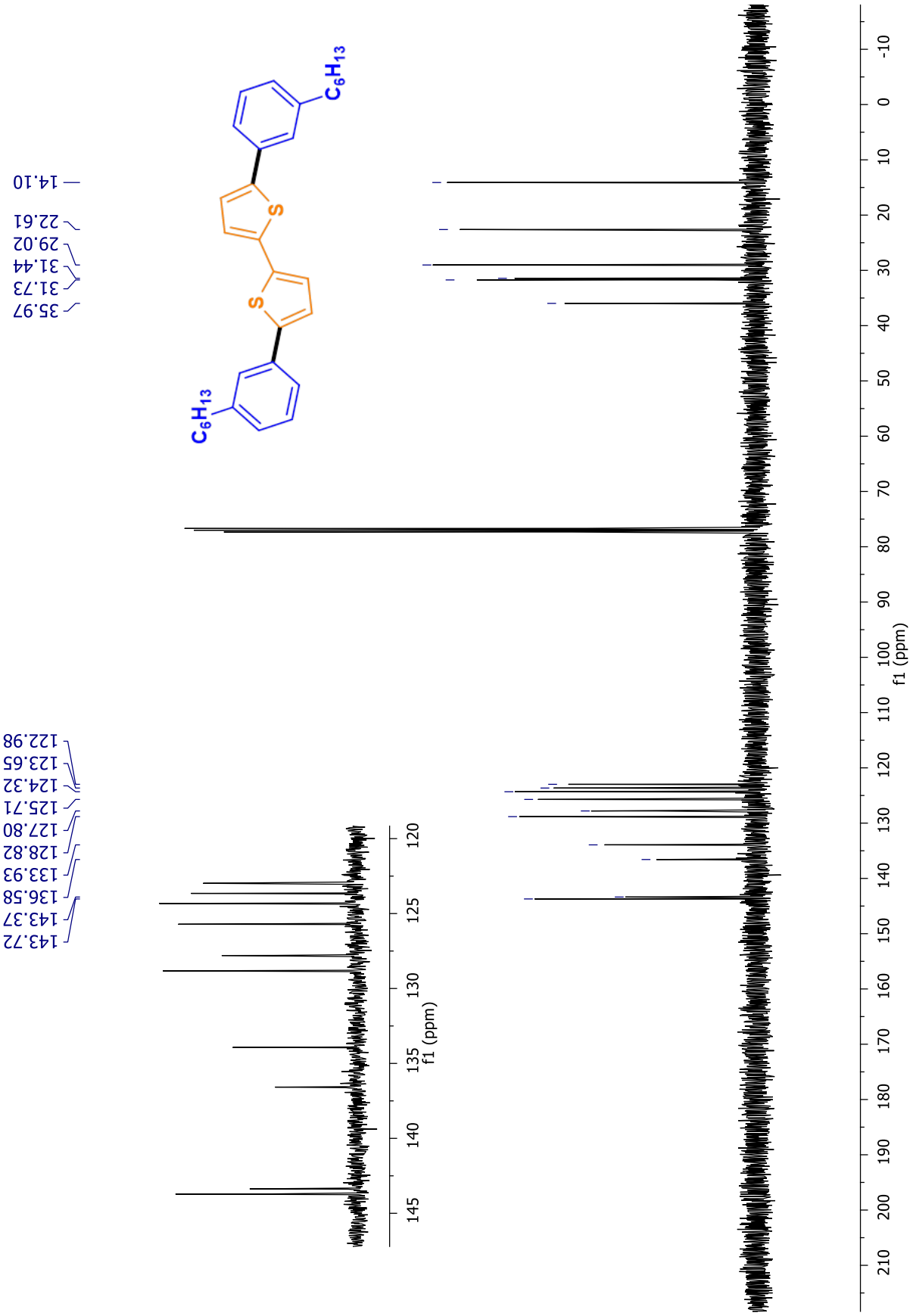

^{13}C-NMR spectrum of derivative 11.

2.5.4.2.6. Synthesis of 2,5-bis(3-hexylphenyl)thieno[3,2-b]thiophene (12)

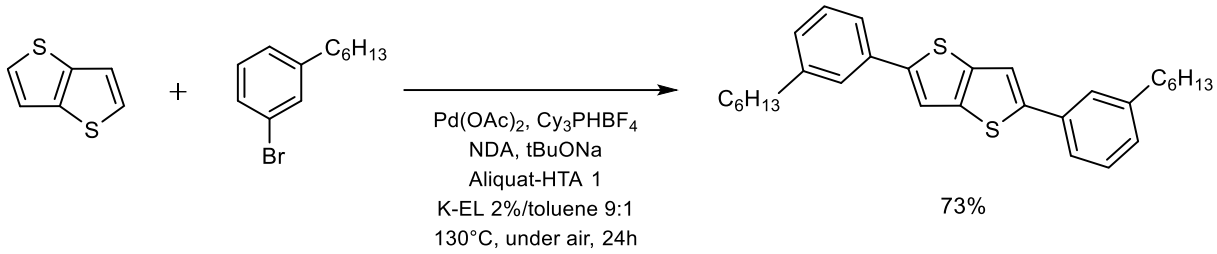

Thieno[3,2-b]thiophene (0.140 g, 1.0 mmol), 1-bromo-3-hexylbenzene (0.482 g, 2.0 mmol), Pd(OAc)2 (0.009 g, 0.04 mmol), Cy3PHBF4 (0.030 g, 0.08 mmol), *t*BuONa (0.288 g, 3.0 mmol), neodecanoic acid (0.104 g, 0.6 mmol), Aliquat HTA-1 35%wt in H2O (0.452 g, 0.6 mmol) are weighted in the pressure-tight 10 mL screw-cap glass tube, then 2 mL of K-EL 2 wt%-toluene (9:1 v/v, 2 mL) oil-in-water emulsion are added. The reaction mixture is stirred and allowed to homogenize for 5 min at RT, subsequently it is heated under stirring at 130°C through oil bath for 24 h. The mixture is cooled, then diluted with 8 mL of methanol and filtered. The crude was purified by filtration on a pad of silica gel (15 g) with CH2Cl2 (30 mL). The product was recrystallized from heptane (20 mL) and isolated as a golden solid in 73% yield (336 mg, 0.73 mmol). Mp: 130-131 °C. Anal. Calcd for $C_{30}H_{36}S_2$: C,78.21; H, 7.88. Found: C, 78.03; H, 7.99.

^{1}H-NMR (400 MHz, CDCl3) δ 7.48 – 7.44 (m, 6H), 7.34 – 7.28 (m, 2H), 7.15 – 7.11 (m, 2H), 2.66 (t, *J* = 7.6 Hz, 4H), 1.71-1.62 (m, 4H), 1.40-1.31 (m, 12H), 0.91 (t, *J* = 7.1 Hz, 6H).

^{13}C-NMR (100 MHz, CDCl3) δ 146.01, 143.76, 139.14, 134.62, 128.87, 127.96, 125.85, 123.17, 115.38, 35.97, 31.72, 31.42, 29.02, 22.61, 14.09.

E-factor calculation for derivative 12

$$E_{factor} = \frac{mass\ of\ reagents + mass\ of\ auxiliaries - mass\ of\ product}{mass\ of\ product} = \\ = \frac{3.4784 + 74.916 - 0.336}{0.336} = 232$$

UV-Vis absorption, PL spectra and DPV plot for derivative 12

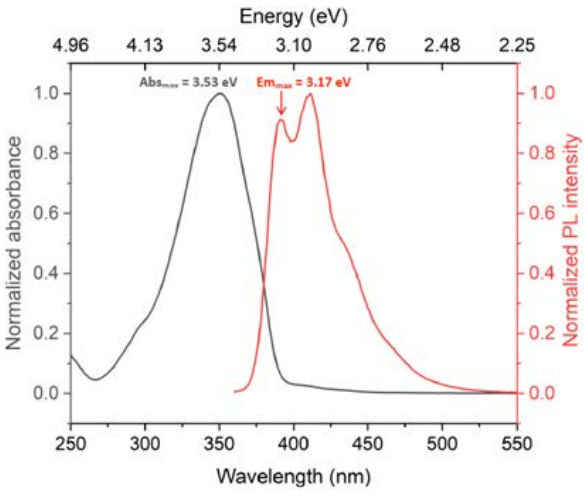

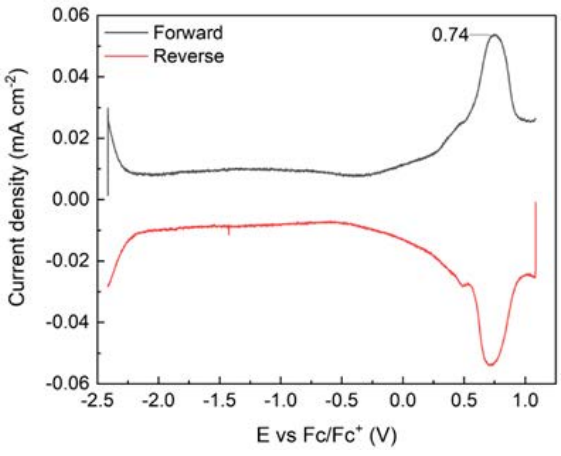

Stokes shift: 0.36 eV.

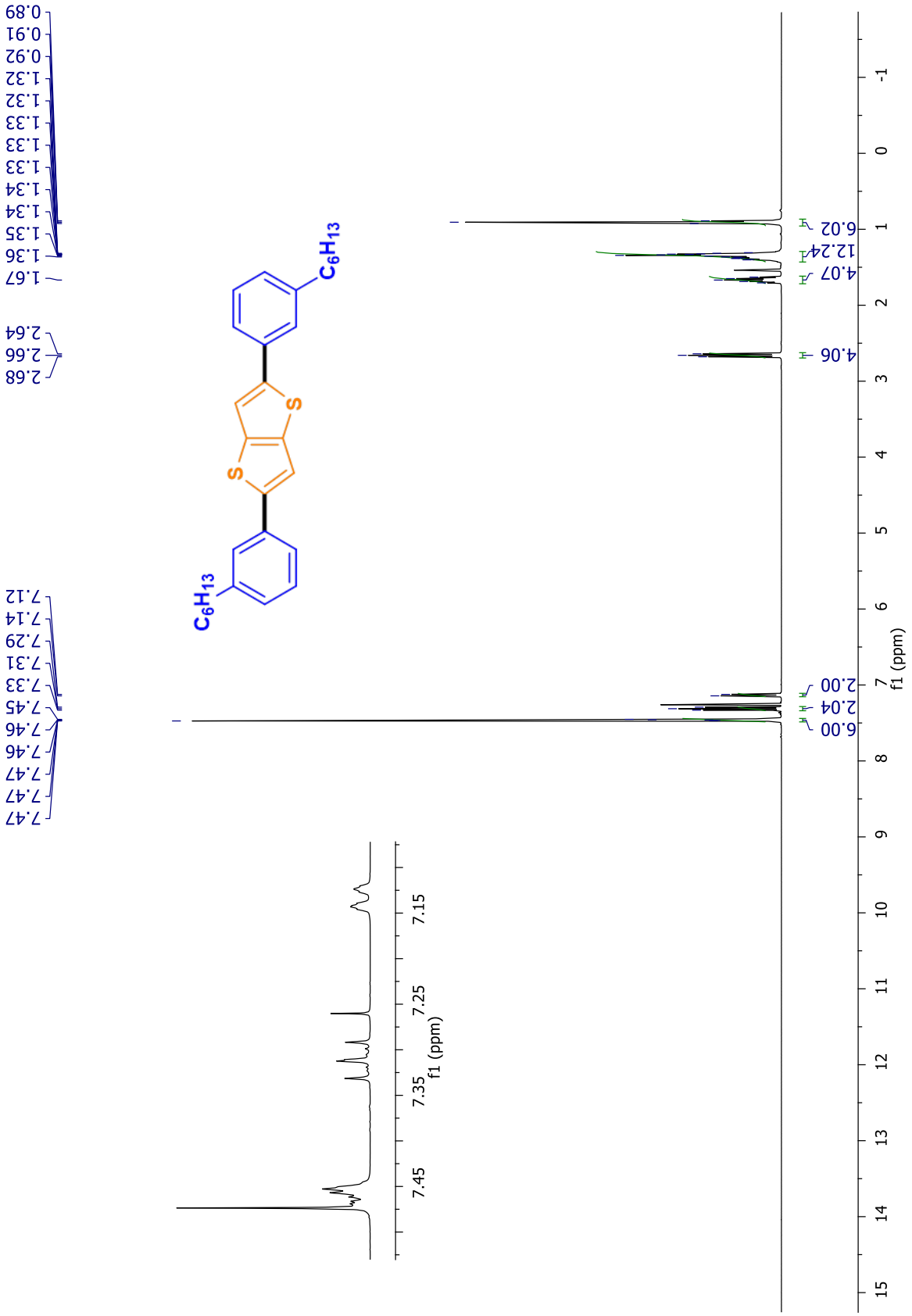

[1]H-NMR spectrum of derivative 12.

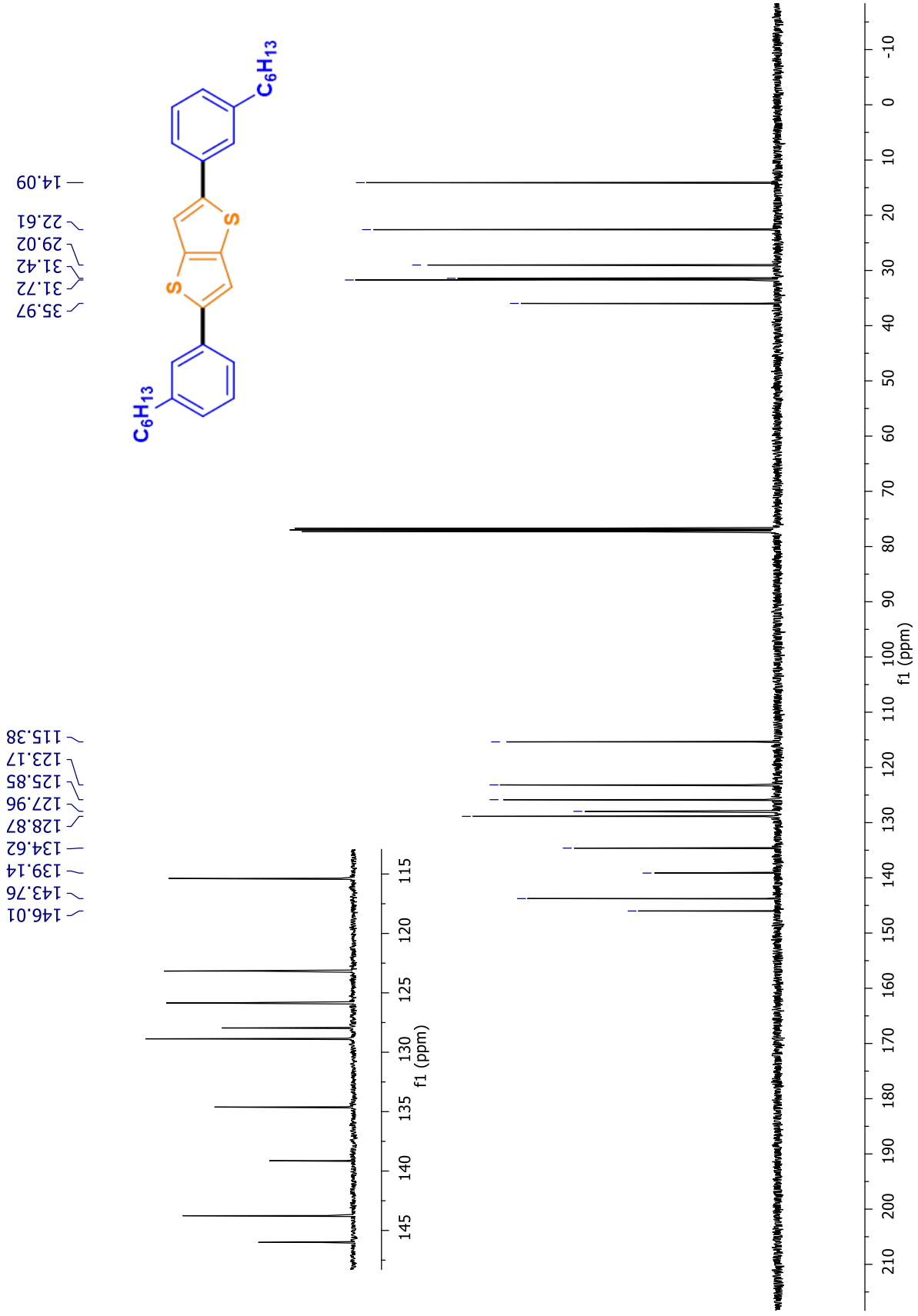

^{13}C-NMR spectrum of derivative 12.

2.5.4.2.7. Synthesis of 9,10-bis(5-hexyl-2-thienyl)anthracene (13)

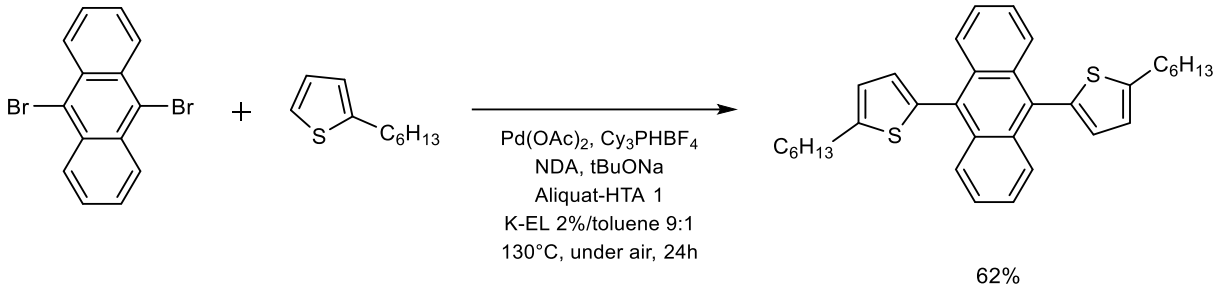

62%

9,10-dibromoanthracene (0.336 g, 1.0 mmol), 2-hexylthiophene (0.337 g, 2.0 mmol), Pd(OAc)2 (0.009 g, 0.04 mmol), Cy3PHBF4 (0.030 g, 0.08 mmol), *t*BuONa (0.288 g, 3.0 mmol), neodecanoic acid (0.104 mg, 0.6 mmol), Aliquat HTA-1 35%wt in H2O (0.452 g, 0.6 mmol) are weighted in the pressure-tight 10 mL screw-cap glass tube, then 2 mL of K-EL 2 wt%-toluene (9:1 v/v, 2 mL) oil-in-water emulsion are added. The reaction mixture is stirred and allowed to homogenize for 5 min at RT, subsequently it is heated under stirring at 130°C through oil bath for 24 h. The mixture is cooled, then diluted with 8 mL of methanol and filtered. The crude was purified by filtration on a pad of silica gel (15 g) with CH2Cl2 (30 mL). The product was recrystallized from heptane (24 mL) and isolated as a yellowish solid in 62% yield (316 mg, 0.73 mmol). Mp: 114-115 °C.

^{1}H-NMR (400 MHz, CDCl3) δ 8.01 – 7.88 (m, 4H), 7.46 – 7.36 (m, 4H), 7.00 (d, J = 3.3 Hz, 2H), 6.97 (dt, J = 3.4, 0.9 Hz, 2H), 2.96 (t, , *J* = 7.6 Hz, 4H), 1.89 – 1.74 (m, 4H), 1.58 – 1.32 (m, 12H), 0.94 (t, J = 7.1 Hz, 6H).

^{13}C-NMR (100 MHz, CDCl3) δ 147.44, 136.11, 131.47, 130.65, 129.16, 126.80, 125.47, 123.92, 31.69, 31.61, 30.28, 28.93, 22.61, 14.09.

E-factor calculation for derivative 13

$$E_{factor} = \frac{mass\ of\ reagents + mass\ of\ auxiliaries - mass\ of\ product}{mass\ of\ product} = \\ = \frac{3.5284 + 77.652 - 0.316}{0.316} = 256$$

UV-Vis absorption, PL spectra and DPV plot for derivative 13

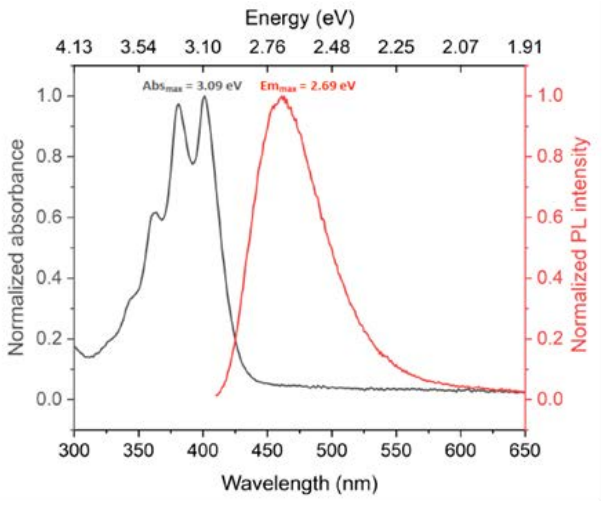

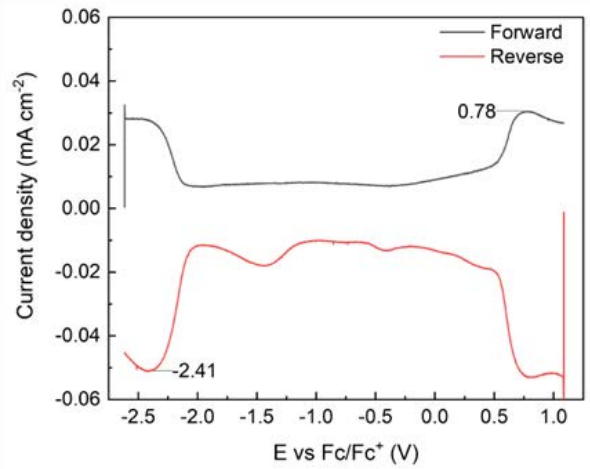

Stokes shift: 0.40 eV.

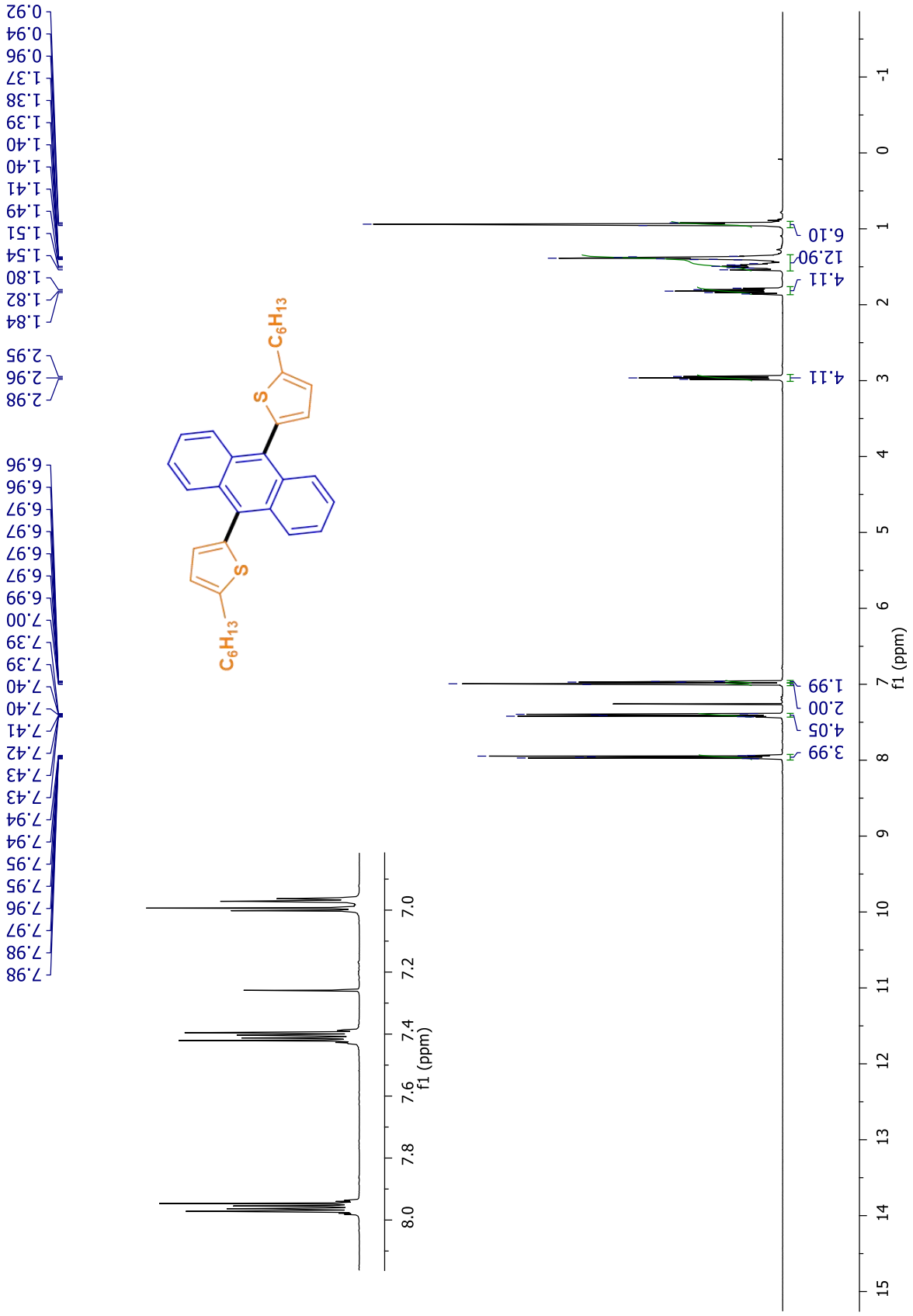

^{1}H-NMR spectrum of derivative 13.

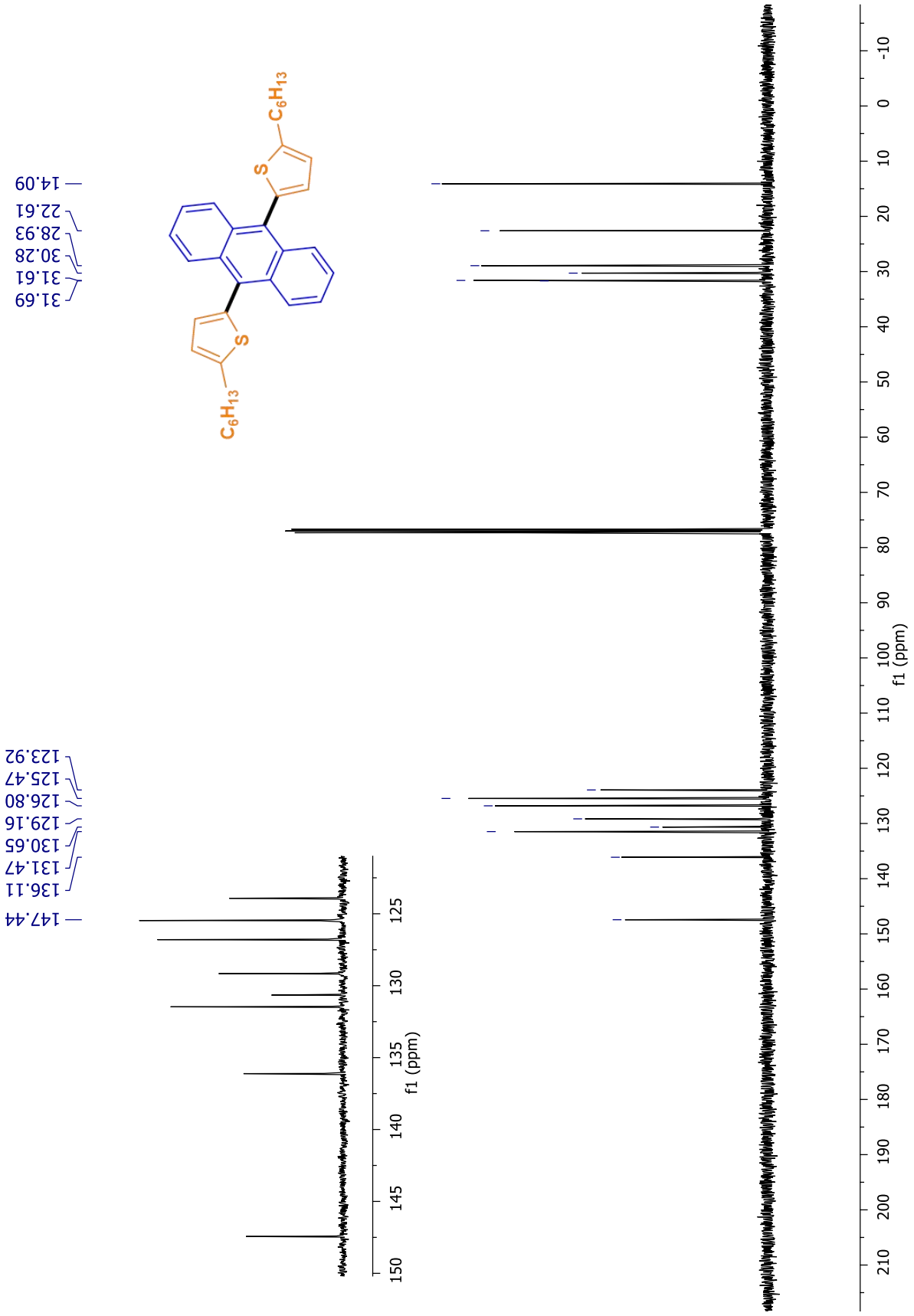

^{13}C-NMR spectrum of derivative 13.

2.5.4.2.8. Synthesis of 4,7-bis(5-hexyl-2-thienyl)benzo[c][1,2,5]thiadiazole (14)

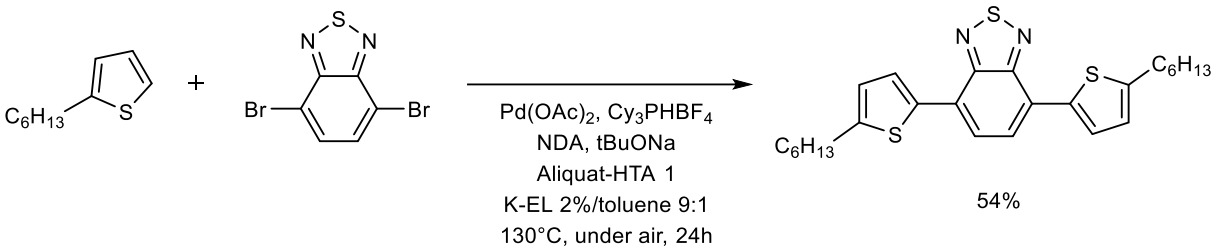

4,7-dibromo-benzo[1,2,5]thiadiazole (0.294 g, 1.0 mmol), 2-hexylthiophene (0.337 g, 2.0 mmol), Pd(OAc)2 (0.009 g, 0.04 mmol), Cy3PHBF4 (0.030 g, 0.08 mmol), *t*BuONa (0.288 g, 3.0 mmol), neodecanoic acid (0.104 mg, 0.6 mmol), Aliquat HTA-1 35%wt in H2O (0.452 g, 0.6 mmol) are weighted in the pressure-tight 10 mL screw-cap glass tube, then 2 mL of K-EL 2 wt%-toluene (9:1 v/v, 2 mL) oil-in-water emulsion are added. The reaction mixture is stirred and allowed to homogenize for 5 min at RT, subsequently it is heated under stirring at 130°C through oil bath for 24 h. The mixture is cooled, then diluted with 8 mL of methanol and filtered. The crude was purified by column chromatography (31.5 g of silica) using a mixture of petroleum ether/dichloromethane 8:2 (126 mL) as eluent. Mp: 75-76 °C. The pure product was isolated as a red solid in 54% yield (254 mg, 0.54 mmol). Anal. Calcd for $C_{28}H_{34}S_3$: C, 72.05; H, 7.34. Found: C, 72.21; H, 7.65.

^{1}H-NMR (400 MHz, CDCl3) δ 7.89 (d, *J* = 3.7 Hz, 1H), 7.67 (s, 1H), 6.84 (dt, *J* = 3.7, 0.9 Hz, 1H), 2.87 (t, *J* = 7.5 Hz, 2H), 1.89 – 1.59 (m, 2H), 1.48 – 1.32 (m, 6H), 0.93 (t, *J* = 7.1 Hz, 3H).

^{13}C-NMR (100 MHz, CDCl3) δ 152.53, 147.60, 136.85, 127.32, 125.61, 125.14, 124.99, 31.64, 31.60, 30.32, 28.90, 22.64, 14.14. Anal. Calcd for C28H34S3: C, 72.05; H, 7.34. Found: C, 72.21; H, 7.65.

E-factor calculation for derivative 14

$$E_{factor} = \frac{mass\ of\ reagents + mass\ of\ auxiliaries - mass\ of\ product}{mass\ of\ product} = \\ = \frac{3.0474 + 137.88 - 0.254}{0.254} = 556$$

UV-Vis absorption, PL spectra and DPV plot for derivative 14

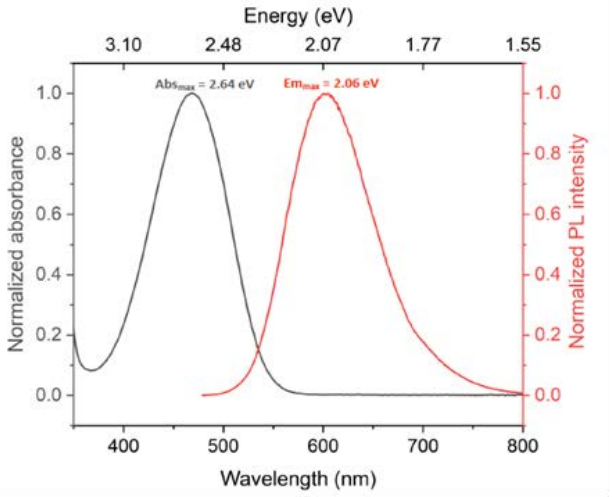

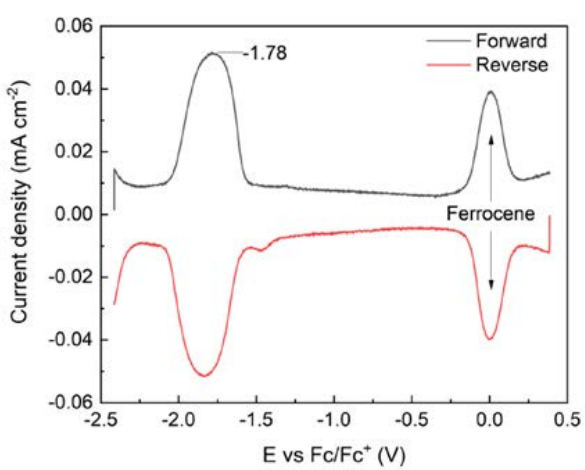

Stokes shift: 0.58 eV.

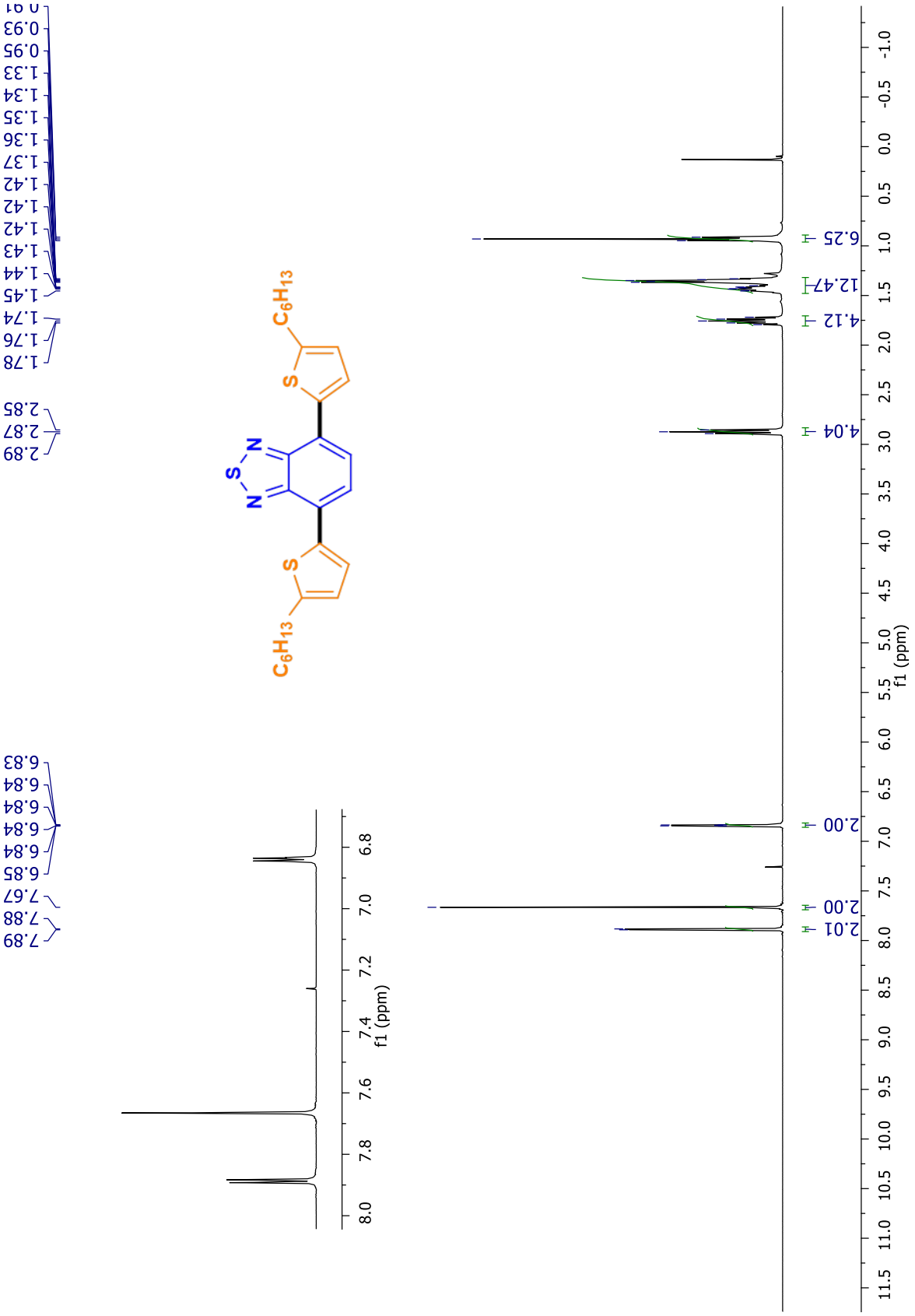

[1]H-NMR spectrum of derivative 14.

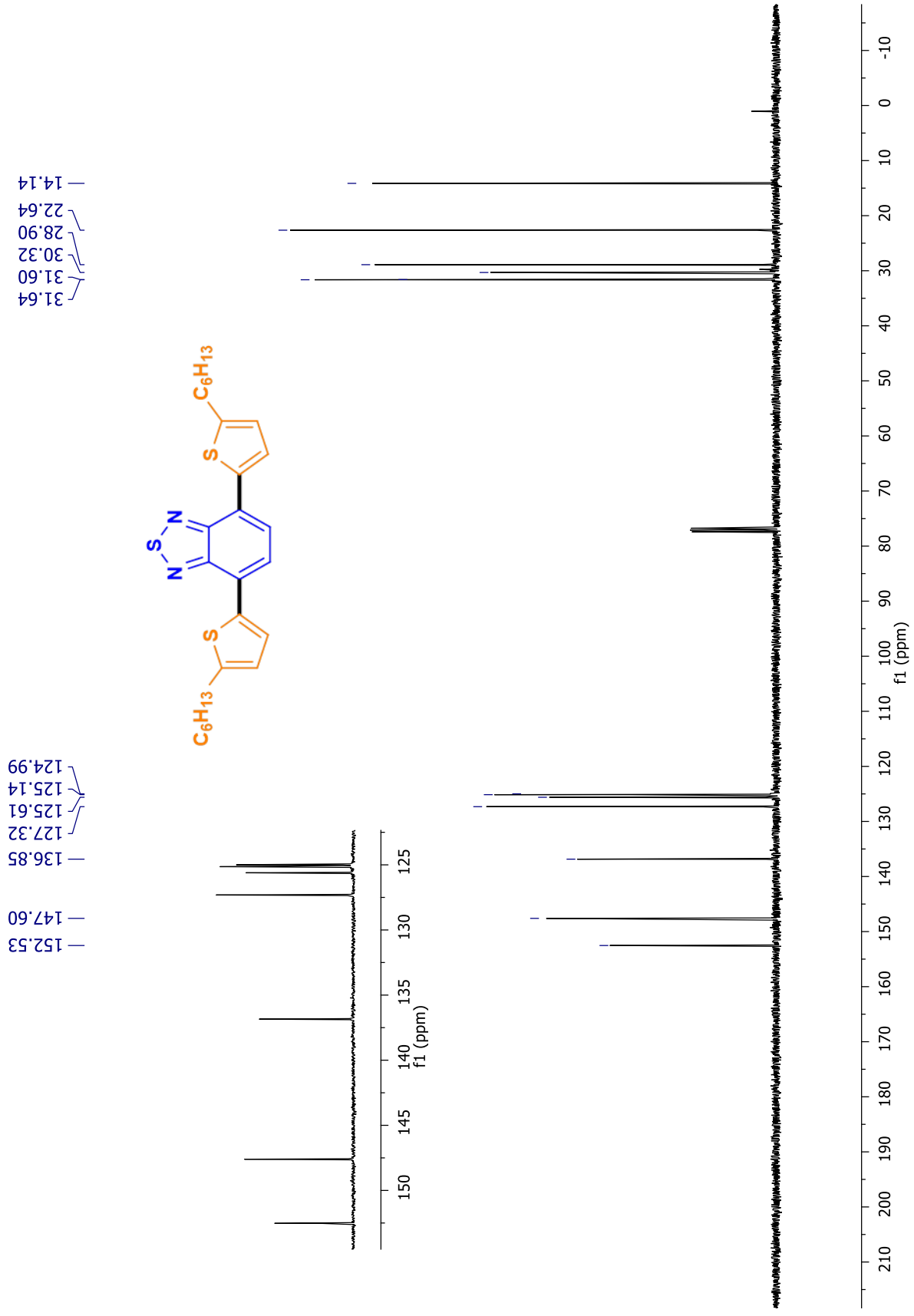

^{13}C-NMR spectrum of derivative 14.

2.5.4.2.9. Synthesis of 1,4'-bis(3-hexylphenyl)-2′,2″,3′,3″,5′,5″,6′,6″-octafluorobiphenyl (15)

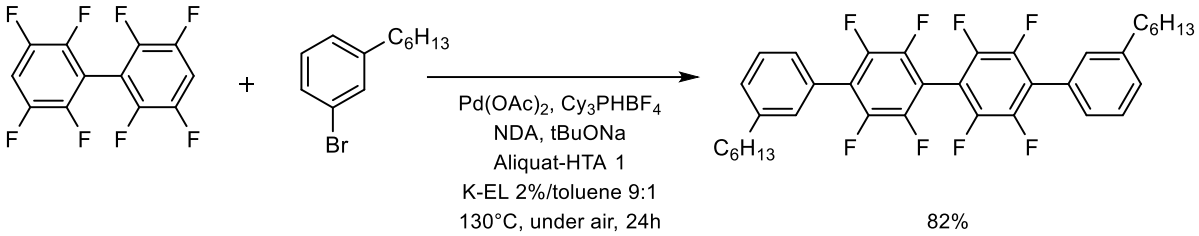

2,2',3,3',5,5',6,6'-octafluorobiphenyl (0.298 g, 1.0 mmol), 1-bromo-3-hexylbenzene (0.482 g, 2.0 mmol), $Pd(OAc)_2$ (0.009 g, 0.04 mmol), Cy3PHBF4 (0.030 g, 0.08 mmol), *t*BuONa (0.288 g, 3.0 mmol), neodecanoic acid (0.104 g, 0.6 mmol), Aliquat HTA-1 35%wt in H_2O (0.452 g, 0.6 mmol) are weighted in the pressure-tight 10 mL screw-cap glass tube, then 2 mL of K-EL 2 wt%-toluene (9:1 v/v, 2 mL) oil-in-water emulsion are added. The reaction mixture is stirred and allowed to homogenize for 5 min at RT, subsequently it is heated under stirring at 130°C through oil bath for 24 h. The mixture is cooled, then diluted with 8 mL of methanol and filtered. The crude was purified by filtration on a pad of silica gel (15 g) with CH_2Cl_2 (30 mL). The product was recrystallized from ethanol (30 mL) and isolated as a white solid in 82% yield (505 mg, 0.82 mmol). Mp: 72-73 °C. Anal. Calcd for $C_{36}H_{34}F_8$: C, 69.89; H, 5.54. Found: C, 70.03; H, 5.64.

^{1}H-NMR (400 MHz, CDCl3) δ 7.47 – 7.41 (m, 2H), 7.37 – 7.29 (m, 6H), 2.70 (t, *J* = 7.6 Hz, 4H), 1.73 – 1.61 (m, 4H), 1.43 – 1.27 (m, 12H), 0.90 (t, *J* = 7.1 Hz, 6H).

^{13}C-NMR (100 MHz, CDCl3): δ 144.4 (dd, J=251.6, 16.7 Hz), 144.1 (d, J=243.5 Hz), 143.5, 130.1, 129.7, 128.6, 127.3, 126.8, 122.9 (t, J=16.7 Hz), 105.9 (m), 35.9, 31.7, 31.3, 28.9, 22.6, 14.1.

E-factor calculation for derivative 15

$$E_{factor} = \frac{mass\ of\ reagents + mass\ of\ auxiliaries - mass\ of\ product}{mass\ of\ product} = \\ = \frac{3.6364 + 84.906 - 0.505}{0.505} = 174$$

UV-Vis absorption, PL spectra and DPV plot for derivative 15

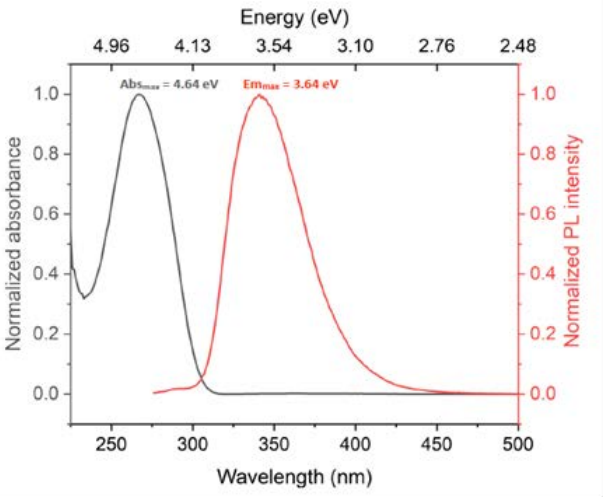

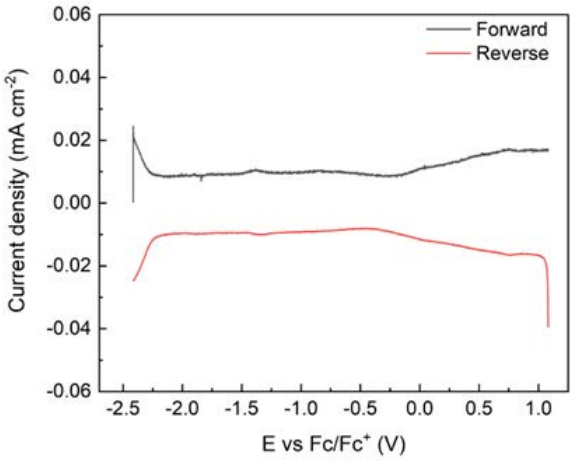

Stokes shift: 1.00 eV.

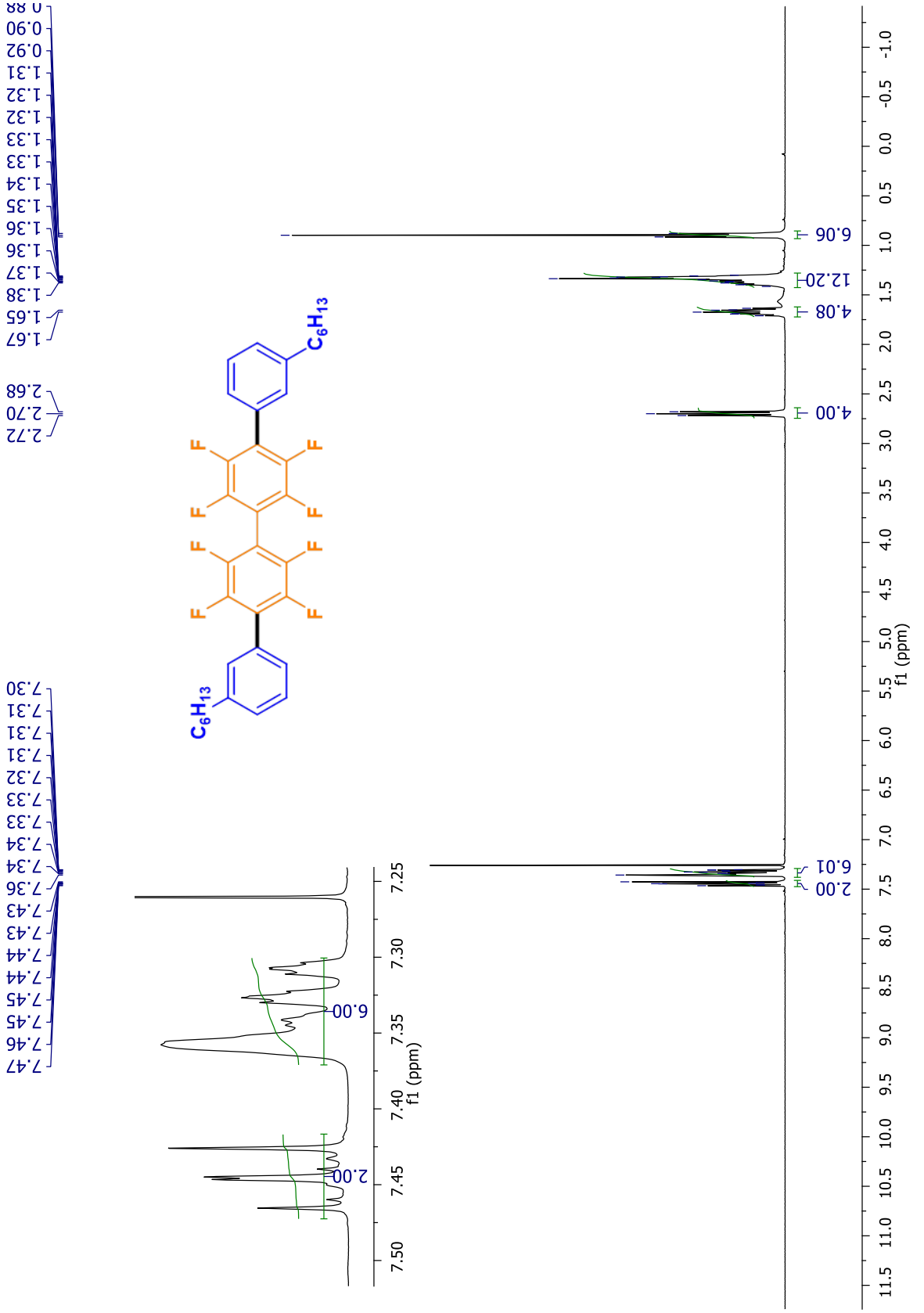

^{1}H-NMR spectrum of derivative 15.

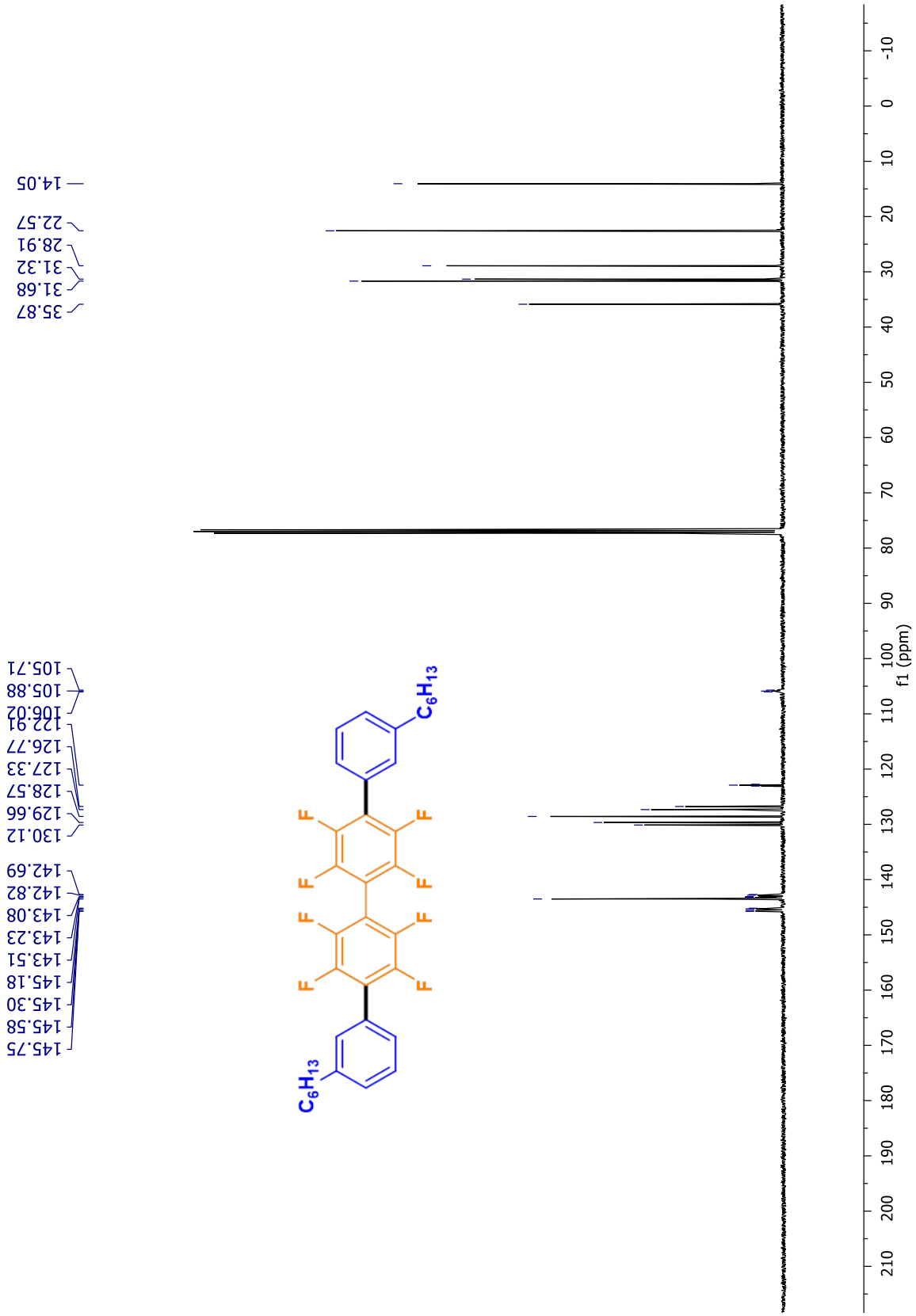

^{13}C-NMR spectrum of derivative 15.

2.6. Micellar Suzuki-Miyaura Synthesis of Symmetrical and Unsymmetrical Benzothiadiazole Luminescent Derivatives in Water and under Air

This work has already been published and it is entitled *"Suzuki-Miyaura Micellar One-Pot Synthesis of Symmetrical and Unsymmetrical 4,7-Diaryl-5,6-Difluoro-2,1,3-Benzothiadiazole Luminescent Derivatives in Water and under Air",* J. Org. Chem. **2018**, 83 (24), 15029–15042. https://doi.org/10.1021/acs.joc.8b02204.[54]

2.6.1. Introduction

The 2,1,3-benzothiadiazole (BT) moiety is a very popular electron-acceptor building block extensively exploited in the syntheses of efficient organic semiconducting materials mainly concerning organic solar cells and organic field-effect transistors.[100–102] To date, various functional molecular an polymeric BT derivatives with tuneable optoelectronic properties have been synthesized by palladium-catalyzed cross-coupling reactions.[101] Further trendy chemical modification of the BT unit includes the fluorination of the 5- and 6-positions (either single- or double-fluorinated BT) imparting different symmetries according to the degree of substitution. The fluorination of BT can decrease the frontier energy levels of the corresponding polymers and enhance the intra- and/or intermolecular interactions.[103] Thus, the fluorinated semiconducting polymers generally show better device performances because of their lower HOMO energy levels, more planar backbones, and higher internal dipole moments than their unsubstituted counterparts.[104]

Among the class of 4,7-diaryl-5,6-difluoro-2,1,3-benzothiadiazole derivatives, the luminescent 4,7-di(thiophene-2-yl)-5,6-difluoro-2,1,3-benzothiadiazole (DTBT) is the most notorious member. According to recent literature, DTBT can be prepared following three different synthetic protocols (**Figure 67**):

a) from reacting 4,7-dibromo-5,6-difluoro-2,1,3-benzothiadiazole (DBBF) with 2-tributylstannylthiophene via Stille coupling in chlorobenzene and under microwave irradiation.[105]

b) from reacting 4,7-diiodo-5,6-difluoro-2,1,3-benzothiadiazole and 2-thienylboronic acid pinacol ester via Suzuki-Miyaura coupling in a water/THF mixture with a moderate to good yield.[106]

c) from reacting 5,6-difluoro-2,1,3-benzothiadiazole and 2-bromothiophene via direct arylation through C−H activation with a modest yield.[107]

However, none of these methods can be considered sustainable. The Stille route is very efficient leading to DTBT in 97% yield, although still involves the use of both toxic halogenated solvent and tin compounds. The Suzuki coupling is known to be particularly tedious for thiophene boronic derivatives due their poor reactivity and pronounced tendency to protodeborylation at working temperatures.[108] Indeed the yield obtained is good but limited at 74% employing iodides as reacting functionalities. The exchange of functionalities between the two counterparts is possible (thus using 2-bromothiophene instead of 2-thienylboronic acid pinacol ester) however this would entail the need of 2,1,3-Benzothiadiazole-4,7-bis(boronic acid pinacol ester), which extremely expensive (174 euro/gram from Merck) and of complex synthetic access. Last, the direct arylation is profitable as it does not require pre-functionalization of one of the two counterparts, however, its generality is limited to substrates having activated C−H bonds lower than those of DFBT, thus limiting product yield to

only 30% due to the activated and reactive 5- position of the 2-bromothiophene counterpart which leads to increased by-products formation.[107]

Micellar catalysis has demonstrated robust efficiency and improved sustainability for C-C couplings, and it is a strong potential candidate to overcome the synthetic access issues of DTBT with a more practical approach.[64] As already pointed, the use of 2% wt K-EL solutions enable to perform Suzuki-Miyaura (S-M) couplings frequently in very mild conditions: in water, at room temperature and under air without the need of removing oxygen from the reaction environment;[64] the idea is to exploit its potential to increase efficiency and sustainability in the synthesis of the widely employed DTBT building block. In this section we show that the careful tuning of reaction conditions, by means modulating the micellar environment through a formulation chemistry approach, enables the preparation of DTBT in high yield, in water, under air, and under very mild conditions by the S-M coupling of DBBF and 2-thienylboronic acid limiting the use of organic solvents.
Additionally, we also show that conditions can be tuned in order to prepare unsymmetrical derivatives holding two different aryl substituents in a one-pot step not requiring the isolation of the monoarylated intermediate. We will show that results are relevant in improving sustainability through a beneficial, simple and industrially scalable synthetic access of valuable luminescent BT derivatives.

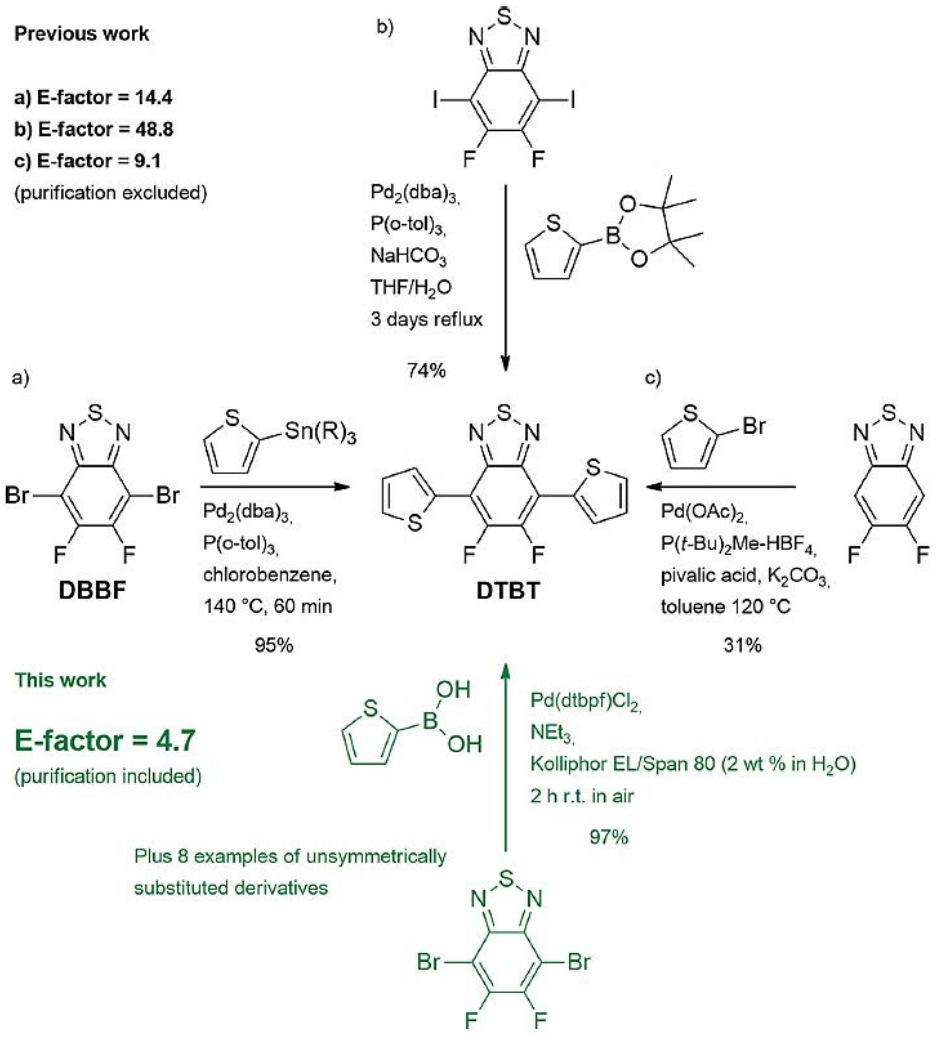

Figure 67. *Literature vs micellar approach for the preparation of DTBT considering yields and E-factors.*

2.6.2. Results and Discussion

2.6.2.1. Micellar Suzuki-Miyaura Synthesis of BT Derivatives

The work started applying the micellar S-M approach to prepare two 4,7-diaryl-2,1,3-benzothiadiazole derivatives (**16** and **17**, **Figure 68**) using a 2 wt % water solution of the industrial surfactant Kolliphor EL and a nominal concentration of 4,7-dibromo-2,1,3-benzothiadiazole of 0.5 M. Most micellar reactions described in the literature suggest the use of a 2−5 wt % solution of surfactant in the presence of 0.5−1.0 M solutions of the reagents. Since working with K-EL solutions, the reactions were performed at room temperature and under air. Derivative **16** with phenyl end-capped groups can be efficiently prepared in quantitative yield in such conditions, employing as catalytic system the well-known $Pd(dppf)Cl_2$ at 2 mol % with respect to equivalent bromide. However, when moving to the synthesis of derivative **17** under the very same conditions, the yield of the isolated product drops significantly.[64] To isolate product **17** with a satisfactory yield the use of the more efficient $Pd(dtbpf)Cl_2$ is essential (**Figure 68**). There is no doubt that this is connected with the poor reactivity of 2-thienylboronic acid. Still, impressively for both the reactions the formation of the monoarylated species was not observed. The reactions were selective toward the formation of the diarylated compounds, even in the case of excess of 4,7- dibromo-2,1,3-benzothiadiazole over the boronic acid employed.

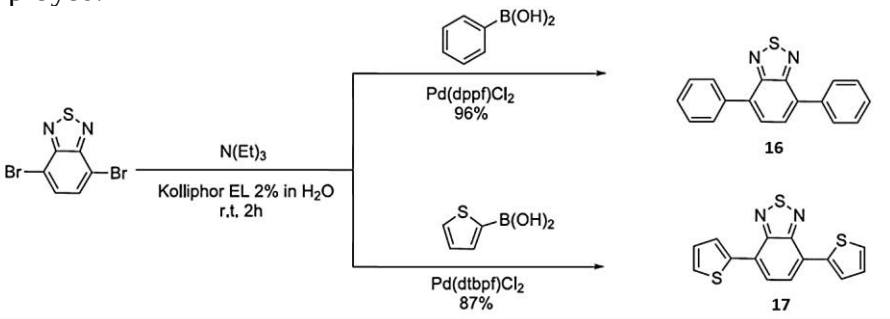

Figure 68. *Reaction scheme for the preparation of derivatives **16** and **17**.*

However, when moving from derivative **16** to the synthesis of DTBT (which is characterized by more relevant optoelectronic properties) the reaction course changes completely. As shown in **Figure 69**, the reaction carried out with $Pd(dppf)Cl_2$ gives very low conversion, mostly leading to the monoarylated specie. When switching to the more reactive $Pd(dtbpf)Cl_2$, the conversion increases substantially yet the reaction does not go to completion even at extended time (no variation in the composition of the reaction mixture was observed).

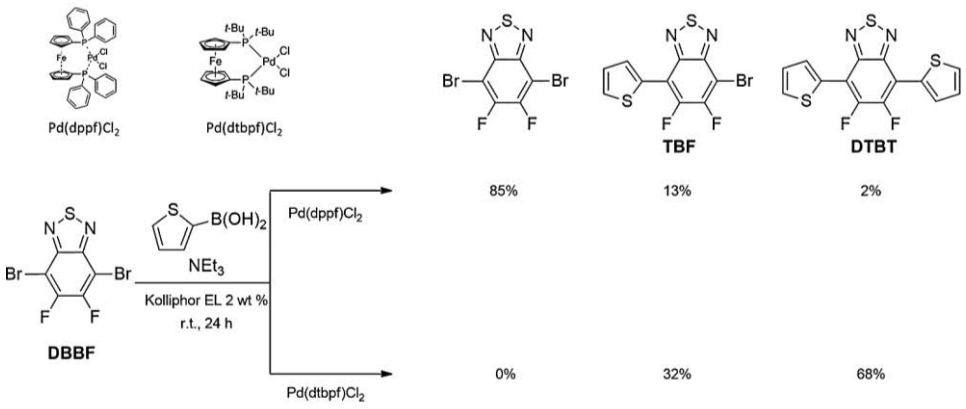

Figure 69. *Chemical composition of the DBBF reaction mixture after 24h using $Pd(dppf)Cl_2$ vs $Pd(dtbpf)Cl_2$.*

In order to investigate the effect of the decreased micellar reactivity towards DBBF we also tested the coupling of DBBF with two additional boronic acids: 3- thienylboronic acid and phenylboronic

acid. Reactions were performed in 2 wt % Kolliphor EL under standardized conditions: 0.5 M DBBF, 1.5 M boronic acid, 3 M NEt_3, and 2 mol % with respect to equivalent bromide of $Pd(dppf)Cl_2$. **Figure 70** shows the results we obtained.

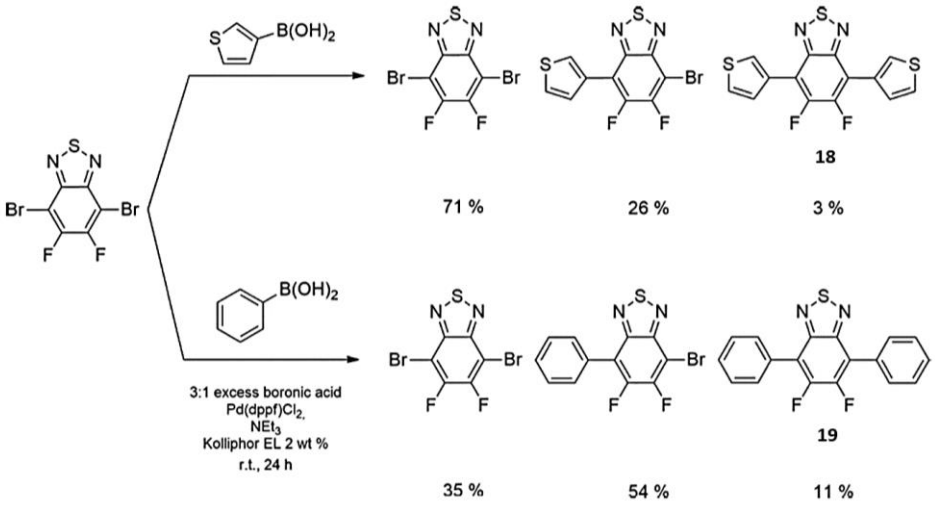

Figure 70. *Examples of micellar S-M reactions carried out on DBBF and leading to limited conversions.*

None of the reactions gave satisfactory conversion, and the monocoupling product was the major component. The use of an organic co-solvent evolving from micellar to emulsion approach may be the right solution. However, such approach is particularly useful to overcome issues related to lack of dispersive efficacy of the reactive species within the reaction mixture that is not in this case. Moreover, the use of a cosolvent remains unsatisfactory from the standpoint of sustainability and E-factor reduction, as the use of organic solvents should be limited as much as possible.

The following part concerns the elucidation of the factors limiting the conversion in the reactions of **Figures 69** and **70**. We thus decided to use the S-M coupling of DBBF and 2-thienylboronic acid as a model case study, evaluating the product distribution as a function of key reaction parameters: the concentration and nature of the surfactant(s), the concentration of the reagents, and the nature of the catalyst. The computationally aided rationalization of the results was finally exploited for the identification of conditions preferentially giving mono- vs double-SM coupling in order to prepare unsymmetrically substituted derivatives in a one-pot procedure.

2.6.2.1.1. Influence of the Surfactant Concentration

The first parameter we explored was the concentration of the surfactant. Literature data mostly refer to a 2 wt % as the best balance between efficiency and cost. In the case of the K-EL the costs are not a big limit; we thus tested 2, 5, 10, and 20 wt % K-EL solutions. The DLS analysis of the surfactant solutions (**Figure 71**) shows that while there is no big difference between 2, 5, and 10 wt % solutions in terms of the dimensions of the micelles obtained, the 20 wt % one also includes aggregates of larger dimensions. The reactions were performed under standardized conditions: 0.5 M DBBF, 1.5 M 2-thienylboronic acid, 3 M NEt_3, and 2 mol % with respect to equivalent bromide of Pd(dppf)Cl2. To start, we purposefully decided to use the less reactive $Pd(dppf)Cl_2$ over $Pd(dtbpf)Cl_2$ in order to better understand and weight the differences between the various reaction conditions employed.

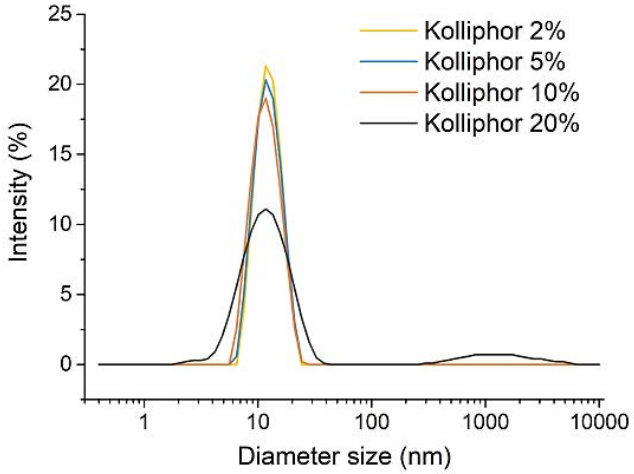

Dispersion	Size (Integrated % intensity)	
	Peak 1	Peak 2
Kolliphor EL 2%	12.7 nm (100%)	-
Kolliphor EL 5%	12.6 nm (100%)	-
Kolliphor EL 10%	12.5 nm (100%)	-
Kolliphor EL 20%	12.6 nm (91%)	1600 nm (9%)

Figure 71. *DLS measurements of K-EL solutions in water as the function of the surfactant concentration.*

All of the reactions were stirred in a standard microwave vessel at room temperature for 12 h, then extracted with CH_2Cl_2, filtered over a pad of silica gel, and submitted to GC–MS characterization. **Table 3** shows the product distributions we obtained. All values are corrected for the instrument response factor for the three different analytes; they thus correspond to the GC–MS yields of the different compounds (see the experimental section 2.6.3. for more details). Data related to the 20 wt% can be excluded as the mixture is out of the micellar regime as evidenced by the DLS data. The results show that the reaction becomes progressively more efficient at higher surfactant concentration and this was expected. However, the reaction is somewhat selective to the monoarylated product even in the presence of a large excess of 2-thienyl-boronic acid. Running the reaction for a longer time and/or under nitrogen atmosphere did not influence the conversion or change the product distribution in any way.

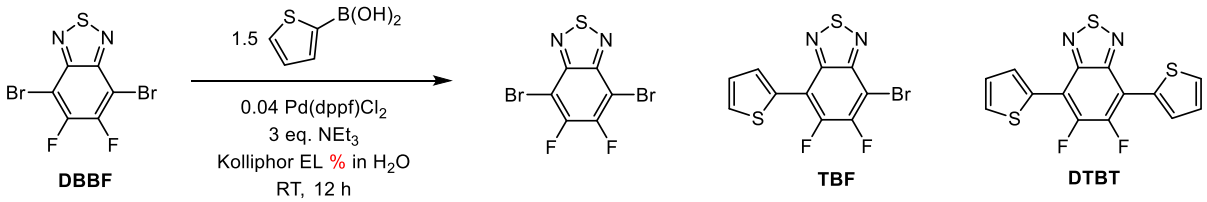

Entry	Surfactant concentration (wt %)	DBBF (mol %)	TBF (mol%)	DTBT (mol %)
1	2	85	13	2
2	5	64	33	3
3	10	28	65	7
4	20	61	34	5

Table 3. *Influence of the surfactant concentration in the S-M coupling reaction between DBBF and 2-thienylboronic acid.*

2.6.2.1.2. Influence of the Reagent's Formal Concentration

Next, we fixed the surfactant concentration at 2 wt % and varied the formal concentration of the limiting reagent DBBF while leaving fixed the respective stoichiometry ratio of 1:3:6:0.04 for DBBF/NEt_3/2-thienylboronic acid /catalyst, respectively. Considering that in micellar reactions most of the reagents and products are just suspended in water, the nominal concentration may not be associated with the stoichiometric ratio within the micelles and/or at the various interphases between reagents, water, and micelles. However, results shown in **Table 4** relate to a low sensitivity towards the variation of the reagents' concentration.

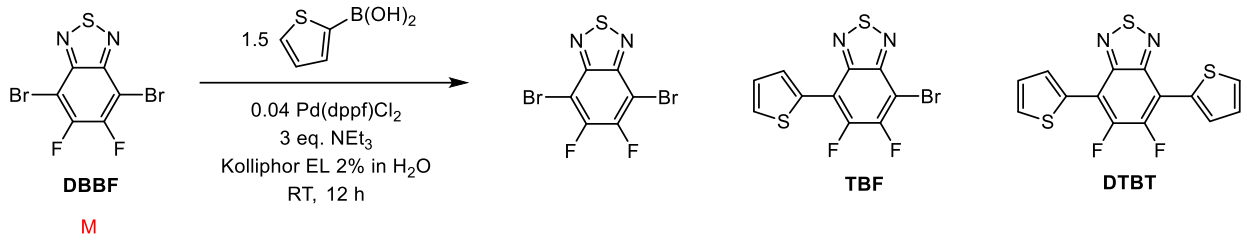

Entry	DBBF (M)	DBBF (mol %)	TBF (mol%)	DTBT (mol %)
1	0.3	84	15	1
2	0.5	85	13	2
3	1	77	21	2
4	1.5	92	8	0

Table 4. *Influence of the reagent's molarity at 2 wt % K-EL concentration in the S-M coupling reaction between DBBF and 2-thienylboronic acid.*

2.6.2.1.3. Influence of the Surfactant's Nature

Despite the wide number of available functional surfactants, concerning both commercial and designer, there are still no general structure-property relationships clearly correlating performances of micellar reactions with the chemical structure and nature of the surfactants. In the case of non-efficient reactions such as the couplings shown in **Figures 69** and **70**, the use of specifically designed surfactants could be of help. Yet, from a sustainable point of view, the synthetic effort required for the preparation of the surfactant should be considered. Some designer surfactants are now commercially available, yet none of them is comparable, in terms of cost and sustainability, with the large number of industrial surfactants constituting the toolbox of the formulation chemist. Moreover, the production of a specific surfactant to suit the needs of every organic substrate is unpractical.

Another well-known strategy of routine practice in formulation chemistry consist in modifying the characteristics of a formulative state through the use of mixtures of surfactants. In this way it is possible to modulate the interactions of the micelles with either the reagents or the products of a given reaction.

Amphiphiles are complex molecules possessing functional groups of different polarity. In the case of polyethoxylated species, like K-EL, they are also intrinsically polydisperse. In order to qualitatively define the affinity of a given surfactant with respect to a phase to be dispersed/emulsified, formulation chemists usually refer to the hydrophilic lipophilic balance (HLB). This parameter is completely empirical (not necessarily linearly correlated with the dielectric constant) and gives a qualitative suggestion of the affinity of a surfactant for water (HLB > 10) or for oil (HLB < 10).[109] It can be assumed that at higher HLB values more polar derivatives will be preferentially dispersed. The HLB

of K-EL is 13.5, which classifies it as water-soluble and appropriate for the preparation of oil in water emulsions. Aiming at tuning the interaction of K-EL with the studied substrates DBBF and 2-thienylboronic acid, we decided to mix it with two other neutral and polyethoxylated industrial surfactants, Tween 80 and Span 80, featuring an HLB of 15 and 4.3, respectively. In both cases, we mixed the surfactants in a 7:3 Kolliphor/co-surfactant wt/wt ratio. This proportion was determined by the limited solubility of Span 80 in water. The HLB values of the two mixtures is defined by the weighted average of the HLB of the pure constituents; thus, the Kolliphor EL/Span 80 mixture has an HLB value of 10.7 and the Kolliphor EL/Tween 80 mixture of 14.0.

Following **Table 5** shows the results we obtained performing the reaction at a 2 wt % surfactant(s) concentration and at a nominal concentration of 0.5M for the bromide. The decision to work at 2 wt % was driven by the limited solubility of Span 80 in water.

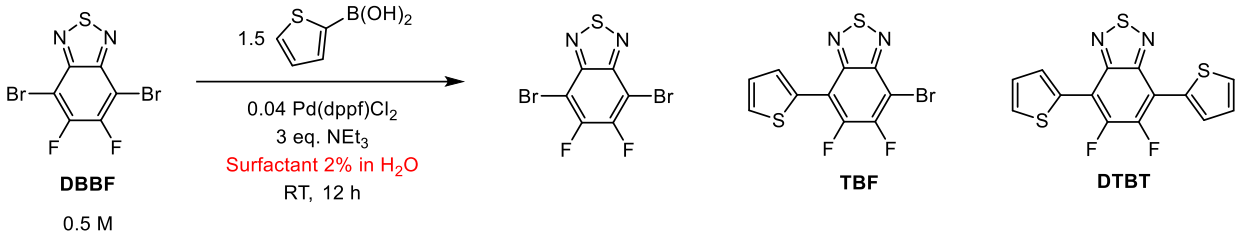

Entry	Surfactant (HLB)	DBBF (mol %)	TBF (mol%)	DTBT (mol %)
1	Kolliphor-EL (13.5)	85	13	2
2	70% Kolliphor EL, 30% Span 80 (10.7)	76	22	2
3	70% Kolliphor EL, 30% Tween 80 (14.0)	95	5	0

Table 5. *Influence of the surfactant's nature at 2 wt % concentration in the S-M coupling reaction between DBBF and 2-thienylboronic acid.*

For all the three cases studied the reaction conversion was low, still slightly better results were observed when working at lower HLB values (entry 2). It would have been interesting explore the effect of even lower HLB values, yet this is technically difficult due to the limited solubility of Span 80 in water, which is homogeneously dissolved till a 7:3 wt/wt mixture with K-EL. Also in this case all reactions were carried out under standard aired environment and no variation in the product distribution was observed working under nitrogen atmosphere.

2.6.2.1.4. Influence of the Catalyst

Pointed that the model reaction works better when using higher surfactant concentration and lower HLB values, we studied the effect of using the more reactive catalyst Pd(dtbpf)Cl_2 instead of Pd(dppf)Cl_2. Following **Table 6** shows the results. Reactions were performed with a stoichiometry ratio of 1:3:6:0.04 for DBBF/NEt_3/2-thienylboronic acid/catalyst, respectively.

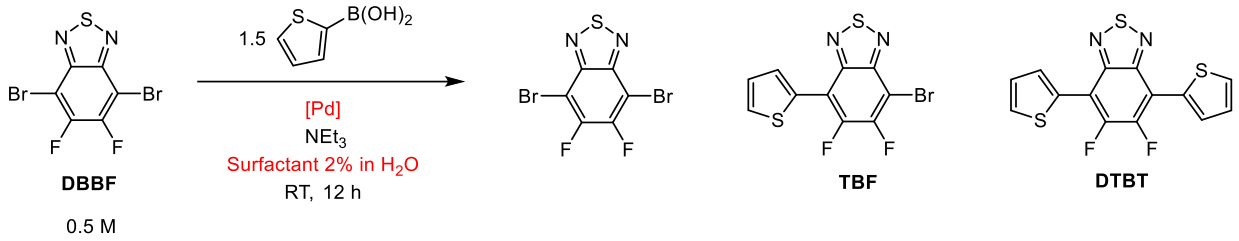

Entry	Surfactant	Catalyst	DBBF (mol %)	TBF (mol%)	DTBT (mol %)
1	Kolliphor-EL	$Pd(dppf)Cl_2$	85	13	2
2	Kolliphor EL	$Pd(dtbpf)Cl_2$	0	32	68
3	70% Kolliphor EL, 30% Span 80	$Pd(dppf)Cl_2$	76	22	2
4	70% Kolliphor EL, 30% Span 80	$Pd(dtbpf)Cl_2$	0	3	97
5	70% Kolliphor EL, 30% Tween 80	$Pd(dppf)Cl_2$	95	5	0
6	70% Kolliphor EL, 30% Tween 80	$Pd(dtbpf)Cl_2$	0	25	75
7	70% Kolliphor EL, 30% Span 80	$Pd(dtbpf)Cl_2$	0	75	25
8a	70% Kolliphor EL, 30% Tween 80	$Pd(dtbpf)Cl_2$	0	83	17
9b	70% Kolliphor EL, 30% Span 80	$Pd(dtbpf)Cl_2$	48	44	8

a: stoichiometry ratio of 1:1.5:3:0.04 for DBBF/NEt_3/2-thienylboronic acid/catalyst, respectively.
b: stoichiometry ratio of 1:3:6:0.01 for DBBF/NEt_3/2-thienylboronic acid /catalyst, respectively.

Table 6. *Influence of the catalyst as the function of reaction formulation in the S-M coupling reaction between DBBF and 2-thienylboronic acid.*

It can be greatly noted that the use of the more reactive $Pd(dtbpf)Cl_2$ significantly improves the reaction outcome for all the conditions explored. Impressively, we obtained DTBT in quantitative yield, at room temperature, under air, and without the use of any cosolvent only in the case of the K-EL/Span80 7:3 mixture, corresponding to the lowest HLB mixture we explored (entry 4[a]). The reaction is so efficient that the product can be isolated at analytical purity directly by filtration of the reaction mixture over a sintered silica filter followed by washing with water and MeOH. Furthermore, again impressively, the mono vs diarylation selectivity can be efficiently controlled by tuning the formulation to much higher HLB values and stoichiometry of the 2-thienylboronic acid. Entry 8[b] of **Table 6** shows that performing the reaction under K-EL/Tween 80 7:3 wt in 1:1.5 stoichiometric ratio of DBBF/2-thienylboronic acid over the larger excess of 1:3 leads to prepare the monoarylated derivative TBF in 83% yield without significant unreacted DBBF and in the presence of only 17% of DTBT. This result opens the way to the preparation of unsymmetrical derivatives. Interestingly, at a

$Pd(dtbpf)Cl_2$ loading of 0.05 mol % in the low HLB surfactant mixture, the obtained results are fully comparable with those obtained with $Pd(dppf)Cl_2$ (entry 9).

2.6.2.1.5. Troublesome DTBT Selectivity and Computational Analysis

The results reported for the model micellar reaction studied so far show how strongly the fomulative effect can be influent in the product distributions and overall conversion. It remains, however, an open question why reactions performed on 4,7-dibromo-2,1,3-benzothiadiazole are selective toward double S-M coupling, while the opposite is true for DBBF. Achievement of satisfactory results requires that a single micelle incorporates reagents, localizes them in the same compartment where the catalyst is also present, assists to their transformation in the product, and eventually releases the latter (according to normal equilibria of micelles) to replace it with a fresh aliquot of the former. This cycle has to be repeated several times, depending on the concentration of the surfactant. Indeed, the conversion degree of the model reaction studied depends linearly upon the amount of surfactant employed. Without a selective affinity from micelles for products vs reagents, these have a probability of being incorporated that will depend on their relative concentration. If, however, the dibrominated substrate (DBBF or 4,7-dibromo-2,1,3-benzothiadiazole) and the corresponding (mono- or di-) arylated product have a markedly different affinity for the micelle compartment where the reactions take place, one of the two will be preferentially incorporated. In the case of micelles preferentially incorporate the di- or mono- bromide above the diarylated product, the reaction will be particularly efficient. On the other hand, if micelles favourably incorporate the diarylated product, the reaction will be severely slowed by saturation of the active sites. The latter effect appears to affect particularly the coupling of DBBF and 2-thienylboronic acid. Besides, the dependency of the mono vs diarylation ratio with the surfactant concentration is less pronounced and it can be assumed that they are almost independent. The data suggest that a saturation effect happens in the coupling between DBBF and boronic acids, which precludes the micelles from performing the coupling reactions multiple times. Conversely, in the case of the coupling using 4,7-dibromo-2,1,3-benzothiadiazole a saturation effect does not happen. To gain further evidence that reactions stops reaching saturation due to selective affinity toward the diarylated DBBF product, we carried out the reaction reported in **Figure 73** at 0.5 M nominal concentration of TBF, in a 2 wt % K-EL solution, and using $Pd(dppf)Cl_2$ as the catalyst. It is noticeable that the formation of DTBT was almost imperceptible.

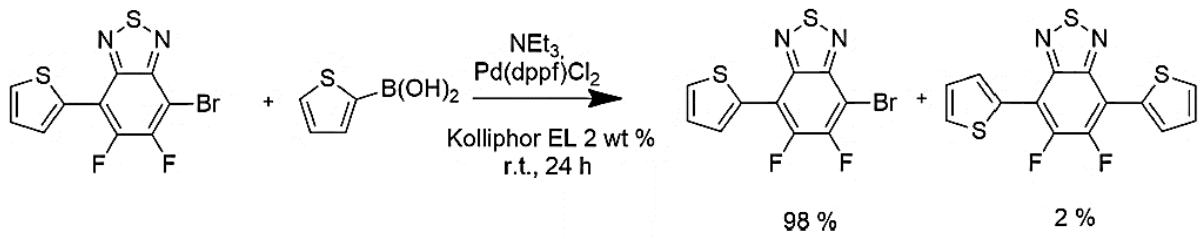

Figure 73. *Micellar S-M reaction of TBF and 2-Thienylboronic acid in 2 wt % K-EL solution, demonstrating the micelle saturation effect.*

Experimentally demonstrated the peculiar incidence of micelle-substate affinity, we carried out a computational analysis in collaboration with Giuseppe Mattioli (CNR - Istituto di Struttura Della Materia, Rome) of the various aryl halides and corresponding products of mono- and di- arylation in order to obtain a quantitative correlation of the dipole moment of the chemical species involved and the HLB of the surfactant(s) employed; this could guide in the elucidation of surfactant/molecules interaction within the micelles. The dipole moments were calculated in water and toluene and

specifically compared between DBBF, 4,7- dibromo-2,1,3-benzothiadiazole, and the corresponding mono and diarylation products. **Figure 72** shows relevant trends in the sign and magnitude of the polarity variation of the different species along the pathway going from reagents to products.

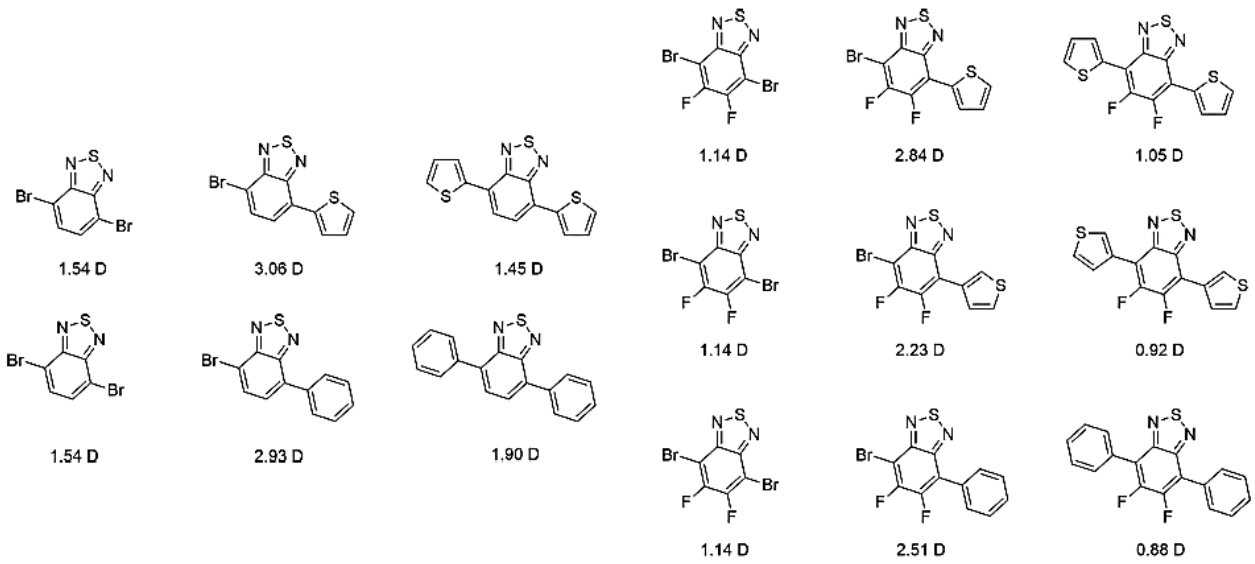

Figure 72. *Calculated dipole moments in toluene for 4,7-dibromo-2,1,3-benzothiadiazole, DBBF, and the corresponding mono- and diarylation products with 2-thienylboronic acid, 3-thienylboronic acid, and phenylboronic acid.*

Without loss of generality, dipole values are averaged on rotational isomers. The computational results differentiate fluorinated from nonfluorinated derivatives on the basis of the polarity of both precursors and reagents. In both cases, the polarity is increased by the first coupling (expected since passing from a symmetric structure to an unsymmetric one) and decreased by the second one (reverting to a symmetrical structure again). Fluorinated derivatives remain, however, in all cases less polar than the corresponding nonfluorinated ones. Even if the calculated values of the dipole moments in water and toluene are different, the same trend is reproduced in both data sets. Only derivatives **16** and **17** (which are both related to the 4,7-dibromo-2,1,3-benzothiadiazole) show a polarity which is similar or higher than that of the corresponding starting dibromide. In all other cases (DBBF derivatives), the diarylation product is sizeably less polar than both the starting bromide and the monoarylated intermediate.

Carrying out reactions with K-EL, which has the relatively high HLB value of 13.5, the emulsification of polar substances over nonpolar ones is generally preferred. In the nonfluorinated series, that are mostly better matched with K-EL's HLB, dibromide and diarylated derivatives possess similar and relatively high polarity. The micelles do not preferentially stabilize either of them, and the reaction can go to completion. The most polar species, that are the monoarylated intermediates, are never observed as they directly react prior to leaving the micelle compartment. On the other hand, in the fluorinated series the polarity of all involved species is smaller than the nonfluorinated ones, thus the emulsification of DBBF is slower with respect to 4,7-dibromo-2,1,3-benzothiadiazole, then the saturation effect takes some time to happen. Moreover, reaction leads to a further reduction of polarity on going from DBBF to the diarylated species. At higher HLB values (14.0 for K-EL/Tween 80 7:3 wt), the reaction does not perform for lack of compatibility. At low HLB values (10.7 for K-EL/Span 80 7:3 wt), the reactions improve, yet the conversion remains limited by the preferential accumulation of diarylation product (the less polar species) over the reagent within the micelles. Furthermore, when using Pd(dppf)Cl_2 the reaction is even slower, and the micelle saturation effect dominate over conversion even more. On the contrary, switching to Pd(dtbpf)Cl_2 the reaction run with remarkably increased kinetics (GC–MS traces after 30 min and 12 h are identical) and proceeded

smoothly in the low HLB mixture (**Table 6** entry 4) and somewhat less smoothly at higher HLB factors (**Table 6**, entries 2 and 6).

The synthesis of DTBT under the best conditions found was scaled up to 20 g of starting DBBF in order to precisely evaluate the E-factor. As the only organic waste produced was the MeOH employed for the final washing step (performed in a Soxhlet continuous extractor), we were able to obtain an E-factor as low as 4.7. The value rise to 10.7 considering that palladium-containing water and surfactants are waste anyway. We decided to not recycle the reaction medium since the crude obtained by fresh micellar solution is of easier and more sustainable purification. The impact on the E-factor is far greater than the benefit obtained recycling the reaction medium. The micellar synthesis of symmetrical BT derivatives concerns E-factor values ranging from 9 to 49 excluding purifications. However, no suitable data are available for all other published routes; an estimate of the E-factors of standard protocols including purification range from 274 to over 1900.

2.6.2.1.6. One-Pot Synthesis of Unsymmetrical Derivatives

Entry 8[b] of Table 6 shows that carrying out the reaction of DBBF and 2-thienylboronic acid in the high-HLB micellar medium K-EL/Tween 80 7:3 wt mixture with tuned stoichiometric ratio between the two counterparts from 1:3 to 1:1.5 enables to control the product distribution, particularly with a marked selectivity towards the monosubstituted intermediate (83% monoarylated vs 17% diarylated). This result opens the way for the preparation of unsymmetrically substituted derivatives in a one-pot procedure. However, according to results of entry 4[a] the only way to drive the reaction to complete diarylation is to use a Kolliphor EL/Span 80 7:3 wt mixture. As such, we developed a two-step, but still one-pot procedure, as no isolation of the intermediate monoarylation product is necessary.

First, we carried out the reaction of DBBF with 2-thienylboronic acid according to the conditions reported in Table 6, entry 8[b] (DBBF/2-thienylboronic acid/NEt_3/Pd(dtbpf)Cl_2 were mixed in a proportion of 1:1.5:6:0.04 working at a 0.5M concentration of DBBF at room temperature and under air). Once we verified by GC-MS analysis that no unreacted DBBF was left (generally after 3h), we added a second aliquot of a different arylboronic acid (1:1.5 TBF/arylboronic acid), and as much Span 80 as needed to reach the HLB value of 10.7 necessary to drive the reaction to completion and thus giving access to unsymmetrically substituted derivatives (12 h, at room temperature and under air). The final unsymmetrically substituted derivatives were isolated from DTBT (generally formed at 15% mol) by unavoidable chromatographic purification of the reaction mixture. **Figure 73** shows the general reaction scheme with the examples of original 4,7-diaryl-5,6-difluoro-2,1,3-benzothiadiazole derivatives synthetized.

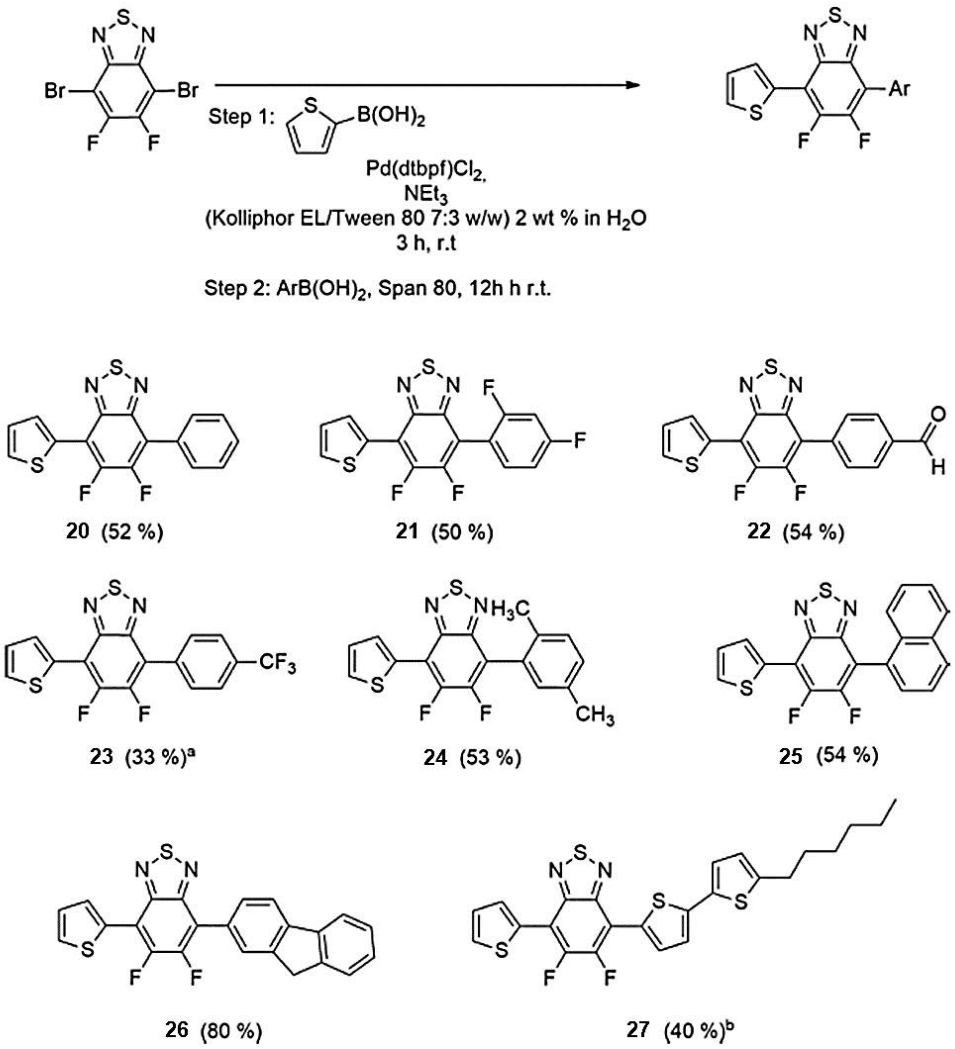

a: low yield due to troublesome chromatographic separation; b: the pinacol ester of the corresponding boronic acid was employed.

Figure 73. *General reaction scheme for the synthesis of unsymmetrical 4,7-diaryl-5,6-difluoro-2,1,3-benzothiadiazole derivatives.*

For all reactions no residual TBF remained from the first step was detected and complete conversion was observed. The moderate to good isolated yields shown in **Figure 73** were limited by the sometimes troublesome (particularly in the case of derivatives **23** and **27**) chromatographic purification of the target product from DTBT.

All unsymmetrically substituted derivatives obtained are original with impressive optical properties, especially for the stokes shifts and emission efficiency, and could have direct applications as luminescent compounds in applications such as luminescent solar collectors, bioimaging, or OLEDs. **Figure 74, Table 7** summarize the most relevant features of the absorption and emission spectra for all the synthetized unsymmetrical BT derivatives.

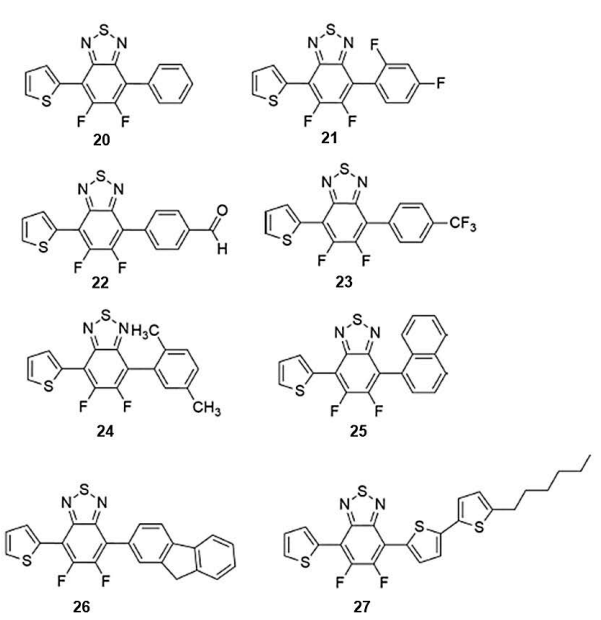

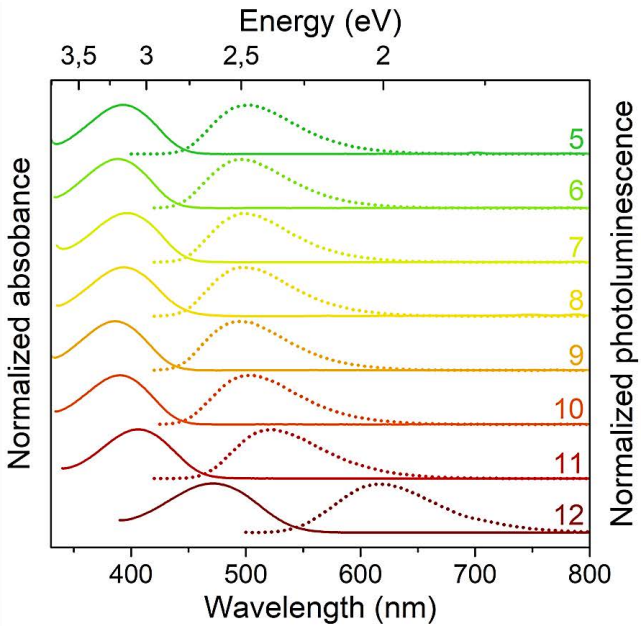

derivative	E_{abs} (eV) / λ_{abs} (nm)	E_{em} (eV)	Stokes shift (eV)	ε ($M^{-1}cm^{-1}$)	Φ [a] (%)
20	3.16/392	2.47	0.69	13 400	83
21	3.19/389	2.50	0.69	10 100	70
22	3.12/396	2.49	0.63	18 000	99
23	3.15/393	2.49	0.66	11 400	74
24	3.21/386	2.52	0.69	9 700	66
25	3.18/390	2.46	0.72	9 100	39
26	3.05/406	2.37	0.68	17 550	90
27	2.63/472	2.01	0.62	24 300	44

a: relative to DTBT (Φ 0.96) as the standard.

Figure 74, Table 7. *Optical properties (absorption and emission maxima, stokes shift, molar extinction coefficient, and emission quantum yield) for derivatives 20-27 in CH_2Cl_2 solution.*

2.6.3. Conclusion

Micro-heterogeneous micellar Suzuki-Miyaura couplings have demonstrated enormous potential in improving sustainability while ensuring efficiency. Particular reactions might require careful tuning of conditions and formulation while moving from standard organic solvent to micellar environment. In the case of the synthesis of symmetrical and unsymmetrical 4,7-Diaryl-5,6-Difluoro-2,1,3-Benzothiadiazole luminescent derivatives, reactions are efficient only when using a suitable formulation with proper micelles-substrates interactions. We demonstrated the possibility to approach complete conversion without requiring the use of organic co-solvents or designer surfactants of multi-step synthesis. Careful selection and mixing of readily available and fully sustainable commercial surfactants lead to DTBT and unsymmetrical BT derivatives in high yields, at room temperature, under air, and with E-factor values markedly low. We particularly focused on Kolliphor EL as the

main micellar forming surfactant and on Tween 80 and Span 80 as hydrophilic and lipophilic co-surfactants, respectively. The collected experimental data, together with the computational analysis suggest that preferential interaction of micellar aggregates with reagents over products of different polarity is essential in order to guarantee complete conversion upon micellar saturation. Within such an optimized micellar environment, it is possible to control the degree of mono- vs di- arylation to the point of being able to prepare unsymmetrically substituted luminescent derivatives by the one-pot sequential reaction of DBBF with two different arylboronic acids. The E-factor values obtained, which are consistent in the 10^1 order for the symmetrical derivatives and in the 10^2 order for the unsymmetrical derivatives including purification, highlight and endorse the industrial compatibility of such protocol considering its strongly reduced environmental impact.

2.6.4. Experimental Section

2.6.4.1. Materials and Instruments

Reagents and solvents were bought from TCI, Fluorochem, and Sigma-Aldrich and used as received. Chromatographic purification were performed using Davisil LC 60A silica gel (pore size 60 Å, 70−200 μm). Composition of solvent mixtures used as eluents are indicated as volume/volume ratios. Melting points were determined using a Buchi M-560 apparatus and are uncorrected. GC-MS spectra were collected on a Clarus 560 S PerkinElmer having an Elite-5MS 30.0 m × 250 μm column. Helium was used as carrier gas. NMR spectra were collected on a Bruker NMR Avance 400 NEO. Absorption spectra of derivatives **20**-**27** were collected on a Cary 60 UV−Vis Agilent spectrophotometer in a 10 mm path length quartz cuvette. Photoluminescence spectra of derivatives **20**-**27** were collected on a Cary Eclipse Fluorescence Agilent spectrophotometer in a 10 mm path length quartz cuvette. DLS experiments were performed on a 90Plus particle size analyzer (Brookhaven Instruments Corp.) with scattering angles of 15° and 90°, equipped with a 35mW solid state 632.8 nm laser and a Brookhaven's TuboCorr correlator with 510 channels.

2.6.4.2. Details on the GC-MS Response Factor Calibration

We quantified the crude product composition in terms of DBBF, TBF and DTBT by gas chromatography coupled with mass spectroscopy (GC-MS). We estimated the reaction mixture composition through area normalization based on response factors method. In order to obtain the relative response factors (f) of the different compounds, we prepared four standard solutions at known concentration of the three pure compounds in dichloromethane in a volumetric flask. Each standard solution was analyzed three times by GC-MS. Averaged areas of each peak A_x were plotted as function of the concentration. Slopes of the linear fitting $S_x = A_x / W_x$ were used to calculate the response factor of compound *x* using the formula:

$$f_x = f_s * \frac{A_s}{A_x} * \frac{W_x}{W_s} = f_s * S_s * \frac{1}{S_x}$$

where the *s* labels the chosen standard. We decided to use DTBT as standard, thus

$$f_s = f_{DTBT} = 1.00 \pm 0.01$$

and using the formula, we found

$$f_{TBF} = 3.1\, f_{DTBT} \pm 0.1$$

$$f_{DBBF} = 1.03\, f_{DTBT} \pm 0.03$$

Full data used to execute the calculations are available from the authors on request. The weight percentage ($Weight\%$:) and the mole percentage ($n/n\%$) of each component in reactions were calculated with the following formulas:

$$Weight\%_X = \left(\frac{f_x A_x^{sample}}{f_{DBBF}A_{DBBF}^{sample} + f_{TBF}A_{TBF}^{sample} + f_{DTBT}A_{DTBT}^{sample}}\right) * 100$$

$$n/n\,\% = \left[\frac{\frac{Weight\%_X}{MM_X}}{\left(\frac{Weight\%_{DBBF}}{MW_{DBBF}} + \frac{Weight\%_{TBF}}{MW_{TBF}} + \frac{Weight\%_{DTBT}}{MW_{DTBT}}\right)}\right] * 100$$

where A_x^{sample} is compound *x* peak area in sample solution and MW is the molecular weight.

2.6.4.3. General Synthetic Procedure for Synthesis of Symmetrical BT Derivatives

Reactions were carried in a test tube which is a 10 mL microwave vial. Depending on the experiment, the boronic acid (**Figures 68, 69** and **70**), the concentration (**Table 3**), amount (**Table 4**), and nature (**Tables 5** and **6**) of surfactant dispersion and the catalyst (**Table 4**) vary. DBBF (165 mg, 0.5 mmol) and the boronic acid (1.5 mmol) were weighed in the vial, and then 1mL of surfactant dispersion in water was added. The mixture was stirred, then NEt_3 (303 mg, 3.0 mmol) was added. The mixture was allowed to homogenize for 5 min before addition of the catalyst (0.02 mmol). All reactions were quenched after 12 h of stirring at room temperature, extracted with CH_2Cl_2, filtered over a pad of silica gel, and submitted to GC-MS characterization.

2.6.4.3.1. Synthesis of 4,7-diphenyl-2,1,3-benzothiadiazole (16)

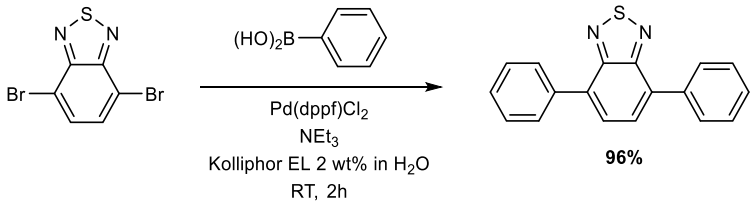

4,7-dibromo-2,1,3-benzothiadiazole (147mg, 0.5 mmol) and phenylboronic acid (183 mg, 1.5 mmol) were weighted in a CEM microwave vial, and then 1 mL of 2 wt % Kolliphor EL dispersion in water was added. The mixture was stirred, and then NEt_3 (303 mg, 3.0 mmol) was added. The mixture was allowed to homogenize for 5 min before addition of $Pd(dppf)Cl_2$ (7.3 mg, 0.01 mmol). After 2 h, the reaction was diluted with water and filtered. The crude was recrystallized from heptane to afford 138 mg of the pure product as bright yellow needles (96 % yield). Characterizations were in agreement with previously published data.

^{1}H-NMR (CDCl3, 500 MHz): δ 7.97 (d, J= 7.78 Hz, 4H), 7.80 (s, 2H), 7.56 (t, J= 7.44 Hz, 4H),7.47(t, J= 7.44 Hz, 2H);

^{13}C-NMR (CDCl3, 125.7 MHz): δ 129.0 ,129.3, 129.5, 130.1, 134.3, 138.3, 155.0.

2.6.4.3.2. Synthesis of 4,7-di(thien-2-yl)-2,1,3-benzothiadiazole (17)

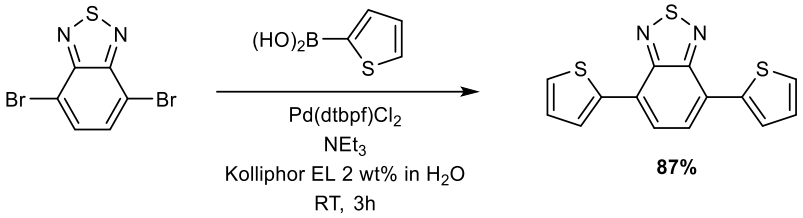

4,7-dibromo-2,1,3-benzothiadiazole (144 mg, 0.5 mmol) and 2-thienylboronic acid (193 mg, 1.5 mmol) were weighted in a CEM microwave vial, and then 1 mL of 2 wt % Kolliphor EL dispersion in water was added. The mixture was stirred, and then NEt_3 (305 mg, 3.0 mmol) was added. The mixture was allowed to homogenize for 5 min before addition of $Pd(dtbpf)Cl_2$ (6.5 mg, 0.01 mmol). After 3 h, the reaction was diluted with water and filtered. The crude was recrystallized from heptane to afford 125 mg of the pure product as bright red needles (96 % yield). Characterizations were in agreement with previously published data.

^{1}H-NMR (400 MHz, CDCl3): δ 7.22–7.24 (dd, J= 5.2, 4Hz, 2H), 7.47–7.48 (dd, J= 5.2, 1.2 Hz, 2H), 7.88 (s, 2H), 8.13–8.14 (dd, J= 3.6, 1.2 Hz, 2H).

^{13}C-NMR (400 MHz, CDCl3): δ 125.8, 126.0, 126.8, 127.5, 128.0, 139.3, 152.6.

2.6.4.3.3. Synthesis of 4,7-di(thiophene-2-yl)-5,6-difluoro-2,1,3-benzothiadiazole (DTBT)

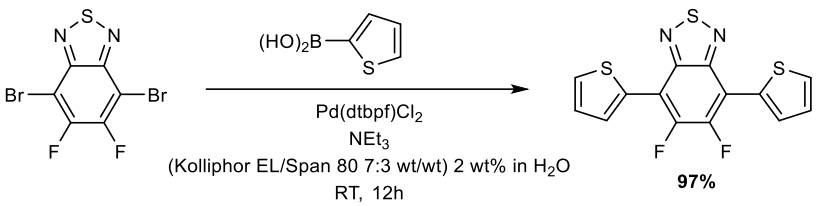

DBBF (20.0 g, 60.6 mmol) and 2-thienylboronic acid (23.3 g, 182 mmol) were weighed in a 500 mL round-bottom flask, and then 121 mL of 2 wt % (Kolliphor EL/Span 80 7:3 w/w) dispersion in water were added. The mixture was stirred with a mechanical stirrer, and then NEt3 (36.7 g, 364 mmol) was added. The mixture was allowed to homogenize before addition of Pd(dtbpf)Cl2 (1.580 g, 2.42 mmol). After 12 h, the reaction mixture was filtered over a sintered silica filter and washed with deionized water. The crude solid was finally purified by hot washing with MeOH (40 mL) in a Soxhlet continuous extractor to remove residual TBF. The product was recovered as a bright yellow solid. (19.8 g, 97% yield). Characterizations were in agreement with previously published data.

^{1}H-NMR (CDCl3, 400 MHz): δ 8.30 (dd, J= 3.9, 1.1 Hz, 2H), 7.62 (dd, J= 5.2, 1.1 Hz, 2H), 7.27 (m, 2H).

^{13}C-NMR (CDCl3, 100 MHz): δ 149.7 (dd, J= 260.0, 20.4 Hz), 148.9 (t, J= 4.4 Hz), 131.5, 130.9 (t, J= 3.9 Hz), 128.9 (t, J= 3.1 Hz), 127.4, 111.8 (d, J= 9.4 Hz).

E-factor calculation for scaled DTBT

$$E\text{-factor} = \frac{\text{mass of byproducts} + \text{mass of solvents}}{\text{mass of product}} =$$

$$= \frac{36.7\ \text{g}\ (NEt_3) + 31.68\ \text{g}\ (\text{MeOH}) + 22.79\ \text{g}\ (\text{boron}) + 121\ \text{g}\ (\text{mic solution})}{19.8\ \text{g}} = 10.7$$

2.6.4.3.4. Synthesis of 4,7-di(thiophene-3-yl)-5,6-difluoro-2,1,3-benzothiadiazole (18)

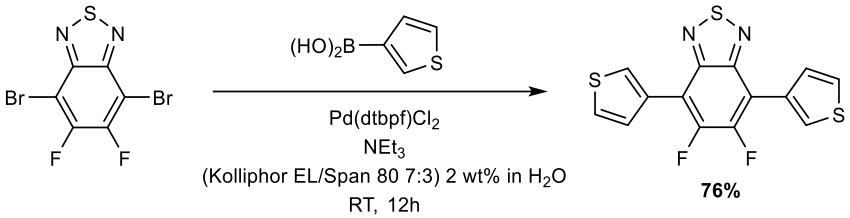

DBBF (165 mg, 0.5 mmol) and 3-thienylboronic acid (192 mg, 1.5 mmol) were weighed in a CEM microwave vial, and then 1 mL of 2 wt % (Kolliphor EL/Span 80 7:3 wt/wt) dispersion in water was added. The mixture was stirred, and then NEt_3 (303 mg, 3.0 mmol) was added. The mixture was allowed to homogenize for 5 min before addition of $Pd(dtbpf)Cl_2$ (13.1 mg, 0.02 mmol). After 5 h, the reaction was diluted with 10 mL of water and filtered. The crude was crystallized from heptane to afford 153 mg of the pure product as yellow needles (91% yield). Mp: 110.9−111.8 °C. Anal. Calcd for $C_{14}H_6F_2N_2S_3$: C, 49.98; H, 1.80; N, 8.33. Found: C, 49.53; H, 1.52; N, 8.02.

^{1}H-NMR (CDCl3, 400 MHz): δ 8.37 (dd, J= 3.0, 1.3 Hz, 2H), 7.94 (dq, J= 5.1, 1.1 Hz, 2H), 7.51 (dd, J= 5.1, 3.0 Hz, 2H).

^{13}C-NMR (CDCl3, 100 MHz): δ 150.5 (dd, J= 258.6, 20.4 Hz), 150.0, 130.2, 128.9 (t, J= 2.9 Hz), 128.2, 125.2, 113.1.

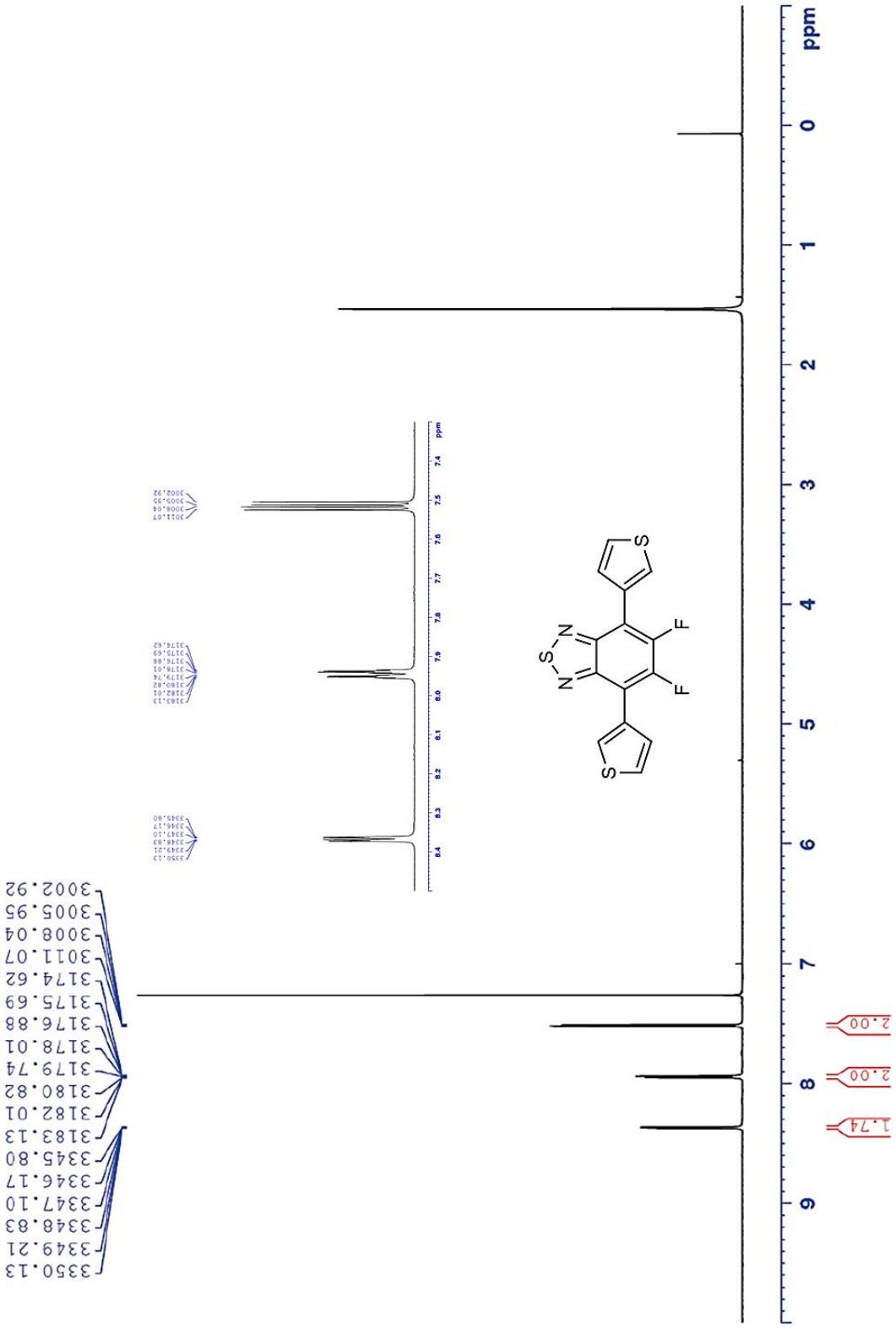

[1]H-NMR spectrum of derivative 18.

^{13}C-NMR spectrum of derivative 18.

2.6.4.3.5. Synthesis of 4,7-diphenyl-5,6-difluoro-2,1,3-benzothiadiazole (19)

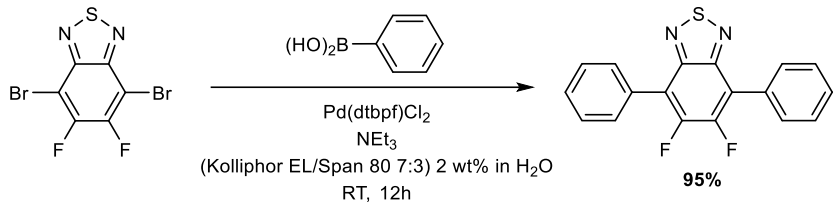

DBBF (165 mg, 0.5 mmol) and phenylboronic acid (183 mg, 1.5 mmol) were weighed in a CEM microwave vial, and then 1 mL of Kolliphor EL 10 wt % dispersion in water was added. The mixture was stirred, and then NEt_3 (303 mg, 3.0 mmol) was added. The mixture was allowed to homogenize for 5 min before addition of $Pd(dtbpf)Cl_2$ (13.1 mg, 0.02 mmol). After 12 h, the reaction was diluted with 10 mL of water and filtered. The crude was crystallized from heptane to afford 153 mg of the pure product as white needles (95% yield). Characterizations were in agreement with previously published data.

^{1}H-NMR (CDCl3, 400 MHz): δ 7.83 (d, J= 7.4 Hz, 4H), 7.59 (t, J= 7.5 Hz, 4H), 7.52 (t, J= 7.4 Hz, 2H).

^{13}C-NMR (CDCl3, 100 MHz): δ 151.4 (t, J = 3.9 Hz), 151.3 (dd, J = 258.6, 20.4 Hz), 131.4, 131.1, 130.0, 129.4, 119.7 (dd, J = 10.5, 4.4 Hz).

2.6.4.3.6. Synthesis of 4-bromo-7-(thiophene-2-yl)-5,6-difluoro-2,1,3-benzothiadiazole (TBF)

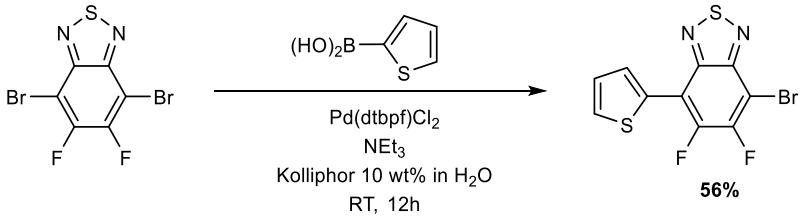

DBBF (330 mg, 1.0 mmol) and 2-thienylboronic acid (192 mg, 1.5 mmol) were weighed in a Biotage microwave vial, and then 2 mL of 10% Kolliphor EL dispersion in water was added. The mixture was stirred, and then NEt_3 (303 mg, 3.0 mmol) was added. The mixture was allowed to homogenize for 5 min before addition of $Pd(dtbpf)Cl_2$ (13.2 mg, 0.02 mmol). After 12 h, the reaction was diluted with 10 mL of water and filtered. The crude was purified by column chromatography using heptane/toluene = 7:3 as eluent. Isolated product: 187 mg (56% yield), yellow powder. Mp: 156.5-157.3. Anal. Calcd for $C_{10}H_3BrF_2N_2S_2$: C, 36.05; H, 0.91; N, 8.41. Found: C, 36.03; H, 0.61; N, 8.32.

^{1}H-NMR (CDCl3, 400 MHz): δ 8.26 (ddd, J = 3.9, 1.1, 0.7 Hz, 1H), 7.64 (dd, J = 5.2, 1.1 Hz, 1H), 7.27 (ddd, J = 5.2, 3.9, 1.4 Hz, 1H).

^{13}C-NMR (CDCl3, 100 MHz): δ 152.4 (dd, J = 256.5, 20.3 Hz), 149.1 (dd, J = 262.3, 19.0 Hz), 149.9 (d, J = 5.1 Hz), 147.9, 131.4 (d, J = 8.7 Hz), 130.8 (dd, J = 5.8, 3.6 Hz), 129.5 (d, J = 6.6 Hz), 127.5, 113.4 (dd, J = 12.3 Hz, 1.4 Hz), 97.1 (dd, J = 21.8, 1.4 Hz).

2.6.4.4. General Procedure for the One-Pot Synthesis of Unsymmetrical BT Derivatives

Reactions were carried in a CEM microwave vial. DBBF (330 mg, 1.0 mmol), 2-thienylboronic acid (192 mg, 1.5 mmol), and $Pd(dtbpf)Cl_2$ (26.3 mg, 0.04 mmol) were weighed in the vessel, and then 2 mL of 2 wt % (Kolliphor/Tween 7:3 w/w) dispersion in water was added. The mixture was allowed to homogenize for 5 min before addition of NEt_3 (607 mg, 6.0 mmol). The reaction was stirred for 3 h, and then 1.5 mmol of the second boronic acid/ester was added in the vessel. Span 80 (20 mg) was added as well. The reaction was stirred overnight and subsequently diluted with 10 mL of water and filtered. The crude was finally purified by column chromatography or recrystallization.

2.6.4.4.1. Synthesis of 4-phenyl-7-(thiophene-2-yl)-5,6-difluoro-2,1,3-benzothiadiazole (20)

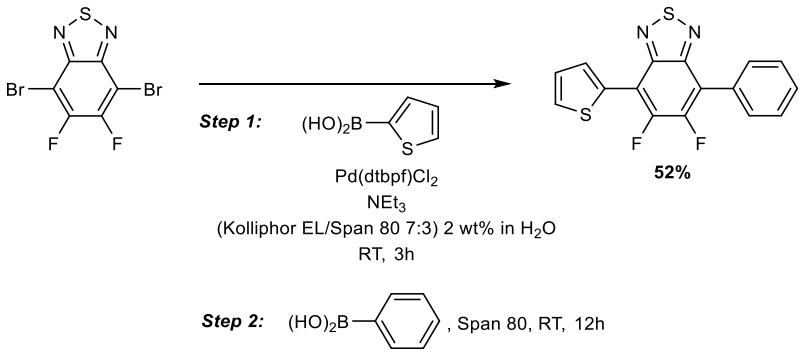

The crude was purified by column chromatography using heptane/DCM = 8:2 as eluent. Isolated product: 172 mg (52%), lime green powder. Mp: 164.7−165.2 °C. Anal. Calcd for $C_{16}H_8F_2N_2S_2$: C, 58.17; H, 2.44; N, 8.48. Found: C, 57.82; H, 2.12; N, 8.45.

^{1}H-NMR (CDCl3, 400 MHz): δ 8.31 (d, J = 3.9 Hz, 1H), 7.82 (d, J = 8.3 Hz, 2H), 7.63 (dd, J = 5.3, 0.9 Hz, 1H), 7.58 (t, J = 7.4, 0.9 Hz, 2H), 7.49−7.52 (m, 1H), 7.29 (m, 1H).

^{13}C-NMR (CDCl3, 100 MHz): δ 151.33 (d, 8.6 Hz), 151.32 (dd, J = 255.9, 19.0 Hz), 150.6 (dd, J = 259.8, 20.0 Hz), 149.9 (d, J = 8.8 Hz), 132.4 (dd, J = 5.4, 3.4 Hz), 131.9 (d, J = 8.3 Hz), 131.4 (d, J = 2.6 Hz), 131.1, 130.0, 129.8 (d, J = 6.4 Hz), 129.4, 128.3, 118.7 (d, J = 14.2 Hz), 113.6 (dd, J = 12.2, 1.2 Hz).

UV-Vis Absorption and PL Spectra of derivative 20

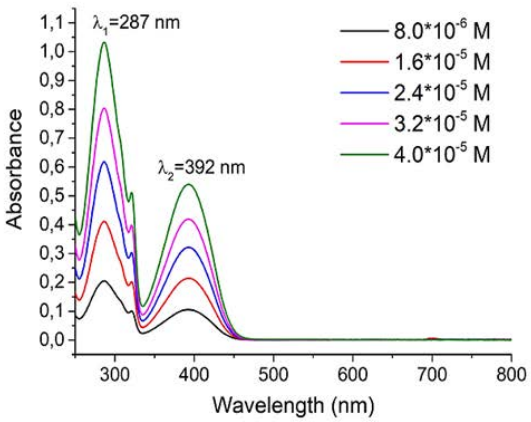

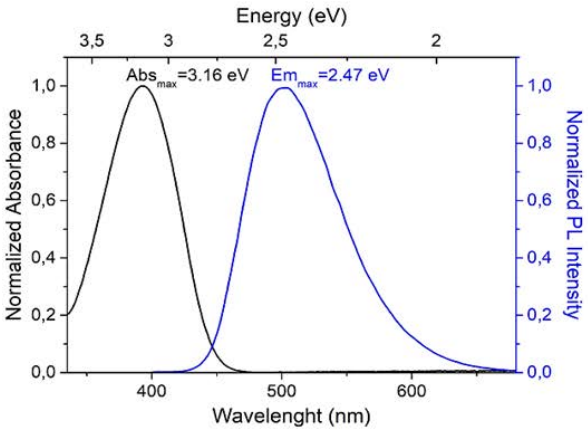

$\varepsilon_{(\lambda 2)}$ = 13 400 (± 200) $M^{-1}cm^{-1}$, solvent CH_2Cl_2. **Stokes shift** = 0.69 eV.

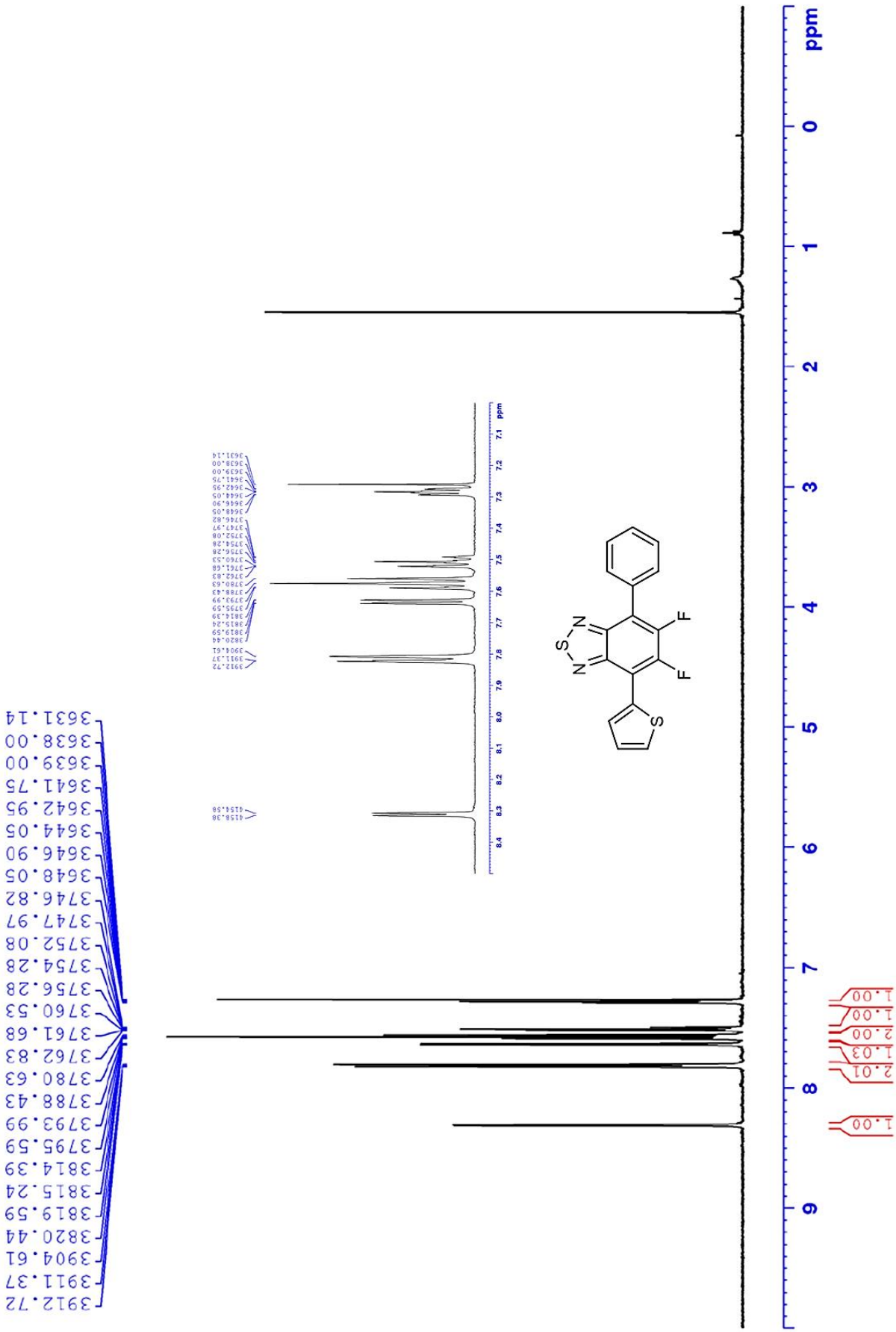

[1]H-NMR spectrum of derivative 20.

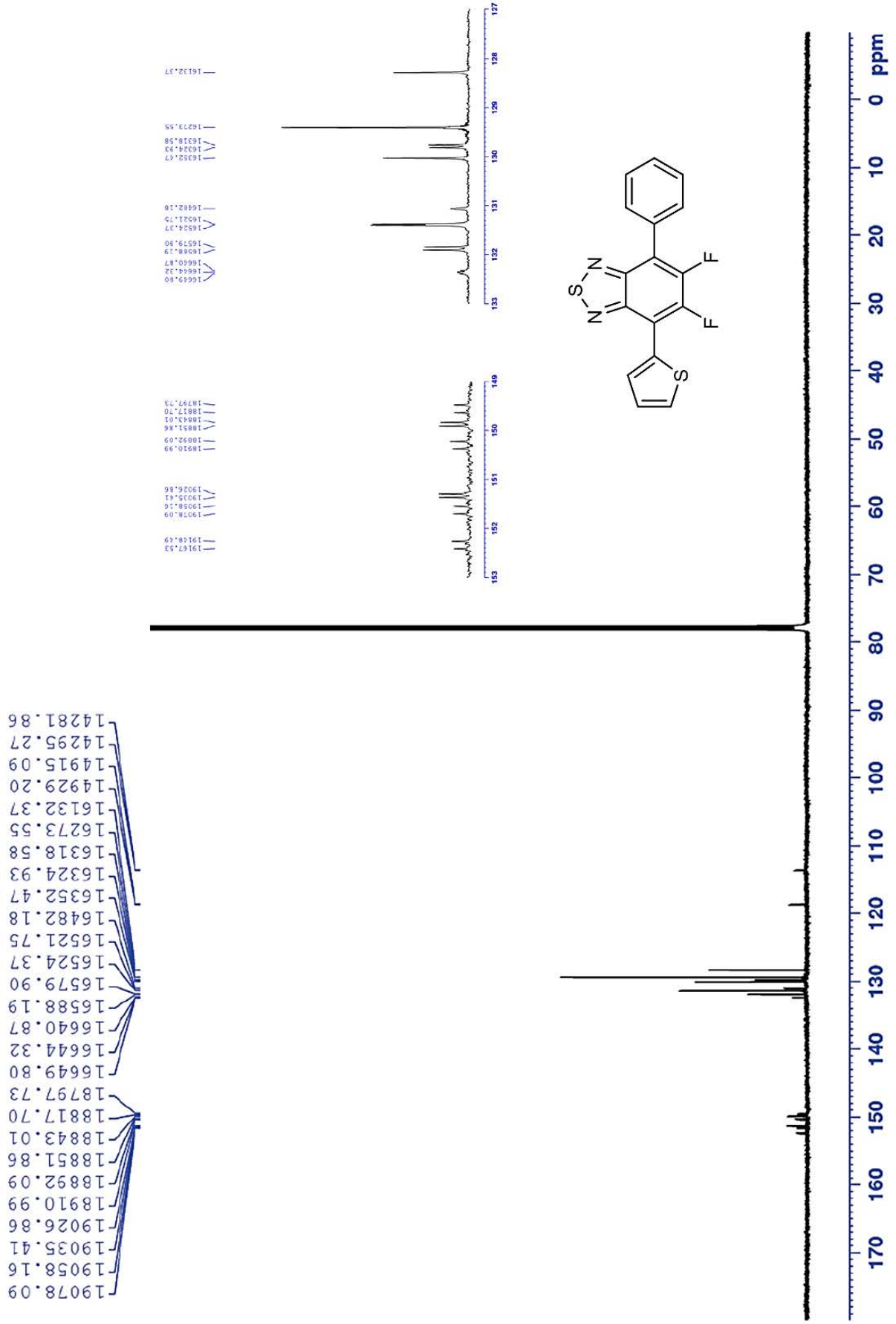

^{13}C-NMR spectrum of derivative 20.

2.6.4.4.2. Synthesis of 4-(2,4-difluorophenyl)-7-(thiophene-2-yl)-5,6-difluoro-2,1,3-benzothiadiazole (21)

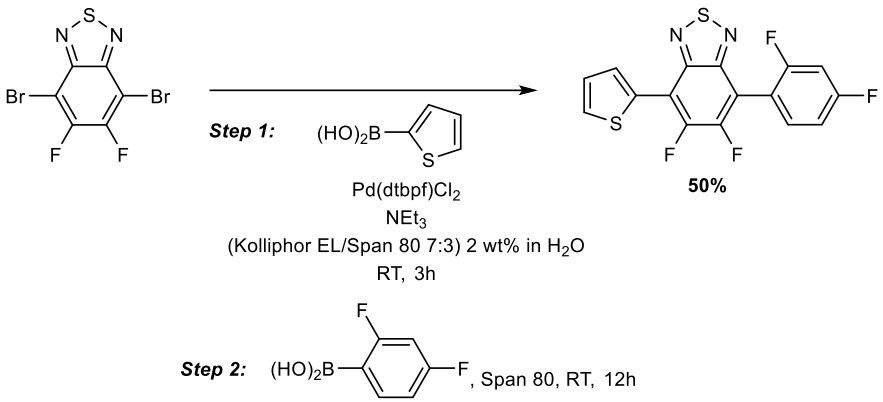

The crude was purified by column chromatography using heptane/toluene = 7:3 as eluent. Isolated product: 183 mg (50%), orange powder. Mp: 166.6−167.8 °C. Anal. Calcd for $C_{16}H_6F_4N_2S_2$: C, 52.45; H, 1.65; N, 7.65. Found: C, 52.07; H, 1.31; N, 7.59.

^{1}H-NMR (CDCl3, 400 MHz): δ 8.35 (ddd, J= 3.8, 1.2, 0.6 Hz, 1H), 7.62−7.68 (m, 2H), 7.31 (ddd, J= 5.2, 3.8, 1.4 Hz, 1H), 7.05−7.15 (m, 2H).

^{13}C-NMR (CDCl3, 100 MHz): δ 163.8 (dd, J= 252.1, 11.6 Hz), 160.5 (dd, J= 253.4, 12.3 Hz), 151.2 (dd, J= 260.7, 21.1 Hz), 150.3 (d, J= 8.8 Hz), 149.4 (dd, J= 265.1, 23.2 Hz), 148.8 (d, J= 8.7 Hz), 133.2 (dd, J= 9.9, 3.7 Hz), 131.4 (d, J= 8.3 Hz), 131.2, 129.3 (d, J= 6.5 Hz), 127.5, 114.1 (d, J= 16.1), 113.8 (d, J= 11.7 Hz), 111.8 (dd, J= 21.7, 3.6 Hz), 111.2 (d, J= 16.0 Hz), 104.7 (t, J= 25.5 Hz).

UV-Vis Absorption and PL Spectra of derivative 21

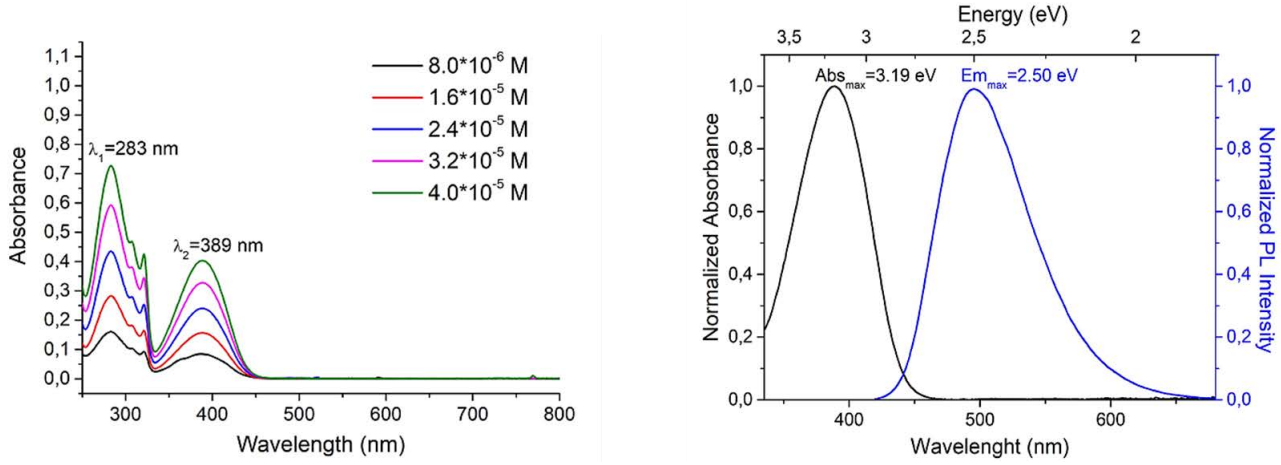

$\varepsilon_{(\lambda 2)}$ = 10 100 (± 200) M $^{-1}$cm^{-1}, solvent CH_2Cl_2. **Stokes shift** = 0.69 eV.

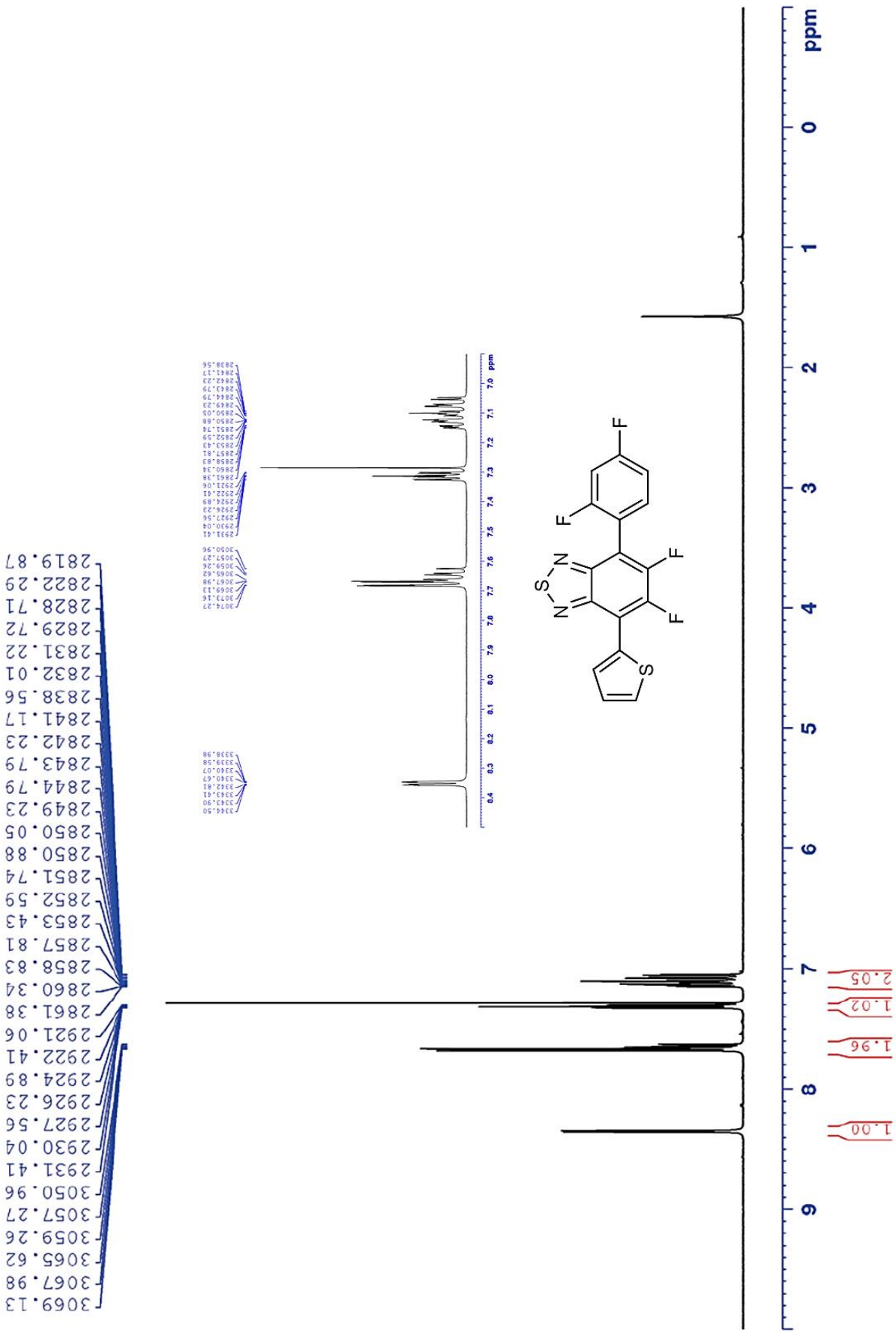

^{1}H-NMR spectrum of derivative 21.

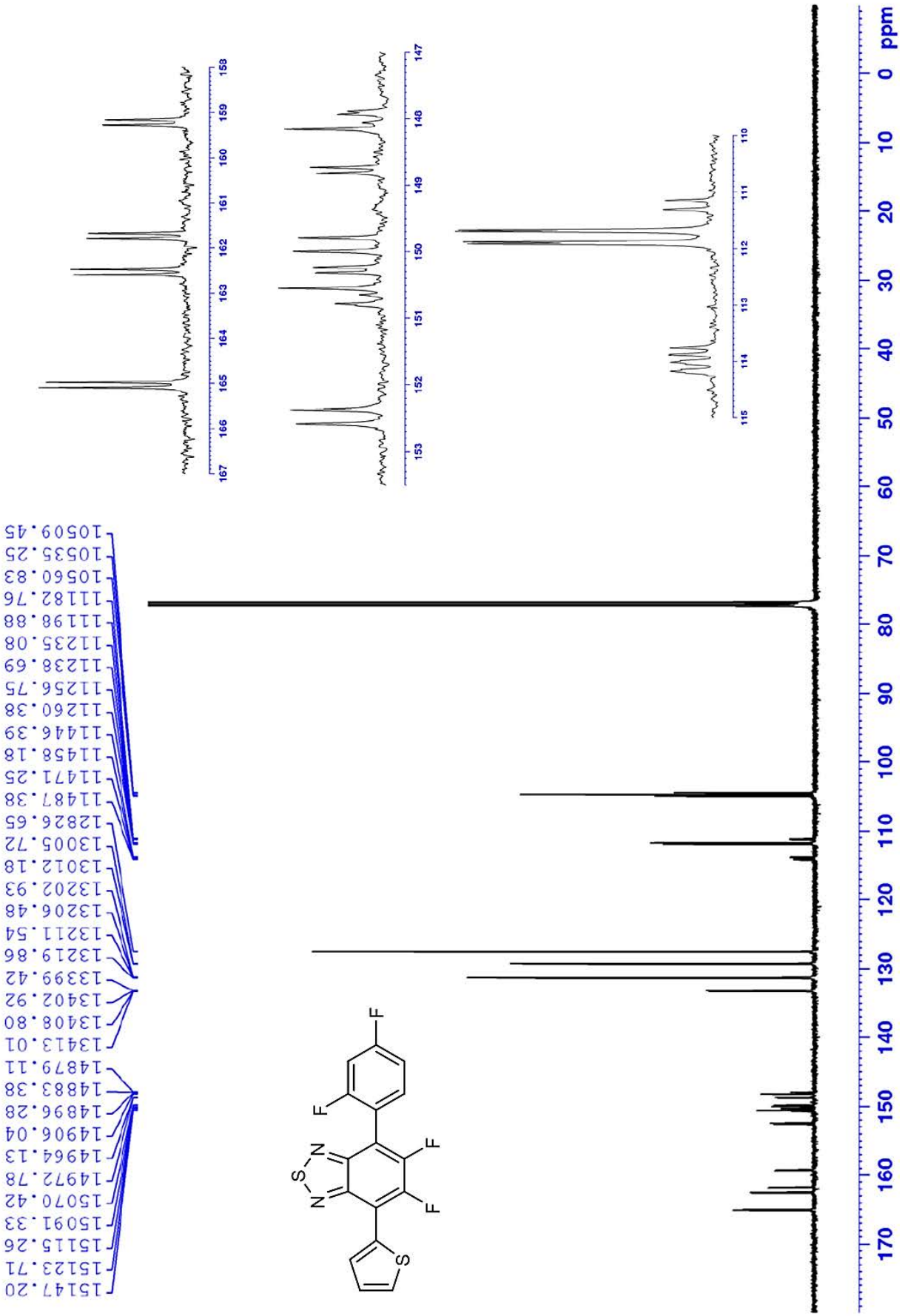

^{13}C-NMR spectrum of derivative 21.

2.6.4.4.3. Synthesis of 4-(4-formylphenyl)-7-(thiophene-2-yl)-5,6-difluoro-2,1,3-benzothiadiazole (22)

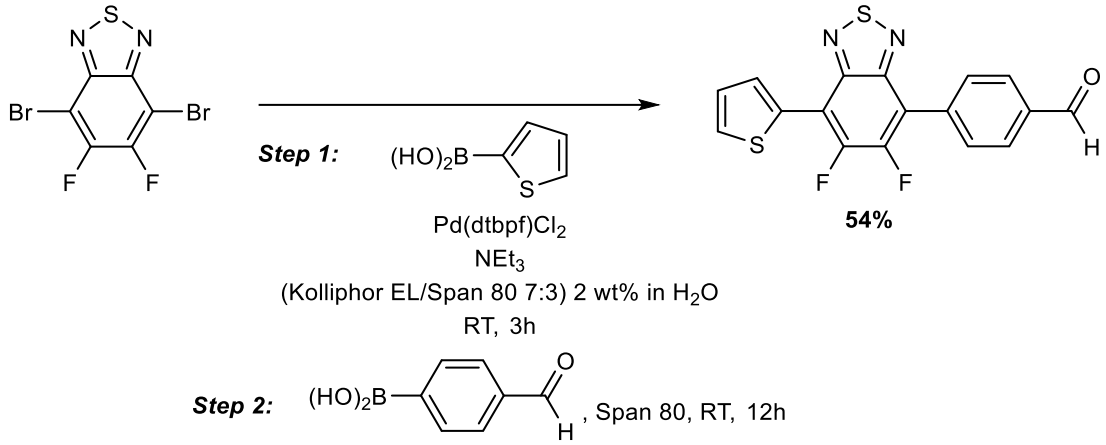

The crude was purified by column chromatography using heptane/DCM = 8:2 as eluent. Isolated product: 194 mg (54%), orange powder. Mp: 171.1−171.4 °C. Anal. Calcd for $C_{17}H_8F_2N_2OS_2$: C, 56.97; H, 2.25; N, 7.82. Found: C, 56.64; H, 1.94; N, 7.77.

^{1}H-NMR (CDCl3, 400 MHz): δ 10.17 (s, 1H), 8.38 (ddd, J= 3.8, 1.1, 0.7 Hz, 1H), 8.09−8.12 (m, 2H), 8.03-8.06 (m, 2H), 7.69 (dd, J= 5.1, 1.1 Hz, 1H), 7.33 (ddd, J= 5.3, 3.9, 1.4 Hz, 1H).

^{13}C-NMR (CDCl3, 100 MHz): δ 191.7, 150.9 (dd, J= 259.3, 19.6 Hz), 149.9 (d, J= 8.0 Hz), 149.4 (dd, J= 260.6, 19.6 Hz), 149.0 (d, J= 8.7 Hz), 136.3, 136.2 (m), 131.5 (d, J= 8.7 Hz), 131.3 (d, J= 2.9 Hz), 131.2, 129.7, 129.5 (d, J= 6.5 Hz), 127.5, 116.2 (d, J= 13.8 Hz), 113.8 (dd, J= 12.5, 2.1 Hz).

UV-Vis Absorption and PL Spectra of derivative 22

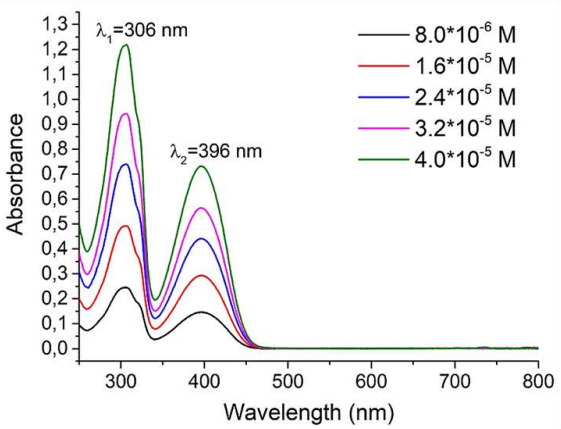

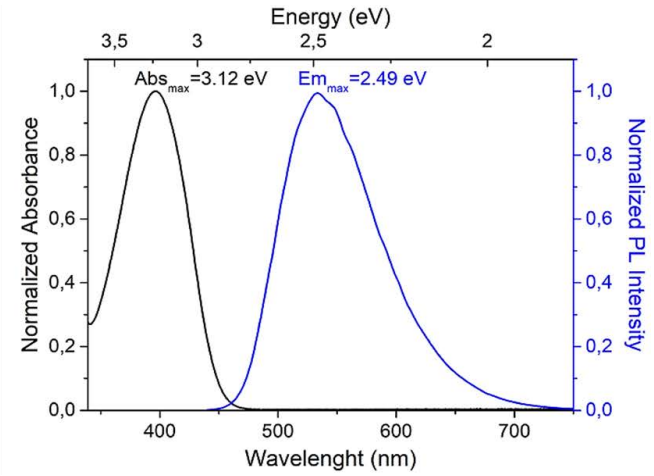

$\varepsilon_{(\lambda 2)}$ = 18 000 (± 400) $M^{-1}cm^{-1}$, solvent CH_2Cl_2. **Stokes shift** = 0.63 eV.

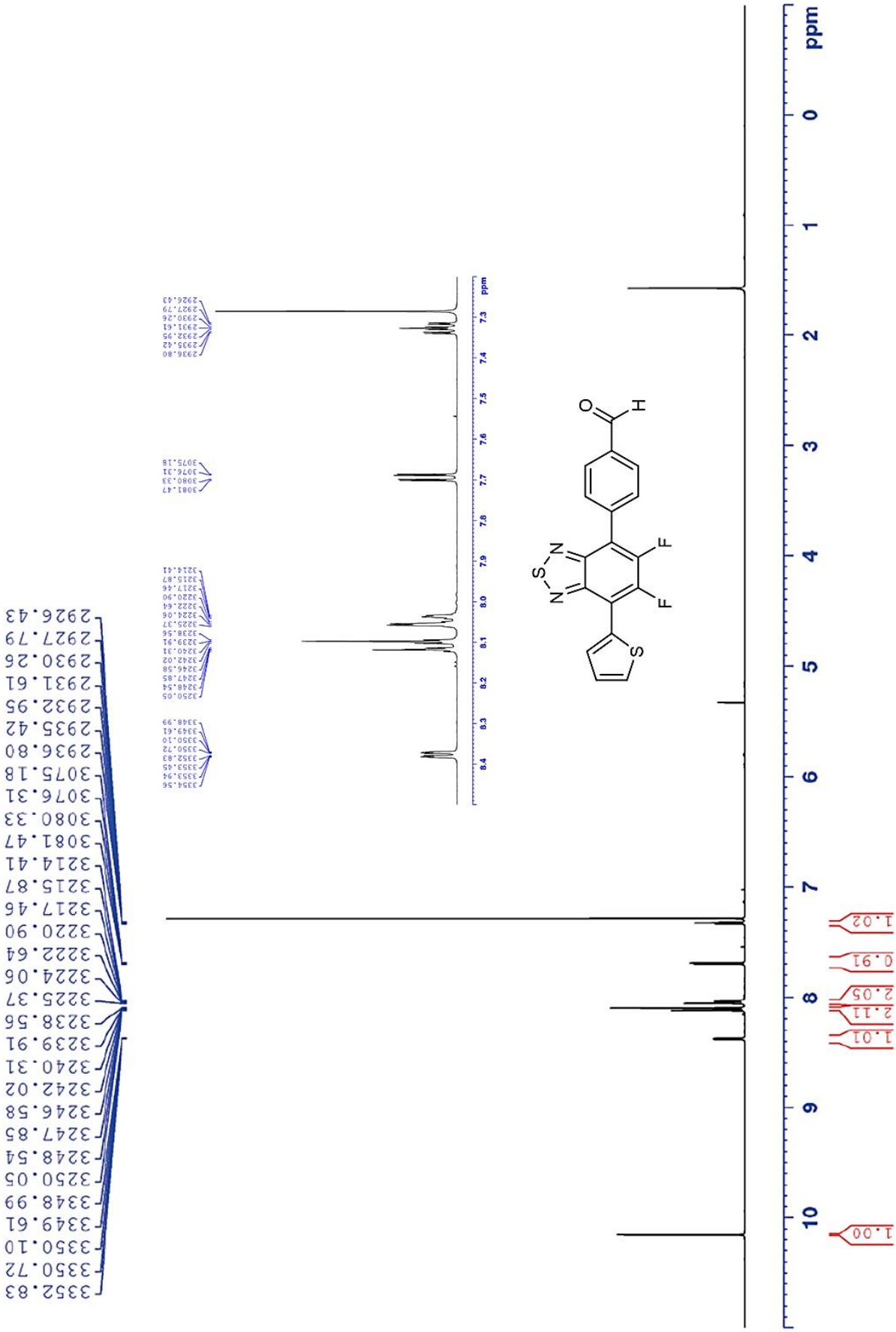

[1]H-NMR spectrum of derivative 22.

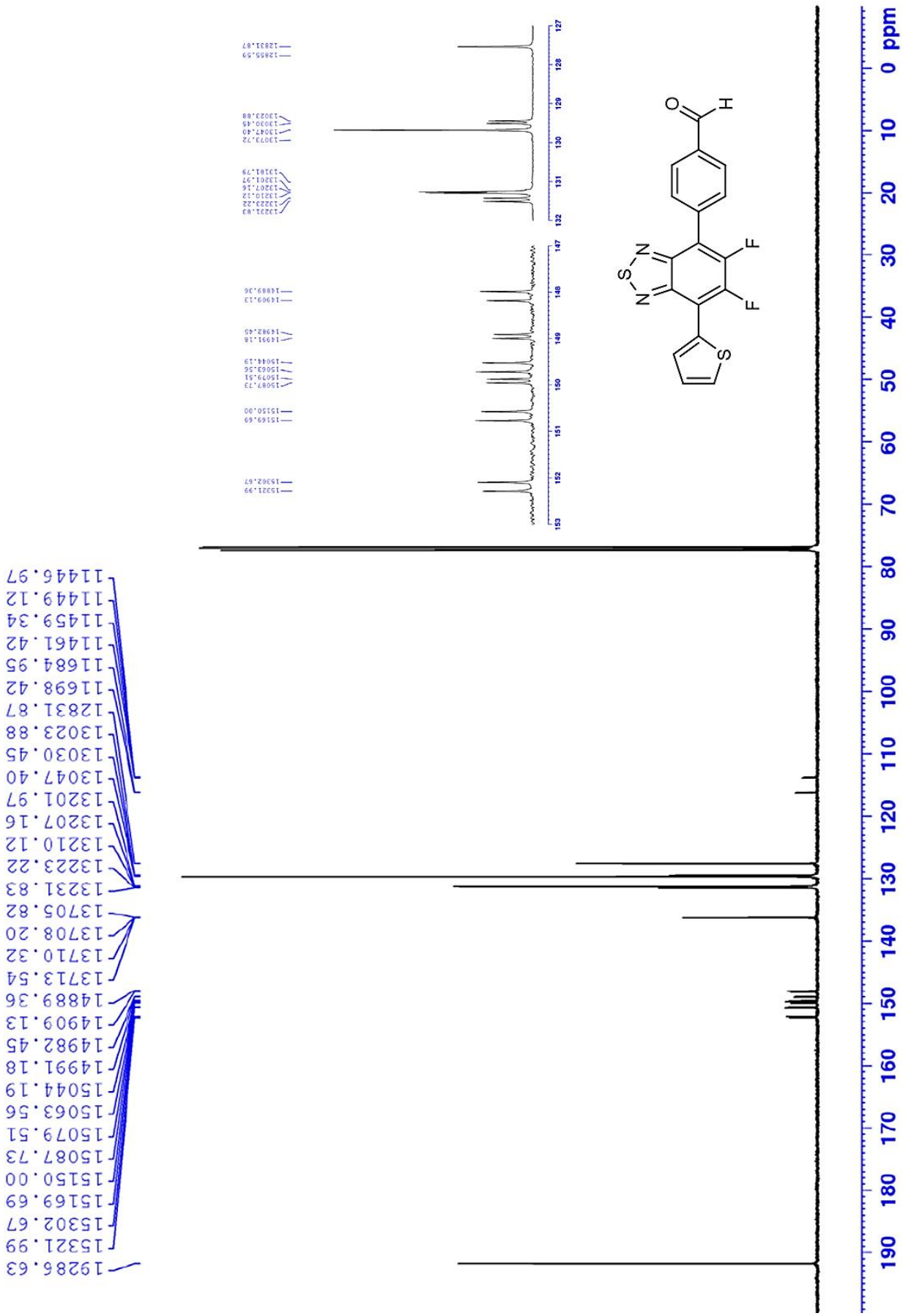

^{13}C-NMR spectrum of derivative 22.

2.6.4.4.4. Synthesis of 4-(4-(trifluoromethyl)phenyl)-7-(thiophene-2-yl)-5,6-difluoro-2,1,3-benzothiadiazole (23)

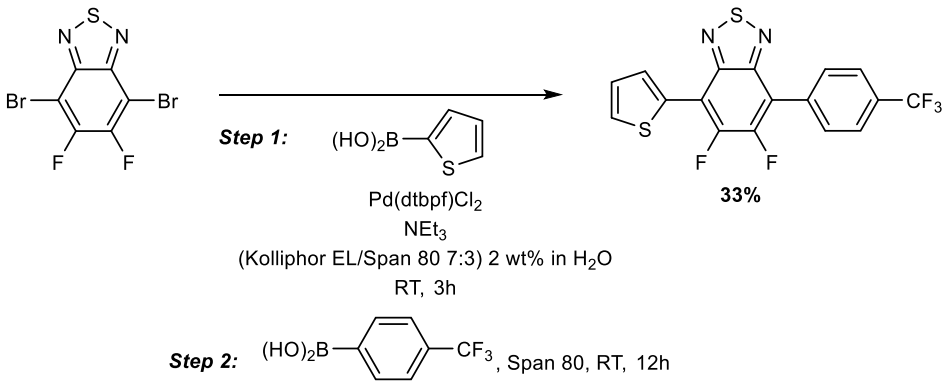

No eluent combination allowed us to separate chromatographically the product from DTBT. Therefore, the crude was refluxed in methanol and hot filtered twice to remove the symmetrical DTBT derivative. The obtained solid was then crystallized three times from heptane. Isolated product: 131 mg (33%), yellow needles. Mp: 124.7–125.3 °C. Anal. Calcd for $C_{17}H_7F_5N_2S_2$: C, 51.25; H, 1.77; N, 7.03. Found: C, 50.90; H, 1.42; N, 6.99.

^{1}H-NMR (CDCl3, 400 MHz): δ 8.37 (ddd, J = 3.8, 1.0, 0.7 Hz, 1H), 7.97–8.00 (m, 2H), 7.84–7.87 (m, 2H), 7.69 (dd, J = 5.1, 1.1 Hz, 1H), 7.33 (ddd, J = 5.2, 3.9, 1.4 Hz, 1H).

^{13}C-NMR (CDCl3, 100 MHz): δ 150.8 (dd, J = 257.9, 18.9 Hz), 150.0 (d, J = 8.7 Hz), 149.3 (dd, J = 260.7, 19.6 Hz), 149.0 (d, J = 8.7 Hz), 133.8 (m), 131.4 (d, J = 8.7 Hz), 131.3 (m), 131.01 (q, J = 32.7 Hz), 130.95 (d, J = 2.9 Hz), 129.4 (d, J = 6.5 Hz), 127.5, 125.5 (q, J = 3.6 Hz), 124.0 (q, J = 272.5 Hz), 116.1 (d, J = 13.8 Hz), 113.7 (dd, J = 12.3, 2.1 Hz).

UV-Vis Absorption and PL Spectra of derivative 23

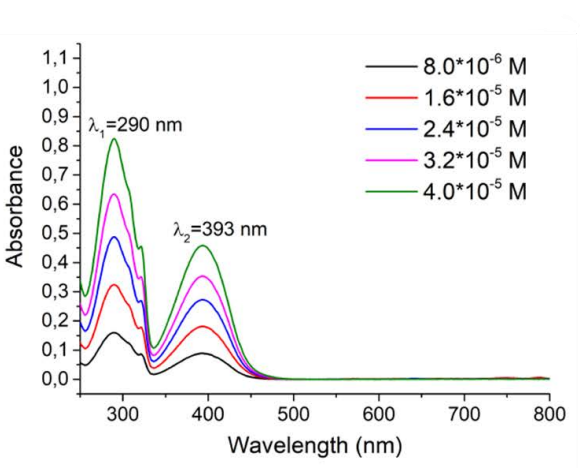

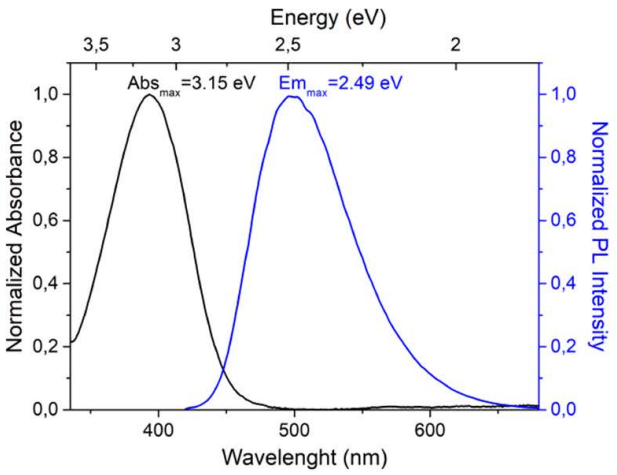

$\varepsilon_{(\lambda 2)}$ = 11 400 (± 200) $M^{-1}cm^{-1}$, solvent CH_2Cl_2. **Stokes shift** = 0.66 eV.

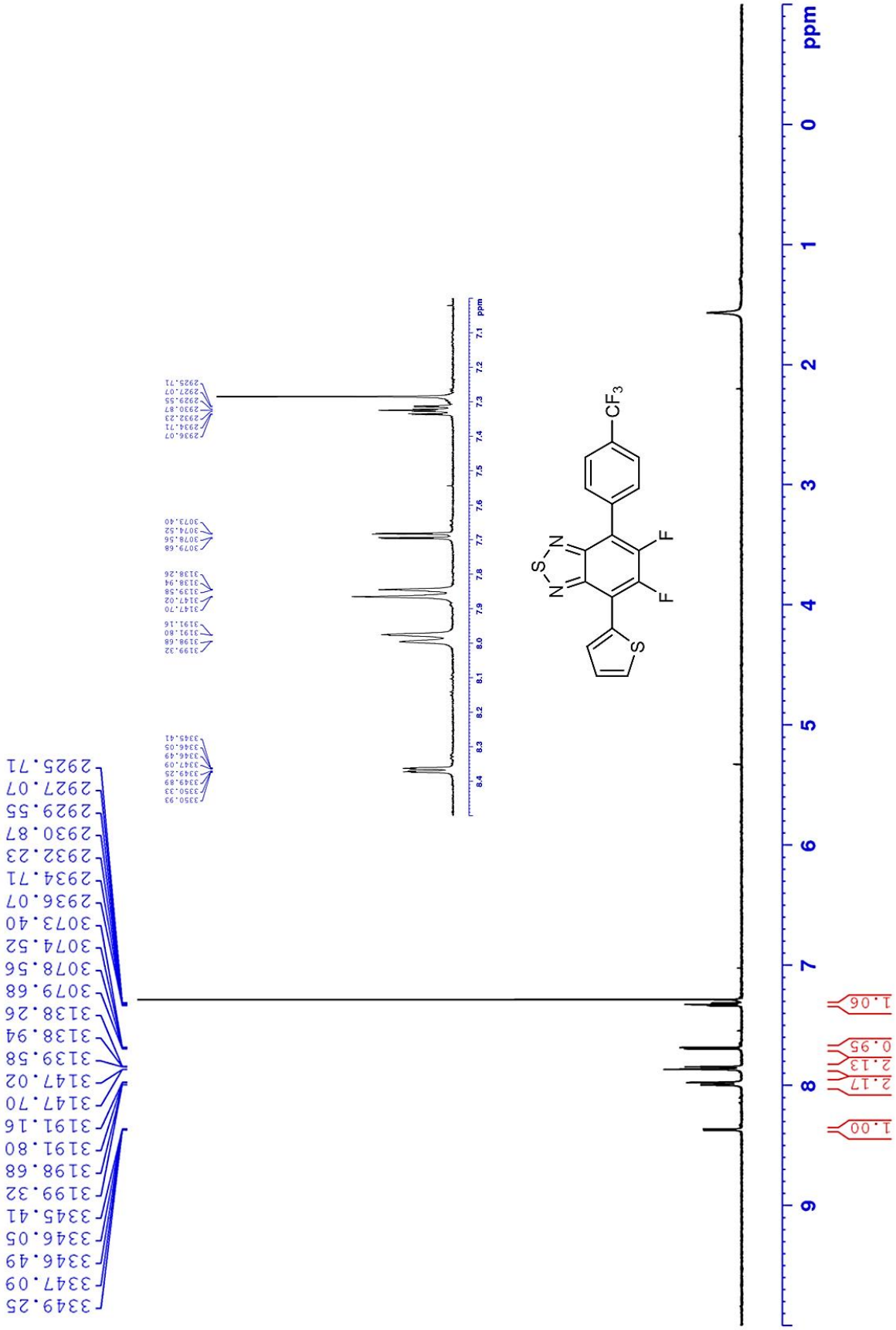

^{1}H-NMR spectrum of derivative 23.

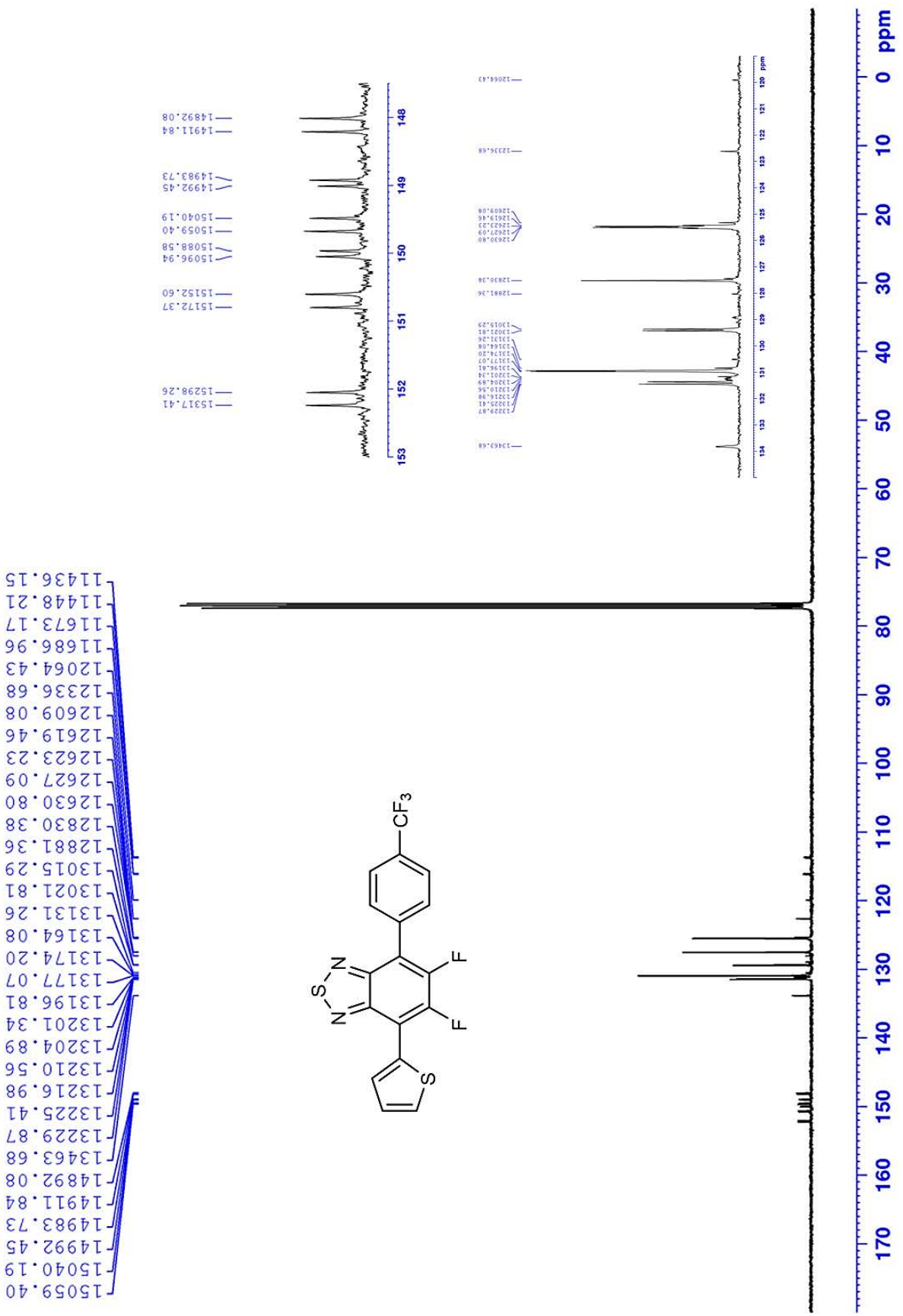

^{13}C-NMR spectrum of derivative 23.

2.6.4.4.5. Synthesis of 4-(2,5-dimethylphenyl)-7-(thiophene-2-yl)-5,6-difluoro-2,1,3-benzothiadiazole (24)

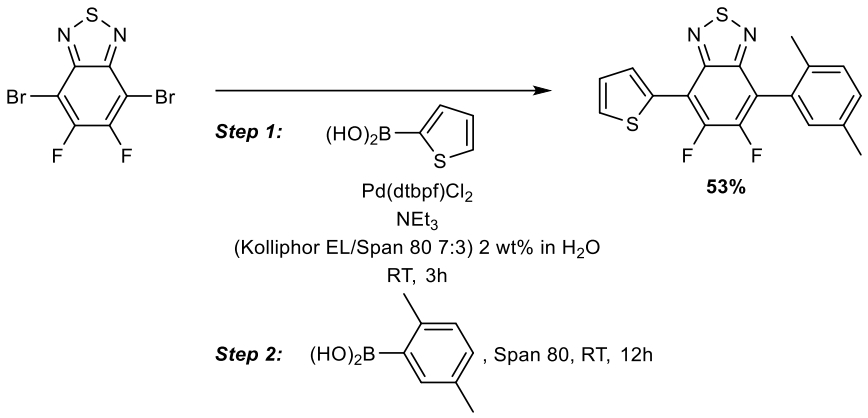

The crude was purified by column chromatography using petroleum ether/toluene = 8:2 as eluent. Isolated product: 190 mg (53%), yellow powder. Mp: 96.8–97.3 °C. Anal. Calcd for $C_{18}H_{12}F_2N_2S_2$: C, 60.32; H, 3.37; N, 7.82. Found: C, 60.46; H, 3.41; N, 7.56.

^{1}H-NMR (CDCl3, 400 MHz): δ 8.33 (ddd, J= 3.8, 1.1, 0.6 Hz, 1H), 7.64 (dd, J= 5.1, 1.1 Hz, 1H), 7.28–7.32 (m, 2H), 7.24–7.26 (m, 1H), 7.20 (s, 1H), 2.41 (s, 3H), 2.15 (s, 3H).

^{13}C-NMR (CDCl3, 100 MHz): δ 150.9 (d, J= 8.7 Hz), 150.4 (dd, J= 255.0, 18.9 Hz), 149.7 (dd, J= 260.9, 19.7 Hz), 148.8 (d, J= 8.7 Hz), 135.4, 134.2, 131.5 (dd, J= 5.8, 3.6 Hz Hz), 131.02, 131.00 (d, J= 8.7 Hz), 130.5, 130.3, 129.4 (d, J= 1.1 Hz), 128.9 (d, J= 6.5 Hz), 127.4, 118.2 (d, J= 16.4 Hz), 112.9 (dd, J= 12.4, 1.4 Hz), 21.0, 19.6 (d, J= 1.5 Hz).

UV-Vis Absorption and PL Spectra of derivative 24

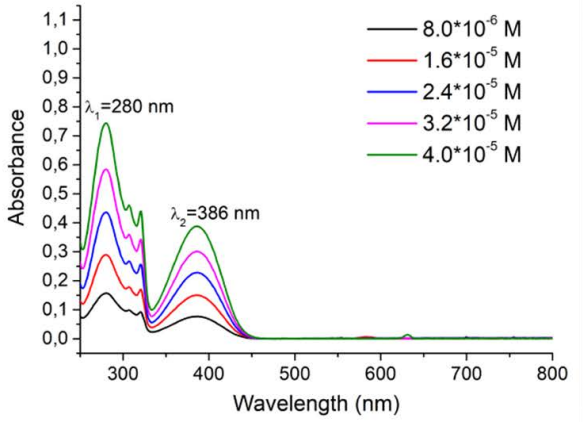

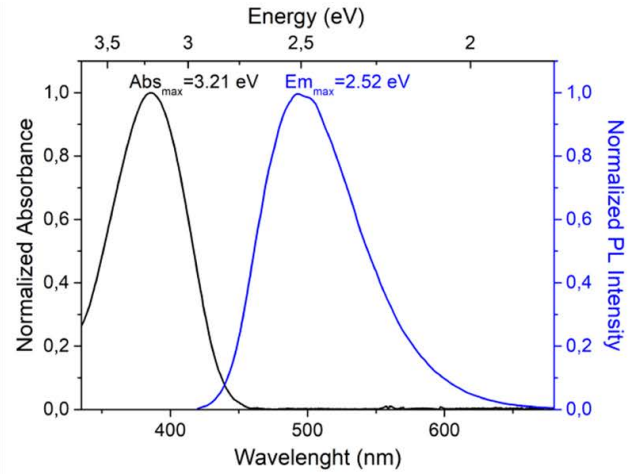

$\varepsilon_{(\lambda 2)}$ = 9 700 (± 200) $M^{-1}cm^{-1}$, solvent CH_2Cl_2. **Stokes shift** = 0.69 eV.

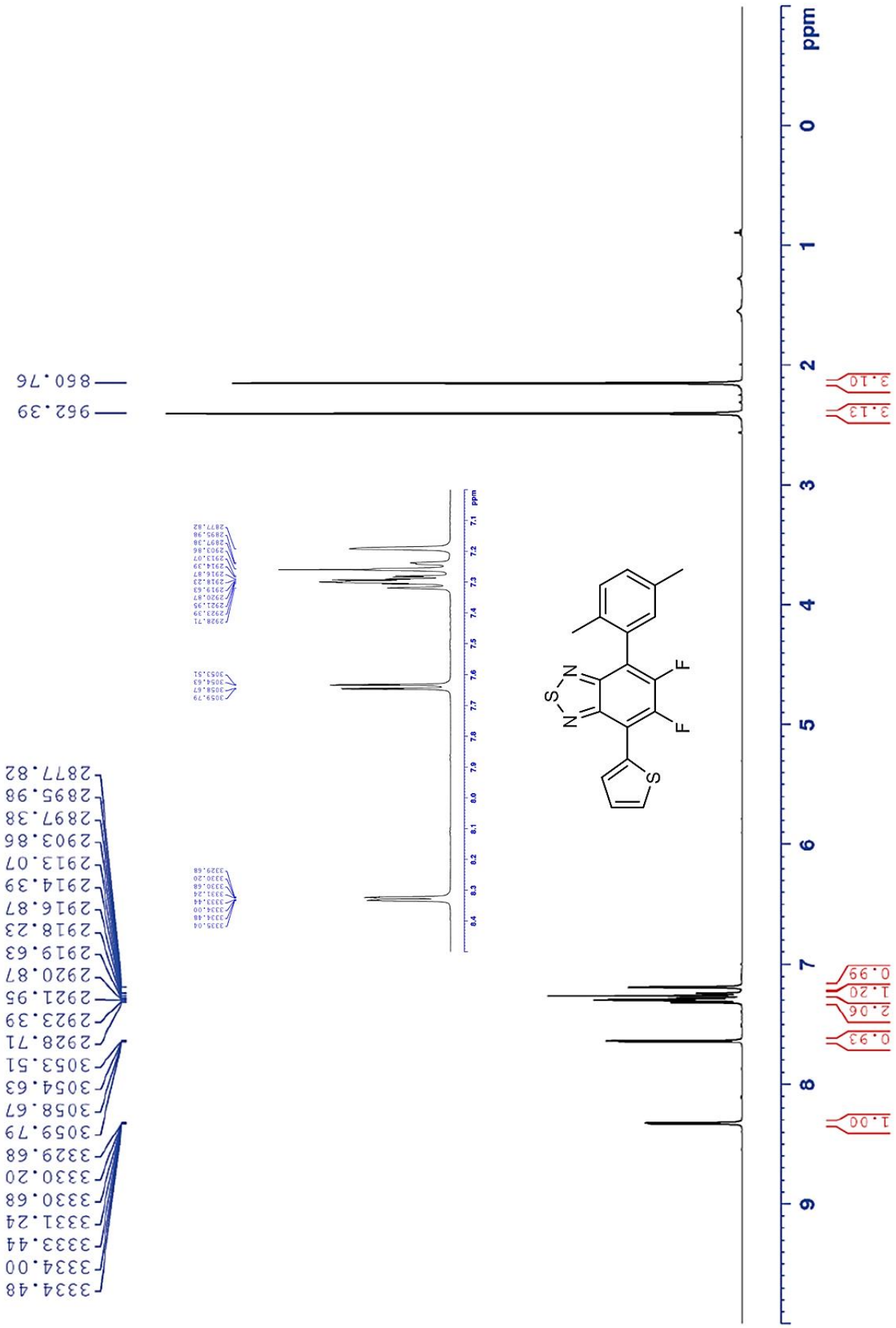

[1]H-NMR spectrum of derivative 24.

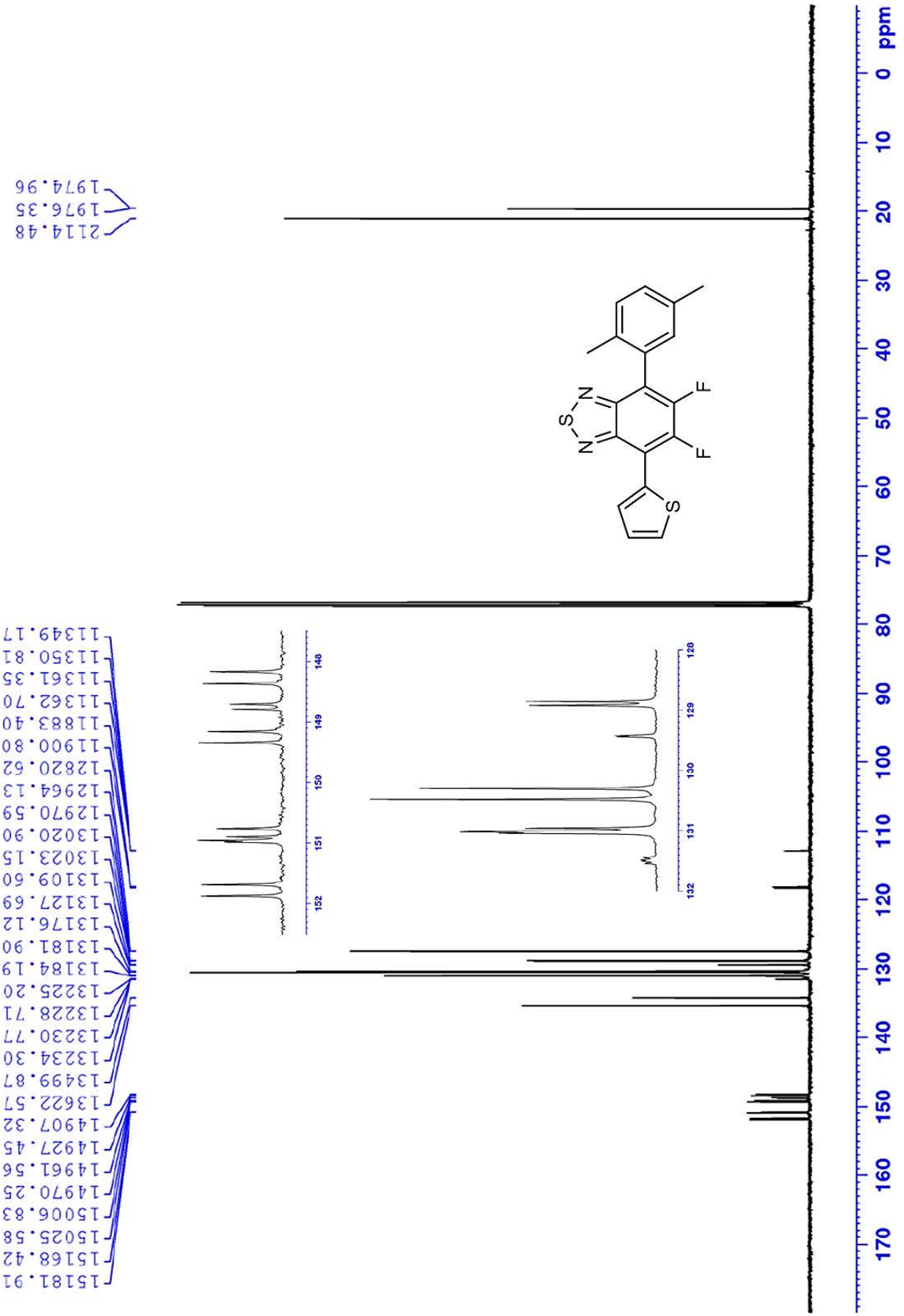

^{13}C-NMR spectrum of derivative 24.

2.6.4.4.6. Synthesis of 4-(naphthalen-1-yl)-7-(thiophene-2-yl)-5,6-difluoro-2,1,3-benzothiadiazole (25)

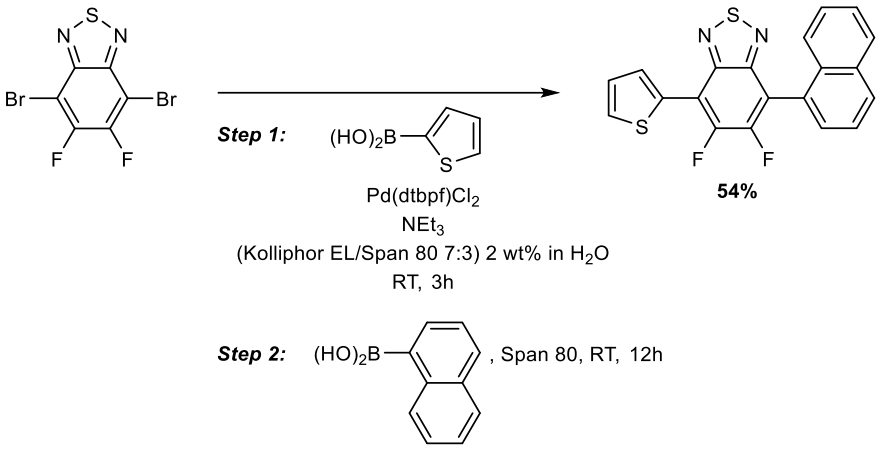

The crude was purified by column chromatographyusing heptane/DCM = 8:2 as eluent. Isolated product: 207 mg (54%), yellow powder. Mp: 149.0−149.5 °C. Anal. Calcd for $C_{20}H_{10}F_2N_2S_2$: C, 63.14; H, 2.65; N, 7.36. Found: C, 63.36; H, 2.94; N, 7.02.

^{1}H-NMR (CDCl3, 400 MHz): δ 8.38 (ddd, J= 3.8, 1.1, 0.6 Hz, 1H), 8.05 (dd, J= 7.0, 2.4 Hz, 1H), 7.98 (d, J= 8.2 Hz, 1H), 7.64−7.69 (m, 3H), 7.54 (ddd, J= 8.3, 6.6, 1.4 Hz, 1H), 7.48−7.51 (m, 1H), 7.43 (ddd, J= 8.5, 6.6, 1.3 Hz, 1H), 7.32 (ddd, J= 5.2, 3.8, 1.3 Hz, 1H).

^{13}C-NMR (CDCl3, 100 MHz): δ 151.4 (d, J= 8.4 Hz), 151.2 (dd, J= 256.8, 20.1 Hz), 149.4 (dd, J= 262.1, 21.4 Hz), 148.8 (d, J= 8.3 Hz), 133.8, 131.6, 131.5 (m), 131.1 (d, J= 8.0 Hz), 129.9, 129.0 (m), 128.7, 127.7 (d, J= 2.5 Hz), 127.4, 126.7, 126.2, 125.30, 125.27, 116.8 (d, J= 16.7 Hz), 113.4 (d, J= 12.0 Hz).

UV-Vis Absorption and PL Spectra of derivative 25

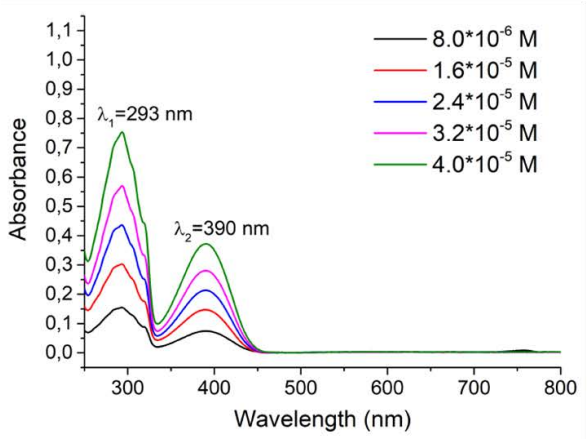

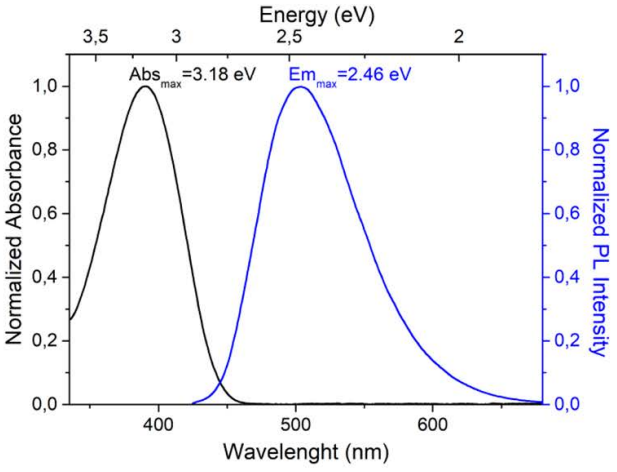

$\varepsilon_{(\lambda 2)}$ = 9 100 (± 300) $M^{-1}cm^{-1}$, solvent CH_2Cl_2. **Stokes shift** = 0.72 eV.

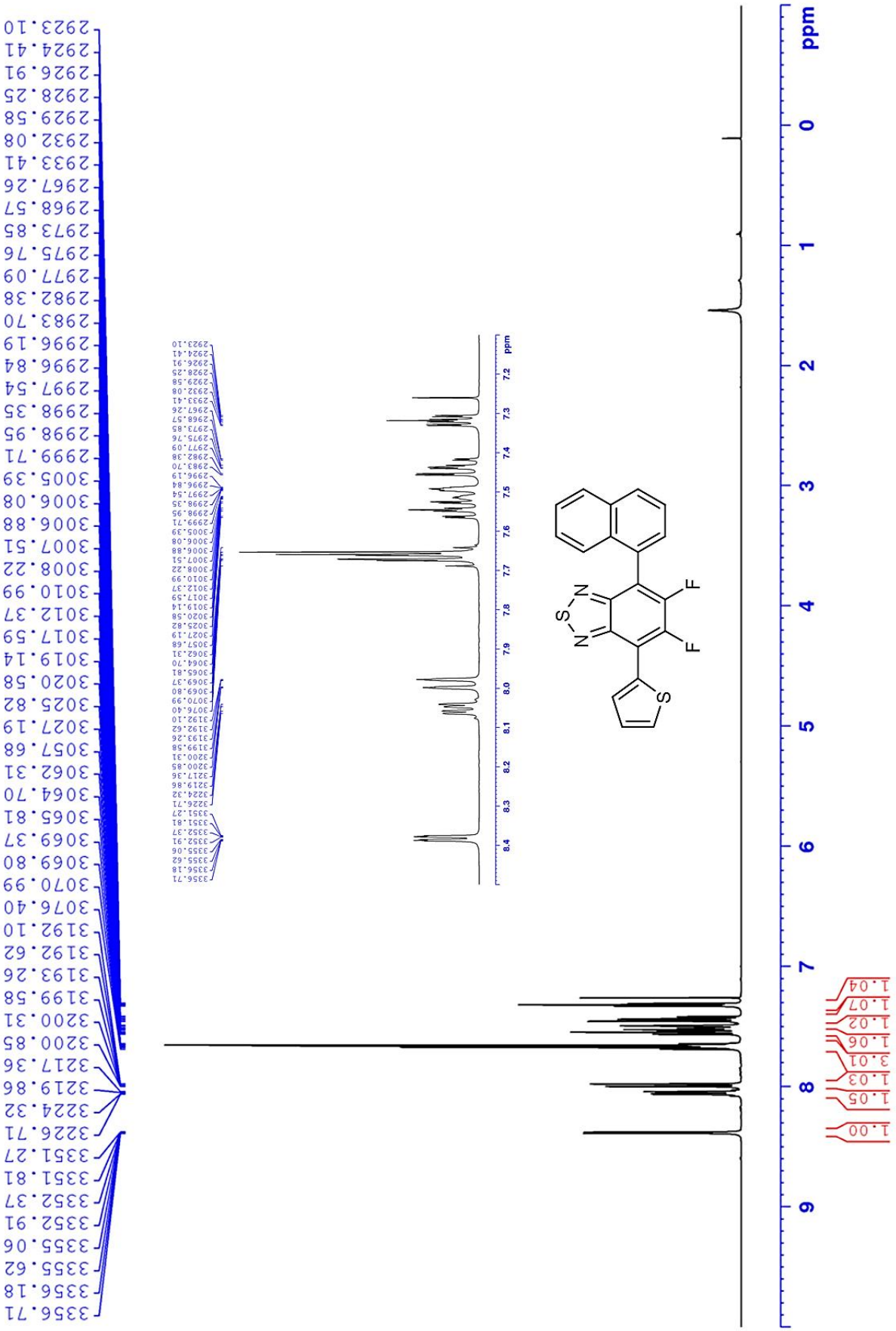

^{1}H-NMR spectrum of derivative 25.

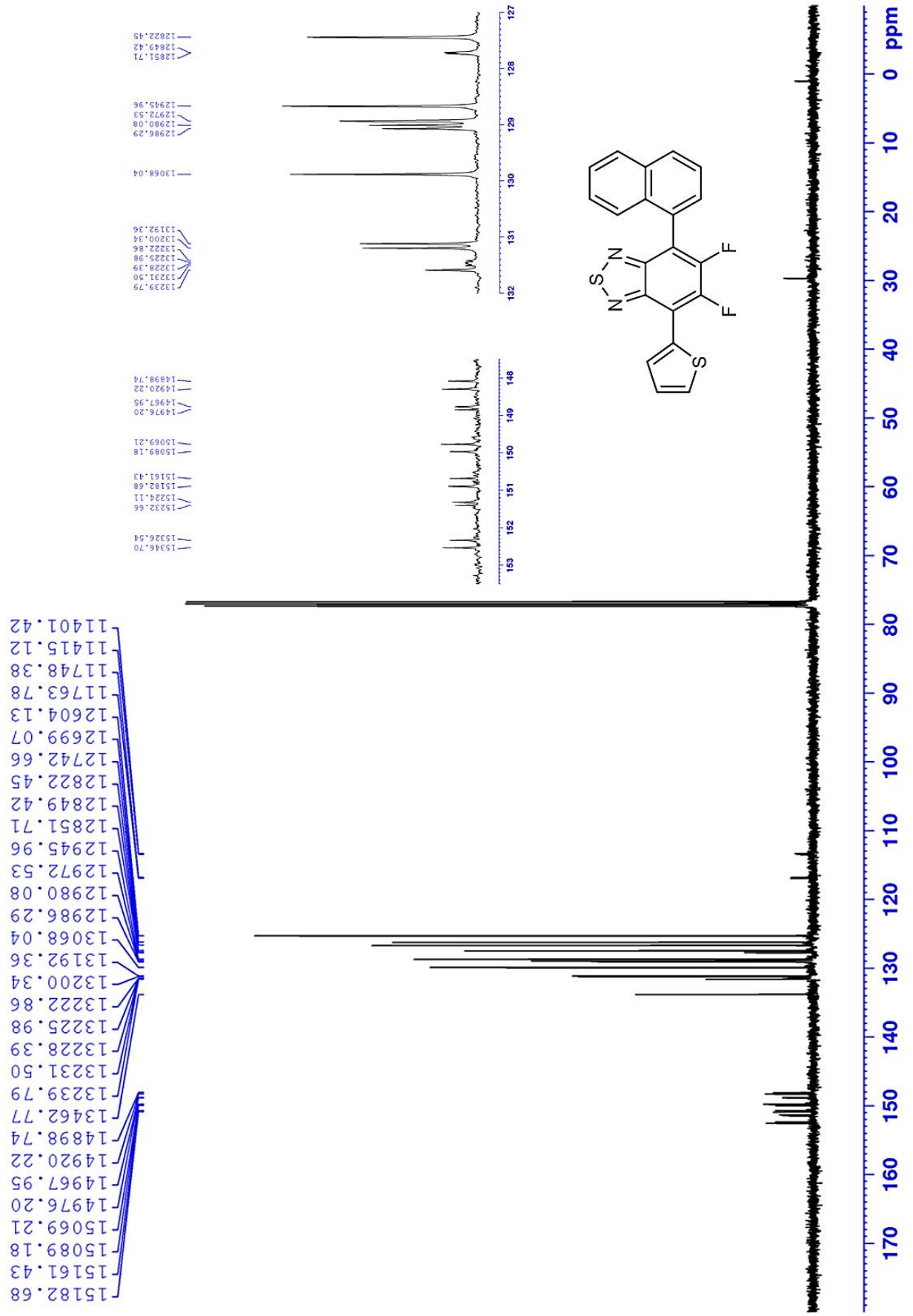

^{13}C-NMR spectrum of derivative 25.

2.6.4.4.7. Synthesis of 4-(9H-fluoren-2-yl)-7-(thiophene-2-yl)-5,6-difluoro-2,1,3-benzothiadiazole (26)

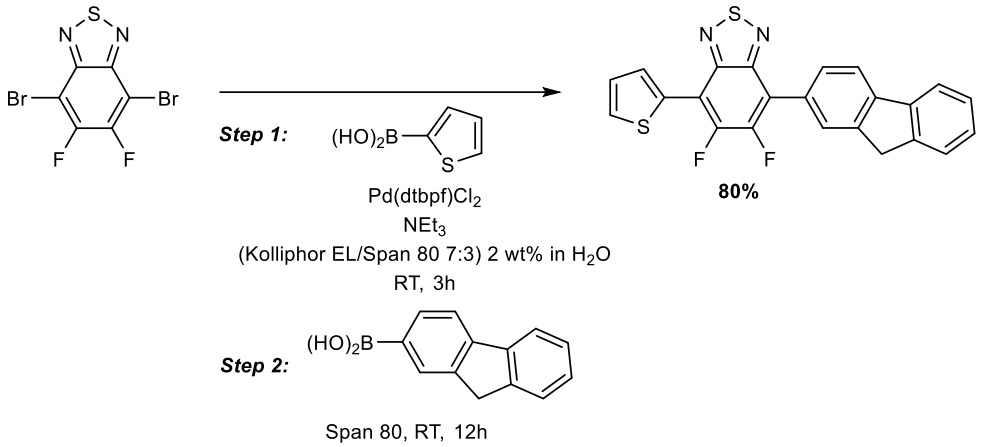

The crude was purified by column chromatography using petroleum ether/toluene = 7:3 as eluent. Isolated product: 335 mg (80%), orange powder. Mp: 196.4−197.0 °C. Anal. Calcd for $C_{23}H_{12}F_2N_2S_2$: C, 66.01; H, 2.89; N, 6.69. Found: C, 65.60; H, 2.67; N, 6.67.

^{1}H-NMR (CDCl3, 400 MHz): δ 8.34 (ddd, J= 3.8, 1.1, 0.6 Hz, 1H), 8.02 (m, 1H), 7.99 (dd, J= 7.9, 0.6 Hz, 1H), 7.85−7.90 (m, 2H), 7.66 (dd, J= 5.2, 1.1 Hz, 1H), 7.61 (d, J= 7.3 Hz, 1H), 7.45 (t, J= 7.5 Hz, 1H), 7.38 (td, J= 7.4, 1.3 Hz), 7.31 (ddd, J= 5.2, 3.9, 1.3 Hz, 1H), 4.05 (s, 2H).

^{13}C-NMR (CDCl3, 100 MHz): δ 150.6 (d, J= 8.7 Hz), 150.4 (dd, J= 255.5, 18.9 Hz), 149.8 (dd, J= 260.7, 20.3 Hz), 149.0 (d, J= 8.7 Hz), 143.8, 143.4, 142.7, 141.1, 131.6 (dd, J= 5.8, 3.6 Hz), 131.0 (d, J= 8.7 Hz), 129.4 (d, J= 2.9 Hz), 128.9 (d, J= 6.5 Hz), 128.4, 127.4, 127.3, 127.1 (d, J= 2.9 Hz), 126.9, 125.1, 120.3, 119.9, 118.2 (d, J= 14.1 Hz), 112.5 (dd, J= 12.4, 1.4 Hz), 37.1.

UV-Vis Absorption and PL Spectra of derivative 26

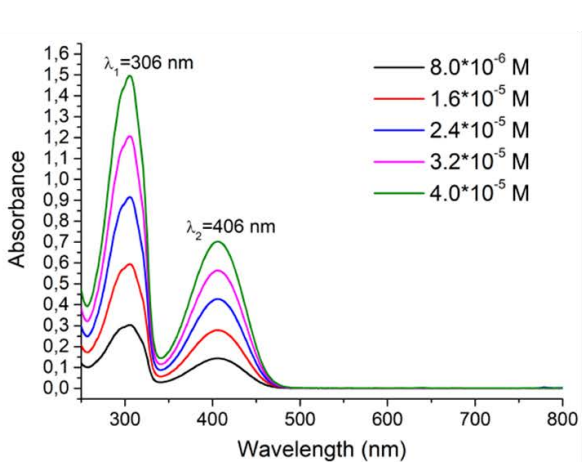

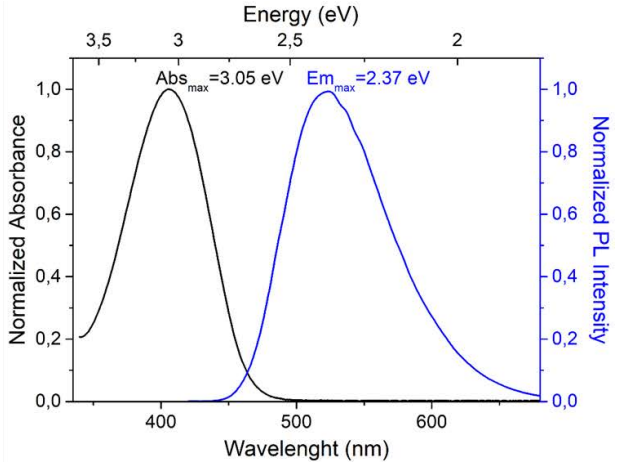

$\varepsilon_{(\lambda 2)}$ = 17 550 (± 140) $M^{-1}cm^{-1}$, solvent CH_2Cl_2. **Stokes shift** = 0.68 eV.

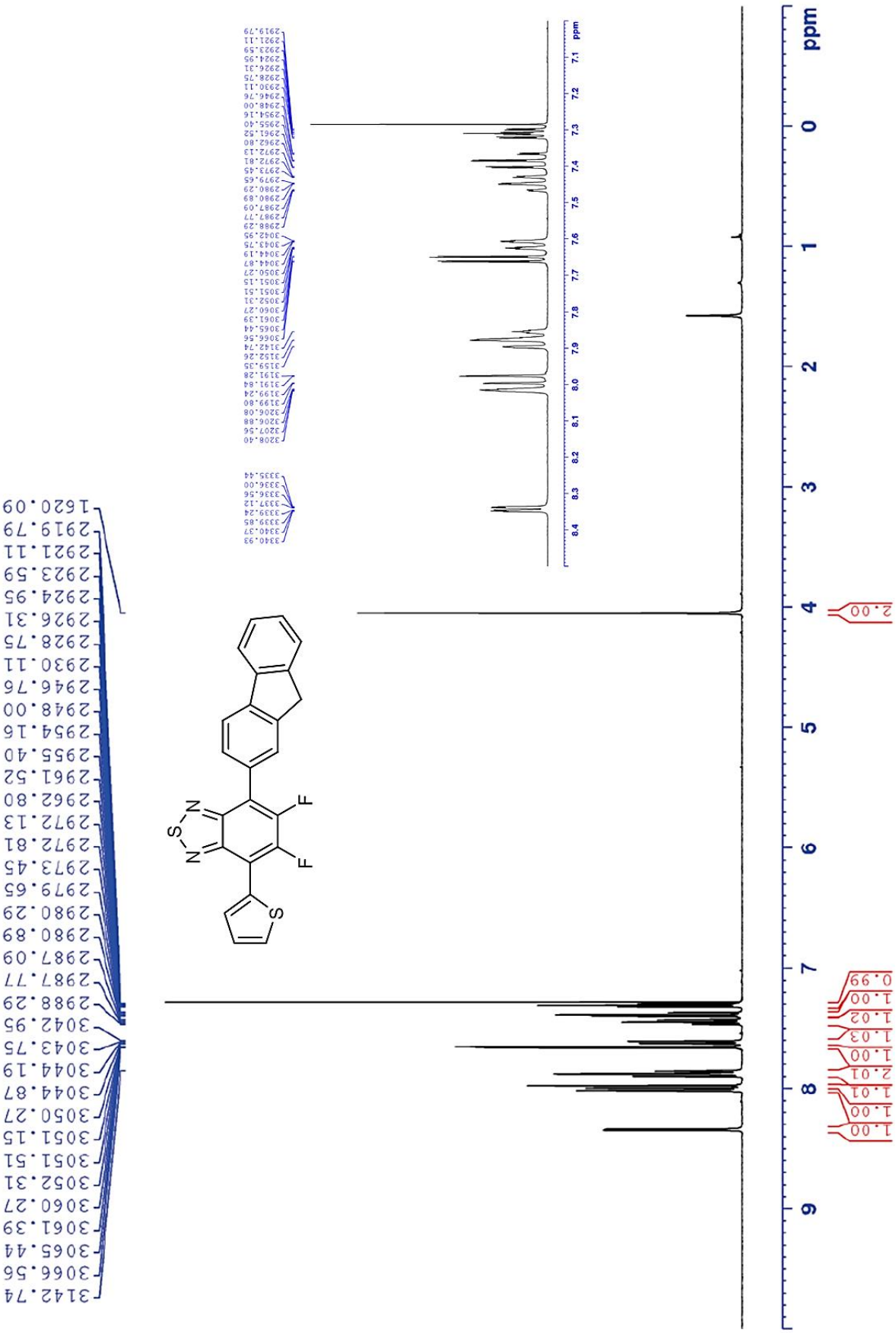

^{1}H-NMR spectrum of derivative 26.

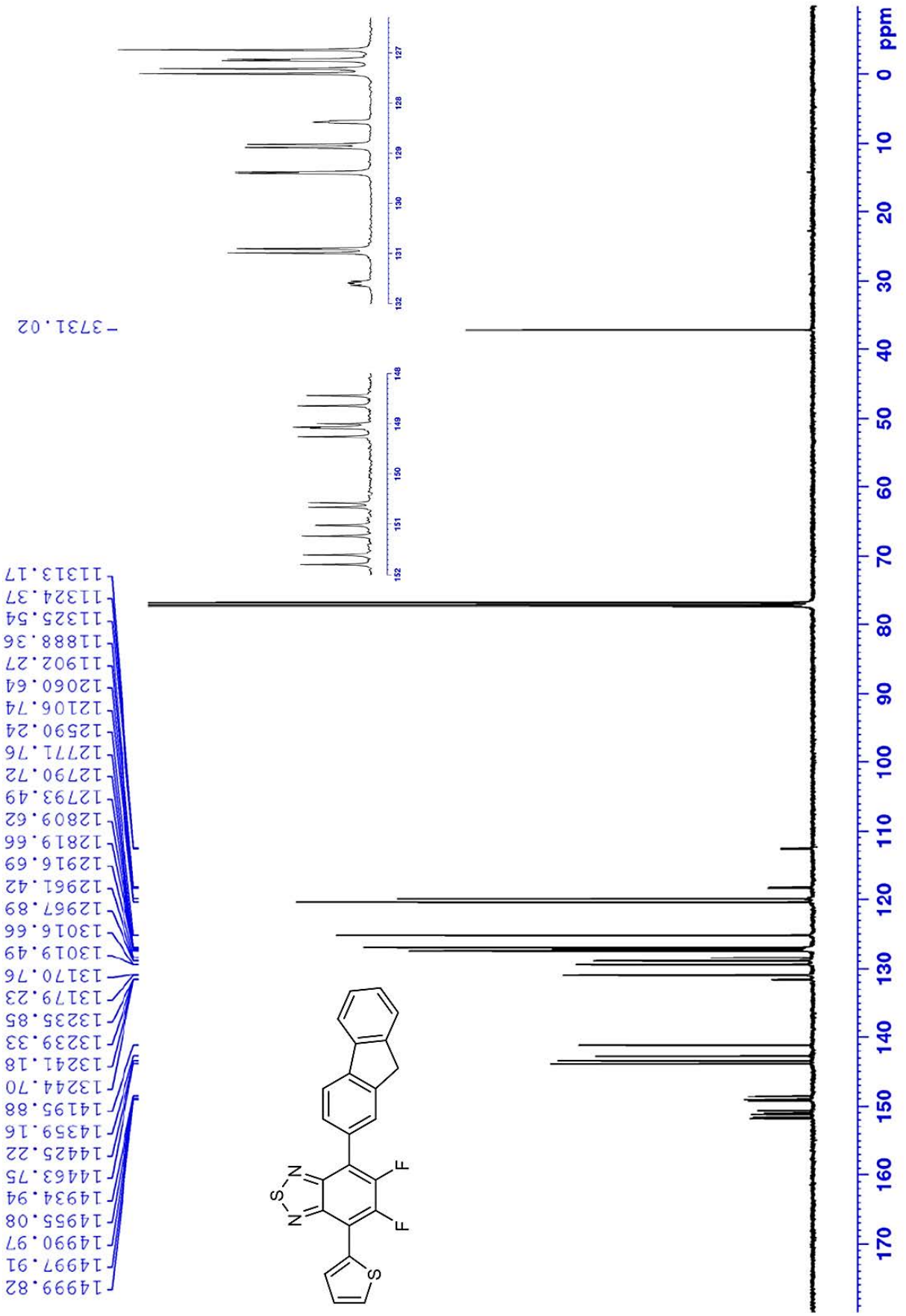

^{13}C-NMR spectrum of derivative 26.

2.6.4.4.8. Synthesis of 4-[5-hexyl-(2,2-bithiophen)-5-yl]-7-(thiophene-2-yl)-5,6-difluoro-2,1,3-benzothiadiazole (27)

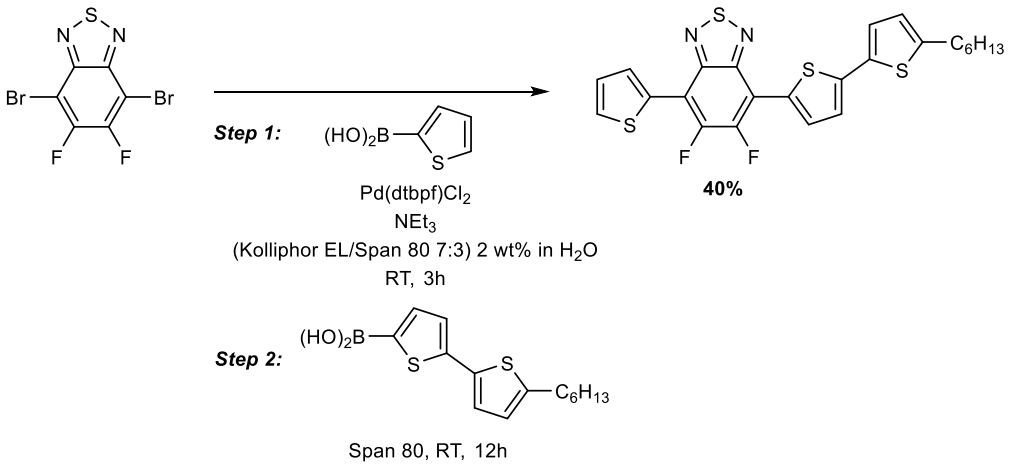

The crude was purified by column chromatography using petroleum ether/toluene = 6:4 as eluent. Isolated product: 201 mg (40%), red powder. Mp: 125.4−126.5 °C. Anal. Calcd for $C_{24}H_{20}F_2N_2S_4$: C, 57.34; H, 4.01; N, 5.57. Found: C, 56.99; H, 3.82; N, 5.40.

^{1}H-NMR (CDCl3, 400 MHz): δ 8.28 (dd, J= 3.8, 1.1 Hz, 1H), 8.19 (d, J= 4.0 Hz, 1H), 7.60 (dd, J= 5.2, 1.2 Hz, 1H), 7.25−7.27 (m, 1H), 7.22 (d, J= 4.1 Hz, 1H), 7.73 (dt, J= 3.6, 1.0 Hz, 1H), 2.82 (t, J= 7.6 Hz, 2H), 1.71 (m, 2H), 1.31−1.43 (m, 6H), 0.91 (t, J= 7.1, 3H).

^{13}C-NMR (CDCl3, 100 MHz): δ 149.9 (dd, J= 260.0, 20.4 Hz), 149.6 (dd, J= 259.4, 20.8 Hz), 148.9, 148.7, 146.6, 141.5 (t, J= 2.9 Hz), 134.2, 131.9 (dd, J= 5.7, 3.6 Hz), 131.7, 130.8 (t, J= 3.6 Hz), 129.7 (d, J= 2.2 Hz), 128.8 (t, J= 2.9 Hz), 127.4, 125.1, 124.2, 123.2, 111.7 (dd, J= 9.5, 3.6 Hz), 111.3 (dd, J= 8.9, 5.1 Hz), 31.6, 31.5, 30.3, 28.8, 22.6, 14.1.

UV-Vis Absorption and PL Spectra of derivative 27

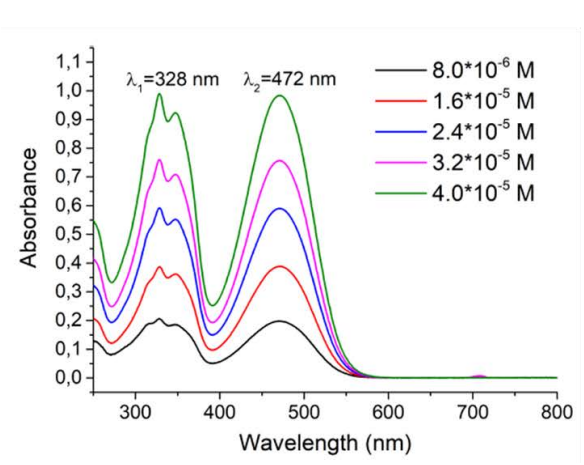

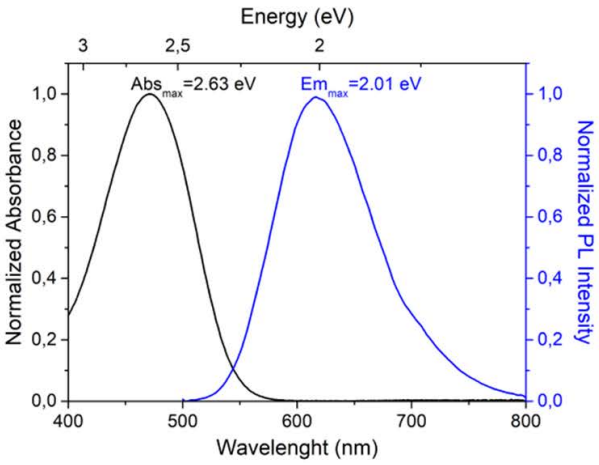

$\varepsilon_{(\lambda 2)}$ = 24 300 (± 600) $M^{-1}cm^{-1}$, solvent CH_2Cl_2. **Stokes shift** = 0.62 eV.

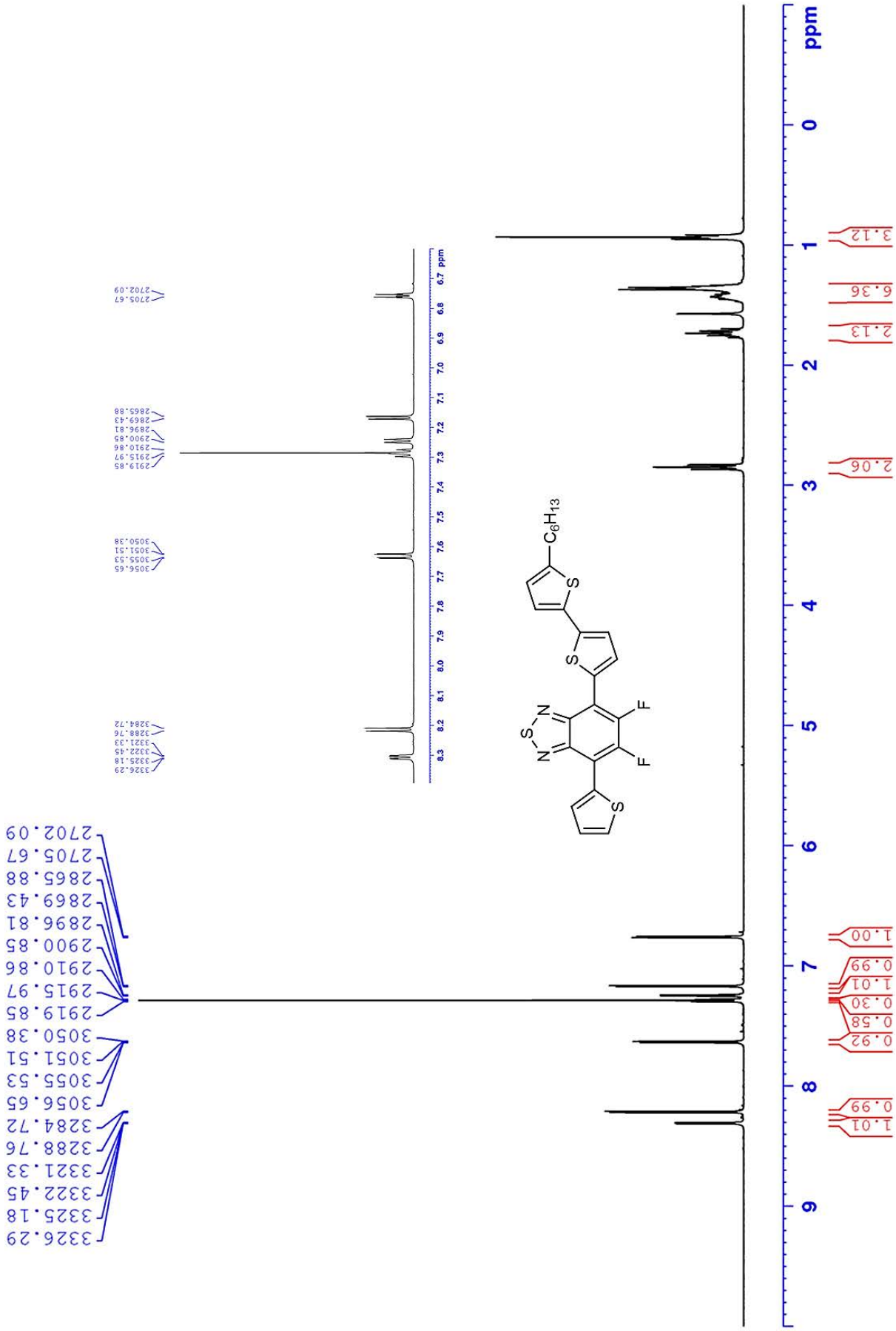

[1]H-NMR spectrum of derivative 27.

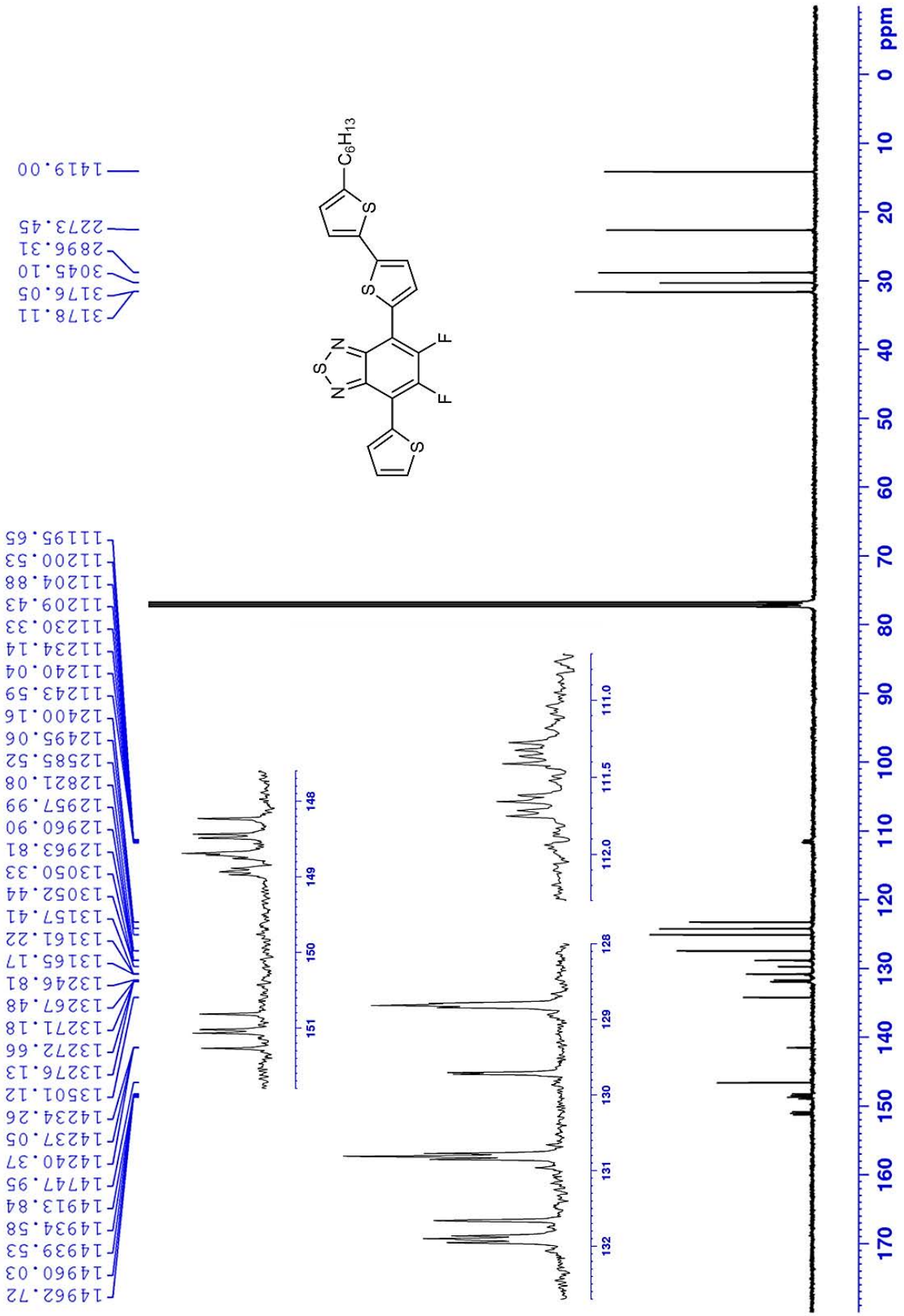

^{13}C-NMR spectrum of derivative 27.

2.7. Suzuki-Miyaura Synthesis of π-Extended [1]BenzoThieno[3,2-b][1]BenzoThiophene (BTBT) Derivatives in an Aromatic Micellar Medium

This work has already been published and it is entitled *"Efficient synthesis of organic semiconductors by Suzuki-Miyaura coupling in an aromatic micellar medium",* Green Chem., **2019**, 21, 4400–4405. https://doi.org/10.1039/C9GC01071H [83]

2.7.1. Introduction

Amongst the most notorious classes of p-type molecular semiconductors for highly-performing OFET devices, [1]benzothieno[3,2-b][1]benzothiophene (BTBT) derivatives represent one of the most promising candidates of major interest.[110,111] The BTBT core is a π-conjugated, completely planar and rigid structure with the strong tendency to form rigidly packed, poorly soluble crystals where cohesive forces are dominated by π-π interactions. Soluble BTBT derivatives can be prepared through alkyl side-chain(s) functionalization. Such functional derivatives are particularly performing semiconductors, with charge carrier mobilities in excess of 10 $cm^2V^{-1}s^{-1}$, [112] precisely because of their highly ordered π-stacked crystal structures that as well lead to highly ordered thin film morphologies.

To date, there is no reference in the literature about the sustainable synthesis of such valuable materials, in particular concerning the micellar catalysis approach. So far, we have seen that inexpensive industrial surfactants, such Kolliphor EL (K-EL), can be efficiently employed to carry out both Suzuki-Miyaura (S-M) and Buchwald-Hartwig (B-H) couplings on aromatic and heteroaromatic organic semiconductors under very mild conditions, in high yield and under a standard laboratory atmosphere.[54,64,69,74] On the other hand, designer surfactants derived from naturally occurring building blocks like Vitamin E containing polyethoxylated derivatives introduced by Prof. Lipshutz are also play a particularly relevant role in improving efficiency besides sustainability. However, yet not specifically designed for the synthesis organic semiconductors.[57] In particular, previous works demonstrated that some particularly tricky reactions involving complex semiconducting structures might require careful tuning of conditions with an appropriate formulation selection (i.e. nature of the surfactant, mixtures of surfactants with controlled HLB, or moving from dispersion/suspension to emulsion) to afford satisfactory conversions and yields while moving from standard organic solvent to micellar environment.[54,70,113] The use of surfactants preferentially stabilizing colloidal dispersions of reagents versus products can also impact on results.[54] Previous experience suggest that more elaborate substrates having consolidated applications may require the use of organic co-solvents.[69,74] Such a strategy is generally successful in the case of poorly dispersible chemicals. Still, crystalline, rigid, and poorly soluble BTBT derivatives are expected to be particularly challenging in the above-mentioned respects. Aiming at reducing the organic solvents consumption, the extension of such a protocol to the sustainable synthesis of BTBT derivatives requires redesigning of the surfactants employed. Surfactants specifically designed to afford specific interactions could provide unique performances, especially in the manufacturing of such highly crystalline π-π rich structures.

This work highlights two new designer surfactants, a naphthalenediimide-containing amphiphile (PiNap-750M) and a BTBT-containing amphiphile (BTBT-750M), both featuring extensive conjugated portions in the hydrophobic compartment, specifically introduced in order to establish specific π-π stacking interactions with the organic semiconducting building blocks. We will show how the exceptional dispersant capabilities of PiNap-750M towards π-extended derivatives featuring

micellar couplings with unprecedented performances in only water, at room temperature and with remarkably short contact times, affording the target compounds with unprecedented high simplicity and sustainability.

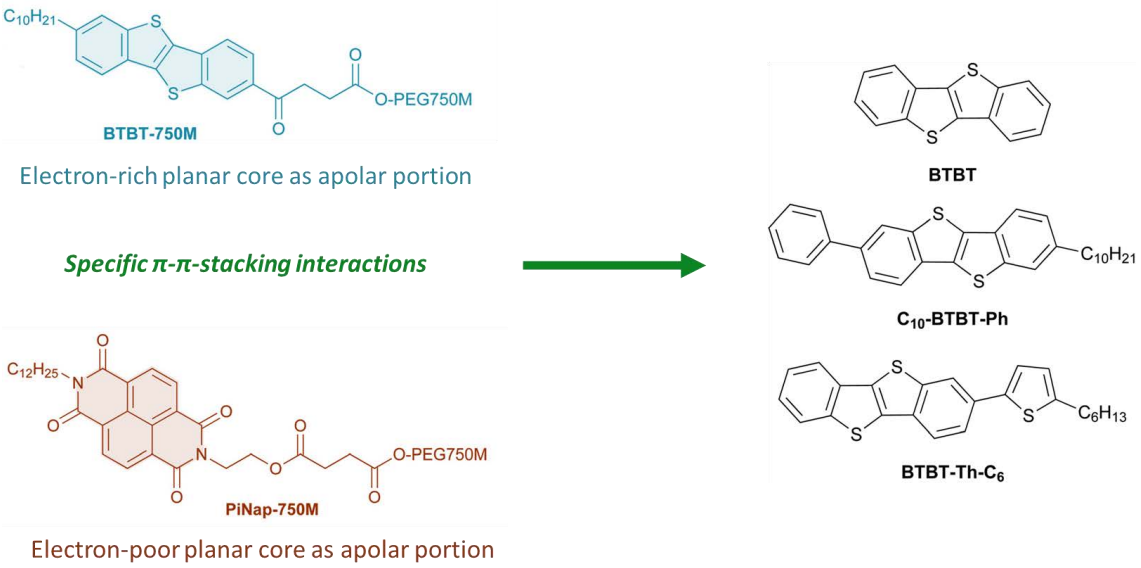

Figure 75. *Representative scheme of the π-conjugated designer surfactant approach for the synthesis of BTBT derivatives.*

2.7.2. Results and Discussion

Amongst the different BTBT derivatives reported in the literature, C_{10}-BTBT-Ph and BTBT-Th-C_6 (**Figure 75**) represent relevant synthetic targets as they are excellent hole carriers and relatively stable materials for highly-performing OFETs.[97,114] Their synthesis involve mainly three steps: first the BTBT core construction, which can be prepared in one-step from commercially available and relatively cheap reagents;[115] then the synthesis of the brominated derivatives (in the case of C_{10}-BTBT-Ph the alkyl chain functionalization is necessary before bromination), and finally the π-conjugation extension through standard cross-coupling reactions concerning Stille and Suzuki–Miyaura (S-M) couplings with appropriate arylboronic and organotin derivatives using organic solvents (**Figure 76)**

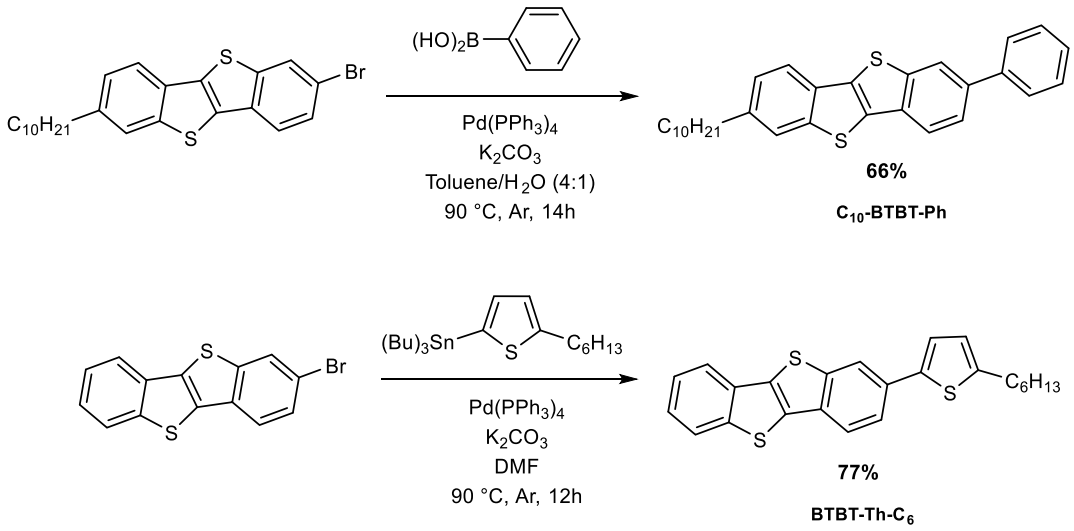

Figure 76. *Chemical structure of BTBT and reaction schemes of literature reported protocols to prepare two relevant structurally related molecular semiconductors C_{10}-BTBT-Ph[114] and BTBT-Th-C6[97].*

According to the generally higher sustainability of the S-M over the Stille reaction, we focused on the optimization of the former in both cases. Yet, prior to deal with the aforementioned targets, we studied the S-M coupling of 2-bromo-[1]benzothieno[3,2-b][1]benzothiophene (BTBT-Br) and phenylboronic acid as a model reaction (**Figure 77**). Reactions were performed with a stoichiometry ratio of 1:1.5:3:0.02 for BTBT-Br/phenylboronic acid/ NEt_3/Pd(dtbpf)Cl_2, respectively.

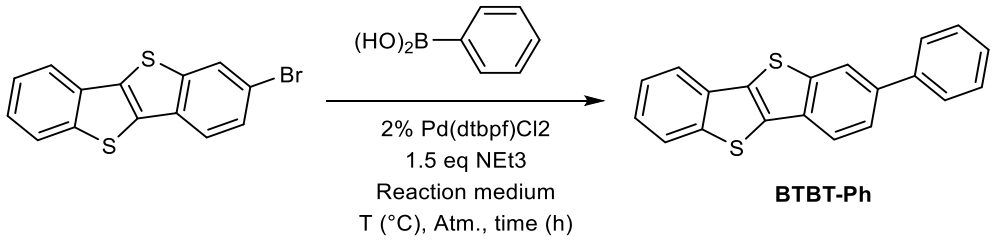

Entry	Medium	Atm.	T (°C)	Time (h)	Yield (%)
1	K-EL 2% wt	Air	25	6	26
2	K-EL 2% wt / THF 9:1 v/v	Air	25	6	50
3	K-EL 2% wt / toluene 9:1 v/v	Air	25	6	45
4	K-EL 2% wt / toluene 9:1 v/v	Air	80	1	90
5	BTBT-750M 2% wt	Air	25	24	73
6	PiNap-750M 2% wt	Air	25	1	78
7	BTBT-750M 2% wt	N_2	25	48	97
8	PiNap-750M 2% wt	N_2	25	1	97
9[a]	PiNap-750M 2% wt	N_2	25	12	97
10[b]	PiNap-750M 2% wt	N_2	25	24	67

a: 0.004 eq. of catalyst used. b: 0.002 eq. of catalyst used. NMR conversion is reported instead of yield.

Figure 77, Table 8. *Screening of the reaction conditions and formulation in the model micellar catalysed S-M coupling of BTBT-Br and phenylboronic acid.*

Again, we selected K-EL as standard surfactant according to our previous experience with S-M couplings of conjugated derivatives. K-EL is a very cheap natural derivative and it has demonstrated to be able to compete with different designer surfactants reported in literature for the synthesis of many relevant compounds without requiring the degassing of the reaction environment.[64] However, as shown in Entry 1 the use of a 2 wt% K-EL water solution as reaction medium displayed unsatisfactory results with only a 26% yield after 6h at room temperature. Prolonging the reaction time does not improve conversion. Convinced that the problem of the poor reactivity was related to the inability of K-EL to efficiently disperse such a highly crystalline derivative as BTBT-Br, we decided to approach the cosolvent strategy, accordingly also with our previous experience[69] and literature results under similar conditions.[73] As shown in Entries 2-4, the use of a cosolvent dramatically improved the reaction. Using a water-miscible cosolvent such as THF, with which the reaction mixture remains in the micellar regime, the yield increased to 50% with the same reaction time than using K-EL only. On the other hand, using a water-immiscible cosolvent such as toluene, with which the reaction mixture turns into an emulsion, results are comparable with THF at room temperature (45% yield) but far better working at 80 °C, leading to 90% yield after just 1 h and working under air. This latter satisfactory result took us to extend the emulsion method using the same conditions to the synthesis of relevant BTBT derivatives, including the aforementioned C_{10}-

BTBT-Ph and BTBT-Th-C_6 (the synthesis of the BTBT core, together with its brominated derivatives is reported in the following experimental section).

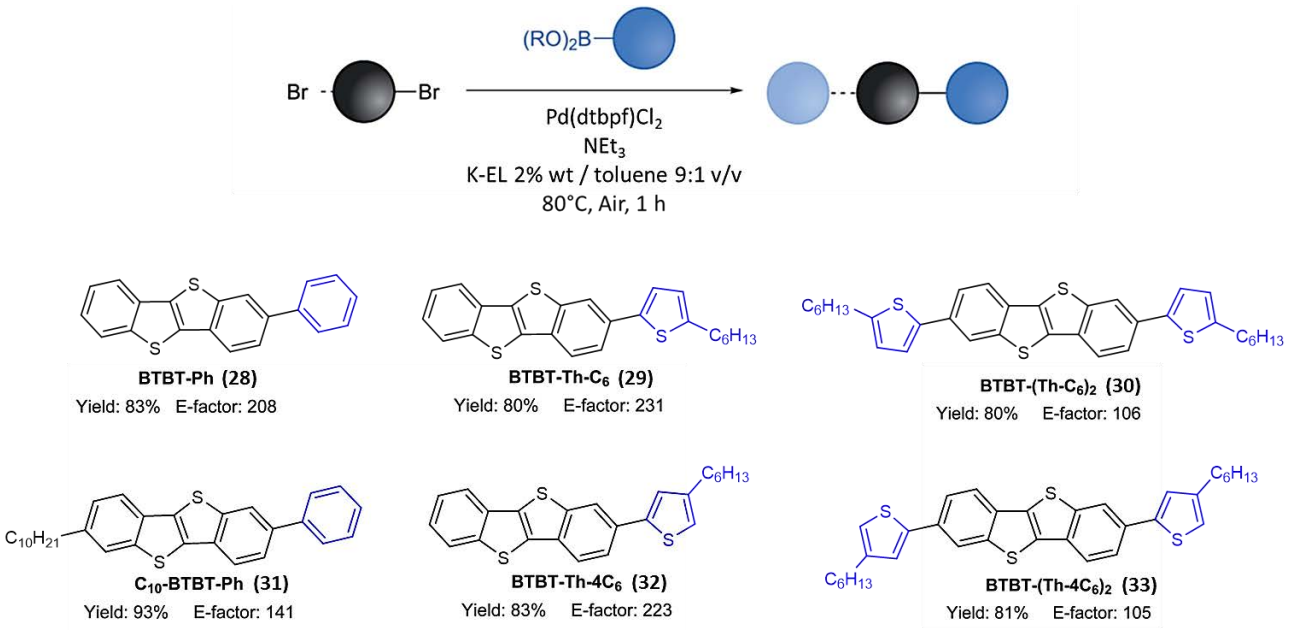

Figure 78. *Screening of the reaction conditions and formulation in the model micellar catalysed S-M coupling of BTBT-Br and phenylboronic acid.*

The emulsion method proved to be suitable for all the BTBT derivatives targets with very satisfactory results leading to 80% to 93% yields and displaying low E-factor values ranging from 105 to 231, demonstrating to be beneficial for both efficiency and sustainability. However, aiming at developing a "totally-green" approach, it is reasonable consider that this method still lacks at using, even if in very small quantities, toluene as organic cosolvent together with prolonged heating. Since toluene does not play a direct role in promoting the couplings, but rather acts as a mixing aid to properly disperse all reagents, we concluded that tailor-designed surfactants could play that role and possibly outperform it.

According to key principles of formulation chemistry, surface-active molecules achieve the best results in dispersing a solid organic substate in water when the lipophilic portion of the amphiphile resembles or at least strongly interacts with the substrate to be dispersed.[116] My group decided to exploit such concepts to specifically design and synthetise two amphiphiles with both the lipophilic portion featuring a conjugated backbone. The first designer surfactant include the electron-rich BTBT core in the structure, while the second incorporate the electron-poor naphthalenediimide (NDI) core. Both the surfactants contain a PEG 750-succinate residue as the lipophilic part of the structure. The idea consist of study the π-π stacking affinity of the BTBT core of the considered substrates with the specifically designed surfactants. These interaction are intended to help achieving a strongly dispersant and stable formulation at all stages of the reaction. In the case of PiNap-750M, the design was guided by the idea of boosted π-π stack interaction between the BTBT and NDI cores by a further donor-acceptor contribution. Indeed, the NDI unit is one of the most established structural motifs in the preparation of electron-deficient organic semiconductors.[117,118] The syntheses of the designer surfactants were carried out by my research group and they are reported in the supporting information of the published article.[83] DLS measurements (**Figure 79**) suggest that BTBT-750M mostly self assembles into micelles having a 15 nm average diameter, while PiNap-750M aggregation in water is more complex, showing the formation of several distinct populations of objects having average hydrodynamic diameters of 60, 1100 and 4300 nm.

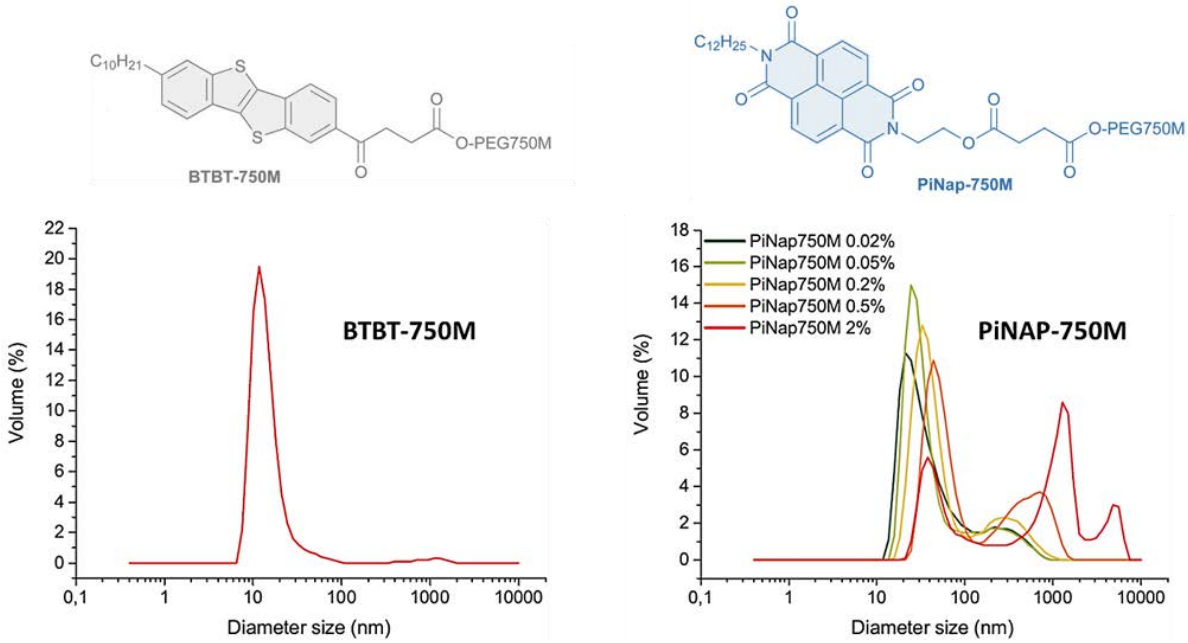

Figure 79. *Left: volume distribution of colloids dimensions in BTBT-750M 2 wt% dispersion in H_2O. Right: volume distribution of colloids dimensions in PiNap-750M 2 wt%, 0.5 wt%, 0.2 wt%, 0.05 wt%, and 0.02 wt% dispersions in H_2O. The decrease in dimensions upon increasing dilution suggests that PiNap-750M forms supramicellar aggregates at high concentration in H_2O.*

As shown in Entries 5-6 of **Table 8, Figure 77** the use of such designer surfactants in only water, at room temperature and under air helped dramatically the efficiency of the S-M couplings compared to K-EL raising the yield of the model reaction to 73% (however requiring 24 h) for BTBT-750M 2% wt solution and to 78% for PiNap-750M 2% wt solution in just 1 h. However, there is no definite reason that designer surfactants should keep oxygen out of the micellar core as is the case with the K-EL. Indeed, if the reaction is carried out under nitrogen atmosphere and with degassed water, the reaction efficiency raise up to quantitative conversion of BTBT-Ph. Still, the main difference between BTBT-750M and PiNap-750M lies on the time required to reach completion; the former requires 48h to reach completion (Entry 7) while the latter only 1h (Entry 8). Thus, the designer surfactant PiNap-750M demonstrated to be a superior performer also compared to the K-EL emulsion approach. One interesting consideration involves the fact that the reaction mixture of the model coupling performed in a 2% wt solution of PiNap-750M assumes a blue colour unlike all the other cases. This is characteristic of the co-presence of NEt3, PiNap-750M and the catalyst (**Figure 80**).

Figure 80. *Picture of the micellar reaction of BTBT-Br with phenylboronic acid in a surfactant dispersion of PiNap-750M (left) and K-EL (right). The blue colour of the reaction performed in PiNap-750M is peculiar, and only seen after the addition of the catalyst and the NEt_3 to the surfactant dispersion.*

Under the very same conditions, we repeated the model reaction by reducing the amount of catalyst from 0.02 to 0.004 and 0.002 equivalents in order to evaluate the optimal required catalyst loading. The reaction reached completion only in the first case (entry 9[a]), but required 12 h. In the latter case conversion was not complete even after 24 h and the conversion was 67% (entry 10[b]).

Encouraged by these latest results, we repeated the syntheses of some BTBT derivatives already synthetized with the emulsion method, in particular BTBT-Th-C6 (29), C_{10}-BTBT-Ph (31), and BTBT-Th-4C_6 (32), under the best condition found with PiNap-750M (entry 8) using 2% mol Pd(dtbpf)Cl_2 and featuring the advantages of no cosolvent and no heating required with respect to the emulsion method (entry 4). Following **Table 9** shows the results.

Entry	Product	Atm.	Time (h)	Yield (%)	E-factor calc. (lit.)
1	BTBT-Ph	N_2	1	97	46.6 (1556)[114]
2	BTBT-Th-C_6 (29)	N_2	1	91	39.2 (1117)[97]
3	C_{10}-BTBT-Ph (31)	N_2	1	94	33.4 (787)[114]
4	BTBT-Th-4C_6 (32)	N_2	1	93	38.4 (-)

Table 9. *Results of couplings carried out in PiNap-750M 2 wt% solutions with the corresponding E factors. A comparison of current E-factors with those from literature procedures is reported where available.*

For all the cases, the observed results were in agreement with those obtained for the model reaction: completion in less than 1 h and yields exceeding the 90%. All the target products were collected just by simply filtration after dilution of the reaction mixture with EtOH. The E-Factors for the couplings were calculated including the not recycled water and purification: ranging from 33 to 47, the method display a two order of magnitude improvement over standard literature procedures.Though, the remarkably better results of PiNap-750M over the BTBT-750M surfactant could be correlated to two different factors. The first one involves the formation of boosted stabilizing NDI-BTBT donor-acceptor interactions improving the capability of PiNap-750M to efficiently disperse electron-rich reagents. This consideration implies that PiNap-750M should have such remarkable performances only for electron-rich bromides. The second possible factor is substrate independent and could be related with the observation of the blue coloration assumed by the reaction mixture. Such phenomenon is observed probably because of a metal to ligand charge transfer after the formation of a peculiar complex between PiNap-750M and the Pd^0 catalyst in the presence of NEt3, improving efficiency in promoting S-M couplings, and never observed in any other formative conditions studied so far.[83] This behaviour and the oxygen sensitivity of the blue species generated by the reduction of Pd(dtbpf)Cl_2 are strong evidence that this could be the case. It should be considered that, unlike the first consideration, this second reason of the enhanced S-M reactivity does not imply any selectivity towards electron-rich bromides: all S-M reactions should be improved in the presence of such blue complex.

Considering the Pd/PiNAP-750M complex theory and in the absence of further evidence, my colleague challenged PiNap-750M in additional S-M couplings on both electron-rich and electron-poor bromides. **Figure 81** shows the results obtained for the coupling of 9,10-dibromoanthracene, 4,7-dibromo-2,1,3- benzothiadiazole, N,N-bis(2-ethylhexyl)-6,6-dibromoisoindigo and N,N-bis(n-octyl)-1,7-dibromo-perylene-3,4:9,10-bis(dicarboximide) with different boronic acids.

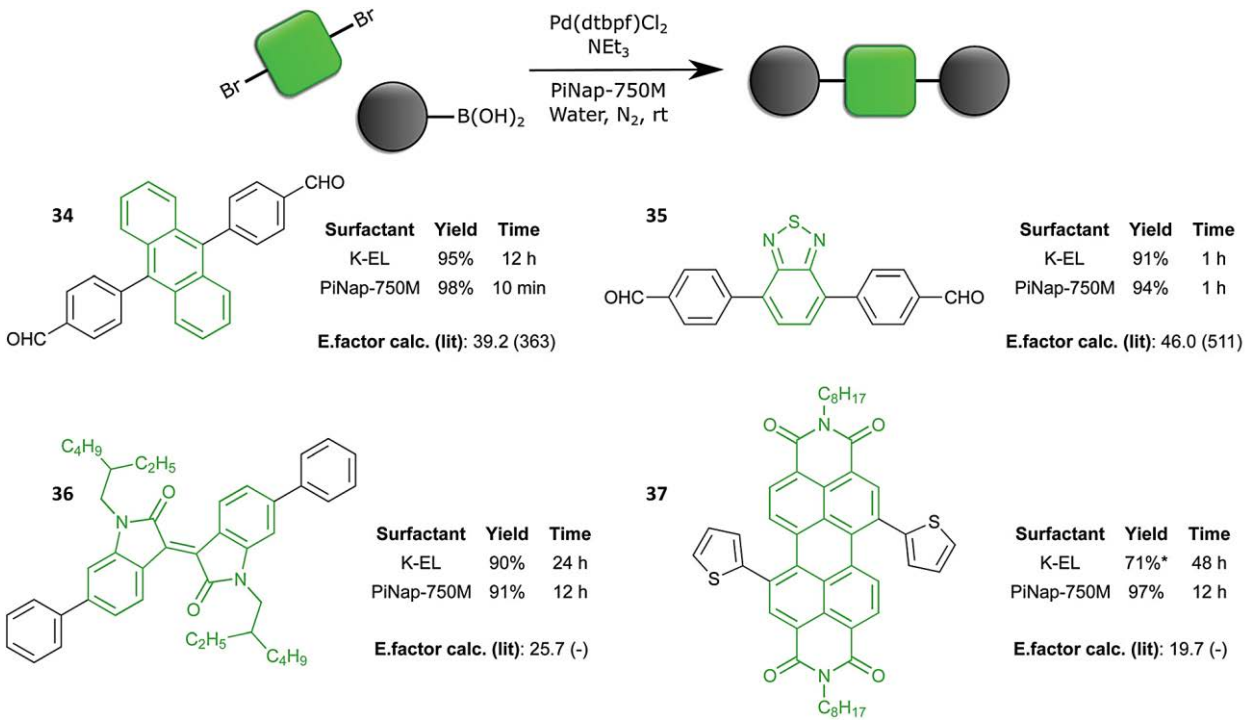

Figure 81. *Couplings of brominated precursors (in green) and arylboronic acids (in black) performed in a 2% wt PiNap-750M solution in deionized water, and their E-factor (comparison with the E-factor from literature procedures is reported where available).*

Rather remarkably, the use of PiNap-750M allows the synthesis of derivatives 34, 35, 36 and 37 in basically quantitative yields at room temperature, without an added cosolvent and in shorter reaction times than those needed for the same reaction to occur in K-EL. Again, E-factors were improved by more than one order of magnitude with respect to reported literature procedures. On the basis of such evidence, PiNap-750M is extremely efficient, regardless of the electron-poor or electron-rich nature of the aromatic core of the starting bromide. Although these results are consistent with the formation of a Pd/PiNap-750M complex, they neither provide clear-cut evidence in support of such an interpretation nor mechanistic insight into its role in enhancing the catalytic activity. Further experimental and computational studies are underway to further substantiate our educated guessing.

2.7.3. Conclusion

The work highlights and prove the needing of modulating the reaction conditions together with the formulation employed in order to achieve satisfactory micellar S-M transformations on highly crystalline substrates such as BTBTs. Relevant BTBT semiconducting derivatives can be efficiently and sustainably prepared under air in high yields and with remarkable reduced E-factors by the emulsion approach requiring the use of organic cosolvents and with prolonged heating, or using a very efficient specific designer surfactant PiNap-750M in only water at room temperature. However, thinking about an industrial reality, it should be balanced the use of a very little amount of organic cosolvent (stoichiometric amounts) and required heating up to 80°C, among the need to synthesize a designer surfactant, which for true is very efficient allowing to perform the reactions in only water and at room temperature, but still requiring an entire multistep synthetic protocol where the quantity of total waste is not negligible. Still, this strategy remains a valid alternative if essential materials are not approachable (completely or partially) with the emulsion method.

2.7.4. Experimental Section

2.7.4.1. Materials and Instruments

Reagents and solvents are bought from TCI, Fluorochem, or Sigma-Aldrich and used as received. Pd(dtbpf)Cl_2 catalyst is purchased from Ark Pharm. Anhydrous solvents are bought from Sigma-Aldrich. Chromatographic purifications are performed using Davisil LC 60A silica gel (pore size 60 Å, 70-200 μm). Composition of solvent mixtures used as eluents are indicated as volume/ volume ratios. Melting points are determined using a Buchi M-560 apparatus and are uncorrected. NMR spectra are collected on a Bruker NMR Avance 400 NEO. DLS experiments are performed on a 90Plus particle size analyzer (Brookhaven Instruments Corp.) with scattering angles of 15° and 90°, equipped with a 35 mW solid state 632.8 nm laser and a Brookhaven's Tubo Corr correlator with 510 channels. Absorption spectra are collected in glovebox under argon atmosphere using a SEC2000 Spectra System UV/Vis single beam spectrophotometer. Sample solutions are prepared using anhydrous acetonitrile and triethylamine, and measurements are performed in a glass cuvette (18 mm pathlenght).

<u>Note:</u> The syntheses of BTBT-750M and PiNAP-750M and their application were carried out by two of my colleagues (Alessandro Sanzone and Sara Mattiello). Specific experimental details are not reported here and can be found in the supporting information of the published article.[83]

2.7.4.2. Synthesis of BTBT and its Brominated Derivatives

2.7.4.2.1. Synthesis of BTBT

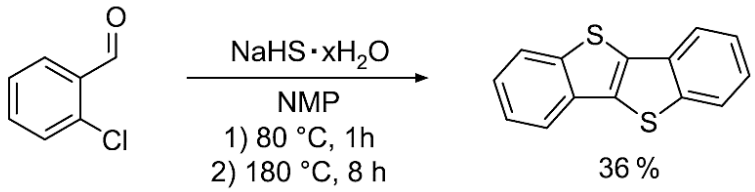

In a 1 L roundbottom flask, 2-chlorobenzaldehyde (250.0 g, 1.778 mol) is put under N_2 atmosphere and subsequently dissolved in NMP (450 mL). The solution is heated to 80 °C, and sodium hydrosulfide hydrate (267.0 g, 2.902 mol) is slowly added to it. Mixture is stirred for 1 hour, and then temperature is raised to 180 °C for 5 hours while distilling water with a Dean-Stark apparatus. During this time, reaction color turns from red to black. Reaction mixture is allowed to warm, and the obtained precipitate is collected on a fritted funnel and washed with water and methanol (1 L). Residual solvent is dried under vacuum to afford the pure product as faint yellow crystals (77.00 g, 36% yield).

^{1}H-NMR (CDCl3, 400 MHz): δ 7.93 (d J= 7.90 Hz, 2H,), 7.89 (d, J= 8.1 Hz, 2H), 7.47 (dd, J= 7.6, 7.3 Hz, 2H), 7.41 (dd, J= 8.0, 7.3 Hz, 2H).

^{13}C-NMR (CDCl3, 100 MHz): δ 143.1, 134.3, 134.0, 125.9, 125.8, 124.9, 123.0.

$$E_{factor} = \frac{m_{reagents} + m_{solvents} - m_{product}}{m_{product}} = \frac{250\,\text{g} + 1250\,\text{g} - 77\,\text{g}}{77\,\text{g}} = 18.5$$

2.7.4.2.2. Synthesis of BTBT-Br

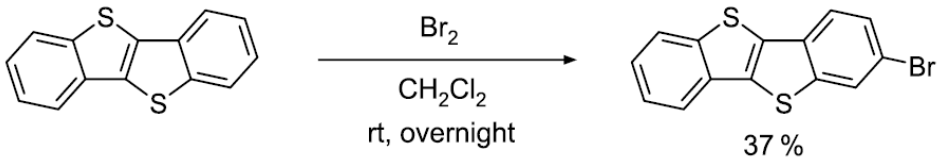

In a 2 L roundbottom flask, BTBT (10.05 g, 41.82 mmol) is dissolved in DCM (600 mL). A solution of Br_2 (7.35 g, 46.0 mmol) in DCM (150 mL) is added dropwise, and the reaction is left stirring at room temperature overnight. A white precipitate forms, which is filtered off. The filtrated is washed with aqueous $NaHSO_3$ (10% w/w) and brine, dried over Na_2SO_4, and the solvent is finally evaporated under reduced pressure. The crude is purified by recrystallization using $CHCl_3$ (200 mL) as solvent. White powder (5 g, 37% yield).

^{1}H-NMR (CDCl3, 400 MHz): δ 8.05 (d, J= 1.7 Hz, 1H), 7.92 (d, J= 7.7 Hz, 1H), 7.88 (dd, J= 7.2, 0.9 Hz, 1H), 7.73 (d, J= 8.5 Hz, 1H), 7.56 (dd, J= 8.4, 1.7 Hz, 1H), 7.49-7.41 (m, 2H).

^{13}C-NMR (CDCl3, 100 MHz): δ 144.5, 143.2, 134.7, 133.8, 133.7, 132.8, 129.2, 127.4, 127.4, 126.2, 125.9, 125.0, 123.4, 122.5, 119.5

$$E_{factor} = \frac{m_{reagents} + m_{solvents} - m_{product}}{m_{product}} = \frac{10.05\,\text{g} + 1296\,\text{g} - 5.01\,\text{g}}{5.01\,\text{g}} = 260$$

2.7.4.2.3. Synthesis of BTBT-Br_2

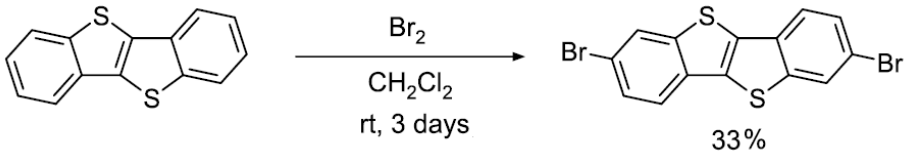

In a 500 mL roundbottom flask, BTBT (2.000 g, 8.322 mmol) is dissolved in DCM (120 mL). A solution of Br_2 (1.46 g, 9.15 mmol) in DCM (30 mL) is added dropwise, and the reaction is left stirring at room temperature overnight. The second Br_2 equivalent (1.46 g in 30 mL of DCM) is therefore added dropwise. Reaction is left stirring at room temperature for two more days. During this time, a white precipitate appears in the flask, which is collected on a Büchner funnel. The white solid is washed with DCM, and aqueous $NaHSO_3$ (10% w/w). This crude (2.830 g) is purified by extraction in a Soxhlet apparatus using DCM as solvent. The pure product recrystallizes in the cold solvent, and it is collected by filtration. Silvery flakes (1.093 g, 33% yield).

^{1}H-NMR (CDCl3, 400 MHz): *d* 8.06 (d, J=1.5 Hz, 1H), 7.74 (d, J=8.6 Hz, 1H), 7.58 (dd, J=8.6, 1.5 Hz, 1H).

^{13}C-NMR (CDCl3, 100 MHz): δ 143.7, 134.3, 131.6, 128.5, 126.5, 122.5, 118. 9.

2.7.4.2.4. Synthesis of C_{10}-BTBT-Br

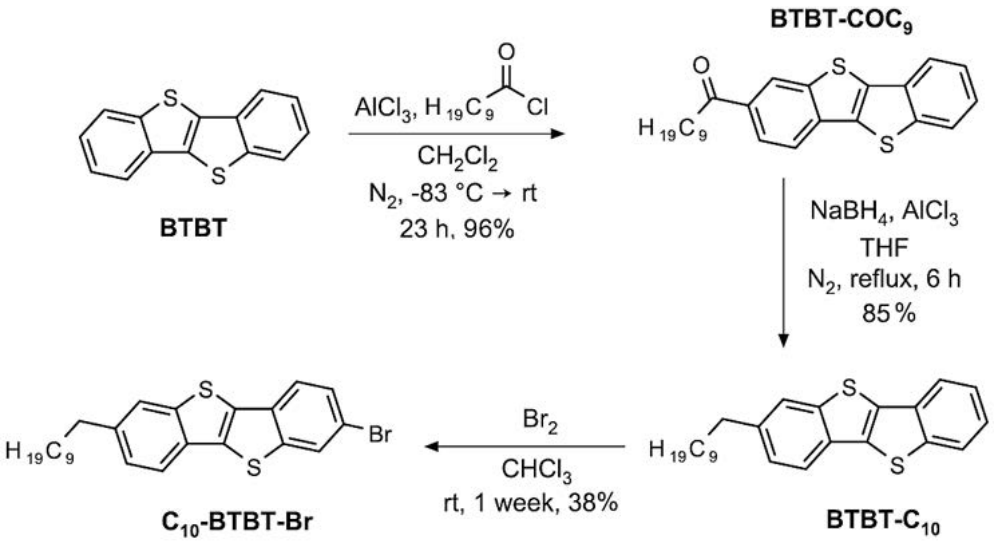

2.7.4.2.4.1. Synthesis of BTBT-COC_9

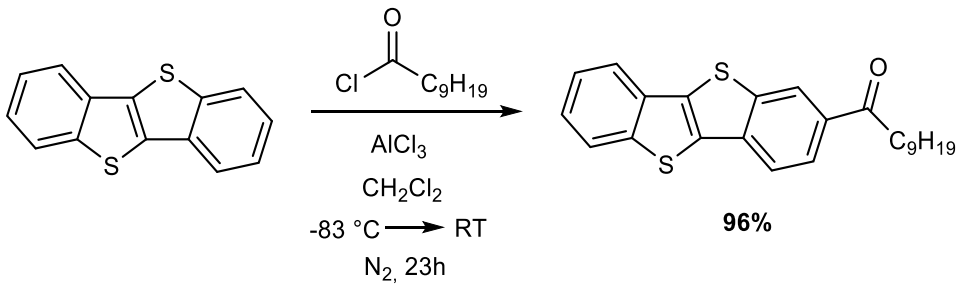

In a three-necked, 1 L roundbottom flask equipped with a thermometer, BTBT (10.008 g, 41.641 mmol) is put under N_2 atmosphere and then dissolved in 400 mL of anhydrous DCM. The solution is cooled to -10 °C and $AlCl_3$ (14.000 g, 105.00 mmol) is added to the flask. The mixture is left stirring for 10 minutes and subsequently cooled with an AcOEt cooling bath. When the mixture reaches -83 °C, decanoyl chloride (7.95 g, 41.7 mmol) is added dropwise. Temperature is kept at -83 °C for 1 h, then the system is allowed to warm at room temperature overnight. Reaction is quenched by careful addition of a 1:1 v/v mixture of H_2O/MeOH (200 mL), and DCM is evaporated at reduced pressure. The obtained dispersion is filtered on a fritted funnel, washed with water and dried under reduced pressure at 70 °C. The obtained solid is hot filtered from toluene (300 mL) and allowed to recrystallize in the cold solvent. Yellow powder (15.700 g, 95.6% yield).

^{1}H-NMR (CDCl3, 400 MHz): δ 8.57 (d, J= 1.5 Hz, 1H), 8.08 (dd, J= 8.4, 1.5 Hz, 1H), 7.99-7.92 (m, 3H), 7.54-7.45 (m, 2H), 3.09 (t, J= 7.0 Hz, 2H), 1.86-1.78 (m, 2H), 1.45-1.31 (m, 14H), 0.91 (t, J= 6.9 Hz, 3H).

^{13}C-NMR (CDCl3, 100 MHz) δ 199.6, 142.8 ,140.2, 136.9, 136.2, 133.6, 133.0, 132.8, 125.8, 125.1, 124.7, 124.5, 124.2, 122.1, 121.4, 38.8, 36.1, 33.3, 31.8, 29.4, 29.2, 26.9, 24.6, 22.7, 14.1.

$$E_{factor} = \frac{m_{reagents} + m_{solvents} - m_{product}}{m_{product}} = \frac{10.008\,\text{g} + 7.95\,\text{g} + 871.2\,\text{g} - 15.700\,\text{g}}{15.700\,\text{g}} = 55.6$$

2.7.4.2.4.2. Synthesis of BTBT-C_{10}

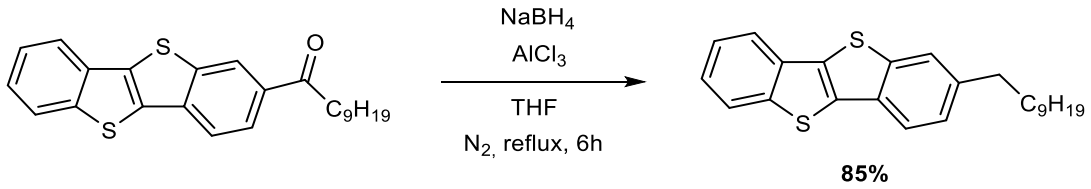

In a two-necked, 1 L roundbottom flask BTBT-COC_9 (15.700 g, 39.788 mmol) is put under N_2 atmosphere and then dissolved in 350 mL of anhydrous THF. The solution is cooled at 0 °C, then $NaBH_4$ (15.000 g, 396.51 mmol) is added, followed by $AlCl_3$ (26.9 g, 202 mmol). Mixture is refluxed overnight. Reaction is quenched with 400 mL of H_2O/MeOH (3:1 v/v), then THF is evaporated and the obtained dispersion is filtered on a fritted funnel. The crude is hot filtered from isopropanol (450 mL) and allowed to recrystallize in the cold solvent. Faint yellow powder (12.882 g, 85.1% yield).

^{1}H-NMR (CDCl3, 400 MHz): δ 7.93 (ddd, J=8.0, 1.2, 0.7 Hz, 1H), 7.89 (ddd, J=7.9, 1.3, 0.7 Hz, 1H), 7.81 (dd, J=8.1, 0.6 Hz, 1H), 7.74 (dd, J=1.5, 0.6 Hz, 1H), 7.47 (ddd, J=7.9, 7.2, 1.2, 1H), 7.41 (ddd, J=8.0, 7.2, 1.3 Hz, 1H), 7.31 (dd, J=8.1, 1.5 Hz, 1H), 2.79 (t, J=7.6 Hz, 2H), 1.76-1.69 (m, 2H), 1.37-1.30 (m, 14H), 0.91 (t, J=6.9 Hz, 3H).
^{13}C-NMR (CDCl3, 100 MHz) δ 146, 141.7 ,139.1, 135.8, 135.1, 132.5, 132.9, 131.7, 124.7, 124.0, 123.6, 123.4, 123.1, 121.0, 120.3, 37.6, 35.1, 32.2, 32.6, 28.4, 26.9, 23.4, 22.7, 22.1, 17.3.

$$E_{factor} = \frac{m_{reagents} + m_{solvents} - m_{product}}{m_{product}} = \frac{15.700\,\text{g} + 744.2\,\text{g} - 12.882\,\text{g}}{12.882\,\text{g}} = 58.0$$

2.7.4.2.4.3. Synthesis of C_{10}-BTBT-Br

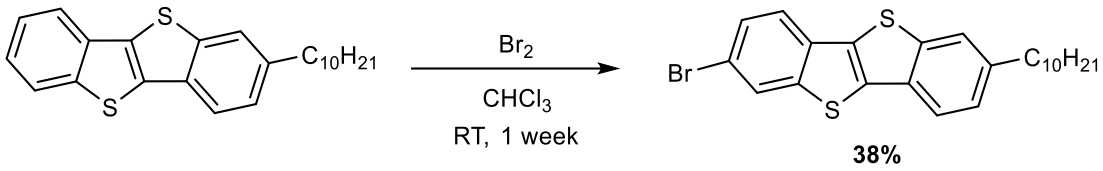

In a two-necked, 500 mL roundbottom flask BTBT-C_{10} (5.000 g, 13.14 mmol) is dissolved in 130 mL of $CHCl_3$. A solution of Br_2 (2.166 g, 13.55 mmol) in $CHCl_3$ (20 mL) is slowly added dropwise. The reaction mixture is allowed to stir for 7 days, over which a precipitate forms. The solid is filtered off and recrystallized from heptane (32 mL) to afford 2.300 g of product as a white powder (38.1% yield)

^{1}H-NMR (CDCl3, 400 MHz): δ 8.06 (dd, J= 1.7, 0.4 Hz, 1H), 7.79 (d, J= 8.1 Hz, 1H), 7.74-7.72 (m, 2H), 7.57 (dd, J= 8.5, 1.8 Hz, 1H), 7.31 (dd, J= 8.1, 1.5 Hz, 2H), 2.80 (t, J= 7.7 Hz, 2H), 1.76-1.68 (m, 2H), 1.37-1.29 (m, 14), 0.90 (t, J= 6.9 Hz, 3H).

^{13}C-NMR (CDCl3, 100 MHz) δ 162.3, 145.3 ,142.3, 138.5, 136.8, 133.5, 132.9, 131.6, 127.9, 124.7, 123.1, 122.2, 120.4, 118.9, 117.8, 39.3, 37.3, 34.5, 32.9, 28.1, 27.4, 25.5, 23.2, 21.9, 20.7.

2.7.4.3. General Procedures for the Preparation of BTBT Derivatives using K-EL Emulsion

1 L of K-EL 2% wt / toluene (9:1 v/v) emulsion is prepared homogenizing a 2 wt% aqueous dispersion of K-EL (18 g of Kolliphor EL in 882 mL of deionized water) with 100 mL of toluene using a T 25 digital ULTRA-TURRAX R until a stable, milky dispersion is obtained.

Procedure for BTBT-Br and C10-BTBT-Br substrates

BTBT bromide (1.00 mmol), boronic acid (or pinacol ester) (1.50 mmol) and $Pd(dtbpf)Cl_2$ (0.02 mmol) are weighted in the vessel, then K-EL 2% wt / toluene (9:1 v/v, 2 mL) is added. The mixture is allowed to homogenize for 5 minutes before addition of triethylamine (3.00 mmol). Reaction is stirred for 1 h at 80 °C. The mixture is diluted with 10 mL of DCM and filtered through a pad of silica (15 g) with a mixture of dichloromethane and ethylacetate (10:1, 22 mL). The filtrated is evaporated under reduced pressure to obtain the product, which eventually is further purified by hot filtration.

Procedure for BTBT-Br_2 substrate

BTBT-Br_2 (398 mg, 1.00 mmol), boronic acid pinacol ester (883 mg, 3.00 mmol) and $Pd(dtbpf)Cl_2$ (26.0 mg, 0.04 mmol) are weighted in the vessel, then K-EL 2% wt / toluene (9:1 v/v, 2 mL) is added. The mixture is allowed to homogenize for 5 minutes before addition of NEt_3 (607 mg, 6.00 mmol). Reaction is stirred for 12 h at 80 °C. The mixture is diluted with 10 mL of ethanol and filtered to obtain the crude product, which is further purified by continuous extraction in a Soxhlet apparatus using $CHCl_3$ (25 mL) as the solvent. The pure product recrystallizes in the cold solvent, and it is recovered by filtration.

2.7.4.3.1. Synthesis of BTBT-Ph

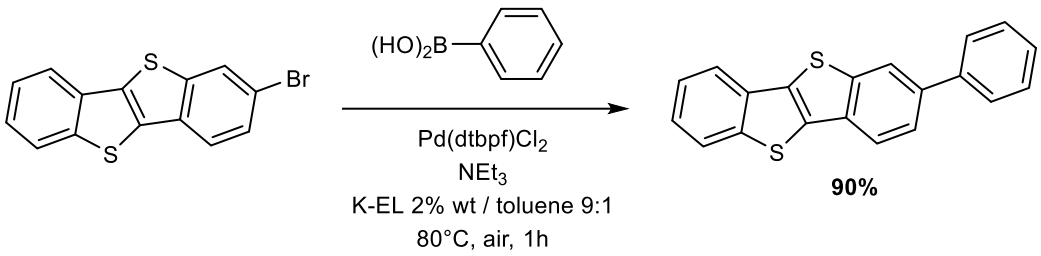

Phenylboronic acid is used as the coupling partner. Pure product is obtained after filtration on silica. White powder, 90% yield. Mp: 248-249 °C.

^{1}H-NMR (CDCl3, 400 MHz): δ 8.16 (dd, J= 1.6, 0.6 Hz, 1H), 7.98-7.95 (m, 2H), 7.93 (ddd, J= 7.8, 1.4, 0.7 Hz, 1H), 7.74-7.71 (m, 3H), 7.54-7.39 (m, 5H).

^{13}C-NMR (CDCl3, 100 MHz): δ 143.06, 142.32, 140.72, 138.39, 133.72, 133.21, 133.13, 132.17, 128.92, 127.48, 127.33, 125.03, 124.92, 124.51, 124.05, 122.35, 121.77, 121.59.

2.7.4.3.2. Synthesis of C_{10}-BTBT-Ph

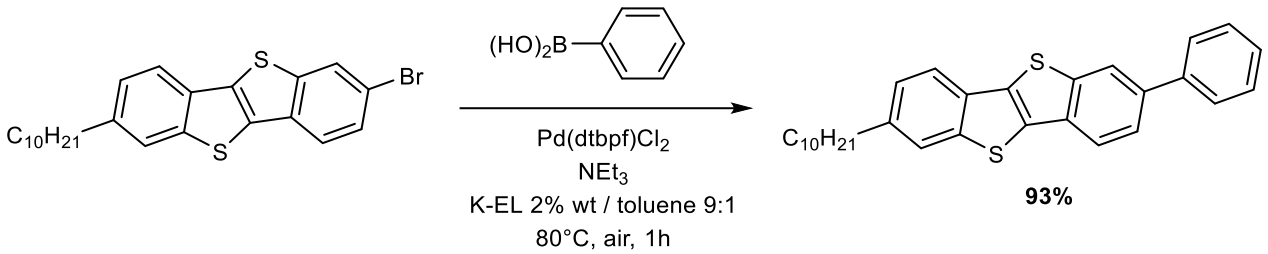

Phenylboronic acid is used as the coupling partner. Pure product is obtained after filtration on silica. White powder, 423 mg, 93% yield. Mp: 212-213 °C.

^{1}H-NMR (CDCl3, 400 MHz): δ 8.12 (dd, J= 1.6, 0.6, 1H), 7.92 (dd, J= 8.3, 0.6 Hz, 1H), 7.80 (dd, J= 8.1, 0.5 Hz, 1H), 7.73 (s, 1H), 7.71-7.68 (m, 3H), 7.51-7.46 (m, 2H), 7.41-7.36 (m, 1H), 7.29 (dd, J= 8.1, 1.5, 1H), 2.77 (t, J= 7.3 Hz, 2H), 1.74-1.67 (m, 2H), 1.35-1.25 (m, 14H), 0.88 (t, J= 6.6 Hz, 3H).

^{13}C-NMR (CDCl3, 100 MHz): δ 142.88, 142.65, 140.79, 140.45, 138.08, 133.69, 132.35, 131.04, 128.91, 127.40, 127.31, 125.96, 124.43, 123.37, 122.32, 121.57, 121.24, 36.14, 31.89, 31.69, 29.61, 29.58, 29.52, 29.32, 29.30, 22.68, 14.11.

2.7.4.3.3. Synthesis of BTBT-Th-C_6

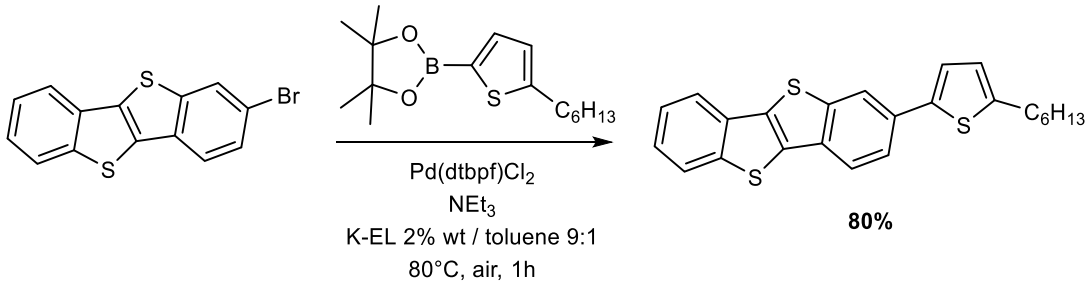

5-Hexyl-2-thiopheneboronic acid pinacol ester is used as the coupling partner. After filtration on silica, product is hot filtered from isopropanol (20 mL), and allowed to crystallize in the cold solvent. White powder, 325 mg, 80% yield. Mp: 184-185 °C.

^{1}H-NMR (CDCl3, 400 MHz): δ 8.08 (d, J= 1.3 Hz, 1H), 7.92 (d, J= 8.0 Hz, 1H), 7.88 (d, J= 7.7 Hz, 1H), 7.84 (d, J= 8.3 Hz, 1H), 7.66 (dd, J= 8.3, 1.6 Hz, 1H), 7.48-7.45 (m, 1H), 7.42-7.38 (m, 1H), 7.22 (d, J= 3.5 Hz, 1H), 6.79 (d, J= 3.6 Hz, 1H), 2.85 (t, J= 7.6 Hz, 2H), 1.75-1.69 (m, 2H), 1.45-1.32 (m, 6H), 0.91 (t, J= 7.2 Hz, 3H).

^{13}C-NMR (CDCl3, 100 MHz): δ 147.10, 143.97, 143.13, 142.04, 134.37, 134.20, 133.99, 132.89, 132.72, 126.11, 125.85, 125.80, 124.90, 123.98, 123.82, 122.61, 122.41, 121.26, 32.50, 32.47, 31.19, 29.67, 23.47, 14.97.

2.7.4.3.4. Synthesis of BTBT-4Th-C_6

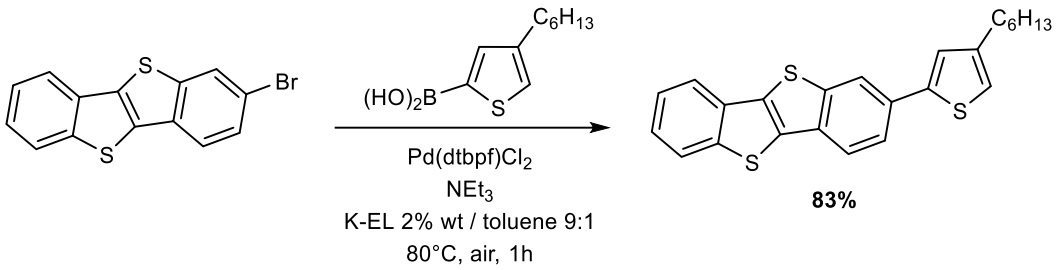

4-Hexyl-2-thiopheneboronic acid pinacol ester is used as the coupling partner. After filtration on silica, product is hot filtered from isopropanol (20 mL), and allowed to crystallize in the cold solvent. White powder, 337 mg, 83% yield. Mp: 172-173 °C. Anal. Calcd for $C_{24}H_{22}S_3$: C, 70.89; H, 5.45. Found: C, 70.51; H, 5.16.

^{1}H-NMR (CDCl3, 400 MHz): δ 8.14 (dd, J=1.6, 0.6 Hz, 1H), 7.94 (ddd, J=7.9, 1.2, 0.7 Hz, 1H), 7.91 (ddd, J=7.9, 1.4, 0.7 Hz, 1H), 7.87 (dd, J=8.3, 0.6 Hz, 1H), 7.71 (dd, J=8.3, 1.6 Hz, 1H), 7.49 (ddd, J=7.8, 7.2, 1.2 Hz, 1H), 7.43 (ddd, J=7.9, 7.2, 1.4 Hz, 1H), 7.28 (m, 1H), 6.94 (m, 1H), 2.67 (t, J=7.2 Hz, 2H), 1.74-1.66 (m, 2H), 1.45-1.34 (m, 6H), 0.94 (t, J=7.7 Hz, 3H).

^{13}C-NMR (CDCl3, 100 MHz): δ 144.56, 143.52, 143.09, 142.30, 133.69, 133.31, 133.11, 132.12, 131.89, 125.05, 124.96, 124.92, 124.05, 123.16, 121.76, 121.58, 120.67, 119.86, 31.73, 30.69, 30.46, 29.05, 22.65, 14.13.

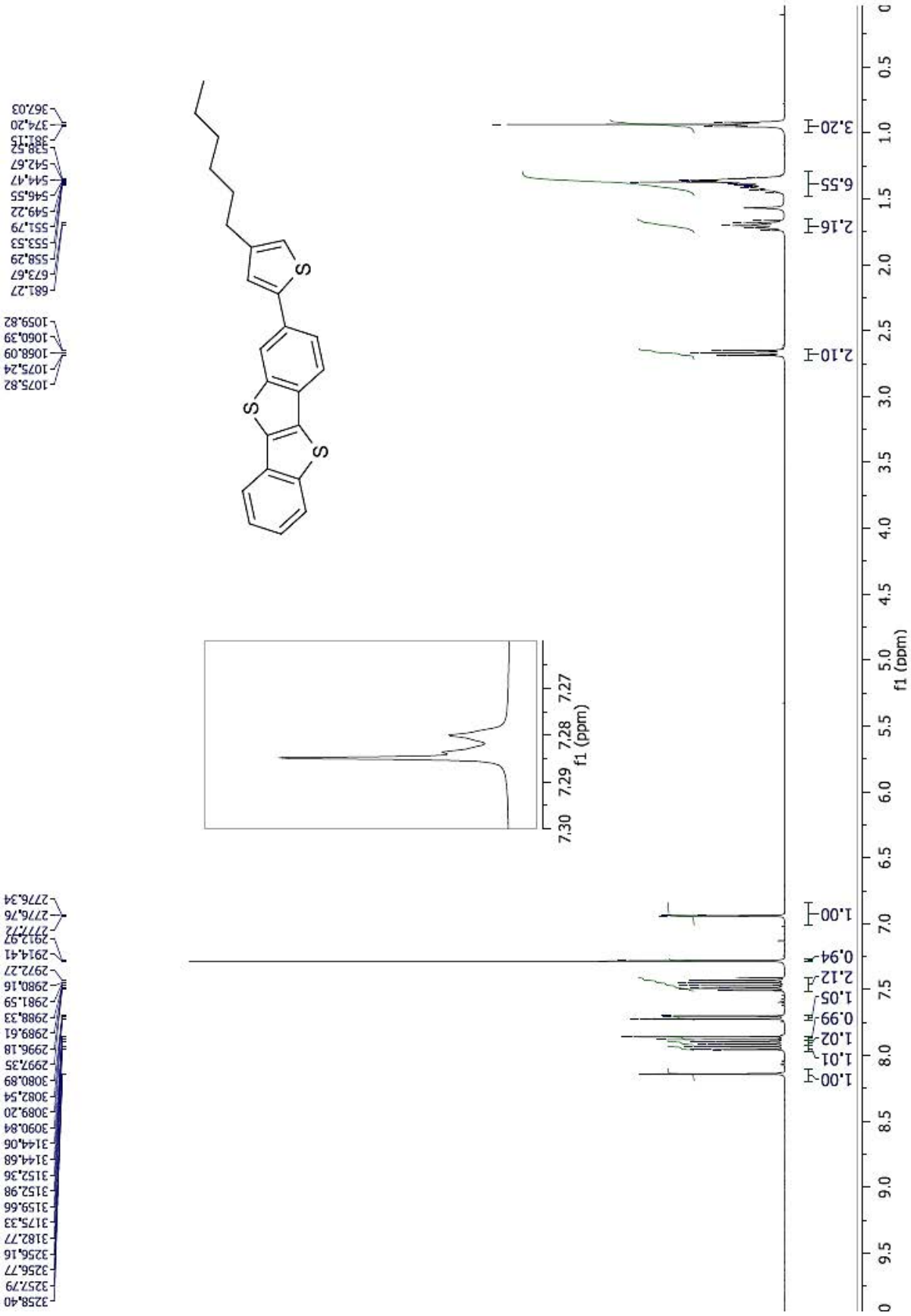

^{1}H-NMR spectrum of BTBT-4Th-C_6.

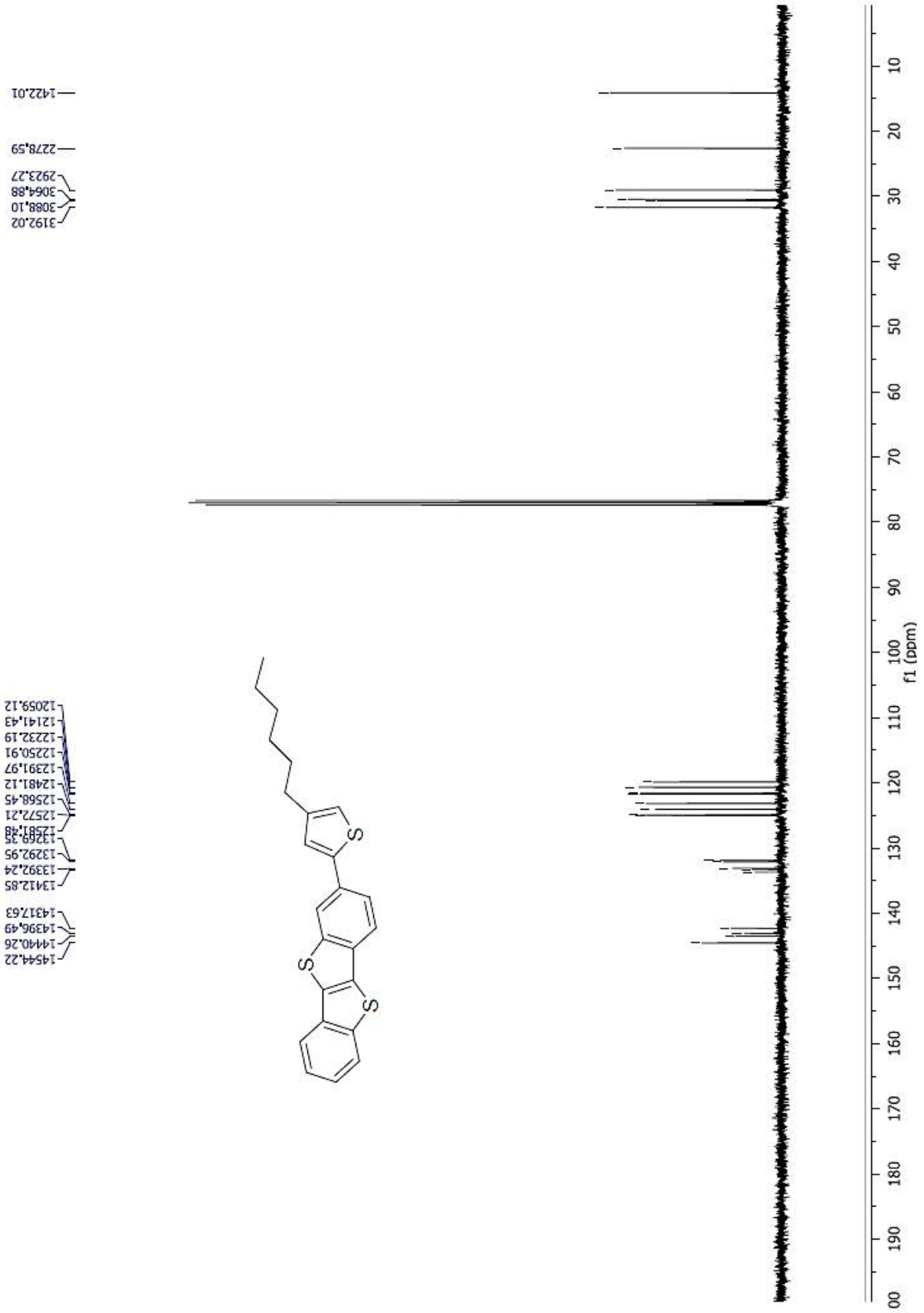

^{13}C-NMR spectrum of BTBT-4Th-C$_6$.

2.7.4.3.5. Synthesis of BTBT-(Th-C_6)$_2$

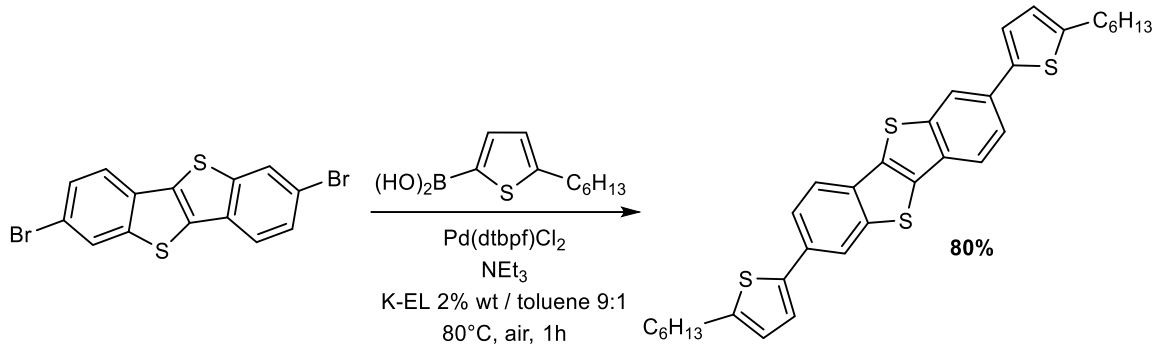

Off-yellow crystals, 458 mg, 80% yield. Mp: 293 °C (degradation). As temperature rises above 270 °C, crystals colour darken; degradation completes over 293 °C. Anal. Calcd for $C_{34}H_{36}S_4$: C, 71.28; H, 6.33. Found: C, 71.54; H, 6.28.

^{1}H-NMR (CDCl3, 400 MHz): δ 8.07 (dd, J=1.6, 0.6 Hz, 2H), 7.83 (dd, J=8.3, 0.6 Hz, 2H), 7.67 (dd, J=8.3, 1.6 Hz, 2H), 7.23 (d, J=3.6 Hz, 2H), 6.79 (dt, J=3.6, 0.9 Hz, 2H), 2.85 (t, J=7.7 Hz, 4H), 1.76 1.69 (m, 4H), 1.43-1.31 (m, 12H), 0.91 (t, J=6.4 Hz, 6H).

^{13}C-NMR (CDCl3, 100 MHz): δ 146.23, 143.75, 141.16, 137.51, 131.97, 131.85, 125.24, 123.09, 122.99, 121.66, 120.35, 31.61, 31.58, 30.31, 28.78, 22.58, 14.08.

2.7.4.3.6. Synthesis of BTBT-(4Th-C_6)$_2$

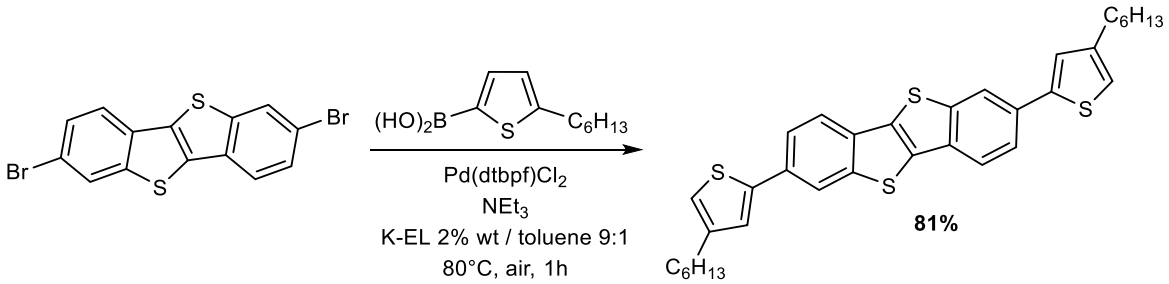

Off-yellow crystals, 464 mg, 81% yield. Mp: 259-261 °C. Anal. Calcd for $C_{34}H_{36}S_4$: C, 71.28; H, 6.33. Found: C, 71.15; H, 6.02.

^{1}H-NMR (CDCl3, 400 MHz): δ 8.12 (dd, J= 1.6, 0.6 Hz, 2H), 7.84 (dd, J= 8.3, 0.6 Hz, 2H), 7.70 (dd, J= 8.3, 1.6 Hz, 2H), 7.26 (m, 2H), 6.92 (dd, J= 2.2, 0.9 Hz, 2H), 2.64 (t, J= 6.8 Hz, 4H), 1.71-1.64 (m, 4H), 1.40-1.31 (m, 12H), 0.91 (t, J= 7.6 Hz, 6H).

^{13}C-NMR (CDCl3, 100 MHz): δ 144.55, 143.47, 143.11, 133.54, 132.08, 131.88, 124.91, 123.20, 121.70, 120.63, 119.87, 31.69, 30.66, 30.44, 29.02, 22.61, 14.10.

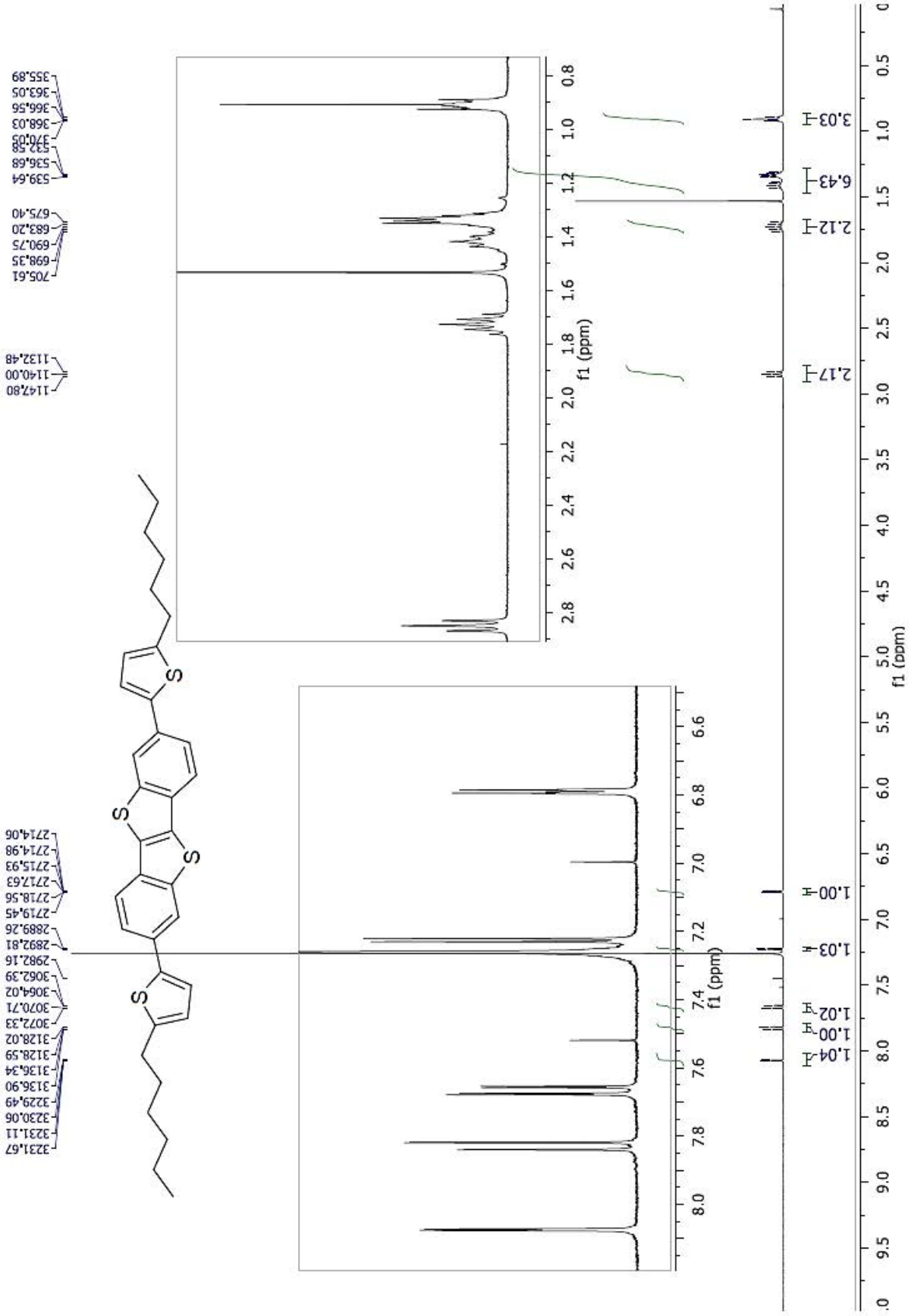

^{1}H-NMR spectrum of BTBT-(Th-C_6)$_2$.

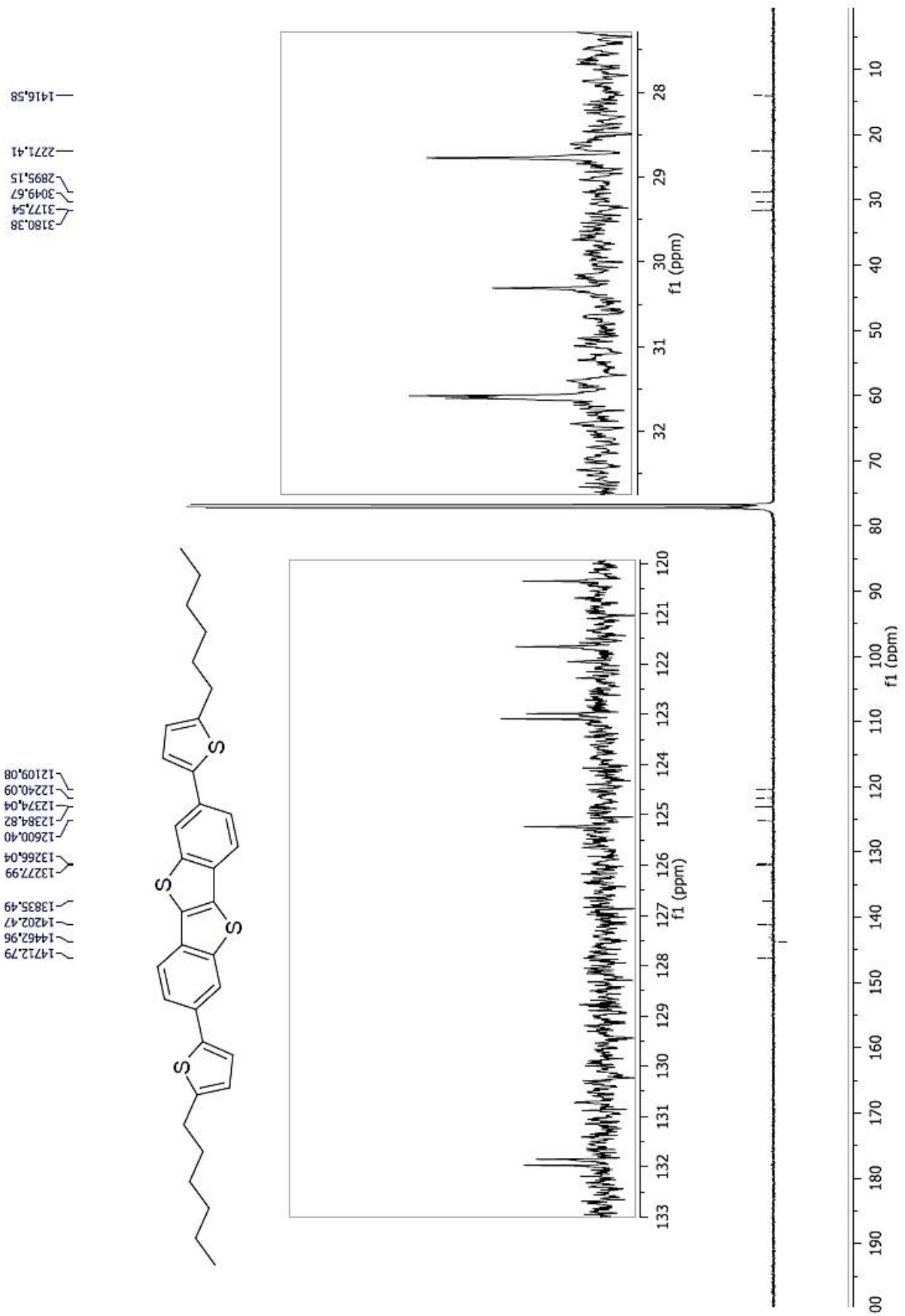

^{13}C-NMR spectrum of BTBT-(Th-C$_6$)$_2$.

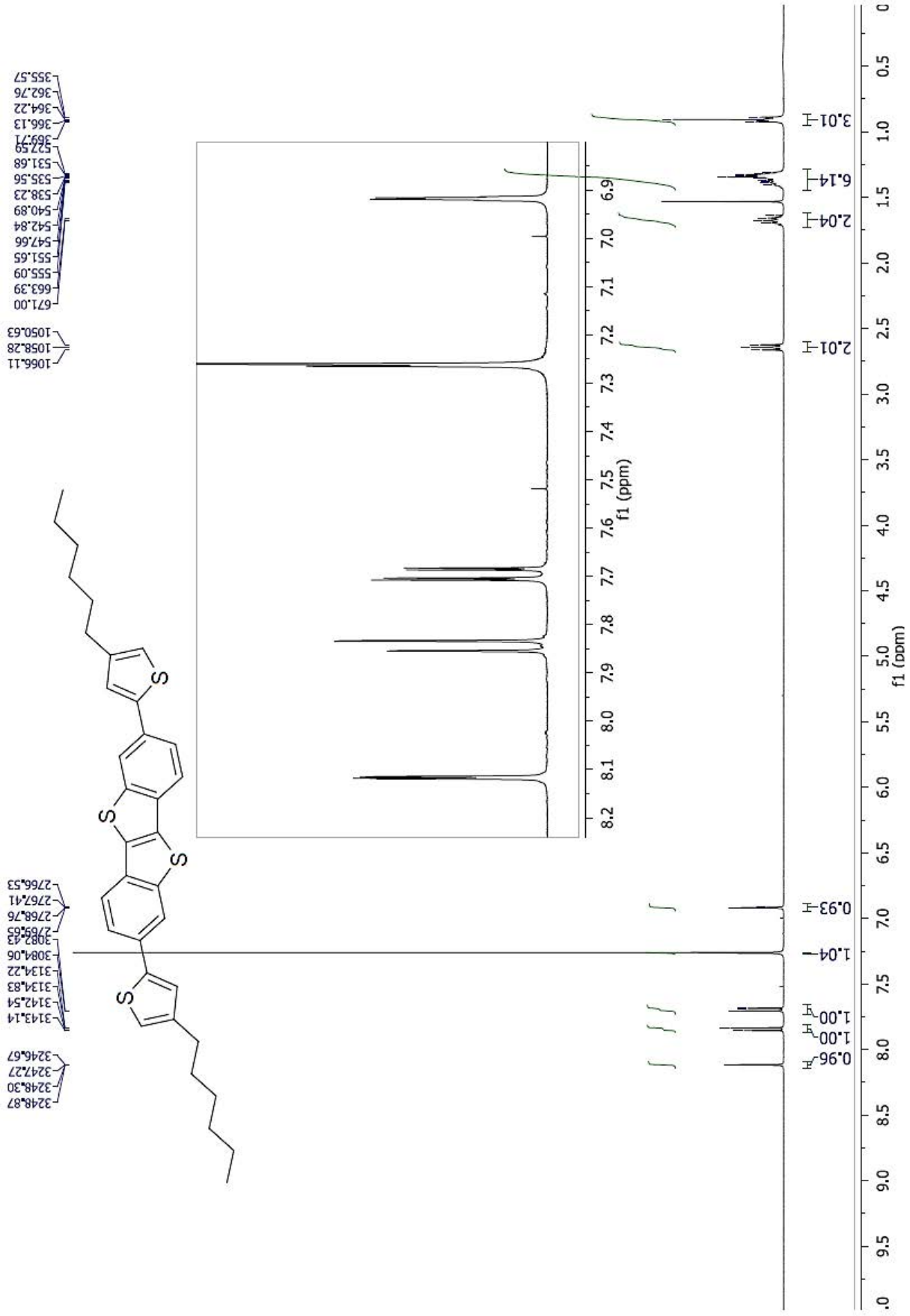

^{1}H-NMR spectrum of BTBT-(4Th-C$_6$)$_2$.

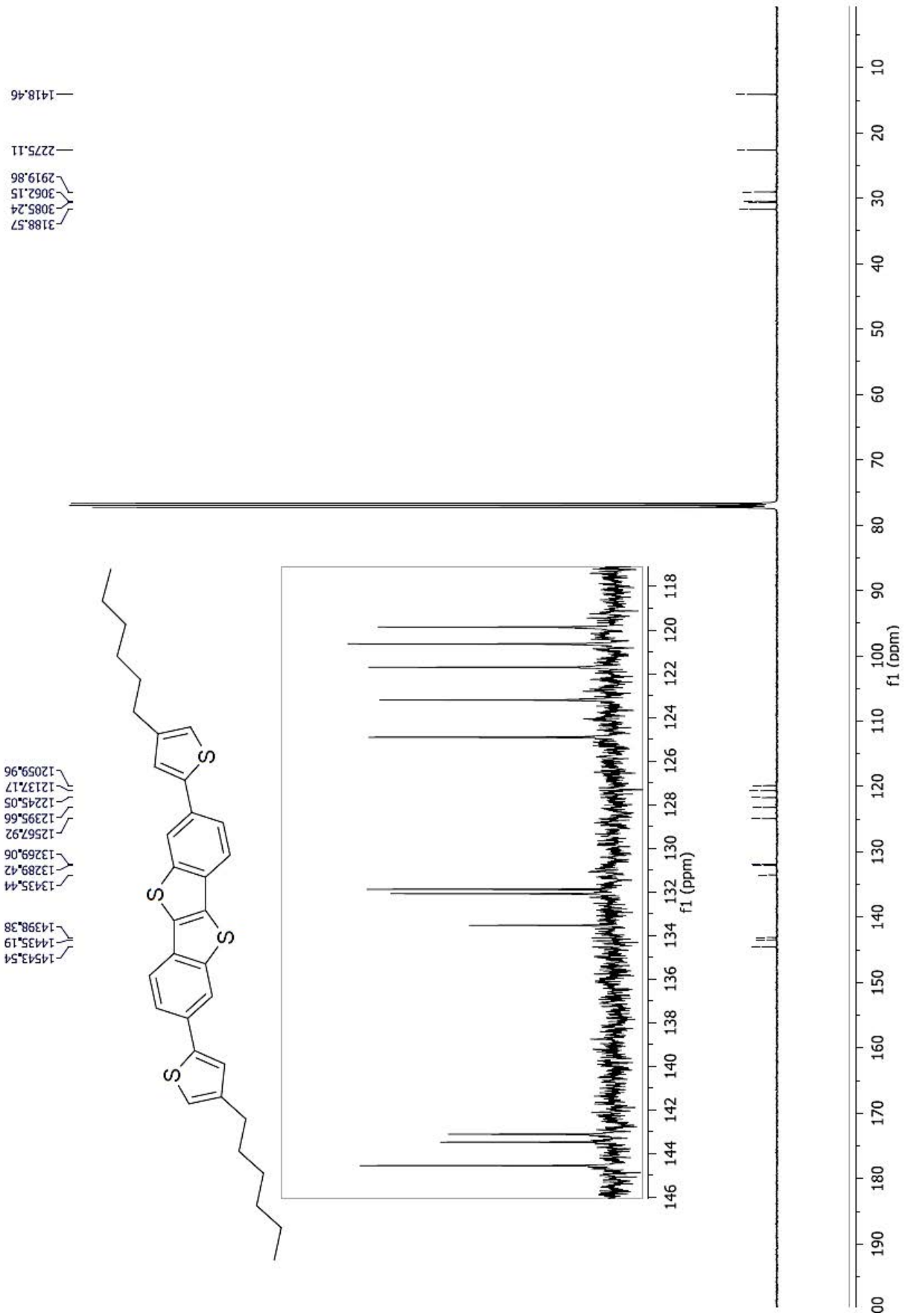

^{13}C-NMR spectrum of BTBT-(Th-C$_6$)$_2$.

2.8. Novel, Fully Sustainable and Cost-Effective Multi-Step Synthesis of Spiro-OMeTAD HTM for Highly Efficient Hybrid Perovskites Solar Cells

2.8.1. Introduction

Spiro-OMeTAD, also known as 2,2',7,7'-tetrakis(N,N-bis-4-methoxyphenylamine)-9,9'-spiro-bifluorene, is a well-established, commercially available, and highly performing organic hole transporting material (HTM) in meso-structured-based Perovskites Solar Cells (PSCs).[119] PSC devices correspond to a particular type of organic-inorganic hybrid photovoltaic cells that use perovskites as an absorbing material for the production of electrical energy. Perovskites are compounds with a crystallographic structure of the ABX_3 type, where usually A is an organic cation (generally methylammonium) placed in the centre of a cube, B is an inorganic cation (generally Pb^{2+}, Sn^{2+}, Ge^{2+}) at the vertices of the cube, and X is a halide (generally Cl^-, Br^-, I^-) that coordinates the inorganic cation according to an octahedral geometry. The photovoltaic cell architecture requires a perovskite layer in contact with two layers: a compact TiO_2 or SnO_2 layer that acts as electron transporting material (ETM), and an organic semiconducting layer that acts as hole transporting material (HTM). Spiro-OMeTAD works effectively on transferring holes from the perovskite to the counter electrode (generally Au or Ag) due to the right match between frontiers energy levels and doping-enhanced mobilities; thus, it minimize the series resistance and interfacial recombination losses in PSCs leading to an enhancement in the fill factor (FF) and open-circuit voltage (V_{OC}).[120] To date, Spiro-OMeTAD-based PSCs are one of the most promising solution-processable organic photovoltaic technologies with power conversion efficiencies (PCEs) exceeding the 20%.[121,122]

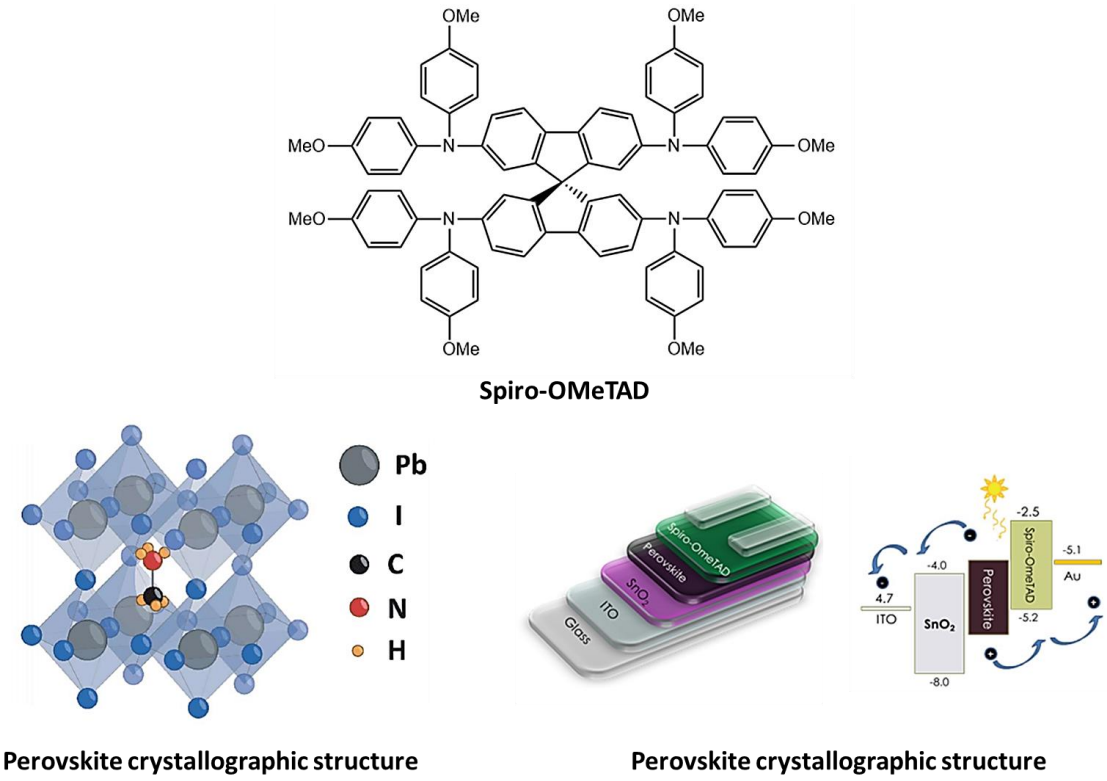

Figure 82. *Top: chemical structure of Spiro-OMeTAD; bottom left: perovskite crystallographic structure concerning the ABX_3 type, the most common cells concerning the $CH_3NH_3PbI_3$ structure; bottom right: general architecture of a perovskite photovoltaic cell and schematic working principle using Spiro-OMeTAD as HTM.*

However, the actual main drawback of this technology is related to the costs required for producing the spiro-OMeTAD, which is markedly expensive due to its lengthy procedures, complex purification processes, and low yielding synthesis[123] The standard production protocol leads to an overall yield of nearly 30%; thus, actually the selling price of Spiro-OMeTAD is around 340 euros/gram by Merck. Moreover, the E-factor value involved in its synthesis is in the 10^3 order. Those factors strongly limit the suitability for large-scale industrial application of Spiro-OMeTAD in PSCs. Therefore, many researchers have tried to develop new 3D spiro-type HTMs based on simpler synthesis and high efficiency to replace the conventional Spiro-OMeTAD in PSC. On the other hand, there are far fewer works seeking an environmentally and economically more efficient synthetic route to replace the actual one.

The Spiro-OMeTAD molecular structure consists of two arylamine moieties perpendicularly linked with a sp^3-hybridized spiro centre (**Figure 82 top**). The rigid spiro structure enables high thermal stability, ensures the formation of a high-quality films, does not compromise solution processability, minimizes the tendency to form aggregates, enhances its glass transition temperature (T_g) without sacrificing the charge transport properties, and provides sufficient energy levels to block electrons and pass holes at the same time.[124] The oxidation potential of spiro-OMeTAD is controlled via the incorporation of methoxy substituents at its diphenylamine moieties. The -OMe group is electron-withdrawing by the inductive effect, but it can also exhibit electron-donating behaviour under resonance stabilization, which in this case is the predominant effect accordingly with Hammett rules as those groups are substituted at the para position.[119]

The most common synthetic route employed to access commercial Spiro-OMeTAD involves five reaction steps starting from commercially available materials with a total yield of the process around 30%. The protocol involves a Grignard's reagent formation and reaction (or alternatively a treatment with tBuLi at -78°C)[125], cyclization, tetra bromination and finally a Pd-catalysed tetra B-H amination reaction.[126] As a result, the time consuming synthesis and high synthetic cost of Spiro-OMeTAD hinder its large-scale commercial application, as it requires hazardous conditions (Grignard reagent) or energetically expensive low temperatures (-78 °C).[126,127]

The first step requires the construction of the 9,9'-spirobifluorene (SBF) core, whose standard synthetic access is reported in literature starting from the commercially available 2-iodobiphenyl and involves three synthetic steps.[128,129] The reaction of 2-iodobiphenyl with metallic magnesium in refluxing THF leads to the formation in situ of the corresponding Grignard reagent, which is then reacted with 9-fluorenone to obtain the intermediate 9-(biphenyl-2-yl)-9-fluorenol (38) in 70% yield (pathway A).[128] Such intermediate can also be prepared starting from the same reagent but using t-BuLi in harsh conditions to promote the lithium-halogen exchange with subsequent quenching with fluorenone affording the aforementioned alcohol in 60% yield (pathway B).[125,130] However, pathway A is the preferred one giving higher yield, and requiring fewer steps under milder reaction conditions. Another variation of the synthetic procedure involves the use of the commercially available 2-bromobiphenyl as starting reagent instead of 2-iodobiphenyl, although the Grignard reaction between 2-bromobiphenyl and magnesium proceeds more slowly but with the same results.[128,131] Finally, a catalytic amount of hydrochloric acid is added to a boiling solution of the carbinol in acetic acid, which leads to a Friedel-Crafts ring-closure reaction and dehydratation, whereupon most of the formed 9,9′-spirobifluorene precipitates on cooling from the solution. For this final step, the authors reported a yield of 84%. The overall yield to construct the SBF structure starting from 2-bromobiphenyl and following the preferred milder pathway A is 59%, while the estimated E-factor accordingly with experimental data is 14 (**Figure 83**).

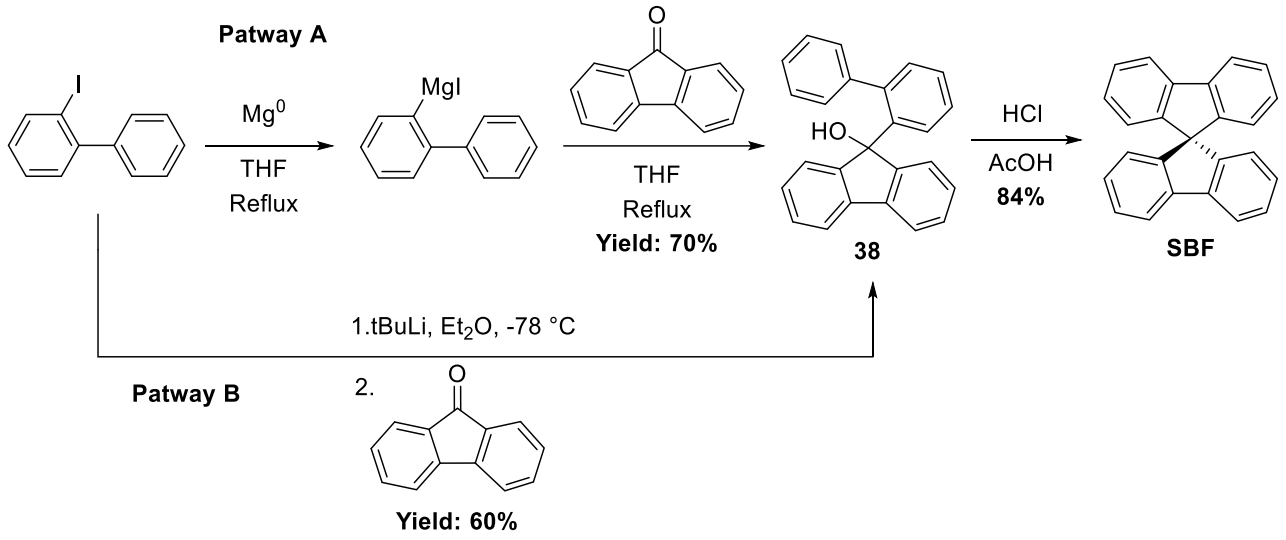

Figure 83. *Synthetic scheme for the construction of the SBF accordingly to standard literature methods.*

More recently, an alternative and valuable procedure to access the SBF core has been reported by Osuka and co-workers.[132] The protocol requires only a single synthetic step starting from commercially available materials. The reactions is an "aromatic metamorphosis" between dibenzo[b,d]thiophene-5,5-dioxide and fluorene in the presence of the strong, non-nucleophilic base $KN(SiMe_3)_2$ resulting in the formation of 9,9'-spirobifluorene in 45% yield after chromatographic purification. According with authors, the transformation would proceed via an intermolecular SNAr reaction followed by intramolecular SNAr cyclization. This protocol has obvious advantages over the aforementioned procedure, including the number of synthetic steps, the atom economy, and the fact that pyrophoric chemicals are not needed, however, the reaction needs a hazard superbase and harsh pressurized conditions (the reaction is performed in dioxane at 150°C for 12h) and the E-factor of the process is around 900.

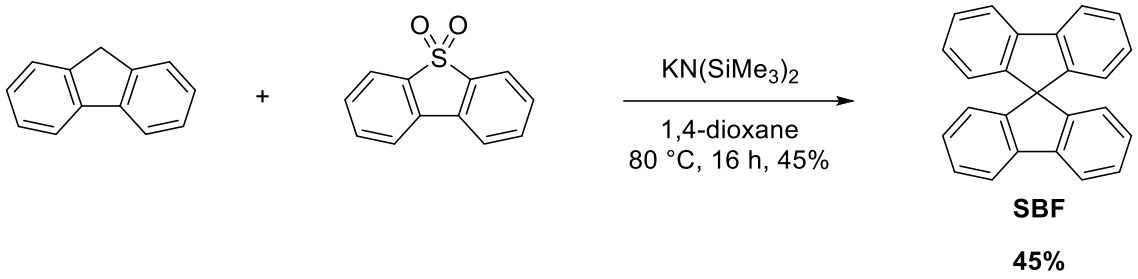

Figure 84. *Reaction scheme for the practical synthesis of SBF in a one-pot procedure developed by Prof. Osuka and co-workers.*

Subsequently, in order to extend the conjugation of the 9,9'-spirobifluorene to access the target compound, it is necessary to synthesize its tetrabrominated derivative 2,2',7,7'-tetrabromospirobifluorene (SBF-4Br). Halogenated compounds are versatile candidates for further substitution like cross-coupling and amination. The standard literature procedure useful to perform the regiospecific 2,2',7,7'-tetrabromination of the SBF core requires the use of at least 4 equivalents of Br_2 as a brominating agent in the presence of $FeCl_3$ as catalysis and chloroform as solvent.[133] The reaction is initially carried out at a temperatures around 0 ° C in order to depress the SBF reactivity and have a better control over the formation of any regioisomers; the bromination proceeds functionalizing the 2, 2', 7 and 7' positions of the 9,9'-spirobifluorene in 90% yield and with an E-factor of the process of 47.[134] However, it should be noted that although the E-factor value is relatively

low, this metric does not take into account the use of toxic halogenated solvents, which should be avoided in an industrial environment.

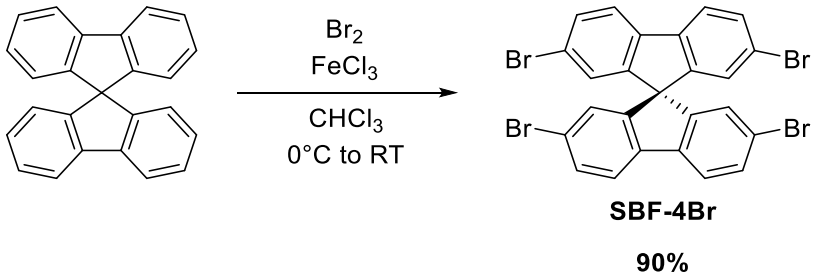

Figure 85. *Reaction scheme for the standard synthesis of 2,2',7,7'-tetrabromospirobifluorene (SBF-4Br).*

Finally, spiro-OMeTAD is synthetized through standard Pd-catalysed Buchwald-Hartwig amination of SBF-4Br with at least 4 equivalents of bis(4-methoxyphenyl)amine, using $Pd_2(dba)_3$ as palladium source, tBuONa as the base, and under inert atmosphere in refluxed toluene for 12 h.[126] The reaction leads to the target product only in 45% yield after careful chromatographic purification. The E-factor of this step including purification is 2040.

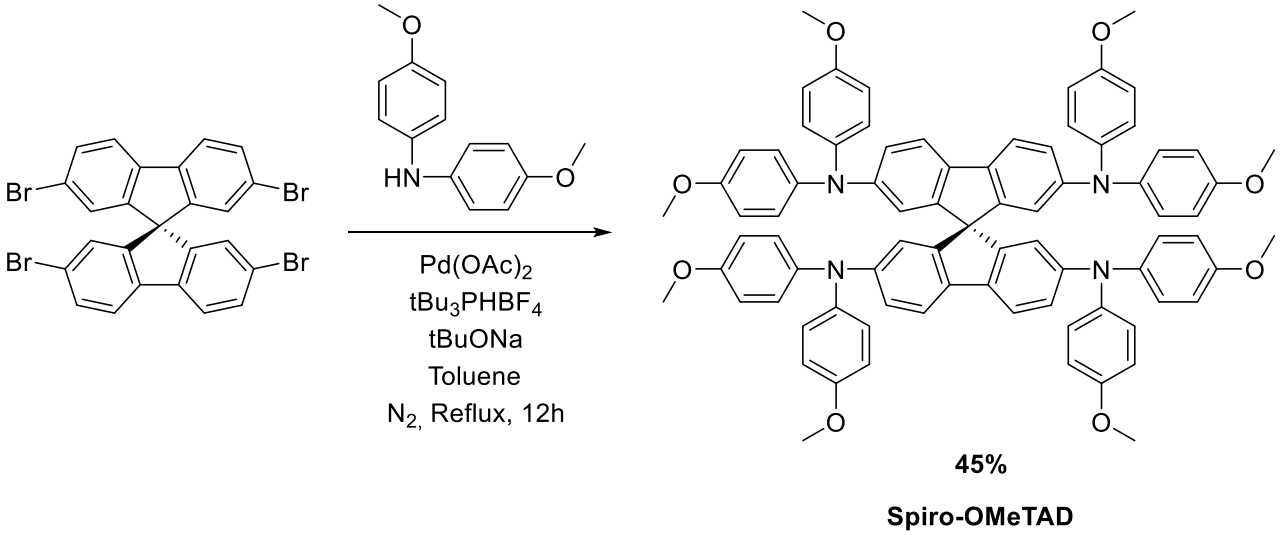

Figure 86. *Reaction scheme for the standard synthesis of spiro-OMeTAD.*

Overall, the synthesis of spiro-OMeTAD from commercially available materials has a yield of 25-30% and an E-factor around 2100. Considering the high environmental and economic impact of the compound, along with its great value within organic solar cells technology, the purpose of this work is to find a new green chemistry compliant synthetic methodology to render spiro-OMeTAD's production industrially feasible. Starting from raw and commercially available materials, we have developed a novel, sustainable and benign alternative route to access spiro-OMeTAD, improved at each step compared to standard protocols reported in the literature. Our protocol enables raising the overall yield of spiro-OMeTAD to 50% and reducing by 1 order of magnitude the overall E-factor, making the compound more economically and environmentally favourable to industry.

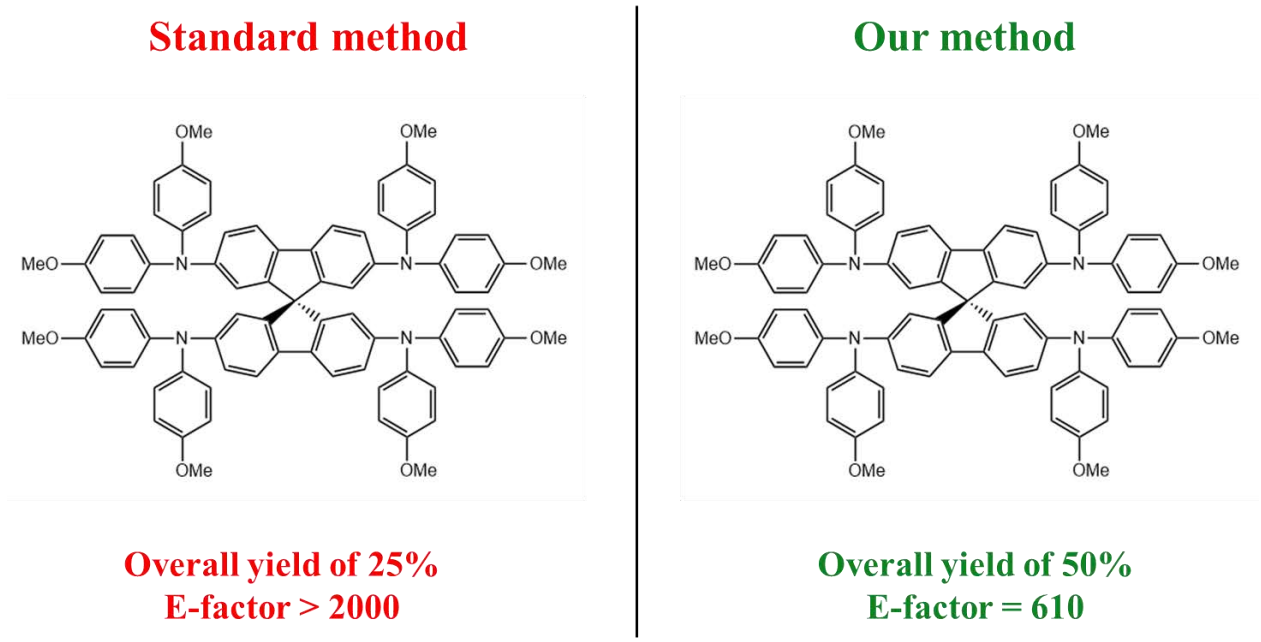

2.8.2. Results and Discussion

2.8.2.1. One-Pot Construction of the SBF Core

At first we started studying the aromatic metamorphosis reaction between dibenzo[b,d]thiophene-5,5-dioxide and fluorene aspired by the work proposed by Prof. Osuka[132]. In these conditions the reaction allow to access the SBF core in moderate yields and in just one synthetic step, avoiding the use of hazardous Grignard reagents, or extremely expensive conditions needed to cool down the reaction at -78°C using pyrophoric tBuLi as previously discussed. Starting from Prof. Osuka's conditions, we developed a sustainable alternative aromatic metamorphosis for the synthesis of the SBF core. The synthetic way we propose uses the melted reagents as mixing medium to perform the reaction "in bulk" without employing any solvent, thus improving the sustainability. Our method uses KOH instead of the superbase $KN(SiMe_3)_2$ (which is not as readily available as KOH) and 18-crown-6 as a phase transfer agent. A small amount of diethylene glycol dimethyl ether (diglyme) is added to obviate the partial sublimation of the fluorene, which otherwise would depose far from the reaction mixture where transformation is happening. The SBF formed can be isolated just filtrating the crude on celite (helping with a little amount of toluene) and sublimating the excess fluorene with a yield of 83%. The E-factor of the process is 10, so greatly reduced compared with that of Prof. Osuka,

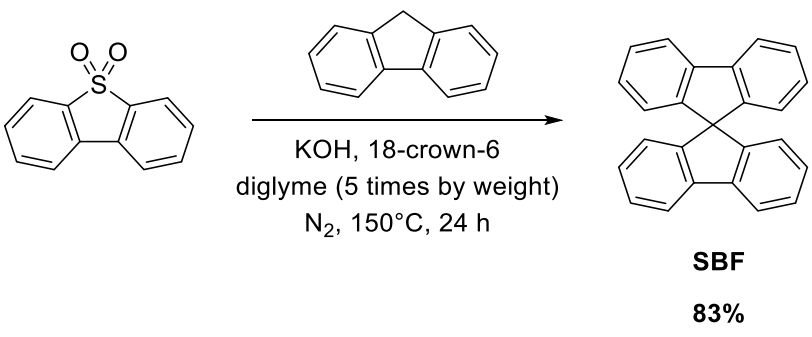

Figure 87. *Reaction scheme for the aromatic metamorphosis we propose.*

Compared with the standard synthesis, this protocol has several advantages: only a single step is required, the yield is fairy higher, the reaction conditions are milder and easily controlled, the quantity of organic solvent is enormously reduced (only a stoichiometric amount employed) and with the possibility of recovering the unreacted fluorene in highly pure grade. The method can be considered an efficient, sustainable, and cost-effective alternative synthetic method to access the SBF core.

2.8.2.2. Micellar Tetra-Bromination Reaction of the SBF

The next step studied involves the synthesis of the SBF-4Br. In the research for a more sustainable protocol, the idea consists of replacing with water the particularly toxic halogenated solvent ($CHCl_3$) used in the standard procedure. The already reported methods of bromination of aromatic compounds in water are scarse and limited to a only few examples such as NaBr-H_2O_2 in H_2O/sc CO_2 biphasic system[135] and H_2O_2-HBr "on water" system,[136] albeit low conversions, high temperature (40 °C), and a very long reaction time (from 8 to 28 h) are some of the concomitant shortcomings. There are also some other reagents that have been developed as a substitute for the harsh Br_2, however, no such reagent is commercialized to date, because of their expensive nature, poor recovery and recycling of spent reagent, disposal of large amounts of HBr waste and that the reagents have a short shelf life, hence they are meant only for laboratory-scale preparations with limited applications.[137] As an alternative, we here propose a bromination methodology for the SBF carried out through the micellar catalysis approach using Br_2 as brominating agent given the very low reactivity of the SBF towards commercially available milder brominating agents. The bromination reaction has been still attracting attention to develop the more practical method suitable for industrial-scale synthesis; this remark enhances the versatility of bromine as an inexpensive, readily available starting material. Moreover, the bromination reaction can take advantage of aqueous micelles as a convenient reaction medium for solubility reasons since aromatic substrates are highly hydrophobic, whereas the electrophile bromonium ion is hydrophilic. In the literature there are already reported some examples of poly-bromination reactions in water using molecular bromine catalysed by micellar solution of sodium dodecyl sulphate (SDS) at room temperature for several aromatics resulting in excellent yields (>90%) and purity.[137] The excellent results with enhanced rates observed can be rationalized in the nature of the surfactant employed: the strong catalytic activity is related to the negatively charged SDS micelles (the SDS is an anionic amphiphile) that are able to specifically interact with the positive brominating electrophilic intermediate Br^+. The reaction between aromatic substrate and bromine occurs immediately at the micellar-water interface (Stern layer)[138,139] by colocalizing the Br^+ (by the surfactant head) to the aromatic substrate which is supposed to be close to the lipophilic tail of the SDS (**Figure 88**).

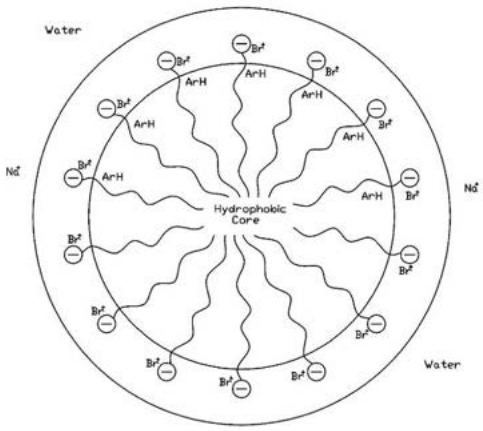

Figure 88. *Representative scheme of the interaction between the positive brominating electrophilic intermediate Br^+ and the negatively charged head of the SDS which brings the two reactants closer.*[137]

Electrophilic aromatic bromination that involves the ionization of a bromine-ring charge transfer-complex is extremely fast in aqueous media in which the formation of the bromonium ion is strongly assisted by electrophilic solvation of the leaving bromide ion (**Figure 89**).[138]

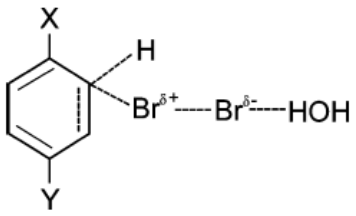

Figure 89. *Bromination transition state assisted by electrophilic solvation of the leaving bromide ion.*

However, the method is restricted to mono, di- and tri- bromination reactions and limited to few simple derivatives. Moreover, considering the more complex tetrabromination reaction of the SBF the choice use of only SDS as surfactant could not be the best option. It should be considered that SDS has a Krafft Point (threshold temperature value below which the formulation is no longer stable and the system demixes) at around 15 °C, thus limiting the possibility to cool down further the reaction in order to have a better control over the formation of undesired regioisomers which are very hard to separate. For this reason, inspired from such impressive earlier results, we still decided to use the effective SDS but mixed with another anionic surfactant, AOT (dioctyl sulfosuccinate sodium salt), which is also supposed to be able to specifically interact with the positively charged intermediate responsible of the bromination process, but characterized by a Krafft Point of 3°C. Thus, we decided to employ a 2% wt solution of AOT/SDS (1:1 wt) mixture as surfactant system to carry out the tetrabromination reaction on the 9,9'-spirobifluorene. The corresponding micellar solution kept stable at around 5°C (ice bath) ensuring satisfactory regioselectivity. **Figure 90, Table 10** shows the results we obtained under the different conditions we tested. Clearly, using water as reaction medium it was not convenient to cool down the reaction below the 5°C. Moreover, we decided to not employ the catalyst $FeCl_3$ since it rapidly hydrolysed and forms $Fe(OH)_3$ when dissolved in water losing its efficacy. Prof. Agarwal reported that the absence of $FeCl_3$ in micellar bromination reaction may require the use of a little excess of bromination agent.[137]

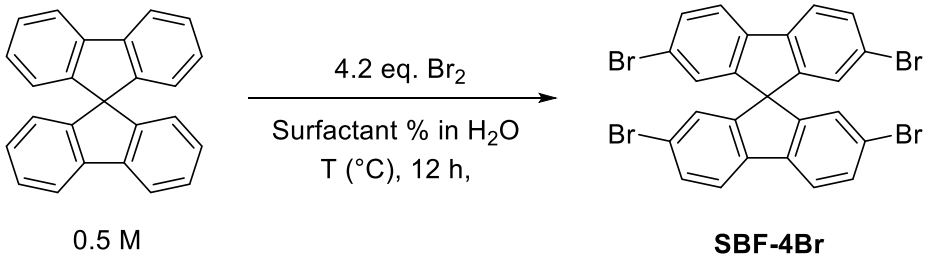

Figure 90. *Reaction scheme for the tetrabromination of SBF in water under the investigated conditions.*

Entry	Surfactant %	Temperature (°C)	SBF-4Br (mol%)
1	SDS 2%	25	55
2	AOT 2%	5 to 25	32

3	SDS/AOT (1:1) 2%	5 to 25	70
4	SDS/AOT (1:1) 8%	5 to 25	76
4[a]	SDS/AOT (1:1) 8%	5 to 25	88 (60% is.)

a: 6 equivalents of Br_2 were employed.

Table 10. *Summarized results for the tetrabromination of SBF in water under the investigated conditions.*

As shown in **table 10** the reaction carried out in an SDS solution at room temperature is somewhat more efficient than using the AOT at lower temperatures (55 vs 32 % of conversion to SBF-4Br for entries 1 and 2, respectively). However, the best solution was the use of the two surfactants mixture SDS/AOT 1:1 starting the reaction at 5°C (entry 3), which gave an increased conversion to SBF-4Br respect to only SDS thanks to the limited formation of the SBF-4Br regioisomer (5 mol%). A possible explanation for the limited conversion observed under these latter conditions may lie in the deterioration of the surfactant(s) by reaction with bromine. To verify this hypothesis, a further test was conducted using a greater quantity of surfactant mixture to contrast the possible degradation, passing from 2 to 8% in water (entry 4). The reaction performed in these conditions led to a slightly better result passing from 70% to 76% of conversion to product. Finally, significantly better results were obtained by working with a marked excess of bromine (entry 4a): passing from 4.2 to 6 equivalents of bromine led to significantly increase from 76 to 88% in the GC-MS yield, however a significant percentage of 11% of regioisomer was still observed. Under these conditions it was possible to isolate the pure product SBF-4Br by simply filtering the reaction mixture, which was then washed with a solution of $NaHSO_3$ to quench an eventual amount of unreacted Br_2, and finally recrystallized from THF in 60% yield. The E-factor of the process is around 30, thus reduced with respect to the literature protocol. The clear improvement in terms of sustainability that accompanies the reaction carried out in a micellar environment is evident.

2.8.2.3. Tetra-Buchwald-Hartwig Amination Reaction

The last synthetic step necessary to obtain the spiro-OMeTAD is the palladium catalysed tetra Buchwald-Hartwig amination reaction of the SBF-4Br with the bis(4-methoxyphenyl)amine. This step is particularly complex, in fact, the standard reaction carried out in refluxing toluene gives spiro-OMeTAD in only 45% and requires a particularly troublesome chromatographic purification. Again, we considered to apply the micellar catalysis approach to replace the use of toxic organic solvent and improve the overall sustainability of the process. Standard micellar catalysis in water solution of a surfactant proved ineffective due to the high temperatures required. Neutral surfactants all feature cloud points in the 40-60°C interval under the strongly basic conditions required by the B-H amination and readily spontaneously demixed. Therefore, in order to find an effective, and at the same time sustainable synthetic protocol, we decided to use an emulsion as a reaction medium. The particular reasons and advantages of using emulsions instead of aqueous micellar solutions have already been described in the previous paragraphs. Specifically, following **Figure 91, Table 11** shows an accurate reaction screening in order to find the most suitable conditions.

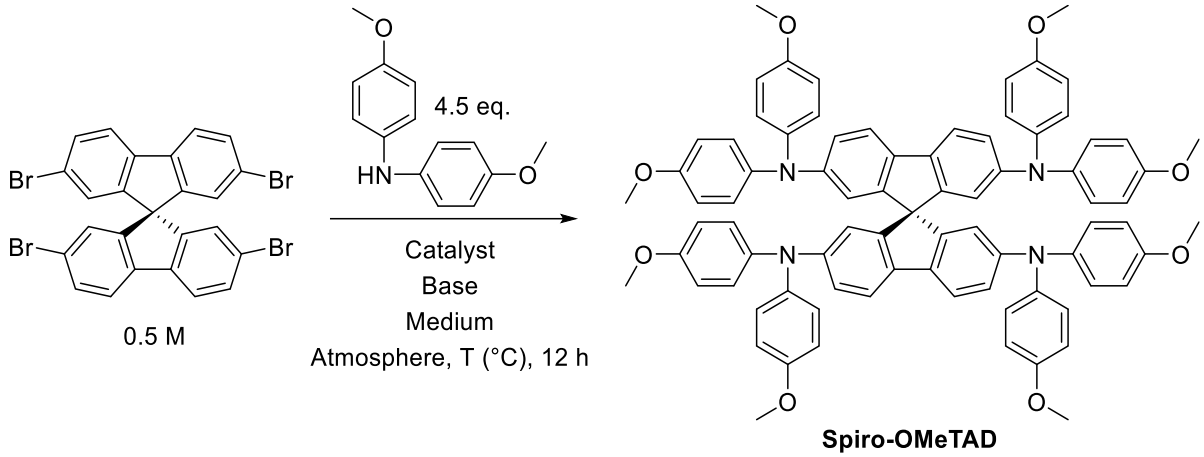

Spiro-OMeTAD

Entry	Medium	Catalyst (8 mol%)	Base (6 eq.)	Atm.	T (°C)	Spiro-OMeTAD (Conversion %)
1	K-EL 2%/toluene 9:1	$Pd(OAc)_2$/ tBu_3PHBF_4	tBuONa	air	80	traces
2	CTAB 2%/toluene 9:1	$Pd(OAc)_2$/ tBu_3PHBF_4	tBuONa	N_2	80	traces
3[a]	CTAB 2%/toluene 9:1	$Pd(OAc)_2$/ tBu_3PHBF_4	tBuONa	N_2	80	traces
4[b]	CTAB 2%/toluene 9:1	$Pd(OAc)_2$/ tBu_3PHBF_4	tBuONa	N_2	80	traces
5	CTAB 2%/toluene 9:1	$Pd(dtbpf)Cl_2$	tBuONa	N_2	80	40 (34 is.)
6	K-EL 2%/toluene 9:1	$Pd(dtbpf)Cl_2$	tBuONa	air	80	21
7	CTAB 2%/toluene 9:1	$Pd(dtbpf)Cl_2$	tBuONa	air	80	37 (32 is.)
8[a]	CTAB 2%/toluene 9:1	$Pd(dtbpf)Cl_2$	tBuONa	air	80	30
9[b]	CTAB 2%/toluene 9:1	$Pd(dtbpf)Cl_2$	tBuONa	air	80	27
10	CTAB 2%/toluene 9:1	$Pd(dtbpf)Cl_2$	NEt_3	air	80	traces
11	CTAB 2%/toluene 9:1	$Pd(dtbpf)Cl_2$	Proton Sponge	air	80	traces
12[c]	CTAB 2%/toluene 9:1	$Pd(dtbpf)Cl_2$	tBuONa	air	110	34
13	/	$Pd(dtbpf)Cl_2$	tBuONa	air	110 to 160	91 (80 is., 55 is)*

a: 30% wt hyperdispersant Jeffsperse X-3503 was employed; b: reaction performed at a nominal concentration of 0.125 M of the SBF-4Br; c: 6 eq. of bis(4-methoxyphenyl)amine were employed. *: 80% yield of isolated product through column chromatography; 55% yield of isolated product without using column chromatography.

Figure 91, Table 11. *Reaction scheme and screening of reaction and formulation conditions for the Pd-catalysed B-H amination of SBF-4Br with bis(4-methoxyphenyl)amine to obtain the Spiro-OMeTAD.*

We started testing the B-H reaction accordingly to standard literature conditions, so with fixed catalytic system $Pd(OAc)_2/tBu_3P^*HBF_4$ and tBuONa as the base, but we replaced the toluene used as solvent with the emulsion obtained by mixing Kolliphor EL 2% wt aqueous solution with toluene 9:1 v/v. The choice of such formulation was motivated by the previous satisfactory results obtained on analogous B-H and S-M reactions on conjugated derivatives.[69,74] Moreover, the reaction was performed under air according to the demonstrated capability of K-EL to provide oxygen free reaction pockets even under standard atmosphere.[69,74] Yet, as reported in entry 1 of **Table 11**, the reaction performed using the K-EL emulsion at 80°C gave unsatisfactory results leading to the desired product Spiro-OMeTAD in only traces. The reaction mixture was inhomogeneous even at simple eye inspectiuon, we thus further tuned formulative conditions. First, we replaced K-EL with the cationic surfactant CTAB (hexadecyltrimethylammonium bromide) in order to verify if the use of a positively charged surfactant could positively influence the course of the reaction by generating specific interactions with the partially negatively charged transient specie $tBuO^-$ (transient because $tBuO^-$ in water rapidly protonate to give tert-butanol) of the base responsible for deprotonation of the amine in the slow stage of the reaction. In this way the CTAB should colocalize the base with the dispersed substate at the oil/water interface helping at closing the catalytic cycle. However, even in this case the product was obtained in only traces (entry 2). Then, we tried to obtain a better formulative state avoiding the demixing of the system as possible candidate for the failing of the reaction. We supposed that the use of a hyper-dispersant stabilizer (polymeric compound used in the industry of organic dyes and pigments to disperse insoluble organic materials) could help improving the formulation thus reaction outcoming. In entry 3[a] we repeated the reaction using the hyperdispersant Jeffsperse X-3503 as co-stabilizer of the emulsifying system. Unfortunately, even under such conditions the reaction was not efficient despite the visually observed improvement of the formulation state with the solid substrates well dispersed. In entry 4[b] we "diluted" the reaction passing from a nominal concentration of the SBF-4Br of 0.5 M to 0.125 M again trying to help the dispersion of the substrates. Even in this case the reaction led to spiro-OMeTAD in only traces despite the better formulative state achieved with respect to entry 3. In entry 5 we decided to exchange the catalytic system replacing the couple $Pd(OAc)_2/tBu_3PHBF_4$ used to generate in situ the Pd^0 specie with $Pd(dtbpf)Cl_2$ which has the phosphine ligand already coordinated to the palladium. Impressively, we observed far better results passing from spiro-OMeTAD traces to 34% yield of isolated product; probably in the previous conditions using the couple $Pd(OAc)_2/tBu_3PHBF_4$ the palladium source and the phosphine ligand could not colocalize in the same compartment of the reaction mixture. These results are not so far compared with the standard literature protocol (34 vs 45% yield of isolated product), however less efficient and unsatisfactory from a sustainable point of view as a chromatographic purification is still required to isolate the product. Then, not satisfied yet, we investigated the use of the K-EL emulsion under air using $Pd(dtbpf)Cl_2$: we observed slightly worse result with a conversion to product of 21% (entry 6). In entry 7 we tested the reaction using the emulsion of CTAB under air without removing oxygen from the reaction environment to verify its impact, and impressively the reaction outcome did not deviate within the experimental error from the result obtained for the reaction carried out under nitrogen atmosphere (entry 5). Probably the amount of oxygen dissolved in water at the working temperature is really small and consequently the catalyst is not poisoned. Considering the results obtained, we decided to continue the screening of the reaction by fixing the CTAB emulsion as the reaction medium. Once the reaction had been improved using a more efficient catalytic system, we continued the study of the reaction returning to consider the formulation aspect. Entry 8[a] shows the results obtained by adding to the reaction a 30% wt of the hyper-dispersant Jeffsperse X3505. However, even if the substrates were well dispersed in water with a very fine particle size of solid

substrates (the appearance was similar to a paint), the reaction did not improve. The other well-defined emulsion was obtained diluting the reaction from 0.5 M to 0.125 M of the SBF-4Br in the emulsion, but again the reaction gave similar results (entry 9[b]). Verified that the incomplete conversion of the reaction is not affected by the formulation, we tried other bases to validate the possibility to improve the reaction in its determining step (coordination of the amine to palladium promoted by its deprotonation). In entry 10 we explored the use of the NEt_3 as the base for two reasons: first, it is known the well-established and efficient activation of the $Pd(dtbpf)Cl_2$ catalyst by the triethylamine, and second, being this base a liquid (the tBuONa is a solid, and even if in water it converts to tBuOH which is also a liquid, not all the base is dissolved at the concentration and conditions used) it helps to better disperse/dissolve the high amount of solid substrates with respect to the liquid components. Unfortunately, the use of such base revealed to be not efficient with the formation of spiro-OMeTAD. In entry 11, we then tested another alternative organic base known as "proton sponge" (N^1,N^1,N^8,N^8-tetramethylnaphthalene-1,8-diamine). This compound is characterized a diamine in which the two dimethylamino groups are attached on the same side (peri position) of a naphthalene ring. This molecule has several very interesting properties; one is its very high basicity. Moreover, being characterized by a melting point of 45 °C, therefore liquid at the reaction temperature of 80 °C, it helps from a formulative point of view. Nevertheless, again the reaction displayed unsatisfactory results with only traces of the product. Once we explored the surfactant and co-stabilizers, the catalytic system, the formulation, the base without even getting close to complete conversion, we finally decided to boost the conditions raising the temperature at 110°C under pressure (the emulsion started boiling around 90 °C) and using a fair excess (6 equivalents instead of 4.5) of the aminating agent (entry 12[c]). The results did not improve, stacking the conversion to product just over the 30%.

Later, we took inspiration from interesting published works of Prof. Nechaev and co-workers related to a highly efficient solvent-free protocol for the Buchwald-Hartwig amination of conjugated (hetero)aryl halides with secondary amines.[140,141] The method avoids the use of further reaction medium (no organic solvents, no water) than the reactants/reagents using an excess of the amine as the solvent. From the sustainability point of view this strategy is extremely advantageous since not even the wasted water would be considered in the E-factor calculation. However, this strategy is not yet reported for complex substrates such as SBF-4Br which require a tetra-functionalizing reaction. We decided to try this strategy for the synthesis of spiro-OMeTAD using melted bis(4-methoxyphenyl)amine (melting point 100-104°C) as the reaction medium, thus working "in bulk". Impressively, as reported in entry 13, the NMR analysis of the crude revealed a conversion to spiro-OMeTAD in 91% in 12h. However, the pure product was obtained in 80% yield using chromatographic purification. Many attempts have been made to isolate the product in a less laborious way, so far without obtaining any success (the product do not recrystallize in many solvents or recrystallizes with impurities, the more influence probably associated with the corresponding trisubstituted structure). Recently, unsatisfied and aiming at finding a more sustainable but still efficient purification strategy, we tested the affinity of the impurity, supposed to be a brominated specie, towards the active charcoal submitting the mixture to a filtration over a pad of SiO_2/active charcoal 1:1 wt/wt. in this way we manage to isolate Spiro-OMeTAD in high purity at 55% yield without the need of requiring a column chromatography. The relevant result greatly exceeds standard literature protocol in terms of both efficiency and sustainability: 55% vs 45% yield of isolated product and E-factor of 610 vs 2040.

2.8.2.4. PSCs Characterization of Newly Synthetized and Commercially available Spiro-OMeTAD HTMs

In collaboration with Prof. Thomas Brown of the University of Rome Tor Vergata, perovskite solar cells with glass/ITO/SnO_2/$Cs_{0.06}(MA_{0.16}FA_{0.78})_{(0.94)}Pb(I_{0.84}Br_{0.16})_3$ (FAMACs)/HTM/Au architecture were fabricated. Three different HTMs were tested: commercial spiro-MeOTAD purchased from Borun New Material Technology LTD as reference cell (labelled as "ref"), and the newly synthesised spiro-OMeTAD HTM of this work, of which it was examined both the highly pure chromatographed sample (labelled as "croma") and the non-chromatographed crude (labelled as "non croma"), in order to verify the impact of impurities of the latter on device performances.

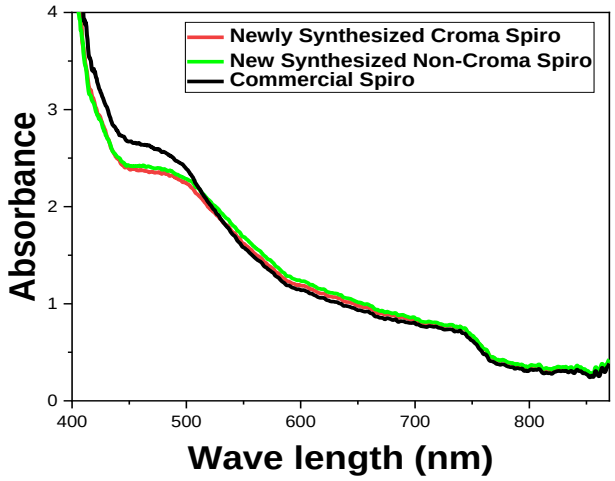

Figure 92. *Comparison of UV absorption spectra of various perovskite devices (New synthesized Spiro and commercial Spiro.*

Devices were characterised under 1 sun (AM1.5G, 100mW/cm²) at room temperature by means of a Keithley 2420 source meter and a ABET sun 2000 solar simulator as light source. During the measurements, the devices were masked with a black tape with 0.1 cm² aperture. External quantum efficiency measurements were carried out with a modular testing platform (Arkeo - Cicci research s.r.l.) consisted of a white LED array (4200 Kelvin) tunable up to 200 $mWcm^{-2}$ of optical power density and a high-speed source meter unit. Stability measurements were carried out and followed by protocols of the International summit on OPV stability (ISOS)-D-1 Shelf testing conditions. Following **Figure 92** shows the absorption spectra of the various perovskite devices (Glass/ITO/SnO2/Perovskite/Spiro/Gold) such as commercial Spiro, new synthesized Spiro (Croma, Non-Croma) illuminated from the HTL side. Absorption spectra of New synthesized Spiro and commercial Spiro HTLs devices have barely any distinction, which is suggesting that the absorption of perovskite films is not affected by newly synthesized Spiro HTLs based perovskite devices at lease for wavelengths below 500nm. As the evidence is obtained from the UV-vis absorption spectra of devices, newly synthesized Spiro does not cause any obvious changes on the optical properties in the perovskite layers.

We then tested the three different materials as HTM for planar perovskite solar cells with glass/ITO/SnO_2/FAMACs/HTM/Au architecture. The results of the device characterisation at STC (AM1.5G, 100mW/cm², 25°C) are shown in **Table 12** and **Figure 93**. The new spiro-type HTM gave similar results in terms of power conversion efficiency (PCE) when compared to reference spiro-MeOTAD cells. Croma-cells delivered an average PCE of 13.81% (PCE_{MAX}= 15.02%), while ref-cells yielded 13.89% average PCE (PCE_{MAX}= 15.02%). Croma devices showed slightly higher open-circuit voltage (V_{OC}), while ref-cells delivered higher currents. Similar fill factors (FF) were observed

for the two types of cells. The main difference among cells fabricated with the new HTM and the ref spiro-MeOTAD was in the hysteresis index (HI), calculated as the ratio $(PCE_{REV}-PCE_{FOR})/PCE_{REV}$ (where PCE_{REV} and PCE_{FOR} are the power conversion efficiencies measured from the reverse and forward scan respectively: around a doubling in HI was observed for croma-devices compared to ref cells (0.09 compared to 0.04), however the HI of croma-devices was below 0.1, which is an acceptable value for PSCs.

The new spiro-type molecule yielded good device performance and acceptable hysteresis, being a promising candidate to replace the commercial spiro-MeTAD HTM. In order to simplify the fabrication process of this new molecule and reduce its cost, we evaluated the effect of the chromatographic purification process of the spiro-type material on the performance of the cells (see **Table 12** and **Figures 93**). "Non-croma"-cells showed 13% reduction in relative terms in average efficiency compared to the purified counterparts, with average PCE of 11.99% (PCE_{MAX}=13.19%). The presence of by-products of the synthetic process in the HTM films mainly determined a remarkable reduction in FF (from 71.6% average of croma-cells to 63.2% of non-croma cells). Hysteresis was also greatly affected by the absence of the purification step, as the HI showed a two-fold increase for non-croma devices (HI=0.21). The variation of PCE between cells with reference HTM and new spiro-type HTM, with was subdued or not to a chromatographic step, is shown in **Figure 93**, where PCE in reverse and forward scans are depicted. Representative J-V curves of the cells, highlighting the hysteresis determined by the different HTMs, are reported in **Figure 94**.

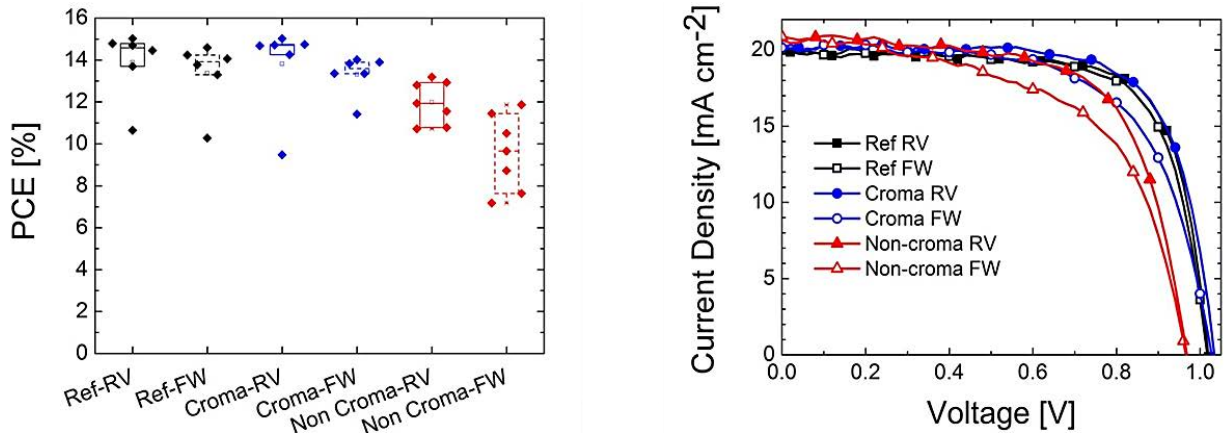

Figure 93. *Left: Power conversion efficiency (PCE) of glass/ITO/SnO_2/FAMACs/HTM/Au cells fabricated with a commercial spiro-MeOTAD HTM "ref" or with a newly synthesised spiro-type HTM "croma" or "non croma". Photovoltaic parameters were extracted either from the reverse (RV) current-voltage scan (from V_{OC} to V=0) and the forwad (FW) current-voltage scan (from V=0 to V_{OC}). Right: Current density vs voltage curves of glass/ITO/SnO_2/FAMACs/HTM/Au cells fabricated with a commercial spiro-MeOTAD HTM "ref", or with a newly synthesised spiro-type HTM "croma" or "non croma". Both reverse (RV) and forwad (FW) scans are reported.*

	V_{OC} [V]	**J_{SC} [mA/cm^2]**	**FF [%]**	**PCE [%]**	**HI**
Ref (rv)	0.998 ± 0.036 (1.027)	19.73 ± 0.28 (20.11)	70.33 ± 6.08 (74.37)	13.89 ± 1.64 (15.02)	0.04 ± 0.01
Ref (fw)	0.996 ± 0.036 (1.022)	19.85 ± 0.19 (20.13)	67.49 ± 5.74 (71.70)	13.37 ± 1.58 (14.59)	
Croma (rv)	1.024 ± 0.023 (1.050)	18.75 ± 2.16 (20.42)	71.61 ± 2.16 (74.34)	13.81 ± 2.14 (15.02)	0.09 ± 0.06

Croma (fw)	1.0023 ± 0.017 (1.045)	18.65 ± 2.17 (20.30)	70.28 ± 4.35 (78.72)	13.31 ± 0.97 (14.02)	0.21 ± 1.11
Non croma (rv)	0.964 ± 0.054 (1.017)	19.74 ± 1.60 (22.28)	63.17 ± 4.04 (67.75)	11.99 ± 1.02 (13.19)	
Non croma (fw)	0.960 ± 0.059 (1.016)	19.12 ± 1.12 (20.87)	51.90 ± 7.01 (62.52)	9.57 ± 1.82 (11.87)	

Table 12. *Photovoltaic parameters of glass/ITO/SnO_2/FAMACs/HTM/Au cells fabricated with a commercial spiro-MeOTAD HTM "ref" cells, or with a newly synthesised spiro-type HTM "croma" or used without any purification step "non croma". Average open circuit voltage (V_{OC}), short circuit current density (J_{SC}), fill factor (FF), power conversion efficiency (PCE) and hysteresis index (HI) were calculated on an average of 6 samples; the maximum values of V_{OC}, J_{SC}, FF and PCE are reported in brackets.*

The external quantum efficiency (EQE) of the cells was evaluated to analyse the different spectral conversion efficiency for the three different HTMs. As shown in **Figure 94**, the EQE spectra had similar shape for the three types of materials. EQE above 80% were observed for ref and croma-cells, while the not purified HTM delivered lower EQE. The integrated JSC calculated from the EQE spectrum was within the experimental error (5% discrepancy) for ref cells (integrated J_{SC}=19.86 mA/cm^2, J_{SC}= 20.11 mA/cm^2 under the sun simulator) and croma cells (20.36 mA/cm2 vs 20.12 mA/cm2); higher error (13%) was observed for non-croma spiro-type HTMs (17.86 mA/cm^2 vs 20.66 mA/cm^2).

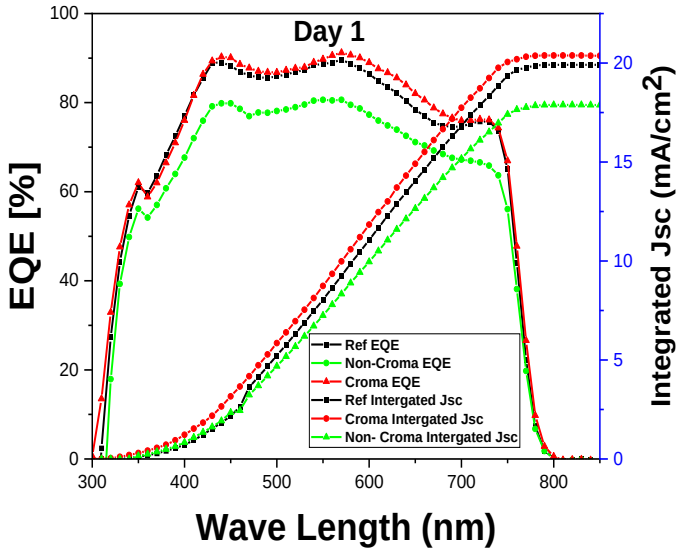

Figure 94. *External quantum efficiency (EQE) of glass/ITO/SnO_2/FAMACs/HTM/Au cells with a commercial spiro-MeOTAD HTM "ref", or with a newly synthesised spiro-type HTM "croma" or "non croma". Also shown is the calculated integrated current from EQE and AM1.5G irradiance spectrum.*

Following **Figures 95** and **96** show the statistics of the photovoltaic parameters of the cells with the three different HTMs under reverse and forward scan. As clearly visible in these figures, the non-purified HTM also shows a higher scattering in the results, with much higher standard deviations compared to reference cells and to their purified counterparts (see **Table 12**).

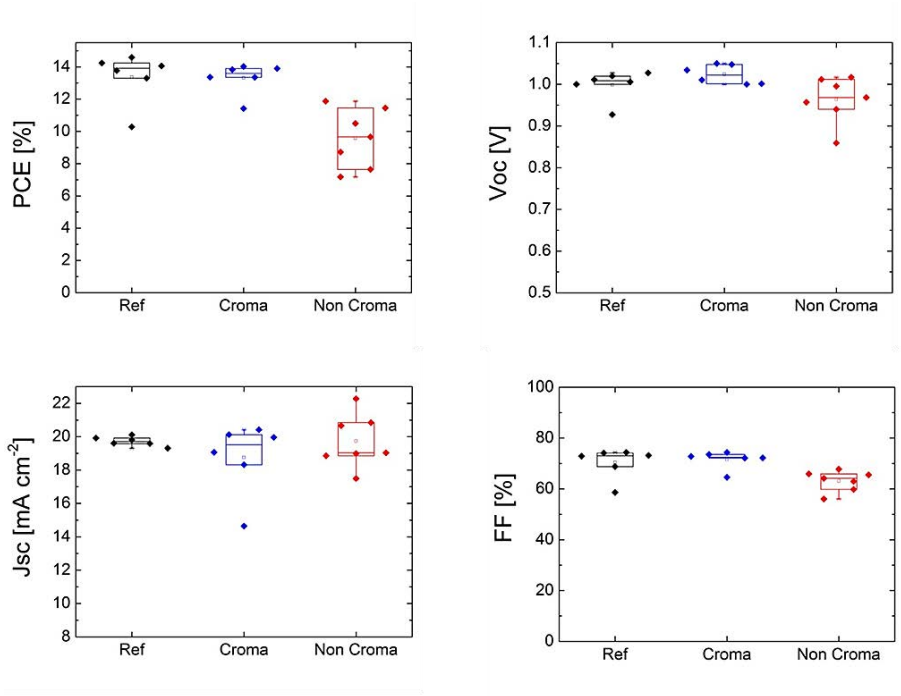

Figure 95. *Photovoltaic parameters, namely power conversion efficiency (PCE), open circuit voltage (V_{OC}), short circuit current density (J_{SC}) and fill factor (FF), of glass/ITO/SnO_2/FAMACs/HTM/Au cells fabricated with a commercial spiro-MeOTAD HTM "ref" cells, or with a newly synthesised spiro-type HTM "croma" or "non croma". The photovoltaic parameters were extracted from the reverse current-voltage scan (from V_{OC} to V=0).*

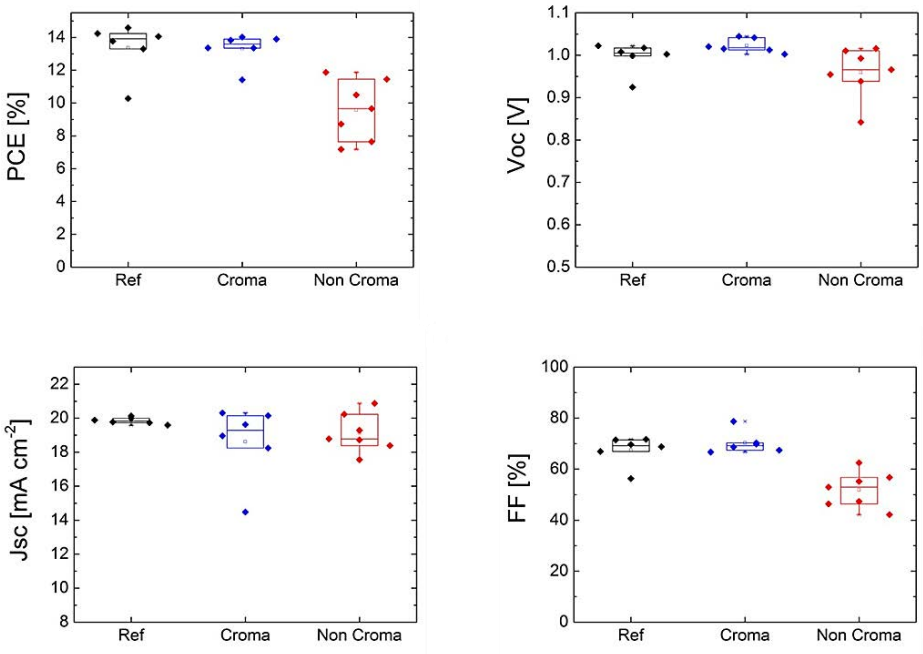

Figure 96. *Photovoltaic parameters, namely power conversion efficiency (PCE), open circuit voltage (V_{OC}), short circuit current density (J_{SC}) and fill factor (FF), of glass/ITO/SnO_2/FAMACs/HTM/Au cells fabricated with a commercial spiro-MeOTAD HTM "ref" cells, or with a newly synthesised spiro-type HTM "croma" or "non croma". The photovoltaic parameters were extracted from the forward current-voltage scan (from V=0 to V_{OC}).*

Following **Figure 97** shows the efficiency of the perovskite solar cells fabricated with different Spiro HTLs over a period of 156 days where the cells were stored in the dry box (RH 30 to 40%) and measurements were done under ambient conditions i.e. STC. The average efficiency of the devices on day 1 for commercial spiro, chroma spiro and non-chroma spiro was 11.94%, 13.43% and 10.50 % respectively calculated over 8 devices.

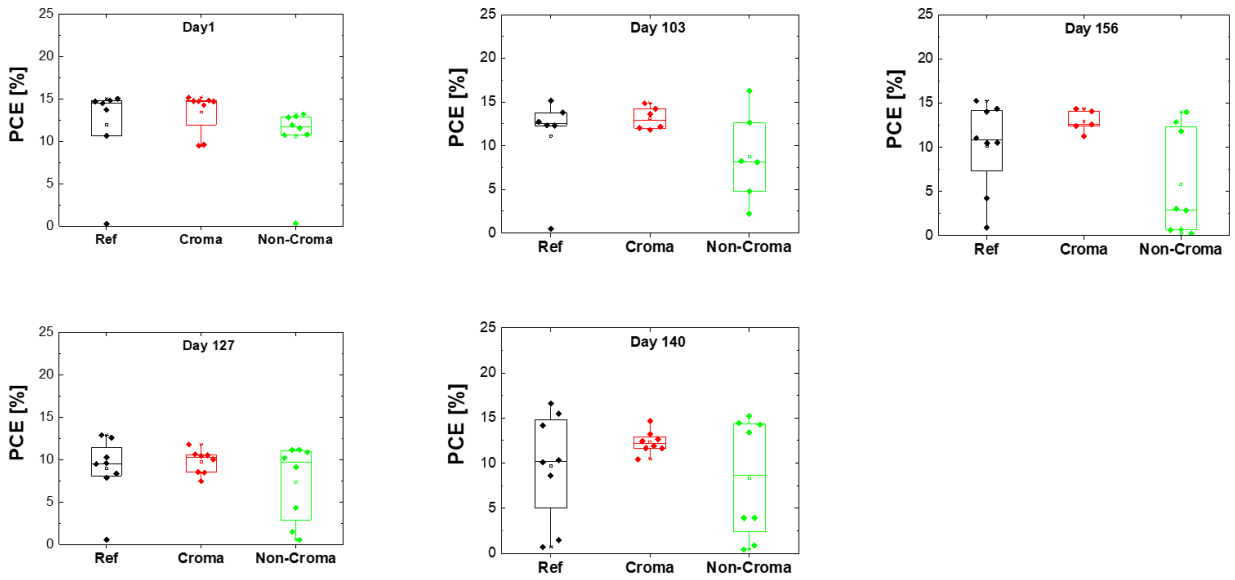

Figure 97. *Box Charts illustrating the statistical distribution of Power conversation efficiency of various perovskite devices (Reference Spiro Devices, newly Synthesized the Chroma Spiro and newly Synthesized the Non-Chroma Spiro) day wise a) day 1, b) day 103, c) day 127, d) day 140 and e) day 156. All cells were stored in the dry box (RH 30 to 40%) and measurements were carried out at standard test conditions (1000 W/m2, 25C and AM1.5G spectrum).*

Following **Figure 98** plots the average PCE with standard deviations as a function of time. It shows that the stability of the chroma spiro and commercial spiro average PCEs are statistically equivalent. In fact, from **Figure 97** one can notice that Chroma spiro devices showed better consistency and reproducibility of performance throughout the experimental period in relation to reference cells, especially after day 127, with 3.66% reduction in efficiency after 156 days. Non-chroma spiro devices instead show a significantly larger scatter in the results with time with the PCE being reduce to 75.2% compared to its value at day 1.

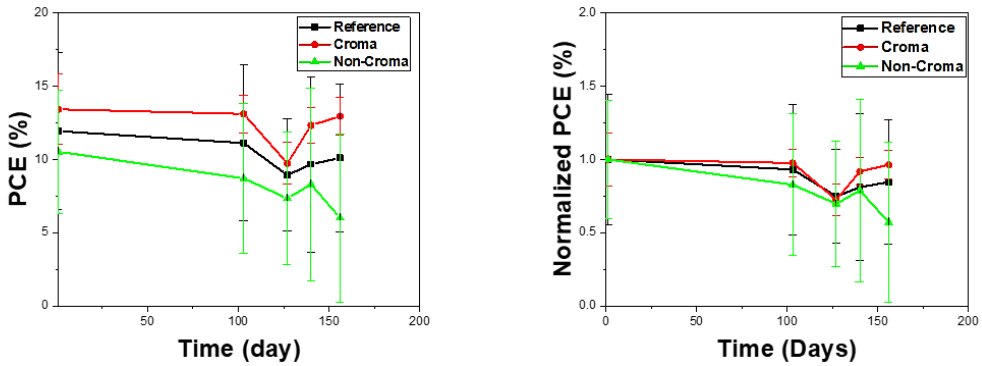

Figure 98. *Illustration shown above is variation of PCE of without encapsulated various devices as a function of time over 156 days stored under dark (RH<40%) at room temperature and all J-V measurements tested Devices were characterised under 1 sun (AM1.5G, 100mW/cm²) at room temperature under ambient environment. a) overall average PCE of all devices Vs Time b) Normalized PCE of all devices Vs Time.*

2.8.3. Conclusions

We developed an efficient, cost-effective, fully-sustainable alternative novel protocol for the synthesis of spiro-OMeTAD starting from commercially available raw materials, making the compound more accessible and suitable to industry for large production. The construction of the SBF core has been addressed in a single synthetic step, in high yield, under milder and cheaper conditions compared with the standard procedure, and with a markedly reduced quantity of the organic solvent employed (only stoichiometric amounts). The synthesis of its tetra-brominated derivative SBF-4Br was efficiently carried out in water as reaction medium, setting aside the use of halogenated solvents which are not compatible with industry. Then, the tetra Buchwald-Hartwig reaction necessary to access spiro-OMeTAD was studied with the sustainable micellar catalysis approach in emulsion conditions, obtaining results comparable with those reported in literature using organic solvents. Further studies, aspired by recent literature on B-H reactions "in bulk", revealed that spiro-OMeTAD can be efficiently synthetized in bulk without employing any organic solvent or water, exploiting the melted amine as mixing medium. The process leads to conversion of target product of 91%, which can be isolated through column chromatography leading 80% yield of pure product with an E-Factor of 1600 or just filtered over a pad of SiO_2/active charcoal 1:1 wt/wt leading 55% of pure product but with an E-factor of 610. Finally, we tested the new spiro-OMeTAD HTMs (both the chromatographed sample and the crude containing impurities) for planar n-i-p perovskite solar cells and we compared the obtained performances with those obtained for the corresponding commercially available reference. Interestingly, the newly synthesised HTM purified by a chromatographic process delivered comparable performance as the reference cells. "Croma"-cells yielded average PCE=13.81%, V_{OC}=1.024, J_{SC}=18.75 and FF=71.61%, as compared to reference devices with delivered PCE=13.89%, V_{OC}=0.998, J_{SC}=19.73 and FF=70.33% when measured at STC. "Croma"-cells showed a higher V_{OC}, but slightly lower J_{SC}. Cells with the new HTM also showed higher hysteresis compared to the reference devices, with HI of 0.09 and 0.04 respectively. The purification process was found to be essential in determining high efficiencies. In fact, cells fabricated with a non-purified HTM showed lower performances (average PCE=11.99%), mainly as the result of the lower fill factors (average FF=63.17%). In addition, "non-croma"-cells showed very high hysteresis (HI=0.21) and larger dispersion in the photovoltaic parameters, the latter accounting for the lower reproducibility of the cells and homogeneity of the HTM films. A crucial factor affecting the development and commercialization of perovskite solar cells is their stability. Stability experiments of devices stored under dark (RH<40%) at room temperature over 256 days (i.e. over 5 months) show that the stability of the average PCE over time is not affected by the HTL. In fact, the "croma" devices show a better cell-to-cell uniformity over time.

In conclusion, our protocol enables to raise the overall yield of spiro-OMeTAD to 50% and reduce by 1 order of magnitude the overall E-factor, making the compound more economically and environmentally favourable to industry. We demonstrated that the spiro-OMeTAD we synthetized represents a valid alternative to the commercial one, as a result of the high efficiencies observed in PSCs, and with similar if not better stability (i.e., cell-to-cell uniformity).

2.8.4. Experimental Section

2.8.4.1. Materials and Instruments

Reagents and solvents are bought from TCI, Fluorochem, or Sigma-Aldrich and used as received. $Pd(dtbpf)Cl_2$ catalyst is purchased from Ark Pharm. Anhydrous solvents are bought from Sigma-Aldrich. Chromatographic purifications are performed using Davisil LC 60A silica gel (pore size 60 Å, 70-200 μm). Composition of solvent mixtures used as eluents are indicated as volume/ volume ratios. NMR spectra are collected on a Bruker NMR Avance 400 NEO. Absorption spectra are collected in glovebox under argon atmosphere using a SEC2000 Spectra System UV/Vis single beam spectrophotometer. PSCs were fabricated with glass/ ITO/ SnO_2/ $Cs_{0.06}(MA_{0.16}FA_{0.78})_{(0.94)}Pb(I_{0.84}Br_{0.16})_3$ (FAMACs)/ HTM/ Au architecture. Glass/ITO substrates (Kintec, 10 ohm/square) were patterned via a laser scribing process and cleaned in ultrasonic bath in acetone, 2-propanol and deionised water for 10 min each. Before deposition of the ETL, glass/ITO substrates were subdued to UV irradiation for 10 min. SnO_2 was deposited by spin-coating a SnO_2 nanoparticle dispersion (15% in water, Alfa Aesar) at 6000 rpm for 35 s. Films were annealed at 100°C for 45 min and subdued to UV irradiation for 10 min. Triple cation precursor solution contained FAI (1 M), PbI_2 (1.2 M), MABr (0.2 M), $PbBr_2$ (0.2 M) and CsI (0.08 M) in anhydrous DMF:DMSO 3.2:1 (v:v). The deposition was carried out in a nitrogen-filled glovebox by spin-coating the precursor solution at 4000 rpm for 23 s; 0.7 mL of chlorobenzene (CB) were dropped on the substrate 7 s before the end of the spin-coating process. Spiro-OMeTAD HTM solutions were prepared by dissolving the compounds at a 73.42 mg/mL concentration in CB and stirred overnight at room temperature; 2 hours prior deposition, the HTM solutions were doped with 16.6 μL/mL LiTFSI stock solution (530 mg/mL in acetonitrile), 26.77 μL/mL TBP and 7.2 μL/mL cobalt(III) complex solution (FK209 from Lumtec). All HTM were spin-coated at 2000 rpm for 20 s. Finally, a 100 nm thick Au electrode was deposited by thermal evaporation. Unless stated otherwise, solvent and reagents were purchased from Sigma Aldrich.

2.8.4.2. Synthesis of 9,9'-spirobifluorene (SBF)

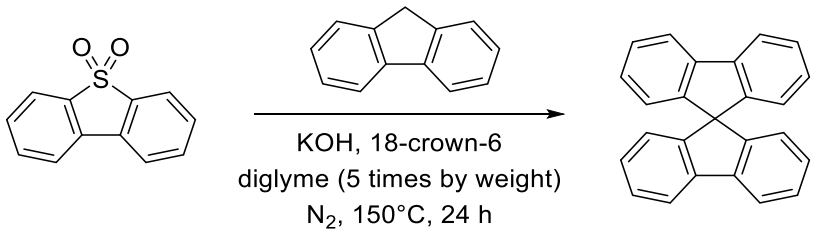

SBF

In a 100 mL two-necked roundbottom flask, dibenzothiophene-5,5-dioxide (2.000 g, 9.25 mmol), fluorene (2.300 g, 13,875 mmol), and KOH 85% wt (2.442 g, 37.0 mmol) were weighted, then the reaction environment was degassed by 3 vacuum/nitrogen cycles and put under N_2 atmosphere. Separately, a solution of 18-corona-6 ether (0.245 g, 0.925 mmol) in 1 ml of anhydrous diglima was prepared and added to the reaction flask, which was then heated at 115 ° C for 3 h and at 160 ° C for 21 h. The reaction was quenched by adding 3,5 mL of anhydrous and degassed MeOH. The reaction was then diluted with 4,0 mL of toluene and filtered over a pad of celite. The reaction crude was purified by sublimation of the unreacted fluorene to afford the pure product as a yellowish powder (2,418 g, 83% yield).

^{1}H-NMR ($CDCl_3$, 400 MHz): δ 7.87 (dd, J= 7.7 Hz, 4H), 7.34 (t, J = 7.7 Hz, 4H), 7.14 (t, J= 7.7 Hz, 4H), 6.75 (d, J= 7.7 Hz, 4H).

^{13}C-NMR ($CDCl_3$, 400 MHz): δ 119.9, 123.9, 127.6, 127.7, 141.6, 148.6, 66.4

2.8.4.3. Synthesis of 2,2',7,7'-tetrabromo-9,9'-spirobifluorene (SBF-4Br)

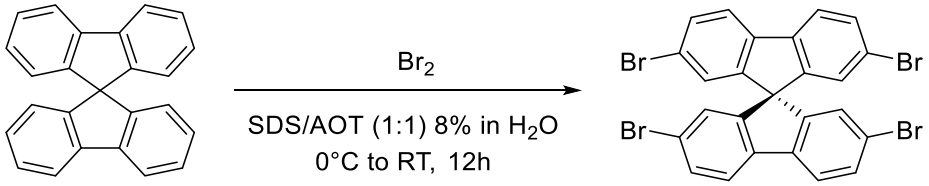

SBF-4Br

In a 100 mL two-necked roundbottom flask the 9,9-spirobifluorene (4.503 g, 14.2 mmol) was weighted, then 30 mL of a solution of SDS/AOT (1:1 wt/wt) 8% in water was added. The mixture was allowed to homogenize for 5 min and put on ice bath until a temperature around 5°C was reached. Then, the bromine (13.62 g, 85.2 mmol) was slowly dripped in the reaction mixture. After 12h the reaction mixture was quenched by adding 30 mL of a $NaHSO_3$ aqueous solution, filtered, and washed with deionised water. The crude was recrystallized from THF to afford the pure product as white crystals (5.372 g, 60%).

^{1}H-NMR ($CDCl_3$, 400 MHz): δ 7.68 (dd, J = 8.2, 0.4 Hz, 4H), 7.54 (dd, J = 8.2, 1.8 Hz, 4H), 6.83 (dd, J = 1.8, 0.4 Hz, 4H).

^{13}C-NMR ($CDCl_3$, 400 MHz): δ 148.79, 139.55, 131.76, 127.32, 122.17, 121.68.

2.8.4.4. Synthesis of 2,2',7,7'-tetrakis(N,N-bis-4-methoxyphenylamine)-9,9'-spirobifluore (spiro-OMeTAD)

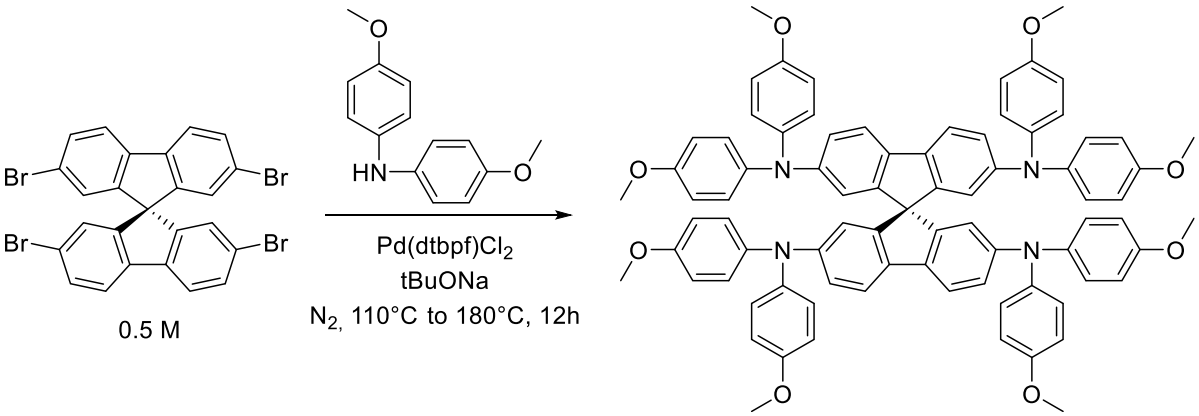

"In Emulsion" Procedure Under Air

1 L of CTAB 2% wt / toluene (9:1 v/v) emulsion was prepared homogenizing a 2 wt% aqueous dispersion of CTAB (18 g of CTAB in 882 mL of deionized water) with 100 mL of toluene using a T 25 digital ULTRA-TURRAX R until a stable, milky dispersion is obtained.

2,2',7,7'-tetrabromo-9,9'-spirobifluorene (0.316 g, 0.5 mmol), bis(4-methoxyphenyl)amine (0.573 g, 2.5 mmol), Pd(dtbpf)Cl_2 (0.026 g, 0.04 mmol), tBuONa (0.288 g, 3.0 mmol) were weighted in a 10mL screw-cap glass tube, then CTAB 2% wt / toluene (9:1 v/v, 1 mL) is added. The mixture is allowed to homogenize for 5 minutes before heating at 80°C. Reaction is stirred for 12 h at 80 °C. The mixture is diluted with 10 mL of MeOH and filtered. The crude was purified through column chromatography using a mixture of heptane/AcOEt 2:1 as eluent. The pure product was obtained as a white powder (0.196 g, 32% yield).

"In bulk" Procedure

In a 10 mL shlenck tube 2,2',7,7'-tetrabromo-9,9'-spirobifluorene (0.316 g, 0.5 mmol), bis(4-methoxyphenyl)amine (0.573 g, 2.5 mmol), Pd(dtbpf)Cl_2 (0.026 g, 0.04 mmol), tBuONa (0.288 g, 3.0 mmol) were weighted, then the reaction environment was degassed by 3 vacuum/nitrogen cycles and put under N_2 atmosphere. The reaction was stirred at 110 °C for 3h and then at 180 °C for further 21h. The reaction mixture is then dissolved in toluene and filtered over a pad of SiO_2/active charcoal 9:1 wt/wt to afford the pure product as a white solid (0.340 g, 55%).

Note: The crude can be submitted to column chromatography using Ept/AcOEt 2:1 as eluent affording the product in 80% yield.

^{1}H-NMR (500 MHz, THF d8) δ 7.40 (d, J = 8.3 Hz, 4H), 6.90 (d, J = 8.9 Hz, 16H), 6.78 (d, J = 8.9 Hz,
20H), 6.52 (d, J = 1.8 Hz, 4H), 3.74 (s, 24H).

^{13}C-NMR (126 MHz, THF d8) δ 153.75, 148.21, 145.64, 139.51, 133.40, 123.25, 120.27, 117.69, 115.55, 112.37, 52.71.

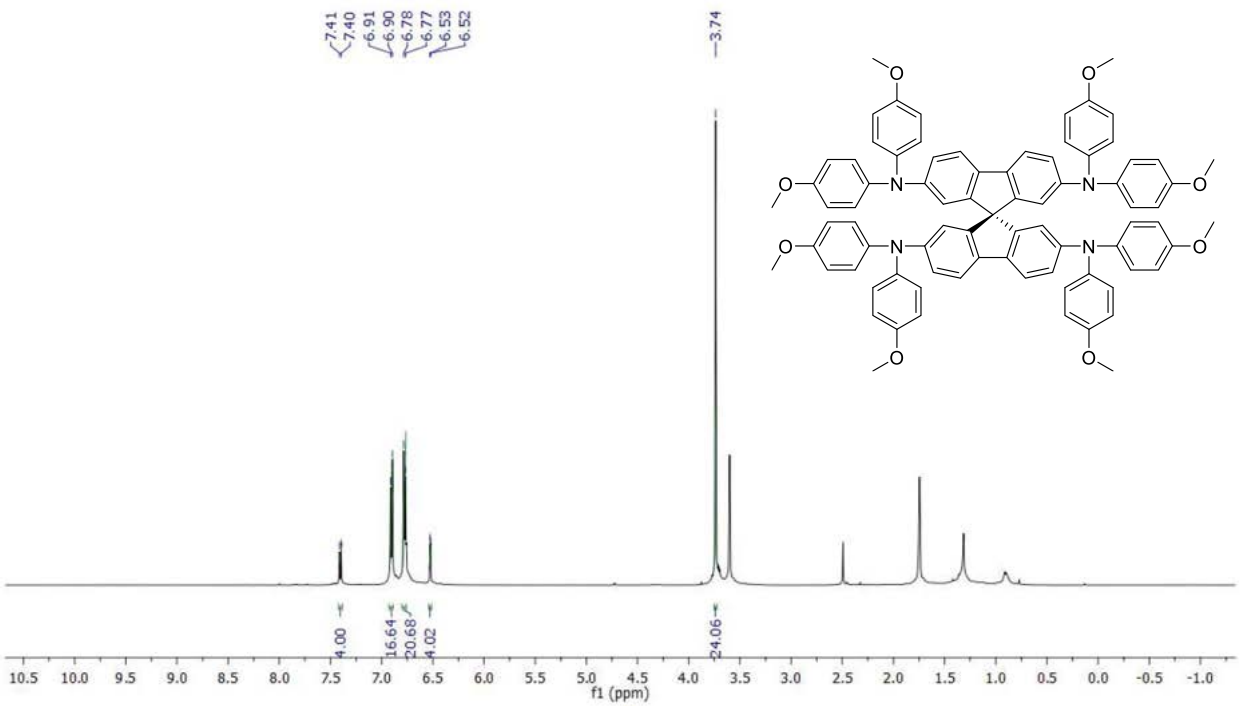

^{1}H-NMR of spiro-OMeTAD.

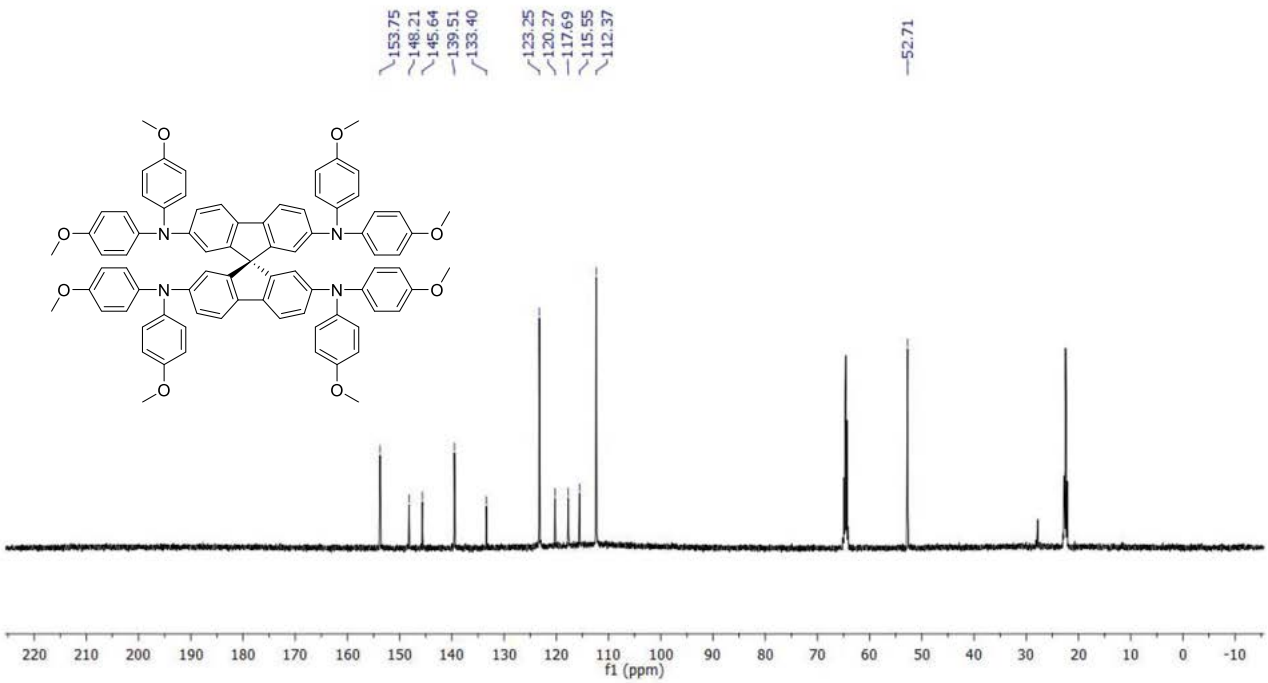

^{13}C-NMR of spiro-OMeTAD.

References

(1) Marrocchi, A.; Facchetti, A.; Lanari, D.; Petrucci, C.; Vaccaro, L. Current Methodologies for a Sustainable Approach to π-Conjugated Organic Semiconductors. *Energy Environ. Sci.* **2016**, *9* (3), 763–786. https://doi.org/10.1039/c5ee03727a.

(2) Phan, S.; Luscombe, C. K. Recent Advances in the Green, Sustainable Synthesis of Semiconducting Polymers. *Trends Chem.* **2019**, *1* (7), 670–681. https://doi.org/10.1016/j.trechm.2019.08.002.

(3) Dwars, T.; Paetzold, E.; Oehme, G. Reactions in Micellar Systems. *Angew. Chemie - Int. Ed.* **2005**, *44* (44), 7174–7199. https://doi.org/10.1002/anie.200501365.

(4) Lipshutz, B. H.; Ghorai, S. Transition-Metal-Catalyzed Cross-Couplings Going Green: In Water at Room Temperature. *Aldrichimica Acta* **2008**, *41* (3), 59–72.

(5) Kirchmeyer, S. The OE-A Roadmap for Organic and Printed Electronics: Creating a Guidepost to Complex Interlinked Technologies, Applications and Markets. *Transl. Mater. Res.* **2016**, *3* (1), 010301. https://doi.org/10.1088/2053-1613/3/1/010301.

(6) Marrocchi, A.; Trombettoni, V.; Sciosci, D.; Campana, F.; Vaccaro, L. *Key Trends in Sustainable Approaches to the Synthesis of Semiconducting Polymers*; Elsevier Ltd., 2019. https://doi.org/10.1016/b978-0-08-102284-9.00002-4.

(7) Po, R.; Bernardi, A.; Calabrese, A.; Carbonera, C.; Corso, G.; Pellegrino, A. From Lab to Fab: How Must the Polymer Solar Cell Materials Design Change?-An Industrial Perspective. *Energy Environ. Sci.* **2014**, *7* (3), 925–943. https://doi.org/10.1039/c3ee43460e.

(8) Po, R.; Bianchi, G.; Carbonera, C.; Pellegrino, A. "all That Glisters Is Not Gold": An Analysis of the Synthetic Complexity of Efficient Polymer Donors for Polymer Solar Cells. *Macromolecules* **2015**, *48* (3), 453–461. https://doi.org/10.1021/ma501894w.

(9) Lee, J.; Park, S. A.; Ryu, S. U.; Chung, D.; Park, T.; Son, S. Y. Green-Solvent-Processable Organic Semiconductors and Future Directions for Advanced Organic Electronics. *J. Mater. Chem. A* **2020**, *8* (41), 21455–21473. https://doi.org/10.1039/d0ta07373c.

(10) Krebs, F. C.; Nyberg, R. B.; Jørgensen, M. Influence of Residual Catalyst on the Properties of Conjugated Polyphenylenevinylene Materials: Palladium Nanoparticles and Poor Electrical Performance. *Chem. Mater.* **2004**, *16* (7), 1313–1318. https://doi.org/10.1021/cm035205w.

(11) Osedach, T. P.; Andrew, T. L.; Bulović, V. Effect of Synthetic Accessibility on the Commercial Viability of Organic Photovoltaics. *Energy Environ. Sci.* **2013**, *6* (3), 711–718. https://doi.org/10.1039/c3ee24138f.

(12) Machui, F.; Hösel, M.; Li, N.; Spyropoulos, G. D.; Ameri, T.; Søndergaard, R. R.; Jørgensen, M.; Scheel, A.; Gaiser, D.; Kreul, K.; Lenssen, D.; Legros, M.; Lemaitre, N.; Vilkman, M.; Välimäki, M.; Nordman, S.; Brabec, C. J.; Krebs, F. C. Cost Analysis of Roll-to-Roll Fabricated ITO Free Single and Tandem Organic Solar Modules Based on Data from Manufacture. *Energy Environ. Sci.* **2014**, *7* (9), 2792–2802. https://doi.org/10.1039/c4ee01222d.

(13) Sanzone, A.; Calascibetta, A.; Monti, M.; Mattiello, S.; Sassi, M.; Corsini, F.; Griffini, G.; Sommer, M.; Beverina, L. Synthesis of Conjugated Polymers by Sustainable Suzuki Polycondensation in Water and under Aerobic Conditions. *ACS Macro Lett.* **2020**, 1167–1171. https://doi.org/10.1021/acsmacrolett.0c00495.

(14) Anastas, P. T.; Kirchhoff, M. M. Origins, Current Status, and Future Challenges of Green Chemistry. *Acc. Chem. Res.* **2002**, *35* (9), 686–694. https://doi.org/10.1021/ar010065m.

(15) Trost, B. M. The Atom Economy - A Search for Synthetic Efficiency. *Science (80-.).* **1991**, *254* (5037), 1471–1477. https://doi.org/10.1126/science.1962206.

(16) Sheldon, R. A. The E Factor: Fifteen Years On. *Green Chem.* **2007**, *9* (12), 1273–1283. https://doi.org/10.1039/b713736m.

(17) Lipshutz, B. H.; Ghorai, S. Transitioning Organic Synthesis from Organic Solvents to Water. What's Your e Factor? *Green Chem.* **2014**, *16* (8), 3660–3679.

https://doi.org/10.1039/c4gc00503a.
(18) Hartmann, S.; Klaschka, U. Interested Consumers' Awareness of Harmful Chemicals in Everyday Products. *Environ. Sci. Eur.* **2017**, *29* (1). https://doi.org/10.1186/s12302-017-0127-8.
(19) Gildner, P. G.; Colacot, T. J. Reactions of the 21st Century: Two Decades of Innovative Catalyst Design for Palladium-Catalyzed Cross-Couplings. *Organometallics* **2015**, *34* (23), 5497–5508. https://doi.org/10.1021/acs.organomet.5b00567.
(20) Zani, L.; Dessì, A.; Franchi, D.; Calamante, M.; Reginato, G.; Mordini, A. Transition Metal-Catalyzed Cross-Coupling Methodologies for the Engineering of Small Molecules with Applications in Organic Electronics and Photovoltaics. *Coord. Chem. Rev.* **2019**, *392*, 177–236. https://doi.org/10.1016/j.ccr.2019.04.007.
(21) Johansson Seechurn, C. C. C.; Kitching, M. O.; Colacot, T. J.; Snieckus, V. Palladium-Catalyzed Cross-Coupling: A Historical Contextual Perspective to the 2010 Nobel Prize. *Angew. Chemie - Int. Ed.* **2012**, *51* (21), 5062–5085. https://doi.org/10.1002/anie.201107017.
(22) *Synthetic Methods for Conjugated Polymers And*.
(23) Ishiyama, T.; Oohashi, Z.; Ahiko, T. A.; Miyaura, N. Nucleophilic Borylation of Benzyl Halides with Bis(Pinacolato)Diboron Catalyzed by Palladium(0) Complexes. *Chem. Lett.* **2002**, No. 8, 780–781. https://doi.org/10.1246/cl.2002.780.
(24) Burke, D. J.; Lipomi, D. J. Green Chemistry for Organic Solar Cells. *Energy Environ. Sci.* **2013**, *6* (7), 2053–2066. https://doi.org/10.1039/c3ee41096j.
(25) Ackermann, L.; Vicente, R.; Kapdi, A. R. Transition-Metal-Catalyzed Direct Arylation of (Hetero)Arenes by C-H Bond Cleavage. *Angew. Chemie - Int. Ed.* **2009**, *48* (52), 9792–9826. https://doi.org/10.1002/anie.200902996.
(26) Mercier, L. G.; Leclerc, M. Direct (Hetero)Arylation: A New Tool for Polymer Chemists. *Acc. Chem. Res.* **2013**, *46* (7), 1597–1605. https://doi.org/10.1021/ar3003305.
(27) Gorelsky, S. I. Reactivity and Regioselectivity of Palladium-Catalyzed Direct Arylation in Noncooperative and Cooperative Processes. *Organometallics* **2012**, *31* (13), 4631–4634. https://doi.org/10.1021/om300230b.
(28) Gorelsky, S. I. Origins of Regioselectivity of the Palladium-Catalyzed (Aromatic)CH Bond Metalation-Deprotonation. *Coord. Chem. Rev.* **2013**, *257* (1), 153–164. https://doi.org/10.1016/j.ccr.2012.06.016.
(29) Pouliot, J. R.; Grenier, F.; Blaskovits, J. T.; Beaupré, S.; Leclerc, M. Direct (Hetero)Arylation Polymerization: Simplicity for Conjugated Polymer Synthesis. *Chem. Rev.* **2016**, *116* (22), 14225–14274. https://doi.org/10.1021/acs.chemrev.6b00498.
(30) Bura, T.; Blaskovits, J. T.; Leclerc, M. Direct (Hetero)Arylation Polymerization: Trends and Perspectives. *J. Am. Chem. Soc.* **2016**, *138* (32), 10056–10071. https://doi.org/10.1021/jacs.6b06237.
(31) Pouliot, J. R.; Grenier, F.; Blaskovits, J. T.; Beaupré, S.; Leclerc, M. Direct (Hetero)Arylation Polymerization: Simplicity for Conjugated Polymer Synthesis. *Chemical Reviews*. 2016. https://doi.org/10.1021/acs.chemrev.6b00498.
(32) Wu, W.; Xin, H.; Ge, C.; Gao, X. Application of Direct (Hetero)Arylation in Constructing Conjugated Small Molecules and Polymers for Organic Optoelectronic Devices. *Tetrahedron Lett.* **2017**, *58* (3), 175–184. https://doi.org/10.1016/j.tetlet.2016.11.126.
(33) Facchetti, A.; Vaccaro, L.; Marrocchi, A. Semiconducting Polymers Prepared by Direct Arylation Polycondensation. *Angew. Chemie - Int. Ed.* **2012**, *51* (15), 3520–3523. https://doi.org/10.1002/anie.201200199.
(34) Suraru, S. L.; Lee, J. A.; Luscombe, C. K. C-H Arylation in the Synthesis of π-Conjugated Polymers. *ACS Macro Lett.* **2016**, *5* (6), 724–729. https://doi.org/10.1021/acsmacrolett.6b00279.
(35) Hendsbee, A. D.; Li, Y. Performance Comparisons of Polymer Semiconductors Synthesized by Direct (Hetero)Arylation Polymerization (DHAP) and Conventional Methods for Organic Thin Film Transistors and Organic Photovoltaics. *Molecules* **2018**, *23* (6). https://doi.org/10.3390/molecules23061255.

(36) Bohra, H.; Wang, M. Direct C-H Arylation: A "Greener" Approach towards Facile Synthesis of Organic Semiconducting Molecules and Polymers. *J. Mater. Chem. A* **2017**, *5* (23), 11550–11571. https://doi.org/10.1039/c7ta00617a.
(37) Bura, T.; Blaskovits, J. T.; Leclerc, M. Direct (Hetero)Arylation Polymerization: Trends and Perspectives. *J. Am. Chem. Soc.* **2016**. https://doi.org/10.1021/jacs.6b06237.
(38) Yu, S.; Liu, F.; Yu, J.; Zhang, S.; Cabanetos, C.; Gao, Y.; Huang, W. Eco-Friendly Direct (Hetero)-Arylation Polymerization: Scope and Limitation. *J. Mater. Chem. C* **2017**, *5* (1), 29–40. https://doi.org/10.1039/C6TC04240F.
(39) Kuwabara, J.; Fujie, Y.; Maruyama, K.; Yasuda, T.; Kanbara, T. Suppression of Homocoupling Side Reactions in Direct Arylation Polycondensation for Producing High Performance OPV Materials. *Macromolecules* **2016**, *49* (24), 9388–9395. https://doi.org/10.1021/acs.macromol.6b02380.
(40) Matsidik, R.; Komber, H.; Luzio, A.; Caironi, M.; Sommer, M. Defect-Free Naphthalene Diimide Bithiophene Copolymers with Controlled Molar Mass and High Performance via Direct Arylation Polycondensation. *J. Am. Chem. Soc.* **2015**, *137* (20), 6705–6711. https://doi.org/10.1021/jacs.5b03355.
(41) Bura, T.; Beaupré, S.; Légaré, M. A.; Quinn, J.; Rochette, E.; Blaskovits, J. T.; Fontaine, F. G.; Pron, A.; Li, Y.; Leclerc, M. Direct Heteroarylation Polymerization: Guidelines for Defect-Free Conjugated Polymers. *Chem. Sci.* **2017**, *8* (5), 3913–3925. https://doi.org/10.1039/c7sc00589j.
(42) Shi, Q.; Tatum, W.; Zhang, J.; Scott, C.; Luscombe, C. K.; Marder, S. R.; Blakey, S. B. The Direct Arylation Polymerization (DArP) of Well-Defined Alternating Copolymers Based On 5,6-Dicyano[2,1,3]Benzothiadiazole (DCBT). *Asian J. Org. Chem.* **2018**, *7* (7), 1419–1425. https://doi.org/10.1002/ajoc.201800232.
(43) Strappaveccia, G.; Ismalaj, E.; Petrucci, C.; Lanari, D.; Marrocchi, A.; Drees, M.; Facchetti, A.; Vaccaro, L. A Biomass-Derived Safe Medium to Replace Toxic Dipolar Solvents and Access Cleaner Heck Coupling Reactions. *Green Chem.* **2015**, *17* (1), 365–372. https://doi.org/10.1039/c4gc01677g.
(44) Bannock, J. H.; Xu, W.; Baïssas, T.; Heeney, M.; de Mello, J. C. Rapid Flow-Based Synthesis of Poly(3-Hexylthiophene) Using 2-Methyltetrahydrofuran as a Bio-Derived Reaction Solvent. *Eur. Polym. J.* **2016**, *80*, 240–246. https://doi.org/10.1016/j.eurpolymj.2016.04.016.
(45) Zhang, S.; Ye, L.; Zhang, H.; Hou, J. Green-Solvent-Processable Organic Solar Cells. *Mater. Today* **2016**, *19* (9), 533–543. https://doi.org/10.1016/j.mattod.2016.02.019.
(46) Nguyen, T. L.; Lee, C.; Kim, H.; Kim, Y.; Lee, W.; Oh, J. H.; Kim, B. J.; Woo, H. Y. Ethanol-Processable, Highly Crystalline Conjugated Polymers for Eco-Friendly Fabrication of Organic Transistors and Solar Cells. *Macromolecules* **2017**, *50* (11), 4415–4424. https://doi.org/10.1021/acs.macromol.7b00452.
(47) Lipshutz, B. H.; Ghorai, S.; Cortes-Clerget, M. The Hydrophobic Effect Applied to Organic Synthesis: Recent Synthetic Chemistry "in Water." *Chem. - A Eur. J.* **2018**, *24* (26), 6672–6695. https://doi.org/10.1002/chem.201705499.
(48) La Sorella, G.; Strukul, G.; Scarso, A. Recent Advances in Catalysis in Micellar Media. *Green Chem.* **2015**, *17* (2), 644–683. https://doi.org/10.1039/c4gc01368a.
(49) Johnsson, M.; Engberts, J. B. F. N. Novel Sugar-Based Gemini Surfactants: Aggregation Properties in Aqueous Solution. *J. Phys. Org. Chem.* **2004**, *17* (11), 934–944. https://doi.org/10.1002/poc.817.
(50) Mandal, S.; Mandal, S.; Ghosh, S. K.; Sar, P.; Ghosh, A.; Saha, R.; Saha, B. A Review on the Advancement of Ether Synthesis from Organic Solvent to Water. *RSC Adv.* **2016**, *6* (73), 69605–69614. https://doi.org/10.1039/c6ra12914e.
(51) Lipshutz, B. H.; Isley, N. A.; Fennewald, J. C.; Slack, E. D. On the Way towards Greener Transition-Metal-Catalyzed Processes as Quantified by e Factors. *Angew. Chemie - Int. Ed.* **2013**, *52* (42), 10952–10958. https://doi.org/10.1002/anie.201302020.
(52) Zhang, X.; Sewell, T. E.; Glatz, B.; Sarupria, S.; Getman, R. B. On the Water Structure at Hydrophobic Interfaces and the Roles of Water on Transition-Metal Catalyzed Reactions: A

Short Review. *Catal. Today* **2017**, *285*, 57–64. https://doi.org/10.1016/j.cattod.2017.02.002.
(53) Bagchi, B. Water Dynamics in the Hydration Layer around Proteins and Micelles. *Chem. Rev.* **2005**, *105* (9), 3197–3219. https://doi.org/10.1021/cr020661+.
(54) Sanzone, A.; Calascibetta, A.; Ghiglietti, E.; Ceriani, C.; Mattioli, G.; Mattiello, S.; Sassi, M.; Beverina, L. Suzuki-Miyaura Micellar One-Pot Synthesis of Symmetrical and Unsymmetrical 4,7-Diaryl-5,6-Difluoro-2,1,3-Benzothiadiazole Luminescent Derivatives in Water and under Air. *J. Org. Chem.* **2018**, *83* (24), 15029–15042. https://doi.org/10.1021/acs.joc.8b02204.
(55) Lorenzetto, T.; Berton, G.; Fabris, F.; Scarso, A. Recent Designer Surfactants for Catalysis in Water. *Catal. Sci. Technol.* **2020**, *10* (14), 4492–4502. https://doi.org/10.1039/d0cy01062f.
(56) Lipshutz, B. H.; Aguinaldo, G. T.; Ghorai, S.; Voigtritter, K. Olefin Cross-Metathesis Reactions at Room Temperature Using the Nonionic Amphiphile "PTS": Just Add Water. *Org. Lett.* **2008**, *10* (7), 1325–1328. https://doi.org/10.1021/ol800028x.
(57) Lipshutz, B. H.; Ghorai, S.; Abela, A. R.; Moser, R.; Nishikata, T.; Duplais, C.; Krasovskiy, A.; Gaston, R. D.; Gadwood, R. C. TPGS-750-M: A Second-Generation Amphiphile for Metal-Catalyzed Cross-Couplings in Water at Room Temperature. *J. Org. Chem.* **2011**, *76* (11), 4379–4391. https://doi.org/10.1021/jo101974u.
(58) Klumphu, P.; Lipshutz, B. H. "nok": A Phytosterol-Based Amphiphile Enabling Transition-Metal-Catalyzed Couplings in Water at Room Temperature. *J. Org. Chem.* **2014**, *79* (3), 888–900. https://doi.org/10.1021/jo401744b.
(59) Handa, S.; Ibrahim, F.; Ansari, T. N.; Gallou, F. π-Allylpalladium Species in Micelles of FI-750-M for Sustainable and General Suzuki-Miyaura Couplings of Unactivated Quinoline Systems in Water. *ChemCatChem* **2018**, *10* (19), 4229–4233. https://doi.org/10.1002/cctc.201800958.
(60) Lee, N. R.; Cortes-Clerget, M.; Wood, A. B.; Lippincott, D. J.; Pang, H.; Moghadam, F. A.; Gallou, F.; Lipshutz, B. H. Coolade. A Low-Foaming Surfactant for Organic Synthesis in Water. *ChemSusChem* **2019**, *12* (13), 3159–3165. https://doi.org/10.1002/cssc.201900369.
(61) Paetzold, E.; Jovel, I.; Oehme, G. Suzuki Reactions in Aqueous Multi-Phase Systems Promoted by Supported Detergents. *J. Mol. Catal. A Chem.* **2004**, *214* (2), 241–247. https://doi.org/10.1016/j.molcata.2003.12.025.
(62) Arcadi, A.; Cerichelli, G.; Chiarini, M.; Correa, M.; Zorzan, D. A Mild and Versatile Method for Palladium-Catalyzed Cross-Coupling of Aryl Halides in Water and Surfactants. *European J. Org. Chem.* **2003**, No. 20, 4080–4086. https://doi.org/10.1002/ejoc.200300356.
(63) Lipshutz, B. H.; Abela, A. R. Micellar Catalysis of Suzuki-Miyaura Cross-Couplings with Heteroaromatics in Water. *Org. Lett.* **2008**, *10* (23), 5329–5332. https://doi.org/10.1021/ol801712e.
(64) Mattiello, S.; Rooney, M.; Sanzone, A.; Brazzo, P.; Sassi, M.; Beverina, L. Suzuki-Miyaura Micellar Cross-Coupling in Water, at Room Temperature, and under Aerobic Atmosphere. *Org. Lett.* **2017**, *19* (3), 654–657. https://doi.org/10.1021/acs.orglett.6b03817.
(65) Mattiello, S.; Monguzzi, A.; Pedrini, J.; Sassi, M.; Villa, C.; Torrente, Y.; Marotta, R.; Meinardi, F.; Beverina, L. Self-Assembled Dual Dye-Doped Nanosized Micelles for High-Contrast Up-Conversion Bioimaging. *Adv. Funct. Mater.* **2016**, *26* (46), 8447–8454. https://doi.org/10.1002/adfm.201603303.
(66) Sassi, M.; Mattiello, S.; Beverina, L. Syntheses of Organic Semiconductors in Water. Recent Advancement in the Surfactants Enhanced Green Access to Polyconjugated Molecules. *European J. Org. Chem.* **2020**, 1–13. https://doi.org/10.1002/ejoc.202000140.
(67) Handa, S.; Andersson, M. P.; Gallou, F.; Reilly, J.; Lipshutz, B. H. HandaPhos: A General Ligand Enabling Sustainable Ppm Levels of Palladium-Catalyzed Cross-Couplings in Water at Room Temperature. *Angew. Chemie - Int. Ed.* **2016**, *55* (16), 4914–4918. https://doi.org/10.1002/anie.201510570.
(68) Handa, S.; Smith, J. D.; Zhang, Y.; Takale, B. S.; Gallou, F.; Lipshutz, B. H. Sustainable HandaPhos-Ppm Palladium Technology for Copper-Free Sonogashira Couplings in Water under Mild Conditions. *Org. Lett.* **2018**, *20* (3), 542–545. https://doi.org/10.1021/acs.orglett.7b03621.

(69) Rooney, M.; Mattiello, S.; Stara, R.; Sanzone, A.; Brazzo, P.; Sassi, M.; Beverina, L. Suzuki-Miyaura Cross-Coupling of Latent Pigments in Water/Toluene Emulsion under Aerobic Atmosphere. *Dye. Pigment.* **2018**, *149* (September 2017), 893–901. https://doi.org/10.1016/j.dyepig.2017.11.044.
(70) Beverina, L.; Rooney, M.; Ruffo, R.; Sassi, M.; Carulli, F.; Luzzati, S.; Resel, R.; Schrode, B. Diketopyrrolopyrrole Latent Pigment-Based Bilayer Solar Cells. *Org. Photonics Photovoltaics* **2019**, *6* (1), 8–16. https://doi.org/10.1515/oph-2018-0002.
(71) Zambounis, J. S.; Hao, Z.; Iqbal, A. Latent Pigments Activated by Heat [1]. *Nature* **1997**, *388* (6638), 131–132. https://doi.org/10.1038/40532.
(72) Głowacki, E. D.; Apaydin, D. H.; Bozkurt, Z.; Monkowius, U.; Demirak, K.; Tordin, E.; Himmelsbach, M.; Schwarzinger, C.; Burian, M.; Lechner, R. T.; Demitri, N.; Voss, G.; Sariciftci, N. S. Air-Stable Organic Semiconductors Based on 6,6′-Dithienylindigo and Polymers Thereof. *J. Mater. Chem. C* **2014**, *2* (38), 8089–8097. https://doi.org/10.1039/c4tc00651h.
(73) Gabriel, C. M.; Lee, N. R.; Bigorne, F.; Klumphu, P.; Parmentier, M.; Gallou, F.; Lipshutz, B. H. Effects of Co-Solvents on Reactions Run under Micellar Catalysis Conditions. *Org. Lett.* **2017**, *19* (1), 194–197. https://doi.org/10.1021/acs.orglett.6b03468.
(74) Vaghi, L.; Sanzone, A.; Sassi, M.; Pagani, S.; Papagni, A.; Beverina, L. Synthesis of Fluorinated Acridines via Sequential Micellar Buchwald-Hartwig Amination/Cyclization of Aryl Bromides. *Synth.* **2018**, *50* (8), 1621–1628. https://doi.org/10.1055/s-0036-1591937.
(75) Vaccaro, G.; Bianchi, A.; Mauri, M.; Bonetti, S.; Meinardi, F.; Sanguineti, A.; Simonutti, R.; Beverina, L. Direct Monitoring of Self-Assembly of Copolymeric Micelles by a Luminescent Molecular Rotor. *Chem. Commun.* **2013**, *49* (76), 8474–8476. https://doi.org/10.1039/c3cc44590a.
(76) Lee, J. S. M.; Cooper, A. I. Advances in Conjugated Microporous Polymers. *Chem. Rev.* **2020**, *120* (4), 2171–2214. https://doi.org/10.1021/acs.chemrev.9b00399.
(77) Calascibetta, A. M.; Mattiello, S.; Sanzone, A.; Facchinetti, I.; Sassi, M.; Beverina, L. Sustainable Access to π-Conjugated Molecular Materials via Direct (Hetero)Arylation Reactions in Water and under Air. *Molecules* **2020**, *25* (16). https://doi.org/10.3390/molecules25163717.
(78) Nishikata, T.; Abela, A. R.; Lipshutz, B. H. Room Temperature C-H Activation and Cross-Coupling of Aryl Ureas in Water. *Angew. Chemie - Int. Ed.* **2010**, *49* (4), 781–784. https://doi.org/10.1002/anie.200905967.
(79) Vaidya, G. N.; Fiske, S.; Verma, H.; Lokhande, S. K.; Kumar, D. A Micellar Catalysis Strategy Applied to the Pd-Catalyzed C-H Arylation of Indoles in Water. *Green Chem.* **2019**, *21* (6), 1448–1454. https://doi.org/10.1039/c8gc03413c.
(80) Daniels, M. H.; Armand, J. R.; Tan, K. L. Sequential Regioselective C − H Functionalization of Thiophenes. **2016**. https://doi.org/10.1021/acs.orglett.6b01205.
(81) Grenier, F.; Goudreau, K.; Leclerc, M. Robust Direct (Hetero)Arylation Polymerization in Biphasic Conditions. *J. Am. Chem. Soc.* **2017**, *139* (7), 2816–2824. https://doi.org/10.1021/jacs.6b12955.
(82) Corti, M.; Minero, C.; Degiorgio, V. Cloud Point Transition in Nonionic Micellar Solutions. *J. Phys. Chem.* **1984**, *88* (2), 309–317. https://doi.org/10.1021/j150646a029.
(83) Sanzone, A.; Mattiello, S.; Garavaglia, G. M.; Calascibetta, A. M.; Ceriani, C.; Sassi, M.; Beverina, L. Efficient Synthesis of Organic Semiconductors by Suzuki-Miyaura Coupling in an Aromatic Micellar Medium. *Green Chem.* **2019**, *21* (16), 4400–4405. https://doi.org/10.1039/c9gc01071h.
(84) Kuwabara, J.; Yamazaki, K.; Yamagata, T.; Tsuchida, W.; Kanbara, T. The Effect of a Solvent on Direct Arylation Polycondensation of Substituted Thiophenes. *Polym. Chem.* **2015**, *6* (6), 891–895. https://doi.org/10.1039/c4py01387e.
(85) Liégault, B.; Lapointe, D.; Caron, L.; Vlassova, A.; Fagnou, K. Establishment of Broadly Applicable Reaction Conditions for the Palladium-Catalyzed Direct Arylation of Heteroatom-Containing Aromatic Compounds Establishment of Broadly Applicable Reaction Conditions

for the Palladium-Catalyzed Direct Arylation of Hetero. *J. Org. Chem.* **2009**, *74* (3), 1826–1834. https://doi.org/10.1021/jo8026565.
(86) Schipper, D. J.; Fagnou, K. Direct Arylation as a Synthetic Tool for the Synthesis of Thiophene-Based Organic Electronic Materials. *Chem. Mater.* **2011**, *23* (6), 1594–1600. https://doi.org/10.1021/cm103483q.
(87) Lombeck, F.; Komber, H.; Gorelsky, S. I.; Sommer, M. Identifying Homocouplings as Critical Side Reactions in Direct Arylation Polycondensation. *ACS Macro Lett.* **2014**, *3* (8), 819–823. https://doi.org/10.1021/mz5004147.
(88) Chen, F.; Min, Q. Q.; Zhang, X. Pd-Catalyzed Direct Arylation of Polyfluoroarenes on Water under Mild Conditions Using PPh 3 Ligand. *J. Org. Chem.* **2012**, *77* (6), 2992–2998. https://doi.org/10.1021/jo300036d.
(89) René, O.; Fagnou, K. Evaluation of Electron-Deficient Phosphine Ligands for Direct Arylation of Heterocycles. *Adv. Synth. Catal.* **2010**, *352* (13), 2116–2120. https://doi.org/10.1002/adsc.201000397.
(90) Iizuka, E.; Wakioka, M.; Ozawa, F. Mixed-Ligand Approach to Palladium-Catalyzed Direct Arylation Polymerization: Effective Prevention of Structural Defects Using Diamines. *Macromolecules* **2016**, *49* (9), 3310–3317. https://doi.org/10.1021/acs.macromol.6b00441.
(91) Novikov, A. A.; Semenov, A. P.; Monje-Galvan, V.; Kuryakov, V. N.; Klauda, J. B.; Anisimov, M. A. Dual Action of Hydrotropes at the Water/Oil Interface. *J. Phys. Chem. C* **2017**, *121* (30), 16423–16431. https://doi.org/10.1021/acs.jpcc.7b05156.
(92) Rudenko, A. E.; Latif, A. A.; Thompson, B. C. Influence of β-Linkages on the Morphology and Performance of DArP P3HT-PC61BM Solar Cells. *Nanotechnology* **2014**, *25* (1). https://doi.org/10.1088/0957-4484/25/1/014005.
(93) Rudenko, A. E.; Thompson, B. C. Influence of the Carboxylic Acid Additive Structure on the Properties of Poly(3-Hexylthiophene) Prepared via Direct Arylation Polymerization (DArP). *Macromolecules* **2015**, *48* (3), 569–575. https://doi.org/10.1021/ma502131k.
(94) Bura, T.; Morin, P. O.; Leclerc, M. En Route to Defect-Free Polythiophene Derivatives by Direct Heteroarylation Polymerization. *Macromolecules* **2015**, *48* (16), 5614–5620. https://doi.org/10.1021/acs.macromol.5b01372.
(95) Mainville, M.; Tremblay, V.; Fenniri, M. Z.; Laventure, A.; Farahat, M. E.; Ambrose, R.; Welch, G. C.; Hill, I. G.; Leclerc, M. Water Compatible Direct (Hetero)Arylation Polymerization of PPDT2FBT: A Pathway Towards Large-Scale Production of Organic Solar Cells. *Asian J. Org. Chem.* **2020**, *9* (9), 1318–1325. https://doi.org/10.1002/ajoc.202000231.
(96) Amaladass, P.; Clement, J. A.; Mohanakrishnan, A. K. Pd-Mediated C-H Arylation of EDOT and Synthesis of Push-Pull Systems Incorporating EDOT. *Tetrahedron* **2007**, *63* (41), 10363–10371. https://doi.org/10.1016/j.tet.2007.07.037.
(97) He, K.; Li, W.; Tian, H.; Zhang, J.; Yan, D.; Geng, Y.; Wang, F. Asymmetric Conjugated Molecules Based on [1]Benzothieno[3,2-b][1]Benzothiophene for High-Mobility Organic Thin-Film Transistors: Influence of Alkyl Chain Length. *ACS Appl. Mater. Interfaces* **2017**, *9* (40), 35427–35436. https://doi.org/10.1021/acsami.7b10675.
(98) Durso, M.; Zambianchi, M.; Zanelli, A.; Lobello, M. G.; De Angelis, F.; Toffanin, S.; Cavallini, S.; Gentili, D.; Tinti, F.; Cavallini, M.; Camaioni, N.; Melucci, M. Synthesis by MW-Assisted Direct Arylation, Side-Arms Driven Self-Assembly and Functional Properties of 9,10-Dithienylanthracene Orthogonal Materials. *Tetrahedron* **2014**, *70* (36), 6222–6228. https://doi.org/10.1016/j.tet.2014.03.010.
(99) Wong, X. L.; Sarjadi, M. S. Synthesis of 4,7-Di(2-Thienyl)-2,1,3-Benzothiadiazole via Direct Arylation. *J. Phys. Conf. Ser.* **2019**, *1358* (1). https://doi.org/10.1088/1742-6596/1358/1/012006.
(100) Crivillers, N.; Favaretto, L.; Zanelli, A.; Manet, I.; Treier, M.; Morandi, V.; Gazzano, M.; Samori, P.; Melucci, M. Self-Assembly and Electrical Properties of a Novel Heptameric Thiophene-Benzothiadiazole Based Architectures. *Chem. Commun.* **2012**, *48* (100), 12162–12164. https://doi.org/10.1039/c2cc36510c.
(101) Wang, Y.; Michinobu, T. Benzothiadiazole and Its π-Extended, Heteroannulated Derivatives:

Useful Acceptor Building Blocks for High-Performance Donor-Acceptor Polymers in Organic Electronics. *J. Mater. Chem. C* **2016**, *4* (26), 6200–6214. https://doi.org/10.1039/c6tc01860b.
(102) Hayashi, S.; Koizumi, T.; Kamiya, N. Elastic Bending Flexibility of a Fluorescent Organic Single Crystal: New Aspects of the Commonly Used Building Block 4, 7-Dibromo-2, 1, 3-Benzothiadiazole. *Cryst. Growth Des.* **2017**, *17* (12), 6158–6162. https://doi.org/10.1021/acs.cgd.7b00992.
(103) Tang, M. L.; Bao, Z. Halogenated Materials as Organic Semiconductors. *Chem. Mater.* **2011**, *23* (3), 446–455. https://doi.org/10.1021/cm102182x.
(104) Bronstein, H.; Frost, J. M.; Hadipour, A.; Kim, Y.; Nielsen, C. B.; Ashraf, R. S.; Rand, B. P.; Watkins, S.; McCulloch, I. Effect of Fluorination on the Properties of a Donor-Acceptor Copolymer for Use in Photovoltaic Cells and Transistors. *Chem. Mater.* **2013**, *25* (3), 277–285. https://doi.org/10.1021/cm301910t.
(105) Uddin, M. A.; Lee, T. H.; Xu, S.; Park, S. Y.; Kim, T.; Song, S.; Nguyen, T. L.; Ko, S. J.; Hwang, S.; Kim, J. Y.; Woo, H. Y. Interplay of Intramolecular Noncovalent Coulomb Interactions for Semicrystalline Photovoltaic Polymers. *Chem. Mater.* **2015**, *27* (17), 5997–6007. https://doi.org/10.1021/acs.chemmater.5b02251.
(106) Li, G.; Kang, C.; Gong, X.; Zhang, J.; Li, C.; Chen, Y.; Dong, H.; Hu, W.; Li, F.; Bo, Z. 5-Alkyloxy-6-Fluorobenzo[c][1,2,5]Thiadiazole- and Silafluorene-Based D-A Alternating Conjugated Polymers: Synthesis and Application in Polymer Photovoltaic Cells. *Macromolecules* **2014**, *47* (14), 4645–4652. https://doi.org/10.1021/ma500417r.
(107) Zhang, J.; Chen, W.; Rojas, A. J.; Jucov, E. V.; Timofeeva, T. V.; Parker, T. C.; Barlow, S.; Marder, S. R. Controllable Direct Arylation: Fast Route to Symmetrical and Unsymmetrical 4,7-Diaryl-5,6-Difluoro-2,1,3-Benzothiadiazole Derivatives for Organic Optoelectronic Materials. *J. Am. Chem. Soc.* **2013**, *135* (44), 16376–16379. https://doi.org/10.1021/ja4095878.
(108) Cox, P. A.; Leach, A. G.; Campbell, A. D.; Lloyd-Jones, G. C. Protodeboronation of Heteroaromatic, Vinyl, and Cyclopropyl Boronic Acids: PH-Rate Profiles, Autocatalysis, and Disproportionation. *J. Am. Chem. Soc.* **2016**, *138* (29), 9145–9157. https://doi.org/10.1021/jacs.6b03283.
(109) Kunieda, H.; Shinoda, K. Evaluation of the Hydrophile-Lipophile Balance of Nonionic Surfactants. **1985**, *107* (1).
(110) Amin, A. Y.; Khassanov, A.; Reuter, K.; Meyer-Friedrichsen, T.; Halik, M. Low-Voltage Organic Field Effect Transistors with a 2-Tridecyl[1] Benzothieno[3,2-b][1]Benzothiophene Semiconductor Layer. *J. Am. Chem. Soc.* **2012**, *134* (40), 16548–16550. https://doi.org/10.1021/ja307802q.
(111) Schweicher, G.; Lemaur, V.; Niebel, C.; Ruzié, C.; Diao, Y.; Goto, O.; Lee, W. Y.; Kim, Y.; Arlin, J. B.; Karpinska, J.; Kennedy, A. R.; Parkin, S. R.; Olivier, Y.; Mannsfeld, S. C. B.; Cornil, J.; Geerts, Y. H.; Bao, Z. Bulky End-Capped [1]Benzothieno[3,2-b]Benzothiophenes: Reaching High-Mobility Organic Semiconductors by Fine Tuning of the Crystalline Solid-State Order. *Adv. Mater.* **2015**, *27* (19), 3066–3072. https://doi.org/10.1002/adma.201500322.
(112) Haase, K.; Teixeira da Rocha, C.; Hauenstein, C.; Zheng, Y.; Hambsch, M.; Mannsfeld, S. C. B. High-Mobility, Solution-Processed Organic Field-Effect Transistors from C8-BTBT:Polystyrene Blends. *Adv. Electron. Mater.* **2018**, *4* (8), 1–9. https://doi.org/10.1002/aelm.201800076.
(113) Brocklehurst, C. E.; Gallou, F.; Hartwieg, J. C. D.; Palmieri, M.; Rufle, D. Microtiter Plate (MTP) Reaction Screening and Optimization of Surfactant Chemistry: Examples of Suzuki-Miyaura and Buchwald-Hartwig Cross-Couplings in Water. *Org. Process Res. Dev.* **2018**, *22* (10), 1453–1457. https://doi.org/10.1021/acs.oprd.8b00200.
(114) Inoue, S.; Minemawari, H.; Tsutsumi, J.; Chikamatsu, M.; Yamada, T.; Horiuchi, S.; Tanaka, M.; Kumai, R.; Yoneya, M.; Hasegawa, T. Effects of Substituted Alkyl Chain Length on Solution-Processable Layered Organic Semiconductor Crystals. *Chem. Mater.* **2015**, *27* (11), 3809–3812. https://doi.org/10.1021/acs.chemmater.5b00810.
(115) Saito, M.; Osaka, I.; Miyazaki, E.; Takimiya, K.; Kuwabara, H.; Ikeda, M. One-Step Synthesis

of [1]Benzothieno[3,2-b][1]Benzothiophene from o-Chlorobenzaldehyde. *Tetrahedron Lett.* **2011**, *52* (2), 285–288. https://doi.org/10.1016/j.tetlet.2010.11.021.
(116) Kiriya, D.; Chen, K.; Ota, H.; Lin, Y.; Zhao, P.; Yu, Z.; Ha, T. J.; Javey, A. Design of Surfactant-Substrate Interactions for Roll-to-Roll Assembly of Carbon Nanotubes for Thin-Film Transistors. *J. Am. Chem. Soc.* **2014**, *136* (31), 11188–11194. https://doi.org/10.1021/ja506315j.
(117) Zhan, X.; Facchetti, A.; Barlow, S.; Marks, T. J.; Ratner, M. A.; Wasielewski, M. R.; Marder, S. R. Rylene and Related Diimides for Organic Electronics. *Adv. Mater.* **2011**, *23* (2), 268–284. https://doi.org/10.1002/adma.201001402.
(118) Suraru, S. L.; Würthner, F. Strategies for the Synthesis of Functional Naphthalene Diimides. *Angew. Chemie - Int. Ed.* **2014**, *53* (29), 7428–7448. https://doi.org/10.1002/anie.201309746.
(119) Teh, C. H.; Daik, R.; Lim, E. L.; Yap, C. C.; Ibrahim, M. A.; Ludin, N. A.; Sopian, K.; Mat Teridi, M. A. A Review of Organic Small Molecule-Based Hole-Transporting Materials for Meso-Structured Organic-Inorganic Perovskite Solar Cells. *J. Mater. Chem. A* **2016**, *4* (41), 15788–15822. https://doi.org/10.1039/c6ta06987h.
(120) Nicholson, B.; Verma, S.; Med, P.; S, S. R Es e a Rc H. **2014**.
(121) Jeon, N. J.; Na, H.; Jung, E. H.; Yang, T. Y.; Lee, Y. G.; Kim, G.; Shin, H. W.; Il Seok, S.; Lee, J.; Seo, J. A Fluorene-Terminated Hole-Transporting Material for Highly Efficient and Stable Perovskite Solar Cells. *Nat. Energy* **2018**, *3* (8), 682–689. https://doi.org/10.1038/s41560-018-0200-6.
(122) Bi, D.; Tress, W.; Dar, M. I.; Gao, P.; Luo, J.; Renevier, C.; Schenk, K.; Abate, A.; Giordano, F.; Correa Baena, J. P.; Decoppet, J. D.; Zakeeruddin, S. M.; Nazeeruddin, M. K.; Grätzel, M.; Hagfeldt, A. Efficient Luminescent Solar Cells Based on Tailored Mixed-Cation Perovskites. *Sci. Adv.* **2016**, *2* (1). https://doi.org/10.1126/sciadv.1501170.
(123) Jeon, N. J.; Lee, J.; Noh, J. H.; Nazeeruddin, M. K.; Grätzel, M.; Seok, S. Il. Efficient Inorganic-Organic Hybrid Perovskite Solar Cells Based on Pyrene Arylamine Derivatives as Hole-Transporting Materials. *J. Am. Chem. Soc.* **2013**, *135* (51), 19087–19090. https://doi.org/10.1021/ja410659k.
(124) Bach, U.; De Cloedt, K.; Spreitzer, H.; Grätzel, M. Characterization of Hole Transport in a New Class of Spiro-Linked Oligofriphenylamine Compounds. *Adv. Mater.* **2000**, *12* (14), 1060–1063. https://doi.org/10.1002/1521-4095(200007)12:14<1060::AID-ADMA1060>3.0.CO;2-R.
(125) Poriel, C.; Ferrand, Y.; Juillard, S.; Le Maux, P.; Simonneaux, G. Synthesis and Stereochemical Studies of Di and Tetra 9,9′- Spirobifluorene Porphyrins: New Building Blocks for Catalytic Material. *Tetrahedron* **2004**, *60* (1), 145–158. https://doi.org/10.1016/j.tet.2003.10.080.
(126) Seok, S. Il. Seok - 2014 - o - Methoxy Substituents in Spiro-OMeTAD for E Ffi Cient Inorganic − Organic Hybrid Perovskite Solar Cells.Pdf. **2014**.
(127) Yang, L.; Xu, B.; Bi, D.; Tian, H.; Boschloo, G.; Sun, L.; Hagfeldt, A.; Johansson, E. M. J. Initial Light Soaking Treatment Enables Hole Transport Material to Outperform Spiro-OMeTAD in Solid-State Dye-Sensitized Solar Cells. *J. Am. Chem. Soc.* **2013**, *135* (19), 7378–7385. https://doi.org/10.1021/ja403344s.
(128) Saragi, T. P. I.; Spehr, T.; Siebert, A.; Fuhrmann-Lieker, T.; Salbeck, J. Spiro Compounds for Organic Optoelectronics. *Chem. Rev.* **2007**, *107* (4), 1011–1065. https://doi.org/10.1021/cr0501341.
(129) Clarkson, R. G.; Gomberg, M. Spirans with Four Aromatic Radicals on the Spiro Carbon Atom. *J. Am. Chem. Soc.* **1930**, *52* (7), 2881–2891. https://doi.org/10.1021/ja01370a048.
(130) Wu, R.; Schumm, J. S.; Pearson, D. L.; Tour, J. M. Convergent Synthetic Routes to Orthogonally Fused Conjugated Oligomers Directed toward Molecular Scale Electronic Device Applications. *J. Org. Chem.* **1996**, *61* (20), 6906–6921. https://doi.org/10.1021/jo960897b.
(131) Kamino, B. A.; Mills, B.; Reali, C.; Gretton, M. J.; Brook, M. A.; Bender, T. P. Liquid Triarylamines: The Scope and Limitations of Piers-Rubinsztajn Conditions for Obtaining

Triarylamine-Siloxane Hybrid Materials. *J. Org. Chem.* **2012**, *77* (4), 1663–1674. https://doi.org/10.1021/jo2020906.
(132) Bhanuchandra, M.; Yorimitsu, H.; Osuka, A. Synthesis of Spirocyclic Diarylfluorenes by One-Pot Twofold SNAr Reactions of Diaryl Sulfones with Diarylmethanes. *Org. Lett.* **2016**, *18* (3), 384–387. https://doi.org/10.1021/acs.orglett.5b03384.
(133) Pei, J.; Ni, J.; Zhou, X. H.; Cao, X. Y.; Lai, Y. H. Head-to-Tail Regioregular Oligothiophene-Functionalized 9,9′-Spirobifluorene Derivatives. 1. Synthesis. *J. Org. Chem.* **2002**, *67* (14), 4924–4936. https://doi.org/10.1021/jo011146z.
(134) Yuan, S.; Kirklin, S.; Dorney, B.; Liu, D. J.; Yu, L. Nanoporous Polymers Containing Stereocontorted Cores for Hydrogen Storage. *Macromolecules* **2009**, *42* (5), 1554–1559. https://doi.org/10.1021/ma802394x.
(135) Ganchegui, B.; Leitner, W. Oxybromination of Phenol and Aniline Derivatives in H2O/ScCO2 Biphasic Media. *Green Chem.* **2007**, *9* (1), 26–29. https://doi.org/10.1039/b609992k.
(136) Podgoršek, A.; Stavber, S.; Zupan, M.; Iskra, J. Environmentally Benign Electrophilic and Radical Bromination "on Water": H2O2-HBr System versus N-Bromosuccinimide. *Tetrahedron* **2009**, *65* (22), 4429–4439. https://doi.org/10.1016/j.tet.2009.03.034.
(137) Kumar, L.; Mahajan, T.; Agarwal, D. D. Aqueous Bromination Method for the Synthesis of Industrially-Important Intermediates Catalyzed by Micellar Solution of Sodium Dodecyl Sulfate (SDS). *Ind. Eng. Chem. Res.* **2012**, *51* (5), 2227–2234. https://doi.org/10.1021/ie2022916.
(138) Ruasse, M. F.; Blagoeva, I. B.; Ciri, R.; Garcia-Rio, L.; Leis, J. R.; Marques, A.; Mejuto, J.; Monnier, E. Organic Reactions in Micro-Organized Media: Why and How? *Pure Appl. Chem.* **1997**, *69* (9), 1923–1932. https://doi.org/10.1351/pac199769091923.
(139) Cordes, E. H.; Bruce Dunlap, R. Kinetics of Organic Reactions in Micellar Systems. *Acc. Chem. Res.* **1969**, *2* (11), 329–337. https://doi.org/10.1021/ar50023a002.
(140) Topchiy, M. A.; Asachenko, A. F.; Nechaev, M. S. Solvent-Free Buchwald-Hartwig Reaction of Aryl and Heteroaryl Halides with Secondary Amines. *European J. Org. Chem.* **2014**, *2014* (16), 3319–3322. https://doi.org/10.1002/ejoc.201402077.
(141) Ageshina, A. A.; Sterligov, G. K.; Rzhevskiy, S. A.; Topchiy, M. A.; Chesnokov, G. A.; Gribanov, P. S.; Melnikova, E. K.; Nechaev, M. S.; Asachenko, A. F.; Bermeshev, M. V. Mixed Er-NHC/Phosphine Pd(Ii) Complexes and Their Catalytic Activity in the Buchwald-Hartwig Reaction under Solvent-Free Conditions. *Dalt. Trans.* **2019**, *48* (10), 3447–3452. https://doi.org/10.1039/c9dt00216b.

Chapter 3

Extension of Sustainable Approaches to the Synthesis of π-Conjugated Polymers

This section concerns with the extension of the previous developed successful sustainable methods, established for the synthesis of some exemplary molecular semiconductors, to the preparation of conjugated polymeric materials. Semiconducting conjugated polymers play a pivotal role in the development of printed (opto)electronics, and there the several advantages in using polymeric versus molecular π-conjugated semiconductors:[1,2]

1. Thin films of polymeric materials are generally exceptionally smooth and uniform, enabling a great control over large-scale of the film structural and morphological characteristics. Printing requires great control of the solution rheological properties, which can be tuned efficiently for polymer-based solutions.

2. Polymer crystalline domains are usually much smaller than the length scale of several optoelectronic devices, resulting in isotropic transport characteristics. This leads to low device-to-device performance variability, which is particularly important, for instance, for integrated circuits.

3. Fabrication of multilayers from solution deposition processes necessitates each stacked layer to be inert to the solvents and processing temperatures that it is exposed to during device manufacture. The reduced solubility of polymers, together with their large bulk viscosity, typically increases the options to find orthogonal solvents for solution deposition on top of polymer layers, thus expanding the choice of materials that can be used in devices.

4. Since polymers do not vaporize before decomposition and hence have negligible vapor pressure, they are not prone to interlayer diffusion during the typical thermal cycles in device fabrication. Furthermore, they typically exhibit robust mechanical properties, making nanometer-thick semiconductor films potentially compatible with roll-to-roll fabrication on flexible substrates.

Polymeric semiconductors for (opto)electronic applications must possess two important structural features.[2] The first is a π-conjugated backbone composed of linked unsaturated units resulting in extended π orbitals along the polymer chain, thus enabling proper charge transport and optical absorption. There is a wide variety of available structural motifs, yet current trends reveal efficient polymers are generally characterized by alternating electron-donating or electron accepting building blocks.[3] The second essential feature is the functionalization of the polymer core with solubilizing substituents, which is of crucial importance for inexpensive manufacture by solution methods as well

as to enhance solid-state interactions.[4] The extent of conjugation, together with the interchain interactions, determine the polymer solution/solid state electronic structure, which in turn control key polymer optical and electrical properties. Other important polymer architecture parameters are the molecular weights distribution (Mn and Mw) and the polydispersity index (PDI) since they impact on properties, solubility, solution aggregation, and formulation rheology, as well as the thin film formation and morphology for both pristine and blended materials. Since when moving from low molecular weights (oligomers) to high molecular weights (polymers) the electronic structure, thermal properties, and microstructure of materials generally vary significantly, it is important to achieve a Mw/PDI regime where a particular property stabilizes and fixes, so that, greater reproducibility of the polymer property from batch to batch can be achieved. This value is likely to be strongly dependent on the polymer structure; however, for most soluble thiophene-based polymers, a number average molecular weight value of about 20-30 kDa and a PD of 1.2-1.8 are reasonable for these threshold values.[5]

Typical methodologies employed to synthesize π-conjugated active polymers in organic (opto)electronics are based on traditional transition metal catalysed step-growth polycondensation and chain growth polymerization reactions In particular, the synthesis of the nowadays most performing alternating copolymers is dominated by Stille and Suzuki-Miyaura (S-M) couplings.[6] As already discussed in the previous chapter, despite their great versatility and wide substrate scope, these reactions have a number of drawbacks, including the number of steps required to prepare the monomeric precursors, the instability of several organometallic reagents employed, poor conversion related to unreactive monomers, difficulties in controlling the polymer architecture (formation of homocouplings and branched defects), prolonged heating, inert atmosphere, the use of toxic and harmful organic solvents, and poor atom economy owing to the formation of stoichiometric amounts by-products. In particular, in the case of the Stille stoichiometric amounts of toxic tin-containing wates are produced, therefore currently excluded as an industrial solution. Improved reaction protocols have been reviewed recently.[7,8] Direct arylation polycondensation (DAP) is emerging as an alternative with improved atom economy. Initial fails regarding regioselectivity and side reactions have been overcome, making this alternative coupling of mostly thiophene-based monomers very resourceful.[9–11] However, DAP shares with S-M polycondensation (SPC), the common feature of requiring the use of organic solvents, eventually generating organic wastes, thus fails in improving the E-Factor of the process.

In the pursuit of a sustainable electronics industry, efforts to implement economically attractive and benign novel approaches to organic semiconductors that minimize the use of solvents and reagents, as well as the number of workup procedures, undoubtedly represent important contributions for the development of the field.[12] In this regard, the development of synthetic approaches to semiconductor materials encompassing the principles of green chemistry is mandatory. Particularly, waste production should be reduced using minimal amounts of reagents and by using easily recoverable/reusable heterogeneous catalytic systems to simplify workup procedures and reduce energy and production times.[12] Particular attention should be directed toward solvents, which are commonly a major input in industrial and lab-based procedures as reaction media, in addition to their use for extraction, separation, and purification. These substances typically comprise the largest fraction of the waste generated (about 90%), as well as presenting significant workplace hazards. Moreover, traditional solvents such as 1-methylpyrrolidone (NMP), dimethylformamide (DMF), and dimethylacetamide (DMA), and chlorinated solvents, which are commonly used as media in condensation polymerizations, increase air pollution; most of them are toxic, flammable, or both. These solvents are not compliant with relevant legislation, ranking high on the list of harmful chemicals. The removal, or at least a sizable reduction, of organic solvents has an immediate impact on sustainability.[13]

3.1. Synthesis of PF8T2 and PF8BT Conjugated Polymers by Sustainable Suzuki-Miyaura Polycondensation in Water and under Air

This work has already been published and it is entitled *"Synthesis of Conjugated Polymers by Sustainable Suzuki Polycondensation in Water and under Aerobic Conditions"*, ACS Macro Lett. **2020**, 9, 1167−1171; https://dx.doi.org/10.1021/acsmacrolett.0c00495.[13]

3.1.1. Introduction

As already discussed in the previous chapter, the use of highly-performing surfactants enables the use of water as the main and often only reaction medium by forming association colloids capable of hosting and promote organic transformations, thus greatly improving the sustainability of the processes. In such nano/micro-heterogeneous environments, organics are accumulated at remarkably high concentration in low polarity domains, thereby they can often efficiently react at high rates, low temperatures, and catalyst ppm levels (this phenomenon is known as "hydrophobic effect").[14,15] The field of organic semiconductors is at its very infancy regarding these new sustainable approaches, but with very promising expectations considering the results obtained in the works described in the previous chapter. For instance, reductions in the E-factor by 1 or even 2 orders of magnitude in the syntheses of relevant molecular semiconductors have been demonstrated using commercially available surfactants.[16–21] However, no reports on the extension of surfactant enhanced S-M couplings to the synthesis of polymeric semiconductors is documented in the literature. The use of water solutions of surfactants is well-known in polymer chemistry but so far is limited to polymerization under miniemulsion conditions for the preparation of conjugated organic nanoparticles. In this case, water is not the reaction medium, but the dispersing phase required for the polymerization of the materials into nanoparticles having specific dimensions and aspect ratio. The process requires the use of enough organic solvent to completely dissolve the reagents and thus is not really beneficial for the reduction of the E-factor of the reaction with respect to homogeneous phase processes. Moreover, all known miniemulsion S-M polymerizations require the use of inert atmosphere.[22,23]

Exemplified by the two well-known and commercially available luminescent polymers poly(9,9-dioctylfluorene-alt-bithiophene) (PF8T2) and poly(9,9-dioctylfluorene-alt-benzothiadiazole) (PF8BT) widely used for the preparation of OLEDs, OPVs, and OFETs, this section describes the first examples of efficient Suzuki-Miyaura polycondensations in water using very minimal amount of organic solvent, under air, and with moderate heating. The synthetic approach enables a reduction of the E-factor by 1 order of magnitude, without negatively affecting molecular weight, dispersity, chemical structure, or photochemical stability of PF8T2 or PF8BT.

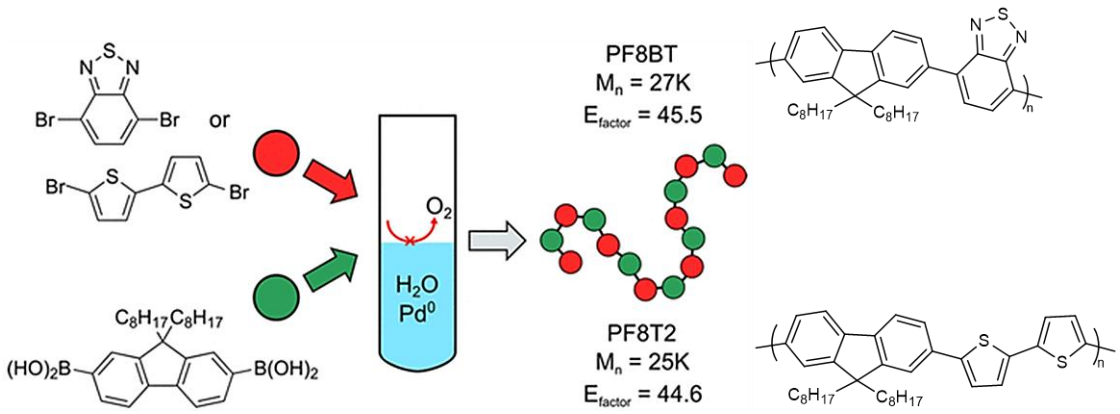

3.1.2. Results and Discussion

To the best of our knowledge, we here present the first study on the use of micellar catalysis as a tool to carry out efficient S-M polymerization reactions with minimal amount of organic solvents and under standard laboratory environment. We decided to apply the method to the preparation of Poly(9,9-dioctylfluorene-alt-bithiophene) (PF8T2) and Poly(9,9-dioctylfluorene-alt-benzothiadiazole) (PF8BT) shown in **Figure 99**. Both copolymers are commercially available active compounds for the preparation of OLEDs, OPVs and OFETs

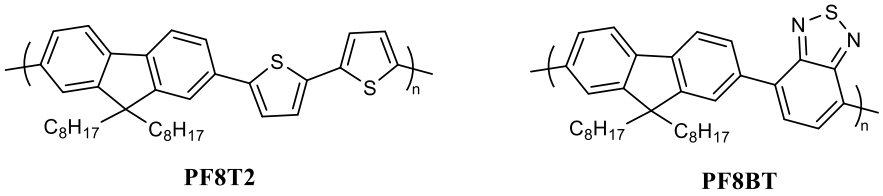

PF8T2 **PF8BT**

Figure 99. *Chemical structures of poly(9,9-dioctylfluorene-alt-bithiophene) (PF8T2) and poly(9,9-dioctylfluorene-alt-benzothiadiazole) (PF8BT).*

For both copolymers, synthetic protocols in organic solvents are well established, thus enabling a direct comparison with our surfactant enhanced approach.

3.1.2.1. Optimization of Formulative Conditions on a Model Small Molecule Compound

Micellar catalyzed reactions are very resourceful but qualitatively different from corresponding transformations carried out in homogeneous phase. As the reaction requires colocalization of counterparts and catalysts within the same pocket of a micro heterogeneous mixture, the hydrophobic/hydrophilic balance and diffusion coefficients of all species are at least as important as the intrinsic reactivity. As such, prior to move to micellar catalyzed polymerizations we investigated the effect of reaction conditions and details of the formulation characteristics on the model reaction between 2,7-dibromo-9,9-dioctylfluorene and thienyl-2-boronic acid, as well as on the same counterparts but with reversed functionalities, 9,9-dioctylfluorene-2,7-diboronic acid and 2-bromothiophene. On doing that, we paid particular attention to reaction conversion and to the side reactions relevant for the formation of defects and terminations during polymerization: homocoupling, dehalogenation and protodeborylation side products. The starting conditions are those that have led to satisfactory results in previous studies. **Figure 100,** Errore. L'origine riferimento non è stata trovata.**3** shows all the results.

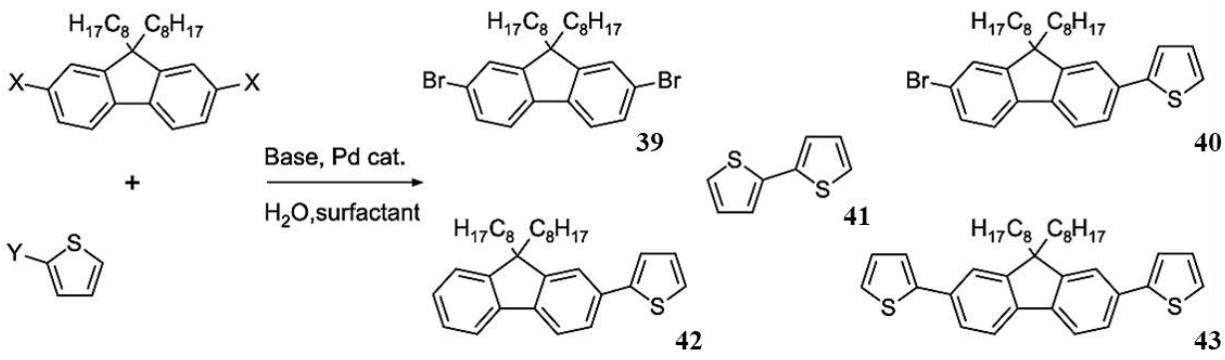

Entry	Medium (wt%)	X	Y	NEt_3 (eq)	[Pd][b] (mol%)	T (°C)	GC peak area (%)				
							39	**40**	**41**	**42**	**43**
1	K-EL (2)	Br	$B(OH)_2$	3	4	25	18	13	3	0	66
2	K-EL(10)	Br	$B(OH)_2$	3	4	25	38	11	3	0	48
3	K-EL(15)	Br	$B(OH)_2$	3	4	25	39	7	3	0	51
4	K-EL (2)	Br	$B(OH)_2$	6	4	25	8	6	2	0	84
5	K-EL (2)	Br	$B(OH)_2$	8	4	25	6	3	0	0	91
6	K-EL (2)	Br	$B(OH)_2$	12	4	25	6	1	0	0	93
7	K-EL (2)	Br	$B(OH)_2$	6	2	25	20	13	4	0	63
8	K-EL (2)	Br	$B(OH)_2$	6	8	25	5	1	1	0	93
9	K-EL/Span80 7/3 (2)	Br	$B(OH)_2$	6	4	25	3	2	1	0	94
10	K-EL/Span80 7/3 (2)	Br	$B(OH)_2$	6	4	40	2	2	1	0	95
11[a]	K-EL/Span80 7/3 (2)	Br	$B(OH)_2$	6	4	25	6	3	1	0	90
12	K-EL (2)	$B(OH)_2$	Br	6	4	25	0	0	0	1	99
13	K-EL/Span80 7/3 (2)	$B(OH)_2$	Br	6	4	25	0	0	0	1	99

[a] Reaction carried out under N_2 atmosphere; [b] $Pd(dtbpf)Cl_2$ used.

Figure 100, Table 13. *Optimization of reaction conditions in the coupling of dioctylfluorene and thiophene. All reactions were carried out in a 5mL glass tube under magnetic stirring at 1000 rpm and at a nominal concentration for fluorene derivative of 0.5 mol/L. Worked up reaction mixtures were characterized by GC-MS using a simple semiquantitative area normalization method.*

We chose Kolliphor EL as the preferred surfactant for our approach as, along with the sizeable benefit of a one order of magnitude reduction in the E-factor of previously studied reactions, such surfactant enables carrying out the cross-coupling reaction under standard laboratory environment.[24] Entries 1-3 show that the increase of the surfactant concentration from the customary 2 wt% to 10 and even 15 wt% does not improve conversion. Entries 4-6 show that the increase in the concentration of the organic base has a profound effect on both conversion and product distribution. The GC-MS yield evolves from 66 % to 84, 91 and eventually 93 % upon increase of the amine stoichiometry from 3, to 6, 8 and 12 equivalents. From the standpoint of the reaction mechanism, such an excess of base should not influence the reaction behavior. The main impact of the amount of NEt_3 is in the nature of the formulation achieved: the amine acts as an organic cosolvent, thus helping in partially dissolving the lipophilic reagents.[25] The concentration of the monoarylated species decreases accordingly. Additionally, no thiophene-thiophene homocoupling is observed when more than 6 equivalents on NEt_3 are employed. Entries 7 and 8 show the expected improvement of conversion and yield upon increase of the catalyst loading. In entry 9 we slightly reduced the Hydrophilic/Lipophilic Balance (HLB) of the surfactant system by mixing K-EL (HLB 13.5) with Span 80 (4.3). We recently demonstrated that the resulting mixture (HLB 10.7) is better suited to work with conjugated donor-acceptor structures.[17] Entry 10 shows that increase of the reaction temperature from 25 (entry 9) to 40 °C has a negligible impact on conversion and yield. Then, entry 11 confirms that carrying out the reaction under nitrogen atmosphere does not impact on yield or product distribution. Finally, we exchanged functionalities between reaction counterparts by using 2-bromothiphene and 9,9-Dioctylfluorene-2,7-diboronic acid under the best conditions identified in the previous entries. Unregarding to the surfactant mixture (K-EL or K-EL/Span 80 7:3) we obtained quantitative

conversion with a 1 % monoarylated species as the only discernible byproduct by GC-MS, in both cases working under standard laboratory atmosphere without removing oxygen from the reaction environment. Satisfied of these two latest promising results, we decided to use these last conditions to carry out the polymerization reactions under study.

3.1.2.2. Surfactant Promoted S-M Polymerization Reactions to Sustainable Access PF8T2 and PF8BT

According to the results obtained with the model reaction, we carried out all polymerizations using 9,9-dioctylfluorene-2,7-diboronic acid, 5,5′-dibromo-2,2′-bithiophene, 2 wt % K-EL in deionized water as the surfactant, 4 mol % $Pd(dtbpf)Cl_2$ as the catalyst, and 6 equivalents of NEt_3 as the base. The purification protocol was the same for all reactions, including the reference one carried out under literature conditions. Following **Figure 101, Table 14** shows all the results obtained for the polymerization reactions.

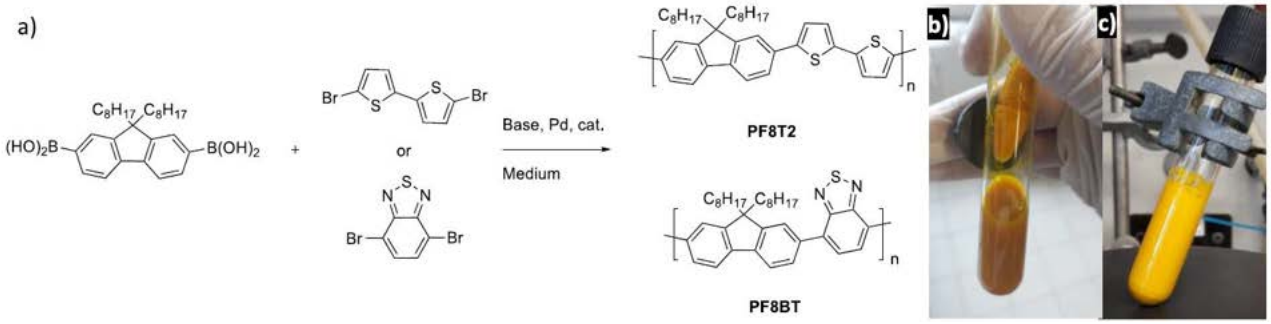

entry/polymer	medium[a]	base	catalyst (mol %)	T (°C)	atm	yield (%)	M_n (kg/mol)	M_w (kg/mol)	Đ
1 - PF8T2	toluene	NaOH	$Pd(PPh_3)_4$ (1)	90	N_2	94	24.2	39.8	1.64
2 - PF8T2	K-EL	NEt_3	$Pd(dtbpf)Cl_2$ (4)	25	air	70	15.9	26.3	1.65
3 - PF8T2	K-EL/Tol .9:1	NEt_3	$Pd(dtbpf)Cl_2$ (4)	25	air	72	20.7	34.8	1.68
4 - PF8T2	K-EL/Tol .9:1	NEt_3	$Pd(dtbpf)Cl_2$ (4)	60	air	72	20.5	37.0	1.81
5 - PF8T2	K-EL/Tol .9:1	NEt_3	$Pd(dtbpf)Cl_2$ (4)	80	air	87	25.2	49.4	1.96
6 - PF8BT	H_2O/Tol .2:1	K_2CO_3	$Pd_2(dba)_3$/P(*o*-Tol)$_3$ (2)	95	N_2	90	11.3	20.1	1.65
7 - PF8BT	K-EL/Tol .9:1	NEt_3	$Pd(dtbpf)Cl_2$ (2)	25	air	77	6.8	11.0	1.54
8 - PF8BT	K-EL/Tol .9:1	NEt_3	$Pd(dtbpf)Cl_2$ (2)	80	air	93	19.7	38.3	1.94
9 - PF8BT	K-EL/Tol .9:1	NEt_3	$Pd(dtbpf)Cl_2$ (4)	80	air	90	26.9	50.9	1.89

[a]K-EL stands for 2 wt % solution of Kolliphor EL in deionized water.

Figure 101, Table 14. *Top:(a) Reaction of 9,9-dioctylfluorene-2,7-diboronic acid with 5,5'-dibromo-2,2'-bithiophene or 4,7-dibromobenzo[c]-1,2,5-thiadiazole via S-M polycondensation to give PF8T2 and PF8BT, respectively; (b) S-M polycondensation in only K-EL: demixing of the system observed (inhomogeneous); (c) S-M polycondensation in K-EL 2%/toluene 9:1, freely stirring. Bottom: Screening of S-M Polycondensation conditions to prepare PF8T2 (Entries 1–5) and PF8BT (Entries 6–9).*

Entry 1 of ***Errore. L'origine riferimento non è stata trovata.*** shows the results we obtained working under literature conditions, that is using toluene as the solvent, 2M NaOH as the base, 1 mol % $Pd(PPh_3)_4$ as the catalyst and heating the reaction under N_2 atmosphere for 24h at 90°C. Under these conditions our data is in line with that previously reported.[26] We performed such polymerization in order to have a standard for comparative characterizations and to gather information for a reliable estimate of the E-factor. Entry 2 shows the results obtained working under the best conditions identified for the test reaction, working in only water using K-EL. We can observe that the reaction is less efficient compared with the literature method, both in terms of yield and molecular weight distributions. The reason for the different behavior of the micellar S-M polymerization with respect

to the test reaction on the model small molecule is likely connected with the opposite formulative behavior we observed in the two cases. In the case of the model compound (**Table 13**, Entry 12), the reaction mixture is at all stages a homogeneous dispersion of the characteristic color of the product (like paint). On the contrary, during the polymerization described in entry 2 of **Table 14** precipitation occurs from the original dispersion, which rapidly turns into a sticky lump wrapped around the stirring bar (see **Figure 101 b**). In general, the success of a micellar enhanced reaction relates to the capability of reagents to reach the active catalytic site within the lipophilic pocket. If mass exchange between the water suspension and the association colloids is precluded, like exactly the case of the phase separation observed in the polymerization reaction, any further chemical evolution is compromised. Literature report similar effects in the case of poorly soluble substrates.[25] Accordingly with our previous experience,[16,18–20] the common solution is the use of small amounts of organic solvents (generally 10 vol% with respect to the water) acting as both dispersants and mixing aid, effectively turning the micellar solution in an emulsion. Such a strategy has a negligible impact on sustainability as the amount of toluene is very small: roughly 20 mg every 100 mg of monomer mixture. We already reported the dynamic light scattering (DLS) characterization: K-EL alone in water gives micelles having a 12 nm average diameter, while the addition of substrates and toluene leads to the formation of an emulsion with average droplet dimension in the 1 μm regime.[16] Thus, in entry 3 of **Table 14** we explored the formulative impact by adding 10 vol% of toluene to the reaction, moving from a micellar regime to an emulsion environment. The results showed that these conditions strongly improve the reaction, which did not display macroscopic phase separation (**Figure 101 c**) and led to both molecular weights and polydispersity much closer to those obtained with the reference reaction (Mw increases moderately from 26.3 to 34.8 kg/mol), while still working under standard laboratory environment under air.

A favorable feature related to the use of emulsions instead of micellar solutions is the possibility to apply a moderate heating to the reaction without facing issues with the low cloud point characterizing most nonionic surfactants in alkaline conditions. Entries 4 and 5 show the effect of the temperature. Working at 60°C has no impact on the yield or molecular weights. However, a further increase of the temperature to 80°C enables to achieve a remarkable Mw of nearly 50 kg/mol with a PDI of 1.96, thus results comparable with literature data for polymerizations carried out under inert atmosphere and with organic solvents.[26,27] We did not continue a study on a further increase in temperature as at higher temperatures the emulsion becomes unstable and macroscopic phase separation is observed. Considering the E-factors of both standard literature and emulsion procedures, the value of the former is 229 (**Table 14**, entry 1) while that of the latter is 45 (**Table 14**, entry 5). In both cases, we did not consider the solvents used during the Soxhlet extraction as they are easily recovered by distillation and recycled. Anyway, the difference in the sustainability index by a factor of 5 is remarkable, especially considering that the same result can be obtained under ambient conditions, which greatly facilitates the entire experimental procedure.

My colleague Alessandro Sanzone then tested, at Chemnitz University of Technology the under the supervision of Prof. Michael Sommer, the generality of our water-based protocol on a structurally related polymer, PF8BT, that is synthesized from the same boronic acid and 4,7- dibromobenzo[c]-1,2,5-thiadiazole via S-M polycondensation as well. The reactions were carried out as the same for the previous case, we initially performed the reaction under literature conditions to get a direct comparison as well as to collect all the information required for the estimate of the E-factor. Entry 6 of **Table 14** shows the results obtained using a biphasic toluene/water 2:1 mixture as the reaction medium, K_2CO_3 as the base and $Pd_2(dba)_3$/$(o\text{-}Tol)_3$ as the catalyst. Entry 7-9 show the results we obtained working in K-EL/toluene 9:1 emulsion, using $Pd(dtbpf)Cl_2$ as the catalysts. As in the case of the PF8T2 polymerization, the best results were obtained working at 80 °C and in the presence of a 10 vol % amount of toluene (**Table 14**, entry 9), achieving a remarkable Mw slightly higher than 50 kg/mol with a PDI of 1.89. The Mw obtained under emulsion conditions is higher than that

achieved in our control experiment using an organic solvent, and in line with the results described in the literature for similar S-M polycondensations in organic solvents.[28–30] The comparison between the E-factors of the two protocol is again in strong favor of the emulsion protocol with a difference by a factor of 4, in fact for the literature procedure we estimated a value of 209 whereas the surfactant enhanced protocol only gave 46.

In order to investigate upon structural integrity of the obtained products, ^{1}H-NMR spectroscopy was performed at 120 °C in $C_2D_2Cl_4$. **Figure 102-a,b** shows the aromatic region of the spectra of PF8T2 obtained from the emulsion method (entry 4 of **Table 14**) and from the standard literature method (entry 1 of **Table 14**), respectively. From this comparison, a difference between the two samples is not noticeable and indications for defects[26] are not seen either, which are further proof for the robustness and advantages of the herein proposed sustainable protocol. The same is true for the comparison between the aromatic regions of the ^{1}H-NMR spectra of the PF8BT emulsion/literature control (**Figure 102-c,d,** respectively corresponding to entries 9 and 6 of **Table 14**). However, one difference between PF8BT made by emulsion polycondensation and in homogeneous medium relies on the presence of OH-termination at the F8 unit for the former at ~6.95 ppm (compare insets of **Figure 102-c,d**). This end group is a result of oxidative deborylation and derives from the presence of oxygen in the reaction medium.[31]

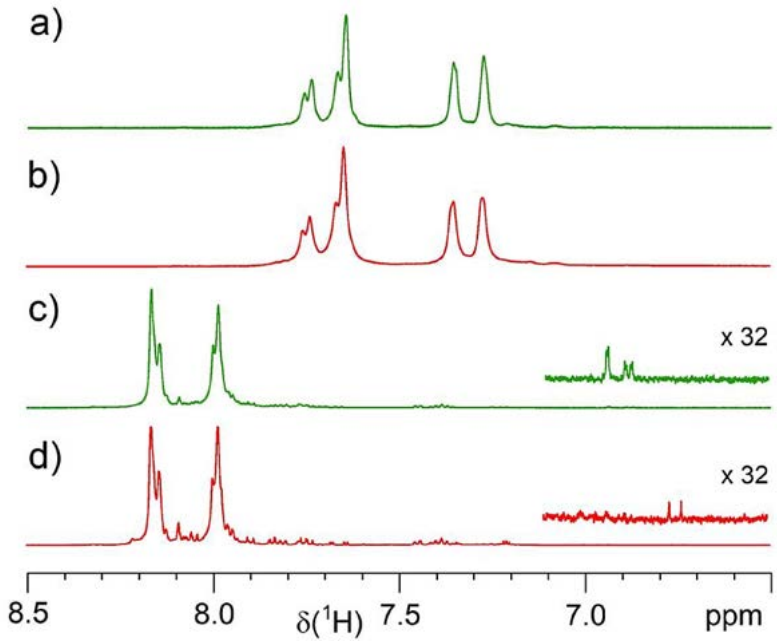

Figure 102. *(a, b) Comparison between the ^{1}H-NMR spectra (regions) of PF8T2 samples. Trace (a) corresponds to Table 1, entry 4, sample polymerized in water; (trace b) is the Table 1, entry 1, control experiment. (c, d) PF8BT samples. Trace (c) corresponds to Table 1, entry 8, sample polymerized in water; trace (d) is Table 1, entry 6, control experiment. The insets in c and d show the intensified region in which OH-termination of the fluorene end groups appears around 6.95 ppm.*

We previously demonstrated that K-EL micelles have an oxygen free core, yet such a characteristic does not include the interphase with the hydrophilic shell.[32] Generally, in micellar-enhanced reactions most of the organic transformations take place in the internal lipophilic core but some of them can also happen close to the interphase region when oxygen can be present. Working with small-molecular materials it is easier to get rid of the few percent of by-products considering the related purification methods allowed. In the case of high molecular weight materials, poisoning of the reacting functionalizations imply chain grow termination, in our case competing with protodeborylation. Such an effect does not alter optical properties (see next paragraph) and does not sizably influence the polymerizations, as the molecular weight are comparable with those obtained

with standard techniques. Further small signals between 7.2 and 8.1 ppm stem from additional end groups both present in entries 6 and 9, which differ in intensity due to their different molar mass.

3.1.2.3. Evaluation of the Emission Efficiency and Photostability of Emulsion vs Homogeneous Phase Polymerized Materials

The data discussed in the previous paragraphs demonstrates that the K-EL enhanced emulsion polymerization of both PF8T2 and PF8BT under standard laboratory conditions and with very limited amounts of organic solvents employed gives materials having polymerization statistics comparable with those of corresponding samples prepared under literature conditions. In a polymeric sample the achievement of high molecular weights is a necessary but not sufficient condition to match performances of materials prepared through different routes. In particular, termination and defectivity can impact on optical properties mostly affecting luminescence quantum yield and photostability. We thus submitted the best samples obtained via emulsion approaches to comparative luminescence and photostability tests with respect to the samples obtained via the literature approach. The work has been performed in collaboration with Prof. Gianmarco Griffini from Politecnico di Milano. In particular, we selected the material obtained under the conditions of entry 5 of **Table 14** as the representative sample of emulsion polymerized PF8T2, and the material obtained by entry 9 of the same table as the representative emulsion polymerized PF8BT sample. We submitted both polymers, along with the corresponding control experiment samples (**Table 14** entry 1 for PF8T2 and Entry 6 for PF8BT) to extended photostability tests. We characterized each sample under three different exposition conditions: a) accelerated weathering tests in a weather-o-meter chamber (SOLARBOX 300E, Co.Fo.Me.Gra. Srl), equipped with a Xenon light and outdoor filter, able to cut out all the wavelengths lower than 280 nm. The total irradiance applied was equal to 550 W/m^2 in the 300-800 nm wavelength range. The temperature was fixed at 35 °C and the relative humidity at 25%; b) UV-A accelerated weathering tests in air, performed using a UV polymerization apparatus (Helios Quartz, POLIMER 400W) equipped with a high-pressure mercury UV-A lamp (Zs type, Helios Quartz) characterized by an emission window between 315 and 400 nm and with radiative power density equal to 300 W/m^2; c) The same test was repeated under nitrogen atmosphere.
Next Errore. L'origine riferimento non è stata trovata.**03** shows that the behavior of PF8T2 spin coated films under SOLARBOX irradiation. The thicknesses of the two samples are comparable (351 nm for **Table 14** entry 1 sample (control experiment PF8T2) and 353 nm for **Table 14** entry 5 sample (emulsion PF8T2). The degradation kinetics is essentially undistinguishable for the two samples both from the standpoint of absorption profiles (**Figure 103-a** and **103-b**) and luminescence spectra (**Figure 103-c** and **103-d**). The lack of photostability of fluorene containing polymers is well established in the literature and we did not expect our samples to be any different.[33,34] It is however clear that the micellar catalyzed polymerization technique does not influence the degradation kinetics.

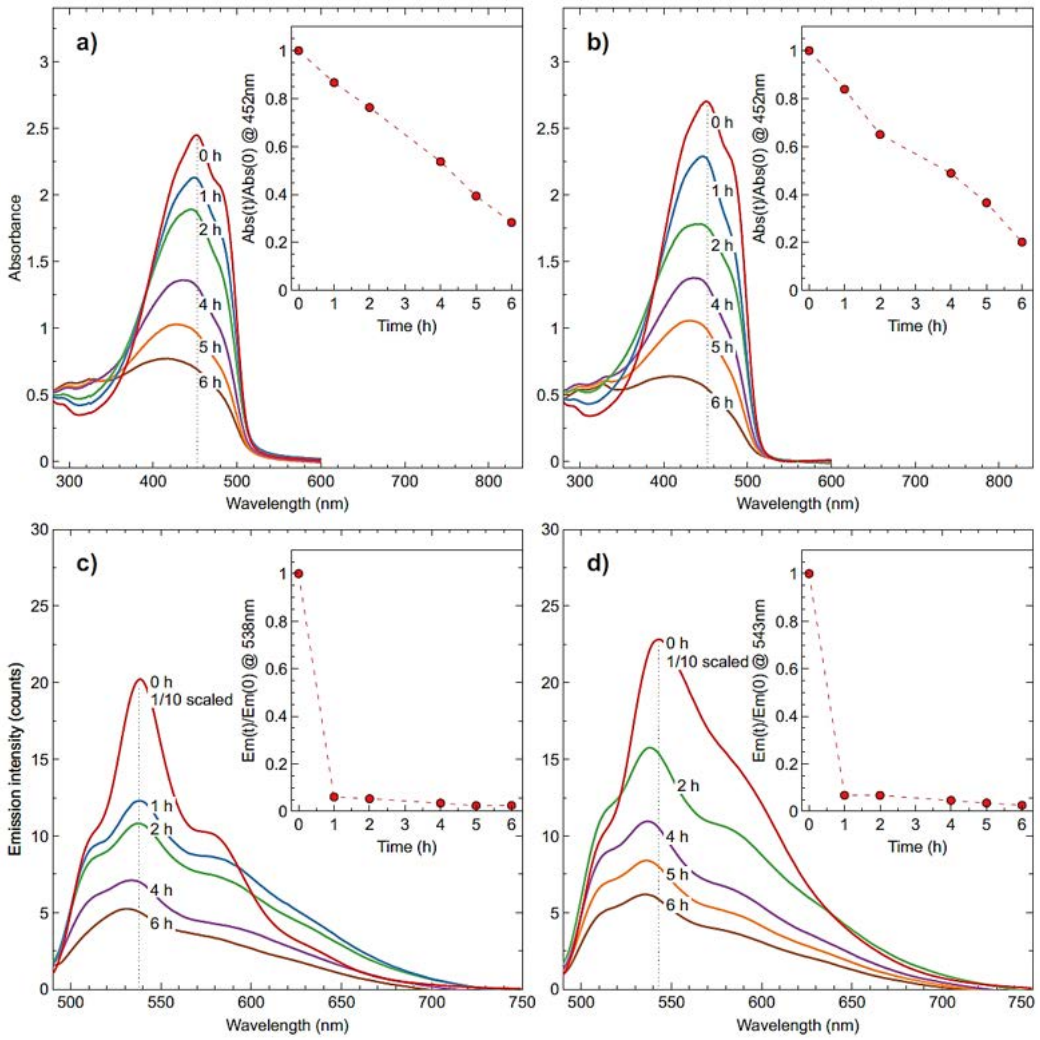

Figure 103. *Top (a and b): UV-Vis absorption spectra as the function of the irradiation time (white-light) in a SOLARBOX for spin coated thin films of Table 14 Entry 1 sample (control experiment PF8T2) (a) and Table 14 Entry 5 sample (emulsion PF8T2) (b). Bottom (c and d): Steady state emission spectra under excitation at 485nm as the function of the irradiation time (white-light) in a SOLARBOX for spin coated thin films of Table 14 Entry 1 sample (control experiment PF8T2) (c) and Table 14 Entry 5 sample (emulsion PF8T2) (d). Emission spectra at 0 h were scaled to 1/10.*

Figure 103-c and **103-d** show that the fluorescence signal is almost immediately quenched, no doubt because of the formation of fluorenone quenching sites. It is however worthwhile noting that the initial luminescence intensity of the two samples is almost the same. As the thicknesses are also essentially identical, it is possible to conclude that the emission efficiency of the two polymers is also similar. Actually, the emulsion polymerized sample is around 10 % more efficient that the control sample.

We then carried out a comparative FT-IR study to verify that the mechanism of degradation is the same for both samples. **Figure 104** shows similar features for both samples. The reduction in intensity at 2925 cm^{-1} and 2850 cm^{-1} is attributed to the loss of alkyl groups connected with the oxidation of the fluorene residue to fluorenone. The interpretation is supported by the appearance of new bands at 1715 cm^{-1}, attributed to carbonyl species. Both spectra also show progressive increase in the intensity of the peak related to sulfoxides and sulphones S=O stretching (1050 cm^{-1} and 1190 cm^{-1} respectively) diagnostics of the oxidation of the thiophene repeating units. The only minor difference between the two spectra is associated with the sulfoxide peak at 1050 cm^{-1}, already evident at time 0 for the control experiment while sizably weaker for the emulsion polymerized one.

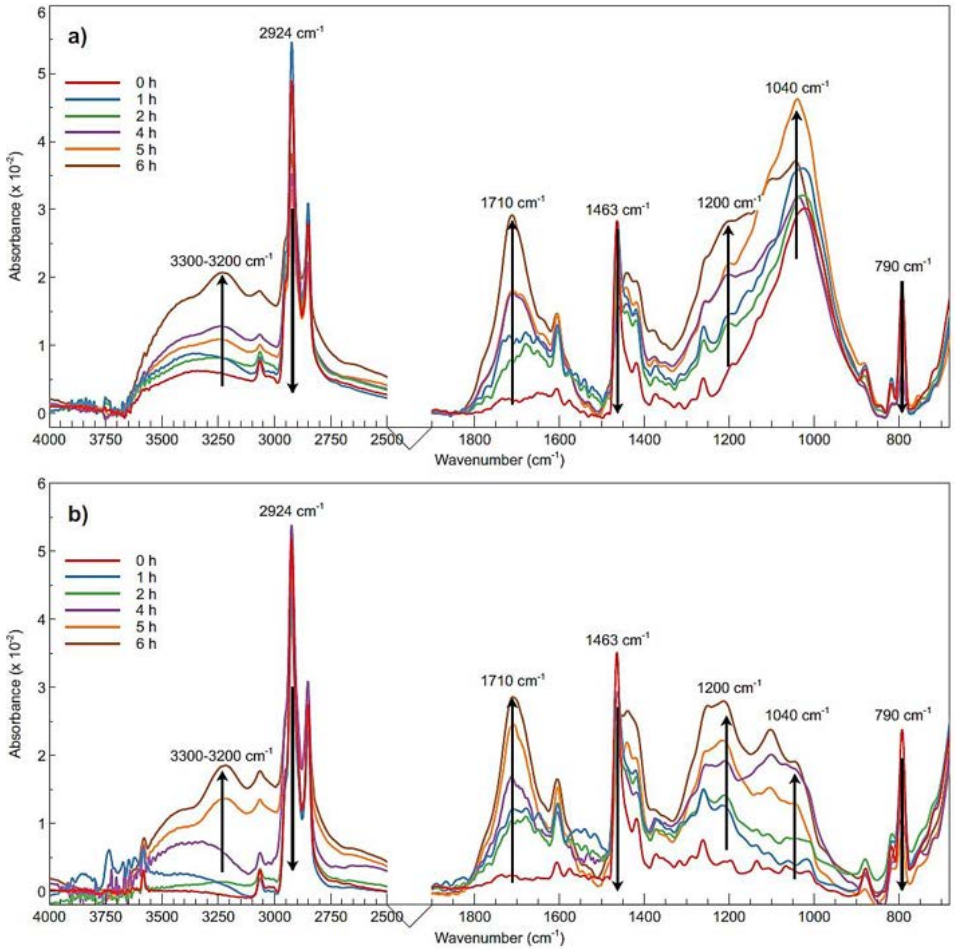

Figure 104. *FT-IR spectra as a function of the irradiation time (white light) for control experiment (a) and emulsion polymerized sample (b).*

Finally, we compared the polymerization statistics before and after weathering by dissolving the exposed films in THF and repeating the GPC characterization. **Table 15** shows that in both cases the light exposure causes a decrease in the molecular weight and a corresponding increase in dispersity. The behavior is very similar for the two samples.

Sample	Weathered	M_n (kg/mol)	Đ	Thickness (nm)
Control[a]	No	24.2	1.64	350.6 ± 19.4
	Yes	18.1	1.99	334.7 ± 21.5
Emulsion[b]	No	25.2	1.96	352.6 ± 9.4
	Yes	18.2	2.23	340.3 ± 13.3

Table 15. *Polymerization statistics for PF8T2 samples before and after weathering test in a SOLARBOX.*

We thus repeated the weathering test using a UV-A light source under air and under nitrogen to ascertain that the light sensitivity of both samples relates to high energy irradiation and that the process is oxygen mediated. The top part of **Figure 105** shows that the degradation kinetics for the control sample (trace a) and the emulsion polymerized sample (trace b) are essentially identical and very similar to those shown in **Figure 103** for the weathering test in the SOLARBOX. Conversely, if the test is performed under nitrogen atmosphere, the degradation is barely noticeable and again essentially identical for both samples.

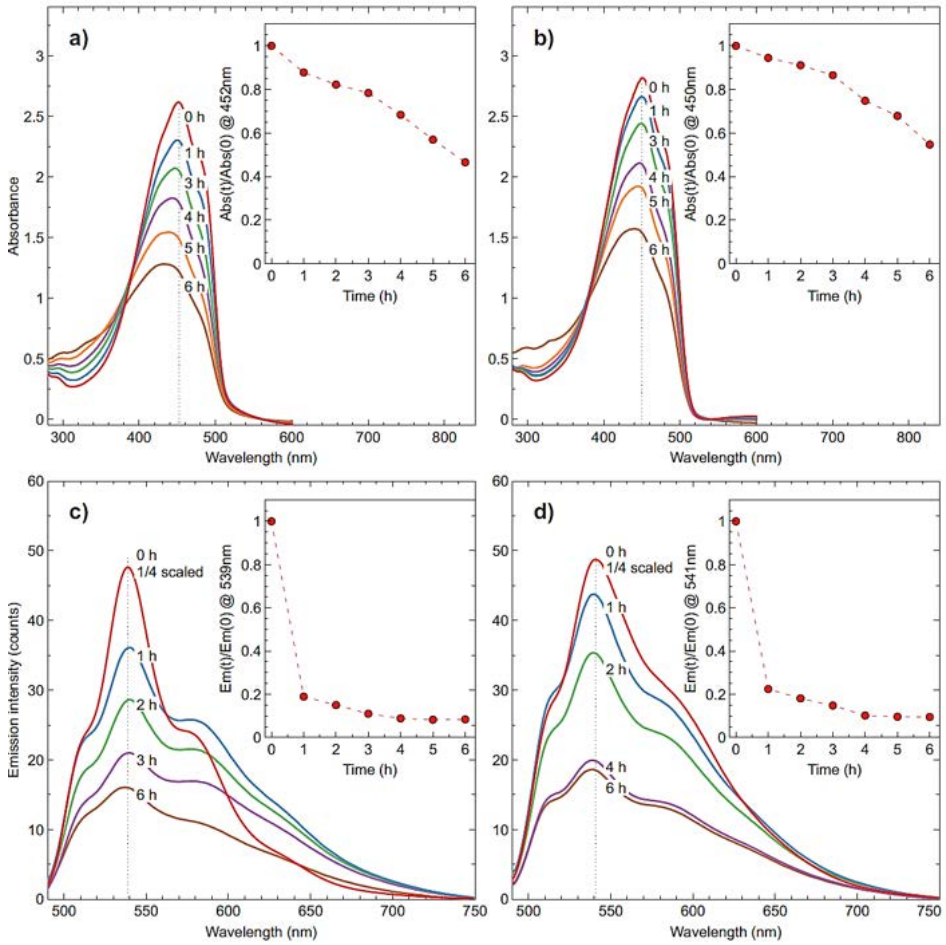

Figure 105. *Top (a and b): UV-Vis absorption spectra as the function of the irradiation time (white-light) under a UVA lamp for spin coated thin films of Table 14 Entry 1 sample (control experiment PF8T2) (a) and Table 14 Entry 5 sample (emulsion PF8T2) (b) under air. Bottom (c and d): Steady state emission spectra under excitation at 485nm as the function of the irradiation time (white-light) in a SOLARBOX for spin coated thin films of Table 14 Entry 1 sample (control experiment PF8T2) (c) and Table 14 Entry 5 sample (emulsion PF8T2) (d). Emission spectra at 0 h were scaled to 1/4.*

We performed the same comparative tests on PF8BT samples (we do not report here all the study for the PF8BT samples since it is parallel and analogous for that performed on PF8T2 samples), with slightly different results. **Figure 106** shows that in this case the degradation kinetics for the two samples (control experiment and emulsion) under SOLARBOX irradiation have similar characteristics but they are not identical. In both cases, the charge transfer band is progressively bleached in intensity blues shifted. However, in the case of the control experiment (**Table 14** entry 6 sample shown in **Figure 106-a**) the intensity at the maximum after 20 h of exposure is 41 % of the initial value, whereas for the emulsion polymerized sample (**Table 14** entry 8 sample shown in **Figure 106-b**) the absorption spectrum retains 66 % of the original intensity. The steady state emission spectra show a similar trend: the emission intensity progressively drops for both polymeric materials, but the emulsion polymerized sample (**Figure 106-c**) retains 34 % of the original efficiency whereas the control sample (**Figure 106-d**) only retains 11 %. As in the previous case, both sample thicknesses (281 nm for control experiment PF8BT sample and 295 nm for emulsion PF8BT sample) and initial emission intensities are comparable. The behavior shown under UV-A irradiation both under air and nitrogen, as well as the changes in the FT-IR spectra are in line with those discussed for PF8T2 samples. The only relevant difference is that PF8BT is in general more resistant to UV-A irradiation

than PF8T2. In agreement with previous literature findings, the main degradation pathway is the formation of fluorenone defects.[30]

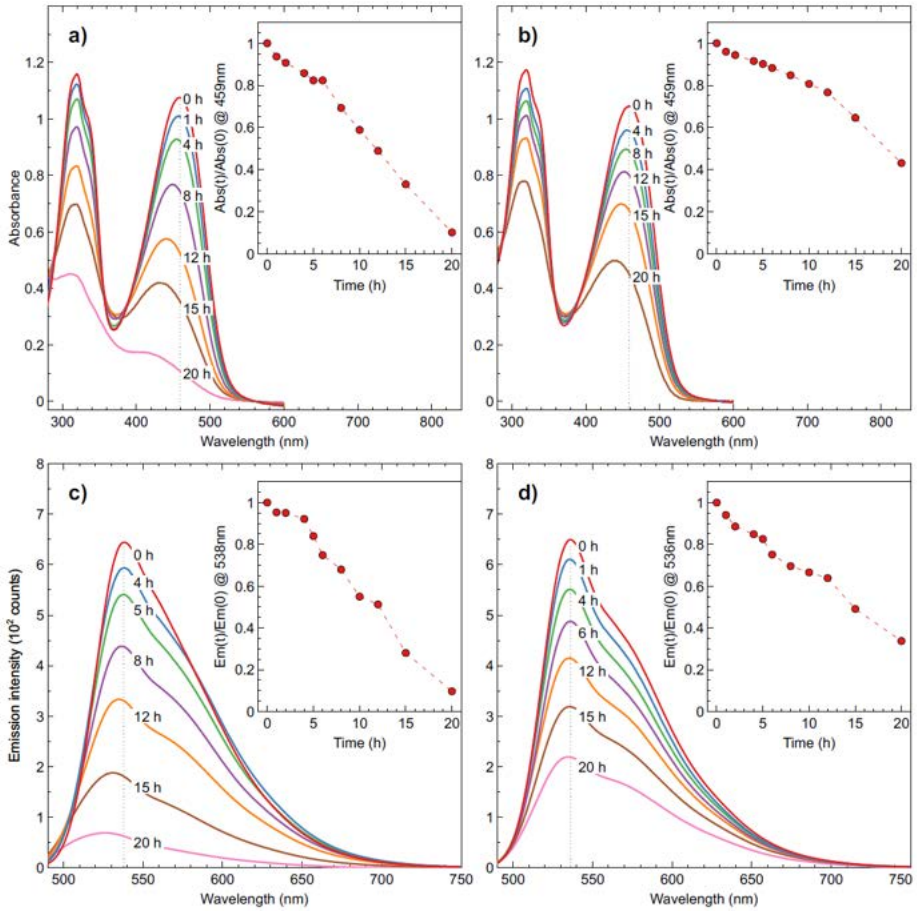

Figure 106. *Top: UV-Vis absorption spectra as the function of the irradiation time (white-light) in a SOLARBOX for spin coated thin films of Table 14 Entry 6 sample (control experiment PF8BT) (a) and Table 14 Entry 8 sample (emulsion PF8T2) (b). Bottom: Steady state emission spectra as the function of the irradiation time (white light) in a SOLARBOX for spin coated thin films of Table 14 Entry 6 sample (control experiment PF8BT) (c) and Table 14 Entry 8 sample (emulsion PF8T2) (d).*

3.1.3. Conclusions

In conclusion, we have shown that the emerging field of surfactant enhanced S-M polycondensations in water is a viable tool for the preparation of established polymeric p-type and n-type organic semiconductors, as respectively exemplified by PF8T2 and PF8BT. In particular, we demonstrated that once reaction conditions are optimized in terms of reaction temperature and formulative conditions, it is possible to prepare samples of both PF8T2 and PF8BT having yields, polymerization statistics, and optical properties comparable where not even better than those that can be obtained with standard protocol based on the use of organic solvents and homogeneous conditions. We chose K-EL as the preferred surfactant for our approach, as it is economic and commercially available, enables a reduced E-factor of the polymerization by 1 order of magnitude, and finally allows to carry out the reaction under ambient conditions. Finally, we tested the stability to visible light and UV-A irradiation of samples prepared in water and in organic solvents with positive results. In the case of PF8T2, control polymer and emulsion polymerized one are essentially identical. In the case of PF8BT samples, the emulsion approach leads to improvement in stability, possibly due to reduced defectivity

during the synthesis. We are presently extending the range of available polymers to more complex derivatives of interest for printed electronics and photovoltaics.

3.1.4. Experimental Section

3.1.4.1. Materials and Instruments

All reagents and chemical compounds were purchased from Aldrich, Fluorochem, or TCI Europe and used without any further purification. ^{1}H-NMR spectra were recorded either using a Bruker Avance 400 NEO spectrometer (for PF8T2 samples) or at 500.13 MHz with a Bruker Avance III spectrometer using a 5 mm BBI gradient probe (for PF8BT samples). PF8T2 samples were measured at 80 °C, PF8BT samples were measured at 120 °C, C2D2Cl4 was used as solvent and for calibration (*d* (1H) = 5.98 ppm). Evolution 600 UV-Vis spectrometer and VISION Pro software (both by Thermo Scientific) were used to collect and analyse data. Measurements were performed in air and at room temperature after the acquisition of a baseline which removes the contribution of air and of eventual contaminants. FTIR spectra were collected with a FT/IR-615 (Jasco Inc.) instrument used in transmission mode, at room temperature and in air. The number of scans performed was 64, the resolution 4 cm^{-1} and the range of the IR analyses was from 4000 cm^{-1} to 600 cm^{-1}. Fluorescence spectra were acquired using a Jasco FP-6600 spectrofluorometer. The tests were carried out to measure both the emission and excitation spectra of the thin-film coatings. Number-average (Mn) and weight-average (Mw) molecular weights were determined by size exclusion chromatography (SEC) and calibrated against polystyrene. Samples of PF8T2 (entries 1 to 5 in Table 1) and PF8BT (entries 6 and 8 in Table 1) were measured at 35 °C on a Waters 510 HPLC system equipped with a Waters 2410 refractive index detector. THF was used as eluent. The sample to analyze (volume 200 µL, concentration in THF 2mg/mL) was injected into a system of columns connected in series (Ultrastyragel models HR 4, HR 3, and HR 2, Waters), and the analysis was performed at a flow rate of 0.5mL/min. Samples of PF8BT (entries 6 to 9 in **Table 14**) were measured on four MZ-Gel SDplus 10E4 Å 5µm columns with pore sizes ranging from 103 to 106 Å (Polymer Standards), connected in series with a RID-20A RI detector and a SPD-20AV UV detector (Shimadzu). THF was used as eluent at 40 °C with a flow rate of 1.0mL/min.

3.1.4.2. General Synthetic Procedure for the Synthesis of the Model Compound 2,7-dithienyl-9,9-dioctylfluorene (43)

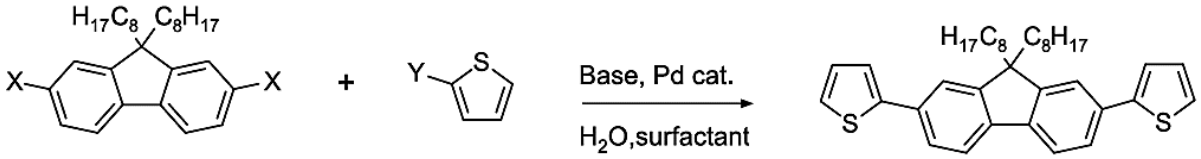

All reactions were carried out in a 5mL CEM microwave glass tube vial under magnetic stirring at 1000 rpm and at a nominal concentration for fluorene derivative of 0.5 mol/L. Depending on the experiment, the surfactant concentration (**Table 13**, entries 1-3), the concentration of the organic base (entries 4-6), the catalyst loading (entries 7-8), the Hydrophilic/ Lipophilic Balance (HLB) of the surfactant system (entry 9), the temperature (entry 10), the atmosphere (entry 11) and the functionalities between reaction counterparts (entries 12-13) vary.

A representative experimental procedure for entry 4 is given as an example: 2,7-dibromo-9,9-dioctylfluorene (137 mg, 0.25 mmol), 2-thienylboronic acid (64 mg, 0.50 mmol) and Pd(dtbpf)Cl2 (6.5 mg, 0.01 mmol) were weighed in the vial and then 0.5mL of Kolliphor EL 2 wt% solution in

water was added. The mixture was stirred and allowed to homogenize for 5 min before addition of the NEt_3 (152 mg, 1.50 mmol). All reactions were quenched after 12 h of stirring at room temperature, extracted with CH_2Cl_2, filtered over a pad of silica gel and submitted to GC-MS characterization. For entry 4 we proceeded with further purification of the product through column chromatography using a mixture of petroleum ether/CH_2Cl_2 (9:1) as eluent. The pure product was obtained in 80% yield (111 mg, 0.20 mmol).

3.1.4.3. General Synthetic Procedure for the Polymerizations

3.1.4.3.1. Synthesis of PF8T2 Control Sample

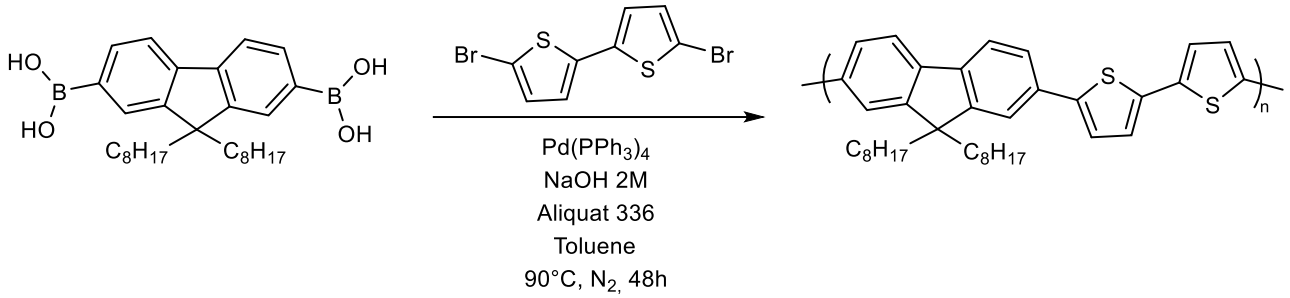

The reaction was carried out according to literature conditions under inert atmosphere using Schlenck technique.

In a 50 mL two-necks round flask 5,5'-dibromo-2,2'-bithiophene (161.8 mg, 0.5 mmol) and 9,9-dioctylfluorene-2,7-diboronic acid (239.2 mg, 0.5 mmol) were dissolved in 11 mL of anhydrous toluene after three vacuum/N2 cycles. Then 13mg of the phase transfer catalyst, Aliquat 336 were added followed by 2mL of 2M aqueous NaOH. After the addition of Pd(PPh3)4 (5.8 mg, 0.005 mmol), the reaction mixture was stirred at 90 °C for 48 h. To provide defined end groups phenylboronic acid (137 mg, 2.2 eq), and after 2 h bromobenzene (176 mg, 2.2 eq) were added. After stirring for further 2 h the polymer was precipitated in methanol (60 mL), filtered and subsequently submitted to soxhlet extraction with MeOH, acetone, heptane and chloroform in order to remove the eccess of end-capping reagents, catalyst residues and oligomers. The polymer was obtained in 94% yield (261 mg, 0.472 mmol).

Calculation of the E-factor

	n (mmol)	mass (g)	volume (mL)	density ($g\,mL^{-1}$)
9,9-dioctylfluorene-2,7-diboronic acid	0.5	0.2392		
5,5′-dibromo-2,2′-bithiophene	0.5	0.1618		
NaOH 2 M in H_2O	4	2.16	2.00	1.08
$Pd(PPh_3)_4$	0.005	0.0058		
Aliquat 336		0.013		
toluene		9.537	11	0.867
Termination and purification				
phenylboronic acid		0.137		
bromobenzene		0.176		
methanol		47.52	60	0.792
PF8T2	0.472	0.261		
Waste and E_{factor}				
Waste (purification excluded): 11.8558 g. $E_{factor} = 45.4$				
Waste (purification included): 59.6888 g. $E_{factor} = 229$				

3.1.4.2.2. Synthesis of PF8BT Control Sample

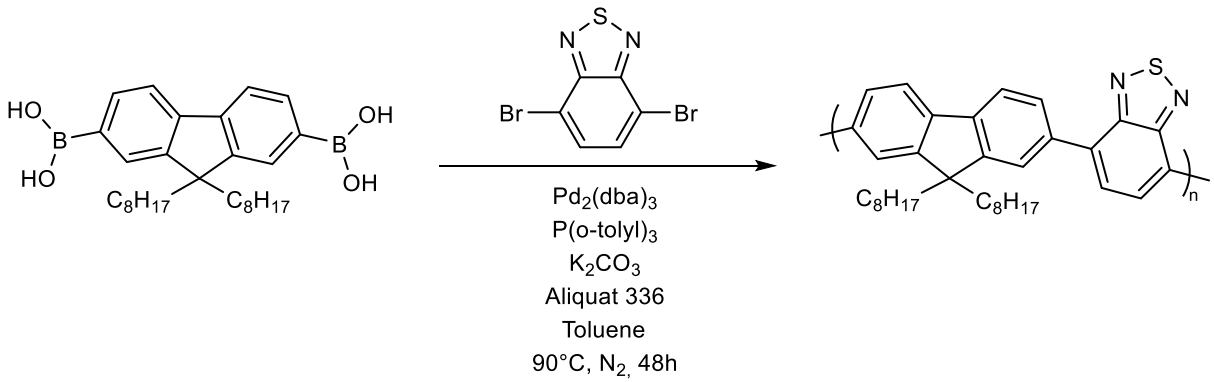

The reaction was carried out according to literature conditions under inert atmosphere using Schlenck technique.
In a 50 mL two-necks round flask 4,7-dibromo-2,1,3-benzothiadiazole (147.7 mg, 0.5 mmol) and 9,9-dioctylfluorene-2,7-diboronic acid pinacol ester (321.7 mg, 0.5 mmol) were dissolved in 3.6 mL of anhydrous toluene after three vacuum/N2 cycles. Then 103mg of the phase transfer catalyst, Aliquat 336 were added followed by 1.25 mL of 3.6 M aqueous K_2CO_3. After the addition of $Pd_2(dba)_3$ (4.6 mg, 0.005 mmol) and P(o-tolyl)$_3$ (3.4 mg, 0.0113 mmol), the reaction mixture was stirred at 90 °C for 48 h. To provide defined end groups phenylboronic acid (646 mg, 10.5 eq), and after 2 h bromobenzene (829 mg, 10.5 eq) were added. After stirring for further 2 h the reaction mixture was diluted with 8 mL of dichloromethane, filtered, and subsequently precipitated in methanol (40 mL). Precipitated polymer was filtered and submitted to soxhlet extraction with MeOH, acetone, heptane and chloroform in order to remove the eccess of end-capping reagents, catalyst residues and oligomers. The polymer was obtained in 90% yield (234 mg, 0.448 mmol).

Calculation of the E-factor

	n (mmol)	mass (g)	volume (mL)	density (g mL^{-1})
9,9-dioctylfluorene-2,7-diboronic acid pinacol ester	0.5	0.3217		
4,7-dibromo-2,1,3-benzothiadiazole	0.5	0.1477		
K_2CO_3 3.6 M in H_2O	4.5	1.725	1.25	1.38
$Pd_2(dba)_3$	0.005	0.0046		
P(*o*−tolyl)$_3$	0.0113	0.0034		
Aliquat 336		0.103		
toluene		3.12	3.6	0.867
Termination and purification				
phenylboronic acid		0.646		
bromobenzene		0.829		
DCM		10.64	8	1.33
methanol		31.68	40	0.792
PF8BT	0.448	0.234		
Waste and E_{factor}				
Waste (purification excluded): 5.1914 g. $E_{factor} = 22.2$				
Waste (purification included): 48.9864 g. $E_{factor} = 209$				

3.1.4.2.3. General Synthetic Procedure for the Optimization of the Polymerization Method in Micellar and Emulsion Environment

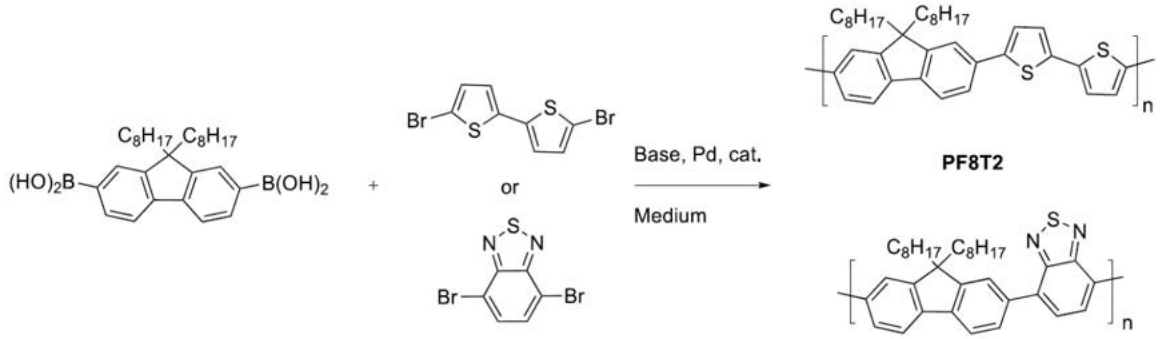

All the polymerizations were carried out in a 5mL CEM microwave glass tube vial under magnetic stirring at 1000 rpm and at a nominal concentration for the monomers of 0.25 mol/L. Depending on the experiment, the medium and the temperature (**Table 14**, entries 2-5 and 7-9) vary.

A representative experimental procedure for entry 5 is given as an example: 9,9-dioctylfluorene-2,7 diboronic acid (239.2 mg, 0.5 mmol), 5,5'-dibromo-2,2'-bithiophene (162.0 mg, 0.5 mmol), and Pd(dtbpf)Cl_2 (13 mg, 0.02 mmol) were weighed in the vial and then 2 mL of Kolliphor EL 2 wt%/toluene 9:1 oil-in-water emulsion was added. The mixture was stirred and allowed to homogenize for 5 min at 80 °C, heating with an oil bath, before addition of the NEt_3 (304 mg, 3.0 mmol). After the addition of the base, the reaction mixture was stirred at 80 °C for 48 h. To provide defined end-groups phenylboronic acid (183 mg, 3 eq.), and after 2 h bromobenzene (157 mg, 3 eq.) were added. After stirring for further 2 h the polymer was precipitated in methanol (10 mL) and then submitted to soxhlet extraction with MeOH, acetone, heptane, and chloroform in order to remove the excess of end-capping groups, catalyst residues and oligomers. The polymer was obtained in 87% yield (240 mg, 0.434 mmol).

Calculation of the E-factor for the Synthesis of PF8T2 in Micellar Conditions

	n (mmol)	mass (g)	volume (mL)	density ($g\,mL^{-1}$)
9,9-dioctylfluorene-2,7-diboronic acid	0.5	0.2392		
5,5′-dibromo-2,2′-bithiophene	0.5	0.1620		
NEt_3	3.0	0.304		
Pd(dtbpf)Cl_2	0.02	0.0130		
Kolliphor EL 2 wt% in water		1.8	1.8	1.0
toluene		0.173	0.2	0.867
Termination and purification				
phenylboronic acid		0.183		
bromobenzene		0.157		
methanol		7.92	10	0.792
PF8T2	0.434	0.240		
Waste and E_{factor}				
Waste (purification excluded): 2.4512 g. $E_{factor} = 10.2$				
Waste (purification included): 10.7112 g. $E_{factor} = 44.6$				

Calculation of the E-factor for the Synthesis of PF8BT in Micellar Conditions

	n (mmol)	mass (g)	volume (mL)	density ($g\,mL^{-1}$)
9,9-dioctylfluorene-2,7-diboronic acid	0.5	0.2392		
4,7-dibromo-2,1,3-benzothiadiazole	0.5	0.1470		
NEt_3	3.0	0.304		
Pd(dtbpf)Cl_2	0.02	0.0130		
Kolliphor EL 2 wt% in water		1.8	1.8	1.0
toluene		0.173	0.2	0.867
Termination and purification				
phenylboronic acid		0.183		
bromobenzene		0.157		
methanol		7.92	10	0.792
PF8BT	0.450	0.235		
Waste and E_{factor}				
Waste (purification excluded): 2.4412 g. $E_{factor} = 10.4$				
Waste (purification included): 10.7012 g. $E_{factor} = 45.5$				

3.2. Synthesis of 3D Conjugated Porous Polymers (CPPs) by Sustainable Suzuki-Miyaura Polycondensation in Water and under Air

3.2.1. Introduction

The last part of this Thesis work entails the extension of the previously developed sustainable synthetic method of surfactant enhanced S-M polycondensations in water to the preparation of conjugated porous polymeric 3D networks. Currently, porous materials cover a large area of applications including gas adsorption, storage, separation, heterogeneous catalysis, biological functions and so forth.[35] Conjugated porous polymers (CPPs) are a peculiar class of porous materials combining extended π-conjugation with (micro)porosity. This feature makes these materials excellent candidates for a wide range of potential applications in energy related areas, such as light-harvesting, fluorescence enhancement, batteries, supercapacitors, photocatalysis, sensing, or solar fuels production.[36] The defining characteristics of CPPs are the surface area and the pore size distribution, together with the electronic structure of the conjugated skeleton. Recently, band-gap control of CPPs with tuneable optical and electrical properties has also been addressed for potential applications in solar cells and OLED devices.[35]

Recent literature describes a wide range of synthetic building blocks and network-forming reactions to construct a wide variety of CPPs with different properties and structures.[35] Considering the enormous potential of such materials on economically favourable organic functional devices for everyday life, they should be readily available at the industrial scale through sustainable processes. A reduction in the E-factor by 1 or even 2 orders of magnitude in the syntheses of CPPs is strictly required to achieve such goal. Actually, no reports on the extension of surfactant enhanced chemistry to the synthesis of CPPs is documented in the literature. Previously, we demonstrated that the use of the lately developed emulsion S-M polycondensation protocol successfully meets these requirements for two well-known representative (opto)electronic linear conjugated polymers - PF8T2 and PF8BT - without altering structural characteristics or properties. Thus, we decided to extend the method to prepare representative CPPs having structural and electronic characteristics closely related to those of PF8T2 and PF8BT.[13] In particular, the synthetized structures are their corresponding 3D networks (**Figure 107**): poly(9,9-spirobifluorene-2,2',7,7'-alt-bithiophene (PSBFT2) and poly(9,9-spirobifluorene-2,2',7,7'-alt-benzothiadiazole (PSBFBT).

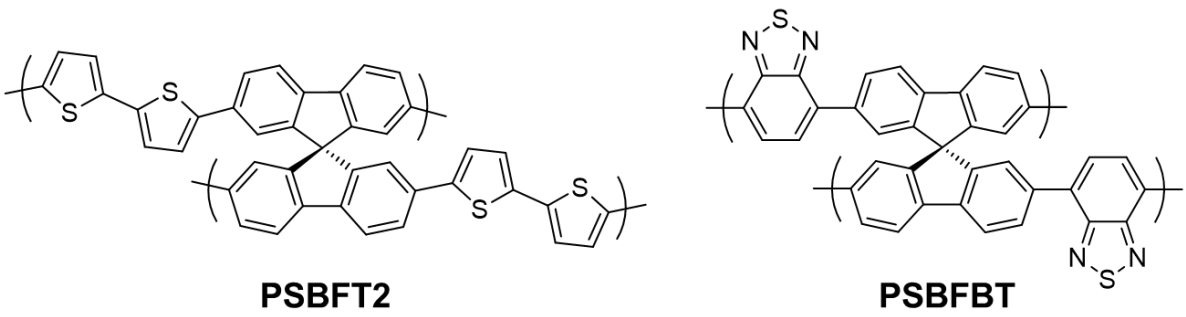

Figure 107. *Chemical structures of poly(9,9-spirobifluorene-2,2',7,7'-alt-bithiophene (PSBFT2) and poly9,9-spirobifluorene-2,2',7,7'-alt-benzothiadiazole) (PSBFBT).*

Subsequently, we synthetized other SBF-based CPPs with chemical structures related to that of PSBFBT (donor-acceptor) but with modulated electronic structures in order to have a more complete

set of materials (full donor, donor-acceptor, and borderline systems) with tuneable (opto)electronic properties and possible selective gas adsorption/storage capabilities. Indeed, the net dipole moment possessed by the building blocks of such networks, given by the alternation of D-A fragments, could lead to a greater efficiency in gas adsorption, storage, and separation, because of specific supramolecular interactions (for example, with CO_2). In details, the functional edge π-blocks of choice were bithiophene (donor), dithienylbenzothiadiazole and dithienyldifluorobenzothiadiazole (boederline systems with different electron donating/releasing capabilities), benzothiadiazole and difluorobenzothiadiazole (acceptors with different strengths). The fluorination effect as already been studied but on different networks. The fluorine atom is isostere of hydrogen, thus electronic structure change without affecting the pore size distribution.[37] Besides, for all the emulsion-synthetized networks, the corresponding linear polymeric structure is reported in literature with well-documented (opto)electronic properties.[38–40]

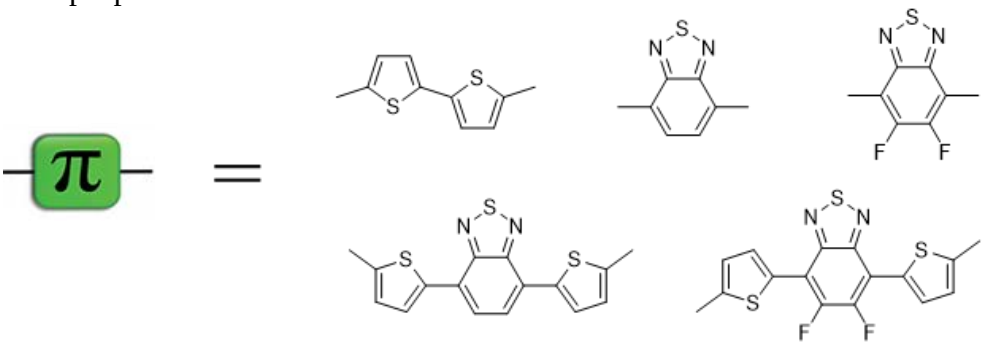

Figure 108. *Chemical structures of the edge building blocks used for the synthesis of the CPPs.*

To the best of our knowledge, we here present the first study on the use of micellar catalysis as a tool to carry out efficient S-M polymerization reactions with minimal amount of organic solvents and under standard laboratory environment for the synthesis of conjugated and porous polymeric materials.

Note: Unfortunately, due to the actual health emergency related to COVID-19, it was not possible to complete the entire study as planned; thus, evaluate if the novel sustainable approach enables to prepare same (or better) quality materials as those prepared in homogenous phase by standard literature protocols, while at the same time reducing the overall E-factor of the process. However, further studies within the research group are still under investigation in order to have a general description and overview for potential applications.

3.2.2. Results and Discussion

The work here presented started at Cardiff University under the supervision of Prof. Davide Bonifazi, where the syntheses of the CPPs and the first part of their characterization were performed. The second part of the work regarding gas adsorption capabilities and pore size measurements were performed in collaboration with Prof. Angiolina Comotti of the University of Milano-Bicocca.

3.2.2.1 Synthesis of the Branch-Core Monomers

The majority of the CPPs reported in the literature have been synthesized by conventional transition-metal-catalysed C-C coupling reactions in organic solvents.[35] The structures and properties of our selected compounds PSBFT2 and PSBFBT have already been reported by very recent literature. The

former compound is reported to be synthetized by standard DHAP protocols or via oxidative polymerization from the tetra-thiophene substituted SBF derivative as the reactive monomer,[41–43] while the latter is reported to be synthetized by standard S-M polycondensation protocol.[44] Both materials possess the SBF core, which acts as branch centre in the final network, alternated at the 2,2',7,7' positions with the 2,2'-bithiophene or 2,1,3-benzothiadiazole unit. The use such building-blocks have been rarely used for synthesis of 3D polymers until recently.[35]

In our previous work related to the synthesis of spiro-OMeTAD (chapter 2, paragraph 2.8.2.1.) we introduced a novel, sustainable and efficient route to access the SBF core in a single reaction step using only a stoichiometric amount of organic solvent. Thus, the method increases the scope of the work considering that the precursor monomer required for the synthesis of the CPPs can in turn be prepared through sustainable approaches. **Figure 109** takes up the reaction under consideration.

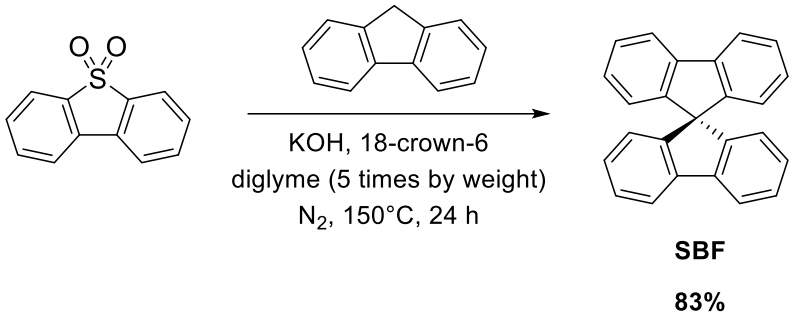

Figure 109. *Reaction scheme of the sustainable aromatic metamorphosis developed to access the SBF core.*

In order to efficiently extend the conjugation of the SBF core through the developed S-M polycondensation emulsion approach it is necessary to functionalize properly the reacting building blocks. Considering our previous study of screening of reaction conditions on the model reaction between the S-M coupling of 9,9-dioctylfluorene and thiophene units, we demonstrated the strong impact of "which unit bears which functionality" on the reaction outcome.[13] In details, we observed that the reaction is particularly efficient (99% of conversion) only when the 9,9-dioctylfluorene unit bears the boronic acid functionality, while the thiophene unit bears the bromide functionality. The rationalization of such observation lies on the well-known tendency of thienyl-2-boronic acid to be susceptible to protodeborylation, thus limiting the possibility to achieve complete conversion. Moreover, considering that we are working on a microheterogeneous environment, where most of the organic transformations are supposed to take place within the internal lipophilic core of the aggregates, it is not excluded that some of them can also happen close to the interphase region. The fact the doubly boronic acid functionalized fluorene unit can most likely be near the interface is coherent. This is because the specie who brings the boronic acid functionality is an ionic specie in the alkaline working conditions (NEt_3 is present), thus a di-anionic fluorene specie is more prone to localize at the interface with water than a mono-anionic thiophene specie. Therefore, in accordance with our previous results, we decided to use the 2,2',7,7'-tetrakis(4,4,5,5-tetramethyl-1,3,2-dioxaborolan)-9,9'-spirobifluorene (SBF-4Bpin) derivative as reactive specie to construct the π-extended porous networks of interest. Such derivative can be prepared by brominating the SBF core, to give 2,2',7,7'-tetrabromo-9,9'-spirobifluorene (SBF-4Br), eventually turned in the tetra boronpinacolate building block SBF-4Bpin by a Miyaura borylation. For the bromination step we already developed a sustainable and efficient alternative protocol to access the SBF-4Br derivative in water using the micellar enhanced approach (all the details are reported in the previous chapter 2, paragraph 2.8.2.2.). **Figure 110** takes up the reaction under consideration.

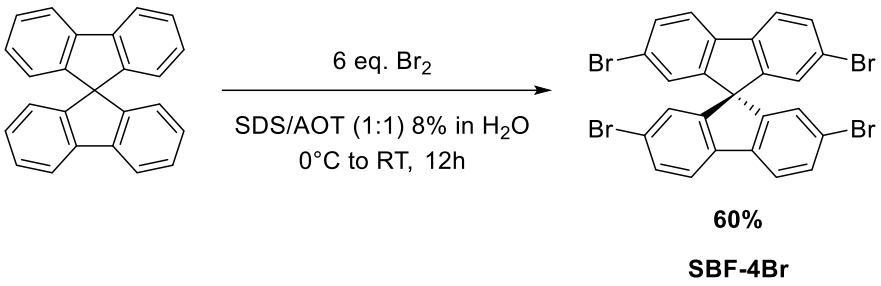

Figure 110. *Reaction scheme of the sustainable tetra-bromination of the SBF core in water.*

Also, for the Miyaura borylation required to access SBF-4Bpin we here propose a sustainable alternative method compared to the classical process reported in the literature.[45] Our method allows to carry out the reaction in very little organic solvent (5 times the weight of the SBF-4Br substrate) leading to a reduction of the E-factor with respect to the literature process by a factor 5. Furthermore, the SBF-4Bpin product is obtained with a higher yield than the reported for the classical method (73% vs 64%).[45] **Figure 111** shows a direct comparison between our method and that reported in the literature for the synthesis of SBF-4Bpin.

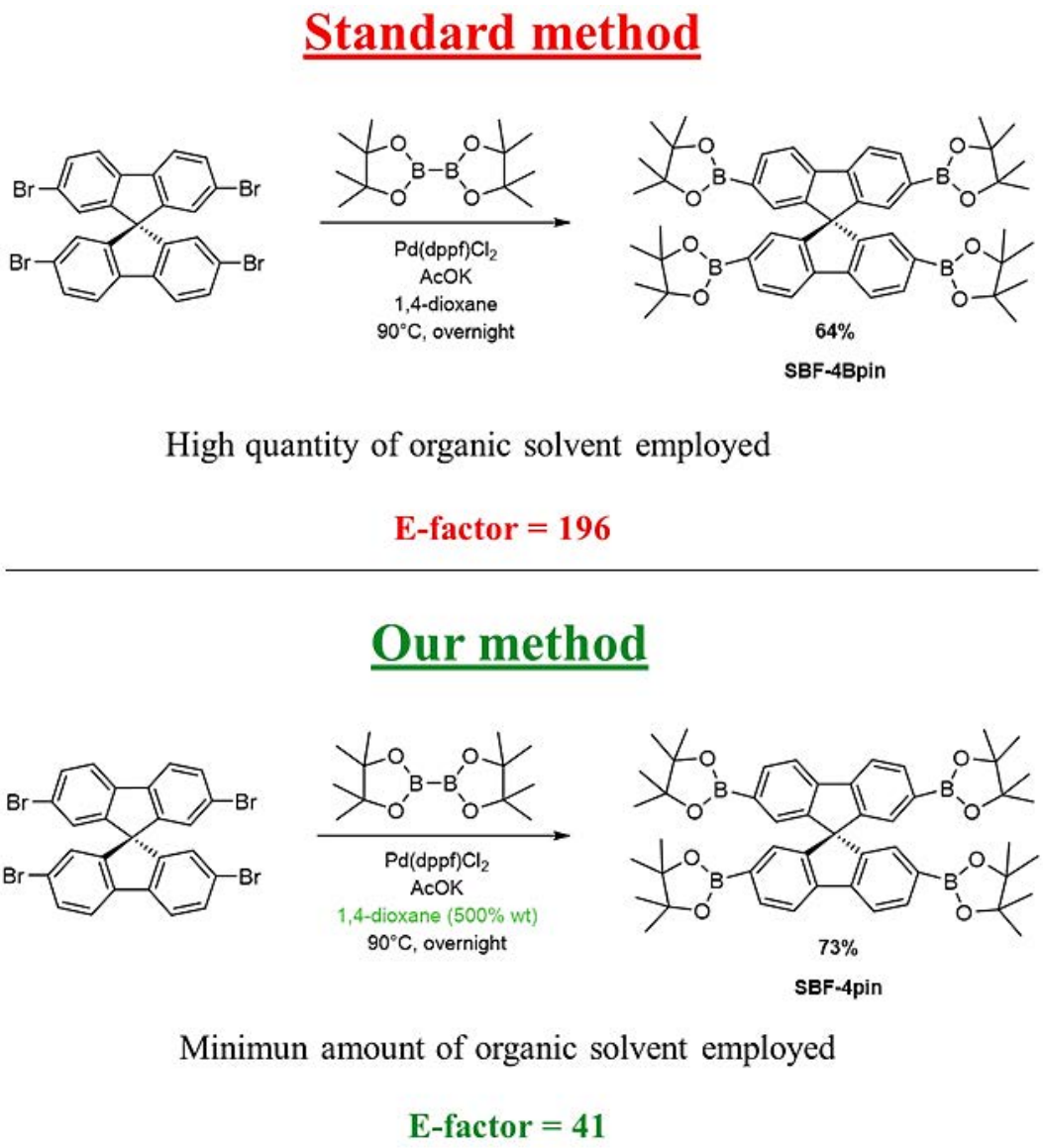

Figure 111. *Reaction scheme of the Miyaura tetra-borylation for the synthesis of SBF-4Bpin of both the literature standard conditions and our method in bulk.*

Then, we decided to prepare another branching center, still based on SBF core but functionalized with a thiophene unit at the reactive positions 2,2',7,7'. As previously explained, in addition to the synthesis of the conjugated and porous polymeric networks PSBFT2 and PSBFBT, we also wanted to extend the method to the preparation of other structurally similar conjugated and porous polymers but having different electronic structures and HOMO/LUMO energy levels (ranging from full donor and donor/acceptor to borderline systems) in order to have a more complete set of materials with tuneable optoelectronic properties and gas-interacting capacities. The second branching unit synthetized is the 2,2′,7,7′-tetrakis(5-bromo-thiophene-2yl)-9,9′-spirobifluorene (SBF-4Th-4Br). We did not proceed with further Miyaura borylation of such derivative since α-thienylboronic acids/esters derivatives are not stable with relative high tendency to protodeborilation under reaction conditions. **Figure 112** show the synthetic scheme for the preparation of SBF-4Th-4Br.

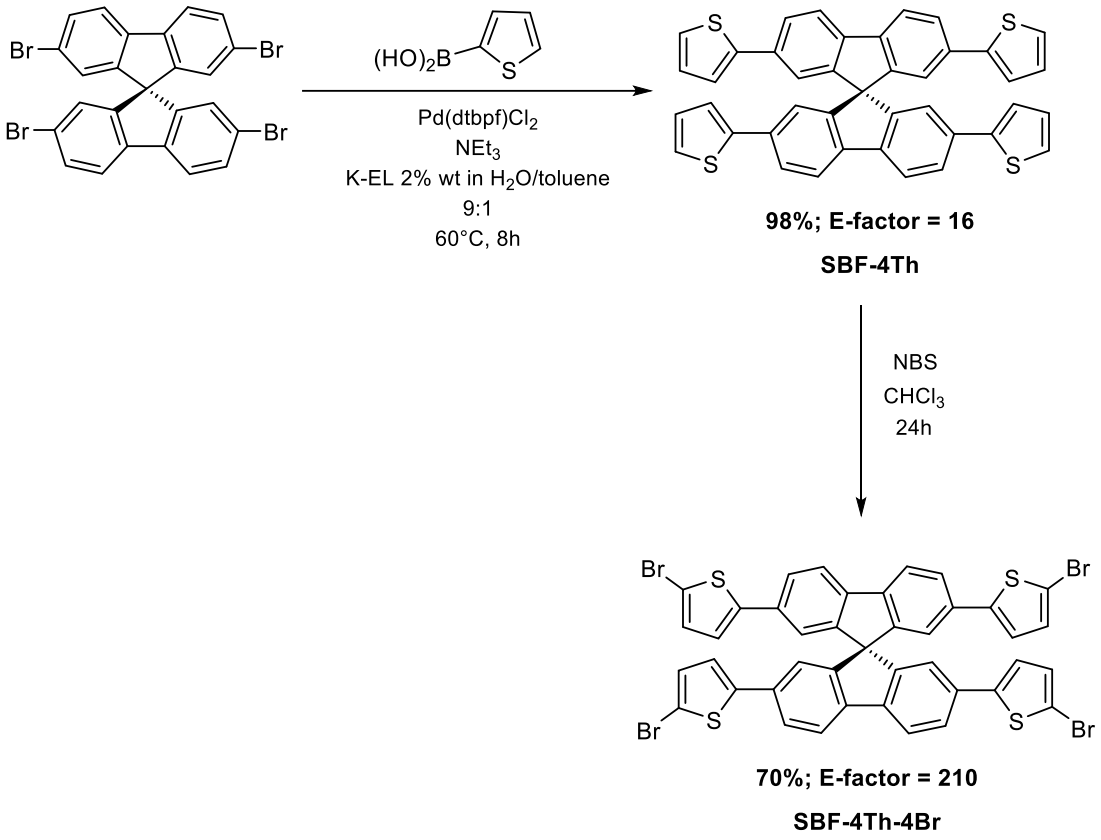

Figure 112. *Reaction scheme of the synthesis of SBF-4Th-4Br as second branch core monomer.*

The first step involves a tetra S-M cross-coupling reaction between SBF-4Br and 2-thienylboronic acid. The reaction was performed using Pd(dtbpf)Cl_2 as catalyst in K-EL 2%/toluene 9:1 v/v emulsion conditions at 60°C for 8h. The product SBF-4Th was obtained in 98% yield and high purity after only a simple filtration over a pad of SiO_2. The E-factor of the process is only 16. For this reaction, the emulsion revealed to be the best choice, since the same reaction performed in both only K-EL or K-EL/Span 80 7:3 gave ^{1}H-NMR conversions to product to nearly 80% and required a column chromatography to isolate the product. The second step is the tetrabromination reaction of SBF-4Th with NBS according to standard procedures. The final branching unit monomer SBF-4Th-4Br was obtained in 70% yield. Our method gave far better results in terms of yield (70% vs 40%) and overall E-factor (226 vs 1415) comparted with that reported in literature.[46] Since the second step is the same as the literature one,[46] all the difference lies on the first step, for which we did not need to recourse to an elaborate chromatographic column.

3.2.2.2 Emulsion S-M Polycondensations to Access CPPs

For the synthesis of the model networks PSBFT2 and PSBFBT we first repeated the standard literature procedures in homogenous phase in order to have a direct comparison with our surfactant enhanced method.[44] Still, the only variation we did with respect to the literature protocol is that we used toluene instead of DMF as organic solvent and we worked at 90°C instead of 150°C. The reason lies on the fact that DMF at 150°C decomposes and moreover, under such condition the parasite protodeborylation side reaction is favoured. On the other hand, working with toluene at 90°C represents a better comparison with respect to our working conditions (oil-in-water emulsion of toluene at 80°C). **Figure 113** shows the S-M couplings in standard toluene/H_2O biphasic conditions for the synthesis of PSBFT2 and PSBFBT networks.

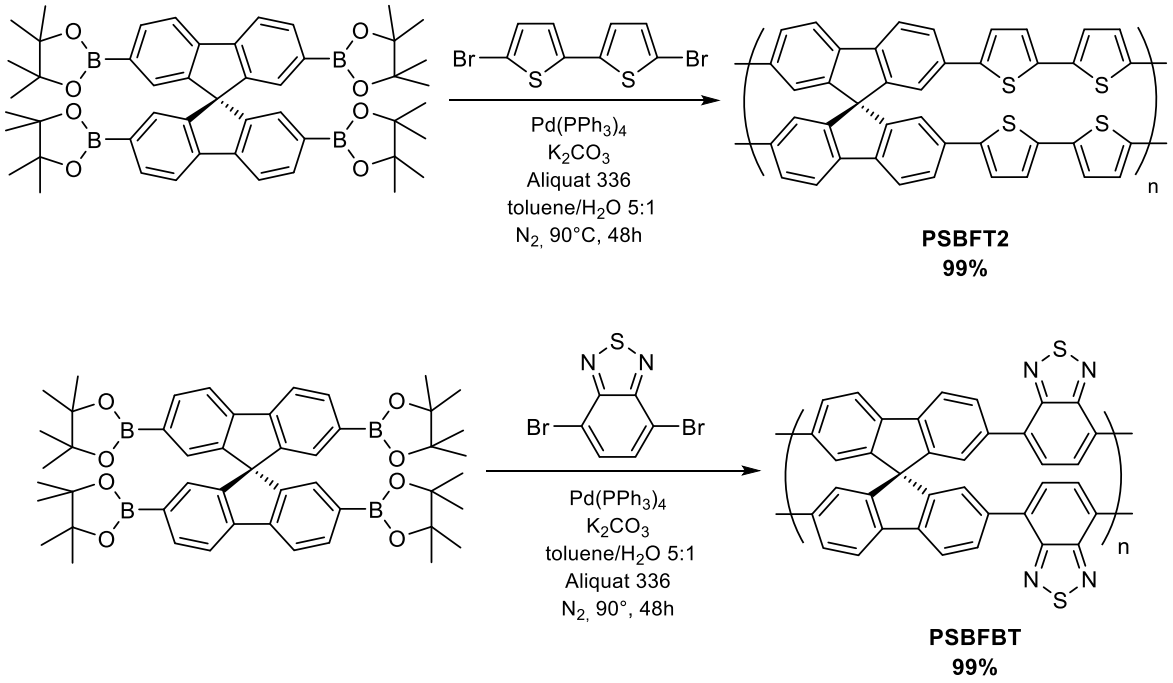

Figure 113. *Reaction schemes for the synthesis of PSBFT2 and PSBFBT in homogenous phase using toluene as solvent and working at 90°C instead of 150°C. Literature reference for the conditions.*[44]

Both the syntheses gave satisfactory results with yields up to 99% and in agreement with corresponding literature.[41,44] The materials were submitted to a purification protocol employed for all the subsequente examples and corresponding to the literature standard: a) all volatiles where removed from the reaction mixture; b) the residue was taken up with MeOH, filtered, washed with water (first at pH=4 using AcOH, then a pH=10 using $NaHCO_3$ and finally at neutral pH), and submitted to Soxhlet extractions (in all of the cases for 10 h) with MeOH, acetone, Heptane, and $CHCl_3$ c) the final polymer was finally taken up with THF and filtered. The recovered material was in all cases an insoluble powder. The E-factor for both polymers is around 300.

Later, we started performing the S-M polycondensations using the best conditions found in the previous work for the synthesis of PF8T2 and PF8BT. We repeated the synthesis of PSBFT2 and PSBFBT, together with other 3D networks with modulated electronic structures. All the polymerizations were carried out using SBF-4Bpin as the branching centre, a dibrominated derivative as edge building block (5,5'-dibromo-2,2'-bithiophene, 4,7-dibromo-2,1,3-benzothiadiazole, 4,7-dibromo-5,6-difluoro-2,1,3-benzothiadiazole, 4,7-bis(5-bromo-thiophene-2yl)-2,1,3-benzothiadiazole, and 4,7-bis(5-bromo-thiophene-2yl)-5,6-difluoro-2,1,3-benzothiadiazole), $Pd(dtbpf)Cl_2$ as the catalyst (2 mol% with respect to equivalent bromide), 6 equivalents of NEt_3 as

the base, and the emulsion obtained by mixing a 2 wt % K-EL solution in deionized water with a 10% vol. of toluene as reaction medium. Following **Figure 114** shows all the CPPs synthetized via the surfactant enhanced approach.

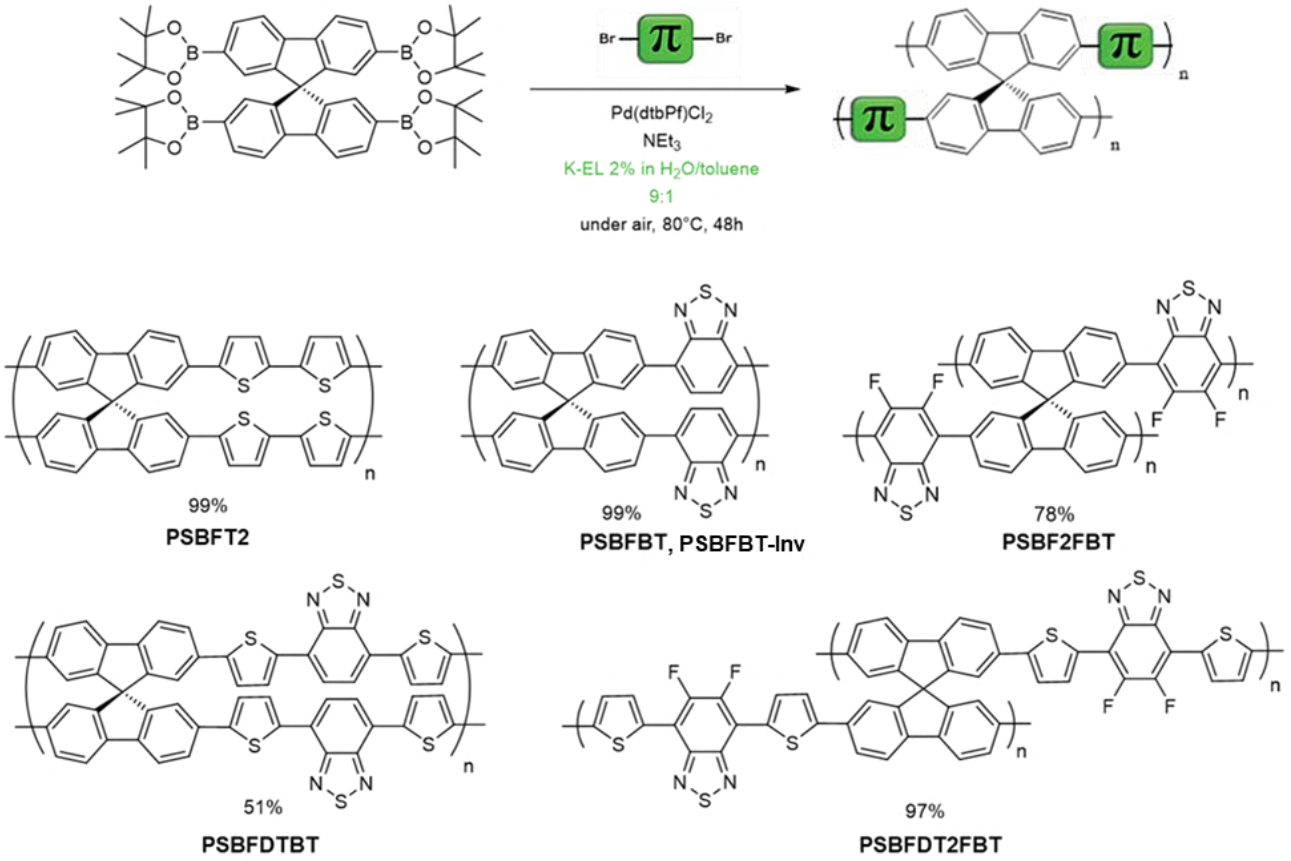

Figure 114. *Emulsion S-M polymerization conditions for the synthesis of CPPs and chemical structures of the synthetized the networks with corresponding yields.*

Compound PSBFBT was also synthetized with inverted functionalities, reacting 2,2',7,7'-tetrabromo-9,9'-spirobifluorene with 2,1,3-benzothiadiazole-4,7-bis(boronic acid pinacol ester, **Figure 115**) in order to investigate if this exchange could have an impact on the final material (labelled as PSBFBT-Inv). For the other CPPs this feature was not explored since the counterpart is thiophene and its corresponding boronic derivative is too much susceptible to protodeborylation. The materials were obtained in moderate to good yields and with E-factor values around 50. To date, the work has progressed to the molecular design and synthesis, structural characterization (see the next experimental section) including FT-IR spectroscopy, solid state ^{13}C-NMR spectroscopy, TGA analysis for thermal stability in both oxygenated and inert atmosphere, powder X-ray diffraction patterns, morphology of CPPs (collection of SEM images), and some prelaminar studies on porosity and gas adsorption characteristics which, however, are currently still under investigation. For these last features, up to now we investigated the samples PSBFT2, PSBFBT-Inv, and PSBF2FBT synthetized with our surfactant enhanced method. For the PSBFBT-Inv sample we studied the porosity by N_2 adsorption experiments. Its N2 adsorption isotherms at 77K is following reported: it exhibits typical type II adsorption−desorption isotherms, featuring a microporous and mesoporous structure.

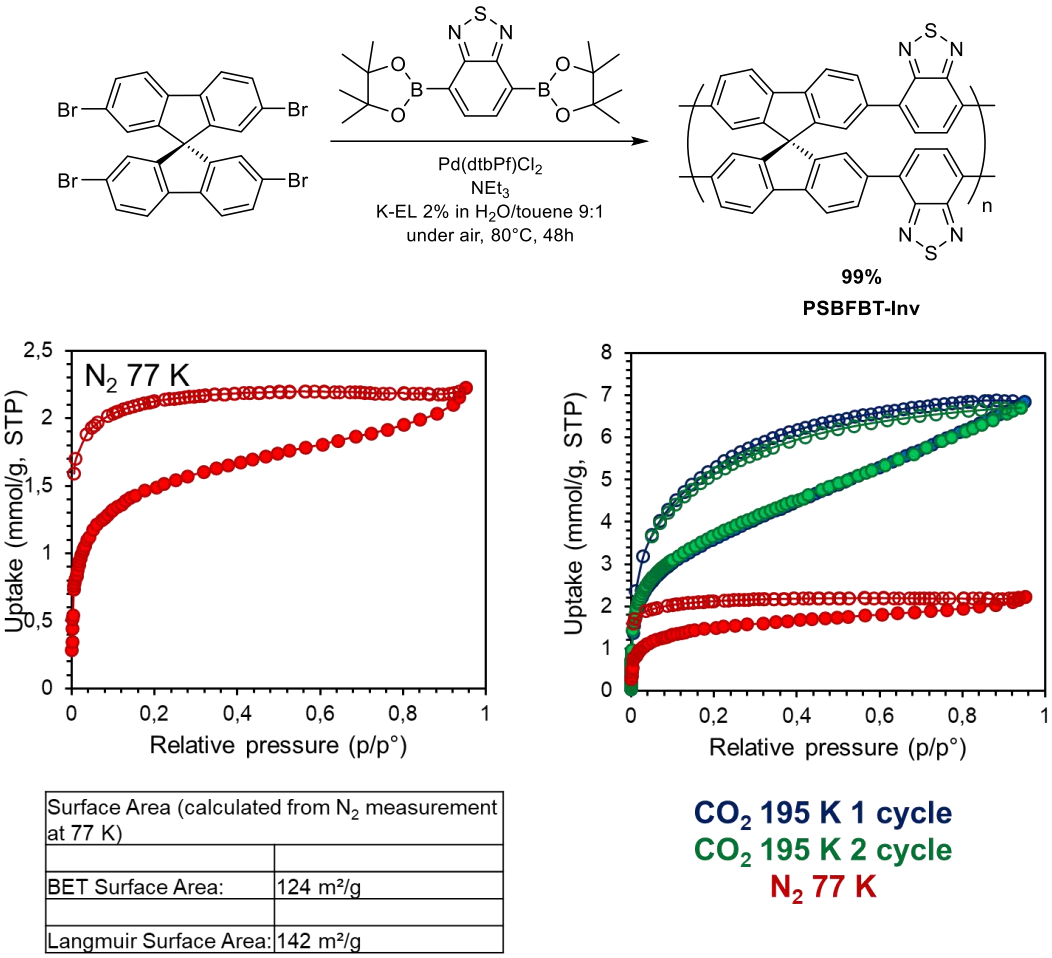

Surface Area (calculated from N_2 measurement at 77 K)	
BET Surface Area:	124 m²/g
Langmuir Surface Area:	142 m²/g

Figure 115. *N_2 adsorption isotherms of PSBFBT-Inv synthetized in emulsion.*

The Nitrogen adsorption isotherms at 77 K display very slow kinetics: the equilibration time has been extended to 20 seconds (usually 5 seconds) in order to reach the equilibrium for the first few points. The calculated surface area from N_2 measurement at 77 K was 124 m^2g^{-1} with the BET method, while 142 m^2g^{-1} with the Langmuir Surface Area method. The result is lower with respect to the literature value (BET= 305 m^2g^{-1} at 77 K)[39] for the same material synthetized in standard homogeneous-phase S-M polycondensation using DMF as solvent and working at 150°C, but in any case, lies in the same range order. However, the same framework displays conventional kinetics for CO_2 adsorption at 195 K. The CO_2 adsorption isotherms display high slope at low relative pressure (**Figure 116**) due to adsorption in accessible micropores (probably ultramicroporous in nature), and an uptake with constant slope (following Henry's law) possibly due to dissolution of CO_2 and swelling effect of the framework. The system can possibly be modelled following "dual-mode adsorption isotherm" considering its behaviour at both the low and high relative pressure regime. Unfortunately, there is not a literature comparison about the CO_2 adsorption characteristics of such material. This data will be compared in the future with our sample model synthesized under classical conditions in the homogeneous phase.

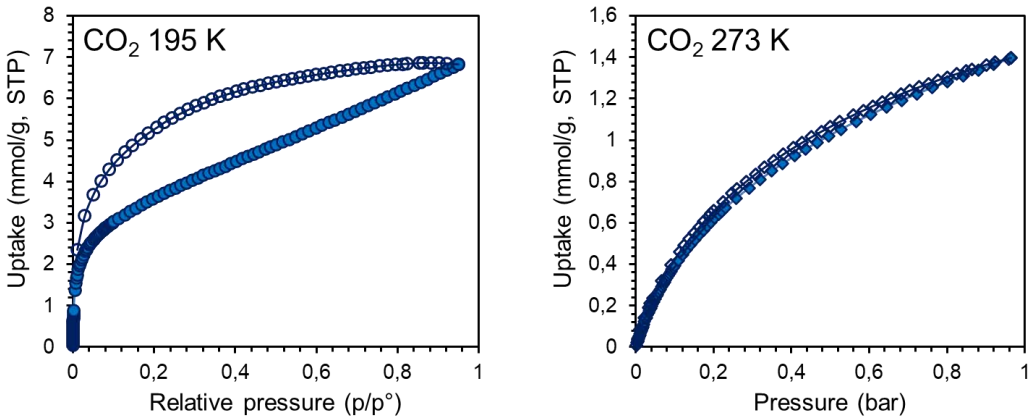

Figure 116. *CO_2 adsorption isotherms of PSBBT-Inv. synthetized in emulsion.*

Given the satisfactory result obtained for this sample concerning the CO_2 capability, we moved to explore the CO_2 absorption/desorption characteristics of the synthetized CPPs. Up to now, we managed to characterize only PSBFT2 and PSBF2FBT as additional materials to PSBFBT-Inv just discussed above. The corresponding CO_2 adsorption isotherms of PSBFT2 and PSBF2FBT are following reported in Figures **117** and **118**.

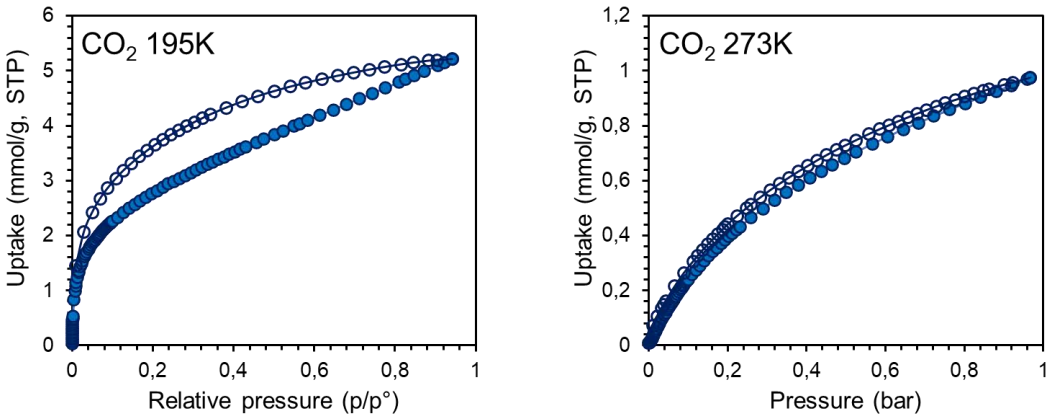

Figure 117. *CO_2 adsorption isotherms of PSBFT2 synthetized in emulsion.*

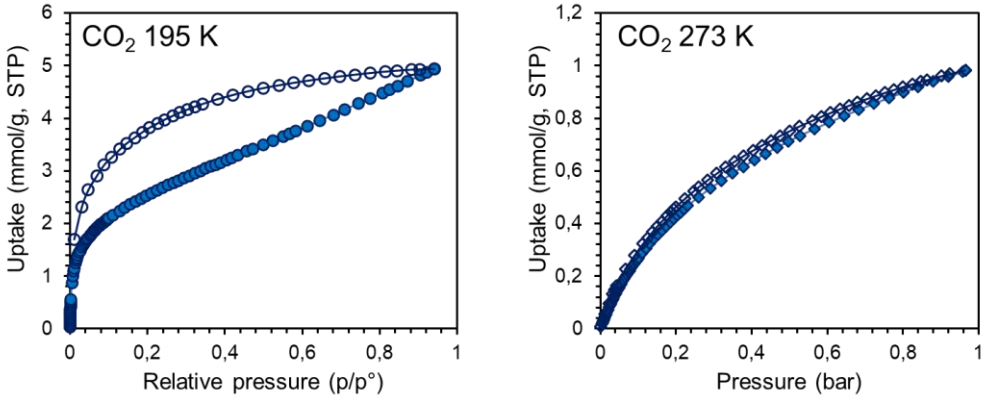

Figure 118. *CO_2 adsorption isotherms of PSBF2FBT synthetized in emulsion.*

This two latter samples PSBFT2 and PSBF2FBT, however, display lower CO_2 adsorption capacities compared with PSBFBT-Inv. The superposition is following reported (**Figure 119**).

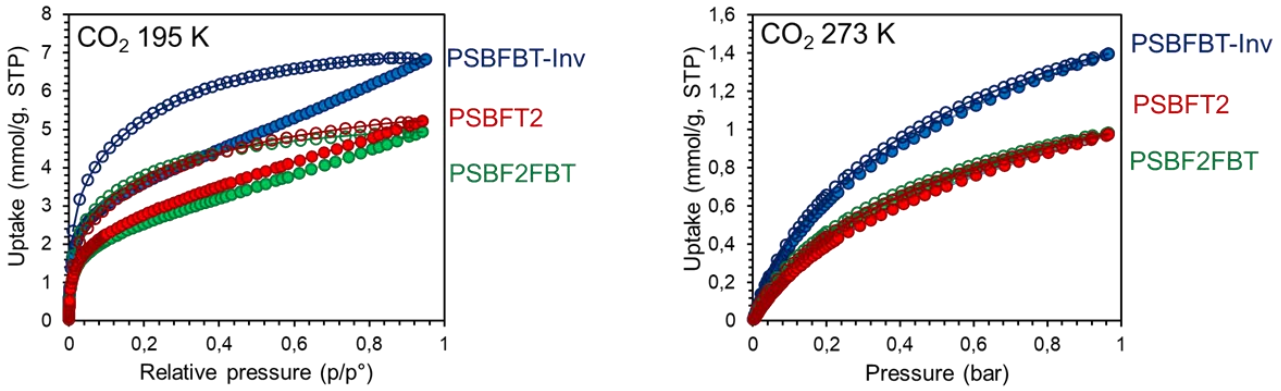

Figure 119. *Superposition of CO_2 adsorption isotherms of PSBFBT-INv, PSBFT2 and PSBF2FBT synthetized in emulsion.*

3.2.3. Conclusions

In conclusion, we have synthetized a set of conjugated porous polymeric networks with different electronic structures through the environmentally benign surfactant enhanced S-M polycondensations approach working in water and under air and leading to moderate to high yields. In particular, the full process can be considered sustainable as the branch core monomer was in turn be prepared through green chemistry compliant processes with an overall E-factor around 90 for all the materials. Structural characterizations of the CPPs are diagnostic and clearly describe the expected characteristics. We started investigating porosity and gas adsorption characteristics for some of the synthetized compounds but however, up to now we managed to collect only few data and work is still in progress. However, from the data we collect so far, we observed microporosity for all the studied materials with very slow kinetics for N_2 adsorption at 77 K. However, the frameworks display conventional kinetics for CO_2 adsorption at 195 K. The CO_2 adsorption isotherms display high slope at low relative pressure due to adsorption in accessible micropores (probably ultramicroporous in nature), and an uptake with constant slope (following Henry's law) possibly due to dissolution of CO_2 and swelling effect of the framework. Furthermore, the system can possibly be modelled following "dual-mode adsorption isotherm" considering its behaviour at both the low and high relative pressure regimes.

3.2.4. Experimental Section

3.2.4.1. Materials and Instruments

All reagents and chemical compounds were purchased from Aldrich, Fluorochem, or TCI Europe and used without any further purification. All solvents were obtained from commercial sources and used as received unless otherwise specified. Solid state 13C magic angle spinning nuclear magnetic resonance (MAS NMR) spectra were collected by a JEOL ECA 400 spectrometer. FT-IR spectra were recorded on a PerkinElmer Spectrum One FT-IR spectrometer. Thermo- gravimetric analyses were performed on a Pyris Diamond TGA (PerkinElmer) instrument, at a heating rate of 10 °C min^{-1} under both air or N_2 atmosphere from 30 to 800 °C. SEM imaging was carried out using a Zeiss SEM. Samples were prepared by depositing dispersion in iPrOH of samples on Si stubs and died under vacuum overnight. Powder X-ray diffraction patterns were obtained at 40 kV and 40 mA on a Bruker

Advanced D8 XRD using Cu−Kα radiation (λ = 1.5418 Å) over 2θ range of 5.0°-6.0° at room temperature. N_2 sorption experiments at 77 K up to 1 bar and CO_2 sorption experiments at 195 K and 273 K up to 1 bar were performed using a Micromeritics ASAP HD 2020 surface area and pore size analyzer. Before sorption analysis, samples were evacuated at 80 °C for 6 hours using a turbo molecular vacuum pump (vacuum pressure below 5 mmHg). Specific surface areas were calculated from N_2 adsorption data by multipoint BET and Langmuir analysis. Ultra-high-purity grade N_2 (99.999%) and CO_2 (99.995%) were used for all adsorption measurements. Helium (99.999%) was used to evaluate the free space.

3.2.4.2. Synthesis of 2,2',7,7'-tetrakis(4,4,5,5-tetramethyl-1,3,2 dioxaborolan)-9,9'-spirobifluorene (SBF-4Bpin)

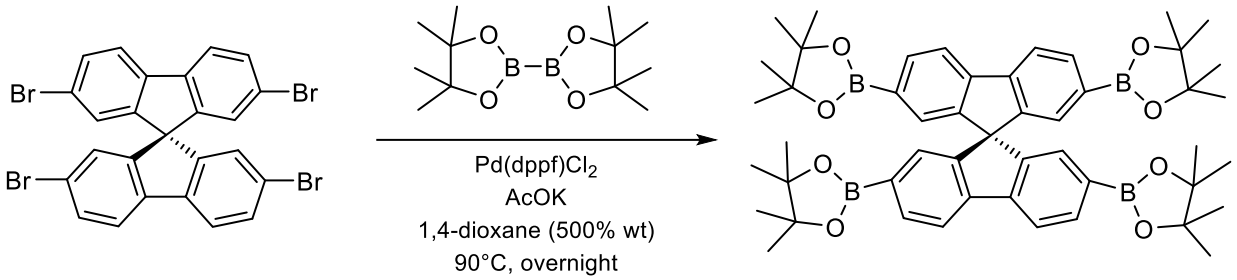

In a two neck round bottom flask 2,2',7,7'-tetrabromo-9,9'-spirobifluorene (6.003g, 9.50 mmol), bis(pinacolato)diboron (14.465g, 56.9 mmol), $Pd(dppf)Cl_2$ (0.556g, 0.76 mmol), AcOK (11.18 g, 119 mmol) were weighted. Then, after three vacuum/N2 cycles they were dissolved in 30 mL of anhydrous toluene. The reaction was heated at 90°C and stirred for 12h. The reaction was cooled and diluted with AcOEt (50 mL) and filter over a pad of celite. After the solvent was evaporated, the crude was recrystallized from THF (60 mL) to give pure product as a white powder (5.689 g, 73%).

^{1}H-NMR (400 MHz, $CDCl_3$): δ 7.85 (m, 8H), 7.09 (s, 4H), 1.25 (s, 48H).

^{13}C-NMR (125 MHz, $CDCl_3$): δ 148.16, 144.68, 134.54, 130.44, 113.68, 83.65, 65.57, 24.78.

3.2.4.3. Synthesis of 2,2′,7,7′-tetrakis(thiophene-2yl)-9,9′-spirobifluorene (SBF-4Th)

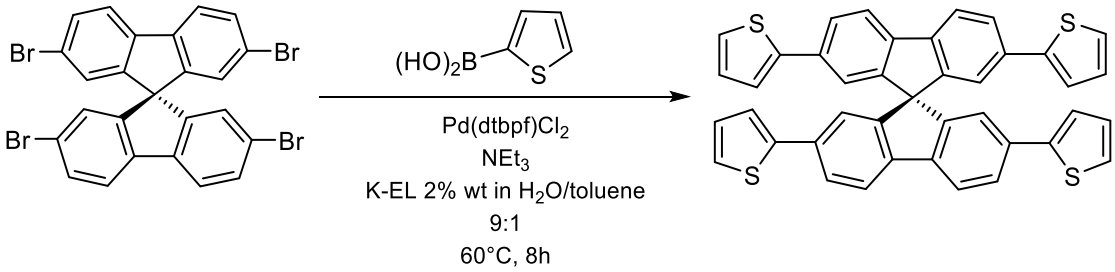

2,2',7,7'-tetrabromo-9,9'-spirobifluorene (1.005g, 1.58 mmol), 2-thienylboronic acid (1,012 g, 7.90 mmol) and $Pd(dtbpf)Cl_2$ (0.082 g, 0.01 mmol) were weighed in the vial and then 3.2 mL of Kolliphor EL 2 wt%%toluene 9:1 v/v emulsion was added. The mixture was stirred and allowed to homogenize for 5 min before addition of the NEt_3 (0.960 g, 9.48 mmol). The reaction was quenched after 8 h of

stirring at 60°C, extracted with CH_2Cl_2 and filtered over a pad of silica gel. The pure product was obtained in 98% yield (0.998 g, 98%).

^{1}H-NMR (400 MHz, $CDCl_3$) δ: 7.86 (d, J= 8.0 Hz, 4H), 7.66 (dd, J= 1.4, 7.8 Hz, 4H), 7.15 (m, 8H), 7.00-7.01 (d, J= 1.6 Hz, 4H), 6.94 (t, J= 4.4 Hz, 4H).

^{13}C-NMR (125 MHz, $CDCl_3$) δ: 149.3, 144.0, 140.5, 134.2, 127.7, 126.0, 124.6, 123.2, 121.3, 121.3, 120.4.

3.2.4.4. Synthesis of 2,2′,7,7′-tetrakis(5-bromo-thiophene-2yl)-9,9′-spirobifluorene (SBF-4Th-4Br)

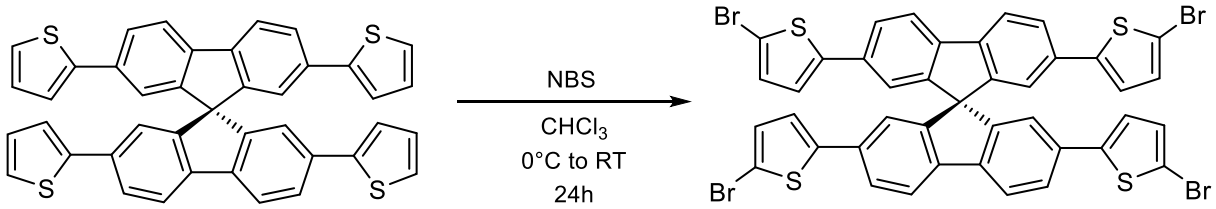

2,2′,7,7′-tetrakis(thiophene-2yl)-9,9′-spirobifluorene (0.900 g, 1.4 mmol) was dissolved in 30 mL of $CHCl_3$ and cooled to 0°C with ice bath. Then NBS (1.120 g, 6.29 mmol) was added slowly in portions. The reaction was stirred at the dark for 24h. The mixture was washed 3 times with 30mL of aq. solution of NaHCO3 and then with 30 mL od deionized water. The crude was dissolved in 40 ml of refluxed $CHCl_3$, then put in the freezer overnight. The pure product recrystallizes as yellow powder (0.928 g, 70%).

^{1}H-NMR (400 MHz, $CDCl_3$) δ: 7.91 (d, J= 8.0 Hz, 4H), 7.66 (dd, J= 1.4, 7.8 Hz, 4H), 6.9 (m, 12H),

^{13}C-NMR (125 MHz, $CDCl_3$) δ: 149.3, 145.4, 140.8, 133.7, 130.8, 126.0, 123.5, 121.0, 120.9, 111.5, 65.80.

3.2.4.5. Synthesis of PSBFT2 Control Sample in Standard Homogeneous Phase Conditions

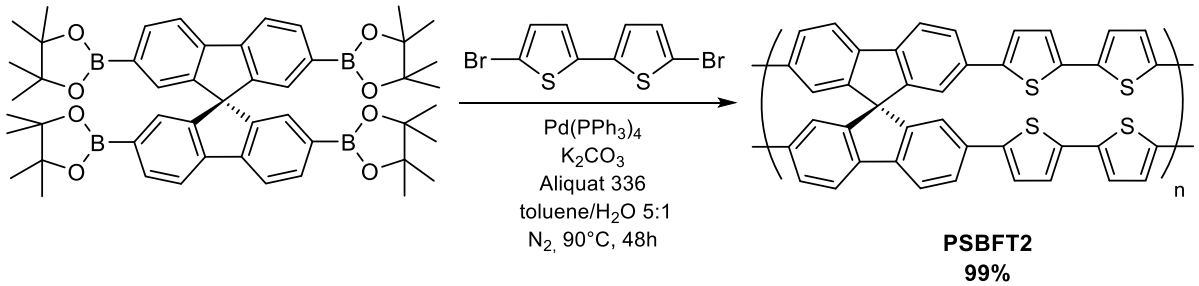

In a 50 mL two-necks round flask and 2,2’,7,7’-tetrakis(4,4,5,5-tetramethyl-1,3,2-dioxaborolan)-9,9’-spirobifluorene (0.500 g, 0.61 mmol) 5,5’-dibromo-2,2’-bithiophene (0.395 g, 1.22 mmol) were dissolved in 12 mL of anhydrous toluene after three vacuum/N_2 cycles. Then 30 mg of the phase transfer catalyst, Aliquat 336 were added followed by 2,5 mL of 2M aqueous K_2CO_3. After the addition of $Pd(PPh_3)_4$ (0.014 g, 0.01 mmol), the reaction mixture was stirred at 90 °C for 48 h. To provide defined end groups phenylboronic acid (137 mg, 2.2 eq), and after 2 h bromobenzene (176

mg, 2.2 eq) were added. After stirring for further 2 h the polymer was precipitated in methanol (60 mL), filtered, washed with water (at pH=4, then at pH=10 and finally neutral) and subsequently submitted to soxhlet extraction with MeOH, acetone, heptane, and chloroform in order to remove the eccess of end-capping reagents, catalyst residues and oligomers. The polymer was dispersed in THF, filtered, and obtained in 99% yield (387 mg, 0.60 mmol).

FT-IR Characterization

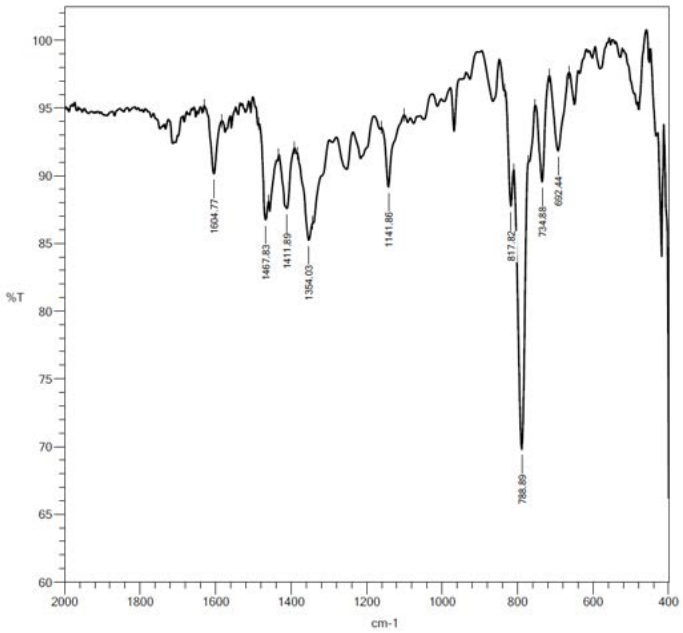

^{13}C Solid-State NMR Characterization

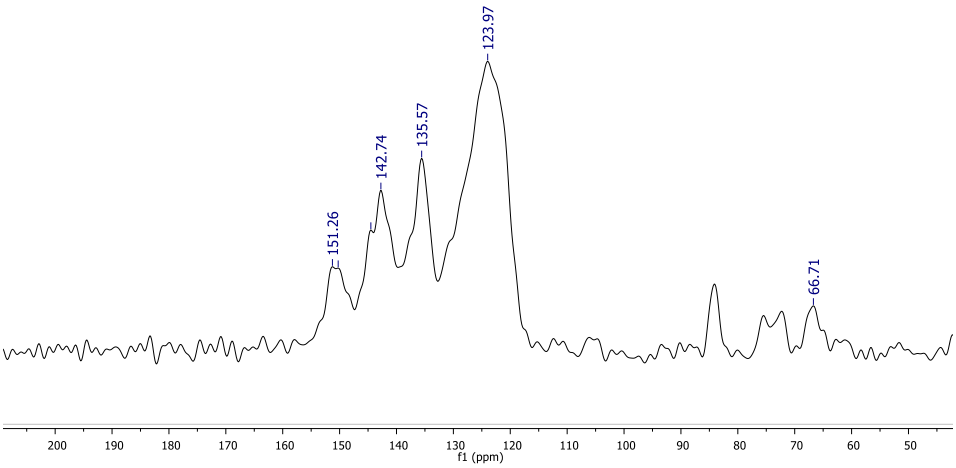

Powder XRD Characterization

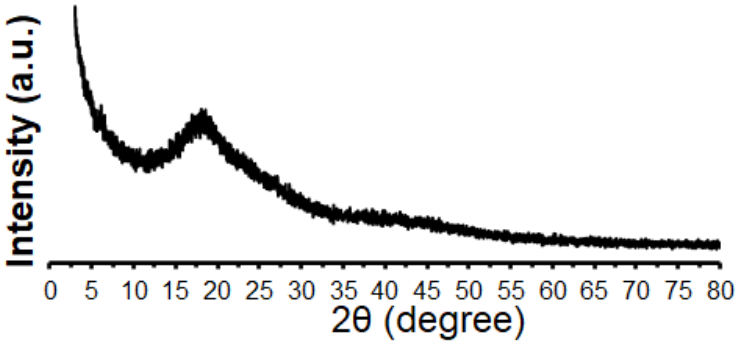

TGA Analysis

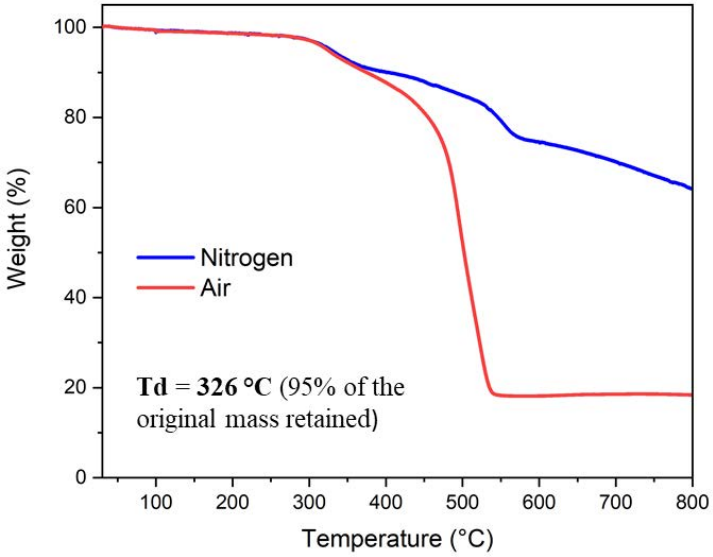

SEM Images

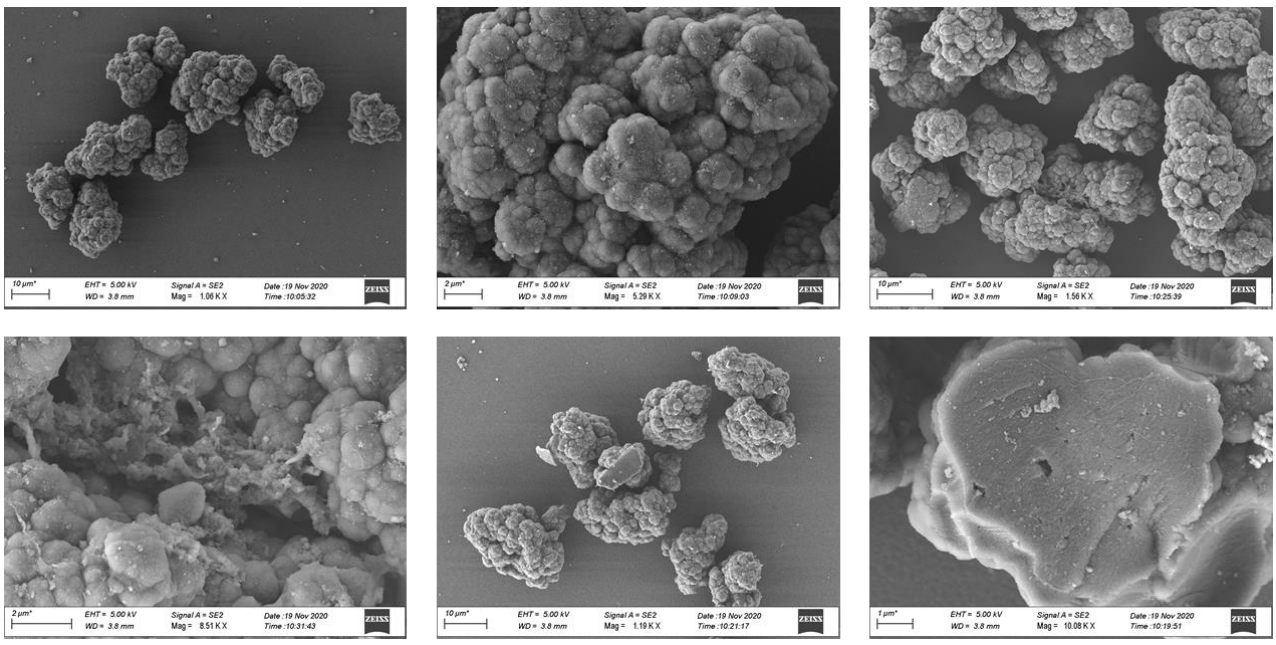

3.2.4.6. Synthesis of PSBFBT Control Sample in Standard Homogeneous Phase Conditions

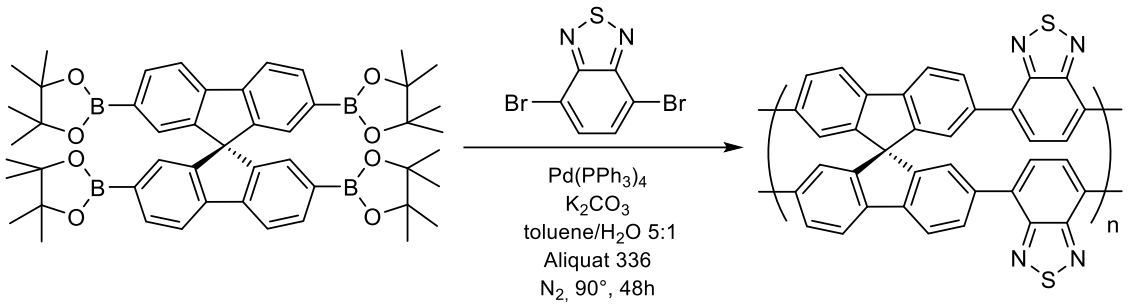

In a 50 mL two-necks round flask and 2,2',7,7'-tetrakis(4,4,5,5-tetramethyl-1,3,2-dioxaborolan)-9,9'-spirobifluorene (0.500 g, 0.61 mmol) 4,7-dibromo-2,1,3-benzothiadiazole (0.358 g, 1.22 mmol) were dissolved in 12 mL of anhydrous toluene after three vacuum/N_2 cycles. Then 30 mg of the phase transfer catalyst, Aliquat 336 were added followed by 2,5 mL of 2M aqueous K_2CO_3. After the addition of $Pd(PPh_3)_4$ (0.014 g, 0.01 mmol), the reaction mixture was stirred at 90 °C for 48 h. To provide defined end groups phenylboronic acid (137 mg, 2.2 eq), and after 2 h bromobenzene (176 mg, 2.2 eq) were added. After stirring for further 2 h the polymer was precipitated in methanol (60 mL), filtered, washed with water (at pH=4, then at pH=10 and finally neutral) and subsequently submitted to soxhlet extraction with MeOH, acetone, heptane, and chloroform in order to remove the eccess of end-capping reagents, catalyst residues and oligomers. The polymer was dispersed in THF, filtered, and obtained in 99% yield (0.312 g, 0.60 mmol).

FT-IR Characterization

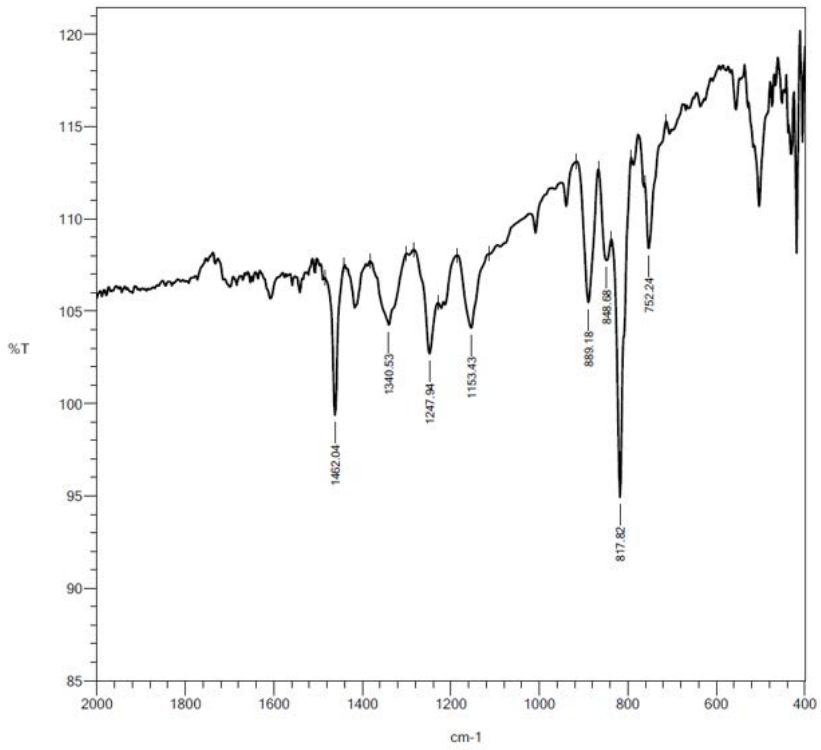

^{13}C Solid-State NMR Characterization

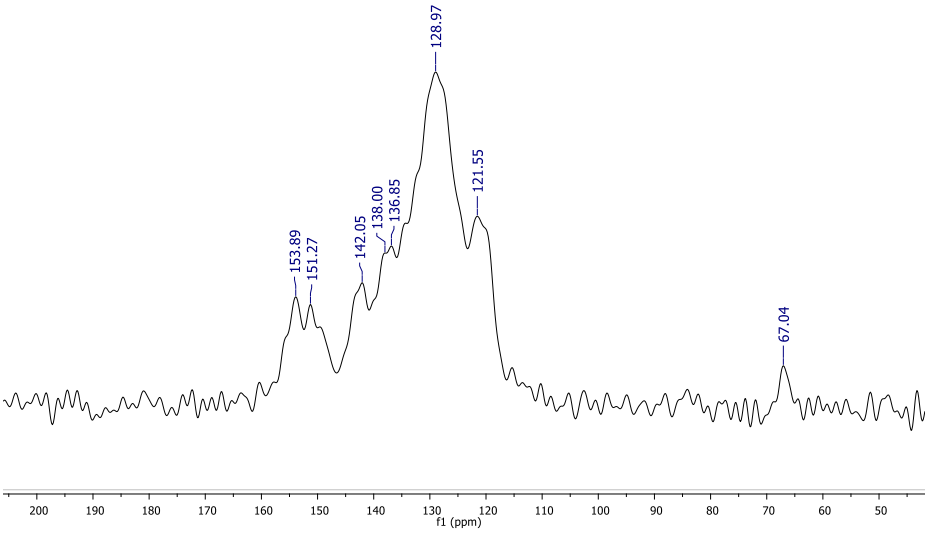

Powder XRD Characterization

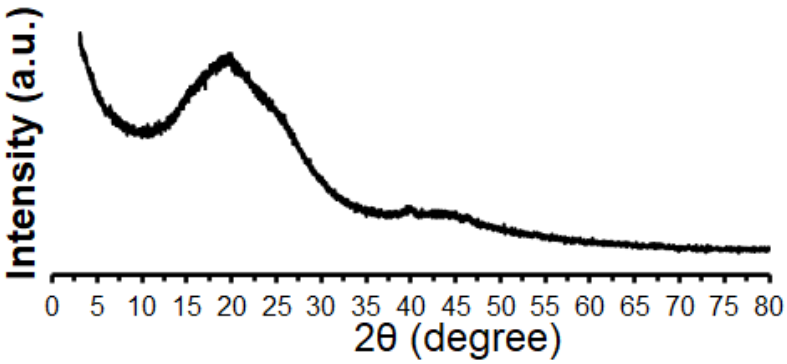

TGA Analysis

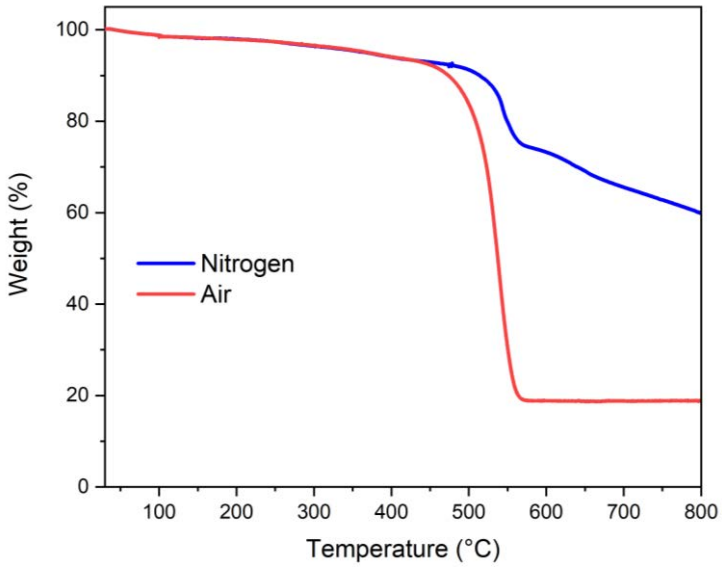

SEM Images

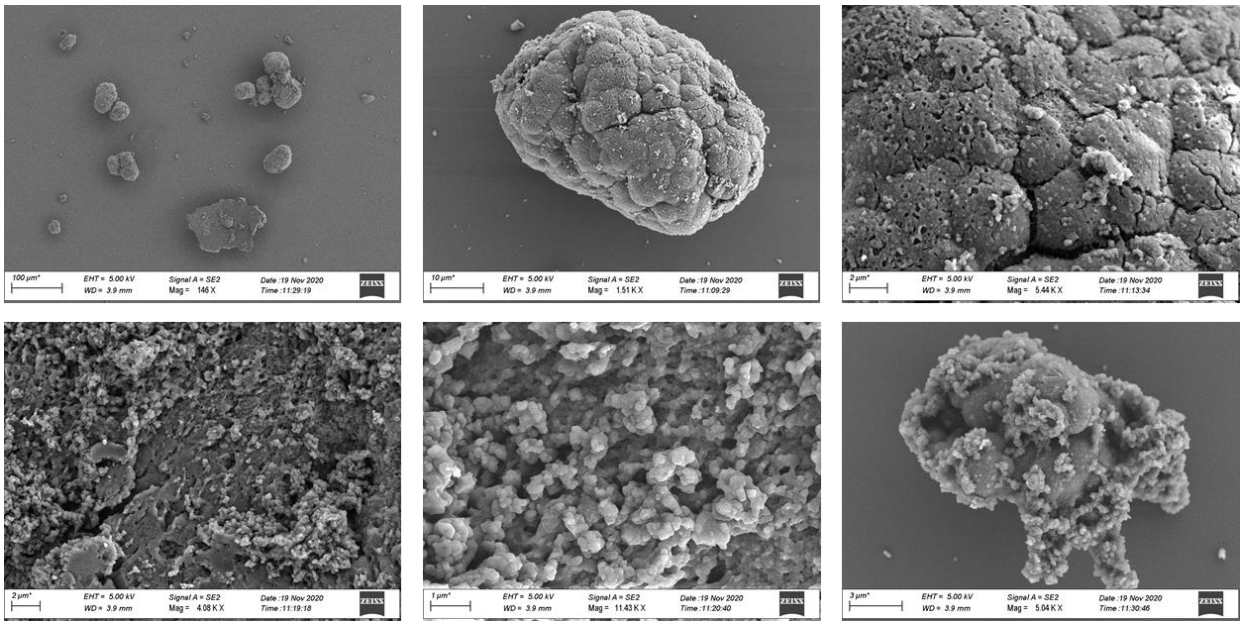

3.2.4.7. General Synthetic Procedure for the Emulsion Polymerizations

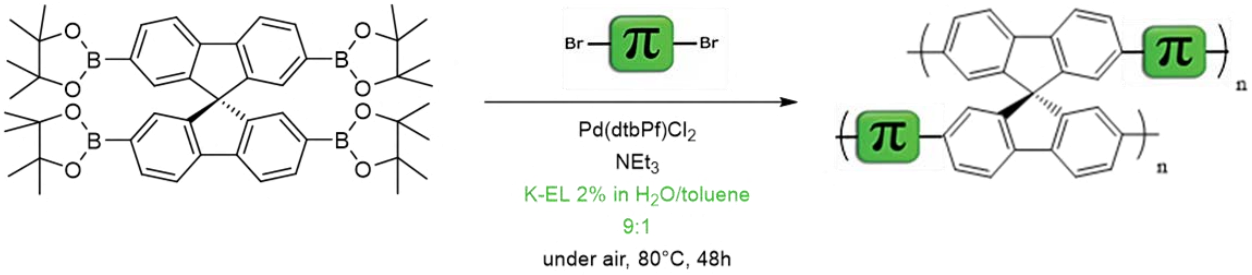

All the polymerizations were carried out in a 5mL CEM microwave glass tube vial under magnetic stirring at 1000 rpm and at a nominal concentration for the monomers of 0.25 mol/L.

A representative experimental procedure for PSBF2FBT is given as an example: 2,2',7,7'-tetrakis(4,4,5,5-tetramethyl-1,3,2-dioxaborolan)-9,9'-spirobifluorene (0.500 g, 0.61 mmol), 4,7-dibromo-5,6-difluoro-2,1,3-benzothiadiazole (0.402 g, 1.22 mmol), and $Pd(dtbpf)Cl_2$ (0.032 g, 0.05 mmol) were weighed in the vial and then 2.4 mL of Kolliphor EL 2 wt%/toluene 9:1 oil-in-water emulsion was added. The mixture was stirred and allowed to homogenize for 5 min at 80 °C, heating with an oil bath, before addition of the NEt_3 (0.370 g, 3.66 mmol). After the addition of the base, the reaction mixture was stirred at 80 °C for 48 h. To provide defined end-groups phenylboronic acid (183 mg, 3 eq.), and after 2 h bromobenzene (157 mg, 3 eq.) were added. After stirring for further 2 h the polymer was precipitated in methanol (10 mL), washed with water (at pH= 4, at pH= 10 and neutral pH) and then submitted to soxhlet extraction with MeOH, acetone, heptane, and chloroform in order to remove the excess of end-capping groups, catalyst residues and oligomers. The polymer was dispersed in THF, filtered, and obtained in 78% yield (0.353 g, 0.48 mmol).

3.2.4.7.1. Characterization of PSBFT2 in Emulsion Conditions

Brown powder, 385 mg, 99%.

FT-IR Characterization

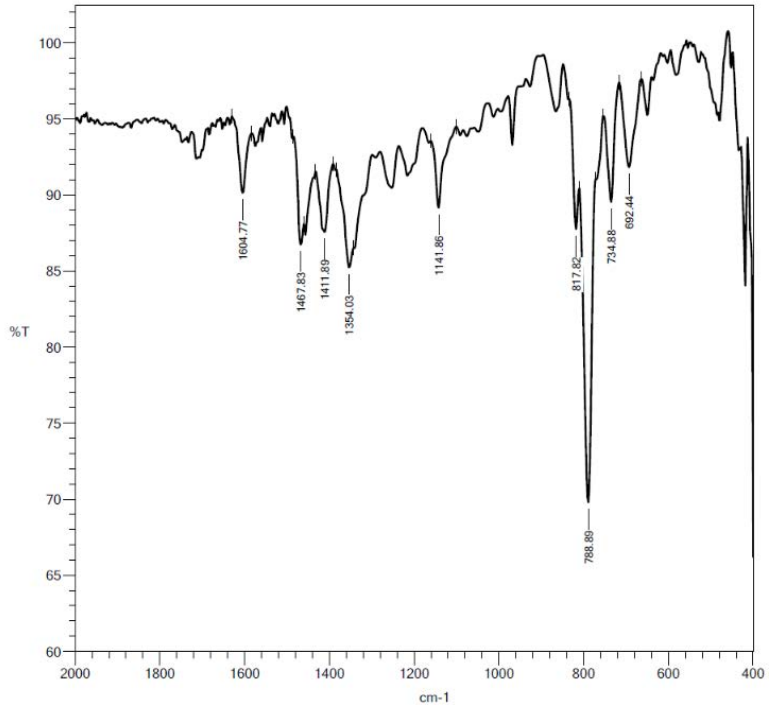

^{13}C Solid-State NMR Characterization

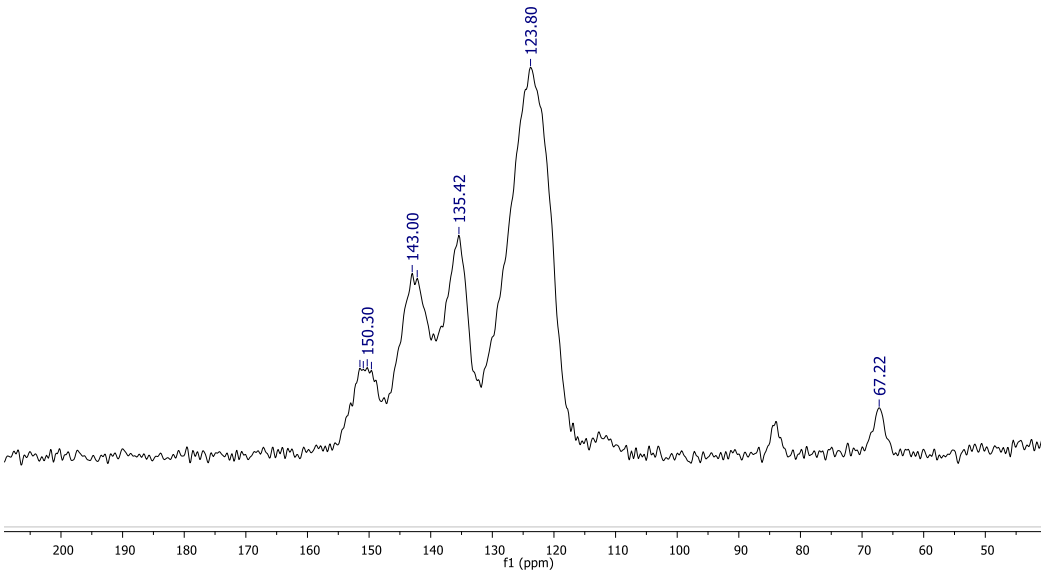

Powder XRD Characterization

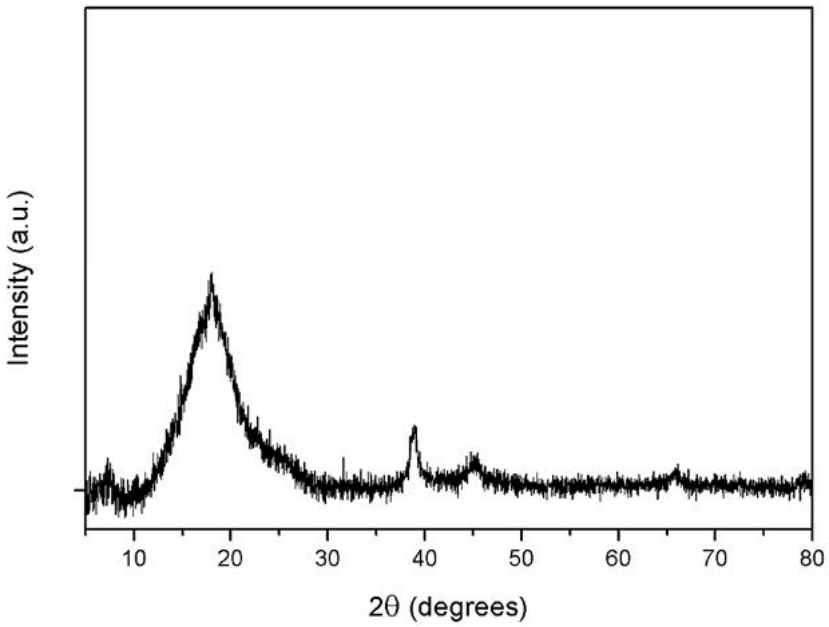

TGA Analysis

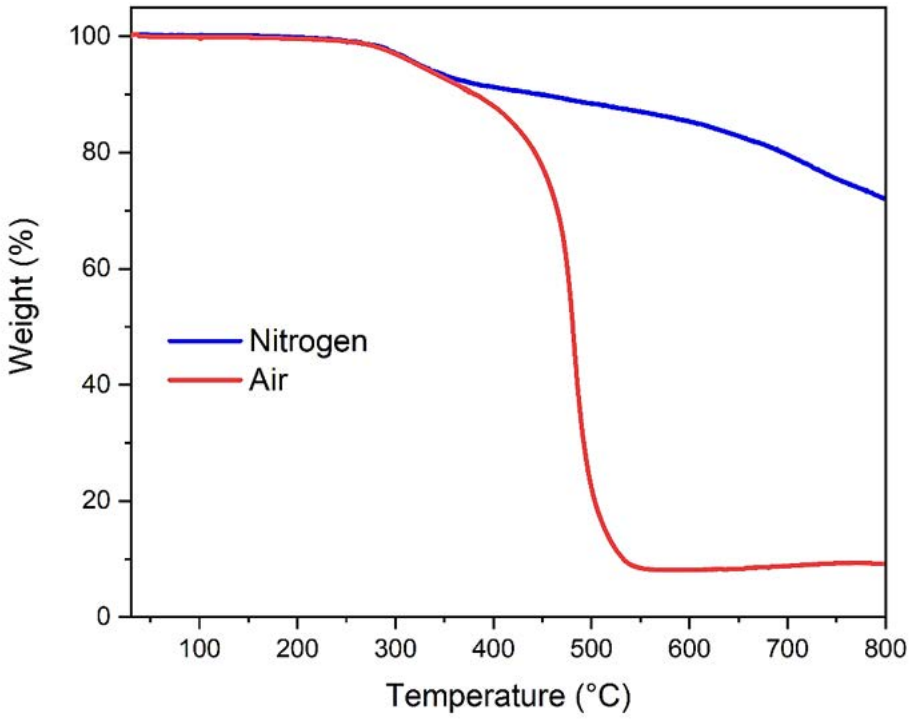

SEM Images

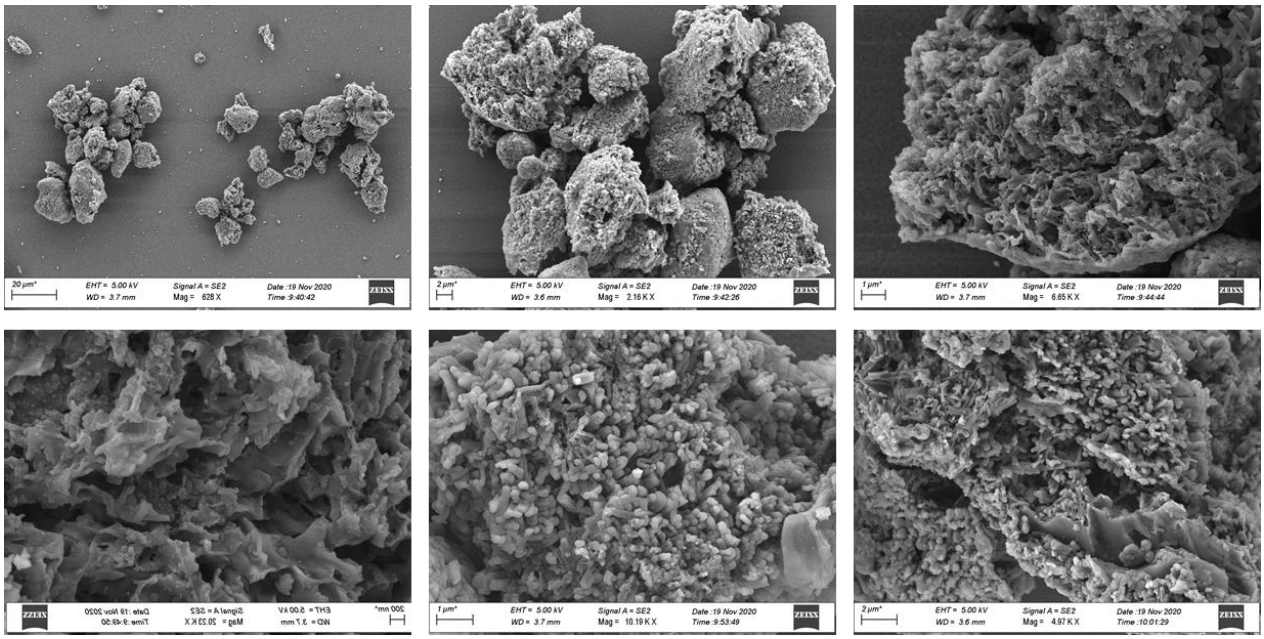

3.2.4.7.2. Characterization of PSBFBT in Emulsion Conditions

Yellow powder, 310 mg, 99%.

FT-IR Characterization

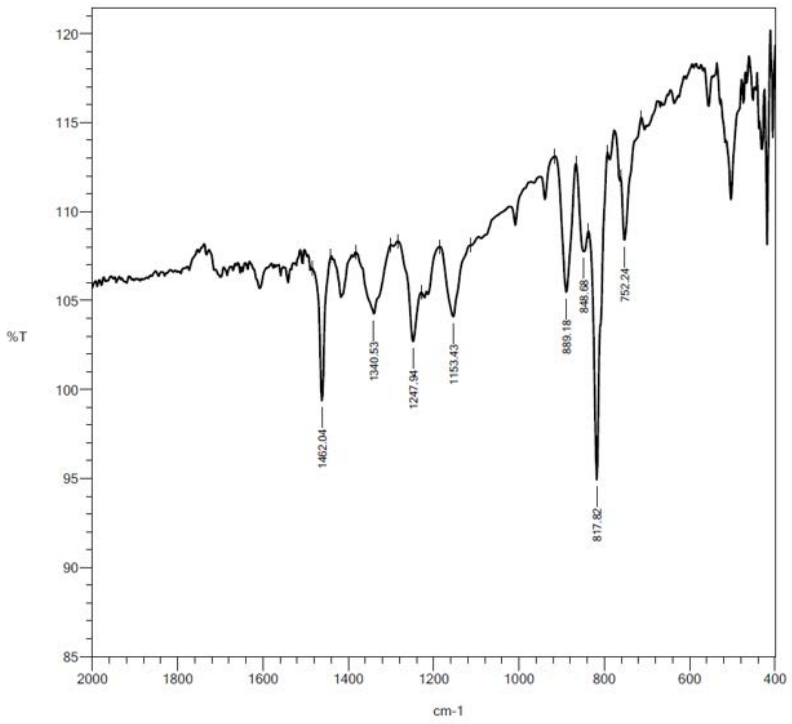

^{13}C Solid-State NMR Characterization

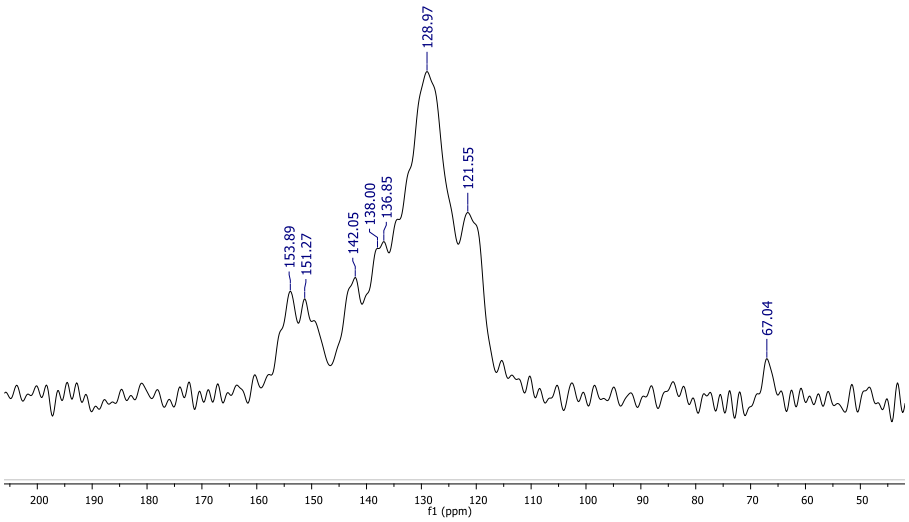

Powder XRD Characterization

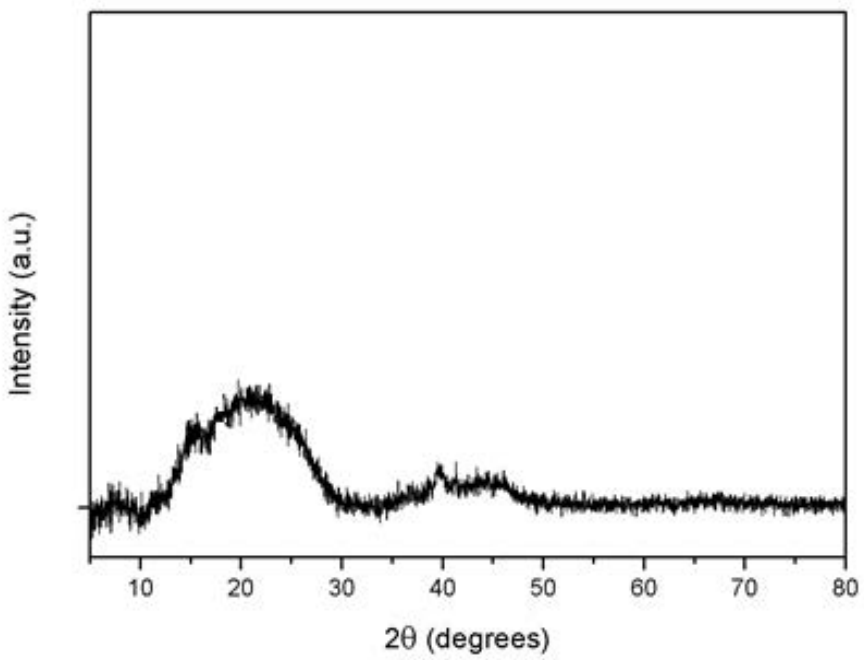

TGA Analysis

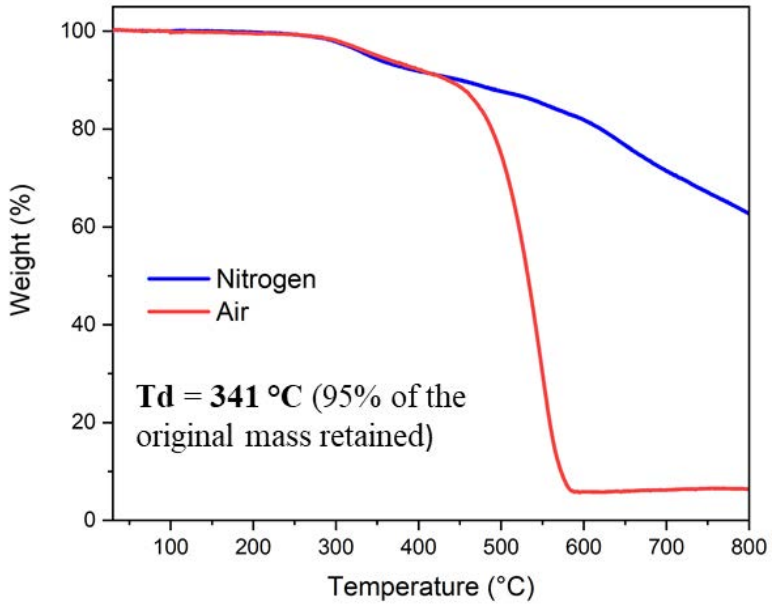

SEM Images

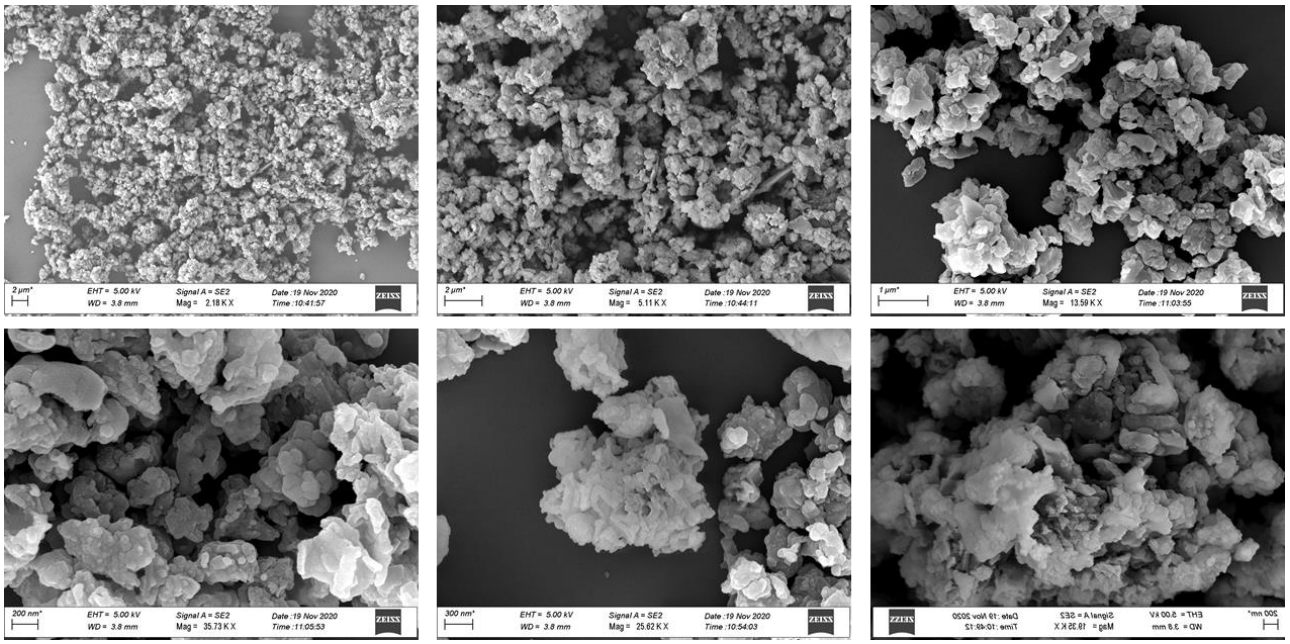

3.2.4.7.3. Characterization of PSBFBT-Inv in Emulsion Conditions

Brown powder, 311 mg, 99%.

FT-IR Characterization

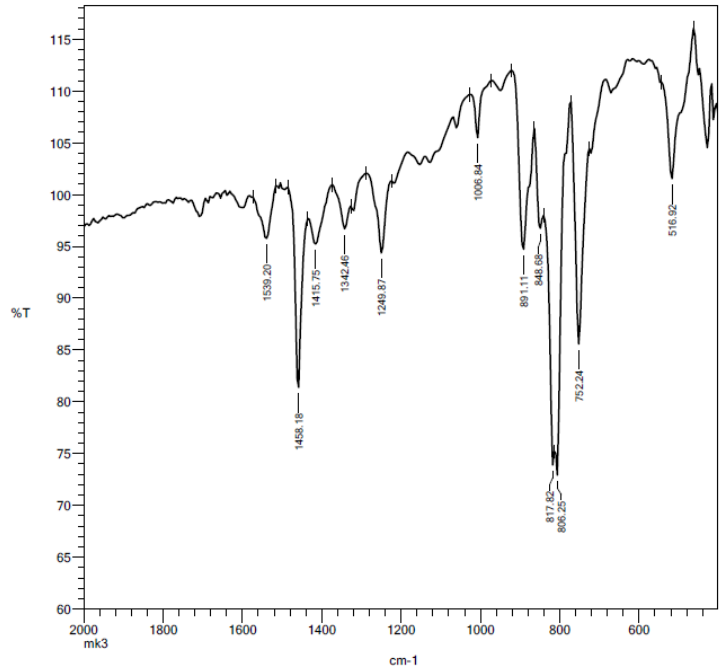

^{13}C Solid-State NMR Characterization

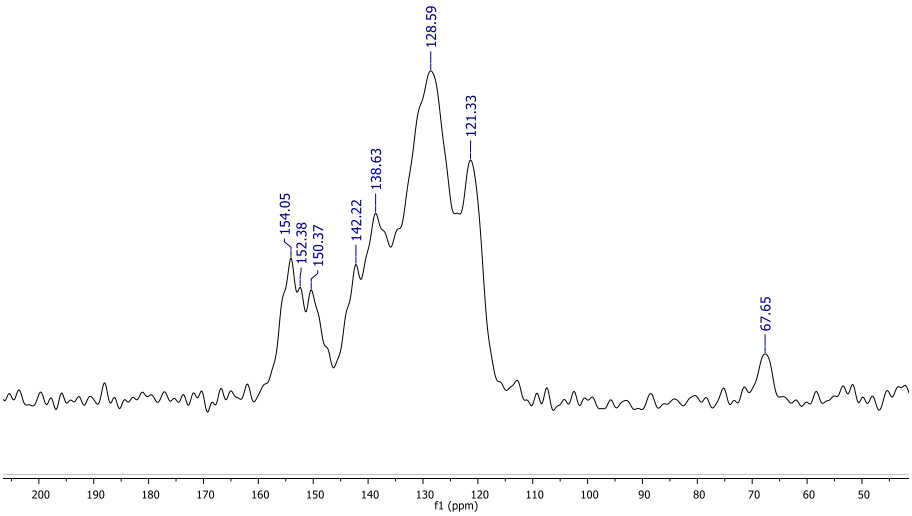

Powder XRD Characterization

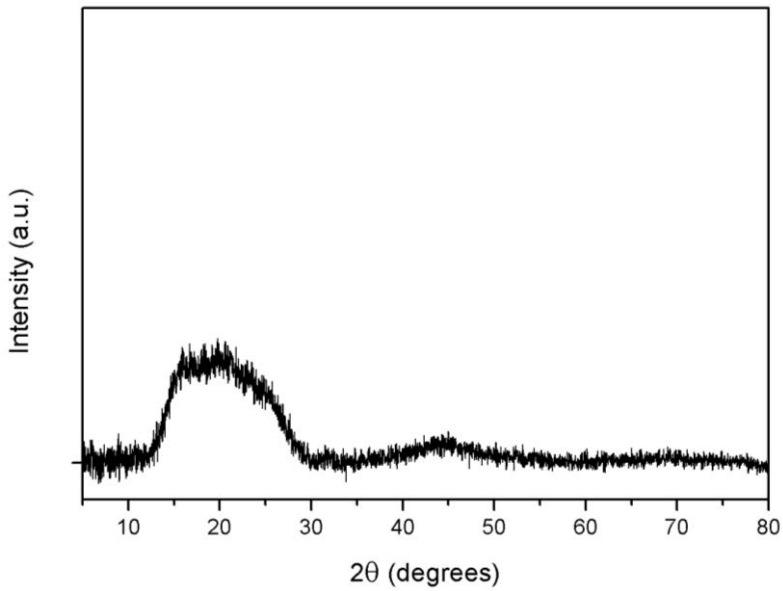

TGA Analysis

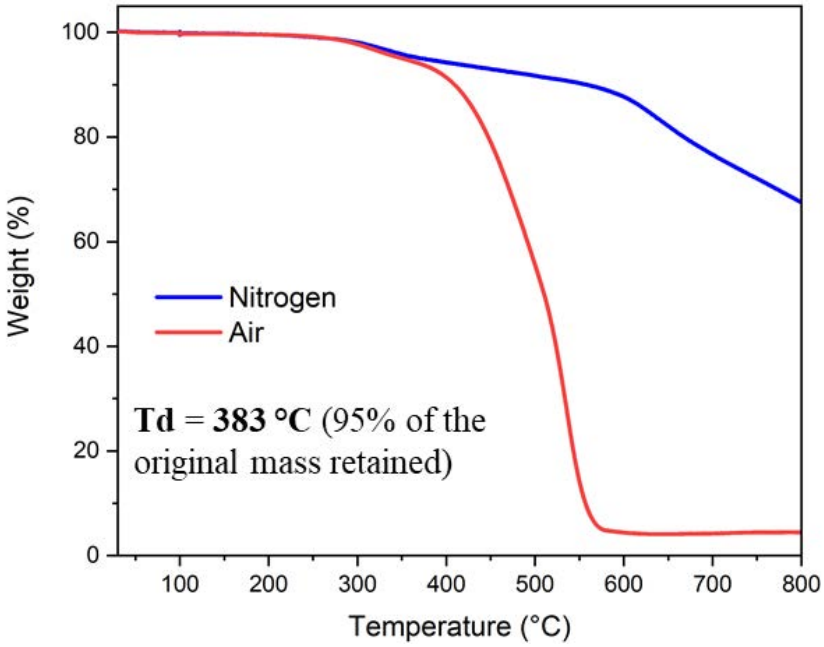

SEM Images

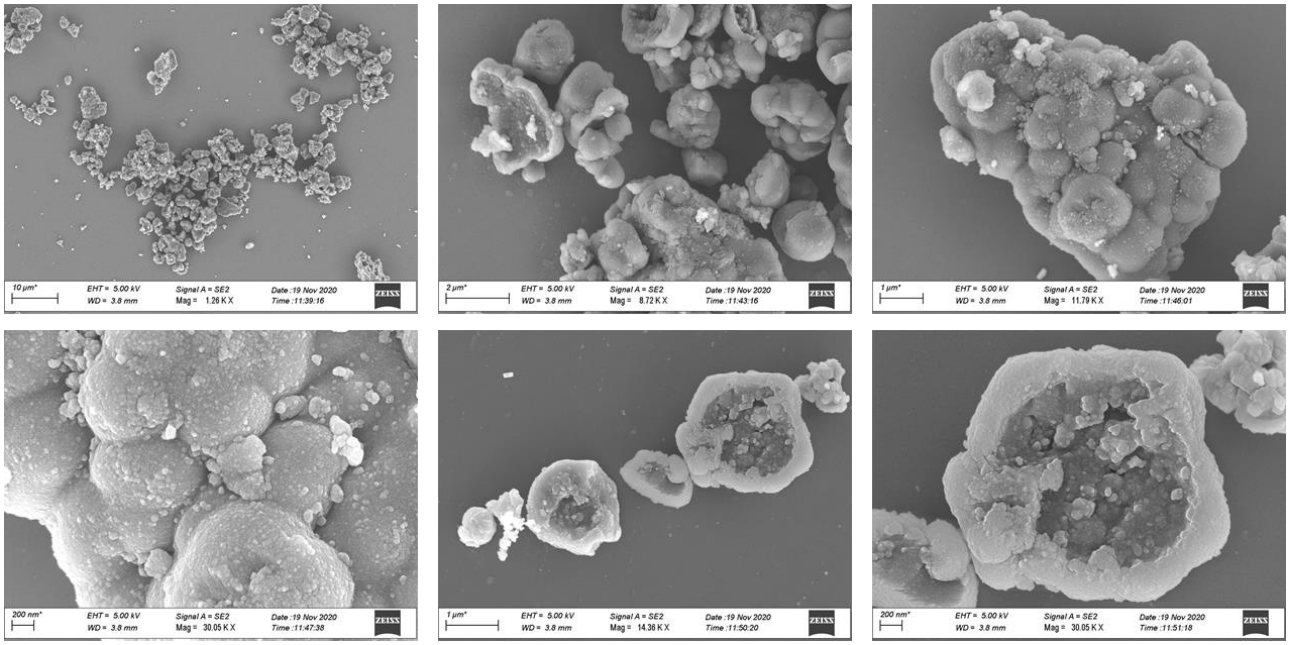

3.2.4.7.4. Characterization of PSBF2FBT in Emulsion Conditions

Dark Yellow powder, 353 mg, 78%.

FT-IR Characterization

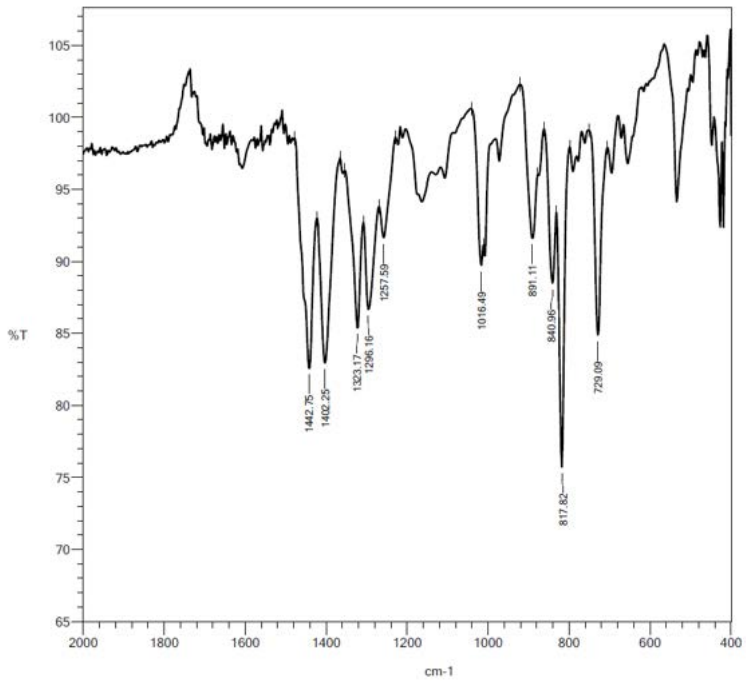

^{13}C Solid-State NMR Characterization

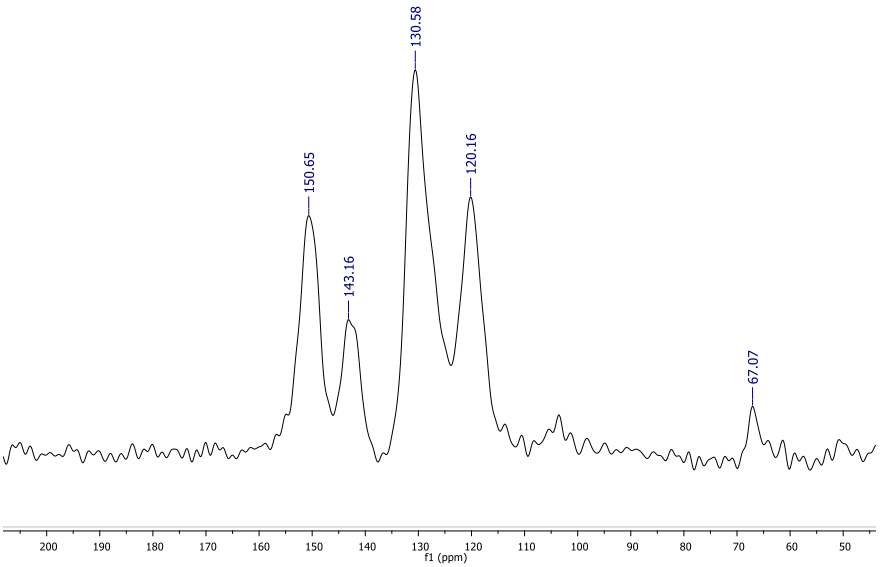

Powder XRD Characterization

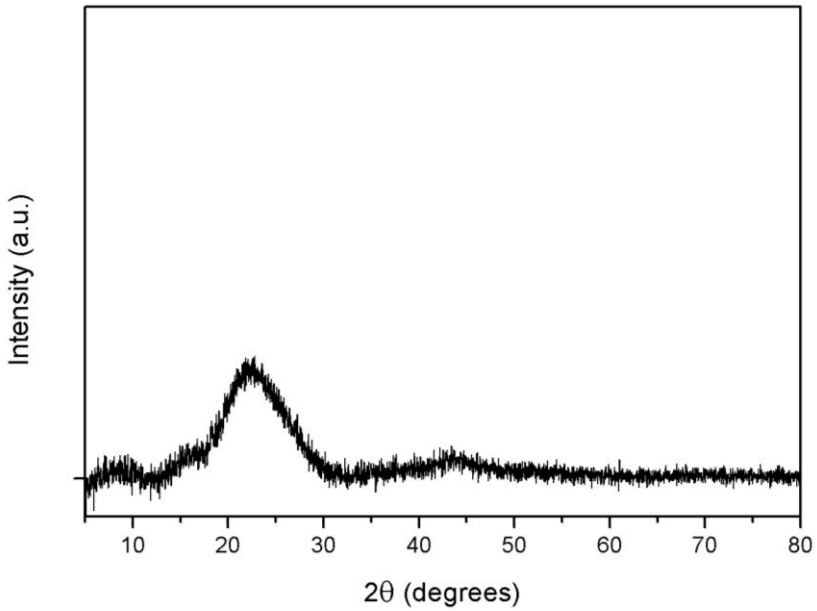

TGA Analysis

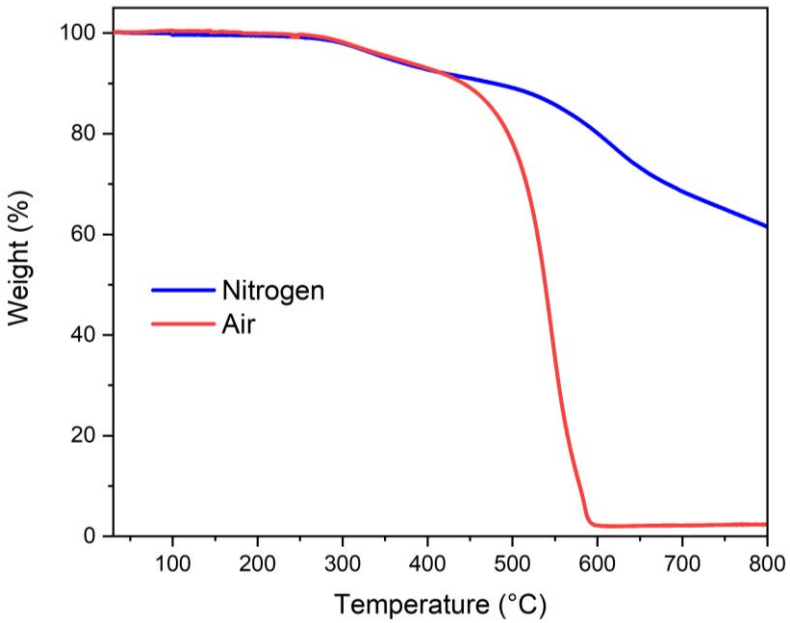

SEM Images

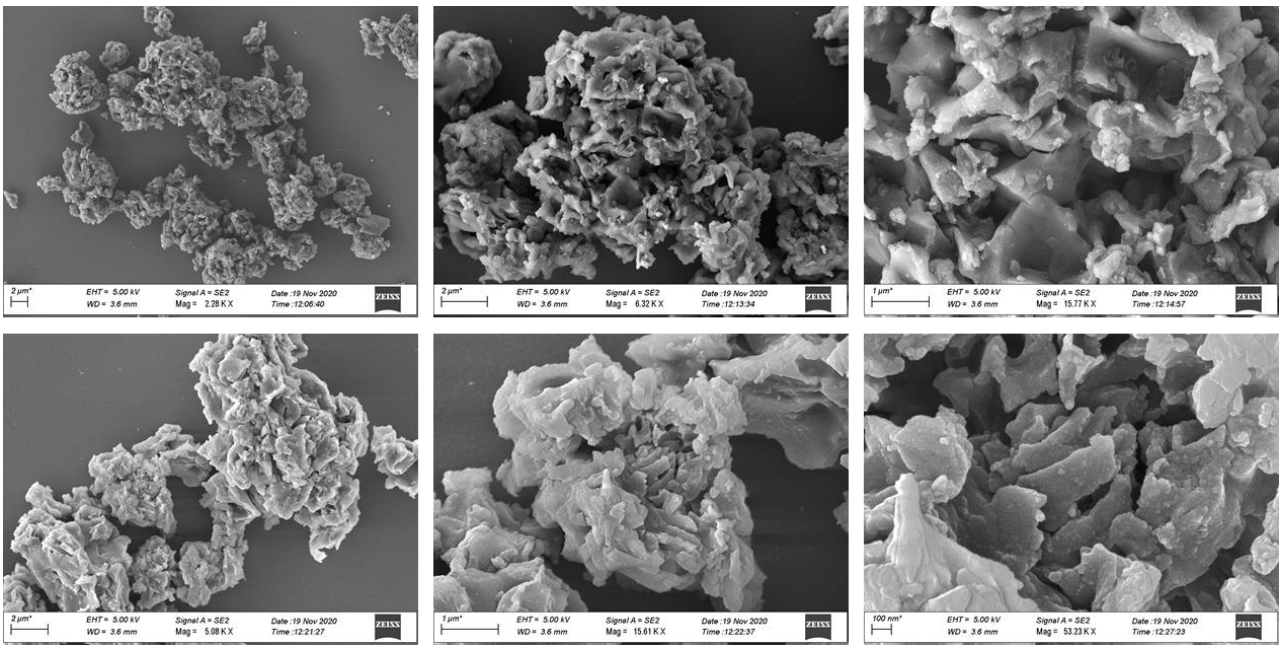

3.2.4.7.5. Characterization of PSBFDTBT in Emulsion Conditions

Red Purpleish powder, 284 mg, 51%.

FT-IR Characterization

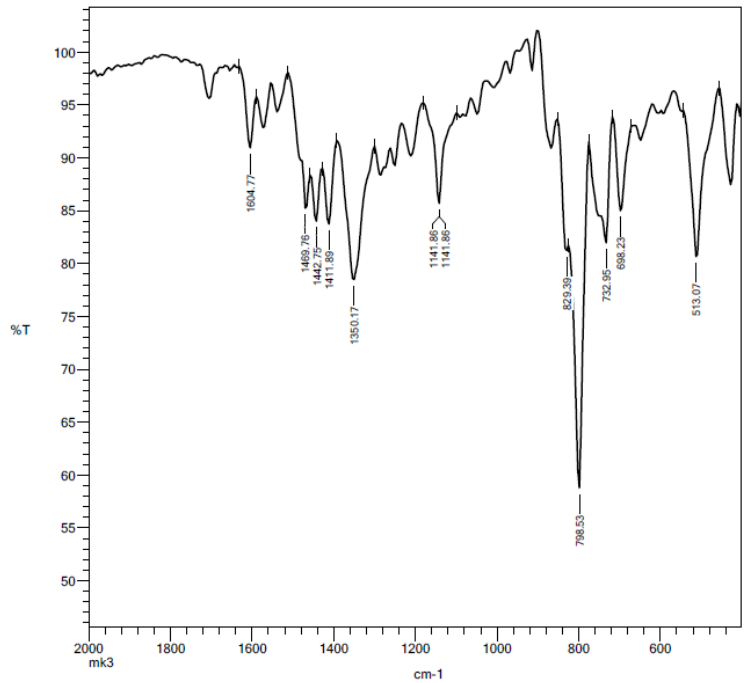

^{13}C Solid-State NMR Characterization

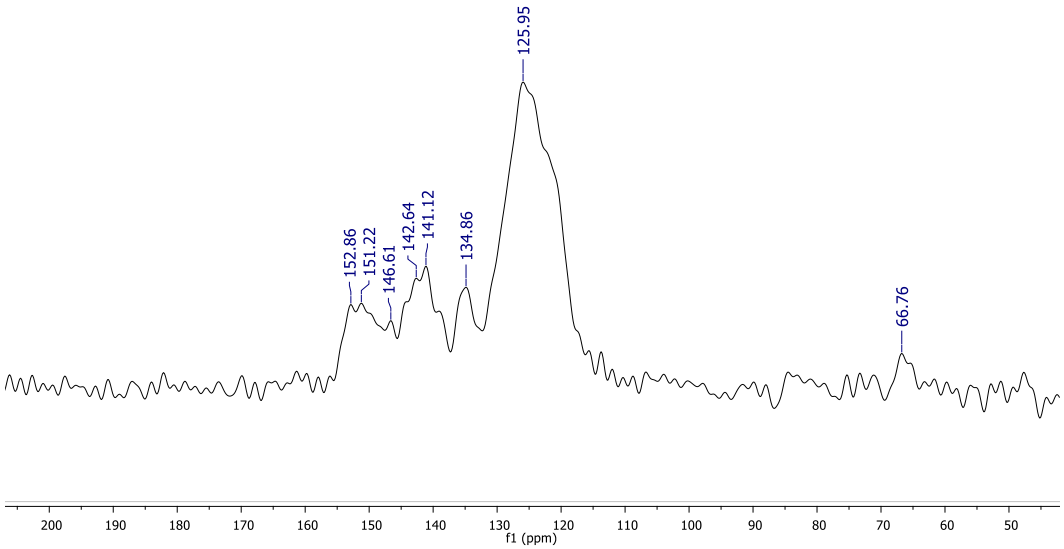

Powder XRD Characterization

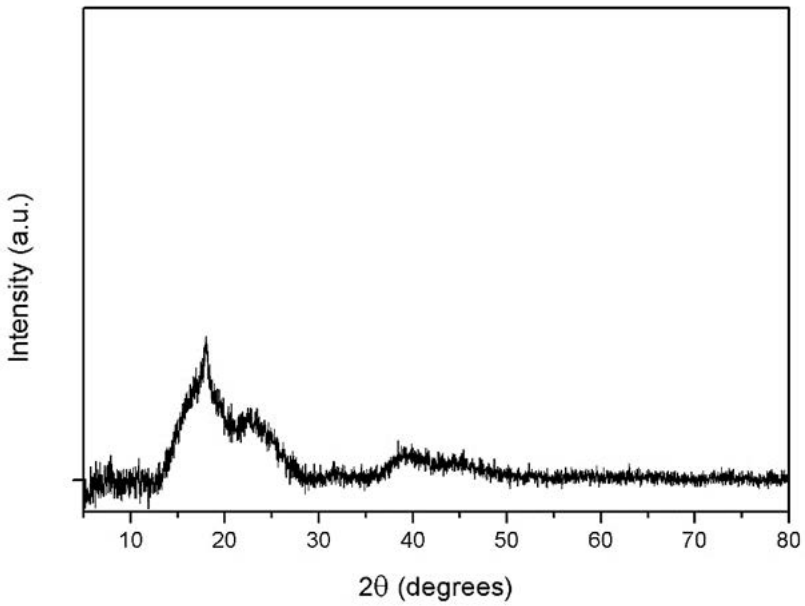

SEM Images

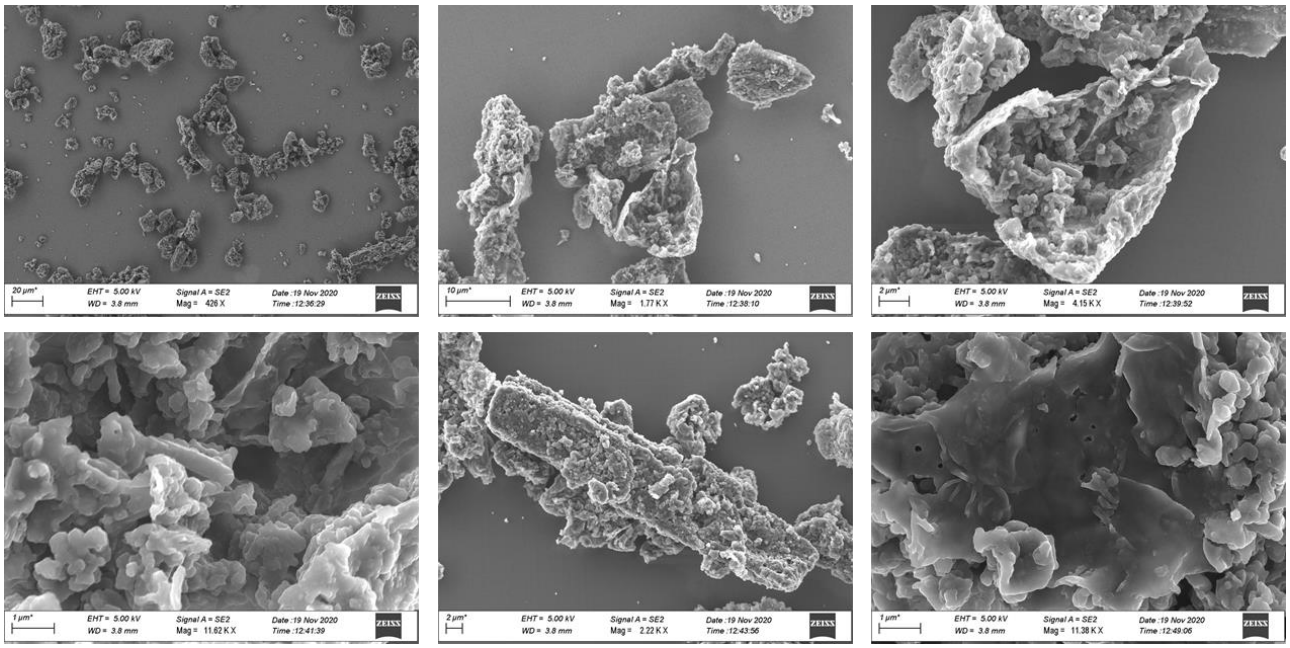

3.2.4.7.6. Characterization of PSBFDT2FBT in Emulsion Conditions

Red powder, 583 mg, 97%.

FT-IR Characterization

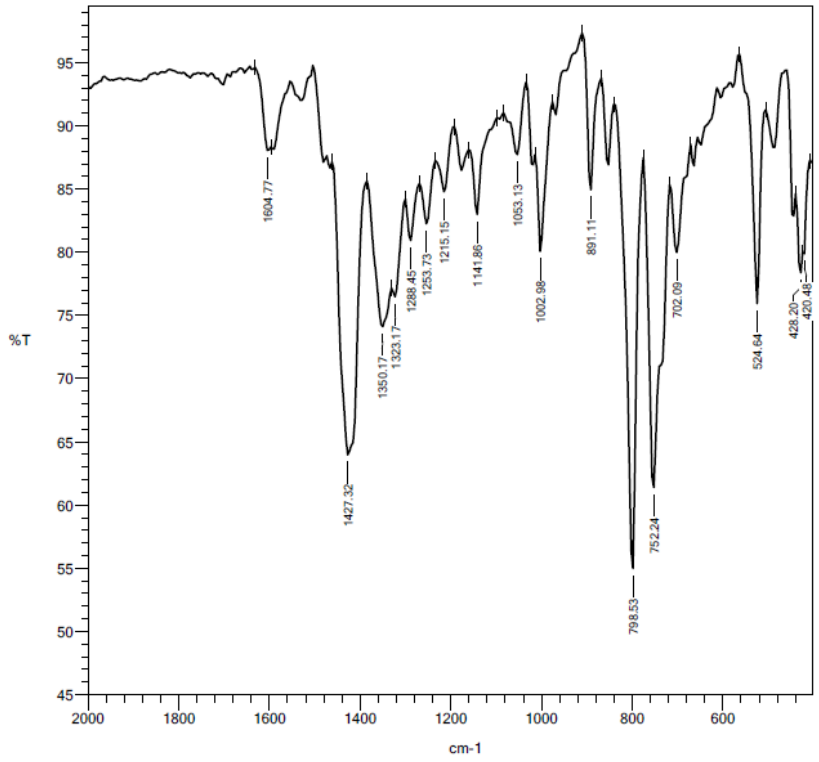

^{13}C Solid-State NMR Characterization

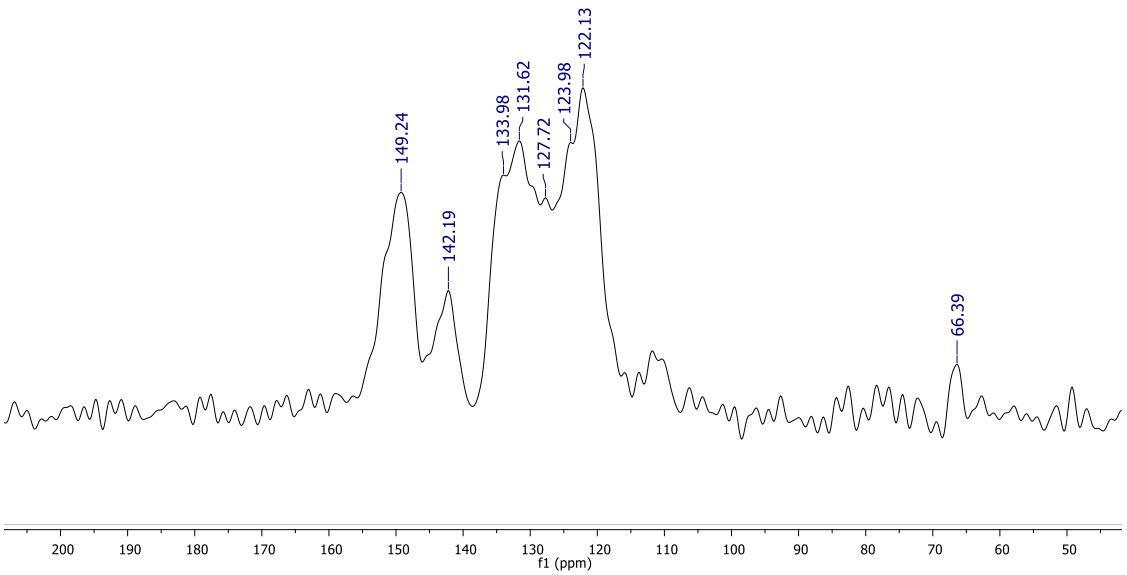

Powder XRD Characterization

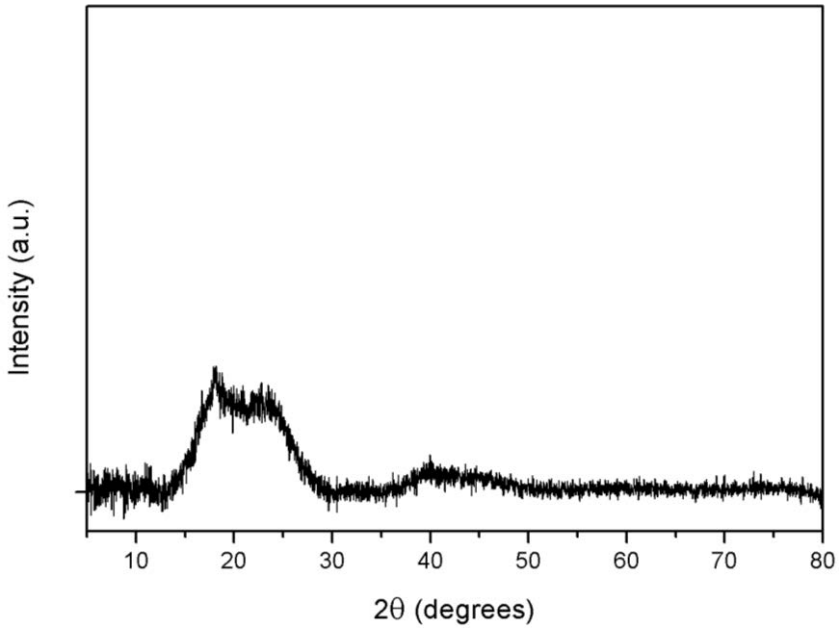

SEM Images

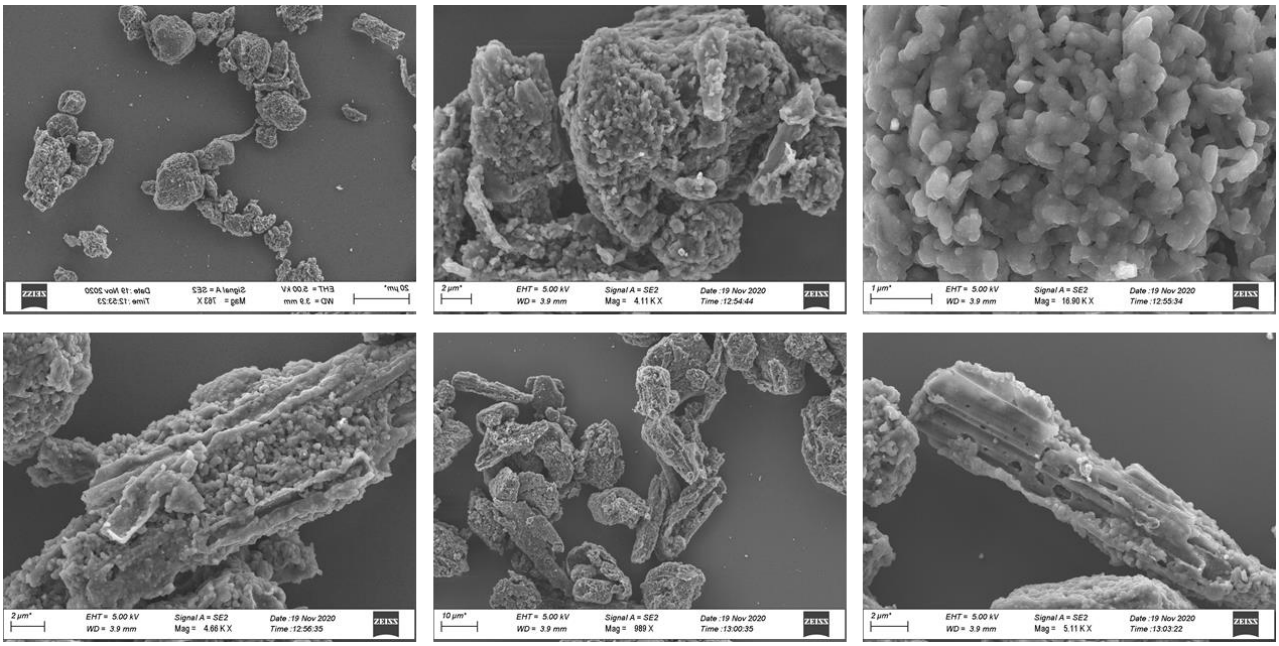

References

(1) Murad, A. R.; Iraqi, A.; Aziz, S. B.; Abdullah, S. N.; Brza, M. A. Conducting Polymers for Optoelectronic Devices and Organic Solar Cells: A Review. *Polymers (Basel).* **2020**, *12* (11), 1–47. https://doi.org/10.3390/polym12112627.

(2) Facchetti, A. π-Conjugated Polymers for Organic Electronics and Photovoltaic Cell Applications. *Chem. Mater.* **2011**, *23* (3), 733–758. https://doi.org/10.1021/cm102419z.

(3) Heeger, A. J. Semiconducting Polymers: The Third Generation. *Chem. Soc. Rev.* **2010**, *39* (7), 2354–2371. https://doi.org/10.1039/b914956m.

(4) Allard, S.; Forster, M.; Souharce, B.; Thiem, H.; Scherf, U. Organic Semiconductors for Solution-Processable Field-Effect Transistors (OFETs). *Angew. Chemie - Int. Ed.* **2008**, *47* (22), 4070–4098. https://doi.org/10.1002/anie.200701920.

(5) Mcculloch, I.; Heeney, M.; Chabinyc, M. L.; Delongchamp, D.; Kline, R. J.; Cölle, M.; Duffy, W.; Fischer, D.; Gundlach, D.; Hamadani, B.; Hamilton, R.; Richter, L.; Salleo, A.; Shkunov, M.; Sparrowe, D.; Tierney, S.; Zhang, W. Semiconducting Thienothiophene Copolymers: Design, Synthesis, Morphology, and Performance in Thin-Film Organic Transistors. *Adv. Mater.* **2009**, *21* (10–11), 1091–1109. https://doi.org/10.1002/adma.200801650.

(6) Marrocchi, A.; Trombettoni, V.; Sciosci, D.; Campana, F.; Vaccaro, L. *Key Trends in Sustainable Approaches to the Synthesis of Semiconducting Polymers*, 2nd ed.; Elsevier Ltd., 2019. https://doi.org/10.1016/b978-0-08-102284-9.00002-4.

(7) Phan, S.; Luscombe, C. K. Recent Advances in the Green, Sustainable Synthesis of Semiconducting Polymers. *Trends Chem.* **2019**, *1* (7), 670–681. https://doi.org/10.1016/j.trechm.2019.08.002.

(8) Zhang, J.; Kang, L. J.; Parker, T. C.; Blakey, S. B.; Luscombe, C. K.; Marder, S. R. Recent Developments in C–H Activation for Materials Science in the Center for Selective C–H Activation. *Molecules* **2018**, *23* (4), 1–13. https://doi.org/10.3390/molecules23040922.

(9) Okamoto, K.; Zhang, J.; Housekeeper, J. B.; Marder, S. R.; Luscombe, C. K. C-H Arylation Reaction: Atom Efficient and Greener Syntheses of π-Conjugated Small Molecules and Macromolecules for Organic Electronic Materials. *Macromolecules* **2013**, *46* (20), 8059–8078. https://doi.org/10.1021/ma401190r.

(10) Rudenko, A. E.; Thompson, B. C. Optimization of Direct Arylation Polymerization (DArP) through the Identification and Control of Defects in Polymer Structure. *J. Polym. Sci. Part A Polym. Chem.* **2015**, *53* (2), 135–147. https://doi.org/10.1002/pola.27279.

(11) Wakioka, M.; Ozawa, F. Highly Efficient Catalysts for Direct Arylation Polymerization (DArP). *Asian J. Org. Chem.* **2018**, *7* (7), 1206–1216. https://doi.org/10.1002/ajoc.201800227.

(12) Marrocchi, A.; Facchetti, A.; Lanari, D.; Petrucci, C.; Vaccaro, L. Current Methodologies for a Sustainable Approach to π-Conjugated Organic Semiconductors. *Energy Environ. Sci.* **2016**, *9* (3), 763–786. https://doi.org/10.1039/c5ee03727a.

(13) Sanzone, A.; Calascibetta, A.; Monti, M.; Mattiello, S.; Sassi, M.; Corsini, F.; Griffini, G.; Sommer, M.; Beverina, L. Synthesis of Conjugated Polymers by Sustainable Suzuki Polycondensation in Water and under Aerobic Conditions. *ACS Macro Lett.* **2020**, 1167–1171. https://doi.org/10.1021/acsmacrolett.0c00495.

(14) Landstrom, E. B.; Handa, S.; Aue, D. H.; Gallou, F.; Lipshutz, B. H. EvanPhos: A Ligand for Ppm Level Pd-Catalyzed Suzuki-Miyaura Couplings in Either Organic Solvent or Water. *Green Chem.* **2018**, *20* (15), 3436–3443. https://doi.org/10.1039/c8gc01356j.

(15) Gabriel, C. M.; Parmentier, M.; Riegert, C.; Lanz, M.; Handa, S.; Lipshutz, B. H.; Gallou, F. Sustainable and Scalable Fe/Ppm Pd Nanoparticle Nitro Group Reductions in Water at Room Temperature. *Org. Process Res. Dev.* **2017**, *21* (2), 247–252. https://doi.org/10.1021/acs.oprd.6b00410.

(16) Mattiello, S.; Rooney, M.; Sanzone, A.; Brazzo, P.; Sassi, M.; Beverina, L. Suzuki-Miyaura Micellar Cross-Coupling in Water, at Room Temperature, and under Aerobic Atmosphere. *Org. Lett.* **2017**, *19* (3), 654–657. https://doi.org/10.1021/acs.orglett.6b03817.

(17) Sanzone, A.; Calascibetta, A.; Ghiglietti, E.; Ceriani, C.; Mattioli, G.; Mattiello, S.; Sassi, M.; Beverina, L. Suzuki-Miyaura Micellar One-Pot Synthesis of Symmetrical and Unsymmetrical 4,7-Diaryl-5,6-Difluoro-2,1,3-Benzothiadiazole Luminescent Derivatives in Water and under Air. *J. Org. Chem.* **2018**, *83* (24), 15029–15042. https://doi.org/10.1021/acs.joc.8b02204.
(18) Rooney, M.; Mattiello, S.; Stara, R.; Sanzone, A.; Brazzo, P.; Sassi, M.; Beverina, L. Suzuki-Miyaura Cross-Coupling of Latent Pigments in Water/Toluene Emulsion under Aerobic Atmosphere. *Dye. Pigment.* **2018**, *149* (September 2017), 893–901. https://doi.org/10.1016/j.dyepig.2017.11.044.
(19) Vaghi, L.; Sanzone, A.; Sassi, M.; Pagani, S.; Papagni, A.; Beverina, L. Synthesis of Fluorinated Acridines via Sequential Micellar Buchwald-Hartwig Amination/Cyclization of Aryl Bromides. *Synth.* **2018**, *50* (8), 1621–1628. https://doi.org/10.1055/s-0036-1591937.
(20) Sanzone, A.; Mattiello, S.; Garavaglia, G. M.; Calascibetta, A. M.; Ceriani, C.; Sassi, M.; Beverina, L. Efficient Synthesis of Organic Semiconductors by Suzuki-Miyaura Coupling in an Aromatic Micellar Medium. *Green Chem.* **2019**, *21* (16), 4400–4405. https://doi.org/10.1039/c9gc01071h.
(21) Calascibetta, A. M.; Mattiello, S.; Sanzone, A.; Facchinetti, I.; Sassi, M.; Beverina, L. Sustainable Access to π-Conjugated Molecular Materials via Direct (Hetero)Arylation Reactions in Water and under Air. *Molecules* **2020**, *25* (16). https://doi.org/10.3390/molecules25163717.
(22) Kuehne, A. J. C.; Gather, M. C.; Sprakel, J. Monodisperse Conjugated Polymer Particles by Suzuki-Miyaura Dispersion Polymerization. *Nat. Commun.* **2012**, *3*. https://doi.org/10.1038/ncomms2085.
(23) Muenmart, D.; Foster, A. B.; Harvey, A.; Chen, M. T.; Navarro, O.; Promarak, V.; McCairn, M. C.; Behrendt, J. M.; Turner, M. L. Conjugated Polymer Nanoparticles by Suzuki-Miyaura Cross-Coupling Reactions in an Emulsion at Room Temperature. *Macromolecules* **2014**, *47* (19), 6531–6539. https://doi.org/10.1021/ma501402h.
(24) Sassi, M.; Mattiello, S.; Beverina, L. Syntheses of Organic Semiconductors in Water. Recent Advancement in the Surfactants Enhanced Green Access to Polyconjugated Molecules. *European J. Org. Chem.* **2020**, *2020* (26), 3942–3953. https://doi.org/10.1002/ejoc.202000140.
(25) Gabriel, C. M.; Lee, N. R.; Bigorne, F.; Klumphu, P.; Parmentier, M.; Gallou, F.; Lipshutz, B. H. Effects of Co-Solvents on Reactions Run under Micellar Catalysis Conditions. *Org. Lett.* **2017**, *19* (1), 194–197. https://doi.org/10.1021/acs.orglett.6b03468.
(26) Kettner, O.; Pein, A.; Trimmel, G.; Christian, P.; Röthel, C.; Salzmann, I.; Resel, R.; Lakhwani, G.; Lombeck, F.; Sommer, M.; Friedel, B. Mixed Side-Chain Geometries for Aggregation Control of Poly(Fluorene-Alt-Bithiophene) and Their Effects on Photophysics and Charge Transport. *Synth. Met.* **2016**, *220*, 162–173. https://doi.org/10.1016/j.synthmet.2016.06.010.
(27) Morin, P. O.; Bura, T.; Sun, B.; Gorelsky, S. I.; Li, Y.; Leclerc, M. Conjugated Polymers à La Carte from Time-Controlled Direct (Hetero)Arylation Polymerization. *ACS Macro Lett.* **2015**, *4* (1), 21–24. https://doi.org/10.1021/mz500656g.
(28) Zhou, X.; Pan, C.; Liang, A.; Wang, L.; Wan, T.; Yang, G.; Gao, C.; Wong, W. Y. Enhanced Figure of Merit of Poly(9,9-Di-n-Octylfluorene-Alt-Benzothiadiazole) and SWCNT Thermoelectric Composites by Doping with FeCl3. *J. Appl. Polym. Sci.* **2019**, *136* (5), 6–11. https://doi.org/10.1002/app.47011.
(29) Liang, A.; Zhou, X.; Zhou, W.; Wan, T.; Wang, L.; Pan, C.; Wang, L. Side-Chain Effects on the Thermoelectric Properties of Fluorene-Based Copolymers. *Macromol. Rapid Commun.* **2017**, *38* (18), 1–6. https://doi.org/10.1002/marc.201600817.
(30) Yu, F.; Wang, Z.; Zhang, S.; Ye, H.; Kong, K.; Gong, X.; Hua, J.; Tian, H. Molecular Engineering of Donor–Acceptor Conjugated Polymer/g-C3N4 Heterostructures for Significantly Enhanced Hydrogen Evolution Under Visible-Light Irradiation. *Adv. Funct. Mater.* **2018**, *28* (47), 1–13. https://doi.org/10.1002/adfm.201804512.
(31) Sommer, M.; Komber, H.; Huettner, S.; Mulherin, R.; Kohn, P.; Greenham, N. C.; Huck, W. T. S. Synthesis, Purification, and Characterization of Well-Defined All-Conjugated Diblock Copolymers PF8TBT- b -P3HT. *Macromolecules* **2012**, *45* (10), 4142–4151. https://doi.org/10.1021/ma300533k.
(32) Mattiello, S.; Monguzzi, A.; Pedrini, J.; Sassi, M.; Villa, C.; Torrente, Y.; Marotta, R.;

Meinardi, F.; Beverina, L. Self-Assembled Dual Dye-Doped Nanosized Micelles for High-Contrast Up-Conversion Bioimaging. *Adv. Funct. Mater.* **2016**, *26* (46), 8447–8454. https://doi.org/10.1002/adfm.201603303.
(33) List, E. J. W.; Gaal, M.; Guentner, R.; De Freitas, P. S.; Scherf, U. The Role of Keto Defect Sites for the Emission Properties of Polyfluorene-Type Materials. *Synth. Met.* **2003**, *139* (3), 759–763. https://doi.org/10.1016/S0379-6779(03)00249-2.
(34) Liu, L.; Tang, S.; Liu, M.; Xie, Z.; Zhang, W.; Lu, P.; Hanif, M.; Ma, Y. Photodegradation of Polyfluorene and Fluorene Oligomers with Alkyl and Aromatic Disubstitutions. *J. Phys. Chem. B* **2006**, *110* (28), 13734–13740. https://doi.org/10.1021/jp062612x.
(35) Lee, J. S. M.; Cooper, A. I. Advances in Conjugated Microporous Polymers. *Chem. Rev.* **2020**, *120* (4), 2171–2214. https://doi.org/10.1021/acs.chemrev.9b00399.
(36) Ren, S.; Dawson, R.; Adams, D. J.; Cooper, A. I. Low Band-Gap Benzothiadiazole Conjugated Microporous Polymers. *Polym. Chem.* **2013**, *4* (22), 5585–5590. https://doi.org/10.1039/c3py00690e.
(37) Cheng, C.; Wang, X.; Lin, Y.; He, L.; Jiang, J. X.; Xu, Y.; Wang, F. The Effect of Molecular Structure and Fluorination on the Properties of Pyrene-Benzothiadiazole-Based Conjugated Polymers for Visible-Light-Driven Hydrogen Evolution. *Polym. Chem.* **2018**, *9* (35), 4468–4475. https://doi.org/10.1039/c8py00722e.
(38) Matsumura, S.; Hlil, A. R.; Lepiller, C.; Gaudet, J.; Guay, D.; Shi, Z.; Holdcroft, S.; Hay, A. S. Stability and Utility of Pyridyl Disulfide Functionality in RAFT and Conventional Radical Polymerizations. *J. Polym. Sci. Part A Polym. Chem.* **2008**, *46* (April), 7207–7224. https://doi.org/10.1002/pola.
(39) Zhang, Z. G.; Wang, J. Structures and Properties of Conjugated Donor-Acceptor Copolymers for Solar Cell Applications. *J. Mater. Chem.* **2012**, *22* (10), 4178–4187. https://doi.org/10.1039/c2jm14951f.
(40) Deng, Z.; Wu, F.; Chen, L.; Chen, Y. Novel Photovoltaic Donor 1-Acceptor-Donor 2-Acceptor Terpolymers with Tunable Energy Levels Based on a Difluorinated Benzothiadiazole Acceptor. *RSC Adv.* **2015**, *5* (16), 12087–12093. https://doi.org/10.1039/c4ra15181j.
(41) Bohra, H.; Wang, M. Direct Arylation Polymerization for Synthesizing a Library of Conjugated Porous Polymers Containing Thiophene-Flanked Building Blocks. *ACS Appl. Polym. Mater.* **2019**, *1* (7), 1697–1706. https://doi.org/10.1021/acsapm.9b00271.
(42) Huang, W. Y.; Shen, Z. Q.; Cheng, J. Z.; Liu, L. L.; Yang, K.; Chen, X.; Wen, H. R.; Liu, S. Y. C-H Activation Derived CPPs for Photocatalytic Hydrogen Production Excellently Accelerated by a DMF Cosolvent. *J. Mater. Chem. A* **2019**, *7* (42), 24222–24230. https://doi.org/10.1039/c9ta06444c.
(43) Schmidt, J.; Weber, J.; Epping, J. D.; Antonietti, M.; Thomas, A. Microporous Conjugated Poly(Thienylene Arylene) Networks. *Adv. Mater.* **2009**, *21* (6), 702–705. https://doi.org/10.1002/adma.200802692.
(44) Zhang, C.; Qiao, Y.; Xiong, P.; Ma, W.; Bai, P.; Wang, X.; Li, Q.; Zhao, J.; Xu, Y.; Chen, Y.; Zeng, J. H.; Wang, F.; Xu, Y.; Jiang, J. X. Conjugated Microporous Polymers with Tunable Electronic Structure for High-Performance Potassium-Ion Batteries. *ACS Nano* **2019**, *13* (1), 745–754. https://doi.org/10.1021/acsnano.8b08046.
(45) Yi, J.; Wang, Y.; Luo, Q.; Lin, Y.; Tan, H.; Wang, H.; Ma, C. Q. A 9,9′-Spirobi[9H-Fluorene]-Cored Perylenediimide Derivative and Its Application in Organic Solar Cells as a Non-Fullerene Acceptor. *Chem. Commun.* **2016**, *52* (8), 1649–1652. https://doi.org/10.1039/c5cc08484a.
(46) Pei, J.; Ni, J.; Zhou, X. H.; Cao, X. Y.; Lai, Y. H. Head-to-Tail Regioregular Oligothiophene-Functionalized 9,9′-Spirobifluorene Derivatives. 1. Synthesis. *J. Org. Chem.* **2002**, *67* (14), 4924–4936. https://doi.org/10.1021/jo011146z.

Final Conclusions

This thesis work walks along with detailed and concrete examples about the current availability of innovative, effective, and sustainable approaches that can be successfully exploited as valid alternative tools for the preparation of industrially feasible active organic semiconductors. The removal or at least the minimization in the use of harmful and toxic organic solvents commonly employed within standard synthetic processes has a decisive impact on safety and sustainability. The field of micellar catalysis and surfactant-enhanced chemistry plays noticeably in improving the sustainability of organic synthesis with the possibility of use water as reaction medium. In this case, organic transformations are no longer carried out in homogeneous phase by solubilizing the substrates, but rather promoted in lipophilic nano/microheterogeneous compartments stabilized by peculiar surface-active agents. The developed methods revealed to be compatible and effective in the production of several classes of semiconducting materials, ranging from small-molecular to polymeric structures, also with different electronic structures and features. Moreover, the Kolliphor-EL colloidal environments, besides being environmentally beneficial, are also practically favourable enabling to perform organic reactions under standard environmentally conditions in air. For all the topics we investigated through, we always verify a reduction of the E-factor at least by a factor 5 compared with corresponding standard procedures using organic solvents. All the calculated E-factors for each topic we investigated are in the range of 10^2 order, which is compatible with a large-scale industrial production. Furthermore, in most cases the target products can be accessed in higher yields with unprecedent efficiency also demonstrating economic benefits.